ISTITUTO NAZIONALE DI FISICA NUCLEARE
Laboratori Nazionali di Frascati

FRASCATI PHYSICS SERIES

LC11: understanding QCD at Linear Colliders in searching for old and new physics
Trento, September 12-16, 2011

Editors:

Francesca Borzumati, Denis Comelli, Gennaro Corcella, Stefania De Curtis, Stefano Moretti, Giulia Pancheri (Coordinator), Orlando Panella.

FRASCATI PHYSICS SERIES

Series Editor
Danilo Babusci

Technical Editor
Debora Bifaretti

Cover by Claudio Federici

Volume LIV

Istituto Nazionale di Fisica Nucleare – Laboratori Nazionali di Frascati
Divisione Ricerca
SIDS – Servizio Informazione e Documentazione Scientifica
Ufficio Biblioteca e Pubblicazioni
P.O. Box 13, I-00044 Frascati Roma Italy
email: sis.publications@lnf.infn.it

ISBN 978–88–86409–60–5

LC11 Workshop: Understanding QCD at Linear Colliders in searching for old and new physics

12-16 September 2011, ECT*, Trento, Italy

Editors
Francesca Borzumati, Tohoku University, Japan
Denis Comelli, INFN Ferrara, Italy
Gennaro Corcella, INFN Frascati National Laboratories, Italy
Stefania De Curtis, INFN Firenze, Italy
Stefano Moretti, Southampton University, UK
Giulia Pancheri (Coordinator), INFN Frascati National Laboratories, Italy
Orlando Panella, INFN Perugia, Italy

Conveners
Higgs physics - Elena Accomando (NExT Institute, Southampton U.)
SUSY - Francesca Borzumati (Tohoku U.)
Tools - Carlo Carloni Calame (NExT Institute, Southampton U.)
Astroparticles - Denis Comelli (INFN Ferrara)
Top and QCD - Gennaro Corcella (LNF Frascati)
Beyond the Standard Model - Aldo Deandrea (IPN, Lyon)
Electroweak physics - Giuseppe Degrassi (Roma III and INFN Roma III) and Massimo Passera (INFN Padova)
Vector boson fusion - Fulvio Piccinini (INFN Pavia)

Contents

Chapter 1

Prologue

This Workshop was part of a series on physics at Linear Colliders (LCs), which is organized in Italy nearly every year with two objectives: to contribute to the international effort for studies and developments of future LCs and to stimulate and gather together the Italian community interested in the physics of such machines. The Workshop, like all others in the series, invited scientists from anywhere in the world to discuss together topical arguments directly and indirectly related to LCs. Previous editions took place in Florence, Perugia and Frascati (twice). Every year the Workshop addresses a different subject, on which to place special emphasis. This year the main topic chosen was Quantum Chromo-Dynamics (QCD) and the role it plays to search for new physics and to increase the precision of Standard Model (SM) measurements.

The particle physics community has recently entered into the the LHC era. Both new and old phenomena are probed with higher luminosities and energies. Together with a study of what is being measured and discussed, it is now the time to look at the future of particle physics and envisage what will be studied in twenty or thirty years from now. Thus the question of which machine can be best to go beyond LHC and its upgrades, whether it be a LC, or a new higher energy electron-proton option, or others. Within the LC options, the energy of the possible accelerator and hence the required technology is still an open issue, whose answer will depend on what we learn from LHC experiments. With the discovery of a light Higgs boson but nothing else, for instance, this would probably encourage an International Linear Collider (ILC) with a moderate beam energy as the best option to study with high precision the Higgs boson properties. In contrast, if other heavy

states are also found, the scenario would probably require a higher energy machine like a Compact LInear Collider (CLIC). Other questions facing particle physics now concern both the potential discoveries as well as how optimal is the present understanding of the background out of which one needs to disentagle the unknown. In addition to studying the Higgs boson, another example is the search for exotic fermions, or technipions, for instance. Some rare processes are characterized by the observation of two, three or more W bosons. In order to distinguish between the Standard Model (SM) production of a number of W bosons, some of which can decay in jets, and the new physics, it is then necessary to have the tools for such calculations, which include not only QCD estimates to higher orders, but also a control of jet phenomenology including the soft part of the event. However, the study of hadronic interactions is not simply a question of background. Indeed, an adequate understanding and description of the hadronic dynamics rely on modelling the large-distance behaviour of QCD. There are many ways to approach the problem. Simulation programs exist, including inputs from many models for the very soft component of the interaction. Along with QCD calculations at Next-to-Leading Order (NLO) or even higher orders, used to describe the part of the interaction leading to jet observables in the final state, Monte Carlo (MC) codes simulate the complexity of LHC events and test different hadronic models. Thus, the LHC allows the tuning of the MC programs and, at the same time, the testing of the modelling of the very soft component of QCD. Other approaches might include studies of the total cross-sections, the inelastic part being measured by all the LHC experiments, or the elastic differential cross section, where the interplay and the transition between the perturbative and non-perturbative part dictates the dependence on the momentum transfer. Another field of investigation where QCD plays a crucial role, both through the known perturbative as well as through the lesser known threshold behaviour, is the physics of the top quark and other heavy flavours. The top quark is still a rather mysterious particle and not all of its behaviour is fully understood. The intense LHC studies will certainly establish some of its properties, as such they will be a guidance in the choice of which future collider to build. To summarize, the major questions which were to be addressed at this Workshop were:

1. What is the status of the projects for the future of particle physics?

2. Are the LHC experiments giving indications for new directions?

3. Which are the possible scenarios for new physics to be discovered either at accelerators or through cosmology?

4. What is the state-of-the-art of QCD concerning our ability to disentangle new physics from SM processes?

5. What messages can we expect from the LHC concerning the large distance behaviour of QCD?

Results and highlights Thanks to speakers who are leaders in the field, the LC11 Workshop presented the state-of-the-art of the different subdisciplines of particle physics: accelerators, experiments, theory and phenomenology. All the participants agreed that the Workshop succeeded in presenting, in a unique combination of talks and discussions, the exciting present, i.e., Tevatron and LHC results, and the planning for the future, for both experiment and theory.

Although not all the questions posed throughout the Workshop could be answered yet, a very good overview of the various problems discussed above was given.

Question 1: Status of future projects for particle physics, including theorical and experimental tools.

The Workshop started with a grand view of the research priorities nowadays in particle physics, as perceived by one of the worldwide experts in beyond the Standard Model (BSM) physics. The presentation spanned from the understanding of the origin of mass and flavour, as testable at particle accelerators and in several underground experiments, to the cosmological implications of the results expected at these apparata and their interplay with the observations gathered by several space probes in the attempt to resolve the mystery of the matter-antimatter asymmetry. The talks transmitted a sense of urgency that made it clear to the audience that we are about to unravel the next layer of particle physics in the upcoming decade or so.

The other talks delivered on the first day were extremely important as they put into context the possible landscape of future LCs, by highlighting the synergies and complementarities existing between the two front-runner projects presently: the aforementioned ILC and CLIC. The physics of these machines was highlighted particularly in view of their potential in accessing new physics signals. Special attention was devoted to the case of a 1 TeV

ILC option. Several testable features of QCD in the TeV regime were discussed in particular. These talks were useful in balancing the often partisan views about either machine, in the direction of recognising that it will be the LHC results that will indicate which LC prototype is best pursuing. In the meantime, the sharing and thus the cross-fertilisation of ideas across the two communities, of ILC and CLIC, will be of the outmost importance.

The two following talks recapped the status of the muon collider project, an alternative (or possibly a successor) to an electron-positron LC, offering the unique opportunity of directly and copiously producing the Higgs boson as a single resonance, thereby affording the unique opportunity of possibly solving this puzzle of current particle physics, i.e., whether Electro-Weak Symmetry Breaking (EWSB) and the ensuing generation of mass is indeed due to the Higgs mechanism and, if so, to which realisation of it.

Questions 2 and 3: LHC results and future scenarios All the LHC experiments presented their results. Great attention was focused on results from ATLAS and CMS and the exclusion limits on the Higgs mass in particular, released shortly before this Workshop, indicating the possibility of a light Higgs. Scenarios for a no-Higgs situation were presented too, highlighting possible strategies for searches for BSM physics and alternative theoretical frameworks, wherein to reconcile EW precision measurements with such scenarios.

One important player in any discussion of new physics is Dark Matter (DM). Since a previous Workshop had been dedicated to this subject, the present Workshop only had one review talk on DM, focusing on the tools for its detection. It was shown that only few multiplets, containing the lightest neutral component automatically stable, can be added to the SM. The ingredients and the recipes for computing signals of TeV-scale DM annihilations and decays in the galaxy and beyond where deeply discussed. For each DM channel, it was shown the energy spectra of electrons and positrons, antiprotons, antideuterons, gamma rays, neutrinos and antineutrinos e, μ and τ at production, computed by high-statistics simulations. The energy spectra of electrons and positrons, antiprotons and antideuterons at the location of the Earth were newly given. All results are available in numerical form and ready to be consumed.

Question 4: State of perturbative QCD : top and jet physics Top quark phenomenology, from both a theoretical and experimental point of view, was thoroughly discussed in the LC11 workshop. We had reviews on the latest results from both Tevatron and LHC experiments, along with discussions on the latest calculations, at fixed order and resummed, as well as MC codes on top quark production and decay at both lepton and hadron colliders. Particular attention was paid to the extraction of the top mass, the forward-backward asymmetry and the top Yukawa coupling. We even had a presentation reviewing the latest results on Soft Collinear Effective Theories (SCETs), taking particular care about the application of the SCET approach to extract the top mass from jet distributions and its relation with the mass parameter implemented in MC generators.

As for resummations, a recent computation of the thrust distribution in electron-positron collisions was also presented and compared with the SCET predictions and experimental data from the ALEPH collaboration. Furthermore, progresses in the implementation of parton showers, as well as NLO MC tools, were also reported. From the experimental side, we heard about the most recent QCD analyses carried out by all the LHC experiments, i.e., ATLAS, CMS, LHCb and ALICE, and by the D0 and CDF collaborations at the Tevatron.

The last three talks of the Workshop were devoted to theoretical and experimental reviews of the present status of QCD, following the lessons learnt from previous and current e^+e^- experiments, Deep Inelastic Scattering (DIS) and hadronic machines. Two talks addressed traditional issues of QCD, from both the theoretical and experimental side, as developed over the years by adopting a perturbative approach formulated within gauge theory, essentially aimed at testing the $SU(3)$ structure of the strong interactions. The third presentation gave instead an overview of recently developed theoretical approaches in describing QCD by exploiting dualities between supersymmetric gauge theories and string theories, chiefly the AdS/CFT correspondence applied to phenomenological aspects of a strongly coupled theory like QCD, including the description of AdS/QCD models of mesons and their application to hadronisation at colliders.

Question 5: Large distance behaviour of QCD QCD at large distance was discussed in the context of total hadronic cross-sections. For LCs, the highlight is on photon-photon interactions, where hadronic production in

both beam-beam interactions and particle-beam interactions can obscure the processes one wants to observe. Progress was reported concerning simulation of both beamstrahlung and bremstrahlung effects at CLIC, using a model developed for proton scattering, where a relevant role is played by emission of infrared gluons, for which a singular but integrable effective coupling is proposed. The infrared region was also discussed from a different viewpoint, namely, in a unified description of both soft and hard interactions, within a framework where the appropriate formalism for high-energy soft interactions is based on Reggeon field theory with a phenomenological (soft) Pomeron, whereas for hard interactions a QCD partonic approach is used in which the (QCD) Pomeron is associated with the Balitsky/Fadin/Kuraev/Lipatov (BFKL) vacuum singularity. In this unified vision the two approaches appear to merge naturally one into the other. That is, the hard partonic approach seems to extend smoothly into the soft hadronic domain. Other approaches to the soft interaction region were discussed within a statistical model. These different approaches indicate a growing awareness in trying to probe the large-distance regime of QCD and its transition to the perturbative region.

In summary, the Workshop succeeded in giving an overview of future projects in particle physics, and of what to expect from physics studies from either e^+e^- or other experiments, depending on our knowledge of QCD. It was discussed how the latter impinges on physics searches of new states of matters or forces, assuming the case of both (multi) Higgs and Higgsless scenarios. Despite the existing variety of approaches to the long distance dynamics of QCD signals that the latter is not yet a complete framework, many excellent presentations showed that clear progress in perturbative QCD and in modelling the non-perturbative regime, both theoretically and phenomenologically, is being made. The format of these Workshops has over the years been proved to be very effective in bringing together theorists and experimentalists for planning the future of particle physics.

Outcomes and Acknowledgments The appreciation of this Workshop by all the participants has been very encouraging and we plan to continue our efforts to explore the physics of future LCs within this format.

In addition to the high level of scientific presentations, the success of the LC11 Workshop was also due to the very efficient organization provided by the ECT* and the very beautiful settings of the venue. Further, we thank the ECT* for providing generous financial support to all the participants and

a wonderful atmosphere for exchange of ideas and discussions. The staff at the Center was extremely helpful and always ready to help us.

We thank INFN for supporting travel for many participants and the workshop secretary M.C. D'amato from INFN Frascati National Laboratories for providing constant help and continuos advice. We also thank colleagues and staff from the INFN Trento and Padova branches (Sezioni) whose help has allowed a smooth and efficient connection between INFN and the ECT*.

One of us, G.P., is grateful to the MIT Center for Theoretical Physics for hospitality through most of the period during which the Workshop was being organized and the Proceedings prepared.

LC11 Organizers and Conveners

Frascati, July 26th, 2012

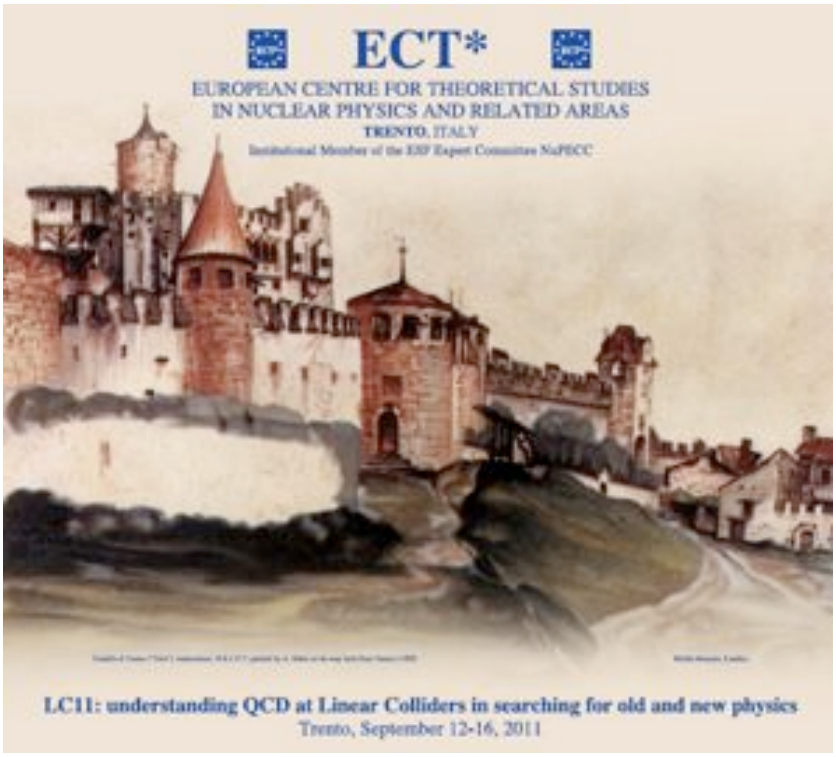

Castello di Trento painted by A. Dürer on his way back from Venice (1495).

Chapter 2

Projects for the future

2.1 F. Richard - Update on ILC

Update on ILC

François Richard
Laboratoire De l'Accélérateur Linéaire d'Orsay
richard@lal.in2p3.fr

Abstract This presentation intends to update the status of ILC project which is close to reaching its major goals, delivering two documents by end of 2012 on the machine and on detectors. Taking the point of view of future users, I will discuss the physics, the overall strategy and the preparation of the detectors.

1 Introduction

The purpose of this presentation is to discuss some key aspects of the ILC activities. It is understood that since Marc Ross [1] will present the machine aspects, I will take the point of view of future 'users' concerned with the physics, the overall strategy and the preparation of the detectors. Ups and downs in the preparation of ILC have been smoothed by a solid organization of the international effort on machine and detectors [2]. Collaboration between ILC and CLIC has become a reality both on machine and detectors. 2012 will be a crucial year for the fruition of these efforts with the production of 2 ILC documents providing the necessary inputs for a political/financial discussion of this program by governments. Beyond that, there will be a phase of active R&D (costs) and siting efforts which can only proceed if one gets significant encouragements from the political bodies. These encouragements could be fueled by a significant discovery made at LHC.

It is clear that my presentation was just a snapshot and that the situation is evolving rapidly. In particular results from LHC on Higgs search are narrowing the mass window for a SM Higgs in the region below 130 GeV. In December 2011, the two experiments have reported a significant excess around 125 GeV which is consistent with a Higgs signal [3]. Also, as recently reported at the plenary ECFA, the status of the ILC project in Japan has made great political progress. The ILC effort which was so far considered as an R&D has reached the Diet and Ministerial levels. Official support for two site studies is underway [4].

The ILC project ILC relies on a well proven technology used to build an XFEL in DESY but with higher gradients $\sim +25\%$ which requires further R&D well underway. ILC therefore does not need a proof of feasibility but rather an active preparation for industrialization to control its major costs. This effort has started with the **KEK Industrial R&D PILOT PLANT**. The **GDE**, an international organization set under B. Barish by ICFA, is about to produce an 'almost' ready for construction project to be proposed to governments in 2013 [1]. ILC works with a large community, ~ 1000 physicists and engineers, preparing detectors and furbishing solid physics arguments in favor of such a project. One of the key features of the future machine and which seriously impacts its optimization is its **flexibility in energy**. This feature is best illustrated with the Higgs study in the

'golden mode' ZH, where, assuming that the Z decays in a pair of muons, one uses the recoil mass technique to achieve a very clean signal as shown in the figure extracted from a full simulation study made by the collaboration ILD [5].

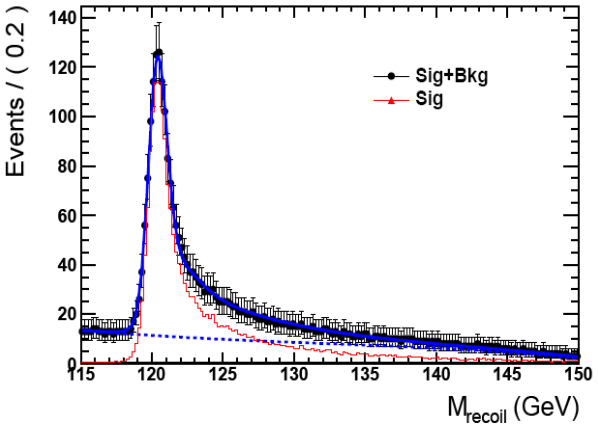

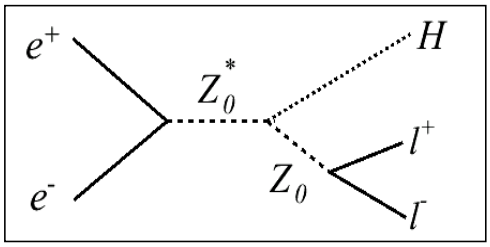

This plot was obtained by running near the ZH threshold meaning, for $m_H = 120\,\text{GeV}$, at $\sqrt{s} \sim 250\,\text{GeV}$. This very narrow mass distribution can only be obtained near threshold where the momenta of the two leptons is minimum giving therefore the best possible resolution on the recoil mass. ILC has therefore been recently [6] re-optimized to reach, at 250 GeV, a luminosity about half the nominal luminosity achieved at 500 GeV. Note that this approach works even if the Higgs decays into invisible or complex modes. It therefore allows a model independent measurement of the HZZ coupling constant with a precision of 1%. The following table allows some meaningful comparisons between the various high energy e^+e^- colliders.

Type	LEP200	SLC100	ILC500	CLIC 500
Vertical size nm	4000	700	5.7	2.3
Total P MW	65	50	216	240
Wall plug transf η%			9.4	4.1
Luminosity 10^{31} cm^{-2} s^{-1}	5	0.2	1500	1400
Interval between bunches ns	>>>	>>>	738	0.5
Polarisation %	No	80	> 80	> 80
Gradient MV/m	8	17	31.5	80

Note that the impressive progress in luminosity from the first linear collider, SLC, requires large electrical power to provide high beam currents and also a dramatic reduction in vertical beam size at the focus point which is only allowed by emittance reduction achieved in damping rings. In spite of using superconductive cavities which provides excellent yield, one needs more than 200 MW from plug power to run such a machine at 500 GeV. As discussed by M. Ross, with improved cavities and

with a different time structure, ILC will be able to run at 1 TeV without exceeding this number. CLIC (see the presentation from R. Corsini at this workshop) has a similar plug transfer efficiency and, using higher gradients, will be able to reach a higher energy. CLIC intends to start a 500 GeV with the aim of reaching 3 TeV with a power consumption of 560 MW. Luminosity can be increased by allowing for a larger energy dispersion but, for the same relative spread, one cannot increase the luminosity with respect to 500 GeV. A critical issue for building ILC is the fabrication of about 16000 SC cavities. This process requires high tech and therefore can be very costly without a careful strategy. PAC, an International Committee under Lynn Evans following ILC activities, has noticed that the European XFEL project under construction at DESY has focused on developing 'expert' companies, that is, few companies capable of mastering the detailed processes required to produce high-gradient cavities, which results in high cost. In the case of LHC, CERN basically assumed responsibility for integrating individual components and for achieving the required performance, significantly relieving risks from industry and hence reducing the cost. In Japan, KEK is building a facility [7] to train industrial partners and share the risks in view of the construction of a LC at reasonable cost. It is highly recommended that the 2 other regions involved in ILC follow the same strategy.

2 Detectors

The two internationally elected ILC detectors, ILD and SiD, should produce a detailed document by end of 2012, in conjunction with the ILC TDR, with a realistic integration of sub-detectors (cables, dead zones, material budget) and full costing. Based on well chosen reference reactions, physics performances will be evaluated at 500 GeV and 1000 GeV center of mass energy. Push-pull studies are progressing well based on CMS experience and switching time between experiments should be below 1 week. CLIC has adopted the same base-line detectors with increased longitudinal dimensions and use of W absorbers in the hadron calorimeter to contain more energetic showers. There is a very large worldwide effort on detector R&D, with large set ups constructed and tested with beams all over the world. CERN is actively participating in this process. There is constant struggle for funding with a recent success just achieved in Japan where a new 5 year plan has been approved.

Below one can see the general structure of the ILD detector, dominated by the iron return yoke for the intense magnetic field, 3.5 T, created by a superconductive solenoid closely following the CMS one. All calorimeters are embedded inside the coil to improve energy reconstruction. A large TPC provides the tracking complemented by high precision Si layers and a very thin micro-vertex Si detectors providing flavor tagging with unprecedented accuracy. This detector achieves full coverage down to 100 mrad for charged and neutral particles. As already mentioned, an important feature is a well organized common effort between CLIC and ILC on detectors. CERN has joined the large international R&D collaborations and now contributes in many aspects, e.g. on testing particle flow algorithms to higher energies, contributing to push-pull studies and costing methods. There is also an active participation of SiD and ILD collaborations to the CLIC CDR [8] document which should appear end of 2011. Of course this collaboration extends on many other machine aspects like damping rings studies (ATF in Japan [1]), beam delivery studies, machine detector interface aspects, civil engineering and cost and schedule issues.

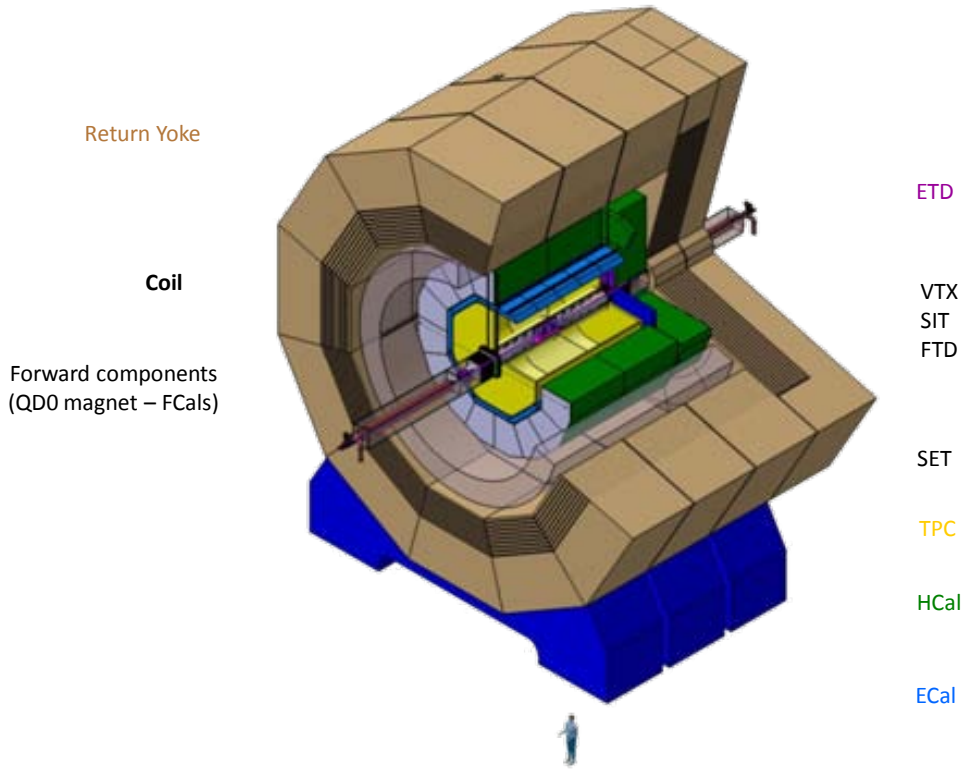

3 Physics landscape

3.1 Higgs

From LEP/SLC/Tevatron precision measurements (PM), one expects a SM Higgs lighter than 150 GeV. With CMSSM, the favored value is 120 GeV but more relaxed SUSY schemes can accommodate heavier values. This prediction needs to be proven by LHC before deciding on future LC given the various competitive models on the market without necessarily a light Higgs and even 'Higgsless'. Present searches from LHC are compatible with a light Higgs ($127 < m_H < 600$ GeV excluded [3]). Both ATLAS and CMS indicate an excess compatible with a SM Higgs at 125 GeV. This evidence can be definitely confirmed with 2012 data. If so, it will be crucial to measure precisely its couplings to bosons and fermions to assess its nature and a LC offers 10 times more precision than LHC which may turn out to be critical to identify new physics. Why do we need such a precision? Taking, as an example, a composite Higgs as suggested by Ref 9, the figure below shows, for $m_H = 125$ GeV, the type of deviation one can expect for such models.

3.2 SUSY

From LHC SUSY searches, there is some 'extension' on the standard scenario CMSSM. However even this scenario is not excluded [10] but hitting the 'naturalness' problem which is the basis for predicting SUSY near the electroweak scale. Several alternative SUSY scenarios are well alive with distinct predictions.

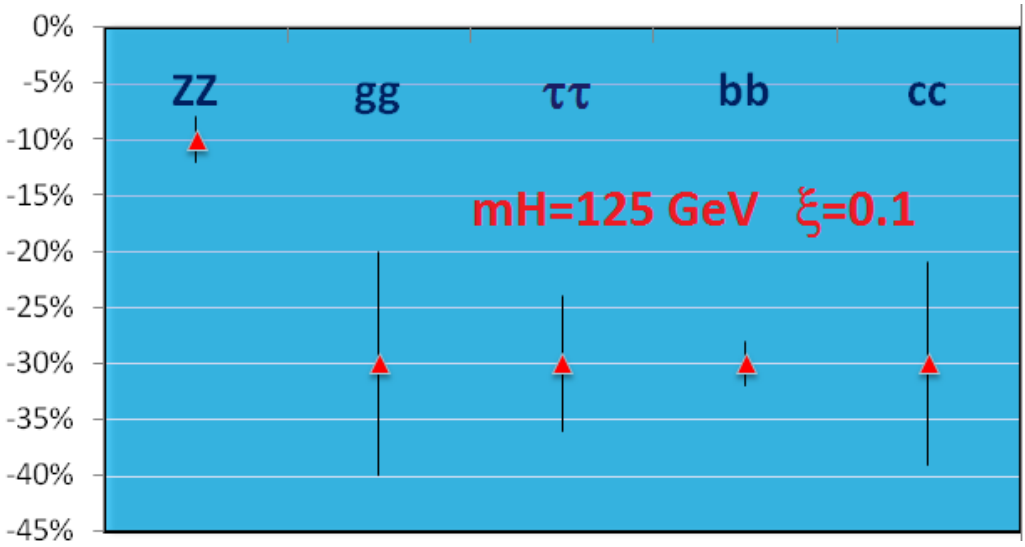

* Keeping alive the 'naturalness' criterion, one can invoke an 'inverted hierarchy' scheme [11] for which only **top and bottom squarks, Higgsinos and gluinos** are 'light' as needed to reduce fine tuning for EWSB

* Other authors [12] give up on the 'naturalness' argument on the basis of the multiverse idea and push up all SUSY masses well beyond the reach of any foreseeable collider, keeping only a light Higgs boson as an indirect proof of SUSY.

* Alternatively one can assume that only part of the SUSY spectrum is very heavy (hence the expression '**split SUSY**') while particles needed for providing dark matter and gauge unification are kept at the TeV scale but not necessarily within the reach of LHC. Exploring such scenarios could require more LHC data than collected in 2012 and, with the 2013-14 shutdown, no stringent answer about SUSY could appear before end of 2015.

3.3 Compositeness

Other views than SUSY are developed, allowing for very different pictures. The well known hierarchy problem can be avoided with a **Composite Higgs** and even with **Higgsless models**. These models are often linked to extra dimensions as, for instance, in the Randall–Sundrum model [13]. The top quark could also be composite like the Higgs boson and precision measurements at ILC could bring invaluable benefits. Longitudinally polarized WL, emerging through the Higgs mechanism, could also be composite. These models also predict deviations in ZLh couplings which can be precisely studied in e^+e^-. In the language of extra dimensions Kaluza–Klein bosons couple preferentially to Higgs, top quarks and longitudinally polarized W/Z generating measurable deviations in couplings to Z boson. As already shown by the TESLA TDR14 a LC collider with electron polarisation can measure with extreme precision effects anomalous diboson couplings (in particular the parameter κz) which could be induced by compositeness. The table below clearly shows how lepton machines provide superior

accuracies for this type of couplings. ILC figures come from the TESLA TDR while LHC numbers are taken from an ATLAS document [15]. It is possible to improve LHC figures with 1000 fb^{-1} but this improvement is modest given that one is already running into systematics.

Coupling Accuracy	LEP200 (PDG)	Tevatron D0	LHC14 100 fb^{-1}	LC500 (TESLA TDR) 500 fb^{-1} P=80%
$\Delta\kappa_Z \times 10^4$	570	5000	400	3
$\Delta g_Z \times 10^4$	200	1000	38	15

New WW studies will be carried out by ILC experimental teams to assess more realistically the possibilities of this important channel which, in particular, allows to extract very precisely the beam polarisation. Recall that the neutrino exchange completely dominates forward production of WW ($> 99\%$) which is only sensitive to left handed polarisation. One therefore simply can write that P AFBW (that is the forward backward charge asymmetry). A LC measuring top, Higgs and WW couplings with excellent accuracies is ideally well suited to observe compositeness effects. LHC can bring very valuable inputs in this sector but it may take well beyond 2012 for a meaningful answer.

4 Next steps for ILC

Machine R&D should go on towards full industrialization to reach acceptable costing. Full realism requires identification of sites (e.g. Japan mountain sites have specific constraints). Results from LHC will play a major part in guiding the choice of LC parameters (energy, technology, options). ILC is not only a 'Higgs factory' but it can also provide very precise and model independent measurements in the top sector. Tevatron has shown hints of deviations in the top sector, the AFBt anomaly, and LHC could bring additional inputs which would motivate a LC operating above the top threshold. ILCSC/ICFA is preparing the governance aspects for the post TDR phase. A procedure will be soon defined on site selection with technical criteria requested for the construction of this machine. Europe will review its global HEP strategy in 2012 (repetition of 2006). There will be an open meeting in September 2012 in Cracow, the analog of the Orsay meeting in 2006. As pointed out by Rolf Heuer on several occasions, CERN is prepared to play its role in particle physics at the energy frontier. Quoting Rolf at Lepton Photon LP11 in Mumbai:

* **CERN participation in global projects independent of location**
* We need to define the most appropriate organizational form for global projects NOW
* CLIC should be part of the new worldwide organization.

5 Conclusions and Prospects

The HEP community has developed a consistent and worldwide strategy to construct an e^+e^- LC. A viable project, ILC, can be presented to the governments from end of 2012. A final decision

(ILC/CLIC) will depend on cost and technology and on physics results from LHC. It also depends on an initiative taken by one country or one region to build this machine and, accordingly, provide the largest part of the resources needed. At this moment there are signs from Japan that this initiative is under way. Active participations of other countries will very much depend on LHC results.

Acknowledgements: It is a pleasure to warmly thank the organizers of LC11 in Trento for the invitation and the very nice atmosphere of this workshop.

References

[1] M. Ross, these proceedings

[2] `http://www.linearcollider.org/cms/` gives all informations about the ILC organization

[3] `https://indico.cern.ch/conferenceDisplay.py?confId=164890` provides the most recent results from LHC on Higgs search

[4] `http://www3.nhk.or.jp/daily/english/20111215_30.html` gives the most recent announcement from Japan

[5] `http://ilcild.org/` is the site of the ILD detector

[6] `http://www.linearcollider.org/interim-report` contains the GDE interim report for ILC

[7] `http://lcdev.kek.jp/STF/` gives some informations about STF the KEK supraconductive test facility

[8] `http://clic-study.org/` describes CLIC activities

[9] G. F. Giudice, C. Grojean, A. Pomarol and R. Rattazzi, JHEP **0706** (2007) 045 [hep-ph/0703164].

[10] O. Buchmueller *et al.*, arXiv:1112.3564 [hep-ph].

[11] A. Pomarol and D. Tommasini, Nucl. Phys. B **466** (1996) 3 [hep-ph/9507462].

[12] See, for instance, G. F. Giudice and A. Strumia, Nucl. Phys. B **858** (2012) 63 [arXiv:1108.6077 [hep-ph]].

[13] See L. Randall and R. Sundrum, Phys. Rev. Lett. **83**, 3370 (1999) [hep-ph/9905221], and K. Agashe, A. Delgado, M. J. May and R. Sundrum, JHEP **0308** (2003) 050 [hep-ph/0308036].

[14] J. A. Aguilar-Saavedra *et al.* [ECFA/DESY LC Physics Working Group Collaboration], TESLA TDR hep-ph/0106315.

[15] B. Dowler *et al.* [ATLAS Liquid Argon HEC Collaboration], Nucl. Instrum. Meth. A **482** (2002) 94.

2.2 N. Armesto - QCD at an electron-hadron collider at CERN: the LHeC project

QCD at an electron-hadron collider at CERN: the LHeC project

Néstor Armesto
Departamento de Física de Partículas and IGFAE, Universidade de Santiago de Compostela, 15706 Santiago de Compostela, Spain
nestor.armesto@usc.es
on behalf of the LHeC Study Group

Abstract. In this contribution I show some of the possibilities for QCD studies offered by the proposed electron-hadron collider at CERN, the Large Hadron-electron Collider. After a brief general introduction and showing some of the possibilities for precision QCD, I will focus on small-x aspects: inclusive measurements and the determination of parton densities, and diffraction. I end by discussing some possibilities for final state studies.

1 Introduction

Quantum Chromodynamics (QCD), as the theory of the strong interaction (see e.g. [1] and references therein), provides the canonical example of a quantum field theory for which all its regimes are accessible in the laboratory. The main open questions in QCD - those related with confinement and hadron structure, and with its high-energy behavior - can be very cleanly investigated in lepton-hadron experiments. DIS studies constitute, since their start in the sixties, one of the three legs, together with lepton annihilation and hadron-hadron colliders, in the high-energy physics experimental program. More specifically, high-energy lepton-hadron colliders offer rich possibilities for understanding the partonic structure of nucleons and nuclei, and the high-energy behavior of QCD through the study of the small-x kinematical regime.

From studies at fixed-target experiments and at the HERA accelerator at DESY, it has been concluded that inclusive and diffractive data at small-x can be described by non-perturbative models and, more interestingly, by different realizations of evolution equations within perturbative QCD: the standard explanation within fixed-order perturbation theory (DGLAP evolution equations), resummation schemes, and non-linear approaches. Concerning the last item, unitarity of QCD as a quantum field theory implies that non-linear phenomena are unavoidable and saturation of partonic densities is expected to occur at high energies or small Bjorken-x. The Color Glass Condensate offers a non-perturbative but weak coupling realization of saturation ideas, see [2] and references therein. The present discussion lies on the relevant kinematical

regime for such phenomena and on the possibilities offered by existing or future experimental data to distinguish among the different available schemes.

Even ignoring such fundamental considerations and focusing merely on practical purposes, our knowledge of the gluon distribution at small x both in protons and nuclei does not suffice for the required precision in predictions within collinear factorization at hadron colliders. For example, gluon densities are among the largest sources of uncertainties for predictions of the Standard Model Higgs cross section through gluon-gluon fusion [3]. Besides, in the lepton-nucleus case and in the semihard region for particle production, collinear factorization is not expected to work and other factorization schemes have been proposed. Both aspects are of great importance for the study of hadronic and nuclear collisions.

The Large Hadron-electron Collider (LHeC [4, 5]) is an electron-proton/ion collider currently under design at CERN, which will collide $20 \div 140$ GeV $e^{\pm}$ against the LHC beams, with a goal luminosity 10^{33} cm^{-2}s^{-1}. The machine is subject, apart from several requirements on detector performance, to the constraints of creating minimal disturbance during construction and working simultaneously to the LHC. Besides electro-weak studies and searches for new physics, this machine will perform precision QCD studies and it should allow an unambiguous access to the novel regime of QCD in which unitarity constraints are at work - the dense region shown in Fig. 1. With the transition between the dilute region and the new phase being a density effect, a two-pronged approach will be pursued: either decreasing x at fixed mass number A and Q^2, or increasing A at fixed x and Q^2. The LHeC will give access to a completely new region of the Q^2-x plane, see Fig. 2.

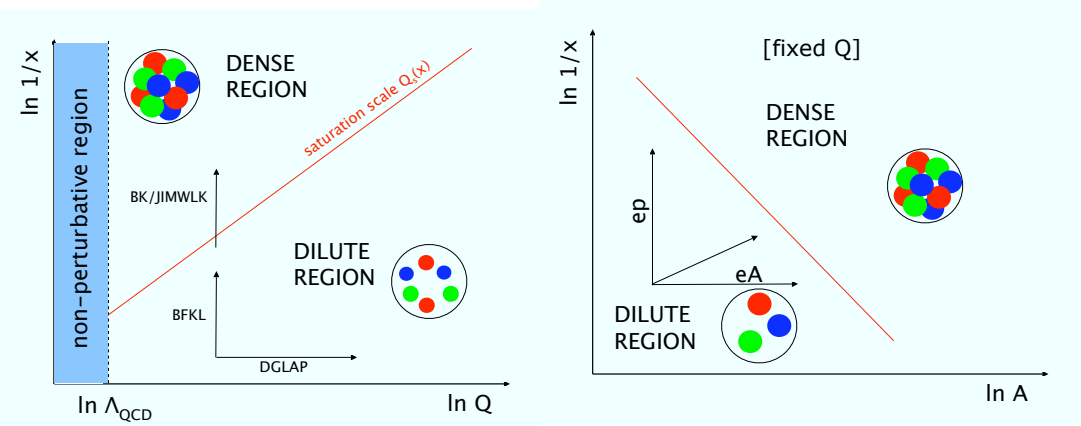

Figure 1: Sketch of the access to the dense partonic region where unitarity effects are essential, from the dilute one where linear evolution is valid. See the text for explanations. (Preliminary, LHeC Design Study Report, CERN 2012.)

In this contribution I will mention some aspects of the QCD studies that may be performed at the LHeC. Due to the limitations of space, I will focus on small-x physics and nuclear targets, which can be addressed with the LHeC. Work on all these aspects is in progress, with the aim of producing a Design Study Report by spring 2012 where extensive information on the accelerator, detector and physics case will be provided. More information can be found in [5], and in related work concerning the proposed Electron-Ion Collider in the USA [6].

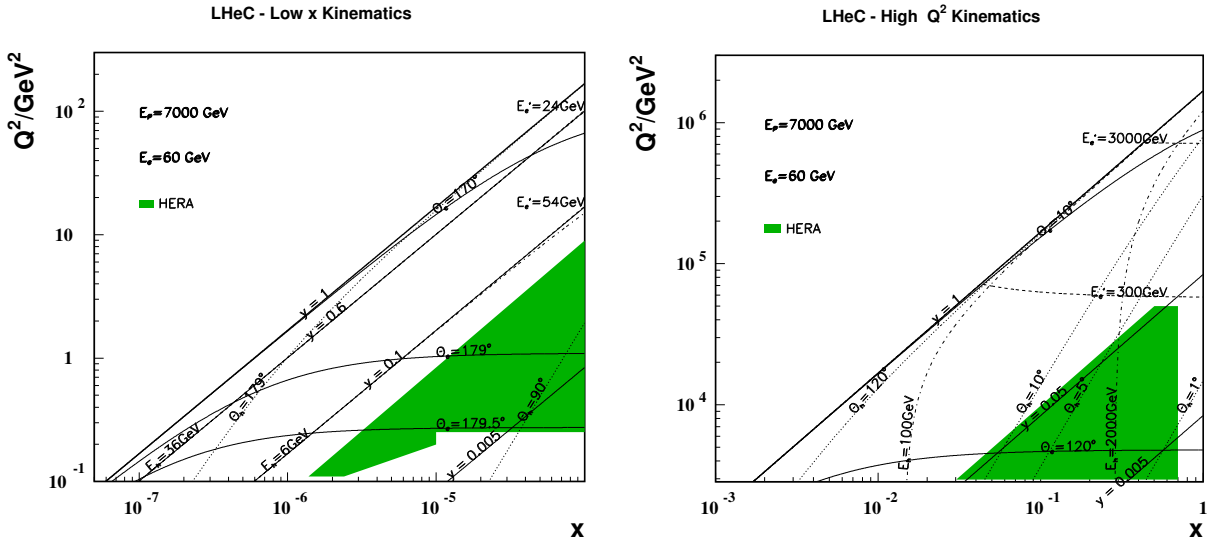

Figure 2: Kinematics of ep scattering at the LHeC at low x (left) and high Q^2 (right). Solid (dotted) curves correspond to constant polar angles θ_e (θ_h) of the scattered electron (hadronic final state). The polar angle is defined with respect to the proton beam direction. Dashed (dashed-dotted) curves correspond to constant energies E'_e (E_h) of the scattered electron (hadronic final state). The shaded (green) area illustrates the region of kinematic coverage in neutral current scattering at HERA. (Preliminary, LHeC Design Study Report, CERN 2012.)

2 Some precision QCD measurements

The LHeC will measure reduced cross sections and the F_2 and F_L structure functions, and their flavor decompositions, with big accuracy in a very large $x-Q^2$ domain. In this way it will allow the extraction of partons densities with unprecedented precision, both in the valence sector and for sea quarks and gluons. For example:

• It will reduce greatly the uncertainties in the strange quark densities through CC measurement and charm tagging.

• It will constrain the treatment of heavy flavors and the contribution of possible intrinsic pieces.
• It will largely reduce the uncertainties in the gluon density both at small and at large x due to the kinematical reach in x and in Q^2, see Fig. 3.
• If deuteron beams become available at the LHC, it will drastically improve our knowledge on the neutron parton densities and reduce the existing uncertainties in the ratio u/d.

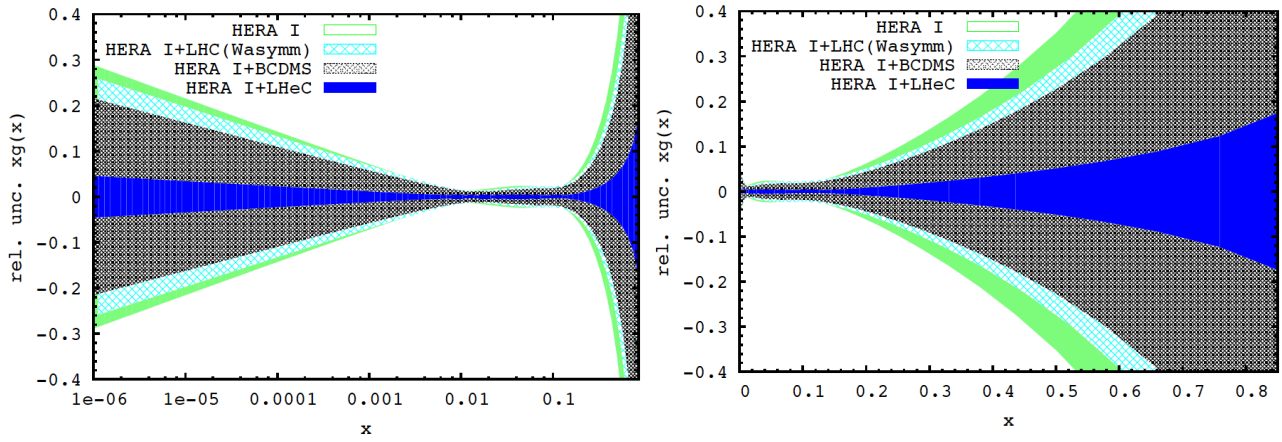

Figure 3: Relative uncertainty of the gluon distribution at $Q^2 = 1.9$ GeV^2, as resulting from an NLO QCD fit to HERA (I) alone (green, outer), HERA and BCDMS (crossed), HERA and LHC (light blue, crossed) and the LHeC added (blue, dark). Left: logarithmic x, right: linear x. (Preliminary, LHeC Design Study Report, CERN 2012.)

Besides, through the measurement of the Q^2-evolution and of jet cross sections, it will allow a determination of the strong coupling constant with such accuracy, up to 1/1000, that will mainly be limited not by experimental but by theoretical considerations (the order of the perturbative expansion and the value of the heavy quark masses), thus triggering new theoretical developments.

Finally, the measurement of the γp cross section will help to constrain models for the high-energy behavior of hadronic cross sections, and the measurement of charge asymmetries will allow to establish the relevance of C-odd exchanges like the odderon.

3 Inclusive observables at small x

The LHeC will give access to a completely new region of the Q^2-x plane, see Figs. 2 and 4. With this huge kinematical lever arm and the possibility to measure not only the total

structure function, F_2, but also its flavor decomposition and the longitudinal one, F_L, (see Fig. 5 for examples of LHeC pseudodata on nuclear ratios of F_2 and F_L), the LHeC offers huge possibilities for:

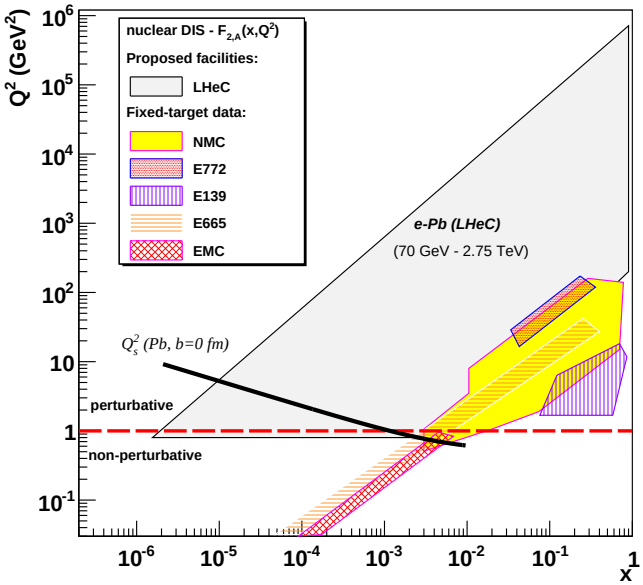

Figure 4: Region of the Q^2-x plane that will be explored with the LHeC in ePb, compared to those achievable at existing eA experiments. An estimation of the saturation scale indicating the dilute-dense transition is shown. (Preliminary, LHeC Design Study Report, CERN 2012.)

• Constraining the parton density functions (PDFs) in DGLAP analysis, both in ep and eA (see [5]), particularly for sea quarks and gluons. For this purpose, the combination of F_2, F_L and $F_{2c,b}$ appears to be very promising. As shown in Fig. 5 for F_2 and F_L in the nuclear case, the expected uncertainty of data is much smaller than the spread of existing models.
• Disentangling fixed-order evolution schemes from resummation or non-linear ones, see [8]. In this respect, the combination of data on F_2 and F_L is required.

4 Diffractive observables

On diffraction[1] [5], the LHeC will explore a new domain of very low β (e.g. down to a few times 10^{-4} for $Q^2 \sim 4$ GeV^2 at $x_P = 0.003$, two orders of magnitude smaller than at HERA,

[1]The diffractive kinematical variables are $x_P = (M_X^2 - t + Q^2)/(W^2 + Q^2)$ and $\beta = x/x_P$, with M_X the diffractive mass, t the transverse momentum squared and W the γ^*-hadron center-of-mass energy.

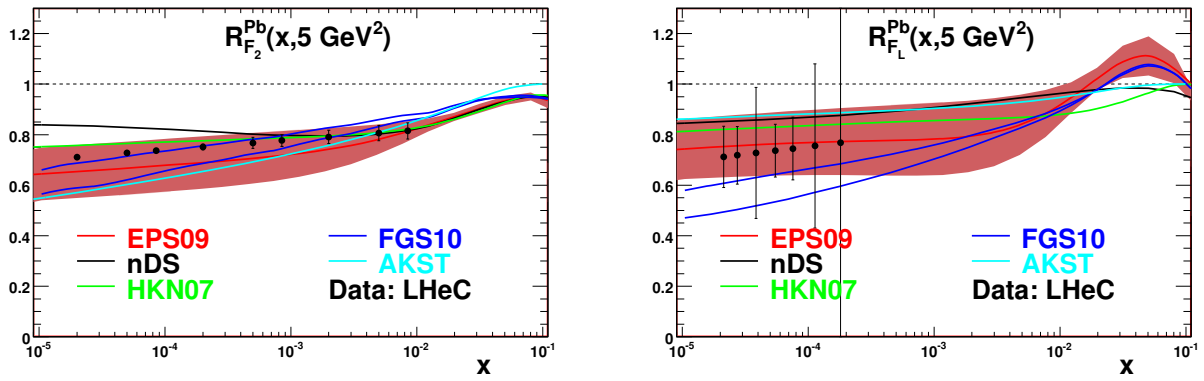

Figure 5: Predictions from different models [7] for the nuclear ratio $R_{F_i}^{\rm Pb} = F_i^{\rm Pb}/(208\,F_i^{\rm p})$, $i = 2, L$, at small x, see the legend on the plots. Circles with error bars are LHeC pseudodata. (Preliminary, LHeC Design Study Report, CERN 2012.)

for the proton, see Fig. 6left; for nuclei, information on diffraction at small x does not exist at all). Several aspects can be highlighted:

• It will give access to diffractive masses as large as 200 GeV, see Fig. 6right, providing data to check models describing the transition from low to high M_X, and to constrain nucleon and nuclear diffractive PDFs in DGLAP analyses.

• For elastic vector meson production or deeply virtual Compton scattering, a huge lever arm in W will be explored (e.g. up to ≈ 1.2 TeV for $E_e = 50$ GeV) with enough precision to disentangle linear evolution schemes from non-linear ones. Besides, the differential spectrum in t will be accessible down to $t \sim -2$ GeV^2. All this will also constrain quark and gluon generalized parton densities (GPDs) at small x where they are presently unknown. Measurements of diffractive production of two vector mesons will allow the determination of helicity-flip GPDs.

• Gribov's relation between diffraction in ep and nuclear shadowing will be checked in a single experimental setup (see e.g. the FGS10 and AKST models in [7] and Fig. 5).

• Diffractive dijets will be measured in DIS with E_T as large as 25-30 GeV, providing a check of collinear factorization for diffractive processes.

The experimental challenge in separating inclusive diffraction ($e + {\rm A} \to e + X + X'$ with a rapidity gap) from coherent ($e+{\rm A} \to e+X+{\rm A}$) and incoherent ($e+{\rm A} \to e+X+Z{\rm p}+[A-Z]{\rm n}$) is under study.

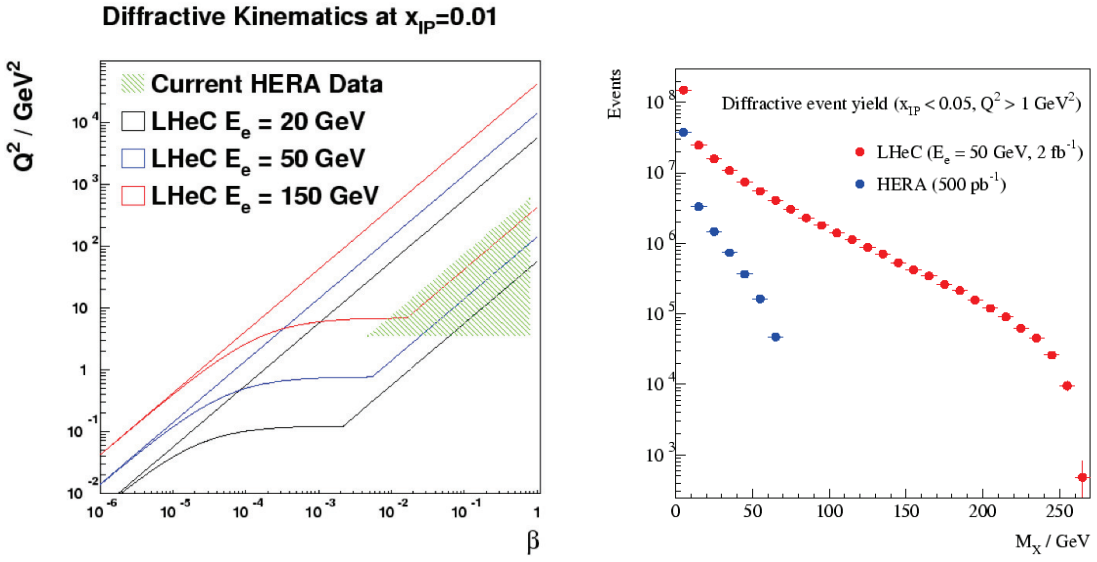

Figure 6: Left: Kinematic range of LHeC in Q^2 and β for different electron energies $E_e = 20, 50, 150$ GeV, for $x_P = 0.01$. 1° acceptance of the detector is assumed. Right: Diffractive event yield versus the mass of the diffractive state, comparing HERA and the LHeC. (Preliminary, LHeC Design Study Report, CERN 2012.)

5 Final states

The LHeC will offer huge possibilities for clarifying the dynamics of QCD radiation and hadronization. For example:

• The dynamics of QCD radiation at small x will be studied through forward jet and particle production, which will be abundant, see Fig. 7.

• The parton/hadron energy loss mechanism in semi-inclusive DIS will be tested by introducing a piece of colored material - the nucleus - which would modify the hadronization pattern i.e. its dependence on the traversed length (by varying either the impact parameter or the nuclear size), its chemical composition,... Energies as high as 10^5 GeV in the rest frame of the nucleus will be accessible and the transition from low to high energies (with hadronization expected to occur inside or outside the nucleus respectively) will be studied.

As an example of the abundant yield of high-energy probes, inclusive jet rates for $Q^2 = 0$ around 10^3 jets per GeV per year are expected [5] with $E_{Tjet} \sim 95$ (80) GeV in ep (ePb).

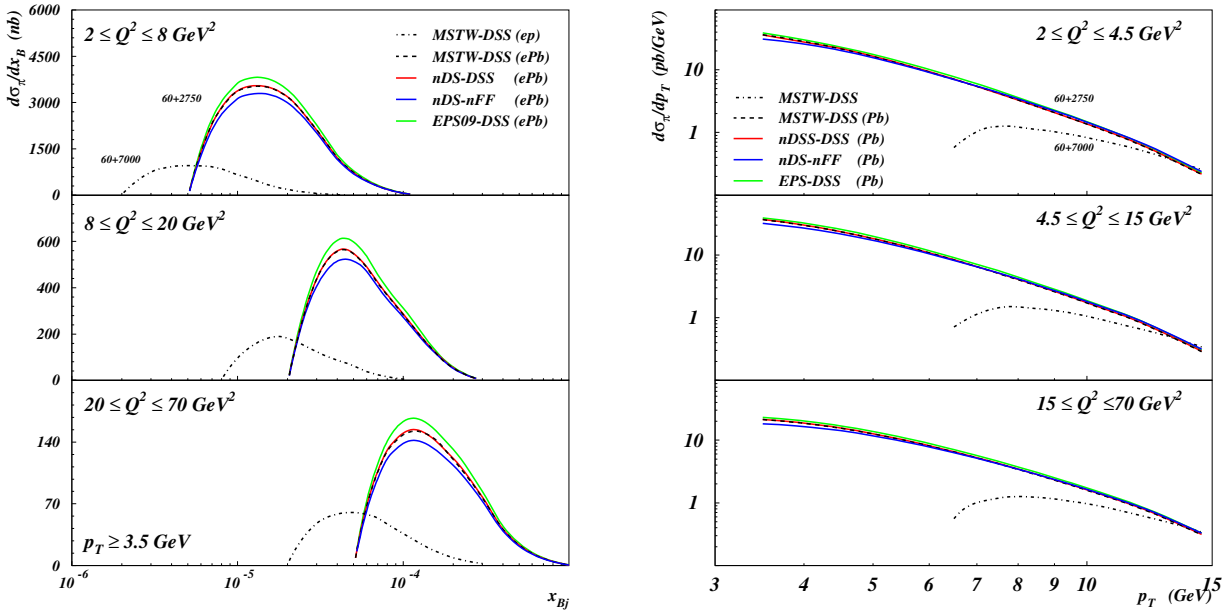

Figure 7: Cross section for inclusive π^0 production versus Bjorken x_{Bj} for $p_T > 3.5$ GeV/c (left) and versus p_T (right), computed in NLO QCD [9]. Dashed-dotted black lines refer to ep collisions. All other line types refer to ePb collisions: dashed black ones to standard nucleon PDFs [10] and fragmentation functions [11], solid red and green ones to nuclear PDFs [7] and nucleon fragmentations functions, and solid blue ones to nuclear PDFs [7] and nuclear fragmentation functions [11]. All cross sections are given per nucleon i.e. divided by 208 for Pb. Cuts: $\theta_\pi \in [5°, 25°]$, $x_\pi = E_\pi/E_p > 0.01$, have been applied. (Preliminary, LHeC Design Study Report, CERN 2012.)

Acknowledgments

NA acknowledges financial support by MICINN of Spain (grants FPA2008-01177 and FPA2009-06867-E), Xunta de Galicia (Consellería de Educación and grant PGIDIT10PXIB 206017PR), project Consolider-Ingenio CPAN CSD2007-00042, and FEDER. He thanks the organizers for the invitation to such a nice meeting.

Note added: during the process of editing these proceedings, the Conceptual Design Report for the LHeC has been published in [12].

References

[1] G. P. Salam, CERN Yellow Report CERN-2010-002, 45-100 [arXiv:1011.5131 [hep-ph]]; B. L. Ioffe, L. N. Lipatov and V. S. Fadin, *Quantum Chromodynamics: Perturbative and Nonperturbative Aspects*, Cambridge University Press 2010.

[2] F. Gelis, E. Iancu, J. Jalilian-Marian and R. Venugopalan, Ann. Rev. Nucl. Part. Sci. **60** (2010) 463.

[3] S. Dittmaier *et al.* [LHC Higgs Cross Section Working Group Collaboration], arXiv:1101.0593 [hep-ph].

[4] M. Klein *et al.*, Proceedings of *11th European Particle Accelerator Conference (EPAC 08)*, Genoa, Italy, 23-27 June 2008, preprint WEOAG01; `http://cern.ch/lhec`.

[5] See the LHeC talks at the *XIX International Workshop on Deep-Inelastic Scattering and Related Subjects (DIS 2011)* in `https://wiki.bnl.gov/conferences/index.php/Future_of_DIS`.

[6] The Electron Ion Collider Working Group Collaboration, C. Aidala *et al.*, *A High Luminosity, High Energy Electron Ion Collider*; `http://web.mit.edu/eicc/`; D. Boer *et al.*, arXiv:1108.1713 [nucl-th].

[7] D. de Florian and R. Sassot, Phys. Rev. D **69** (2004) 074028; M. Hirai, S. Kumano and T. H. Nagai, Phys. Rev. C **76** (2007) 065207; K. J. Eskola, H. Paukkunen and C. A. Salgado, JHEP **0904** (2009) 065; V. Guzey and M. Strikman, Phys. Lett. B **687** (2010) 167; N. Armesto, A. B. Kaidalov, C. A. Salgado and K. Tywoniuk, Eur. Phys. J. C **68** (2010) 447.

[8] J. Rojo and F. Caola, arXiv:0906.2079 [hep-ph].

[9] A. Daleo, D. de Florian and R. Sassot, Phys. Rev. D **71** (2005) 034013.

[10] A. D. Martin, W. J. Stirling, R. S. Thorne and G. Watt, Eur. Phys. J. C **63** (2009) 189.

[11] D. de Florian, R. Sassot and M. Stratmann, Phys. Rev. D **75** (2007) 114010; Phys. Rev. D **76** (2007) 074033; R. Sassot, M. Stratmann and P. Zurita, Phys. Rev. D **81** (2010) 054001.

[12] J. L. Abelleira Fernandez *et al.* [LHeC Study Group Collaboration], J. Phys G **39** (2012) 075001.

2.3 M. Cirelli - Tools for Dark Matter indirect detection

Tools for Dark Matter Indirect Detection

Marco Cirelli
CERN Theory Division, CH-1211 Genève, Switzerland &
IPhT, CNRS, URA 2306 & CEA/Saclay, F-91191 Gif-sur-Yvette, France
marco.cirelli@cea.fr, marco.cirelli@cern.ch

Abstract I discuss ingredients and recipes for computing signals of TeV-scale Dark Matter annihilations and decays in the Galaxy and beyond: the energy spectra of electrons and positrons, antiprotons, antideuterons, gamma rays, neutrinos and antineutrinos e, mu, tau at production, the propagation functions for charged particles in the Galaxy, the energy spectra at the location of the Earth, the gamma ray fluxes from the Galaxy and from beyond. All results discussed here are available in numerical form and ready to be consumed.
[*Report number: Saclay T12/007, CERN-PH-TH/2012-032*]

1 Introduction

Cosmology and astrophysics provide several convincing **evidences of the existence of Dark Matter** (DM). The observation that some mass is missing to explain the internal dynamics of galaxy clusters and the rotations of galaxies dates back respectively to the '30s and the '70s. The observations from weak lensing, for instance in the spectacular case of the so-called 'bullet cluster', provide evidence that there is mass where nothing is optically seen. More generally, global fits to a number of cosmological datasets (Cosmic Microwave Background, Large Scale Structure and also Type Ia Supernovae) allow to determine very precisely the amount of DM in the global energy-matter content of the Universe at $\Omega_{\rm DM}h^2 = 0.1123 \pm 0.0035$.

All these signals pertain to the gravitational effects of Dark Matter at the cosmological and extragalactical scale. Searches for explicit manifestation of the DM particles that are supposed to constitute the halo of our own galaxy (and the large scale structures beyond it) have instead so far been giving negative results, but this might be on the point of changing.

Indirect searches for Dark Matter aim at detecting the signatures of the annihilations or decays of DM particles in the fluxes of Cosmic Rays (CRs), intended in a broad sense: charged particles (electrons and positrons, protons and antiprotons, deuterium and antideuterium), photons (gamma rays, X-rays, synchrotron radiation), neutrinos. In general, a key point of all these searches is to look for channels and ranges of energy where it is possible to beat the background from ordinary astrophysical processes. This is for instance the basic reason why searches for charged particles focus on fluxes of antiparticles (positrons, antiprotons, antideuterons), much

less abundant in the Universe than the corresponding particles, and searches for photons or neutrinos have to look at areas where the DM-signal to astro-noise ratio can be maximized.

Pioneering works have explored indirect detection (ID) as a promising avenue of discovery since the late-70's. Since then, innumerable papers have explored the predicted signatures of countless particle physics DM models. In the past 3 years or so, however, the field has experienced a significant burst of activity, mainly due to the results presented by a few very well performing experiments, above all the PAMELA satellite, the FERMI satellite and the HESS telescope. It is fair to say that the field has passed, for better or for worse, from a theory-driven state to a data-driven phase.

The next few years promise to be even richer of data from Dark Matter Indirect Searches (certainly in terms of further explorations of the parameter spaces, and hopefully even with a positive detection). It will therefore be useful to have at disposal a **set of consistent tools** that can allow to interpret these data in a model independent way and cross-check between different channels. This is what we have aimed at realizing in [1] and that I am going to briefly present in this text. While the complete discussions can be found in [1], here I will focus only on some aspects and on the general infrastructure, leaving most of the formulae outside. All the results are available in numerical form in [2].

2 Fluxes at production

The first ingredients that one needs to compute DM ID signatures are of course the **fluxes of stable Standard Model particles** ($e^{\pm}, \bar{p}, \bar{d}, \gamma, \overset{(-)}{\nu}_{e,\mu,\tau}$) originating from DM annihilations, or decays. We want to be as model independent as possible and so we consider DM annihilations (parameterized by the DM DM cross section σv) and decays (described by the DM decay rate $\Gamma = 1/\tau$) into a large number of primary channels:

$$\begin{array}{l} e^+_L e^-_L,\ e^+_R e^-_R,\ \mu^+_L \mu^-_L,\ \mu^+_R \mu^-_R,\ \tau^+_L \tau^-_L,\ \tau^+_R \tau^-_R, q\bar{q},\ c\bar{c},\ b\bar{b},\ t\bar{t},\ \gamma\gamma,\ gg, \\ W^+_L W^-_L,\ W^+_T W^-_T,\ Z_L Z_L,\ Z_T Z_T, \\ h_{115}h_{115},\ h_{135}h_{135},\ h_{170}h_{170},\ h_{200}h_{200},\ h_{300}h_{300},\ h_{400}h_{400},\ h_{500}h_{500}, \\ \nu_e\bar{\nu}_e,\ \nu_\mu\bar{\nu}_\mu,\ \nu_\tau\bar{\nu}_\tau, VV \to 4e,\ VV \to 4\mu,\ VV \to 4\tau, \end{array} \tag{1}$$

where $q = u, d, s$ denotes a light quark and h_m is the Standard Model (SM) Higgs boson, with m being its mass in GeV. The last three channels denote models in which the annihilation or decay first happens into some new (light) boson V which then decays into a pair of leptons, along the lines of the models proposed in [3, 4].

All the spectra are available on [2]. Here I want to discuss two general issues: i) the intrinsic uncertainty in computing those spectra with numerical methods and ii) the impact of ElectroWeak radiation.

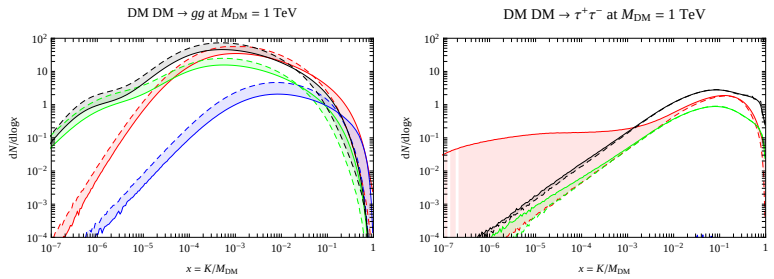

Figure 1: Comparison between Monte Carlo results: PYTHIA is the continuous line, HERWIG is dashed. Photons (red), $e^{\pm}$ (green), $\bar{p}$ (blue), $\nu = \nu_e + \nu_\mu + \nu_\tau$ (black).

2.1 MonteCarlo 'uncertainty'

Almost every DM indirect search analysis uses the collider MonteCarlo code PYTHIA to compute the annihilation spectra, despite the fact that other codes are available and that in any case all codes have been designed and calibrated for the collider environment and in an energy range which (until recently) was much lower than the multi-TeV one of interest for some DM models.

In order to get a feeling of the intrinsic uncertainty related to these issues, in [1] we employed the two most widely used MonteCarlo simulation programs: PYTHIA [5] (version 8.135) and HERWIG [6] (version 6.510). In fact, the algorithms implemented in HERWIG and PYTHIA are quite different, in both parton showers and hadronization.

The discrepancies can be tentatively quoted at $\pm 20\%$, although bigger surprises are possible for some channels. In particular, fig. 1 (right panel) shows a case in which the predictions from HERWIG largely underestimate the flux of photons at low energy. This is due to the fact that the latter does not include photon emission off leptons.

2.2 ElectroWeak radiation

The emission of W's and Z's from the final (or initial!) states is enhanced by one or more powers of $\ln(M/M_{W,Z})$, with $M \gg M_{W,Z}$, not depending on the DM model. For large M, these can be important and lead to significant modifications of the spectra. First, the weak emission entails the presence of further unstable hadrons in the final state, and therefore it significantly modifies the flux of γ's and $e^{\pm}$ at energies $E \ll M$, M being the DM mass. Moreover, W/Z radiation leads to a $\bar{p}$ contribution, even in annihilation channels that would be completely leptonic if EW radiation is neglected. For instance, a DM DM $\to \nu\bar{\nu}$ channel also yield $e^{\pm}$'s, γ's and $\bar{p}$'s, rather counter-intuitively.

3 Propagation of charged cosmic rays

The e^-, e^+ and $\bar{p}$ produced in any given point of the halo **propagate** immersed in the turbulent galactic magnetic field. The field consists of random inhomogeneities that act as scattering centers for charged particles, so that their journey can effectively be described as a diffusion process from an extended source (the DM halo) to some final given point (the location of the Earth, in the case of interest). While diffusing, charged CRs experience several other processes, and in particular energy losses due to synchrotron radiation, Inverse Compton Scattering (ICS) on the low energy photons of the CMB and starlight, Coulomb losses, bremsstrahlung, nuclear spallations... . Quantitatively, the steady-state number density $n_f(\vec{x}, E)$ per unit energy E of the cosmic ray species f $(= e^+, e^-, \bar{p})$ in any given point $\vec{x}$ obeys to a diffusion-loss equation [7]

$$\begin{aligned} -\mathcal{K}(E)\cdot\nabla^2 n_f - \frac{\partial}{\partial E}\left(b(E,\vec{x})\, n_f\right) \;&+\; \frac{\partial}{\partial z}\left(\mathrm{sign}(z)\, V_{\rm conv}\, n_f\right) \\ &= Q(E,\vec{x}) - 2h\,\delta(z)\,\Gamma\, n_f\,. \end{aligned} \tag{2}$$

The first term accounts for diffusion, with a coefficient conventionally parameterized as $\mathcal{K}(E) = \mathcal{K}_0(E/\mathrm{GeV})^\delta$. The second term describes energy losses: the coefficient b is position-dependent since the intensity of the magnetic field (which determines losses due to synchrotron radiation) and the distribution of the photon field (which determines losses due to ICS) vary across the galactic halo. It also has a dependence on energy which is equal to E^2 only as long as ICS is approximated with Thomson scattering. It is normalized by the value of the typical loss timescale at 1 GeV at the location of the Earth $\tau_\odot = 5.7\times10^{15}$ sec. This is illustrated in fig. 2. The third term deals with convection while the last term accounts for nuclear spallations, that occur with rate Γ in the disk of thickness $h \simeq 100$ pc. The source, DM annihilations, is given by $Q = 1/2\,(\rho(\vec{x})/M)^2 \sum_i \mathrm{BR}_i \langle\sigma v\rangle\ (dN_f^i/dE)$, where σv is the total annihilation cross section and the sum runs over all primary channels i in which the cosmic ray species f is produced. dN_f^i/dE) are the spectra discussed in Sec. 2. $\rho(\vec{x})$ is the DM density distribution in the galactic halo. The different processes described above have a different importance depending on the particle species: the journey of electrons and positrons is primarily affected by synchrotron radiation and inverse Compton energy losses, while for antiprotons these losses are negligible and convection and spallation dominate.

Eq. (2) is usually solved numerically in a diffusive region with the shape of a solid flat cylinder that sandwiches the galactic plane, with height $2L$ in the z direction and radius $R = 20\,\mathrm{kpc}$ in the r direction. The location of the solar system corresponds to $\vec{x}_\odot = (r_\odot, z_\odot) = (8.33\,\mathrm{kpc}, 0)$. Boundary conditions are imposed such that the number density n_f vanishes on the surface of the cylinder, outside of which the charged cosmic rays freely propagate and escape. The values of the propagation parameters δ, K_0, $V_{\rm conv}$ and L are deduced from a variety of (ordinary) cosmic ray data and modelizations.

In the usual solution scheme, the energy loss coefficient b is considered as constant in space

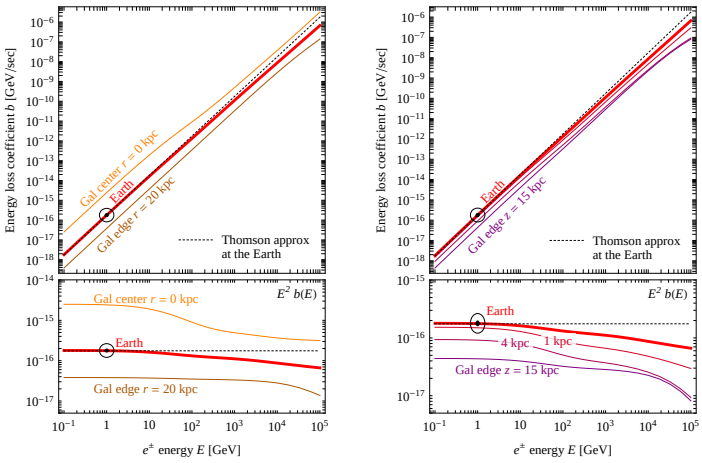

Figure 2: Energy loss coefficient function for electrons and positrons in the Milky Way. Left panel: at several locations along the galactic radial coordinate r, right panel: above (or below) the location of the Earth along the coordinate z. The dot points at the value of $\tau_\odot$.

and proportional to E^2. In [1], we improved the numerical solution by including the correct space and energy dependence. This involves defining a set of energy-dependent 'halo functions' (see [1] for more details).

Once the propagation is performed, one obtains the fluxes of charged cosmic rays at the location of the Earth. Depending on the choices for the propagation parameters, the resulting spectra can differ by more than one order of magnitude. Two representative examples can be found in fig. 3: positrons on the left and antiprotons on the right. The MIN, MED, MAX labels refer indeed to different sets of propagation parameters. The positron panel also reports the spectrum obtained by the old approximated propagation method (black line). All numerical spectra are available in [2].

4 Galactic γ rays

Dark Matter produces high energy gamma rays both by direct ('prompt') emission during annihilation or decay and by Inverse Compton Scattering of $e^\pm$ produced by DM on the ambient light ('secondary'). The former are included in the fluxes discussed in Sec. 2. The latter have to be computed by folding the maps of propagated $e^\pm$ with the maps of target light, in particular in the Galaxy.

One of the best features of these fluxes of ICS γ rays as possible signatures of DM is that

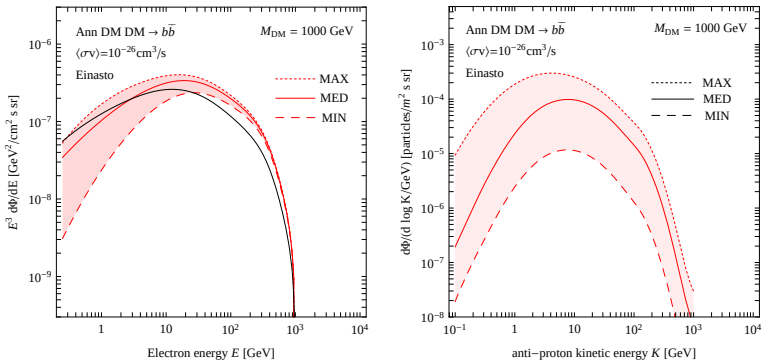

Figure 3: Examples of propagated fluxes of charged CRs at the location of the Earth. Positrons on the left and antiprotons on the right.

they originate from 'everywhere' in the diffusion volume of the galactic halo, including regions where the astrophysical background is reduced (e.g. at high latitudes). Moreover, other energy losses (such as synchrotron radiation) are sub-dominant with respect to Inverse Compton energy losses essentially everywhere, so that, thanks to energy conservation, the resulting ICS γ flux suffers only moderate astrophysical uncertainties.

In [1] we presented a compact formalism to compute galactic ICS γ-ray fluxes, employing a set of functions similar to the halo functions that are introduced for the propagation of charged cosmic rays (briefly discussed above). An example of the resulting fluxes is reported in fig. 4, left. This example chooses a specific DM model and a small but not too small observational rectangular window of 5° around the Galactic Center. The fluxes are plotted for different choices of DM profile, showing that variations of two orders of magnitude are possible. Again, all numerical spectra can be computed with the tools available in [2].

5 Extragalactic γ rays

The γ-rays emitted by DM annihilations or decays in all the extragalactic structures and (in principle) all along the history of the Universe reach us in the form of an isotropic contribution to the total γ-ray intensity. In [1] we discuss in detail how to compute it. With respect to the galactic case, there are a few main differences: (i) one has to include the effect of the 'cosmological dimming' due to the expansion of the Universe, (ii) one has to include the fact that, unlike in the galactic environment, on cosmologically large distances one can not neglect the absorption of gamma-rays and finally (iii) one has to account for the history of formation of DM structures. Fig. 4, right, shows an example of the resulting fluxes. One also sees that,

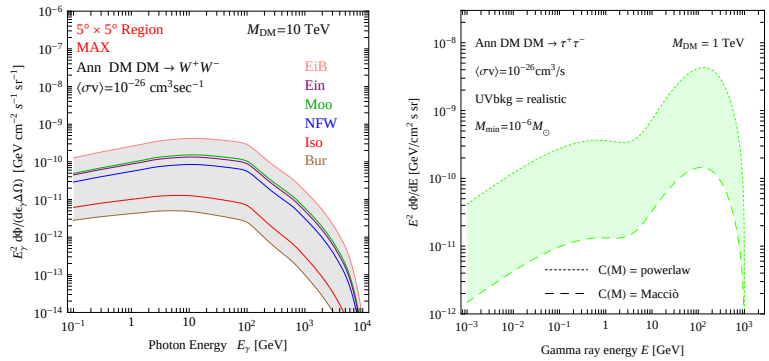

Figure 4: Left: example of fluxes of ICS γ-rays from the Galaxy, for different choices of the DM galactic profile. Right: example of fluxes of extragalactic γ-rays, illustrating the impact of changing the assumption for the concentration parameter.

varying the choice for the concentration function $C(M)$ (one of the parameters associated to the history of halo formation), the spread can be almost 2 orders of magnitude.

6 Conclusions

The next few years will be rich of data in the field of indirect searches for Dark Matter. It will be interesting, from a phenomenological and model-independent point of view, to have at disposal all the tools needed to quickly interpret and cross check them. This is what we aimed at providing in [1]. We make all numerical results downloadable from [2]. The main innovations introduced in the paper are: (i) a comparison between different MCs, (ii) an improved semi-analytical propagation for $e^\pm$ in the Galaxy, (iii) a set of 'halo functions' for computing ICS γ-ray fluxes, (iv) a thorough analysis of the uncertainties that affect extragalactic γ-ray fluxes.

Acknowledgements

I thank all my coauthors of [1], on which the work presented here is based, and for useful discussions. My work is supported in part by the French national research agency ANR under contract ANR 2010 BLANC 041301 and by the EU ITN network UNILHC.

References

[1] M. Cirelli, G. Corcella, A. Hektor, G. Hutsi, M. Kadastik, P. Panci, M. Raidal and F. Sala *et al.*, "PPPC 4 DM ID: A Poor Particle Physicist Cookbook for Dark Matter Indirect Detection," JCAP **1103** (2011) 051, arXiv:1012.4515 [hep-ph].

[2] www.marcocirelli.net/PPPC4DMID.html

[3] N. Arkani-Hamed, D. P. Finkbeiner, T. R. Slatyer, N. Weiner, Phys. Rev. D79 (2009) 015014, arXiv:0810.0713.

[4] M. Pospelov, A. Ritz, Phys. Lett. B671 (2009) 391-397, arXiv:0810.1502.

[5] T. Sjostrand, S. Mrenna and P.Z. Skands, Comput. Phys. Commun. 178 (2008) 852.

[6] G. Corcella et al., JHEP 0101 (2001) 010.

[7] P. Salati, *Indirect and direct dark matter detection*, Proceedings of the 2007 Cargèse Summer School: Cosmology and Particle Physics Beyond the Standard Models, PoS(cargese)009, pos.sissa.it/cgi-bin/reader/conf.cgi?confid=49

Chapter 3

Precision physics at e^+e^- colliders

3.1 F. Jegerlehner - Implications of low and high energy measurements on SUSY models

Implications of low and high energy measurements on SUSY models

Fred Jegerlehner
Institut für Physik, Humboldt Universität zu Berlin, Newtonstrasse 15, D-12489 Berlin, Germany
Deutsches Elektronen-Synchrotron (DESY), Platanenallee 6, D-15738 Zeuthen, Germany
fjeger@physik.hu-berlin.de

Abstract
New Physics searches at the LHC have increased significantly lower bounds on unknown particle masses. This increases quite dramatically the tension in the interpretation of the data: low energy precision data which are predicted accurately by the SM (LEP observables like M_W or loop induced rare processes like $B \to X_s\gamma$ or $B_s \to \mu^+\mu^-$) and quantities exhibiting an observed discrepancy between SM theory and experiment, most significantly found for the muon $g-2$ seem to be in conflict now. $(g-2)_\mu$ appears to be the most precisely understood observable which at the same time reveals a 3-4 σ deviation between theory and experiment and thus requires a significant new physics contribution. The hints for a Higgs of mass about 125 GeV [1, 2], which is precisely what SUSY extensions of the SM predict, seem to provide a strong indication for SUSY. At the same time it brings into serious trouble the interpretation of the $(g-2)_\mu$ deviation as a SUSY contribution.

1 Minimal Super Symmetric extensions of SM

The Standard Model (SM), although doing surprisingly well in describing most of the precision data at the quantum level, is incomplete as it does not incorporate dark matter (DM) for example and it has fine tuning problems most notably it predicts a vacuum energy contribution induced by the Higgs condensate which is 50 orders of magnitude too large and also the Higgs mass is not protected from being much heavier than other SM particles. As we know all SM states are protected either by chiral or by gauge symmetries, except from the Higgs. Supersymmetry (SUSY) imposing an invariance under the exchange of bosons/fermions with fermions/bosons in a field theory in principle is able to cure these problems if it would not be broken. As we know from observation, any SUSY extensions of the SM must be broken in such a way that all sparticles are heavier than all SM particles. Still, for the Higgs a minimal SUSY extensions of the SM predicts a light Higgs $m_h < M_Z$ + radiative corrections $\leq$ 140 GeV and finding a Higgs in this range is a strong argument in favor of SUSY (see the blue-band plot Fig. 3 in [3]).

A viable Minimal Supersymmetric extensions of the SM (MSSM) is possible only if we supplement the SM with an additional Higgs doublet (2HDM). One reason is supersymmetry itself, the other

is anomaly cancellation of the SUSY partners of the Higgses. We thus have the SM with two scalars, a lighter h and a heavier H, a pseudoscalar A and the charged Higgses $H^\pm$ the spectrum of which is doubled by the SUSY completion, the sparticles. The vacuum expectation values of the two scalars $v_i =< H_i >\ (i = 1, 2)$ define the new parameter $\tan\beta = v_1/v_2$. In the minimal SUSY models the masses of the extra Higgses at tree level are severely constrained by mass- and coupling-relations. Only two independent parameters are left, which we may choose to be $\tan\beta$ and m_A. Very important is the fact that the SM gauge structure is not touched when going to the MSSM and gauge and Yukawa couplings of the sparticles are completely fixed by the gauge couplings of the SM.

In general 2HDMs do not exhibit the phenomenologically well established "minimal flavor violation" (MFV) constraint, which demands FCNC and CP patterns to be close to what we have in the SM [4]. The trick which saves the peculiar SM features is R-parity, a Z_2 symmetry between the two Higgs doublet fields $H_1 \leftrightarrow H_2$. As a byproduct SUSY+R-parity implies a stable lightest SUSY particle (LSP) which is a good candidate for the astrophysically established dark matter. The LSP usually is the lightest neutralino $\tilde{\chi}_1^0$, but also a gravitino can be a viable DM candidate.

Even with the constraints mentioned, SUSY extensions of the SM allow for a large number ~ 100 of free symmetry breaking parameters. Free parameters typically are masses and mixings of the neutralinos, the higgsino mass μ ($+\mu H_1 H_2$ term of the 2HDM Higgs potential) and $\tan\beta$.

This changes if one marries SUSY with GUT ideas, in fact SUSY-GUTs (e.g. as based on SU(5)) are the only theories which allow for grand unification broken at a low scale (~ 1 TeV). This provides strong constraints on the SUSY breaking mechanism, specifically we distinguish the constrained CMSSM a SUSY-GUT with soft breaking masses universal at the GUT scale. The NUHM is as CMSSM with non-universal Higgs masses. Minimal super gravity (mSUGRA) exhibits super gravity induced SUSY breaking with $m_{3/2} = m_0$ at the bare level. These models assume many degeneracies of masses and couplings in order to restrict the number of parameters. Typically, SM parameters are supplemented by $m_{1/2}$ (scalar-matter mass, like $m_{\tilde{q}}$, $m_{\tilde{\ell}}$), m_0 (the $U(1)_Y \otimes SU(2)_L$ gaugino masses, $m_{\tilde{\gamma}}$, $m_{\tilde{Z}}$, $m_{\tilde{W}}$ and gluino mass $m_{\tilde{g}}$), $\text{sign}(\mu), \tan\beta, A$ (trilinear soft breaking term), and more for less constraint models.

2 Low energy monitor: the muon anomaly

Formally a_μ is one of the simplest observables one can imagine, just the electromagnetic vertex $(-ie)\ \bar{u}(p')\left[\gamma^\mu F_1(q^2) + i\frac{\sigma^{\mu\nu}q_\nu}{2m_\mu}F_2(q^2)\right]u(p)$ in the static limit where $F_1(0) = 1,\ \ F_2(0) = a_\mu$. And it has a simple experimental consequence, it is responsible for the Larmor precession of a muon circulating in a homogeneous magnetic field and which can be measured very precisely. Presently we have [5, 6, 7, 8, 9]

$$a_\mu^{\text{Exp.}} = 1.16592080(63) \times 10^{-3} \qquad a_\mu^{\text{The.}} = 1.16591797(60) \times 10^{-3} \tag{1}$$

$$\delta a_\mu = a_\mu^{\text{Exp.}} - a_\mu^{\text{The.}} = (283 \pm 87)\ \cdot 10^{-11}\ , \tag{2}$$

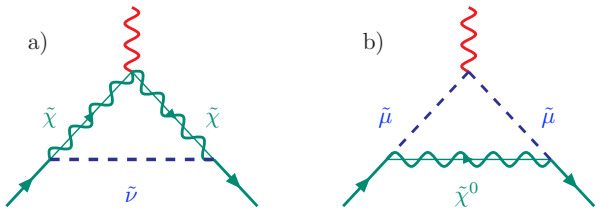

Figure 1: Leading SUSY contributions to $g-2$ in supersymmetric extension of the SM. For subleading corrections see [11].

which is a 3.3 σ deviation. If we take quoted errors and uncertainties to be estimated correctly and if we assume it is not a statistical fluctuation we have to conclude that we see physics beyond the SM: $\delta a_\mu = \Delta a_\mu^{\rm NP}$.

Nevertheless, the status of the theory must be examined. In particular the estimates of hadronic effects is by no means always 100 % certain. Recently, it has been shown that taking into account properly $\rho-\gamma$ mixing, which is absent in τ-decay, actually accounts for the τ versus e^+e^- discrepancy [7]. It means that τ data have to be corrected according to $v_0(s) = r_{\rho\gamma}(s)\, R_{\rm IB}(s)\, v_-(s)$ with a mixing correction $r_{\rho\gamma}(s)$ which had not been taken into account in previous analyses [8]. These findings have been obtained/confirmed in a different approach based on the Hidden Local Symmetry model [10].

The muon is particularly interesting because possible contributions from unknown heavier states yield contributions

$$a_\mu^{\rm NP} = C\, m_\mu^2/M_{\rm NP}^2 \tag{3}$$

where naturally $C = O(\alpha/\pi)$ ($\sim$ lowest order $a_\mu^{\rm SM}$). Typical New Physics scales required to satisfy $\Delta a_\mu^{\rm NP} = \delta a_\mu$ are $M_{\rm NP} = 2.0^{+0.4}_{-0.3}$ TeV, 100^{+21}_{-13} GeV and 5^{+1}_{-1} GeV for $C = 1$, α/π and $(\alpha/\pi)^2$, respectively.

Different extensions of the SM yield very different effects in a_μ such that a_μ is a very good monitor to look for physics beyond the SM. It is not so easy to get substantial effects with obvious new physics possibilities: in view that the τ yields $a_\mu(\tau) \simeq 42\cdot 10^{-11}$ only, and bounds like $m_L > 100$ GeV for a heavy lepton or $m_{b'} \gtrsim 200$ GeV for a heavy quark show that sequential fermions (4th family) would not be able to give a substantial effect. Similarly, possible Z', W' or leptoquarks, which have to satisfy bounds like $M_{Z',W'} > 600-800$ GeV, depending on the GUT scenario yield tiny effects only. They can be estimated by rescaling the weak SM contribution with $(M_W/M_{W'})^2 \sim 0.01$, which gives 1% of $19.5\cdot 10^{-10}$, too small to be of relevance. More examples have been reviewed in [6].

Before the recent results from the LHC, constraints on the mass spectrum from LEP and the Tevatron already excluded sufficiently light new states which could produce a 3-4 σ effect, unless the coupling is unusually strong, with the risk that perturbative arguments fail to be reliable.

The most promising New Physics scenarios are provided by SUSY extensions of the SM because in these models the muon Yukawa coupling is enhanced by $\tan\beta = v_1/v_2$ which naturally may be

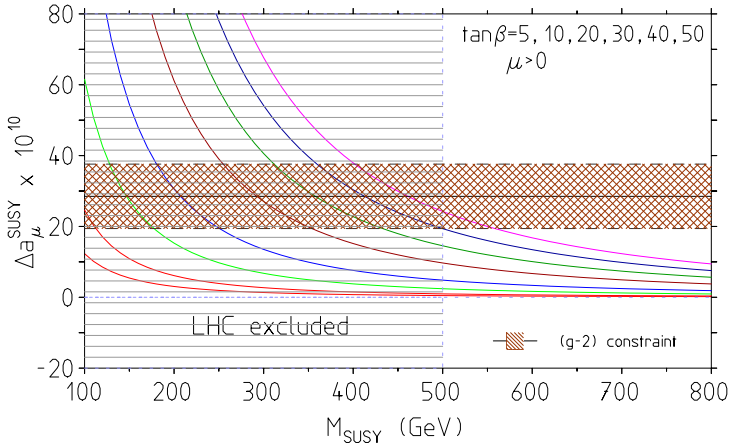

Figure 2: Constraint on large $\tan\beta$ SUSY contributions as a function of $M_{\rm SUSY}$. The horizontal band shows $\Delta a_\mu^{\rm NP} = \delta a_\mu$. The region left of $M_{\rm SUSY} \sim 500$ GeV is excluded by LHC searches. If $m_h \sim 125 \pm 1.5$ GeV actually $M_{\rm SUSY} > 800$ GeV depending on details of the stop sector ($\{\tilde{t}_1, \tilde{t}_2\}$ mixing and mass splitting) and weakly on $\tan\beta$.

expected to be as large as the top to bottom quark mass ratio (assuming $y_t = y_b$) $\tan\beta = v_1/v_2 = m_t/m_b \sim 40$. Such enhanced supersymmetric contributions to a_μ stem from sneutrino–chargino and smuon–neutralino loops as shown in Fig. 1. The renormalization group improved 1-loop MSSM result is given by

$$a_\mu^{\rm SUSY} \simeq \frac{{\rm sign}(\mu M_2)\,\alpha(M_Z)}{8\pi \sin^2\Theta_W}\,\frac{\left(5+\tan^2\Theta_W\right)}{6}\,\frac{m_\mu^2}{M_{\rm SUSY}^2}\,\tan\beta\left(1-\frac{4\alpha}{\pi}\ln\frac{M_{\rm SUSY}}{m_\mu}\right) \tag{4}$$

with $M_{\rm SUSY}$ a typical SUSY loop mass and the sign is determined by the Higgsino mass term μ. Obviously, the 3-4 σ deviation in muon $g-2$ (if real) requires sign(μ) positive and $\tan\beta$ preferably large. These are clear cut constraints which cannot be obtained easily based on LHC data alone. In GUT constrained models where neutralino masses are constrained by limits on the colored sector from the LHC, typically now $M_{\rm SUSY} > 500$ GeV. If we assume $\delta a_\mu = \Delta a_\mu^{\rm SUSY}$ we find $\tan\beta \simeq M_{\rm SUSY}^2/(65.5\ {\rm GeV})^2$, which for $M_{\rm SUSY} \simeq 500$ GeV requires $\tan\beta \simeq 58$ (see Fig. 2), which is in conflict with a Higgs near 125 GeV as we will see below.

3 High energy precision physics: LEP, B-physics

Here we are looking at SM precision observables like G_F (muon lifetime), Z observables M_Z, Γ_Z, g_V, g_A, $\sin^2\Theta_{\rm eff}$ (LEP1/SLD) W and top observables M_W, Γ_W, m_t and Γ_t (LEP2/Tevatron). An important observable is the W mass given by

$$M_W^2\left(1-\frac{M_W^2}{M_Z^2}\right) = \frac{\pi\alpha}{\sqrt{2}G_F}\,(1+\Delta r) \tag{5}$$

where $\Delta r = f(\alpha, G_F, M_Z, m_t, \cdots)$ represents the radiative correction to the tree level mass-coupling relation, which depends on the independent parameters of the theory. They differ from the SM by additional contributions in extensions of the SM and thus allow to constrain the parameter space of the extended model. In SUSY models M_W is sensitive to the top/stop sector parameters and actually M_W is essentially the only observable which slightly improves in MSSM fits (see Fig. 25 of [12]) while

$$\sin^2\Theta_{\rm eff} = \frac{1}{4}\left(1 - {\rm Re}\,\frac{v_{\rm eff}}{a_{\rm eff}}\right) \tag{6}$$

remains unaffected [3] (see Figs. 14 and 15 of [13] and Fig. 1 of [14] and Fig. 4 of [3]). The global fit of LEP data [15] does not improve when going from the SM to the MSSM, i.e. SUSY effects are strongly constrained here. MSSM results merge into SM results for larger SUSY masses, as decoupling is at work.

Data on the penguin loop induced $B \to X_s\gamma$ transition yields another strong constraint on deviations from the SM [16]. Indeed, the SM prediction [17] $\mathcal{B}(b \to s\gamma)_{\rm NNLL} = (3.15 \pm 0.23)\cdot 10^{-4}$ is consistent within 1.2 σ with the experimental result [18] $\mathcal{B}(b \to s\gamma) = (3.55 \pm 0.24 \pm 0.09)\cdot 10^{-4}$. It implies that SUSY requires heavier $m_{1/2}$ and/or m_0 in order not to spoil the good agreement.

The very rare box loop induced decay $B_s \to \mu^+\mu^-$ is very interesting because SUSY contributions (box contributions with W's replaced by charged Higgses $H^\pm$) are able to enhance the SM value

$$\mathcal{B}(\bar{B}_s \to \mu^+\mu^-) = (3.1 \pm 1.4)\times 10^{-9} \tag{7}$$

by two orders of magnitude, especially in scenarios with non-universal Higgs masses (NUHM). The best bound obtained recently by LHCb [20] is

$$\mathcal{B}(\bar{B}_s \to \mu^+\mu^-) < 1.4\times 10^{-8}\,, \tag{8}$$

and gets closer to the SM value again constraining too large effects from beyond the SM.

In SUSY+R-parity scenarios the dark matter relict density [21] $\Omega_{\rm CDM}h^2 = 0.1126 \pm 0.0081$ represents a tough constraint for the relic density of neutralinos produced in the early universe. A DM neutralino is a WIMP DM candidate. The density predicted is [22]

$$\Omega h^2 \sim \frac{0.1\,{\rm pb}}{\langle\sigma v\rangle} \sim 0.1\left(\frac{M_{\rm WIMP}}{100{\rm GeV}}\right)^2\,, \tag{9}$$

where $\langle\sigma v\rangle$ is the relativistic thermally averaged annihilation cross-section. Note that except from $\Omega_{\rm CDM}$ all observables prefer heavier SUSY masses such that effects are small by decoupling. The muon $g-2$ in contrast requires moderately light SUSY masses and in the pre-LHC era fitted rather well with expectations from SUSY (see e.g. Fig. 2 of [23] and [24]).

4 Implications of LHC data

Direct LHC search limits have been taken into account above in some cases. LHC events most directly test the colored sector of the MSSM. In models like the CMSSM and NUHM, constrained by coupling unification at the GUT scale, the colored sector parameters get closely related to the uncolored sector. Consequently one obtains model dependent constraints on physics controlled via standard precision tests. Typically, in constrained models LHC data have a strong influence on a large part of SUSY parameter space [25]. The impact is very well illustrated e.g. in Figs. 1 of [26, 27].

A particular role is played by the mass of the light Higgs. At tree level in the MSSM $m_h \leq M_Z$. This bound receives large radiative corrections from the $t/\tilde{t}$ sector, which changes the upper bound to [28]

$$m_h^2 \sim M_Z^2 \cos^2 2\beta + \frac{3\sqrt{2}G_\mu m_t^4}{2\pi^2 \sin^2\beta} \ln\left(\frac{m_{\tilde{t}_1} m_{\tilde{t}_2}}{m_t^2}\right) + \cdots \tag{10}$$

which in any case is well below 200 GeV. A given value of m_h fixes the value of $m_{1/2}$ represented by $\{m_{\tilde{t}_1}, m_{\tilde{t}_2}\}$. Global frequentist fits to the CMSSM and NUHM1 scenarios predict $m_h \sim 119$ GeV in fits incorporating the $(g-2)_\mu$ constraint and ~ 126 GeV without it. If $m_h \simeq 125$ GeV as suggested by most recent LHC Higgs searches [1, 2] $m_{1/2}$ would be fixed around 800 to 950 GeV. Together with the narrow bound from the cosmic relict density in the CMSSM one would also fix m_0 at a relatively low value depending sensitively on $\tan\beta$, however.

As we see, the present LHC data have a quite dramatic impact on SUSY scenarios. The main outcome is that in constrained models like CMSSM, NUHM1, mSUGRA or NUHM2 all allowed parameter points with $m_h \sim 125$ GeV are inconsistent with the observed $(g-2)_\mu$ [29, 27] ! However, in unconstrained SUSY extensions of the SM, only direct searches for sneutrino, chargino, smuon and neutralino states (or corresponding mass bounds) can lead to definite conclusions.

5 Comments and Outlook

SUSY is the natural mechanism to tame the cosmological constant problem as well as the Higgs hierarchy problem of the SM. However, to make a SUSY extension of the SM not to spoil phenomenologically established minimal flavor patterns of the SM one has to supplement it by assuming R-parity as an extra symmetry. Most of the popular MSSM scenarios assume in addition GUT to be at work which heavily constrains the parameter ambiguities in the possible soft SUSY breakings. One should be aware of the fact that SUSY and GUT are uncorrelated symmetry concepts, GUT assumptions almost always made in SUSY extensions of the SM may not be realistic. Unlike chiral symmetry, gauge symmetry and super symmetry gauge unification is not imposed to protect light states since the GUT scale is only two or three orders of magnitude below $M_{\rm Planck}$.

Another comment concerns the nature of dark matter. DM is quite commonly assumed to consist of one or several species of elementary particle. In the SUSY+R-parity framework the LSP is an elementary particle. Here we should keep in mind that normal matter in the universe is dominated by nucleons, i.e., the normal matter density is 99% frozen energy and the light fermion masses generated in electroweak symmetry breaking represent a minor correction only. What if dark matter is not the result of the existence of a stable heavy elementary particle, but again mostly a form of frozen energy? One could think of unflavored SU(4) confined states. Such dark matter would be bosonic with no new fermionic matter which would form DM stars. Stability of such matter would be natural similar to B conservation for normal baryonic matter. In this context direct DM searches [30] are extremely important and progress in this field will bring more light into the DM puzzle.

Before the LHC was in operation one was expecting that SUSY improves agreement with experiment for observables like a_μ and marginally for M_W. After the first LHC results the expectations have changed. The situation looks somewhat disturbing. If a Higgs of mass near 125 GeV would be confirmed one would have a strong point for SUSY at work. But the $(g-2)_\mu$ deviation requires unexpectedly large $\tan\beta$ now. It would mean that the top-bottom Yukawa coupling get an inverse hierarchy relative to the masses, which to me looks quite unnatural.

I start to worry about the muon anomaly result in the sense that it is not 100% clear to me whether experiments measure what theoreticians calculate, namely $a_\mu = F_2(0)$? The fact that perfect charged one-particle states do not exist, due to the infrared problem of QED, could affect the measurement at the level of precision we are dealing with. To my knowledge, in deriving the equations of motion of the muon in the external field the radiation field is neglected. The possible problem has been investigated at leading order in [31] some time ago, but no higher order results have been worked out so far. At the given level of precision this is an issue which should be investigated more carefully.

Within the next 5 years a new muon $g-2$ experiment will go into operation at Fermilab (E989) [32]. It will be an upgraded Brookhaven experiment (E821) working with ultra-relativistic magic energy muons. An alternative project is being designed at J-PARC which will work with ultra-cold muons [33]. The experiment will have very different systematics and therefore will provide a very important crosscheck of the storage ring experiments. The accuracy attempted is $\delta a_\mu = 16 \cdot 10^{-11}$. Provided the deviation (2) is real and the central value would not move, and provided theory is able to reduce theoretical uncertainties accordingly, the 3σ would turn into a 9σ deviation. If SUSY or 2HDM would be at work this experiment would provide invaluable information about the sign of the parameter μ and pin down $\tan\beta$ like no other experiment [34].

One has to be aware that much of the tension in the interpretation of the data we are confronted with, may be a result of too special model assumptions used in analyzing the data. First LHC data primarily constrain the colored sector. In those SUSY models which do not assume a strong correlation between the colored and the uncolored sector a future ILC(1000) would play a prominent role in disentangling the true structure beyond the SM. For much more detailed discussions I refer to the articles quoted earlier and the references therein.

Acknowledgments

I am grateful to the organizers for the kind invitation, for the support and the kind hospitality at the ECT* Trento.

References

[1] ATLAS Collaboration Higgs search status report, http://www.atlas.ch/news/2011/status-report-dec-2011.html

[2] CMS Collaboration Higgs search status report, http://cdsweb.cern.ch/record/1406347/files-static/HIG-11-032-pas.pdf

[3] O. Buchmueller et al., Phys. Lett. B **657** (2007) 87.

[4] G. D'Ambrosio, G. F. Giudice, G. Isidori, A. Strumia, Nucl. Phys. B **645** (2002) 155.

[5] G. Bennett et al., Phys. Rev. Lett. **92** (2004) 161802; Phys. Rev. **D 73** (2006) 072003.

[6] F. Jegerlehner, A. Nyffeler, Phys. Rept. **477** (2009) 1.

[7] M. Davier, A. Hoecker, B. Malaescu, Z. Zhang, Eur. Phys. J. C **71** (2011) 1515.

[8] F. Jegerlehner, R. Szafron, Eur. Phys. J. C **71** (2011) 1632.

[9] J. Miller, E. de Rafael, B. Roberts, Rept. Prog. Phys. **70** (2007) 795; J. Prades, E. de Rafael, A. Vainshtein, arXiv:0901.0306 [hep-ph]; K. Hagiwara, R. Liao, A. D. Martin, D. Nomura, T. Teubner, J. Phys. G G **38** (2011) 085003.

[10] M. Benayoun, P. David, L. DelBuono, F. Jegerlehner, Eur. Phys. J. C **72** (2012) 1848.

[11] S. Heinemeyer, D. Stöckinger, G. Weiglein, Nucl. Phys. B **699** (2004) 103; D. Stöckinger, J. Phys. G **34** (2007) R45;

[12] S. Heinemeyer, W. Hollik, D. Stöckinger, A. M. Weber, G. Weiglein, JHEP **0608** (2006) 052.

[13] S. Heinemeyer, W. Hollik, A. M. Weber, G. Weiglein, JHEP **0804** (2008) 039.

[14] O. Buchmueller et al., Phys. Rev. D **81** (2010) 035009.

[15] ALEPH, CDF, D0, DELPHI, L3, OPAL, SLD Collaborations, the LEP Electroweak Working Group, the Tevatron Electroweak Working Group and the SLD electroweak and heavy flavour groups, arXiv:1012.2367 [hep-ex],

[16] S. Bertolini, F. Borzumati, A. Masiero, G. Ridolfi, Nucl. Phys. B **353** (1991) 591.

[17] M. Misiak et al., Phys. Rev. Lett. **98** (2007) 022002.

[18] D. Asner et al., The Heavy Flavor Averaging Group, arXiv:1010.1589 [hep-ex].

[19] G. Isidori, P. Paradisi, Phys. Lett. B **639** (2006) 499; G. Isidori, F. Mescia, P. Paradisi, D. Temes, Phys. Rev. D **75** (2007) 115019.

[20] R. Aaij et al. [LHCb Collaboration], arXiv:1112.1600 [hep-ex].

[21] E. Komatsu et al. [WMAP Collaboration], Astrophys. J. Suppl. **192** (2011) 18;

[22] G. Belanger, F. Boudjema, A. Pukhov, A. Semenov, Comput. Phys. Commun. **176** (2007) 367; **149** (2002) 103; **174** (2006) 577.

[23] K. A. Olive, Eur. Phys. J. C **59** (2009) 269.

[24] J. Ellis, K. A. Olive, P. Sandick, New J. Phys. **11** (2009) 105015.

[25] O. Buchmueller et al., arXiv:1110.3568 [hep-ph].

[26] K. A. Olive, arXiv:1202.2324 [hep-ph].

[27] J. Ellis, K. A. Olive, arXiv:1202.3262 [hep-ph].

[28] H. E. Haber, R. Hempfling, Phys. Rev. Lett. **66** (1991) 1815.

[29] H. Baer, V. Barger, A. Mustafayev, arXiv:1112.3017 [hep-ph].

[30] E. Aprile *et al.* [XENON100 Collaboration], Phys. Rev. Lett. **107** (2011) 131302 and references therein.

[31] O. Steinmann, Commun. Math. Phys. **237** (2003) 181.

[32] R. M. Carey, K. R. Lynch, J. P. Miller, B. L. Roberts, W. M. Morse, Y. K. Semertzides, V. P. Druzhinin and B. I. Khazin *et al.*, FERMILAB-PROPOSAL-0989.

[33] N. Saito et al., `http://phipsi11.inp.nsk.su/talks/Phipsi2011-saito.pdf`

[34] D. W. Hertzog, J. P. Miller, E. de Rafael, B. Lee Roberts, D. Stöckinger, arXiv:0705.4617 [hep-ph].

3.2 G. Venanzoni - Latest on the g-2 from experiment

Latest on the muon g-2 from experiment

Graziano Venanzoni
Laboratori Nazionali di Frascati dell' INFN, Frascati, Italy
graziano.venanzoni@lnf.infn.it

Abstract We review the latest experimental achievements on the hadronic cross section measurements at low energy which are of fundamental importance for a precise evaluation of the hadronic contribution to the $g-2$ of the muon. We also discuss the new proposed muon $g-2$ experiments, with particular emphasis on E989 at Fermilab which plans to improve the experimental uncertainty by a factor of 4 with respect to the previous E821 experiment at BNL.

1 The Muon anomaly as a precision test of the Standard Model

The muon anomaly $a_\mu = (g-2)/2$ is a low-energy observable, which can be both measured and computed to high precision [1]. Therefore it provides an important test of the Standard Model (SM) and allows a sensitive search for new physics [2]. Since the first precision measurement of a_μ from the E821 experiment at BNL in 2001 [3], there has been a discrepancy between its experimental value and the SM prediction. This discrepancy has been slowly growing due to recent impressive theory and experiment achievements. Figure 1 (from Ref. [4]) shows an up-to-date comparison of the SM predictions by different groups and the BNL measurement for a_μ. Evaluations of different groups are in very good agreement, showing a persisting $3\,\sigma$ discrepancy (as, for example, $26.1 \pm 8.0 \times 10^{-10}$[4]). It should be noted that both theoretical and experimental uncertainties have been reduced by more than a factor of two in the last ten years[1].

The accuracy of the theoretical prediction ($\delta a_\mu^{\rm SM}$, between 5 and 6 $\times 10^{-10}$) is limited by the strong interaction effects which cannot be computed perturbatively at low energies. Table 1 shows their contribution to the error for three recent estimates [6, 7, 4][2]. The leading-order hadronic vacuum polarization contribution, $a_\mu^{\rm HLO}$, gives the main uncertainty (between 4 and 5 $\times 10^{-10}$). It can be related by dispersion integral to the measured hadronic cross sections, and it is known with a fractional accuracy of 0.7%, i.e. to about 0.4 ppm. The $O(\alpha^3)$ hadronic light-by-light contribution, $a_\mu^{\rm HLbL}$, is the second dominant error in the theoretical evaluation. It

[1] In 2001 this discrepancy was $(23.1 \pm 16.9) \times 10^{-10}$ [5].
[2] Ref. [6] uses a more conservative error analysis.

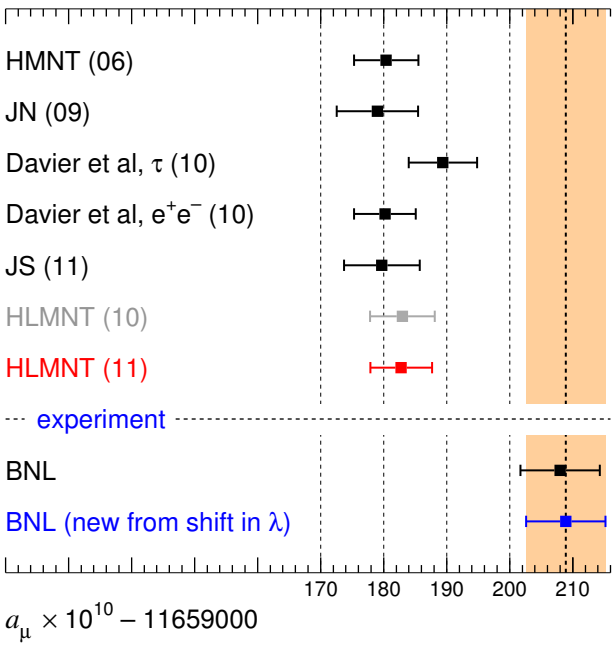

Figure 1: Standard Model predictions of a_μ by several groups compared to the measurement from BNL (from Ref. [4]).

cannot at present be determined from data, and relies on specific models. Although its value is almost one order of magnitude smaller than $a_\mu^{\rm HLO}$, it is much worse known (with a fractional error of the order of 30%) and therefore it still gives a significant contribution to $\delta a_\mu^{\rm SM}$ (between 2.5 and 4 $\times 10^{-10}$). From the experimental side, the error achieved by the BNL E821 experiment is $\delta a_\mu^{\rm EXP} = 6.3 \times 10^{-10}$ (0.54 ppm) [8]. This impressive result is still limited by the statistical error, and experiments to measure the muon $g-2$ with a fourfold improvement in accuracy have been approved at Fermilab [9] and J-PARC [10].

2 Recent progress on the hadronic contribution to a_μ

Differently from the QED and Electroweak contributions to a_μ, which can be calculated using perturbation theory, and therefore are well under control, the hadronic ones (LO VP and HLbL) cannot be computed reliably using perturbative QCD. The lowest order hadronic contribution $a_\mu^{\rm HLO}$ can be computed from hadronic e^+e^- annihilation data via a dispersion relation, and therefore its uncertainty strongly depends on the accuracy of the experimental data. For the

Error	[6]	[7]	[4]	prospect
$\delta a_\mu^{\rm SM}$	6.5	4.9	4.9	3.5
$\delta a_\mu^{\rm HLO}$	5.3	4.2	4.3	2.6
$\delta a_\mu^{\rm HLbL}$	3.9	2.6	2.6	2.5
$\delta(a_\mu^{\rm SM} - a_\mu^{\rm EXP})$	8.8	8.0	8.0	4.0

Table 1: Estimated uncertainties δa_μ in units of 10^{-10} according to Refs. [6, 7, 4] and (last column) prospects in case of improved precision in the e^+e^- hadronic cross section measurement (the prospect on $\delta a_\mu^{\rm HLbL}$ is an *educated guess*). Last row: Uncertainty on Δa_μ assuming the present experimental error of 6.3 from BNL-E821 [8] (first two columns) and of 1.6 (last column) as planned by the future $(g-2)$ experiments [9, 10].

hadronic Light-by-Light contribution $a_\mu^{\rm HLbL}$ there is no direct connection with data and therefore only model-dependent estimates exist. As the hadronic sector dominates the uncertainty on the theoretical prediction $a_\mu^{\rm SM}$, considerable effort has been put on it by experimental and theoretical groups, reaching the following main results:

- A precise determination of the hadronic cross sections at the e^+e^- colliders (VEPP-2M, DAΦNE, BEPC, PEP-II and KEKB) which allowed a determination of $a_\mu^{\rm HLO}$ with a fractional error below 1%. These efforts led to the development of dedicated high precision theoretical tools, like the inclusion of high-order Radiative Corrections (RC) and the non-perturbative hadronic contribution to the running of α (i.e. the vacuum polarisation, VP) in Monte Carlo (MC) programs used for the analysis of the data [11];

- Use of *Initial State Radiation* (ISR) [12, 13, 14] which opened a new way to precisely obtain the electron-positron annihilation cross sections into hadrons at particle factories operating at fixed beam-energies [15, 16];

- A dedicate effort on the evaluation of the Hadronic Light-by-Light contribution, where two different groups [17, 6] found agreement on the size of the contribution (with slightly different errors), and therefore strengthening our confidence in the reliability of these estimates;

- An impressive progress on QCD calculation on the lattice, where an accuracy better than 3% was reached on the two-flavor QCD correction to $a_\mu^{\rm HLO}$ [18];

- Better agreement between the e^+e^- and the τ based evaluation of $a_\mu^{\rm HLO}$, thanks to improved isospin corrections [7]. These two sets of data are eventually in agreement (with τ data moving towards e^+e^- data) after including vector meson and $\rho-\gamma$ mixing [19, 20].

3 σ_{had} measurements at low energy

In the last few years, big efforts on e^+e^- data in the energy range below a few GeV led to a substantial reduction in the hadronic uncertainty on $a_\mu^{\rm HLO}$. Figure 2 shows an up-to-date compilation of these data. The main improvements have been achieved in the region below

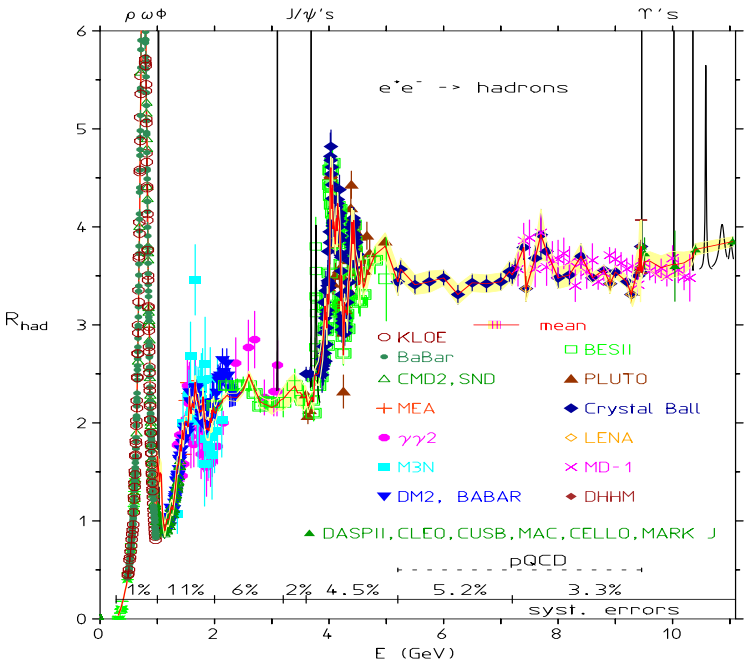

Figure 2: An updated compilation of R measurements. In the bottom line the overall uncertainties of the different regions are reported (*courtesy of Fred Jegerlehner*).

5 GeV: between 2 and 5 GeV (where the data are now closer to the prediction of pQCD), the BESII collaboration reduced the error to ∼7% [21] (before it was ∼15%); between 1 and 4.5 GeV BaBar measured various final states with more than two hadrons with a systematic accuracy between 3% and 15%, as shown in Tab. 3; below 1 GeV, the CMD-2 [22, 23, 24] and SND [25] collaborations at Novosibirsk, KLOE [26, 27, 28] at Frascati and BaBar [29] at Stanford measured the pion form factor in the energy range around the ρ peak with a systematic error of 0.8%, 1.3%, 0.9%, and 0.5%, respectively.

The CMD-2 and SND collaborations at Novosibirsk and BESII in Beijing were performing the hadronic cross section measurements in a traditional way, i.e., by varying the e^+e^- beam energies. KLOE, BaBar, and more recently Belle used ISR (also called *radiative return*) as reviewed in Refs. [11, 15, 16]. Figure 2 shows that, despite the recent progress, the region between 1 and 2 GeV is still poorly known, with a fractional accuracy of ∼6%. Since about

Process	Systematic accuracy
$\pi^+\pi^-\pi^0$	(6-8)%
$2\pi^+2\pi^-$	(3-8)%
$2\pi 2\pi^0$	(8-14)%
$2(\pi^+\pi^-)\pi^0, 2(\pi^+\pi^-)\eta$	(7-10)%
$3\pi^+3\pi^-, 2\pi^+2\pi^-2\pi^0$	(6-11)%
$KK\pi, KK\eta$	(5-6)%
$K^+K^-\pi\pi$	(8-11)%
$K^+K^-\pi^+\pi^-\pi^0$, $K^+K^-\pi^+\pi^-\eta$	(5-10)%
$2(K^+K^-)$	(9-13)%

Table 2: Systematic accuracy on more than two hadrons processes studied by BaBar in the energy range $1< \sqrt{s} < 4.5$ GeV using ISR.

50% of the error squared, $\delta^2 a_\mu^{\rm HLO}$ comes from this region (see Fig. 3), it is evident how desirable an improvement on the hadronic cross section of this region is.

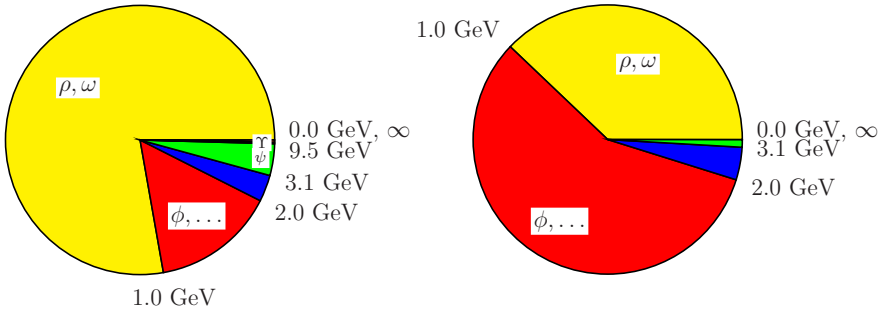

Figure 3: The distribution of contributions (left) and errors (right) in % for $a_\mu^{\rm HLO}$ from different energy regions. The error of a contribution i shown is $\delta_{i\,\rm tot}^2 / \sum_i \delta_{i\,\rm tot}^2$ in %. The total error combines statistical and systematic errors in quadrature (from Ref. [6]).

3.1 Measurement of $\sigma_{\pi\pi}$ below 1 GeV

The region below 1 GeV is dominated by the two-pion channel which accounts for 70% of the contribution to $a_\mu^{\rm HLO}$, and for 40% to the total squared error of a_μ (see Fig. 3). Therefore due to its particular importance, it has been studied by different experiments as shown in Fig. 4. CMD-2 and SND have performed an energy scan at the e^+e^- collider VEPP-2M ($\sqrt{s} \in [0.4–1.4]$ GeV) with $\sim 10^6$ and $\sim 4.5\times 10^6$ events respectively, and systematic fractional errors from 0.6%

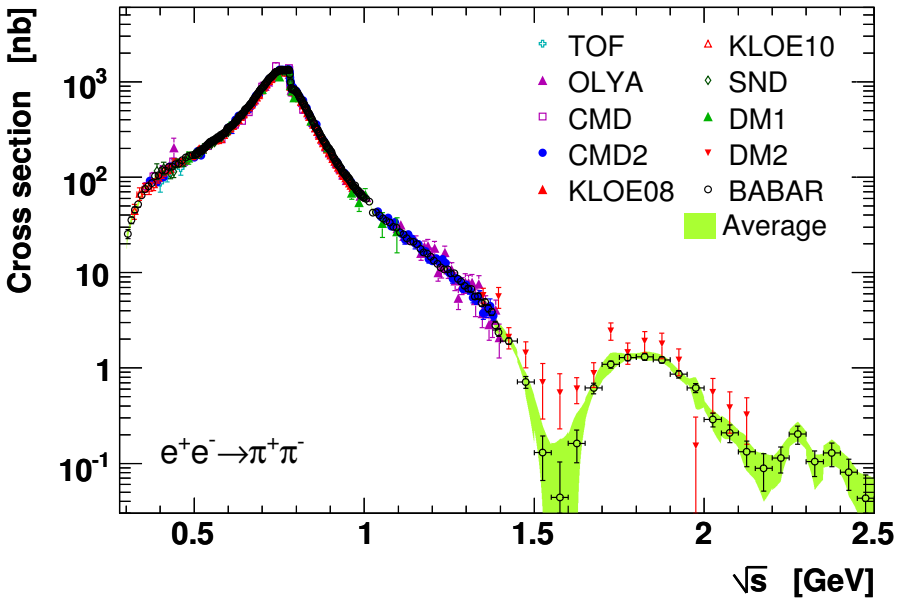

Figure 4: Cross section of $e^+e^- \to \pi^+\pi^-$ as measured by different experiments (from Ref. [7]).

to 4% in the cross sections, depending on $\sqrt{s}$. The pion form factor has also been measured by KLOE and more recently by BaBar, both using ISR. KLOE collected more than 3.1 million events, corresponding to an integrated luminosity of 240 pb^{-1}, leading to a relative error of 0.9% in the energy region [0.6–0.97] GeV dominated by systematics. BaBar has performed a $\pi^+\pi^-(\gamma)$ cross section measurement based on half a million selected events. The pion form factor is obtained by the ratio $\pi^+\pi^-(\gamma)$ to $\mu^+\mu^-(\gamma)$ which allows a systematic error of 0.5% in the ρ region increasing to 1% outside. The threshold region $[2m_\pi - 0.5$ GeV] provides 13% of the total $\pi^+\pi^-$ contribution to the muon anomaly: $a_\mu^{\rm HLO}\ [2m_\pi - 0.5\ {\rm GeV}] = (58.0 \pm 2.1) \times 10^{-10}$. To overcome the lack of precision data at threshold energies, the pion form factor is extracted from a parameterization based on ChPT, constrained by spacelike data [30]. The most effective way to measure the cross section near the threshold in the timelike region is provided by ISR events, where the emission of an energetic photon allows to study the two pions at rest. BaBar has achieved an error between 0.8 and 1.4% in this region, while KLOE has achieved a larger error (up to 7%) dominated by the point-like model uncertainty for FSR.
There is a fair agreement between the four experiments in the region below 1 GeV, with a discrepancy of about 2-3% between KLOE (lowest cross section) and BaBar (highest cross section) at the ρ peak, and CMD2 and SND somehow in the middle. Although small, this difference is larger than the claimed systematic error and can be a limitation for further improvements of $a_\mu^{\rm SM}$. As BaBar and KLOE (published) data use a different normalization (to muon pair and to Bhabha events, respectively) it may be that part of this difference can come from the normalization procedure itself. In order to check this possibility, the KLOE experiment has recently

presented a new *preliminary* measurement of the pion form factor derived from the bin-by-bin $\pi^+\pi^-\gamma/\mu^+\mu^-\gamma$ ratio [31] as done in BaBar. As can be shown in Fig. 5, good agreement is found

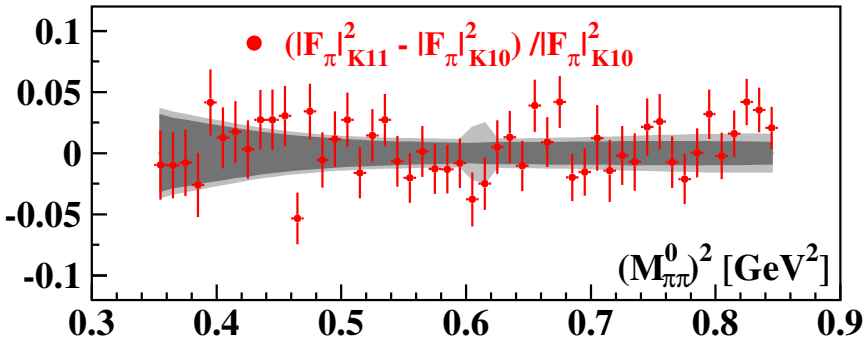

Figure 5: Fractional difference between the published KLOE measurement normalized to Bhabha events [26] and the new *preliminary* one derived from the bin-by-bin $\pi^+\pi^-\gamma/\mu^+\mu^-\gamma$ ratio.

between the two spectra, which excludes possible problems in the normalization procedure used in KLOE.

3.2 Measurement of σ_{had} above 1 GeV

The region [1–2.5] GeV, with an uncertainty on σ_{had} between 6 and 10%, is the most poorly known, and contributes about 55% of the uncertainty on $a_\mu^{\rm HLO}$ (see Fig. 3). In this region BaBar using ISR has published results on e^+e^- into three, four, five and six hadrons, with a general improvement with respect to the much less precise measurements from M3N, DM1 and DM2. For several channels, BaBar measured lower cross sections with respect to older experiments, resulting in a reduced contribution from this energy region to $a_\mu^{\rm HLO}$. Recently CMD-3 and SND experiments at the upgraded VEPP-2000 collider in Novosibirsk have presented new measurements on multihadron channels [32]. With about 20 pb^{-1} of collected data, they have achieved a statistical error comparable to ISR data from B-factories. VEPP-2000 plans to collect an integrated luminosity of 1 fb^{-1}, which would allow a significant improvement for many channels in the region below 2 GeV.
With a specific luminosity of 10^{32}cm^{-2}s^{-1}, DAΦNE upgraded in energy, could perform a scan in the region from 1 to 2.5 GeV, collecting an integrated luminosity of 20 pb^{-1} per point corresponding to few days of data taking for each energy bin [33]. By assuming an energy step of

25 MeV, the whole region would be scanned in one year of data taking. The statistical yield would be one order of magnitude higher than what would have been achieved with 1 ab^{-1} at BaBar, and better than what is to be expected at BESIII with 10 fb^{-1} at 3 GeV.
Finally, prospects of reaching an integrated luminosity by a factor of 30-100 exceeding that of the present machines appear at Super B-Factories. Such machines will improve accuracy for many processes whose studies are now statistically limited.

4 Measuring a_μ

The muon anomaly a_μ has been measured with better and better accuracy during the last 50 years. The E821 experiment at Brookhaven has reached an impressive 14-fold improvement in precision with respect to the pioneering measurements performed at CERN. Two new experiments with a goal of fourfold improvement in accuracy are underway: the approved E989 at Fermilab [9], and the J-PARC proposal [10] that has recently received stage-one approval. E989 is based on the well known magic-momentum concept and uses the BNL storage ring as a key element. The proposal at J-PARC uses a new approach with ultra-slow muons at off-magic momentum. We will now discuss how the measurement of a_μ is done, describing the E821 experiment, and its upgrade E989.
The measurement of a_μ uses the spin precession resulting from the torque experienced by the magnetic moment when placed in a magnetic field. An ensemble of polarized muons is introduced into a magnetic field, where they are stored for the measurement period. The rate at which the spin rotates relative to the momentum vector is given by the difference in frequency between the spin precession and cyclotron frequencies. Because electric quadrupoles are used to provide vertical focusing in the storage ring, their electric field is seen in the muon rest frame as a moving magnetic field that can affect the spin precession frequency. In the presence of both $\vec{E}$ and $\vec{B}$ fields, and in the case that $\vec{\beta}$ is perpendicular to both, the anomalous precession frequency (*i.e.* the frequency at which the muons spin advances relative to its momentum) is

$$\begin{aligned} \vec{\omega_a} &= \omega_S - \omega_C \\ &= -\frac{q}{m}\Big[a_\mu \vec{B} - \Big(a_\mu - \frac{1}{\gamma^2-1}\Big)\frac{\vec{\beta}\times\vec{E}}{c}\Big] \end{aligned} \tag{1}$$

The experimentally measured numbers are the muon spin frequency ω_a and the magnetic field, which is measured with proton NMR, calibrated to the Larmor precession frequency, ω_p, of a free proton. The anomaly is related to these two frequencies by

$$a_\mu = \frac{\tilde{\omega_a}/\omega_p}{\lambda - \tilde{\omega_a}/\omega_p} = \frac{R}{\lambda - R}, \tag{2}$$

where $\lambda = \mu_\mu/\mu_p = 3.183345137(85)$ (determined experimentally from the hyperfine structure of muonium), and $R = \tilde{\omega_a}/\omega_p$. The tilde over ω_a means that it has been corrected for the electric-field and pitch ($\vec{\beta}\cdot\vec{B} \neq 0$) corrections [3]. The magnetic field in Eq. 1 is an average that can be expressed as an integral of the product of the muon distribution times the magnetic field distribution over the storage region. Since the moments of the muon distribution couple to the respective multipoles of the magnetic field, either one needs an exceedingly uniform magnetic field, or exceptionally good information on the muon orbits in the storage ring, to determine the $< B_\mu >$ distribution to sub-ppm precision. This was possible in E821 where the uncertainty on the magnetic field averaged over the muon distribution was 30 ppb (parts per billion). The coefficient of the $\vec{\beta} \times \vec{E}$ term in Eq. 1 vanishes at the "magic" momentum of 3.094 GeV/c; where $\gamma = 29.3$. Thus a_μ can be determined by a precision measurement of ω_a and B. At this magic momentum, the electric field is used only for muon storage and the magnetic field alone determines the precession frequency. The finite spread in beam momentum and vertical betatron oscillations introduce small (sub ppm) corrections to the precession frequency. These are the only corrections made to the measurement.
The experiment consists of repeated fills of the storage ring, each time introducing an ensemble of muons into a magnetic storage ring, and then measuring the two frequencies ω_a and ω_p. The muon lifetime at the magic momentum is 64.4 μs, and the data collection period is typically 700 μs. The $g-2$ precession period is 4.37 μs, and the cyclotron period ω_C 149 ns.

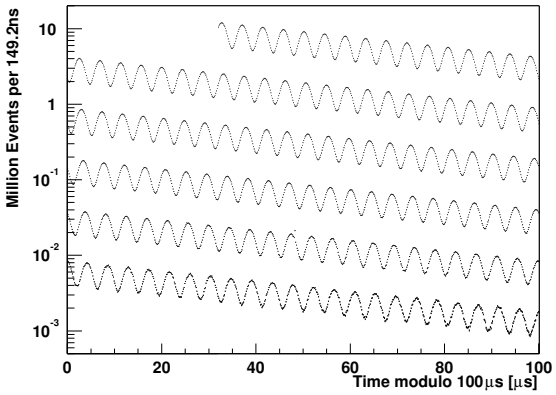

Figure 6: Distribution of electron counts versus time for the 3.6 billion muon decays. The data are wrapped around modulo 100 μs [8].

Because of parity violation in the weak decay of the muon, a correlation exists between the muon spin and the direction of the high-energy decay electrons. Thus as the spin rotates relative to the momentum, the number of high-energy decay electrons is modulated by the frequency ω_a,

as shown in Fig. 6. The E821 storage ring was constructed as a super-ferric magnet, meaning that the iron determined the shape of the magnetic field. Thus the magnetic field needed to be well below saturation and was chosen to be 1.45 T. The resulting ring had a central orbit radius of 7.112 m, and 24 detector stations were placed symmetrically around the inner radius of the storage ring. The detectors were made of Pb/SciFi electromagnetic calorimeters which measured the decay electron energy and time of arrival. The detector geometry and number were optimized to detect the high energy decay electrons, which carry the largest asymmetry, and thus information on the muon spin direction at the time of decay. In this design, many of the lower-energy electrons miss the detectors, reducing background and pileup.

5 The Fermilab proposal: E989

The E989 collaboration at Fermilab plans to measure a_μ with an uncertainty of 1.6×10^{-10} (0.14 ppm), corresponding to a 0.10 ppm statistical error and roughly equal 0.07 ppm systematic uncertainties on ω_a and ω_p.

The proposal efficiently uses the unique properties of the Fermilab beam complex to produce the necessary flux of muons, which will be injected and stored in the (relocated) muon storage ring. To achieve a statistical uncertainty of 0.1 ppm, the total data set must contain more than 1.8×10^{11} detected positrons with energy greater than 1.8 GeV, and arrival time greater than 30 μs after injection into the storage ring. The plan uses 6 out of 20 of the 8-GeV Booster proton batches, each subdivided into four bunches of 10^{12} p/bunch. The proton bunches fill the muon storage ring at a repetition rate of 15 Hz, to be compared to the 4.4 Hz at BNL. The proton bunch hits a target, producing a 3.1 GeV/c pion beam that is directed along a greater than 1 km decay line. The resulting pure muon beam is injected into the storage ring. The muons will enter the ring through a new superconducting inflector magnet, which will replace the existing one, which is wound in such a manner that the coils intercept the beam on both ends of the magnet. The new inflector will result in a higher muon storage efficiency. Once entering the ring, an optimized pulse-forming network will energize the storage ring kicker to place the beam on a stable orbit. The pion flash (caused by pions entering the ring at injection) will be decreased by a factor of 20 from the BNL level, and the muon flux will be significantly increased because of the ability to take zero-degree muons. The stored muon-per-proton ratio will be increased by a factor of 5 to 10 over BNL.

The E821 muon storage will be relocated to Fermilab, in a new building with a stable floor and good temperature control, neither of which were available at Brookhaven.

The new experiment will require upgrades of detectors, electronics and data acquisition equipment to handle the much higher data volumes and slightly higher instantaneous rates. High-density segmented tungsten/scintillating-fibers [34] and crystals are considered as possible choice for the calorimeter. In-vacuum straw drift tubes have been developed to determine

the stored muon distribution from decay positron tracks and to provide data for a greatly improved muon electric dipole moment measurement, which can be obtained in parallel [35]. A modern data acquisition system will be used to read out waveform digitizer data and store it so that both the traditional event mode and a new integrating mode of data analysis can be used in parallel. The systematic uncertainty on the precession frequency is expected to improve by a factor 3 thanks to the reduced pion contamination, the segmented detectors, and an improved storage ring kick of the muons onto orbit. The storage ring magnetic field will be shimmed to an even more impressive uniformity, and improvements in the field-measuring system will be implemented. The systematic error on the magnetic field is halved by better shimming, relocations of critical NMR probes, and other incremental changes.
In less than two years of running, the statistical goal of 4×10^{20} protons on target can be achieved for positive muons. A follow-up run using negative muons is possible, depending on future scientific motivation. Two additional physics results will be obtained from the same data: a new limit on the muon's electric dipole moment (up to 100 times better); and, a more stringent limit on possible CPT or Lorentz violation in muon spin precession. A technically driven schedule permits data taking to begin in 2016.

6 Prospects on a_μ

With the new experiments planned at Fermilab and J-PARC the uncertainty of the difference Δa_μ between the experimental and the theoretical value of a_μ will be dominated by the uncertainty of the hadronic cross sections at low energies, unless new experimental efforts at low energy are undertaken. The last column of Table 1 shows a future scenario based on realistic improvements in the $e^+e^- \to hadrons$ cross sections measurements. Such improvements could be obtained by reducing the uncertainties of the hadronic cross sections from 0.7% to 0.4% in the region below 1 GeV and from 6% to 2% in the region between 1 and 2 GeV as shown in Table 3.

	$\delta(\sigma)/\sigma$ present	$\delta a_\mu^{\rm HLO}$ present	$\delta(\sigma)/\sigma$ prospect	$\delta a_\mu^{\rm HLO}$ prospect
$\sqrt{s} < 1$ GeV	0.7%	3.3	0.4%	1.9
$1 < \sqrt{s} < 2$ GeV	6%	3.9	2%	1.3
$\sqrt{s} > 2$ GeV		1.2		1.2
total		5.3		2.6

Table 3: Overall uncertainty of the cross-section measurement required to get the reduction of uncertainty on $a_\mu^{\rm HLO}$ in units 10^{-10} for three regions of $\sqrt{s}$ (from Ref. [36]).

In this scenario the overall uncertainty on Δa_μ could be reduced by a factor 2. In case the central value would remain the same, the statistical significance would become 7-8 standard deviations, as it can be seen in Fig. 7.

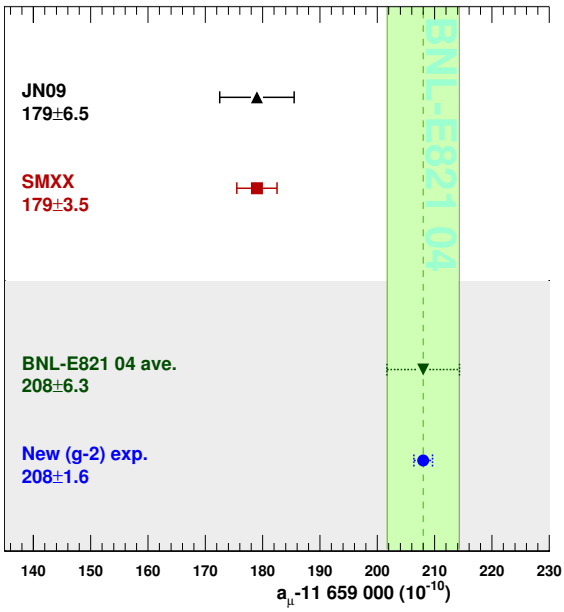

Figure 7: Comparison between $a_\mu^{\rm SM}$ and $a_\mu^{\rm EXP}$. "JN09" is the current evaluation of $a_\mu^{\rm SM}$ using Ref. [6]; "SMXX" is the same central value with a reduced error as expected by the improvement on the hadronic cross section measurement (see text); "BNL-E821 04 ave." is the current experimental value of a_μ; "New $(g-2)$ exp." is the same central value with a fourfold improved accuracy as planned by the future $(g-2)$ experiments [9, 10].

The effort needed to reduce the uncertainties of the $e^+e^- \to hadrons$ cross-sections according to Table 3 is challenging but possible, and certainly well motivated by the excellent opportunity the muon $g-2$ is providing us to unveil (or constrain) "new-physics" effects. A long-term program of hadronic cross section measurements at low energies is clearly warranted and fortunately it has been already started at VEPP-2000. In addition, recent theoretical activities focused on lattice calculation have already reached a mature stage and have real prospects to match the future experimental precision.
With the expected reduction of the error on $a_\mu^{\rm HLO}$, and the planned improved precision of the new $g-2$ experiments, the hadronic Light-by-Light contribution could become the main limitation for further progress on $a_\mu^{\rm SM}$. Although there isn't a direct connection with data, $\gamma\gamma$ measurements performed at e^+e^- colliders will help us to constrain form factors [37]. Lattice

calculation could help as well.

7 Conclusion

The measurements of the muon anomaly a_μ have been a important benchmark for the development of QED and the Standard Model. In the recent years, following the impressive accuracy (0.54 ppm) reached by the E821 experiment at BNL, a worldwide effort from different theoretical and experimental groups has significantly improved the SM prediction. At present there appears to be a 3σ difference between the experimental value and the SM prediction of a_μ. This discrepancy, which would fit well with SUSY expectations, is a valuable constraint in restricting physics beyond the Standard Model, guiding the interpretation of LHC results. In order to clarify the nature of the observed discrepancy between theory and experiment, and eventually firmly establish (or constrain) new physics effects, new direct measurements of the muon $g-2$ with a fourfold improvement in accuracy have been proposed at Fermilab by E989 and J-PARC. First results from E989 could be available around 2017/18.

Acknowledgments

It's a pleasure to thank the LC11 local organizing committee, particularly G. Pancheri, for running a smooth and productive meeting in a very friendly atmosphere. I thank D. Hertzog and L. Roberts for useful discussions on the E821 and E989 experiments, and S. Eidelman, F. Jegerlehner, W. Kluge, M. Passera and L. Roberts for a careful reading of the manuscript. Support from ECT* is warmly acknowledged.

References

[1] F. Jegerlehner, "The anomalous magnetic moment of the muon," Berlin, Springer (2008) 426 p (Springer tracts in modern physics. 226)

[2] D. Stöckinger, "Muon (g-2) and physics beyond the standard model," In Roberts, Lee B., Marciano, William J. (eds.): Lepton dipole moments 393-438 (Advanced series on directions in high energy physics. 20)

[3] H. N. Brown *et al.* [Muon g-2 Collaboration], Phys. Rev. Lett. **86** (2001) 2227

[4] K. Hagiwara, R. Liao, A. D. Martin, D. Nomura and T. Teubner, J. Phys. G **38** (2011) 085003

[5] J. Prades, hep-ph/0108192.

[6] F. Jegerlehner and A. Nyffeler, Phys. Rept. **477** (2009) 1

[7] M. Davier, A. Hoecker, B. Malaescu and Z. Zhang, Eur. Phys. J. C **71** (2011) 1515

[8] G. W. Bennett *et al.* [Muon G-2 Collaboration], Phys. Rev. D **73** (2006) 072003

[9] The New Muon (g - 2) Collaboration, R.M. Carey *et. al.*, see http://lss.fnal.gov/archive/testproposal/0000/fermilab-proposal-0989.shtml

[10] J. Imazato, Nucl. Phys. Proc. Suppl. **129** (2004) 81.

[11] S. Actis *et al.* [Working Group on Radiative Corrections and Monte Carlo Generators for Low Energies Collaboration], Eur. Phys. J. C **66** (2010) 585

[12] M. S. Chen and P. M. Zerwas, Phys. Rev. D **11** (1975) 58

[13] S. Binner, J. H. Kuhn and K. Melnikov, Phys. Lett. B **459** (1999) 279

[14] M. Benayoun, S. I. Eidelman, V. N. Ivanchenko and Z. K. Silagadze, Mod. Phys. Lett. A **14** (1999) 2605

[15] W. Kluge, Nucl. Phys. Proc. Suppl. **181-182** (2008) 280

[16] V. P. Druzhinin, S. I. Eidelman, S. I. Serednyakov and E. P. Solodov, Rev. Mod. Phys. **83**, (2011) 1545

[17] J. Prades, E. de Rafael and A. Vainshtein, (Advanced series on directions in high energy physics. 20)

[18] X. Feng, K. Jansen, M. Petschlies and D. B. Renner, arXiv:1103.4818 [hep-lat]

[19] F. Jegerlehner and R. Szafron, Eur. Phys. J. C **71** (2011) 1632

[20] M. Benayoun, P. David, L. Del Buono and F. Jegerlehner, Eur. Phys. J. C **72** (2012) 1848

[21] J. Z. Bai *et al.* [BES Collaboration], Phys. Rev. Lett. **88** (2002) 101802

[22] R. R. Akhmetshin *et al.* [CMD-2 Collaboration], Phys. Lett. B **648** (2007) 28

[23] R. R. Akhmetshin *et al.* [CMD-2 Collaboration] JETP Lett. **84** (2006) 413 [Pisma Zh. Eksp. Teor. Fiz. **84** (2006) 491]

[24] R. R. Akhmetshin *et al.* [CMD-2 Collaboration], Phys. Lett. B **578** (2004) 285

[25] M. N. Achasov *et al.*, J. Exp. Theor. Phys. **103** (2006) 380

[26] F. Ambrosino *et al.* [KLOE Collaboration], Phys. Lett. B **700** (2011) 102

[27] F. Ambrosino *et al.* [KLOE Collaboration], Phys. Lett. B **670** (2009) 285

[28] A. Aloisio *et al.* [KLOE Collaboration], Phys. Lett. B **606** (2005) 12

[29] B. Aubert *et al.* [BABAR Collaboration], Phys. Rev. Lett. **103** (2009) 231801

[30] S. R. Amendolia *et al.* [NA7 Collaboration], Nucl. Phys. B **277** (1986) 168

[31] The KLOE Coll., in the proceedings of EPS Conference

[32] E. P. Solodov, presentation at the International Workshop on e+e- collisions from Phi to Psi (PHIPSI11), September 19-22 2011, Novosibirsk; S. I. Serednyakov presentation at the International Workshop on e+e- collisions from Phi to Psi (PHIPSI11), September 19-22 2011, Novosibirsk

[33] D. Babusci *et al.*, arXiv:1007.5219 [hep-ex].

[34] R. McNabb *et al.*, ,Nucl. Instrum. Meth. A **602** (2009) 396

[35] G. W. Bennett *et al.* [Muon (g-2) Collaboration], Phys. Rev. D **80** (2009) 052008

[36] F. Jegerlehner, Nucl. Phys. Proc. Suppl. **181-182** (2008) 26.

[37] D. Babusci *et al.*, arXiv:1109.2461 [hep-ph]

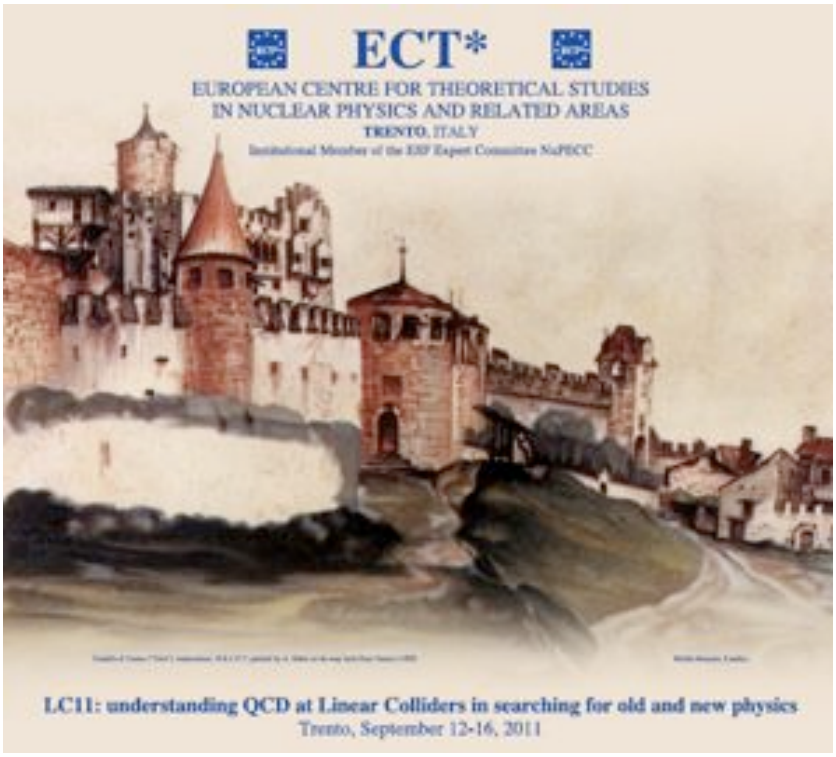

Castello di Trento painted by A. Dürer on his way back from Venice (1495).

Chapter 4

Photon-photon physics

4.1 R.M. Godbole, K. Mohan and G. Pancheri - Hadronic backgrounds due to two photon processes at CLIC

Hadronic backgrounds due to two photon processes at CLIC

Rohini M. Godbole [1] *and Kirtimaan Mohan*
Centre for High Energy Physics, Indian Institute of Science, Bangalore 560 012, India
rohini@cts.iisc.ernet.in, kirtimaan@cts.iisc.ernet.in

Giulia Pancheri
INFN Frascati National Laboratory, Via E. Fermi 40, I00044 Frascati, Italy
giulia.pancheri@lnf.infn.it

Abstract Hadronic backgrounds coming from two photon processes are studied at CLIC energies and beam parameters. We determine these backgounds as predicted by various models and fits to experimental data and show that the beamstrahulng induced backgrounds at CLIC are considerably large.

1 Introduction

The experiments at the LHC are expected to close in on the Higgs sector of the SM in the coming months and then one hopes to get glimpses of the physics beyond the SM in these experiments.However a search for signals beyond the SM seems to be heavily dependent on precise measurements of various quantities. The requirement for high levels of precision hard to acheive at a hadron collider and the construction of an e^+e^- linear now appears to be a growing necessity [1, 2]. Historically, progress in particle physics has been achieved by the working of a hadronic and a leptonic collider in tandem. The required high precision for the studies at the e^+e^- colliders has been made possible due to the very clean environment that they have traditionally provided. However, at high energy and high luminosity linear colliders, the "cleanliness" of this environment may be threatened by large hadronic two-photon interaction rates [3, 4]. In addition to the energy distribution of the photons participating in the two photon interactions, a good knowledge of the energy dependence of $\sigma^{\rm tot}(\gamma\gamma \to \text{hadrons})$ is of utmost importance to be able to assess the issue. These backgrounds are under control at the International Linear Collider (ILC) for the energies and the designs under consideration [1, 5]. The Compact Linear Collider (CLIC) is a machine that has been proposed to be built to study e^+e^- collisions at centre of mass energy of about 3 TeV [6]. These backgrounds are expected to be larger for an e^+e^- collider operating in this higher energy range [7] and will affect the

[1] Speaker

study of various BSM scenarios [8]. It is therefore important to revisit the issue and obtain an estimate of the range of expected backgrounds, based on the current understanding of the energy dependence of $\sigma^{\rm tot}(\gamma\gamma \to \text{hadrons})$. An in depth analysis of these backgrounds has been carried out in [9]. Various detector and beam effects and the direction and momentum distributions of the hadrons produced two photon processes were considered in the simulation. Two models for $\sigma^{\rm tot}(\gamma\gamma \to \text{hadrons})$ were used and it was pointed out that there was a 15% difference arising from the use of these models. In our study we try to determine the spread of predictions that one will get from various theoretical models.

In the following we estimate the contributions from $\gamma\gamma \to$ hadrons to backgrounds at CLIC. We first review the current status of data and models on the total photon-photon cross-sections and the predictions for these cross-sections at the nominal CLIC centre of mass energy of 3 TeV. We then determine the number of hadronic events expected at CLIC from these processes. It may be mentioned here that a good understanding of hadron production in two photon processes may play a role also in the context of either the heavy ion collisions [10] or the two photon processes to be studied at the high luminosity LHC [11].

2 Status of Currently available data and models for $\sigma^{had}_{\gamma\gamma}$

Data for the process $\gamma\gamma \to hadrons$ come from e^+e^- colliders MD-1 [12], PETRA [13], TPC(1984) [14] , TPC(1989) [15], L3 [16] and OPAL [17]. A plot of the data points is shown in Fig.1. Note that the data shows a typical behaviour of total cross-sections with an initial decrease followed by an increase. The data for the decreasing part of the cross-section has large errors and spread from various experiments, however the increasing part from L3 and OPAL experiments is the most consistent available data set. Experimentally, all total cross-sections rise asymptotically with energy, but it is not clear whether the rate of increase is the same for all processes. Phenomenologically, the LEP data seem to indicate that the slope with which the total $\gamma\gamma$ cross-section rises is not the same as in the proton case[18]. This difference would spoil the simplicity of the so-called Regge-Pomeron model, in which the high energy rise is described through a single universal term [19].

Various models exist which attempt to explain these total cross-sections. These can be broadly divided into two classes: the "proton-like" models in which the photon is assumed to behave like a proton and QCD inspired models. Fig. 1 shows a collection of data for the total hadronic cross-section $\sigma(\gamma\gamma \to \text{hadrons})$ from the various e^+e^- experiments in comparison with the predictions from a number of theoretical models [20, 21, 22, 23, 24, 25, 26, 27, 28]. Examples of predictions of "proton-like" models, Aspen[22] as well as some QCD inspired models such as BKKS[25] and EMM [26, 27, 28] are shown. The band referred to as "Proton Factorized" is infact the average proton-proton and proton-antiproton cross-section $(\sigma_{pp}+\sigma_{p\bar{p}})/2$ as calculated in the EMM-BN model[29, 30, 31] and divided by a factor of 330^2 [28]. All models predict a

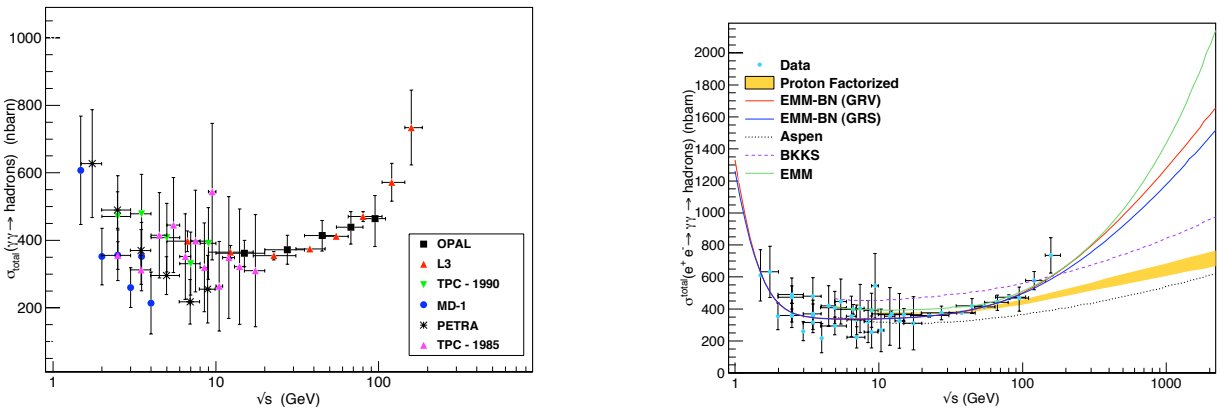

Figure 1: The Figure on the left shows data from various experiments. The Figure on the right shows predictions from factorization (proton like) models [22] and a QCD structure function model [25] together with those from the EMM[26, 27, 28] are compared with the present data.

rise of the cross-section with the collision energy $\sqrt{s_{\gamma\gamma}}$, but with very different slopes.

Donnachie and Landshoff [19] first carried out fits to the total pp and $p\bar{p}$ cross-sections in the framework of Regge theory. One observes a similar behaviour in pp,$p\bar{p}$ and γp total cross-sections. In fact Regge theory predicts that the shapes of these total cross-sections should be process independent. With this in mind, we perform fits of the available $\gamma\gamma$ data with a similar form.

We try to fit the available data to a Regge-Pomeron inspired form

$$\sigma_{total}(\gamma\gamma \to hadrons) = As^{\epsilon} + Bs^{-\eta} + Cs^{\epsilon_1} \tag{1}$$

Note that originally only one pomeron was used to fit the pp and $p\bar{p}$ data, but as Donnachie and Landshoff have shown recently [32], the data are better described with the inclusion of a hard pomeron (Cs^{ϵ_1}).

Table 1: Results of fits to the OPAL and L3 total $\gamma\gamma$ cross sections, of the form $Bs^{-\eta}+As^{\epsilon}+Cs^{\epsilon_1}$.

Data	A (nb)	B (nb)	C (nb)	ϵ, ϵ_1	χ^2
L3+OPAL	51 ± 14	1132 ± 158	–	$\epsilon = 0.240 \pm 0.032$	4.0
L3+OPAL	187 ± 4	310 ± 91	–	$\epsilon = 0.093$ fixed	26
L3+OPAL	103 ± 18	934 ± 156	5.0 ± 1.0	$\epsilon = 0.093$,fixed	
				$\epsilon_1 = 0.418$, fixed	2.8

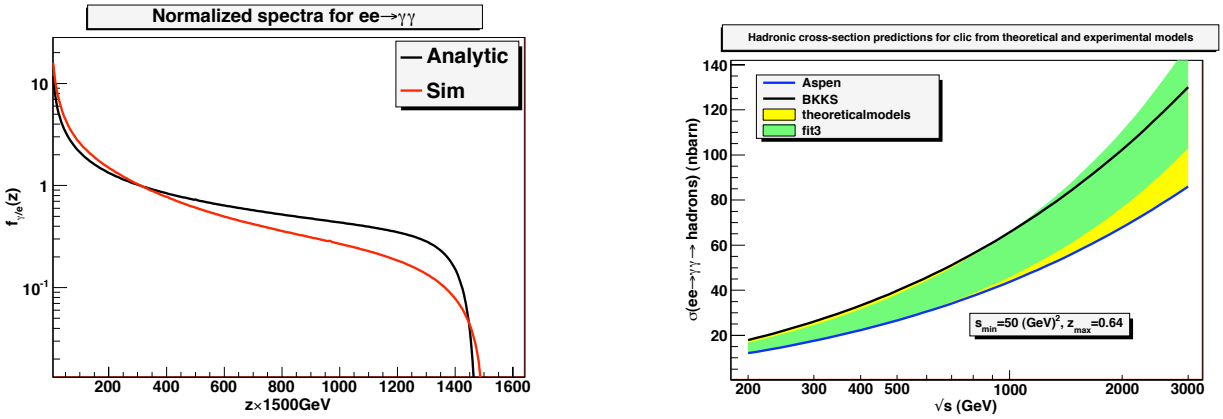

Figure 2: Figure on the left shows the two photon spectra that were used. The Figure on the right is a comparison of the predictions coming from models and that from experimental fits to data.

We see that the rate of increase of the total cross-section is parametrized by ϵ and this appears to be higher than in the proton case, indicative of different physics. Note that inclusion of the hard pomeron does give us a slightly better fit but only marginally. However, this is not conclusive evidence in favour of the second pomeron in the $\gamma\gamma$ case. Only more data at higher energies can tell us this.

3 Predictions for CLIC

In linear colliders, if the outgoing and incoming leptons in a hard scattering process are almost collinear, the calculation of the corresponding cross-section can be considerably simplified by use of the Weizsacker-Williams (WW)[33] approximation or equivalent photon approximation. This approximation gives us an energy spectrum of photons that are generated through bremsstrahlung radiation. One should also note that linear colliders such as CLIC (3 TeV)[34] require dense particle bunches in order to obtain large luminosities. As a result electrons and positrons experience transverse acceleration due to strong electromagnetic fields and radiate what is known as "beamstrahlung" photons. In the WW approximation, the energy spectrum of the exchanged photons is given by [35]

$$f_{\gamma/e}(z) = \frac{\alpha_{\rm em}}{2\pi z}\left[(1+(1-z)^2)\ln\frac{P^2_{max}}{P^2_{min}} - 2(1-z)\right], \qquad (2)$$

where $P^2_{max} = s_{ee}/2*(1-\cos\theta_{tag})(1-z)$, $P^2_{min} = m_e^2\frac{z^2}{(1-z)}$. Here, using θ_{tag} the maximal scattering angle for the outgoing electron, we have taken anti-tagging into account following *ref.* [18].

To select $e^+e^- \to e^+e^-$hadrons events, a minimum value of $s_{\gamma\gamma}$ is required, selecting a region such that the value of $s_{\gamma\gamma}$ can be corrected for smearing and losses with sufficient precision.

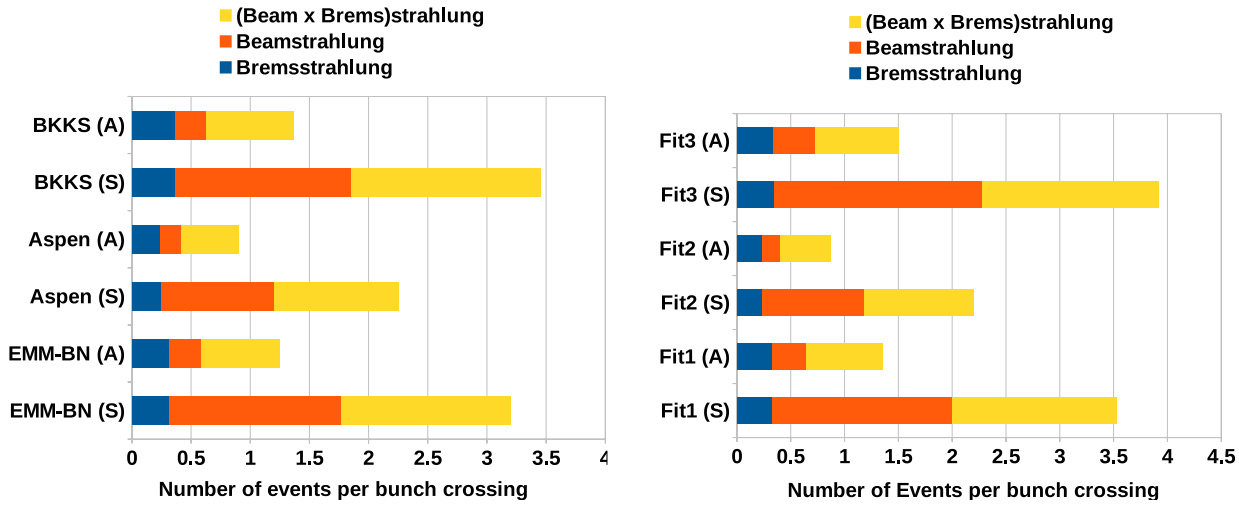

Figure 3: The Figure on the left shows predictions from theoretical models and the Figure on the right shows predictions from fits to data for the number of events per BX for 2 photon backgrounds at CLIC.

Also a maximum value is imposed, because the events resemble annihilation events for too large a value of $s_{\gamma\gamma}$ and cannot be easily separated. We choose the region 50 GeV^2 $< s_{\gamma\gamma} < 0.64 s_{ee}$ following *ref.* [18].

For the beamstrahlung contributions we use two different spectra of photons.

- An analytic form of the beamstrahlung photons [36].
- Spectrum generated by simulation using GUINEAPIG, which we refer to as Sim [37].

We show the folded cross-sections for various energies and models using only the WW contribution in Fig. 2. We see that there is a broad range of predictions but current experimental data is not precise enough to rule out any of the models.

We calculate the number of events in the following way; if b1=beamstrahlung spectra of beam1, b2=beamstrahlung spectra from beam2, w1=bremsstrahlung spectra from beam1, and w2=bremsstrahlung spectra for beam2, then, we calculate the following event numbers;
Including only bremsstrahlung contribution: $n_{brem} = \mathcal{L}_{ee} \times w1 \times w2$,
Including only beamstrahlung contribution: $n_{beam} = \mathcal{L}_{\gamma\gamma} \times b1 \times b2$,
Including beamstrahlung and bremsstrahlung: $n_{bb} = \left(\frac{\mathcal{L}_{\gamma e} + \mathcal{L}_{e\gamma}}{2}\right)(b1 \times w2 + b2 \times w1)$.
Where, $\mathcal{L}_{ee} = 4.3146609 \times 10^{34} m^{-2}$, $\mathcal{L}_{\gamma\gamma} = 2.9678426 \times 10^{34} m^{-2}$, $\mathcal{L}_{\gamma e} = 3.37706 \times 10^{34} m^{-2}$, $\mathcal{L}_{e\gamma} = 3.3754 \times 10^{34} m^{-2}$, are the integrated luminosities per bunch crossing [37].

Figure 3 present the expected number per bunch crossing of hadronic events from $\gamma\gamma$ collisions at CLIC energies (3 TeV), for various model predictions and fits . The beamstrahlung spectra given by simulations and available from *ref.* [37], have been normalised to unity and the necessary normalisation information is contained in the $\mathcal{L}_{\gamma\gamma}$ and $\mathcal{L}_{e\gamma}$ factors. When one uses the analytic expression for these spectra instead, then the necessary normalisation is included in the spectrum itself and hence use of $\mathcal{L}_{ee}$ gives the necessary event rates.

4 Conclusions

Thus we see that depending on which model gives the right high energy description, we expect between 2-4 hadronic events per bunch crossing at CLIC. The beamstrahlung photons completely dominate the $\gamma\gamma$ luminosity and its inclusion increases the expected number of events by a factor of 10 more than those calculated from WW photons alone. However, about half of these events come from the cross term between beamstrahlung and bremsstrahlung.

Another important point to note is that the spectrum of photons being large at low energies means that the dominant contribution to the background will come from low energy photons. However the cuts we have applied on the energy mean that the we cannot see the contibution of photons colliding with $\sqrt{s} < 8GeV$. The EMM-BN model predicts lower cross-sections at lower energies as compared to the BKKS model and the reverse at higher energies as can be seen from Fig1. In spite of this the BKKS model predicts higher backgrounds at CLIC. This means that the region between $10 - 100$ GeV is the most important for predicting backgrounds at CLIC. Greater analysis is needed to gauge the contribution of various energies of photons to the backgrounds. Currently work is in progress to include this range of predictions on the analyses of new physics.

5 Acknowledgements

K.A.M. thanks CSIR for financial support. R.M.G. wishes to acknowledge the Department of Science and Technology of India, for financial support under the J.C. Bose Fellowship scheme under grant no. SR/S2/JCB-64/2007 and CERN, Theory Division, for hospitality where part of this work was done. We would also like to thank M. Battaglia for discussions and clarifications regarding the photon spectrum.

References

[1] J. A. Aguilar-Saavedra *et al.* [ECFA/DESY LC Physics Working Group Collaboration], *"TESLA: Technical design report. Part 3. Physics at an e^+e^- linear collider,"* hep-

ph/0106315.

[2] G. Aarons *et al.* [ILC Collaboration], arXiv:0709.1893 [hep-ph].

[3] M. Drees, R.M. Godbole, Phys. Rev. Lett **67**, 1189 (1991).

[4] M. Drees and R.M. Godbole, Zeit. Phys. **C59** (1993) 591.

[5] P. Chen,T. L. Barklow, M. E. Peskin, Phys. Rev. **D49** (1994) 3209.

[6] M. Battaglia, A. De Roeck, J. Ellis, D. Schulte, hep-ph/0412251 v1.

[7] R.M. Godbole, A. Grau, K.A. Mohan, G. Pancheri, Y.N. Srivastava, Nuovo Cim. **034C** (2011) 129.

[8] M. Battaglia, F. Bogert, A. Ferrari, J. Relefors and S. Zalusky, arXiv:1203.0668 [hep-ex].

[9] LCD-Note-2011-020, T. Barklow , D. Dannheim , M. O. Sahin , D. Schulte, 2012.

[10] See for example, M. Klusek-Gawenda, A. Szczurek, M. V. T. Machado, V. G. Serbo, Phys. Rev. **C83**, 024903 (2011), [arXiv:1011.1191 [nucl-th]].

[11] See for example, E. Chapon, C. Royon, O. Kepka, Phys. Rev. **D81**, 074003 (2010). [arXiv:0912.5161 [hep-ph]].

[12] S. E. Baru, M. V. Beilin, A. E. Blinov, V. E. Blinov, A. E. Bondard, A. D. Bukin, S. I. Eidelman and Y. .I. Eidelman *et al.*, Z. Phys. C **53** (1992) 219.

[13] C. Berger *et al.* [PLUTO Collaboration], Phys. Lett. B **149** (1984) 421.

[14] D. Bintinger *et al.* [TPC/Two Gamma Collaboration], Phys. Rev. Lett. **54** (1985) 763.

[15] H. Aihara *et al.* [TPC/Two Gamma Collaboration], Phys. Rev. D **41** (1990) 2667.

[16] M. Acciarri *et al.* [L3 Collaboration], Phys. Lett. B **519** (2001) 33 [hep-ex/0102025].

[17] G. Abbiendi *et al.* [OPAL Collaboration], Eur. Phys. J. C **14** (2000) 199 [hep-ex/9906039].

[18] R.M. Godbole, A De Roeck, A. Grau, G. Pancheri, J. High Energy Phys. 0306, 061 (2003).

[19] A. Donnachie and P. V. Landshoff, Phys. Lett. B **296** (1992) 227 [hep-ph/9209205].

[20] A. Donnachie and P. Landshoff, Phys. Lett. **B437** (1998) 408.

[21] G. Schuler and T. Sjöstrand, Zeit. Phys. **C68** (1995) 607; Phys. Lett. **B376** (1996) 193; Zeit Phys. **C73** (1997) 677.

[22] M.M. Block, E.M. Gregores, F. Halzen and G. Pancheri, Phys.Rev. **D58** (1998) 17503; M. Block, E.M. Gregores, F. Halzen and G. Pancheri, Phys.Rev. **D60** (1999) 54024.

[23] C. Bourelly, J. Soffer and T.T. Wu, Mod.Phys.Lett. **A15** (2000) 9.

[24] E. Gotsman, E. Levin, U. Maor, E. Naftali, Eur.Phys.J. **C14** (2000) 511, hep-ph/0001080.

[25] B. Badelek, M. Krawczyk, J. Kwiecinski and A.M. Stasto, Phys.Rev. **D62** (2000) 074021; e-Print Archive: hep-ph/0001161.

[26] A. Corsetti, R.M. Godbole and G. Pancheri, Phys.Lett. **B435** (1998) 441.

[27] R. M. Godbole, G. Pancheri, Eur. Phys. J. **C19** (2001) 129, hep-ph/0010104.

[28] R. M. Godbole, A. Grau, G. Pancheri, Y. N. Srivastava, Eur. Phys. J. **C63** (2009) 69-85. [arXiv:0812.1065 [hep-ph]].

[29] A. Grau, G. Pancheri and Y. N. Srivastava, Phys. Rev. D **60** (1999) 114020

[30] R.M. Godbole, A. Grau, G. Pancheri, Y.N. Srivastava,Phys.Rev.D 72 076001 (2005), hep-ph/0408355v3.

[31] A. Achilli, R. M. Godbole, A. Grau, R. Hegde, G. Pancheri and Y. Srivastava, Phys. Lett. B **659** (2008) 137 [arXiv:0708.3626 (hep-ph)].

[32] A. Donnachie and P. V. Landshoff, arXiv:1112.2485 [hep-ph].

[33] C.F. v. Weizsäcker, Z. Phys. **88**,(1934) 612; E.J. Williams, Phys. Rev. **45** (1934) 729.

[34] CLIC, A linear collider based on CLIC technology, the CLIC study team, G. Guignard (Editor), CERN-2000-08.

[35] See for example, S. Frixione, M.L. Mangano, P. Nason and G. Ridolfi, Phys. Lett. **B319** (1993) 339.

[36] P. Chen, Phys. Rev. **D46** (1992) 3.

[37] M. Battaglia, private communication and http://clic-beam-beam.web.cern.ch/clic-beam-beam/.

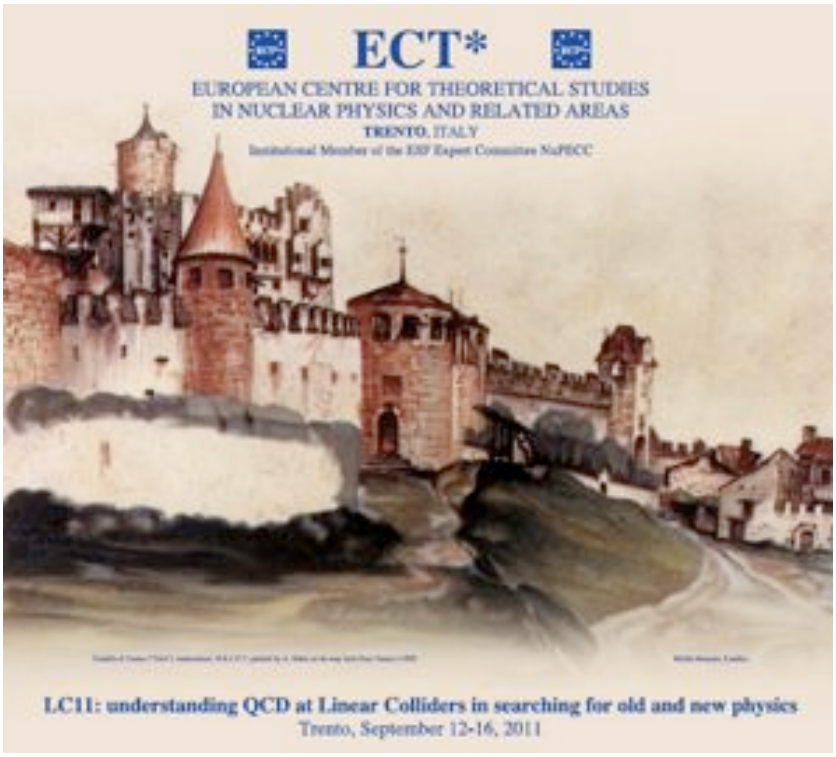

Castello di Trento painted by A. Dürer on his way back from Venice (1495).

4.2 A. Finch - What Can Two Photons Tell Us About QCD?

What Can Two Photons Tell Us About QCD?

Alex J. Finch
Physics Dept., Lancaster University, United Kingdom
A.Finch@lancaster.ac.uk

Abstract
The contribution to testing QCD made by the study of two photon interactions at former and future colliders is briefly reviewed.

1 Introduction

The study of photon photon interactions was a significant part of the physics program at electron positron colliders such as LEP, KEKB and PETRA, and will also be a part of the program at a future linear collider. The main contribution of such studies is in understanding QCD. In the following I will briefly review existing results and even more briefly describe possible future work. Oher reviews are available, notably in the Photon XX conference series [2]

2 How can a photon look like a hadron?

A photon does not carry colour so how could two photon collisions tell us anything about QCD? The answer of course is that quarks also carry electric charge, so a virtual photon can fluctuate into a quark antiquark pair. Given enough time this pair can interact via the exchange of gluons to become increasingly hadron like. A second photon may interact directly with one of the quarks in this virtual photon, or may itself transform into a hadroninc object and the two objects may then interact via the exchange of glouns. This is the basis of using two photon data to test QCD. Of course if QCD could be calculated exactly then any measurement we chose to make could be compared to theory. In practice however we are largely reliant on perturbative QCD and this means we need to find processes in which there is a hard scale which will ensure that α_s is sufficiently small that perturbative calculations are valid. Some terminology that it is important to understand in this field is that of 'direct' and 'resolved' photons. In direct processes, all of the photon's energy goes into the hard scattering process. In resolved processes, the photon has already become a virtual hadronic state, and hard scattering is off a component of this hadronic state, leaving some remnant beam pipe or spectator jet.

3 Where do we get two photon data?

As I have already mentioned, the existing two photon data is obtained at electron positron colliders. The primary purpose of such machines is of course to study events where an electron and a positron annihilate, however there are many more interactions where the electron and positron scatter off of each other and some of their energy goes into the production of new matter, in other words ineleastic electron positron collisions. These processes can be viewed as being the result of two virtual photons interacting. In the results presented below the production mechanism is sometimes factored out so that what is measured is a photon photon process. In others the result is actually for the full process including the beam electrons, but it is interpreted in terms of photon photon collisions. The spectrum of photon energies produced at these machines is predominantly at low energies so although the total cross section may be large the number of interesting events at higher energies which can test QCD is much lower.

4 Some definitions

In two photon collisions we define $Q^2 = -q^2$, as minus the virtuality squared of one photon, and $P^2 = -p^2$, as minus the virtuality of other photon, where $P^2 < Q^2$ by definition. If neither electron is "tagged", i.e. observed, then P^2 and Q^2 are both close to zero. In $\sim 10\%$ of events one electron is tagged so Q^2 is non-zero, while P^2 is close to zero. In rare events both electrons are tagged.

5 Perturbative QCD

As previously stated, in order to test perturbative QCD one requires a hard scale somewhere in the event. Examples of processes which contain a hard scale are:

- photon structure function measurements,
- high transverse momentum jets or hadrons,
- high mass exclusive pairs of hadrons,
- high mass quarks i.e. charm or beauty.

6 The Photon Structure Function

This is the classic measurement in two photon physics, it requires one tagged electron, to produce a probing high Q^2 photon, which then measures the structure of the other "nearly

real" photon. Experimentally the measurement is plagued by problems converting from visible final state mass to true final state mass. As only one scattered electron is observed, in order to measure $x = Q^2/(W^2 + Q^2 + P^2)$ in single tag events one must measure W, but this is poorly measured as a large part of the final state goes in the forward direction where there are either no detectors, or those that are located there are electromagnetic spectrometers, which are poor at measuring hadronic energy. This results in a strong dependence of the result on the poorly undertood soft processes in the Monte Carlo models.

These acceptance issues were studied in a combined measurement by all of the four LEP experiments [3]. Single tagged data was corrected to the hadron level to produce a plot of "energy flow" as a function of pseudorapidity. This data has been published so as to provide an input for future Monte Carlo writers to try to improve their models. The data showed that the existing Monte Carlo programs overestimate the energy going into the forward region. The result of this poor ability to measure the final state is that one has to apply an unfolding technique in order to find the distribution in true W. This results in strong correlations between the measured points. A comprehensive summary of all the structure function results is maintained by Richard Nisius [4]. The results are well described by QCD, however as the "hadronic" region at low x and Q^2 is barely accessible, they can be nearly as well described by QPM.

7 High Transverse Momentum Jets and Hadrons

Studies of high transverse momentum processes have the advantage of relatively large statistics, as they do not require a tagged electron. The momenta are not very high however. In the case of jet measurements there is the usual question as to how to compare the jets measured by experiment to theory's partons. As is usual in these cases, both are corrected to the hadron level in the hope that one is then comparing like with like. Compared to the photon structure function measurements, high transverse momenum jets are more sensitive to the resolved photon and hence the hadronic part of photon structure function. The experiment which has studied this most extensively is OPAL. They have made a measurement [5] of di-jet events. They used an inclusive k_T clustering algorithm and measured cross sections as a function of mean jet transverse energy (E_T) of the two leading (highest E_T) jets and as a function of

$$x_\gamma^\pm = \frac{\sum_{jet1,2} E \pm p_z}{\sum_{hadrons} E \pm p_z},$$

which measures the fraction of the photon's momentum which was carried by the parton which produced the observed jets. The variable x_γ is used experimentally to define regions where the photon is mostly involved in 'direct' processes, or 'resolved' processes. One finds from Monte Carlo studies that events with $x_\gamma > 0.75$ are predominantly direct events while those with $x_\gamma < 0.75$ are predominantly resolved events. OPAL observed good agreement with a next to

leading order QCD calculation for the full data sample, and the single resolved sample, with a slight discrepancy in the double resolved events. Similar results have been found by DELPHI [6]

L3 have published measurements of jet and hadron production as a function of transverse momentum (p_t) [7], and their data show a large excess above NLO QCD predictions at high values of p_t where one would expect the theory to work best. Most of the excess comes from events with $W_{\gamma\gamma} > 50\,\mathrm{GeV/c^2}$, a region where the other three LEP experiments find it hard to make a measurement due to backgrounds from annihilation processes. OPAL have attempted to reproduce the L3 measurement [8] using the same cuts and they see a slight excess at the highest p_t point in hadron production, but not in jet production. DELPHI have also measured hadron production [9] and with their preferred cuts, requiring $W_{\gamma\gamma} < 35\mathrm{GeV/c^2}$ they see no excess but if they use L3 cuts there is an excess at high p_t, however that region is dominated by annihilation processes, not two photon ones.

8 Heavy Flavour Production

In two photon physics one can measure inclusive charm and beauty production. In this case the quark mass reduces the theoretical uncertainty somewhat. Charm quarks can be identified by D^* production and high p_t lepton production. Beauty quarks have been identified by high p_t lepton production and lifetime tags.

A popular way to detect the presence of charm is the so called "D^* trick" in which one looks for a D^* decaying to a D^0 and a soft pion. Due to the kinematics of this decay, a plot of the mass difference of a candidate D^* and D^0 shows a clear peak close to threshold. This technique has been used by many experiments to measure charm production [10] and the result is in beautiful agreement with NLO QCD predictions. The second method for detecting heavy flavour quarks is by looking at the p_t of electrons or muons with respect to a jet direction. The higher mass of the charm and beauty quarks results in some leptons from their decays being at higher p_t than those from light quarks. This is however not an event tagging method so one must fit to p_t distributions to extract the fraction of heavy quarks in the sample. This has been used to extract total cross sections for both charm and beauty production [11]. In the case of charm production the result is again in agreement with theory, but in beauty production L3 reported a large excess above the theoretical expectation. This has been provisionaly confirmed by DELPHI and OPAL in conferences but they have never published these results. ALEPH however used the method of lifetime tagging [12] to detect beauty quark production, and their measurement is in agreement with QCD, although at the high side of the predictions. As a by-product of this measurement ALEPH are able to measure x_γ in their beauty tagged events and show a nice separation into direct and single resolved events.

Another handle on charm production is via inclusive J/ψ production measurements. DELPHI have measured this and find it only has contributions from diffractive or resolved pro-

cesses [13]. They found 36 events at LEP II, and after fitting to p_t^2 they found that 74% of the events were from the resolved process. The diffractive processes only contributes to the region $P_t^2 < 3$. It has been reported [14] that the colour singlet model prediction for this process is one order of magnitude too low while NRQCD prediction agrees well with the data.

9 Exclusive Pair Production

The exclusive production of pairs of mesons or baryons has been promoted for a long time as a clean test of QCD [15]. The calculation involves convoluting a perturbatively calculable hard scattering process with some non perturbative "Wave function" or "Distribution Amplitudes". It is argued that while these are not calculable, they should be the same for a given hadron in different production mechanisms, so that combining several measurements will give unambiguos predictions. This is only true at asymptotic values of the hadron pair mass, and at lower values other models are required. For mesons there is the "handbag" model [16] while for baryons there is the diquark model [17].

Measurements of charged pion and kaon pair production have been made by Belle and ALEPH [18][19] and the shape is well described by QCD. The ratio of kaon pair to pion pair production is consistent with the prediction of Benayoun and Chernyak [20], but not with that of Brodsky and Lepage [15]. The difference in these predictions derives from the different distribution amplitudes they adopt. Belle have also measured $\pi^0\pi^0$ production [21]. It is around 0.32 of the rate of $\pi^+\pi^-$ production which is much larger than typical QCD predictions which are of the order of a few percent.

Belle have also measured $K_s^0 K_S^0$ production [22] and find a W dependence which is not consistent with the QCD prediction. The ratio of this to K^+K^- production approaches the QCD prediction at high W and is inconsistent with the handbag model prediction. L3, OPAL and Belle have also measured $p\bar{p}$ production [23]. The data does not appear to be consistent with QCD at presently available energies.

10 Two Photon Physics at a Linear Collider

Should a linear electron positron collider ever be built it is safe to assume that much of the two photon physics studies performed at earlier machines will be repeated. Typical specifications for such a machine would see luminosities 1000 times that of LEP and energies more than double. The analysis is slightly more complicated at a linear collider as one needs to take account of beamstrahlung for example, however this should not present insurmountable difficulties. The increased energy and luminosity will open up some studies unavailable at LEP. There are in fact not many studies published in the literatrure of the standard measurements as perforformed at LEP as they are not deemed important enough to effect the design of the collider. The really

exciting prospect at a future linear collider would be the construction of a photon linear collider. This is created by firing laser pulses at the incoming electron beams just as they are about to collide [24] and converting them into photon beams. There are many technical difficulties to be overcome in realising such a plan, and it is only if it can be shown to contribute significant knowledge to something like the Higgs boson that it will be built.

If only one of the two beams was converted into photons then it would allow a far better measurement of the Photon Structure Function to be performed, and this has been studied [25]. It has also been proposed that the much higher luminosity would allow the charm photon structure function to be measured [26] which would be a stringent test of QCD.

11 Conclusions

The measurements in two photon physics made at LEP and Belle represent major improvements of our understanding of two photon physics. In general the results are well described by QCD. There are however a few exceptions, namely

- L3's measurements of hadrons and Jets;
- L3's measurement of beauty production;
- the normalisation of exclusive pair production;
- the ratio of $\pi^0\pi^0$ to $\pi^+\pi^+$ production.

The photon structure function is extensively measured, and parameterised but it is hard to measure and the experimentally accessible x region is dominated by QPM. Other processes, for example jets, heavy flavours etc. are more sensitive to the hadronic or 'resolved' part of the photon and easier to measure. They are generally in agreement with QCD. A future linear collider will allow these results to be improved further and new measurements will become possible. In addition a photon linear collider would provide a unique opportunity to measure the hadronic nature of a photon and test QCD.

Acknowledgments

I would like to thank the conference organisers for arranging such an enjoyable and informative conference and in their generous support that enabled me to attend.

References

[1] Proceedings of Photon 2009, DESY-PROC-2009-03.

[2] A.Finch, *Nucl. Phys. B (Proc. Suppl.)* 126 (2004) 399-413.

[3] ALEPH, L3 and OPAL Collaborations, *Eur. Phys. J. C* 23 (2002) 2, 201.

[4] R. Nisius, *Phys. Rept.* 332 (2000) 165.

[5] OPAL Collaboration, *Eur. Phys. J. C* 31 (2003) 3.

[6] DELPHI Collaboration, *Eur. Phys. J. C* 58 (2008) 531.

[7] L3 Collaboration, *Phys. Lett.* B 554 (2003) 105,
L3 Collaboration, *Phys. Lett. B* 602 (2004) 157.

[8] OPAL Collaboration, *Phys. Lett. B* 658 (2008) 185,
OPAL Collaboration, *Phys. Lett. B* 651 (2007) 92.

[9] DELPHI Collaboration, *Phys. Lett. B* 678 (2009) 444.

[10] OPAL Collaboration, *Eur. Phys. J* C16 (2000) 597,
L3 Collaboration, *Phys. Lett. B* 535 (2002) 59,
A. A. Sokolov, for DELPHI Collaboration, *AIP Conf. Proc.* 619 (2002) 799,
ALEPH Collaboration, *Eur. Phys. J. C* **28** (2003) 437.

[11] L3 Collaboration, *Phys. Lett.* B 453 (1999) 83,
DELPHI Collaboration, *Nucl. Phys. Proc. Suppl.* 126 (2004) 185.

[12] ALEPH Collaboration, *JHEP* 0709 (2007) 102.

[13] DELPHI Collaboration, *Phys. Lett. B* 565 (2003) 76.

[14] M. Klasen, B. A. Kniehl, L. N. Mihaila and M. Steinhauser, *Phys. Rev. Lett.* 89 (2002) 032001.

[15] S.J. Brodsky and G.P. Lepage, *Phys. Rev.* D24 (1981) 1808.

[16] M. Diehl, P. Kroll and C. Vogt, *Phys. Lett.* B532 (2002) 99,
A. Szczurek and J. Speth, hep-ph/p207265.

[17] C. F. Berger and W. Schweiger, *Fizika* B8 (1999) 371.

[18] Belle Collaboration, *Phys. Lett. B* 615 (2005) 39.

[19] ALEPH Collaboration, *Phys. Lett. B* 569 (2003) 140.

[20] M. Benayoun and V.L. Chernyak, *Nucl. Phys. B* 329 (1990) 209.

[21] Belle Collaboration, *Nucl. Phys. Proc. Suppl.* 184 (2008) 215.

[22] Belle Collaboration, *Phys. Lett. B* 651 (2007) 15.

[23] CLEO Collaboration, *Phys. Rev. D* 50 (1994) 5484,
VENUS Collaboration, *Phys. Lett. B* 407 (1997) 185,
OPAL Collaboration, *Eur. Phys. J. C* 28 (2003) 45,
OPAL Collaboration, *Phys. Lett. B* 571 (2003) 11,
Belle Collaboration, *Phys. Lett. B* 621 (2005) 41.

[24] I.F. Ginzburg, G.L. Kotkin, V.G. Serbo, and V.I. Telnov, *Pizma ZhETF* 34 (1981) 514 ,
I.F. Ginzburg, G.L. Kotkin, V.G. Serbo, V.I. Telnov, *Nucl. Instrum. Meth.* 205 (1983) 47,
I.F. Ginzburg, G.L. Kotkin, S.L. Panfil, V.G. Serbo, and V.I. Telnov., *Nucl. Inst. Meth. A* 219 (1984) 5.

[25] A. Vogt (Leiden U.), A. De Roeck (CERN), 2nd ECFA/DESY Study 1998-2001, 1814.

[26] E. Laenen and S. Riemersma, *Phys. Lett. B* 376 (1996) 169.

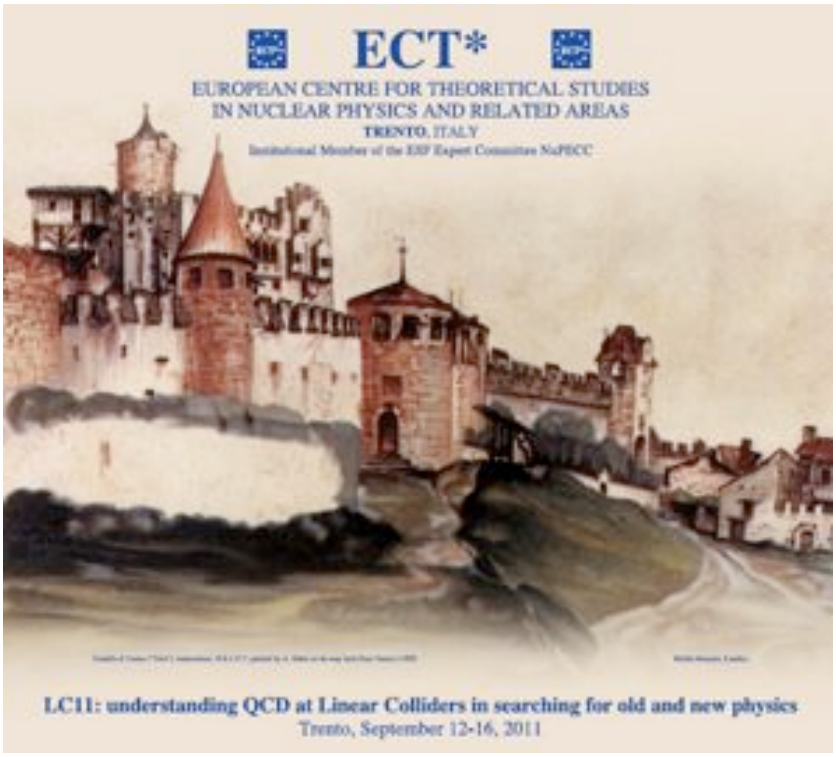

Castello di Trento painted by A. Dürer on his way back from Venice (1495).

4.3 F. Kapusta and W. da Silva - Color factors and color basis in $\gamma\gamma$, γg and $gg \to q\bar{q}Q\bar{Q}$

Color factors and color basis in $\gamma\gamma$, γg and $gg \to q\bar{q}Q\bar{Q}$

Frédéric Kapusta [1]
CNRS/IN2P3 , LPNHE Paris, France
kapusta@in2p3.fr

Wilfrid da Silva
University of Paris 6 , LPNHE Paris, France
dasilva@in2p3.fr

Abstract Computing QCD helicity amplitudes requires the knowledge of color bases. The construction of such bases by iteration is explicitly described. $gg \to q\bar{q}$ is given as a template.

1 Introduction

At Photon2007 it was shown that computing QCD helicity amplitudes involving gluons and quark-antiquark pairs need to get explicit color bases [1]. The projection operator technique misses useful information coming from the various amplitudes recombination such as the separation of gauge invariant QED-like and pure QCD terms.

$SU(3)$ irreducible representations $\left[\begin{array}{c} p \\ q \end{array} \right]$ are realized through the irreducible superspinor components $\psi^{i_1 i_2 \ldots i_p}_{j_1 j_2 \ldots j_q}$ with p contravariant and q covariant components. Its rank cannot be lowered anymore by contractions like $\delta^{j_1}_{i_1}$ and antisymmetrisations like $\epsilon^{j_1 j_2 i}$. The number of independent components of such an irreducible spinor is $N_{pq} = \frac{1}{2}(p+1)(q+1)(p+q+2)$.

2 Color Factors

Color factors of amplitudes with n gluons and m quark-antiquark pairs are of the type $(t^{a_1})^{i_1}_{j_1}(t^{a_2})^{i_2}_{j_2} \ldots (t^{a_n})^{i_n}_{j_n}(\lambda^{k_1}_{l_1})^{k'_1}_{l'_1} \ldots (\lambda^{k_m}_{l_m})^{k'_m}_{l'_m}$ where $(\lambda^k_l) = (A_0)^k_l t^0 + \sum_{a=1}^{a=8}(A_a)^k_l t^a$ with "universal" A coefficients such that $\sum_j^i \frac{1}{2}\sum_{a_3=1}^{a_3=8}(A^*_{a_3})^i_j(A_{a_3})^i_j = N^2 - 1 = 8$ and $\sum_j^i (A^*_0)^i_j (A_0)^i_j = 1$.

In terms of representations $\left[\begin{array}{c} 1 \\ 0 \end{array} \right] \left[\begin{array}{c} 0 \\ 1 \end{array} \right] = \left[\begin{array}{c} 0 \\ 0 \end{array} \right] + \left[\begin{array}{c} 1 \\ 1 \end{array} \right]$ and the first orthonormal basis is given by $\left[\begin{array}{c} 0 \\ 0 \end{array} \right]^{i_1}_{j_1} = (t^0)^{i_1}_{j_1} = \frac{1}{\sqrt{N}}\delta^{i_1}_{j_1}$ and $\left[\begin{array}{c} 1 \\ 1 \end{array} \right]^{i_1}_{j_1} = \sqrt{2}(t^{a_1})^{i_1}_{j_1}$

[1] Speaker

Computing traces, the number of color factors is given by the number of singlets in $\left[\begin{array}{c}1\\1\end{array}\right]^n$. These color factors should be recast as a fixed ordered product of color matrices times a weighted sum of orthogonal singlet tensors. We consider now $\left[\begin{array}{c}1\\1\end{array}\right]\left[\begin{array}{c}q\\r\end{array}\right]$ and proceed by iteration.

From $\psi^a_b\varphi^{c_1c_2.....c_q}_{d_1d_2....d_r}$ we get one $\left[\begin{array}{c}q+1\\r+1\end{array}\right]$, if $q\geq 1$ from $\psi^a_{c_1}\varphi^{c_1c_2.....c_q}_{d_1d_2....d_r}$ one $\left[\begin{array}{c}q\\r\end{array}\right]$, and if $r\geq 1$ from $\psi^{d_1}_b\varphi^{c_1c_2.....c_q}_{d_1d_2....d_r}$ another $\left[\begin{array}{c}q\\r\end{array}\right]$, and if $r\geq 1$ and $q\geq 1$ one $\left[\begin{array}{c}q-1\\r-1\end{array}\right]$ from $\psi^{d_1}_{c_1}\varphi^{c_1c_2.....c_q}_{d_1d_2....d_r}$. If $q\geq 1$ from $\epsilon_{eac_1}\psi^a_b\varphi^{c_1c_2.....c_q}_{d_1d_2....d_r}$ one $\left[\begin{array}{c}q-1\\r+2\end{array}\right]$, and if $q\geq 2$ from $\epsilon_{eac_1}\psi^a_{c_2}\varphi^{c_1c_2.....c_q}_{d_1d_2....d_r}$ one $\left[\begin{array}{c}q-2\\r+1\end{array}\right]$. Similarly if $r\geq 1$ from $\epsilon^{ebd_1}\psi^a_b\varphi^{c_1c_2.....c_q}_{d_1d_2....d_r}$ one $\left[\begin{array}{c}q+2\\r-1\end{array}\right]$ and if $r\geq 2$ from $\epsilon^{ebd_1}\psi^{d_2}_b\varphi^{c_1c_2.....c_q}_{d_1d_2....d_r}$ one $\left[\begin{array}{c}q+1\\r-2\end{array}\right]$.

We thus obtain the two following useful tools :

- The basic iteration formula

$$\left[\begin{array}{c}1\\1\end{array}\right]\left[\begin{array}{c}q\\r\end{array}\right]=\left[\begin{array}{c}q+1\\r+1\end{array}\right]+\left[\begin{array}{c}q\\r\end{array}\right][\Theta(q-1)+\Theta(r-1)]+\left[\begin{array}{c}q-1\\r-1\end{array}\right]\Theta(q-1)\Theta(r-1)+$$
$$\left[\begin{array}{c}q-2\\r+1\end{array}\right]\Theta(q-2)+\left[\begin{array}{c}q-1\\r+2\end{array}\right]\Theta(q-1)+\left[\begin{array}{c}q+1\\r-2\end{array}\right]\Theta(r-2)+\left[\begin{array}{c}q+2\\r-1\end{array}\right]\Theta(r-1) \quad (1)$$

- The "Checksum"
  Taking into account the dimensions of the irreducible representations, we get for example interesting arithmetical relations for cubic polynomials with $p\geq 2$.

$$6N_{p(p+3r)}=N_{(p+1)(p+1+3r)}+N_{(p+1)(p+1+3(r-1))}+N_{(p-1)(p-1+3r)}+$$
$$N_{(p-1)(p-1+3(r+1))}+N_{(p-2)(p-2+3(r+1))}+N_{(p+2)(p+2+3(r-1))} \quad (2)$$

Applying these tools to octet products $\left[\begin{array}{c}1\\1\end{array}\right]^n$ we easily get :

$$\left[\begin{array}{c}1\\1\end{array}\right]^2=\left[\begin{array}{c}2\\2\end{array}\right]+2\left[\begin{array}{c}1\\1\end{array}\right]+\left[\begin{array}{c}0\\0\end{array}\right]+\left(\left[\begin{array}{c}3\\0\end{array}\right]+\left[\begin{array}{c}0\\3\end{array}\right]\right) \quad (3)$$

$$\left[\begin{array}{c}1\\1\end{array}\right]^3=\left[\begin{array}{c}3\\3\end{array}\right]+6\left[\begin{array}{c}2\\2\end{array}\right]+8\left[\begin{array}{c}1\\1\end{array}\right]+2\left[\begin{array}{c}0\\0\end{array}\right]+4\left(\left[\begin{array}{c}3\\0\end{array}\right]+\left[\begin{array}{c}0\\3\end{array}\right]\right)+2\left(\left[\begin{array}{c}4\\1\end{array}\right]+\left[\begin{array}{c}1\\4\end{array}\right]\right) \quad (4)$$

$$\left[\begin{array}{c}1\\1\end{array}\right]^4 = \left[\begin{array}{c}4\\4\end{array}\right] + 12\left[\begin{array}{c}3\\3\end{array}\right] + 33\left[\begin{array}{c}2\\2\end{array}\right] + 32\left[\begin{array}{c}1\\1\end{array}\right] + 8\left[\begin{array}{c}0\\0\end{array}\right] + 20\left(\left[\begin{array}{c}3\\0\end{array}\right] + \left[\begin{array}{c}0\\3\end{array}\right]\right) + 15\left(\left[\begin{array}{c}4\\1\end{array}\right] + \left[\begin{array}{c}1\\4\end{array}\right]\right) + 3\left(\left[\begin{array}{c}5\\2\end{array}\right] + \left[\begin{array}{c}2\\5\end{array}\right]\right) + 2\left(\left[\begin{array}{c}6\\0\end{array}\right] + \left[\begin{array}{c}0\\6\end{array}\right]\right) \tag{5}$$

By inspection of the iteration one can infer that :
$\left[\begin{array}{c}1\\1\end{array}\right]^n = \sum_{p=0}^{p=n} A_p^n \left[\begin{array}{c}p\\p\end{array}\right] + \sum_{p,r} B_{p,r}^n \left(\left[\begin{array}{c}p+3r\\p\end{array}\right] + \left[\begin{array}{c}p\\p+3r\end{array}\right]\right)$

with non zero coefficients obtained when $n = 2m+1$ for $(1 \le r \le m, 0 \le p \le 2(m-r)+1)$ and when $n = 2m$ for $(1 \le r \le m, 0 \le p \le 2(m-r))$

$$\left[\begin{array}{c}1\\1\end{array}\right]^n = \sum_{p=0}^{p=n} A_p^n \left[\begin{array}{c}p\\p\end{array}\right] + \sum_{(1\le r\le[\frac{n}{2}], 0\le p\le n-2r)} B_{p,r}^n \left(\left[\begin{array}{c}p+3r\\p\end{array}\right] + \left[\begin{array}{c}p\\p+3r\end{array}\right]\right) \tag{6}$$

The coefficients will be stored in tables ${}_{(m+1)^2}T^{2m}_{2m(m+1)+1}$ and ${}_{(m+1)(m+2)}T^{2m+1}_{2(m+1)^2}$, the lower left index being the total numer of coefficients and the lower right the number of irreducible representations.

$${}_2\mathcal{T}_2^1 = \left(\begin{array}{cc} A_0 & A_1 \end{array}\right) = \left(\begin{array}{cc} 0 & 1 \end{array}\right) \tag{7}$$

$${}_4\mathcal{T}_5^2 = \left(\begin{array}{ccc} A_0 & A_1 & A_2 \\ B_{0,1} & & \end{array}\right) = \left(\begin{array}{ccc} 1 & 2 & 1 \\ 1 & & \end{array}\right) \tag{8}$$

$${}_6\mathcal{T}_8^3 = \left(\begin{array}{cccc} A_0 & A_1 & A_2 & A_3 \\ B_{0,1} & B_{1,1} & & \end{array}\right) = \left(\begin{array}{cccc} 2 & 8 & 6 & 1 \\ 4 & 2 & & \end{array}\right) \tag{9}$$

$${}_9\mathcal{T}_{13}^4 = \left(\begin{array}{ccccc} A_0 & A_1 & A_2 & A_3 & A_4 \\ B_{0,1} & B_{1,1} & B_{2,1} & & \\ B_{0,2} & & & & \end{array}\right) = \left(\begin{array}{ccccc} 8 & 32 & 33 & 12 & 1 \\ 20 & 15 & 3 & & \\ 2 & & & & \end{array}\right) \tag{10}$$

$${}_{12}\mathcal{T}_{18}^5 = \left(\begin{array}{cccccc} A_0 & A_1 & A_2 & A_3 & A_4 & A_5 \\ B_{0,1} & B_{1,1} & B_{2,1} & B_{3,1} & & \\ B_{0,2} & B_{1,2} & & & & \end{array}\right) = \left(\begin{array}{cccccc} 32 & 145 & 180 & 94 & 20 & 1 \\ 100 & 100 & 36 & 4 & & \\ 20 & 5 & & & & \end{array}\right) \tag{11}$$

$${}_{16}\mathcal{T}_{25}^6 = \left(\begin{array}{ccccccc} A_0 & A_1 & A_2 & A_3 & A_4 & A_5 & A_6 \\ B_{0,1} & B_{1,1} & B_{2,1} & B_{3,1} & B_{4,1} & & \\ B_{0,2} & B_{1,2} & B_{2,2} & & & & \\ B_{0,3} & & & & & & \end{array}\right) = \left(\begin{array}{ccccccc} 145 & 702 & 999 & 660 & 215 & 30 & 1 \\ 525 & 630 & 315 & 70 & 5 & & \\ 161 & 70 & 9 & & & & \\ 5 & & & & & & \end{array}\right) \tag{12}$$

$\left[\begin{array}{c}1\\1\end{array}\right]^{n+1} = \left[\begin{array}{c}1\\1\end{array}\right]\left[\begin{array}{c}1\\1\end{array}\right]^{n}$ give useful relations between n and $n+1$ coefficients, and is the basis of ongoing studies.
Since $A_0^n \propto (n-1)!$, the number of color factors grows rapidly with n. For processes involving n gluons and and m quark-antiquark pairs, the number of color factors is :

$$N_{n,m} = \sum_{p=0}^{p=m} C_{\ m}^{\ p} A_0^{n+m-p} \tag{13}$$

We consider here a few examples :
$\gamma g \to q\bar{q}$, $n=1$, $m=1$, $N_{1,1} = A_0^2 + A_0^1 = 1$,
$\gamma g \to q\bar{q}Q\bar{Q}$, $n=1$, $m=2$, $N_{1,2} = A_0^3 + 2A_0^2 + A_0^1 = 4$
$gg \to q\bar{q}$, $n=2$, $m=1$, $N_{2,1} = A_0^3 + A_0^2 = 3$
$gg \to q\bar{q}Q\bar{Q}$, $n=2$, $m=2$, $N_{2,2} = A_0^4 + 2A_0^3 + A_0^2 = 13$
$gg \to q\bar{q}q'\bar{q}'Q\bar{Q}$, $n=2$, $m=3$, $N_{2,3} = A_0^5 + 3A_0^4 + 3A_0^3 + A_0^2 = 63$

3 Bases Construction

We start with the tensorial basis of $\left[\begin{array}{c}1\\1\end{array}\right]^2$ to give details of the iterative procedure needed for the example of the next section.

Traceless tensors obtained via symmetrisation, antisymmetrisation and counterterms.
Starting from the singlet term $Tr(t^{a_1}t^{a_2}) = (t^{a_1})_{i_1}^{j_1}(t^{a_2})_{i_2}^{j_2}\delta_{j_2}^{i_1}\delta_{j_1}^{i_2}$, we define
$\left[\begin{array}{c}0\\0\end{array}\right]_{j_1j_2}^{i_1i_2} = \frac{1}{\sqrt{N^2-1}}(\delta_{j_2}^{i_1}\delta_{j_1}^{i_2} - \frac{1}{N}\delta_{j_1}^{i_1}\delta_{j_2}^{i_2})$ such that $\left[\begin{array}{c}0\\0\end{array}\right]_{j_1j_2}^{i_1i_2}\left[\begin{array}{c}0\\0\end{array}\right]_{j_1j_2}^{i_1i_2} = 1.$

We can now write $Tr(t^{a_1}t^{a_2}) = \sqrt{N^2-1}(t^{a_1})_{i_1}^{j_1}(t^{a_2})_{i_2}^{j_2}\left[\begin{array}{c}0\\0\end{array}\right]_{j_1j_2}^{i_1i_2}$

Using $\sum_{a=1}^{a=N^2-1}(t^a)_j^i(t^a)_{i'}^{j'} = \frac{1}{2}\delta_{i'}^i\delta_j^{j'} - \frac{1}{2N}\delta_j^i\delta_{j'}^{i'}$ we can check that

$\sum_{a_1,a_2} Tr(t^{a_1}t^{a_2})Tr(t^{a_1}t^{a_2})^* = (N^2-1)(t^{a_1})_{i_1}^{j_1}(t^{a_2})_{i_2}^{j_2}(t^{a_2})_{j_2'}^{i_2'}(t^{a_1})_{j_1'}^{i_1'}\left[\begin{array}{c}0\\0\end{array}\right]_{j_1j_2}^{i_1i_2}\left[\begin{array}{c}0\\0\end{array}\right]_{j_1'j_2'}^{i_1'i_2'} =$

$(N^2-1)\frac{1}{2}\frac{1}{2}\left[\begin{array}{c}0\\0\end{array}\right]_{j_1j_2}^{i_1i_2}\left[\begin{array}{c}0\\0\end{array}\right]_{j_1j_2}^{i_1i_2} = (N^2-1)\frac{1}{4}$ in agreement with $Tr(t^{a_1}t^{a_2}) = \frac{1}{2}\delta^{a_1a_2}$

We notice that $\left[\begin{array}{c}0\\0\end{array}\right]_{j_1j_2}^{i_1j_1} = \sqrt{\frac{N^2-1}{N}}\left[\begin{array}{c}0\\0\end{array}\right]_{j_2}^{i_1}$ and $\left[\begin{array}{c}0\\0\end{array}\right]_{j_1}^{i_1}\left[\begin{array}{c}0\\0\end{array}\right]_{j_1j_2}^{i_1i_2} = 0$

Now with one contraction we construct two $\left[\begin{array}{c}1\\1\end{array}\right]$ in the following way :

$$\left[\begin{array}{c}1\\1\end{array}\oplus\right]^{i_1i_2}_{j_1j_2} = A\{\delta^{i_1}_{j_2}\left[\begin{array}{c}1\\1\end{array}\oplus\right]^{i_2}_{j_1} + \delta^{i_2}_{j_1}\left[\begin{array}{c}1\\1\end{array}\oplus\right]^{i_1}_{j_2} - \tfrac{2}{N}\delta^{i_1}_{j_1}\left[\begin{array}{c}1\\1\end{array}\oplus\right]^{i_2}_{j_2} - \tfrac{2}{N}\delta^{i_2}_{j_2}\left[\begin{array}{c}1\\1\end{array}\oplus\right]^{i_1}_{j_1}\}$$

$$\left[\begin{array}{c}1\\1\end{array}\ominus\right]^{i_1i_2}_{j_1j_2} = B\{\delta^{i_1}_{j_2}\left[\begin{array}{c}1\\1\end{array}\ominus\right]^{i_2}_{j_1} + \delta^{i_2}_{j_1}\left[\begin{array}{c}1\\1\end{array}\ominus\right]^{i_1}_{j_2} - \tfrac{2}{N}\delta^{i_1}_{j_1}\left[\begin{array}{c}1\\1\end{array}\ominus\right]^{i_2}_{j_2} - \tfrac{2}{N}\delta^{i_2}_{j_2}\left[\begin{array}{c}1\\1\end{array}\ominus\right]^{i_1}_{j_1}\}$$

where $\left[\begin{array}{c}1\\1\end{array}\oplus\right]^{i_1}_{j_1} = (t^{a_1})^{i_1}_{l}(t^{a_2})^{l}_{j_1} + (t^{a_1})^{l}_{j_1}(t^{a_2})^{i_1}_{l} - Tr(t^{a_1}t^{a_2})\frac{2}{N}\delta^{i_1}_{j_1}$

and $\left[\begin{array}{c}1\\1\end{array}\ominus\right]^{i_1}_{j_1} = (t^{a_1})^{i_1}_{l}(t^{a_2})^{l}_{j_1} - (t^{a_1})^{l}_{j_1}(t^{a_2})^{i_1}_{l}$. Using

$$\left(\left[\begin{array}{c}1\\1\end{array}\oplus\right]^{i_1i_2}_{j_1j_2}\right)^* = \left[\begin{array}{c}1\\1\end{array}\oplus\right]^{j_1j_2}_{i_1i_2} \text{ and } \left(\left[\begin{array}{c}1\\1\end{array}\ominus\right]^{i_1i_2}_{j_1j_2}\right)^* = -\left[\begin{array}{c}1\\1\end{array}\ominus\right]^{j_1j_2}_{i_1i_2}$$

together with $(t^{a_1})^{i}_{j}(t^{a_2})^{j}_{k} = \frac{1}{2N}\delta^{a_1a_2}\delta^{i}_{k} + \frac{1}{2}(d^{a_1a_2a_3} + if^{a_1a_2a_3})(t^{a_3})^{i}_{k}$

$$\left[\begin{array}{c}1\\1\end{array}\oplus\right]^{i_1i_2}_{j_1j_2}\left[\begin{array}{c}1\\1\end{array}\oplus\right]^{j_1j_2}_{i_1i_2} = A^2 d^{a_1a_2a_5}d^{a_1a_2a_5} \text{ giving } A = \tfrac{1}{\sqrt{D}} \text{ with } D = \tfrac{(N^2-1)(N^2-4)}{N}$$

$$\left[\begin{array}{c}1\\1\end{array}\ominus\right]^{i_1i_2}_{j_1j_2}\left[\begin{array}{c}1\\1\end{array}\ominus\right]^{j_1j_2}_{i_1i_2} = B^2 f^{a_1a_2a_5}f^{a_1a_2a_5} \text{ implying } B = \tfrac{1}{\sqrt{F}} \text{ with } F = N(N^2-1)$$

With σ and τ being permutations, we complete the basis with :

$$\left[\begin{array}{c}2\\2\end{array}\right]^{i_1i_2}_{j_1j_2} \propto \sum_{\sigma\tau}\left\{(t^{a_1})^{i_{\sigma(1)}}_{j_{\tau(1)}}(t^{a_2})^{i_{\sigma(2)}}_{j_{\tau(2)}} - \tfrac{1}{N+2}\delta^{i_{\sigma(1)}}_{j_{\tau(1)}}\left[\begin{array}{c}1\\1\end{array}\oplus\right]^{i_{\sigma(2)}}_{j_{\tau(2)}} - \tfrac{1}{N(N+1)}\delta^{i_{\sigma(1)}}_{j_{\tau(1)}}\delta^{i_{\sigma(2)}}_{j_{\tau(2)}}\left[\begin{array}{c}0\\0\end{array}\right]\right\}$$

$$\left[\begin{array}{c}3\\0\end{array}\right]^{i_1i_2}_{j_1j_2} \propto \epsilon_{j_1j_2i_3}\sum_{\sigma}(t^{a_1})^{i_{\sigma(1)}}_{k_1}(t^{a_2})^{i_{\sigma(2)}}_{k_2}\epsilon^{k_1k_2i_{\sigma(3)}}$$

or

$$\left[\begin{array}{c}3\\0\end{array}\right]^{i_1i_2}_{j_1j_2} \propto 3[(t^{a_1})^{i_1}_{k_1}(t^{a_2})^{i_2}_{k_2} + (t^{a_1})^{i_2}_{k_1}(t^{a_2})^{i_1}_{k_2}]\epsilon^{k_1k_2}_{j_1j_2}$$

$$-\delta^{i_1}_{j_1}\left[\begin{array}{c}1\\1\end{array}\ominus\right]^{i_2}_{j_2} - \delta^{i_2}_{j_1}\left[\begin{array}{c}1\\1\end{array}\ominus\right]^{i_1}_{j_2} + \delta^{i_1}_{j_2}\left[\begin{array}{c}1\\1\end{array}\ominus\right]^{i_2}_{j_1} + \delta^{i_2}_{j_2}\left[\begin{array}{c}1\\1\end{array}\ominus\right]^{i_1}_{j_1}$$

Define $\left[\begin{array}{c}0\\3\end{array}\right]^{j_1j_2}_{i_1i_2}$ as $\left(\left[\begin{array}{c}3\\0\end{array}\right]^{i_1i_2}_{j_1j_2}\right)^*$ which gives $\left[\begin{array}{c}0\\3\end{array}\right]^{j_1j_2}_{i_1i_2} \propto 3[(t^{a_1})^{k_1}_{i_1}(t^{a_2})^{k_2}_{i_2} + (t^{a_1})^{k_1}_{i_2}(t^{a_2})^{k_2}_{i_2}]\epsilon^{j_1j_2}_{k_1k_2}$

$$+\delta^{j_1}_{i_1}\left[\begin{array}{c}1\\1\end{array}\ominus\right]^{j_2}_{i_2} + \delta^{j_1}_{i_2}\left[\begin{array}{c}1\\1\end{array}\ominus\right]^{j_2}_{i_1} - \delta^{j_2}_{i_1}\left[\begin{array}{c}1\\1\end{array}\ominus\right]^{j_1}_{i_2} - \delta^{j_2}_{i_2}\left[\begin{array}{c}1\\1\end{array}\ominus\right]^{j_1}_{i_1}$$

and $\left[\begin{array}{c}3\\0\end{array}\right]^{i_1i_2}_{j_1j_2}\left(\left[\begin{array}{c}0\\3\end{array}\right]^{i_1i_2}_{j_1j_2}\right)^* = 0$

We need now the singlets of $\left[\begin{array}{c}1\\1\end{array}\right]^3$, basically the two $\left[\begin{array}{c}0\\0\end{array}\right]^{i_1i_2i_3}_{j_1j_2j_3}$

which arise from $\left[\begin{array}{c}1\\1\end{array}\oplus\right]^{i_1i_2}_{j_1j_2}\left[\begin{array}{c}1\\1\end{array}\right]^{i_3}_{j_3}$ and $\left[\begin{array}{c}1\\1\end{array}\ominus\right]^{i_1i_2}_{j_1j_2}\left[\begin{array}{c}1\\1\end{array}\right]^{i_3}_{j_3}$.

Thus we build $[(t^{a_1})^{i_1}_{i_2}(t^{a_2})^{i_2}_{i_3}-(t^{a_2})^{i_2}_{i_1}(t^{a_1})^{i_1}_{i_3}](t^{a_3})^{i_3}_{i_1}$ and $[(t^{a_1})^{i_1}_{i_2}(t^{a_2})^{i_2}_{i_3}+(t^{a_2})^{i_2}_{i_1}(t^{a_1})^{i_1}_{i_3}](t^{a_3})^{i_3}_{i_1}$ which leads to

$\left[\begin{array}{c}0\\0\end{array}\ominus\right]^{i_1i_2i_3}_{j_1j_2j_3}=A(\delta^{i_1}_{j_3}\delta^{i_2}_{j_1}\delta^{i_3}_{j_2}-\delta^{i_1}_{j_2}\delta^{i_2}_{j_3}\delta^{i_3}_{j_1})$ and

$\left[\begin{array}{c}0\\0\end{array}\oplus\right]^{i_1i_2i_3}_{j_1j_2j_3}=B\{(\delta^{i_1}_{j_3}\delta^{i_2}_{j_1}\delta^{i_3}_{j_2}+\delta^{i_1}_{j_2}\delta^{i_2}_{j_3}\delta^{i_3}_{j_1})-\frac{1}{N}\sum_\sigma\delta^{i_{\sigma(1)}}_{j_{\sigma(1)}}[-\frac{1}{N}\delta^{i_{\sigma(2)}}_{j_{\sigma(2)}}\delta^{i_{\sigma(3)}}_{j_{\sigma(3)}}+\delta^{i_{\sigma(2)}}_{j_{\sigma(3)}}\delta^{i_{\sigma(3)}}_{j_{\sigma(2)}}]-\frac{2}{N^2}\delta^{i_1}_{j_1}\delta^{i_2}_{j_2}\delta^{i_3}_{j_3}\}$

the counter terms being there to impose a null trace. The normalisation is given by : $\left[\begin{array}{c}0\\0\end{array}\ominus\right]^{i_1i_2i_3}_{j_1j_2j_3}\left[\begin{array}{c}0\\0\end{array}\ominus\right]^{i_1i_2i_3}_{j_1j_2j_3}=2N(N^2-1)A^2$ or $A=\frac{1}{\sqrt{2F}}=\frac{1}{4\sqrt{3}}$ and similarly

$\left[\begin{array}{c}0\\0\end{array}\oplus\right]^{i_1i_2i_3}_{j_1j_2j_3}\left[\begin{array}{c}0\\0\end{array}\oplus\right]^{i_1i_2i_3}_{j_1j_2j_3}=2\frac{(N^2-1)(N^2-4)}{N}B^2$ or $B=\frac{1}{\sqrt{2D}}=\frac{1}{4}\sqrt{\frac{3}{5}}$

4 An explicit example

We explicit here the $gg\to q\bar{q}$ case.

The three amplitudes are with evident notations :

$$\begin{aligned}
M_1 &= u_j t^{a_1}t^{a_2}v^i(-ig_s)\bar{u}_q\gamma(\epsilon_1)\frac{i(\gamma(q-k_1)+m)}{(q-k_1)^2-m^2+i\epsilon}(-ig_s)\gamma(\epsilon_2)v_{\bar{q}}=ig_s^2c_1L_1\\
M_2 &= u_j t^{a_2}t^{a_1}v^i(-ig_s)\gamma(\epsilon_2)\frac{i(\gamma(k_1-\bar{q})+m)}{(k_1-\bar{q})^2-m^2+i\epsilon}(-ig_s)\gamma(\epsilon_1)v_{\bar{q}}=ig_s^2c_2L_2\\
M_3 &= ig_s^2\left(if^{a_1a_2a_3}u_jt^{a_3}v^i\right)\frac{1}{(q+\bar{q})^2}((2k_1+k_2)\cdot\epsilon_2\bar{u}_q\gamma(\epsilon_1)v_{\bar{q}}\\
&\quad-(k_1+2k_2)\cdot\epsilon_1\bar{u}_q\gamma(\epsilon_2)v_{\bar{q}}-\epsilon_1.\epsilon_2\bar{u}_q\gamma(k_1-k_2)v_{\bar{q}})=ig_s^2c_3L_3
\end{aligned}$$

$c_1=t^{a_1}t^{a_2}\lambda^i_j=(A_0)^i_j(t^{a_1})^{j_1}_{i_1}(t^{a_2})^{i_1}_{i_3}(t^0)^{i_3}_{j_1}+(A_{a_3})^i_j(t^{a_1})^{j_1}_{i_1}(t^{a_2})^{i_1}_{i_3}(t^{a_3})^{i_3}_{j_1}$

$c_1=(A_0)^i_j(t^{a_1})^{j_1}_{i_1}(t^{a_2})^{j_2}_{i_2}\sqrt{\frac{N^2-1}{N}}\left[\begin{array}{c}0\\0\end{array}\right]^{i_1i_2}_{j_1j_2}+$

$(A_{a_3})^i_j(t^{a_1})^{j_1}_{i_1}(t^{a_2})^{j_2}_{i_2}(t^{a_3})^{j_3}_{i_3}\frac{1}{2}\left\{\sqrt{2D}\left[\begin{array}{c}0\\0\end{array}\oplus\right]^{i_1i_2i_3}_{j_1j_2j_3}+\sqrt{2F}\left[\begin{array}{c}0\\0\end{array}\ominus\right]^{i_1i_2i_3}_{j_1j_2j_3}\right\}=d_1+d_2+d_3$

$c_2=d_1+d_2-d_3$

$c_3=(A_0)^i_j[(t^{a_1})^{j_1}_{i_1}(t^{a_2})^{i_1}_{i_3}-(t^{a_2})^{j_1}_{i_1}(t^{a_1})^{i_1}_{i_3}](t^0)^{i_3}_{j_1}+(A_{a_3})^i_j(t^{a_1})^{j_1}_{i_1}(t^{a_2})^{j_2}_{i_2}(t^{a_3})^{j_3}_{i_3}\sqrt{2D}\left[\begin{array}{c}0\\0\end{array}\ominus\right]^{i_1i_2i_3}_{j_1j_2j_3}=2d_3$

$c_1L_1+c_2L_2+c_3L_3=(d_1+d_2)(L_1+L_2)+d_3(L_1-L_2+2L_3)$

The amplitude is expressed as a sum of "QED-like" and "QCD" amplitudes.

By construction with $(t^{a'_3})^{j'_3}_{i'_3}\left[\begin{array}{c}0\\0\end{array}\right]^{i_1i_2}_{j_1j_2}\left[\begin{array}{c}0\\0\end{array}\oplus\right]^{i_1i_2i'_3}_{j_1j_2j'_3}=0$

$\overline{|c_1L_1+c_2L_2+c_3L_3|^2}=(|d_1|^2+|d_2|^2)\overline{|L_1+L_2|^2}+|d_3|^2\overline{|L_1-L_2+2L_3|^2}$

$d_3{}^*d_3=(A^*_{a_3})^i_j(A_{a'_3})^i_j(t^{a_1})^{i_1}_{j_1}(t^{a_2})^{i_2}_{j_2}(t^{a_3})^{i_3}_{j_3}(t^{a_1})^{j'_1}_{i'_1}(t^{a_2})^{j'_2}_{i'_2}(t^{a'_3})^{j'_3}_{i'_3}\frac{F}{2}\left[\begin{array}{c}0\\0\end{array}\ominus\right]^{i_1i_2i_3}_{j_1j_2j_3}\left[\begin{array}{c}0\\0\end{array}\ominus\right]^{i'_1i'_2i'_3}_{j'_1j'_2j'_3}$

and then summing over the color indices

and using the identity $\sum_{a=1}^{a=N^2-1}(t^a)^i_j(t^a)^{j'}_{i'}=\frac{1}{2}\delta^i_{i'}\delta^{j'}_j-\frac{1}{2N}\delta^i_j\delta^{i'}_{j'}$ we get

$\overline{d_3{}^*d_3}=\sum^i_j(A^*_{a_3})^i_j(A_{a'_3})^i_j(t^{a_3})^{i_3}_{j_3}(t^{a'_3})^{j'_3}_{i'_3}\frac{1}{2}\frac{1}{2}\frac{F}{2}\left[\begin{array}{c}0\\0\end{array}\ominus\right]^{i_1i_2i_3}_{j_1j_2j_3}\left[\begin{array}{c}0\\0\end{array}\ominus\right]^{i_1i_2i'_3}_{j_1j_2j'_3}$

Since $\left[\begin{array}{c}0\\0\end{array}\ominus\right]^{i_1i_2i_3}_{j_1j_2j_3}\left[\begin{array}{c}0\\0\end{array}\ominus\right]^{i_1i_2i'_3}_{j_1j_2j'_3}=\frac{1}{N^2-1}(\delta^{i'_3}_{i_3}\delta^{j_3}_{j'_3}-\frac{1}{N}\delta^{i_3}_{j_3}\delta^{i'_3}_{j'_3})$

$\overline{d_3{}^*d_3}=\sum^i_j(A^*_{a_3})^i_j(A_{a'_3})^i_j(t^{a_3})^{i_3}_{j_3}(t^{a'_3})^{j_3}_{i_3}\frac{1}{2}\frac{1}{2}\frac{F}{2}\frac{1}{N^2-1}=\frac{1}{2}\frac{1}{2}\frac{F}{2}=\frac{N(N^2-1))}{8}=N$

$\overline{d_1^*d_1}=\frac{1}{2}\frac{1}{2}(A^*_0)^i_j(A_0)^i_j\sqrt{\frac{N^2-1}{N}}\left[\begin{array}{c}0\\0\end{array}\right]^{i_1i_2}_{j_1j_2}\sqrt{\frac{N^2-1}{N}}\left[\begin{array}{c}0\\0\end{array}\right]^{i_1i_2}_{j_1j_2}=\frac{N^2-1}{4N}=\frac{2}{3}$

$\overline{d_2^*d_2}$ is obtained as $\overline{d_3^*d_3}$ with F replaced by D,

$\overline{d_2^*d_2}=\frac{D}{8}=\frac{(N^2-1)(N^2-4)}{8N}=\frac{5}{3}$ and $\overline{d_1^*d_1}+\overline{d_2^*d_2}=\frac{(N^2-1)(N^2+1)}{4N}=\frac{7}{3}$

Finally we have : $\overline{|c_1L_1+c_2L_2+c_3L_3|^2}=\frac{7}{3}\overline{|L_1+L_2|^2}+3\overline{|L_1-L_2+2L_3|^2}$

The global mechanism is then checked on this example where the QED-like term is separated from the pure QCD contribution taking care of the color factors.

5 Conclusions

We have shown here a tool to get an explicit decomposition of QCD amplitudes. There is still an interesting problem to solve : the explicit expression of A^n and B^n. Another ongoing activity being the automatic iterated bases construction using Mathematica.

Acknowledgments

We thank all the organizers for allowing us to participate to such an interesting Workshop and we thank also N. Arteaga for his valuable help.

References

[1] W. da Silva and F. Kapusta,"Four fermion two pair production from PLC to LHC", Proceedings of the International Conference on the Structure and Interactions of the Photon, Including the 17th International Workshop on Photon-Photon Collisions and the International Workshop on High Energy Photon Linear Colliders,PHOTON 2007, Nuclear Physics **B184**(2008)302306.

[2] Wolfram Mathematica.

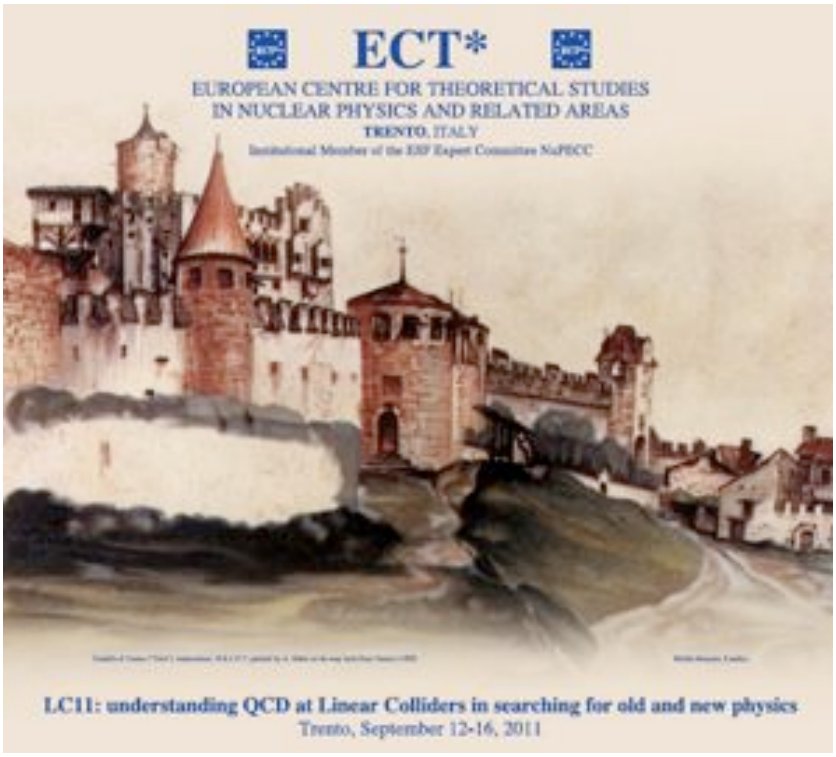

Castello di Trento painted by A. Dürer on his way back from Venice (1495).

4.4 W. da Silva and F. Kapusta- Two fermion pair production in photon-photon, photon-gluon and gluon-gluon collisions

Two fermion pair production in photon-photon, photon-gluon and gluon-gluon collisions

W. da Silva [1]
University of Paris 6, LPNHE Paris, French
dasilva@in2p3.fr

F. Kapusta
CNRS/IN2P3, LPNHE Paris, French
kapusta@in2p3.fr

Abstract For the first time, at our knowledge, we have obtained some analytical asymptotic formulae at Born level for the $\gamma\gamma$ production of lepton and pion pair and also for the production of pion and kaon pair without any approximation on particle masses. All these results are in agreement with computations using mass approximations. The computation method is the same as we proceeded for the production of two lepton pair with equal or unequal masses. We also presented a Monte-Carlo based on the impact factor method, which gives a crude estimate of the production rate of this kind of events at the Photon Collider, LHC and the future Linear Collider.

1 Introduction

The total cross section of two identical lepton pair production at infinite energy in $\gamma\gamma$ collisions has been computed long time ago [1, 2, 4, 5]. The corresponding total and differential cross sections of different two pair produced has already been obtained with logarithmic approximation and including $\gamma\gamma$ polarisation [7]. Two types of diagrams contribute : peripheral and bremsstrahlung [9] . At the level of the total cross section, only the first ones give a non null constant value [5]. The main ingredients used in our present approach are the Factorisation Formula and the Helicity Amplitudes Computation [10]. The result is obtained in a closed form and details of interest are given.

1.1 The factorization formula

The differential cross-section corresponding to the peripheral contribution is given by [9] :

$$\frac{d\sigma}{dtdW^2dW'^2} = \frac{W^2W'^2}{8\pi^3 s^2 t^2}((1+ch^2\theta)\sigma_T\sigma'_T + sh^2\theta(\sigma_T\sigma'_L + \sigma_L\sigma'_T) + ch^2\theta\sigma_L\sigma'_L) \quad (1)$$

[1] Speaker

where s is the $\gamma\gamma$ invariant mass squared, W and W' the two pair masses, m and m' the two lepton masses and $-t$ the exchanged space-like photon squared mass. σ_T and σ_L are the transverse and longitudinal cross sections of virtual photoproduction [11] at one vertex :

$$\sigma_T = \frac{4\pi\alpha^2\beta W^2}{(W^2+t)^2}(\beta^2 - 2 + 2\frac{2t}{W^2} - \frac{t^2}{W^4} + \frac{3-\beta^4+2t^2/W^4}{2\beta}\mathcal{L}) \tag{2}$$

$$\sigma_L = \frac{16\pi\alpha^2\beta t}{(W^2+t)^2}(1 - \frac{1-\beta^2}{2\beta}\mathcal{L}), \quad \mathcal{L} = \ln(\frac{1+\beta}{1-\beta}), \quad \beta = \sqrt{1-\frac{4m^2}{W^2}} \tag{3}$$

and σ'_T, σ'_L the analogous ones at the other vertex. θ is the imaginary rotation angle between the two vertices planes [10] and $t_{min}(t_{max})$ the lower (upper) value of t. Taking

$$sh^2\theta = \frac{4st(t-t_{min})(t_{max}-t)}{(W^2+t)^2(W'^2+t)^2} \tag{4}$$

and we have for large center of mass energy : $sh^2\theta \simeq ch^2\theta$. In that case, the right hand side member of equation (1) gets a simple factorized expression :

$$\frac{d\sigma}{dtdW^2dW'^2} = \frac{W^2W'^2}{2\pi^3}\frac{(\sigma_T+\sigma_L)}{(W^2+t)^2}\frac{(\sigma'_T+\sigma'_L)}{(W'^2+t)^2} \tag{5}$$

2 Analytic formula for two pairs production at $\gamma\gamma$ infinite energy

2.1 Two lepton pairs production

After integrating over the invariant mass of each pair of different masses leptons, we obtain when the $\gamma\gamma$ invariant mass goes to infinity :

$$\sigma = \frac{8\alpha^4}{\pi}\int_0^\infty f(t,m)f(t,m')dt \tag{6}$$

where

$$f(t,m) = \int_{4m^2}^\infty \frac{W^2\left(\sigma_T+\sigma_L\right)}{4\pi\alpha^2\left(W^2+t\right)^2}\,dW^2 = \frac{1}{3t}\left(1+\frac{1}{2}v\left(5-\frac{1}{v^2}\right)\ln\left(\frac{1+v}{1-v}\right)\right),\ v = \sqrt{\frac{t}{t+4m^2}} \tag{7}$$

Making the following variable change :

$$t = \frac{4m^2\left(1-z\right)^2y^2}{\left(1-y^2\right)\left(1-z^2y^2\right)}, \quad z = \frac{m-m'}{m+m'}, \quad 0 \le y \le 1 \tag{8}$$

we obtain an easier integrable expression where the product of logarithms has now disappeared and only logarithms and logarithms squared appear :

$$\sigma = \frac{8\alpha^4}{\pi}\int_0^1 c(y,z)g(y,z)g(y,-z)dy \tag{9}$$

with

$$c(y,z) = \frac{1}{18mm'(1-z^2)y^3}, \quad g(y,z) = a(y,z) + b(y,z)\ln\left(\frac{(1+y)(1-zy)}{(1-y)(1+zy)}\right) \tag{10}$$

$$a(y,z) = 1 - zy^2, \quad b(y,z) = \frac{y^2\left((5-y^2)z^2 - 8z + 5\right) - 1}{2(1-z)y} \tag{11}$$

Now the integration is straightforward. All our calculations were tested with Mathematica [17]. We finally obtain the total cross section for the two lepton pair production in $\gamma\gamma$ at infinite energy :

$$\sigma^{\gamma\gamma\to 2l2L} = \frac{4\alpha^4}{9\pi mm'}\left\{\frac{19}{16}\left[2\left(\frac{1}{u}-u\right)\ln u - \left(\frac{1}{u}+u\right)\left(2+\ln^2 u\right)\right] + \left[\frac{25}{4} + \frac{19}{32}\left(\frac{1}{u}-u\right)^2\right]P(u)\right\} \tag{12}$$

where

$$P(u) = P\left(\frac{1}{u}\right) = \Lambda_3(u) - \Lambda_3(-u), \quad \Lambda_n(z) = \int_0^z \frac{\ln^{n-1}|t|}{1+t}\,dt \text{ (Kummer function [12])} \tag{13}$$

$$P(u) = \ln^2(u)\ln\left(\frac{1+u}{1-u}\right) - 2\ln(u)\left(Li_2(u) - Li_2(-u)\right) + 2\left(Li_3(u) - Li_3(-u)\right), u = \frac{m'}{m} \le 1 \tag{14}$$

When the two masses are very different, i.e. $m \gg m'$ in our case, the cross section given by Eq. (15)

$$\sigma \simeq \frac{28\alpha^4}{27\pi m^2}\left(\ln^2 u^2 - \frac{103}{21}\ln u^2 + \frac{485}{63}\right) \tag{15}$$

is in agreement with the computation of [7] . For equal masses, dividing by 2 the expression obtained in order to take into account the effect of identical particles, we get :

$$\sigma = \frac{\alpha^4}{\pi m^2}\left(\frac{175}{36}\zeta(3) - \frac{19}{18}\right) \tag{16}$$

This result (16) coincides with the well-known formula for identical pair production [1, 2, 18].

2.2 Lepton and charged pion or kaon pairs production

In order to obtain an analytical asymptotic formula for the $\gamma\gamma$ production of lepton and pion pairs we compute the transverse (Eq. (17)) and longitudinal (Eq. (18)) cross sections of virtual photoproduction of two charged pions depicted as scalar point-like particles in QED [8].

$$\sigma_T^{\gamma\gamma^\star\to\pi^+\pi^-} = \frac{2\pi\alpha^2\beta u}{(u+t)^2}\left[3-\beta^2+\frac{-3+2\beta^2+\beta^4}{2\beta}\ln\left(\frac{1+\beta}{1-\beta}\right)\right] \tag{17}$$

$$\sigma_L^{\gamma\gamma^\star\to\pi^+\pi^-} = \frac{4\pi\alpha^2\beta t}{(u+t)^2}\left[-3+\frac{3-\beta^2}{2\beta}\ln\left(\frac{1+\beta}{1-\beta}\right)\right], \quad L=\ln(\frac{1+\beta}{1-\beta}), \quad \beta=\sqrt{1-\frac{4m_\pi^2}{W}} \tag{18}$$

The transverse and longitudinal cross sections of virtual photoproduction of two leptons remain unchanged given by Eq. (2) and Eq. (3). Using the change of variables depicted by Eq. (8) the integration of Eq. (5) can be made and the total cross section for the production of lepton and pion pair at infinite energy is obtained taking $u=\frac{m_l}{m_\pi}$ (m_l is the lepton mass) :

$$\sigma^{\gamma\gamma\to 2l2\pi} = \frac{\alpha^4}{72\pi m_\pi m_l}\left[-2\left(\frac{19}{u}+5u\right)\ln u+\left(\frac{19}{u}-5u\right)\left(2+\ln^2 u\right)+\left(\frac{5u^2}{2}+27-\frac{19}{2u^2}\right)P(u)\right] \tag{19}$$

The production of lepton and kaon pairs is also described by Eq. (19), above, exchanging pion mass with kaon mass. When the two masses are very different, which is the case of electron and pion pair production ($m_\pi \gg m_e$), we obtain Eq. (20) below

$$\sigma \simeq \frac{16\alpha^4}{27\pi m_\pi^2}\left[\ln^2\left(\frac{m_e}{m_\pi}\right)-\frac{8}{3}\ln\left(\frac{m_e}{m_\pi}\right)+\frac{163}{72}\right] \tag{20}$$

which is in agreement with [8].

2.3 Charged pion and kaon pair production

Function of $u=\frac{m_\pi}{m_K}$, the total cross section for the production of charged kaon and charged pion pairs in $\gamma\gamma$ collisions at infinite energy (Eq. (21)) is obtained replacing Eq. (2) and Eq. (3) respectively by Eq. (17) and Eq. (18) with the kaon mass used instead of the pion mass.

$$\sigma^{\gamma\gamma\to 2\pi 2K} = \frac{5\alpha^4}{144\pi m_\pi m_K}\left[2\left(u-\frac{1}{u}\right)\ln u+\left(\frac{1}{u}+u\right)\left(2+\ln^2 u\right)+\left(\frac{4}{5}-\frac{1}{2}\left(\frac{1}{u}-u\right)^2\right)P(u)\right] \tag{21}$$

2.4 Two charged pion pair production

For equal masses, dividing by 2 the expression (21) in order to take into account the effect of identical particles, we get Eq. (22) below,

$$\sigma^{\gamma\gamma\to 4\pi} = \frac{\alpha^4}{144\pi m_\pi^2}\,(7\zeta(3)+10) \tag{22}$$

which coincides with the formula for identical charged pions pair production [3]

3 Pseudo pairs configuration Monte Carlo

In order to estimate the experimental production rate of two pairs including cuts, we have built a Monte-Carlo fully integrated in ROOT [13]. The pseudo pairs configuration space phase event is made using the Cellular Monte Carlo Event Generator FOAM [14]. In the case of electron and muon pairs production in $\gamma\gamma$ collision, upper right in fig. 4 shows perfect agreement between first, Helicity Amplitudes computed without approximation (red triangles) and the numerical integration of the factorization formulae (1) (blue and pink (with invariant mass cut) lines), second Impact Factor Method which gives us the dominant term at low angle and high energy (black points) and formula (12) (green curve) at infinite energy.

3.1 ILC result's

As an example of our Monte Carlo results, we show in fig. 3, for a future linear collider, the pseudo-rapidity distribution (η). This is an important variable that allows to check if the pairs are contained in the detector. Fig. 3 shows that pions ($|\eta_{\mathrm{MAX.}}| \simeq 4$ (top, middle, lower figure, blue line)), electrons ($|\eta_{\mathrm{MAX.}}| \simeq 6.5$ (top figure,red line)), muons ($|\eta_{\mathrm{MAX.}}| \simeq 4$ (middle figure, red line)) and products of $u\bar{u}$ fragmentation (lower figure, green line) can be seen in very forward detector (FTD and VTX). As a conclusion, due to the mass of particles composing the pseudo pairs, many particles are produced in the beam pipe, but a significant fraction can be seen at low angle. The cross section was computed using the expression (23) below

$$\sigma = \int_{z_{min}}^{z_{max}} dz\; 2z \int_{\frac{z^2}{z_{max}}}^{z_{max}} \frac{dy}{y}\; f_{\gamma/e}(y) f_{\gamma/e}(\frac{z^2}{y}) \sigma^{\gamma\gamma\to\ \pi^+\pi^- l^+ l^-}\left(z\sqrt{S_{e^+e^-}}\right), \quad y = \frac{E_\gamma}{E_{beam}} \tag{23}$$

where $f_{\gamma/e}(y)$ is the equivalent photon approximation flux [6, 10]. Fig. 4 lower right shows the production of pion and muon pairs as a function of electron-positron center of mass energy. This kind of plot is relevant when the energy $\sqrt{S_{e^+e^-}}$ is high as this is the case for a the future linear collider. We think that in an environment where the production of pions is very high,

due to a lot of production processes, lepton pairs can be used for tagging pion pairs coming from this particular mode of production. But as we see in fig. 4 lower right, there is a strong dependence of the visible cross section to the angular and energy cuts applied. Event if we do not want to detect specially this kind of $\gamma\gamma$ production, more studies have to be made, because this is a potential background for detectors at very low angle, and for the time being, it is never taken into account.

3.2 LHC result's

To study mechanisms of pion pair production at LHC in $\gamma\gamma \rightarrow \ \pi^+\pi^- l^+ l^-$, the cross section is computed in this way

$$\sigma = \int_{z_{min}}^{z_{max}} dz 2z \int_{\frac{z^2}{z_{max}}}^{z_{max}} \frac{dy}{y} f_{\gamma/p}(y) f_{\gamma/p}(\frac{z^2}{y}) \sigma^{\gamma\gamma \rightarrow \ \pi^+\pi^- l^+ l^-}(W_{\gamma\gamma}) \tag{24}$$

where

$$f_{\gamma/p}(y, \mu^2) = f_{\gamma(el)/p}(y) + f_{\gamma(inel)/p,Q^2}(y) \tag{25}$$

$y = \frac{E_\gamma}{E_{beam}}$ and Q^2 is the resolution scale at which the proton is probed. We use for the photon content of the proton, the elastic and inelastic contributions given respectively by [15] and [16]. Fig. 4 upper left, shows few events, depending strongly on experimental cuts. But in the elastic case the signature is clear. To proceed and conclude on a realistic estimation of the number of events, we need the simulation of all background event in order to reject them. The use of Roman Pots to tag the proton can help a lot, but the statistics can decrease drastically.

In the case where the pion pair is accompanied by a beauty pair, for example see lower left part of fig. 4, we use for the gluon content of the proton, the CTEQ6 parton density function and the expression of the central cross section is :

$$\sigma^{\gamma g \rightarrow \ \pi^+\pi^- Q\bar{Q}} = \frac{1}{8} 4 e_Q^2 \frac{\alpha_s}{\alpha} \frac{1}{2} \sigma^{\gamma\gamma \rightarrow \ l\bar{l}Q\bar{Q}} \tag{26}$$

We need also in this case a realistic LHC estimation of background (pion decay in flight, simulation, pile-up ,$\cdots$) to see if we can extract this type of signal. Anyway this kind of events has to be estimated, because the pseudo pair configuration can lead to some "strange" events. Considering a pion pair and a $Q\bar{Q}$ pair, produced at low angle, back to back in the γg center of mass, once boosted to the laboratory system, some pion pairs might escape the detector, while $Q\bar{Q}$ pairs are still visible from one side of the detector.

4 Conclusions

For the first time, at our knowledge, we have obtained analytical asymptotic formulae (12, 19, 21) at Born level for the $\gamma\gamma$ production of two lepton pairs, pion and lepton pairs and pion and

kaon pairs respectively, without any approximation on particle masses. In the case where the masses are equals or very different these formulas (15, 16, 20, 22) coincide with the literature. We think that this work is the basis for further studies, including the threshold behavior and the global approach of QED production of four leptons or mixed QED QCD processes at future colliders, as well as the gluon-gluon case which is under study. We have also presented a Monte-Carlo which can generate this type of pseudo-pair events. The studies are in progress in order to evaluate some realistic numbers of expected event at LHC, PLC and the future colliders.

Acknowledgments

We thank all the organizers for allowing us to participate to the Workshop and also N. Arteaga, a "Paul Kessler Group" member, for all his valuable help.

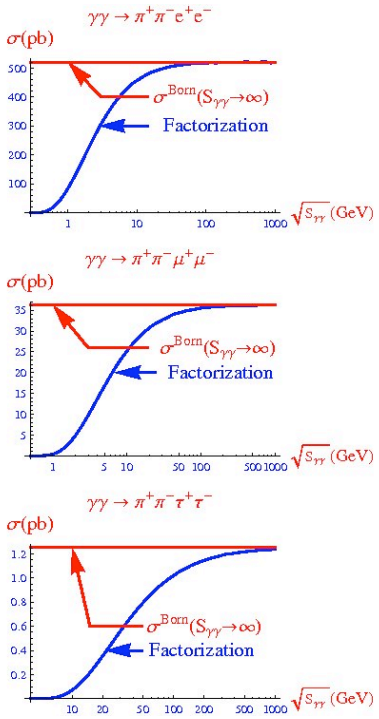

Figure 1: $\gamma\gamma$ production of pion and lepton pair - formula (19) (red curve)- numerical integration of formula (1) (blue curve)

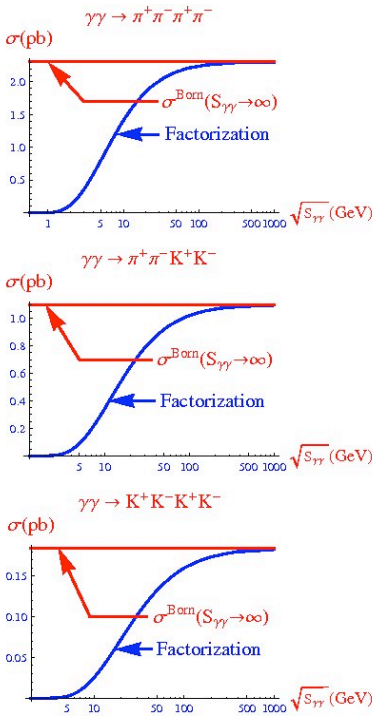

Figure 2: $\gamma\gamma$ production of pion and kaon pairs - formulas (22) and (21) (red curve)- numerical integration of formula (1) (blue curve)

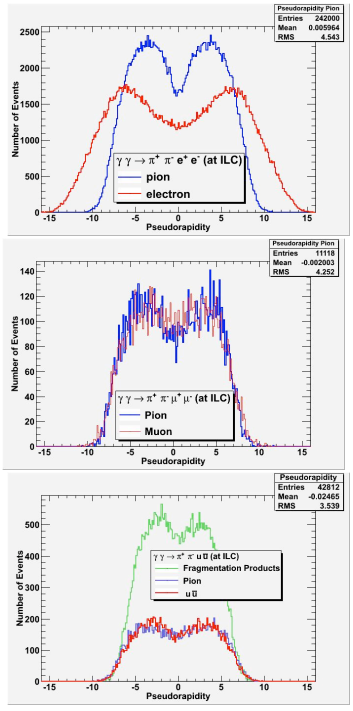

Figure 3: Pion and lepton (or u-quark) pair production at ILC (details are explained in the text)

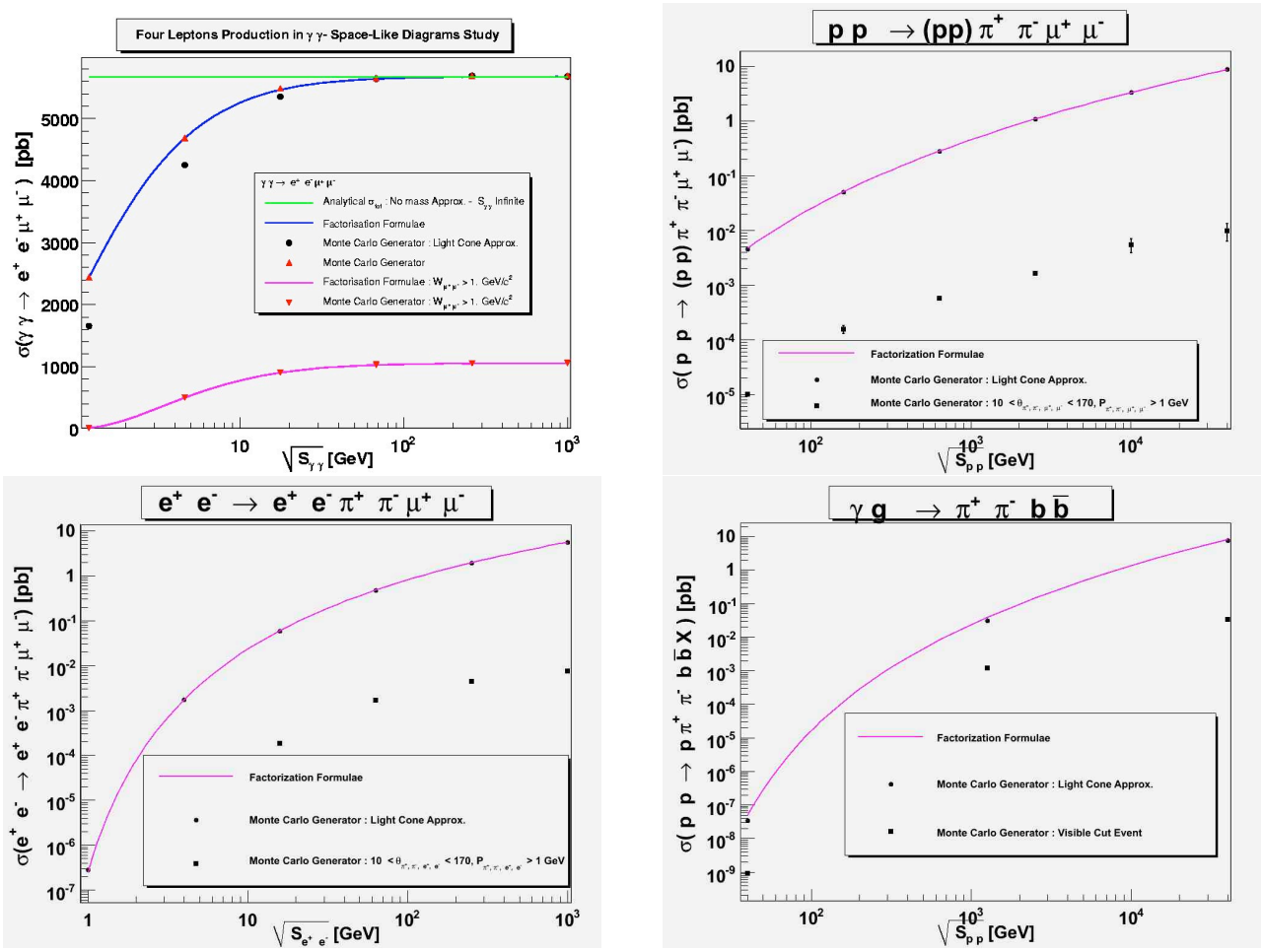

Figure 4: Electron and muon pair production at PLC (upper right) - pion and muon pair production at ILC (lower right) - pion and muon pair production at LHC (upper left) - pion and beauty quark pair production at LHC (lower left) - details are explained in the text.

References

[1] L.N. Lipatov and G.V. Frolov, ZhETF Pis. Red.**10** 399(1969), JETP Letters **10** 254(1969)

[2] H. Cheng and T.T. Wu, Phys. Rev.**D1** 3414 (1970)

[3] H. Cheng and T.T. Wu, Phys. Rev.**D2** 2103 (1970)

[4] V. G. Serbo, ZhETF Pis. Red. 12 (1970) 39

[5] Brown, Hunt, Mikaelian , Muzinich, Phys. Rev.**D9** vol 8 (1973) 3083

[6] V.M. Budnev *et al.*, Phys. Rept. **15C**, 181 (1975).

[7] E.A. Kuraev, A. Schiller and V. G. Serbo, Nucl. Phys.**B256** (1985) 189

[8] E.A. Kuraev, A. Schiller and V. G. Serbo, Nucl. Phys.**B256** (1985) 211

[9] C. Carimalo, G. Cochard, P. Kessler, J. Parisi and B. Roehner, Phys. Rev.**D10** (1974) 1561

[10] The Paul Kessler Group Legacy : P. Kessler, Acta Physica Austriaca, 41 (1975) 141 C. Carimalo, G. Cochard, P. Kessler, J. Parisi and B. Roehner, Phys. Rev.**D10** (1974) 3414 C. Carimalo, P. Kessler and J. Parisi, Phys. Rev.**D18** 2443 (1978) C. Carimalo, Thèse de Doctorat d'Etat, Mai 1977, Université Paris VI (unpublished)

[11] L.N Hand, Phys. Rev. 129 (1963) 1834

[12] L.Lewin (Ed.) (1991). Structural Properties of Polylogarithms, Mathematical Surveys and Monographs 37, Providence RI, Amer. Math. Soc.

[13] R. Brun and F. Rademakers, ROOT - an object oriented data analysis framework, Proceedings AIHENP'96 Workshop, Lausanne, Sept. 1996, Nucl. Inst., Meth. in Phys. Res. A 389 (1997) 81-86, See also http://root.cern.ch/.

[14] S. Jadach, Comput.Phys.Commun. 152 (2003) 55-100

[15] Bernd A. Kniehl *Phys. Lett.* B (1991) 254-267

[16] M. Glück, M. Stratmann and W. Vogelsang, *Phys. Lett.* B (1995) 343-399

[17] Wolfram Mathematica

[18] W. da Silva, F. Kapusta, Proceedings of the International Conference on the Structure and Interactions of the Photon, Including the 17th International Workshop on Photon-Photon Collisions and the International Workshop on High Energy Photon Linear Colliders - PHOTON 2007, Nucl. Phys.**B184** (2008) 302-306

4.5 D. Lopez-Val - Single Higgs-boson production at a photon-photon collider: a 2HDM/MSSM comparison

Single Higgs boson production at a photon-photon collider: a 2HDM/MSSM comparison

David López-Val
Institut für Theoretische Physik,Universität Heidelberg
Philosophenweg 16, D-69120 Heidelberg, Germany
lopez@thphys.uni-heidelberg.de

Abstract We consider the loop-induced production of a single Higgs boson from direct $\gamma\gamma$-scattering at a photon collider. A dedicated analysis of the total cross section $< \sigma_{\gamma\gamma\to h} >$ (for $h = \mathrm{h}^0, \mathrm{H}^0, \mathrm{A}^0$), and the relative strength of the effective $h\gamma\gamma$ coupling $r \equiv g_{\gamma\gamma h}/g_{\gamma\gamma H_{SM}}$, is carried out within the general Two-Higgs-Doublet Model (2HDM) and the Minimal Supersymmetric Standard Model (MSSM). We systematically survey representative regions over the parameter space, in full agreement with brought-to-date theoretical and phenomenological restrictions, and obtain production rates up to 10^4 Higgs boson events per 500fb^{-1} of integrated luminosity. We identify trademark phenomenological profiles for the different $\gamma\gamma \to h$ channels and trace them back to the distinctive dynamical features characterizing each of these models – most significantly, the enhancement potential of the Higgs self-interactions in the general 2HDM. The upshot of our results illustrates the possibilities of $\gamma\gamma$-physics and emphasizes the relevance of linear colliders for the Higgs boson research program.

1 Introduction

The LHC is now truly laying siege to the Higgs boson. The diphoton and gauge boson pair excesses recently reported by ATLAS and CMS [1] may indeed constitute, if confirmed, a first solid trace of its existence. In the meantime, the currently available data keeps narrowing down the mass range and the phenomenological portray under which the Higgs boson may manifest. On the other hand, strong theoretical motivation supports of the idea that Electroweak Symmetry Breaking (EWSB) is realized by some mechanism beyond that of the Standard Model (SM), viz. of a single, fundamental spinless field. One canonical example of the latter is the general 2HDM [2]. Here, the addition of a second scalar $SU_L(2)$ doublet tailors a rich and disclosing phenomenology [3]. The 2HDM can be fully set along in terms of the the physical Higgs boson masses; the ratio $\tan\beta \equiv \langle H_2^0\rangle/\langle H_1^0\rangle$ of the two Vacuum Expectation Values (VEVs) giving masses to the up- and down-like quarks; the mixing angle α between the two CP-even states, $\mathrm{h}^0, \mathrm{H}^0$; and, finally, one genuine Higgs boson self-coupling, which we shall denote λ_5.

The Higgs sector of the MSSM corresponds to a particular (supersymmetric) realization of the general (unconstrained) 2HDM [4]. For further details we refer the reader to Ref. [5], where all the notation, model setup and restrictions are discussed at length.

Following the eventual discovery of the Higgs boson(s) at the LHC, of crucial importance will be to address the precise experimental determination of its quantum numbers, mass spectrum and couplings to other particles. A linear collider (linac) can play a central role in this enterprise [6]. Dedicated studies have exhaustively sought for the phenomenological imprints of the basic 2HDM Higgs boson production modes, such as e.g. i) triple Higgs, $e^+e^- \to 3h$ [7]; ii) inclusive Higgs-pair through EW gauge boson fusion, $e^+e^- \to V^*V^* \to 2h+X$ [8]; iii) exclusive Higgs-pair $e^+e^- \to 2h$ [5,9]; and iv) associated Higgs/gauge boson $e^+e^- \to hV$ [10], with $h \equiv h^0, A^0, H^0, H^\pm$ and $V \equiv Z^0, W^\pm$ [1]. As a common highlight, all these studies report sizable production rates and large quantum effects, arising from the potentially enhanced Higgs self-interactions. These self-couplings, unlike their MSSM analogues, are not anchored by the gauge symmetry, and may thus be strengthened as much as allowed by the unitarity bounds. Interestingly enough, Higgs boson searches at an e^+e^- collider may benefit from alternative operation modes, particularly from $\gamma\gamma$ scattering. In this vein, single ($\gamma\gamma \to h$) and double ($\gamma\gamma \to 2h$) Higgs boson pair production are examples of $\gamma\gamma$-induced processes which entirely operate at the quantum level. The effective (loop-mediated) Higgs/photon interaction $g_{\gamma\gamma h}$ can be regarded as a direct probe of non-standard (charged) degrees of freedom coupled to the Higgs sector. The aforementioned single Higgs channels have been considered in the framework of the SM [12], the 2HDM [13] and the MSSM [14,15] and are known to exhibit excellent experimental prospects, not only due to the clean environment inherent to a linac machine, but also owing to the high attainable $\gamma\gamma$ luminosity, and the possibility to tune the γ-beam polarization as a strategy to enlarge the signal-versus-background ratios[2].

2 Numerical analysis

2.1 Computational setup

In this contribution we present a fully updated analysis of the process $\gamma\gamma \to h$ ($h = h^0, H^0, A^0$) and undertake a comparison of the 2HDM – versus the MSSM results. We focus our attention on the following two quantities: **i)** the total, spin-averaged cross section,

$$\langle \sigma_{\gamma\gamma\to h} \rangle(s) \;=\; \sum_{\{ij\}} \int_0^1 d\tau \, \frac{d\,\mathcal{L}_{ij}^{ee}}{d\tau} \, \hat{\sigma}_{\eta_i\,\eta_j}(\hat{s}) \,, \tag{1}$$

[1] For related work in the context of MSSM Higgs boson production see e.g. [11].

[2] Analogue studies for the $\gamma\gamma \to hh$ mode are available e.g. in Ref. [16].

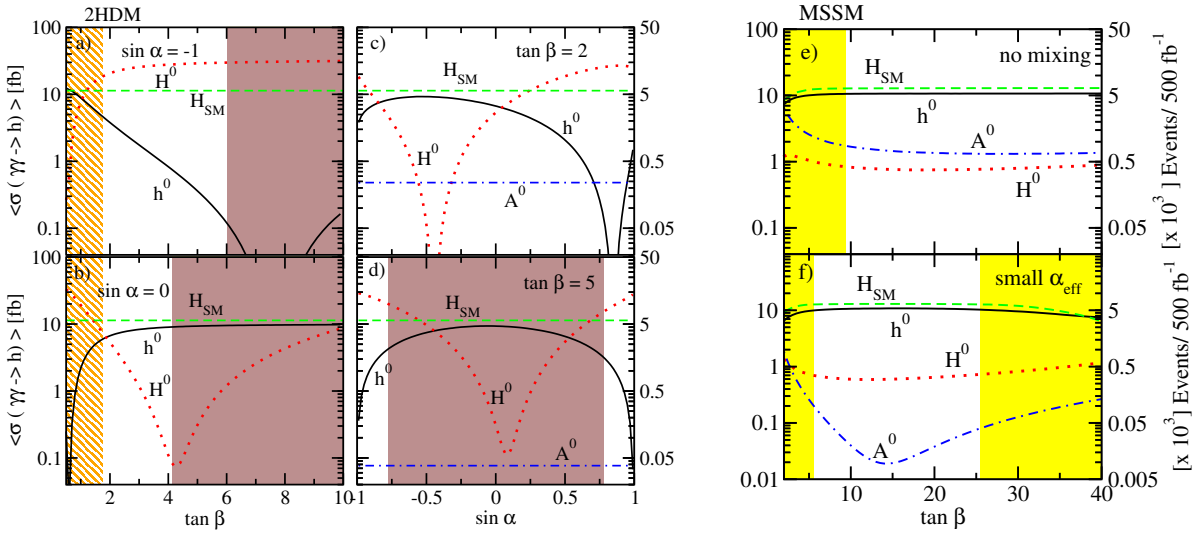

Figure 1: **Left panels (a-d):** Total spin-averaged cross-section $\langle\sigma_{\gamma\gamma\to \mathrm{h}^0}\rangle(s)$ and number of Higgs boson events, as a function of $\tan\beta$ (a,b) and $\sin\alpha$ (c,d) within the 2HDM. The shaded (resp. dashed) areas are excluded by unitarity (resp. $B_d^0 - \bar{B}_d^0$ mixing). The Higgs boson masses are fixed as follows: $M_{\mathrm{h}^0} = 115\,\mathrm{GeV}$; $M_{\mathrm{H}^0} = 165\,\mathrm{GeV}$; $M_{\mathrm{A}^0} = 100\,\mathrm{GeV}$; $M_{\mathrm{H}^\pm} = 105\,\mathrm{GeV}$, with $\lambda_5 = 0$. **Right panels (e-f):** $\langle\sigma_{\gamma\gamma\to \mathrm{h}^0}\rangle(s)$ within the MSSM, as a function of $\tan\beta$, for both the *no-mixing* and the *small-α_{eff}* benchmark points [17]. The dashed regions are ruled out by $b \to s\gamma$ data. The linac center-of-mass energy is kept at $\sqrt{s} = 500\,\mathrm{GeV}$.

where $\hat{\sigma}_{\eta_i\,\eta_j}$ stands for the "hard" scattering cross section, $\hat{s} = \tau\, s$ being the partonic center-of-mass energy; while $d\,\mathcal{L}_{ij}^{ee}/d\tau$ denotes the (differential) photon luminosity distributions, by which we describe the effective $e^\pm \to \gamma$ conversion of the primary linac beam. In turn, $\eta_{i,j}$ accounts for the respective polarization of the resulting photon beams; and **ii)** the $\gamma\gamma h$ coupling strength, $r \equiv g_{\gamma\gamma h}/g_{\gamma\gamma H_{SM}}$ – that we normalize to the SM, identifying $\mathrm{h}^0 \equiv \mathrm{H}_{SM}$. We compare the distinct phenomenological patterns that emerge from the 2HDM and the MSSM and spell out the specific dynamical features that may help to disentangle both models. Further details may be found in Refs. [13, 14].

Throughout our study we make use of the standard algebraic and numerical packages FeynArts, FormCalc and LoopTools [18]. Updated experimental constraints (stemming from the EW precision data, low-energy flavor-physics and the Higgs mass regions ruled out by the LEP, Tevatron and LHC direct searches), as well as the theoretical consistency conditions (to wit: perturbativity, unitarity and vacuum stability) are duly taken into account – cf. [19–24]. The photon luminosity distributions are obtained from [25], while the MSSM Higgs mass spectrum is provided by FeynHiggs [26].

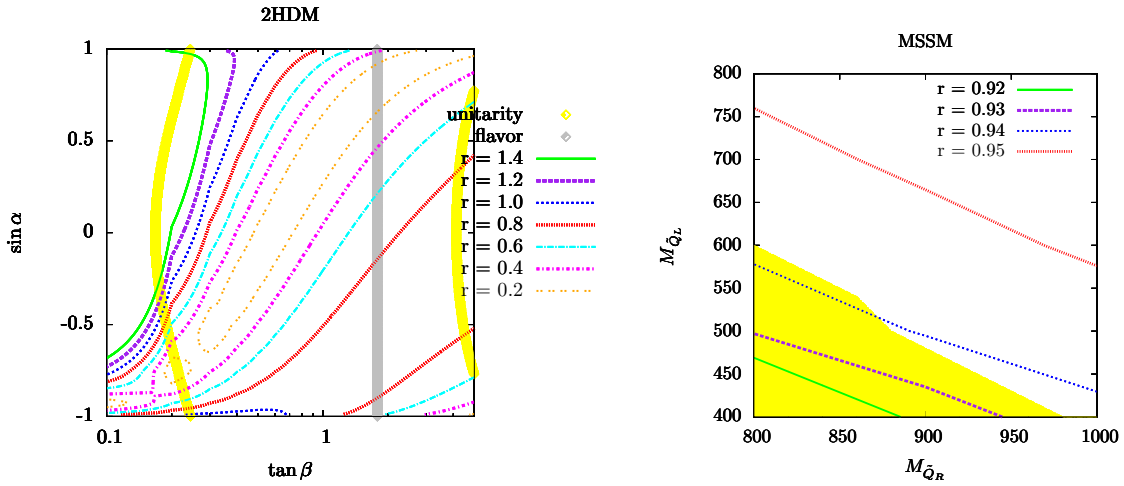

Figure 2: Contour plots of the ratio $r \equiv g_{\gamma\gamma h}/g_{\gamma\gamma H_{SM}}$ that measures the effective $\gamma\gamma h$ coupling strength normalized to the SM, for representative parameter space configurations, comparing the 2HDM (left panel) and MSSM (right panel). The 2HDM calculation is carried out assuming type-I Higgs/fermion Yukawa couplings, $\lambda_5 = 0$ and the same set of Higgs boson masses as in Fig. 1. The yellow strips on the left plot denote the lower and upper bounds ensuing from unitarity, while the grey vertical band displays the restrictions stemming from $B_d^0 - \bar{B}_d^0$. As for the MSSM parameter setup, we employ $\tan\beta = 2$, $M_{\mathrm{A}^0} = 600$ GeV, $\mu = 500$ GeV, $A_t = 1800$ GeV, $M_2 = 500$ GeV. The dashed area is ruled out by $b \to s\gamma$. The linac center-of-mass energy is kept at $\sqrt{s} = 500\,\mathrm{GeV}$.

2.2 Profiling $\gamma\gamma \to h$ within the 2HDM

The upshot of our numerical analysis is displayed on the left panels of Figs. 1 - 2. There we illustrate the behavior of $< \sigma_{\gamma\gamma\to h} >$ and the ratio r over representative regions of the 2HDM parameter space. For definiteness, we perform our calculation for a type-I 2HDM structure and for relatively light Higgs boson masses (as quoted in the Figure caption). The pinpointed trends, however, do not critically depend on the previous assumptions – see Ref. [13,14] for an extended discussion. Our results neatly illustrate the interplay of the charged Higgs boson, $\mathrm{W}^{\pm}$ boson and fermion loops, whose respective contributions to $g_{\gamma\gamma h}$ undergo a highly characteristic destructive interference. The strength of the Higgs self-coupling $\lambda_{h\mathrm{H}^+\mathrm{H}^-}$, which is primarily modulated by $\tan\beta$ and λ_5, determines whether the overall rates may become enhanced ($r > 1$) or suppressed ($r < 1$) relatively to the SM expectations. Scenarios yielding $r > 1$ could in principle be met for $\lambda_{h\mathrm{H}^+\mathrm{H}^-} \sim \mathcal{O}(10^3)$ GeV and $M_{\mathrm{H}^\pm} \sim \mathcal{O}(100)\,\mathrm{GeV}$ (due to strongly boosted $\mathrm{H}^{\pm}$-mediated loops) or $\tan\beta < 1$ (which enhances the top-mediated loops through the Higgs-top Yukawa coupling, $g_{\mathrm{h}^0 t\bar{t}} \sim \sin\alpha/\sin\beta$). In practice, however, both situations are disfavored by the combined effect of the unitarity and vacuum stability conditions, together with the flavor physics constraints (mostly from $B_d^0 - \bar{B}_d^0$). Instead, the 2HDM regions with $\lambda_{h\mathrm{H}^+\mathrm{H}^-} \sim \mathcal{O}(10^2)\,\mathrm{GeV}$ give rise to

a trademark suppression of the single Higgs boson rates, and pull the relative $h\gamma\gamma$ coupling strength down to values of $r \sim -50\%$. Away from these largely subdued domains, we retrieve total cross sections in the ballpark of $< \sigma_{\gamma\gamma\to h} > \sim 1 - 50$ fb – this is to say, up to a few thousand neutral, CP-even, single Higgs boson events, for the light (h^0) and the heavy (H^0) states alike. Finally, if the Higgs self-interactions are even weaker – or, alternatively, the charged Higgs bosons are very massive – then the $\mathrm{H}^\pm$-mediated corrections become subleading. In such instances we are left with $r \lesssim 1$, as a reflect of the fact that the $g_{\gamma\gamma h}$ coupling is now essentially determined by a SM-like combination of $\mathrm{W}^\pm$ and fermion-mediated loops. It is also worth underlining the complementary nature of the production rates for the two neutral CP-even Higgs channels $\gamma\gamma \to \mathrm{h}^0/\mathrm{H}^0$, which ensues from the inverse correlation of the respective couplings to the charged Higgs, namely of $\lambda_{\mathrm{h}^0\mathrm{H}^+\mathrm{H}^-}$ with respect to $\lambda_{\mathrm{H}^0\mathrm{H}^+\mathrm{H}^-}$ – see the σ_{h^0} and σ_{H^0} curves from panels a-d in Fig. 1. We also observe that the results for $\gamma\gamma \to \mathrm{H}^0$ tend to be slightly above the SM yields, whereas $\gamma\gamma \to \mathrm{h}^0$ stays usually below. This follows from the kinematic structure of the total cross section, $< \sigma_{\gamma\gamma\to h} > \sim M^4_{M_h}/M^2_W$, which implies $\sigma_{\mathrm{H}^0} > \sigma_{\mathrm{h}^0}$ as $M_{\mathrm{H}^0} > M_{\mathrm{h}^0} \equiv M_{\mathrm{H}_{SM}}$. In contrast, and owing to its CP-odd nature, $\gamma\gamma \to \mathrm{A}^0$ is essentially featureless and entails a minor numerical impact.

2.3 Profiling $\gamma\gamma \to h$ within the MSSM

Let us now turn our attention to the MSSM. On the right panels of Figs. 1-2 we survey the behavior of the purported quantities $< \sigma_{\gamma\gamma\to h} >$ and r for the representative MSSM parameter setups that are quoted below [17]:

	M_{A^0} [GeV]	M_{SUSY} [GeV]	μ [GeV]	$X_t \equiv A_t - \mu/\tan\beta$ [GeV]	M_2 [GeV]	M_3 [GeV]
no-mixing	400	2000	200	0	200	1600
small α_{eff}	300	800	2000	-1100	500	500

We note that GUT relations between M_1 and M_2, as well as universal trilinear couplings ($A_t = A_b = A_\tau$), are assumed throughout. Likewise, we duly account for the impact of the different sets of constraints, most significantly stemming from $\mathcal{B}(b \to s\gamma)$ (dashed areas, in yellow) and the Higgs boson and squark mass bounds settled by direct exclusion limits.

In this SUSY setup, non-standard contributions to the effective $g_{h\gamma\gamma}$ interaction may emerge from a twofold origin. On the one hand we have a panoply of the 2HDM one-loop diagrams mediated by the interchange of virtual charged Higgs bosons. In the present framework, however, these terms do no longer bear any enhancement capabilities, since the corresponding Higgs self-interactions are completely tied to the gauge couplings – as a consequence of the underlying SUSY invariance. On the other hand we find the squark-mediated quantum corrections. Their imprints on $g_{\gamma\gamma h}$ are mostly visible for relatively light squarks (with masses of few hundred GeV), hand in hand with sizable mass splittings between their respective left and right-handed components and large trilinear couplings to the Higgs bosons [3]. In prac-

[3]The phenomenological implications of this kind of Yukawa, and Yukawa-like couplings have been addressed

tice, however, the combination of the different experimental restrictions effectively tames the abovementioned enlargement power.

We can thus conclude that realistic MSSM scenarios encompass rather mild departures from the SM loop-induced mechanism ($r \sim -5\%$), rendering overall production rates again in the ballpark of $< \sigma_{\gamma\gamma\to h} > \sim \mathcal{O}(10)$ fb for the lightest CP-even state $h = \mathrm{h}^0$– while its heavier companions $\mathrm{H}^0, \mathrm{A}^0$ lie typically one order of magnitude below [14].

3 Discussion and concluding remarks

In this contribution we have reported on the single Higgs boson production through $\gamma\gamma$ scattering in a TeV-range linear collider. The process $\gamma\gamma \to h$ is driven by an effective, loop-induced $h\gamma\gamma$ interaction, a mechanism that is directly sensitive to the eventual presence of new charged degrees of freedom. We have computed the total cross section, $< \sigma_{\gamma\gamma\to h} >$, alongside with the effective (normalized) coupling strength $r \equiv g_{\gamma\gamma h}/g_{\gamma\gamma H_{SM}}$, within both the 2HDM and the MSSM. We have disclosed characteristic phenomenological profiles and spelt out their main differences, which mostly stem from the respective Higgs self-interaction structures. In the MSSM, the aforementioned self-couplings are anchored by the gauge symmetry, while in the 2HDM they can be as large as permitted by the combined set of experimental and theoretical restrictions – most significantly unitarity. We have identified a sizable depletion of $< \sigma_{\gamma\gamma\to h} >$ (corresponding to values of $r \sim -50\%$) for those 2HDM configurations in which a relatively large $\lambda_{h\mathrm{H}^+\mathrm{H}^-}$ interaction is capable to thrust the $\mathrm{H}^\pm$-mediated contribution to $g_{\gamma\gamma h}$, and subsequently to maximize the destructive interference that operates between the different $\mathrm{H}^\pm$, W^+ and fermion-mediated loops. A smoking gun of underlying 2HDM physics would thus manifest here as a missing number of single Higgs boson events. On the MSSM side, departures from the SM are comparably much tempered ($r \simeq -5\%$) and essentially driven by the squark-mediated corrections, which are relatively suppressed by the mass scale of the exchanged SUSY particles and further weakened by the stringent experimental bounds. An additional distinctive feature of both models might manifest from the simultaneous observation of $\gamma\gamma \to \mathrm{h}^0$ and $\gamma\gamma \to \mathrm{H}^0$. Situations where both channels yield $\mathcal{O}(10^3)$ events per 500 fb^{-1} could only be attributed to a non-standard, non-SUSY Higgs sector, since the mass splitting between the two neutral, CP-even Higgs states is typically enforced to be larger in the MSSM – so that the corresponding $\gamma\gamma \to \mathrm{H}^0$ rates are comparably smaller.

The clean environment of a linac offers excellent prospects for the tagging and identification of the single Higgs boson final states through the corresponding decay products. The latter should arise in the form of either i) highly energetic, back-to-back heavy-quark dijets ($h \to jj$, with $jj \equiv c\bar{c}, b\bar{b}$); ii) lepton tracks from gauge boson decays ($h \to \mathrm{W}^+\mathrm{W}^- \to 2l + \not{E}_T, \mathrm{Z}^0\mathrm{Z}^0 \to 4l$); iii) in the specific case of the MSSM, and if kinematically allowed, also the Higgs decays

in the past in a wide variety of processes, see e.g. [27].

into chargino pairs ($h \to \tilde{\chi}_1\tilde{\chi}_2 \to jj + \not{E}_T$). Precise Higgs boson mass measurements could then be conducted upon the reconstruction of the dijet – or dilepton – invariant masses and should broaden the present coverage of the LHC. For instance, they would enable to sidestep the so-called "LHC wedge", namely the $M_{\mathrm{A}^0} \gtrsim 200\mathrm{GeV}$ and $\tan\beta \sim \mathcal{O}(10)$ domains of the MSSM parameter space [28]. The dominant backgrounds, corresponding to the processes $\gamma\gamma \to b\bar{b}/\mathrm{W}^+\mathrm{W}^-$, could be handled not only by means of standard kinematic cuts, but also through a suitable tuning of the photon beam polarization [15].

A future generation of linac machines, and of $\gamma\gamma$ facilities in particular, should therefore be instrumental for a precise experimental reconstruction of the EWSB mechanism; namely for the measurement of the Higgs boson mass, couplings and quantum numbers, if not for the discovery of the Higgs boson itself – if its mass and/or its coupling pattern fell beyond the reach of the LHC and the $\mathrm{e}^+\mathrm{e}^-$ colliders. Photon-photon physics may well furnish a most fruitful arena in which to carry the Higgs boson research program to completion.

Acknowledgements It is a pleasure to thank Joan Solà for the fruitful and enduring collaboration over the past years. I would also like to express my gratitude to the organizers of the LC 2011 workshop at ETC-Trento for the kind invitation to present this review, and for the kind atmospheare and enlightening time we all shared at the meeting.

References

[1] ATLAS Collaboration, ATLAS-CONF-2011-157; CMS Collaboration, CMS-PAS-HIG-11-03.

[2] J.F. Gunion, H.E. Haber, G.L. Kane, S. Dawson, *The Higgs hunter's guide*, Addison-Wesley, Menlo-Park, 1990; G. C. Branco, P.M. Ferreira, L. Lavoura, M.N. Rebelo, M. Sher, J. P. Silva, *Theory and phenomenology of two-Higgs-doublet models*, arXiv:1106.0034.

[3] M. Moretti, F. Piccinini, R. Pittau, J. Rathsman, JHEP 1011 (097) 2010, M. Aoki et al, arXiv:1104.3178; G. Bhattacharyya, P. Leser, H. Pas, *Phys. Rev.* **D83** (2011) 011701; S. Chang, J. A. Evans, M. A. Luty, Phys. Rev. D **84** (2011) 095030

[4] H.P Nilles, *Phys. Rept.* **110** (1984) 1; H.E. Haber, G.L. Kane, *Phys. Rept.* **117** (1985) 75; S. Ferrara, ed., *Supersymmetry*, vol. 1-2 (North Holland, World Scientific, 1987).

[5] D. López-Val, J. Solà, *Phys. Rev.* **D81** (2010) 033003; *Fortsch. Phys.* **G58** (2010) 660; PoS RADCOR2009, 045 (2010).

[6] *ILC Reference Design Report Volume 2: Physics at the ILC*, arXiv:0709.1893; G. Weiglein *et al.*, *Physics interplay of the LHC and the ILC.*, *Phys. Rept.* **426** (2006) 47, hep-ph/0410364.

[7] G. Ferrera, J. Guasch, D. López-Val, J. Solà, *Phys. Lett.* **B659** (2008) 297; PoS **RADCOR2007**, 043 (2007), arXiv:0801.3907.

[8] R. N. Hodgkinson, D. López-Val, J. Solà, *Phys. Lett.* **B673** (2009) 47.

[9] A. Arhrib, G. Moultaka, *Nucl. Phys.* **B558** (1999) 3; A. Arhrib, M. Capdequi Peyranère, W. Hollik, G. Moultaka, *Nucl. Phys.* **B581** (2000) 34; J. Guasch, W. Hollik, A. Kraft, *Nucl. Phys.* **B596** (2001) 66.

[10] D. López-Val, J. Solà, N. Bernal, *Phys. Rev.* **D81** (2010) 113005; D. López-Val, J. Solà, PoS **RADCOR2009**, 045 (2010); Fortsch. Phys. 58 (2010) 660.

[11] See e.g. P. Chankowski, S. Pokorski, J. Rosiek, *Nucl. Phys.* **B423** (1994) 437; V. Driesen, W. Hollik, *Zeitsch. f. Physik* **C68** (1995) 485; A. Djouadi, H.E. Haber, P.M. Zerwas, *Phys. Lett.* **B375** (2003) 1996; A. Djouadi, W. Kilian, M. Mühlleitner, P. M. Zerwas, *Eur. Phys. J* **C10** (1999) 27; S. Heinemeyer, W. Hollik, J. Rosiek and G. Weiglein, *Int. J. of Mod. Phys.* **19** (2001) 535; H. E. Logan, S.-f. Su, *Phys. Rev.* **D66** (2003) 035001; E. Coniavitis, A. Ferrari, *Phys. Rev.* **D75** (2007) 015004; O. Brein, T. Hahn, *Eur. Phys. J* **C52** (2007) 397.

[12] D. L. Borden, D. A. Bauer, D. O. Caldwell, Phys. Rev. D **48**, 4018 (1993); P. Niezurawski, A. F. Żarnecki, M. Krawczyk, Acta Phys. Polon. B **34**, 177 (2003)

[13] N. Bernal, D. López-Val, J. Solà, *Phys. Lett.* **B677** (2009) 38.

[14] D. López-Val, J. Solà, *Phys. Lett.* **B702** (2011) 246; J. Solà, D. López-Val, Nuovo Cim. **C34** (2011) 57.

[15] B. Grzadkowski, J.F. Gunion, *Phys. Lett.* **B294** (1992) 361; J. F. Gunion, H.E. Haber, *Phys. Rev.* **D48** (1993) 5; S-h. Zhu, C-s. Li, C-s. Gao, *Chin. Phys. Lett.* 15 (1998) 2; M. Mühlleitner, M. Krämer, M. Spira, P. Zerwas, *Phys. Lett.* **B508** (2001) 311; D. M. Asner, J. B. Gronberg, J.F. Gunion, *Phys. Rev.* **D67** (2003) 035009; M. Krawczyk, hep-ph/0307314; P. Niezurawski, A.F. Żarnecki, M. Krawczyk, *Acta Phys. Polon.* **B** 37 (2006) 1187.

[16] see e.g. F. Cornet and W. Hollik, *Phys. Lett.* **B669** (2008) 58; E. Asakawa, D. Harada, S. Kanemura, Y. Okada and K. Tsumura, *Phys. Lett.* **B672** (2009) 354; A. Arhrib, R. Benbrik, C.-H. Chen, R. Santos, *Phys. Rev.* **D80** (2009) 015010; E. Asakawa, D. Harada, S. Kanemura, Y. Okada, K. Tsumura, *Phys. Rev.* **D82** (2010) 115002.

[17] M. Carena, S. Heinemeyer, C. Wagner, *Eur. Phys. J* **C26** (2003) 601.

[18] T. Hahn, Comput. Phys. Commun. 140, 418 (2001); T. Hahn, C. Schappacher,*Com. Phys. Comm.* **G143** (2002) 54; T. Hahn and M. Pérez-Victoria, *Com. Phys. Comm.* **G118** (1999) 153.

[19] A. Wahab El Kaffas, P. Osland, O. M. Greid, *Phys. Rev.* **D76** (2007) 095001; H. Flächer, M. Goebel, J. Haller, A. Höcker, K. Mönig, J. Stelzer, *Eur. Phys. J* **C60** (2009) 543; N. Mahmoudi, O. Stål, *Phys. Rev.* **D81** (2010) 035016; S. R. Juárez, D. Morales, P. Kielanowski, arXiv:1201.1876

[20] F. Mahmoudi, *http://superiso.in2p3.fr*; F. Mahmoudi, *Comput. Phys. Commun.* **178** (2008) 745; *Comput. Phys. Commun.* **180** (2009) 1579.

[21] S. Kanemura, T. Kubota and E. Takasugi, *Phys. Lett.* **B313** (1993) 155; A. Akeroyd, A.Arhrib, E.-M. Naimi, *Phys. Lett.* **B490** (2000) 119. See also Sect. III of Ref. [5].

[22] M. Sher, *Phys. Rept.* **179** (1989) 273; S. Nie and M. Sher, *Phys. Lett.* **B449** (1999) 89; S. Kanemura, T. Kasai, Y. Okada, *Phys. Lett.* **B471** (1999) 182; P.M. Ferreira, D.R.T. Jones, JHEP 08 (2009) 069.

[23] D. Eriksson, J. Rathsman, O. Stål, *Com. Phys. Comm.* **G181** (2010) 189, *http://www.isv.uu.se/thep/MC/2HDMC/.*

[24] P. Bechtle, O. Brein, S. Heinemeyer, G. Weiglein, K. E. Williams, *Com. Phys. Comm.* **G181** (2010) 138; arXiv:1102.1898, *http://www.ippp.dur.ac.uk/HiggsBounds.*

[25] V. I. Telnov, *Acta Phys. Polon.* **B** 37 (2006) 633; A. F. Żarnecki, *Acta Phys. Polon.* **B**34 (2003) 2741.

[26] S. Heinemeyer, W. Hollik and G. Weiglein, *Com. Phys. Comm.* **G124** (2000) 76; S. Heinemeyer, W. Hollik and G. Weiglein, *Eur. Phys. J* **C9** (1999) 343; G. Degrassi, S. Heinemeyer, W. Hollik, P. Slavich, *Eur. Phys. J* **C28** (2003) 133; M. Frank et al., JHEP 02 ((2007)) 047.

[27] J.A. Coarasa, D. Garcia, J. Guasch, R.A. Jiménez, J. Solà, *Eur. Phys. J* **C2** (1998) 373; *Phys. Lett.* **B425** (1998) 329; D. Garcia, W. Hollik, R.A. Jiménez, J. Solà, *Nucl. Phys.* **B427** (1994) 53; S. Béjar, J. Guasch, D. López-Val, J. Solà, *Phys. Lett.* **B668** (2008) 364.

[28] H. Haber, *J. Phys. Conf. Ser.* **G259** (2010) 012017.

4.6 G. Pancheri, A. Grau, R.M. Godbole, et al. - Probing confinement and asymptotia in hadronic cross-sections at LHC

Probing confinement and asymptotia in hadronic cross-sections at LHC

Giulia Pancheri [1]
INFN Frascati, Via E. Fermi, I00044 Frascati Italy
giulia.pancheri@lnf.infn.it

Rohini M. Godbole
Centre for High Energy Physics, Indian Institute of Science, Bangalore, 560 012, India
rohini@cts.iisc.ernet.in

Agnes Grau
Departamento de Física Teórica y del Cosmos,Universidad de Granada, 18071 Granada, Spain
igrau@ugr.es

Olga Shekhovtsova
IFIC,Universitat de Valencia-CSIC, Apt. Correus 22085, E-46071, Valencia, Spain
olga.shekhovtsova@ific.uv.es

Yogendra N. Srivastava
Physics Department, University of Perugia, Italy
yogendra.srivastava@pg.infn.it

Abstract We present our model for the total hadronic cross-section. This model allows to probe confinement through an impact parameter distribution derived from soft gluon k_t-resummation in the infrared region. We compare our results with data and discuss whether the limiting asymptotic behaviour from the Froissart bound has been reached. Considerations about connections between existence of hidden dimensions and asymptotia in the total cross-section are given.

1 Introduction

TOTEM measurements at LHC indicate that the total cross-section is rising faster than $\log s$ [1] and the dip in the elastic differential cross-section has reappeared [2]. These results have a number of important consequences. If asymptotia has been reached [3], then the existence of hidden extra dimensions [4, 5] can be excluded in the present energy range [6], and, according to [7] even beyond, if the Froissart bound is saturated.

[1] Speaker

The behaviour of the total cross-section at high energy is regulated by the Froissart-Martin bound [8, 9], according to which asymptotically

$$\sigma_{\rm total} \lesssim \log^2 s \tag{1}$$

Such limiting behaviour is related to the existence of a cut-off in impact parameter space, typically of exponential or gaussian type. The cut-off reflects the property of confinement to a region limited by the hadron sizes. From the point of view of hadron constituent dynamics, scattering of quarks and gluons becomes ineffective at very high energy: there are so many gluons packed in the interaction region that partons cannot see each other, and a saturation effect takes over.

In the model for total cross-section we have developed through the years [10], the saturation effect, by which too many gluons screen the interaction, is obtained through soft-gluon k_t-resummation pushed into the infrared region (IR) coupled to an ansatz for the effective gluon coupling reflecting a confining one-gluon exchange potential.

In the following we shall first highlight our model [10] for probing confinement through the total cross-section. We then present our description of the energy behaviour of the total and inelastic cross-sections from lower energy up the present LHC measurements.

2 The Bloch-Nordsiek model for total cross-section

Our model for the high energy behaviour of the total cross-section is based on three steps: i) eikonal representation for the scattering amplitude, which allows to resum an infinite number of single scattering processes, ii) high energy rising behaviour, at center of mass energies such that $\sqrt{s} \geq 10\ GeV$, dominated of medium- and low-p_t parton-parton processes, i.e. final state partons with $p_t \geq 1\ GeV$, asa *mini-jets*, which can be described by perturbative QCD through parton-parton cross-sections and parton density functions (PDFs), iii) resummation in transverse momentum of soft gluon emission during each single scattering process, down into the infrared region. The first step has been standard practice in total cross-section models, and the second one is used in MonteCarlo simulations of minimum bias events, having been proposed more than 25 years ago [11, 12, 13, 14]. Conversely, the last step, resummation down into the infrared momentum region, is so far specific to our model, and, in our understanding, crucial to establish the asymptotic behavior of the cross-section. This is why we have labeled it as *Bloch Nordsieck model (BN)*, to stress the importance of the infinite sum of soft quanta in dealing with any collision between charged (colour in QCD) particles. It is through the last step that we establish the connection between the high energy behaviour of the total cross-section, confinement and the infrared behaviour of soft gluon coupling.

Two are the major properties of the high energy behaviour of the total cross-section, the fast rise, observed for the first time at the CERN Intersecting Storage Rings (ISR), and the

subsequent leveling off into a smooth behaviour consistent with a logarithmic rise. We attribute the rise in general to mini-jets contributions and the leveling off to be a manifestation of confinement. In the following, we shall describe the model we use and how it relates these properties in a physicallty transparent way.

Writing the scattering amplitude in impact parameter space as

$$\mathcal{F}(s,t) = \frac{i}{2\pi}\int d^2\mathbf{b}e^{i\mathbf{q}\cdot\mathbf{b}}[1-e^{i\chi(b,s)}] \tag{2}$$

with $t=-q^2$, the optical theorem allows to write the total cross-section as

$$\sigma_{total}(s) = 2\int d^2\mathbf{b}[1-\cos\Re e\chi(b,s)e^{-\Im m\chi(b,s)}] \tag{3}$$

where $\mathbf{b}$ is the impact parameter, $\sqrt{s}$ is the CM energy and the function $\chi(b,s)$ depends on the model. Since the total cross-section is dominated by large b-values, and ρ, the ratio of the real to the imaginary part of the amplitude at $t=0$ is very small, we use the approximation $\Re e\chi(b,s)\approx 0$. Our model is then built on the fact that QCD provides a natural mechanism for the rise of the number of parton-parton collisions, and that the eikonal formalism can relate this number to the rise with energy of the total cross-section. To introduce parton-parton scattering, we consider the inelastic cross-section, obtained as

$$\sigma_{inel} = \sigma_{total} - \sigma_{elastic} = \int d^2\mathbf{b}[1-e^{-2\Im m\chi(b,s)}] \tag{4}$$

As commented in a later section, the above expression is also obtained as the sum of all inelastic independent processes, Poisson distributed around an average number of collisions $\bar{n}(b,s)$. If the parton momenta are in the perturbative or semi-perturbative region, i.e. partons exit the collision region with $p_t \geq p_{tmin}$ with $p_{tmin}\sim 1\ GeV$, these collisions can be calculated using perturbative QCD for the parton-parton cross-section. We include both low and high energy processes by writing

$$2\Im m\chi(b,s) = \bar{n}(b,s) = \bar{n}_{soft}(b,s) + \bar{n}_{hard}(b,s) \tag{5}$$

The average number of collisions at a given CM energy $\sqrt{s}$, is obtained as the parton density at impact parameter $\mathbf{b}$ times the cross-section for collisions between partons. In our model, for the high energy component, we write

$$\bar{n}_{hard}(b,s) = A(b,s)\sigma_{jet}(s,p_{tmin}) \tag{6}$$

where $A(b,s)$ is the normalized probability of finding a parton at impact parameter $\mathbf{b}$. This function describes the average location of the partons during the scattering process. We relate it to the acollinearity of initial state partons, as we describe in the following.

To find a parton, we need a colllision to take place, hence a probe, such as the scattering. The scattering implies soft gluon emission, which introduces acollinearity in the initial state, since, to Leading Order (LO) in the collision, partons are all collinear. Soft gluon emission has a logarithmic dependence on the energy of the emitting particles and the acollinearity is then energy dependent.

Resummation of medium-large soft guon momenta [15, 16, 17] is a standard practice in hadronic physics, except that, of norm, the integration is extended only down to an infrared safe cut-off, and the remaining infrared contributions are embedded into an intrinsic transverse momentum. The expression for the overall transverse momentum K_t imparted to an initially collinear parton pair reads

$$d^2P(K_t) = d^2K_t \int \frac{d^2\mathbf{b}}{(2\pi)^2} e^{i\mathbf{K_t}\cdot\mathbf{b} - h(b)} \tag{7}$$

where $h(b)$ is the regularized single gluon spectrum. Taking the Fourier transform to impact parameter space, resummation leads to an impact parameter distribution due to soft gluon emission given as

$$A(b,s) = \frac{e^{-h(b)}}{\int d^2\mathbf{b} e^{-h(b)}} \propto e^{-\int d^3\bar{n}_g(k)[1-e^{-i\mathbf{b}\cdot\mathbf{k}}]} \tag{8}$$

Notice, in Eq. (8), the factor $1 - e^{-i\mathbf{b}\cdot\mathbf{k}}$, which in QED cancels the infrared divergence, and which is usually approximated to 1 in QCD applications, where the infrared limit is not accessed. However, this is precisely the region where one can expect confinement to arise. Indeed, the above equation allows to introduce the direct link between confinement and the smooth high energy behaviour of the total cross-section. Asymptotically, when $2\Im m\chi(b,s) \simeq \bar{n}_{hard}(b,s)$, the large b-behaviour of A(b,s), and hence of the amplitude in $\mathbf{b}$-space, is dominated by the low k_t behaviour of $d^3\bar{n}_g(k)$, the (infrared singular) distribution of single gluons emitted in the scattering. This distribution depends on the soft gluon coupling to hard gluons and quarks. However the infrared region does not admit a perturbative expression for this coupling. To study the infrared region, from which confinement effects such as the intrinsic transverse momentum of hadrons arise, we have long since proposed an ansatz [18], which allows us to probe Eq. (8) down to $k_t = 0$, i.e.

$$d^3\bar{n}_g(k) = constant \frac{d^2k_t}{k_t^2}\frac{dk_L}{k_L}\alpha_s(k_t) \sim_{k_t\to 0} \frac{d^2k_t}{k_t^2}\frac{dk_L}{k_L}k_t^{-2p} \tag{9}$$

with $p < 1$ for the k_t-integral to converge. To obtain a smooth transition between the asymptotic freedom region and the infrared momenta, we proposed the expression

$$\alpha_{eff}(k_t) = \frac{12\pi}{11N_f - 2N_c}\frac{p}{\log[1 + p(k_t/\Lambda)^{2p}]} \tag{10}$$

The above expression corresponds to a gluon spectrum which is singular but integrable. By taking a Fourier transform of the corresponding one-gluon exchange expression, the corresponding potential can be seen to have a large distance limit $V(r) \sim r^{2p-1}$, namely rising with distance as long as $p > 1/2$. The limit $p = 1$ correspond to the linearly rising case. Thus the overall condition is $1/2 < p < 1$.

Coupling soft gluon k_t-resummation to LO parton-parton scattering cross-sections, evaluated through library available LO parton density functions in PDFLIB 8.04 [19], provides construction of $\bar{n}_{hard}(b, s)$ based on current phenomenology. To actually construct the total cross-section with this model we need a further input, i.e. $\bar{n}_{soft}(b, s)$, for which we have no microscopic description at present and which we parametrize [10].

The energy dependence of the total cross-section is then obtained by combining our proposed impact parameter distribution with the power-like $s-$behaviour of the minijet cross-sections, since, at LO, one has $\sigma_{jet}(s) \sim s^{\epsilon}$ with $\epsilon \sim 0.3$. Such high energy behaviour is a direct consequence of current LO parametrizations of the gluon densities at small x, the parton energy fraction, and it has been one of the problems encountered in using mini-jets as seeds of the high energy rise: mini-jets could describe the beginning of the rise of the total cross-section, but as the energy increases this rise is too fast. However, as we have shown in [20], our ansatz for the effective quark-gluon coupling, introduces a cut-off in impact paramer space which leads to

$$\sigma_{total} \sim constant\ [\log s]^{1/p} \tag{11}$$

a behaviour consistent with the Froissart bound, because of the condition $1/2 < p < 1$.

3 Phenomenology of the total cross-section

In this section, we compare our total cross-section description to data, from lower CM energies up to LHC energies. Application of the model described in the previous section leads to the results shown in Table 1 from [10] and to Fig. 1, with the parameters as described, and σ_0 determining the low energy normalization as discussed in [10].

The normalization of the curves in Fig. 1 depends on the parametrization of lower energy data, i.e. the choice for $\bar{n}_{soft}(b, s)$ which defines the region $\sqrt{s} \lesssim 10\ GeV$. Two different models have been used: the one labelled *BN* in the left hand panel, corresponds to an impact parameter distribution for the soft part as in Eq. (8), with an *ad hoc* parametrization of the maximum energy available to single soft gluon emission as described in our 2005 article [10]. The second model, indicated in the figure by the dashed curve, is a power-law type parametrization for the low energy part (with minimization in presence of mini-jets for the high energy part). Not all available sets of LO PDFs [19] give a satisfactory description of data. Presently, in addition to GRV and MRST, whose results are reproduced in the table, CTEQ densities are also available.

Table 1: Values of σ_{tot} for p_{tmin}, σ_0 and p corresponding to different parton densities in the proton, for which our model [10] gives a satisfactory description of the total cross-section.

PDF	p_{tmin} (GeV)	$\sigma_0(mb)$	p	σ_{tot} $\sqrt{s} = 7\ TeV$	σ_{tot} (mb) $\sqrt{s} = 8\ TeV$	σ_{tot}(mb) $\sqrt{s} = 14\ TeV$
GRV	1.15	48	0.75	92	93	100
GRV94	1.10	46	0.72	96	98	104
	1.10	51	0.78	83	85	90
GRV98	1.10	45	0.70	95	97	102
	1.10	50	0.77	82	83	88
MRST(72)	1.25	47.5	0.74	86	88	96
	1.25	44	0.66	98	100	111

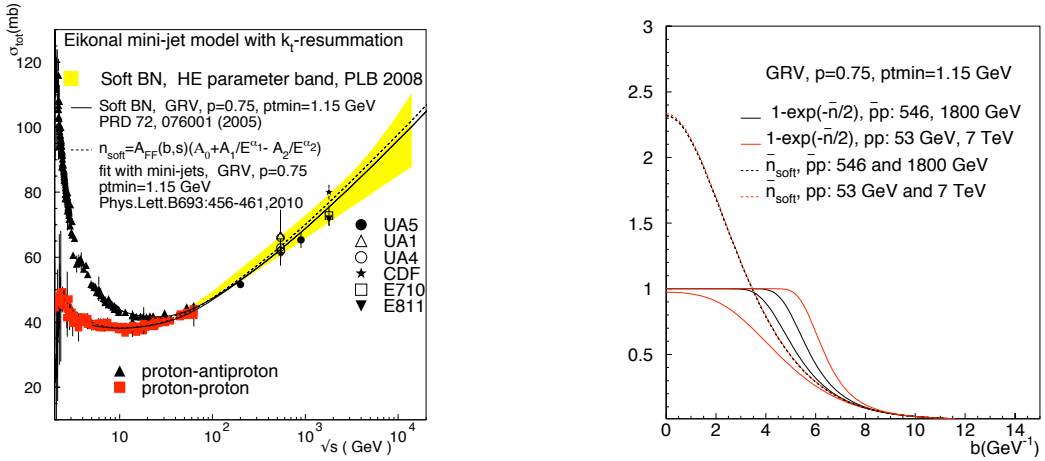

Figure 1: At left, our description of the total cross-section from [10], with LHC values as in the Table. At right, with low energy parametrization for the soft part, we show the elastic amplitude $1 - exp[-\bar{n}(b,s)/2]$, in impact parameter space, according to our model for a chosen set of high energy parameters and different c.m. energies. Also plotted is the average number of soft collisions, $\bar{n}_{soft}(b,s)$, which sets the normalization of the cross-section at lower energies, i.e. before the onset of mini-jets.

However, their low-x behaviour does not give results which can be used in our LO model for an asymptotic rise of the cross-section [21].

Limiting our choice of parameters to GRV and MRST densities, we obtain the band shown in the left panel of Fig. 1. We notice that the curve describing the upper edge of the band is consistent with the TOTEM result and with the CDF result at the TeVatron as well as with the measurements at CERN $S\bar{p}pS$.

The results of this model for the elastic amplitude in **b**-space are detailed in the right panel of Fig. 1. One can see that as the energy increases, the amplitude becomes closer and closer to the black disk limit. In this figure, we have chosen a particular QCD parametrization of the high energy effects,. i.e. LO GRV parton densities, $p_{tmin} = 1.15\ GeV$ and $p = 0.75$. Very

similar results are obtained with MRST.

Our phenomenology is based on LO parton density functions (PDFs) and LO parton-parton cross-section to describe the rise due to minijets, coupled to implementation of our model for quark-gluon coupling in the IR.Table 1 shows that an adequate description of recent TOTEM data for the total cross-section is obtained with $p = 0.66 \sim 2/3$. According to the discussion in [20], this corresponds to an asymptotic behaviour

$$\sigma_{\rm total} \sim [\log s]^{3/2} \tag{12}$$

namely a behaviour midway between a simple logarithm and saturation of the Froissart bound. Data at higher energy can of course change our estimate for the singularity parameter p, which is based on an LO QCD parametrization, as described.

4 The inelastic cross-section

The eikonal model can also be used to describe the inelastic total cross-section. In its simplest form, $\sigma_{\rm inel}$ is given by Eq. (4). However, we notice the following.

It is possible to obtain the expression for the inelastic total cross-section given by Eq. (4) through a semi-classical argument, based on the hypothesis that the scattering between hadrons takes place through multiple parton-parton collisions which are independently distributed. This corresponds to assuming a Poisson distribution around an average number of collisions $\bar{n}$, namely

$$P(\{n, \bar{n}\}) = \frac{(\bar{n})^n e^{-\bar{n}}}{n!} \tag{13}$$

Calculating the scattering at each impact parameter value b between the scattering hadrons, summing on all possible number of collisions and integrating over the impact parameter space leads to

$$\sigma_{inel}(s) = \sum_{n=1} \int d^2\mathbf{b}\ P(\{n, \bar{n}\}) = \int d^2\mathbf{b}[1 - e^{-\bar{n}(b,s)}] \tag{14}$$

Comparing Eq.(4) with Eq.(14) leads to the identification $\bar{n}(b, s) = 2\Im m\chi(b, s)$, but also implies that Eq. (4) only sums independent processes. What then happens to the single and double diffractive processes, for which strong correlations between final state hadrons are at play? Our interpretation, confirmed by the comparison with data shown in Fig. 2, is that in a two component eikonal model, such as the one examined here which distinguished only between elastic and inelastic processes, diffraction, single and double, is counted as part of the elastic cross-section. Indeed, when one applies Eqs. (3) and (4) using the same set of parameters for $\chi(b, s)$ to describe both the total and the inelastic cross-section, the result is generally short of reported data for the difference $\sigma_{\rm inel} = \sigma_{\rm total} - \sigma_{\rm elastic}$, as we show in the figure.

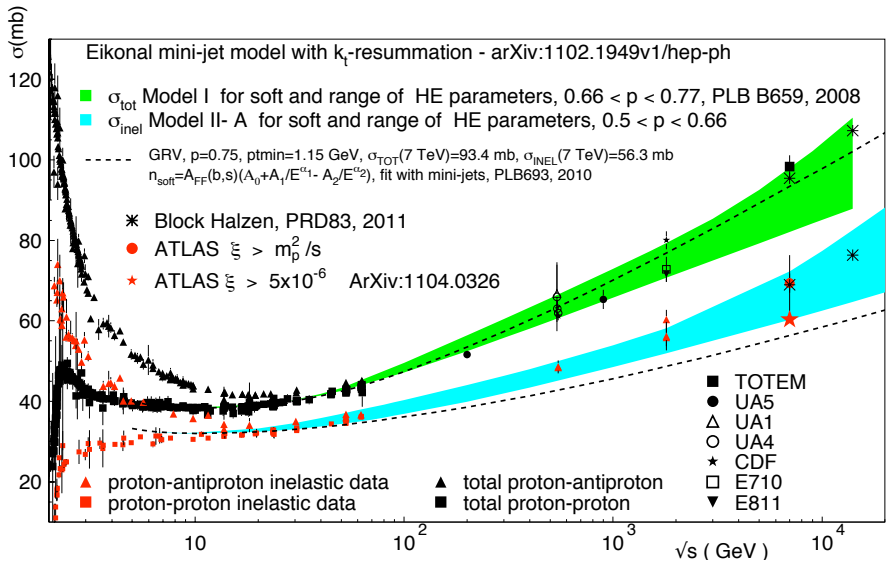

Figure 2: Data for the total and inelastic cross-sections compared with our model, as described in the text.

Basically, to summarize, in a two component model, the same eikonal function describes the elastic, the total and the inelastic cross-section. The failure of such model is however clearly shown in Fig. 2 from [21] where we compare our results with recent data by TOTEM [1] and ATLAS [22]. In this figure, the dashed line corresponds to use the same eikonal function (namely same set of parameters) for both the inelastic and the total cross-section. A discrepancy of the model prediction with the lower energy data obtained from

$$\sigma^{exp}_{inelastic} \equiv \sigma^{exp}_{total} - \sigma^{exp}_{elastic} \tag{15}$$

makes the point. The dashed line indeed describes well the cross-section for inelastic processes in the central region, but fails to account for the totality of inelastic events, confirming our interpretation.

By relaxing the request of having a unique set of parameters defining the eikonal function in the inelastic and the total cross-section expression, one can accomodate both the data for the inelastic total cross-section as given by Eq. (15) and extrapolations from the CMS (released as CMS-PAS-FWD-11-001) and ATLAS experiments [22]. Such exercises are shown by the two bands in the figure. For different proposals to calculate the inelastic cross-section, see for instance [23] and [24].

5 Asymptotic high energy total cross sections in theories with extra dimensions

The rate at which cross sections grow with energy is sensitive to the presence of extra dimensions in a rather model-independent fashion. This allows for a systematic search of extra dimensions which is largely unaffected by single events that might, due to statistical fluctuations, support some model with higher dimensions. In [6], how rates would be expected to grow if there are more spatial dimensions than 3 appearing at some energy scale $\sqrt{s_1}$, was examined making connections with black hole physics and string theory. These results may be summarized as follows.

For $n = (D-4)$ extra dimensions, the total cross-section at a high energy $\sqrt{s}$ reads

$$\sigma_{tot}(s) \sim \ \sigma_o[ln(s/s_o) + f_n(s/s_1)^{(n+1)/4}]^2, \tag{16}$$

where f_n is the strength of the elastic amplitude due to extra n-dimensions open at a threshold $\sqrt{s_1}$. Hence, while the cross-section would follow the familiar Froissart-Martin $(ln(s/s_o)^2)$ rise below the opening of the threshold for extra dimensions, for energies beyond, they would grow as a power law in s

$$\sigma_{tot}(s) \rightarrow \ (s/s_1)^{(n+1)/2}; \ \ (s > s_1). \tag{17}$$

High quality accelerator total cross-section data are available from $\sqrt{s} \sim \ 5\ GeV$ up to recent data from the LHC TOTEM group at $\sqrt{s} = 7\ TeV$. An analysis -including that from the cosmic ray energy data from the Auger Collaboration up to $\sim 50 - 60\ TeV$- are all consistent with the traditional Froissart-Martin bound for the $D = 4$ case. In fact, a strong case for a $(ln(s/s_o)^2)$ rise, and hence saturating up to 100 TeV, has been made by Block and Halzen[7] confirming this result.

6 Conclusions

We have described a model for the total cross-section which relates saturation of the Froissart bound to the infrared behaviour of soft gluons emitted during the scattering processes which contribute to the total cross-section. We have also shown the limitations of the two component eikonal model and compared the predictions of the soft gluon resummation model (BN model) with data. This model is able to accomodate the recent TOTEM data for the total cross-section. The resulting set of parameters indicates a rise with energy not yet saturating the Froissart bound.

This model can be adapted to photon processes as well, in particular to studies of the hadronic background in $\gamma\gamma$ collisions at linear colliders, as discussed in ref. [25].

Acknowledgments

G.P. is grateful to the Center for Theoretical Physics of MIT for hospitality, while this work was prepared. Work partially supported by Spanish MEC (FPA2006-05294, FPA2010-16696) and by Junta de Andalucia (FQM 101). This work has been supported in part by the Spanish Consolider Ingenio 2010 Programme CPAN (CSD2007-00042).Y.S. would like to thank his colleagues on the Auger Collaboration for discussions. This project is partially supported by MEC (Spain) under grants FPA2007-60323 and FPA2011-23778, by the Spanish Consolider-Ingenio 2010 Programme CPAN (CSD2007-00042). This research of OS was supported by a Marie Curie Intra European Fellowship within the -7th European Community Framework Programme (FP7-PEOPLE-2009-IEF) PIEF-GA-2009-253329.

References

[1] G. Latino et al., *First Results from the TOTEM Experiment*, arXiv:1110.1008 [hep-ex].

[2] G. Antchev et al., *Europhys.Lett.* **96** (2011) 21002; e-Print: arXiv:1110.1395 [hep-ex]

[3] M. Block and F. Halzen, *Phys.Rev.Lett.***107** (2011) 212002 e-Print: arXiv:1109.2041 [hep-ph].

[4] D. Amati, M. Ciafaloni, and G. Veneziano, preprint S.I.S.S.A. 121 EP, Sep. 1988.

[5] K. Agashe and A. Pomarol, *New J. Phys.* **12** (2010) 075010; doi: 10.1088/1367-2630/12/7/075010 (2010).

[6] J. Swain, A. Widom and Y. Srivastava, *Asymptotic High Energy Total Cross Sections and Theories with Extra Dimensions*, arXiv:hep-ph:1104.2553 [submitted for publication].

[7] M. Block and F. Halzen, *'Soft' Hadronic Cross Sections Challenge Hidden Dimensions*, e-Print: arXiv:1201.0960 [hep-ph] [submited for publication].

[8] M. Froissart, Phys. Rev. **123** (1961) 1053.

[9] A. Martin, Phys. Rev. **129** (1963) 1432-1436; A. Martin and F. Cheung, "Analyticity Properties and Bounds of the Scattering Amplitudes", Eq.(6.7), page 34, Gordon and Breach Science Publishers, N. Y., (1970).

[10] Over the years, the work has been done in collaboration with A. Achilli, R. Godole, A.Corsetti, and O. Shekhovotsova. Some general references are: *Phys.Lett.* **B693**(2010) 456; e-Print: arXiv:1008. 4119[hep-ph]; *Eur.Phys.J.* **C63**(2009) 69; e-Print:

arXiv:0812.1065 [hep-ph]; *Phys.Lett.* **B659**(2008) 137; e-Print: arXiv:0708.3626 [hep-ph]; *Phys.Rev.* D72(2005) 076001; e-Print: hep-ph/0408355; *Phys.Rev.* **D60**(1999) 114020; e-Print: hep-ph/9905228;*Phys.Lett.* **B382** (1996)282; e-Print: hep-ph/9605314.

[11] G. Pancheri and C. Rubbia, *Nucl.Phys.* **A418** (1984) 117C-138C.

[12] T.K. Gaisser and F. Halzen *Phys.Rev.Lett.* **54** (1985).

[13] L. Durand and Pi Hong, *Phys.Rev.Lett.***58** (1987) 303-306.

[14] G. Pancheri and Y. Srivastava, *Phys.Lett.* **B182** (1986) 199-207.

[15] Y. L. Dokshitzer, D. Diakonov, S.I. Troian, *Phys.Lett.* **B79** (1978)269-272.

[16] G. Parisi and R. Peronzio, *Nucl.Phys.* **B154** (1979).

[17] G. Altarelli, R.K. Ellis, M. Greco, and G. Martinelli, *Nucl.Phys. B246* (1984)12.

[18] A. Nakamura, G. Pancheri and Y.N. Srivastava, *Z.Phys.* **C21** (1984)243.

[19] H. Plothow-Besch, W5051 PDFLIB 2000.04.17, CERN-PPE.

[20] A. Grau, R. M. Godbole, G. Pancheri, Y. N. Srivastava, *Phys. Lett.* **B682** (2009) 55, e-Print: arXiv:0908.1426 [hep-ph].

[21] A. Achilli, R. Godole, A.Corsetti, and O. Shekhovotsova, *Phys. Rev.* **D84** (2011), arXiv:1102.1949 [hep-ph].

[22] G. Aad *et al.*, *Measurement of the Inelastic Proton-Proton Cross-Section at* $\sqrt{s} = 7$ *TeV with the ATLAS Detector,* arXI:1104.0326 [hep-ex].

[23] P. Lipari and M. Lusignoli, *Phys. Rev.* **D80** (2009) 074014, e-Print: arXiv:0908.0495 [hep-ph].

[24] V.A. Khoze, A.D. Martin and M. Ryskin, these Proceedings and references therein.

[25] R.M. Rohini, K. Mohan and G. Pancheri, these Proceedings.

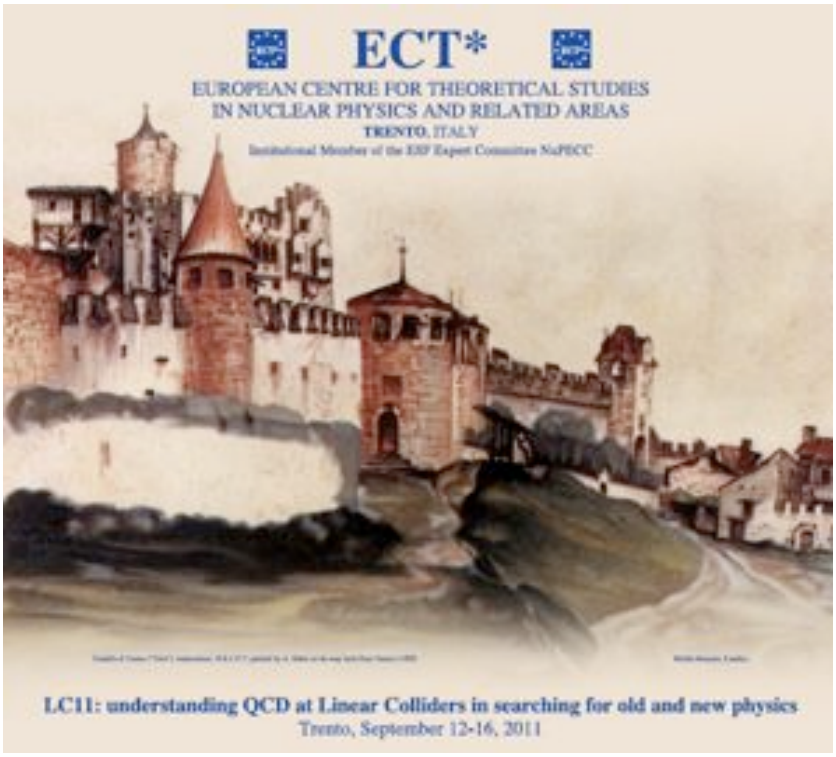

Castello di Trento painted by A. Dürer on his way back from Venice (1495).

Chapter 5

QCD

5.1 G. Bellettini - QCD Highlights from CDF (and D0)

QCD Highlights from CDF (and D0)

Giorgio Bellettini
Dipartimento di Fisica and INFN, Pisa
Fermilab
giorgiob@fnal.gov

Abstract We review a number of hadron physics results at the Fermilab Tevatron collider, paying special attention to some anomalies observed recently in vector boson events with associated jets.

Introduction

The main features of hadron interactions were studied with priority in the early times of the Tevatron collider. The results from those times will stay for always in the Particle Data Book. A revival of interest on them can be expected when the analysis of minimum bias data collected in a few runs at reduced Tevatron energies of 300 and 900 GeV, just before the shutdown of the collider, will be performed by CDF and D0. The 900 GeV data of CDF will be the largest statistics of minimum bias ever collected at hadron colliders. We shall mention only a few classical QCD measurements which were continued during the Tevatron Run II (2001-2011). At this point in time hadron jets are the primary objects of interest in searches on heavy flavor, vector boson, top quark and searches for New Physics. Most of my talk will discuss measurements of jet properties in associated vector boson production.

Physics results from D0 and CDF

The running strong coupling constant α_s and the point-like quarks Taking advantage of the wide and rather uniform coverage of their calorimeter, the D0 Collaboration has measured the inclusive jet cross section over a large range of polar angle and transverse momentum. Their recent data are displayed in Fig. 1 [1]. These data can be interpreted by convoluting structure functions of the primaries and parton-parton scattering amplitudes with α_s-dependent couplings, as depicted in Fig. 2. The coupling constant α_s can thus be measured.

To illustrate the running of α_s, D0 data are merged with previous HERA measurements and plotted as a function of transverse momentum p_t in Fig. 3 [2].

Production of jets at small center of mass angles θ^* is dominated by gluon exchange amplitudes, which generate a cross section as $d\sigma/dcos\theta^* \simeq 1/(1-\cos\theta^*)^2$ with a Rutherford-like

dependence on θ^*. A possible new interaction at a higher energy scale Λ can be tested by assuming an additional four fermion point-like interaction amplitude. This amplitude would generate in the cross section a term as $d\sigma/dcos\theta^* \simeq 1/\Lambda(1+\cos\theta^*)^2$, thereby smoothing the forward angular dependence. It became customary to display the angular cross section as a function of $\chi = (1+\cos\theta^*)/(1-\cos\theta^*)$ rather than of θ^* directly, since this makes the distribution more sensitive to a possible Λ-dependent term, as illustrated in Fig. 4. Assuming the less favorable interference sign between the contact and the QCD interaction amplitudes, the D0 analysis excludes $\Lambda < 2.58\ TeV$ at 95% c.l. [3].

Searches for new particles New heavy particles decaying into two quarks are expected in many models, like those which predict a new intermediate boson Z'. The result of a search for a $t-\bar{t}$ resonance in the $m_{t\bar{t}}$ spectrum by CDF using the of 106 pb^{-1} integrated luminosity collected in run1 is shown in Fig. 5. The inset shows a simulation of a narrow, vector-like Z' resonance of mass 500 GeV/c^2. These early data left room for hopes. However, the CDF search for di-quark resonances in run2 gave negative results in the $t-\bar{t}$ spectrum as well as in any other dijet channel. The inclusive dijet mass distribution with 1.13 fb^{-1} excludes bumps up to $m_{jj} \sim 1.25\ TeV/c^2$ [5] (Fig. 6). The limits obtained on a number of exotic processes are also shown in Fig. 6.

The features of additional jets in W, Z production events are now raising great interest. Observing a second intermediate boson decaying into two jets in these events is the natural training lane towards the search for associated production of a light Higgs boson, as $W(Z)H \rightarrow W(Z)bb$. The integral jet production rate above a 30 GeV energy cut in Z+jets events measured by CDF is shown in Fig. 7 [5]. While the leading order calculation predicts less rate and requires a normalization factor of 1.46 in order to fit the data, the NLO calculation fits well the entire distribution. Since the simulation of jet production in W events is very similar to production in Z events, this agreement gives confidence on the simulation of the features of the QCD background in a search for diboson events.

In a search for light Higgs $\rightarrow b\bar{b}$ the ultimate background will b-jets production by non-resonant QCD processes. Simulating reliably this background is of utmost importance. Tagging of a secondary vertex due to late decay of beauty hadrons has been exploited since a long time for assigning b-flavor to jets. CDF has developed a technique by which b-jet flavor tagging is improved by measuring the mass of the track system associated to delayed vertices within a jet. However, such secondary vertices can be generated also by charmed hadron decays. Also, because of decays of unstable hadrons and of measurement errors ('fakes'), light jets can feature secondary vertices as well. Given the dominance of light flavor and gluon jets in inclusive production, fakes can produce a very significant tag rate. Fig. 8 shows the simulated vertex mass distribution of b and lighter quark vertices and a CDF fit to the vertex mass of b-tagged jets in Zjj data in 7.8 fb^{-1}, in terms of b-signal and background [7]. The relatively

larger mass of b-vertices can be used to improve the purity of b tagging. The measured b-jet rates fit reasonably well with theory expectation in terms of relative rates to total Z production and to inclusive Z+jets:

$$\frac{\sigma(Z+b)}{\sigma(Z)} = (2.84 \pm 0.29 \pm 0.29) \times 10^{-3} \quad (1)$$

to be compared with theory expectations varying between 2.3×10^{-3} and 2.8×10^{-3} depending on the Q^2 scale,

$$\frac{\sigma(Z+b)}{\sigma(Z+jets)} = (2.24 \pm 0.24stat \pm 0.27syst) \times 10^{-2} \quad (2)$$

to be compared with theory expectations between 1.8×10^{-2} and 1.9×10^{-2}. We expect jet production dynamics to be very similar in W+jets as in Z+jets. Therefore one is confident in simulation of jet production in W events as well. This is the jet production Standard Model picture on which the search for rare diboson processes and for possible new phenomena in W with final state jets is based.

Finding dibosons in fully leptonic final states is relatively easy. CDF observation of $ZZ \to llll$ in 4 charged leptons (Fig. 9) dates from 2009 [8]. The statistics is not very large, but the ZZ component is clear. Of course, the four charged leptons final state provides the clearest signature for ZZ production. If one studies final states with jets, WZ, WW pairs mix with ZZ and generate an inclusive signal. This inclusive diboson signal has the largest rate and was the first to be observed by CDF in the sample of large $E_{t,miss}$ +2jets, where the prime contribution is from $Z \to \nu\bar{\nu}$ (also W leptonic decays generate $E_{t,miss}$ when the charged lepton is not detected). The jj invariant mass in this sample [9] is shown in Fig. 10. More recently, associated $W/Z \to jj$ production in events with a charged lepton and $E_{t,miss}$ was also observed [10], as shown in Fig.11 ($Z \to ll$ events contribute to these events when a lepton escapes detection).

The slightly inaccurate fit in Fig. 11 to the distribution around $m_{jj} = 150\ GeV$ triggered CDF to a deeper study of this process above $m_{jj} = m_Z$. Events with exactly two $E_t > 30\ GeV$ jets were selected and $P_{T,jj} > 40\ GeV$ of the jet pair was required in order to allow a more reliable background calculation. The result of this analysis is shown in Figs. 12a and 12b [11]. The expected rate was simulated according to the SM cross sections for the known processes (inclusive W+jets being the dominant backgroud, as listed in the inset), but the fit to the spectrum was poor. A bump of over 3 σ significance about 40 GeV wide around $m_{jj} = 145\ GeV$ was left unexplained. The rate in the bump corresponds to a cross section of $3.1 \pm 0.8\ pb$, i.e. to a 3.3σ effect.

When confronted with the problem of understanding this anomaly, one is troubled by the limited information available on hadron jets. Jets are defined by a cone algorithm and their energy is integrated within some range of pseudorapidity-athimuthal angle ($\Delta R = \sqrt{\Delta\eta^2 + \Delta\phi^2} =$

0.4 in this analysis). Corrections for detector defects, out-of-cone energy losses, in-cone energy contributed by underlying event are applied only in average. When aiming to spectroscopy of hadron jet systems, we suffer because with this definition jet energy resolution is too poor. Jet energy calibration should be personalized and be flavor specific for optimal discrimination of signal versus background. A new state may decay into a pair of light quark jets, s-jets, c-jets, b-jets. Background jets have their own flavor composition, often with dominance of gluon jets. Therefore signal/background would depend on flavor, and flavor tagging would allow separate studies in flavor channels. Combining separate analyses in different flavor channels would improve the overall S/B discrimination. Hopefully, personalized corrections will be possible in future experiments.

In absence of more detailed information, several important checks were made on data of this spectrum. The b-tag rates for jets in the bump and in adjacent m_{jj} ranges, at $m_{jj} < 120\ GeV$ and $m_{jj} > 160\ GeV$, were compared and found to be the same within statistical errors. The overall mass of the W+jj system was studied. Although the fit to the SM contribution was not perfect (Fig. 13), no evidence for a mother resonance was found [12].

The same m_{jj} distribution was studied by D0 [13] who did not see any evidence for a bump (Fig. 14). The p-value for a bump at 145 GeV with cross section as large as 3 pb is $< 10^{-3}$. Fitting for a bump, D0 finds a cross section $\sigma_{D0} = 0.4 + 0.8 - 0.4\ pb$, consistent with 0 within 0.5σ. This is 2.5σ apart from the CDF value of $3.1 \pm 0.8\ pb$, with a 0.6% probability of being consistent with it. On comparing directly the event rates of the two experiments, CDF (Fig. 15) concluded that they are not fully incompatible [14]. In the range $120 < m_{jj} < 300\ GeV$ both CDF and D0 see a $\sim 4\ \sigma$ rate excess above SM simulation. The D0 excess is 200 ± 50 events, CDF excess is 370 ± 70 events. The difference is 170 ± 86 events, about 2σ. At the time being, CDF is increasing the statistics of the measurement to the full available integrated luminosity and searching for the anomaly in other channels where the effect, if it is real, should also appear.

A step forward in the hunt for the light Higgs boson is studying b-jets in W/Z events. The process W(Z)+bb with two b-jets produced incoherently in association to a W or Z boson is an irreducible background for the process$W(Z)H \rightarrow l\nu b\bar{b}$. A step in this direction is made by CDF searching for heavy flavored jet pairs in W/Z events (Fig. 16). Charm is tagged with an efficiency of ~ 6 %, beauty with an efficiency of ~ 40%. Because of the larger rate of WW production than WZ, the observed 3σ excess is mostly due to $W \rightarrow cs$. However, some rate is also contributed by $Z \rightarrow b\bar{b}$ [15]. A search for exclusive beauty jets will come next.

Conclusions

We have discussed D0 and CDF results in jet production and the search for new particles at the TeVatron. In order to fully exploit the jet internal structure one must compare data

to jet fragmentation theory. In addition, the job for theorist would include interpreting the kinematical structure of multi-jet states. These are hard jobs since these phenomena are in part non-perturbative. It must be faced since we must expect that the branching ratios of new states of higher and higher mass into multi-jets will become dominant. We will be forced to tackle multi-jets spectroscopy. One can advocate a vital role of theory in this project. In a joint effort between experimentalists and theorists, the role of hard interaction theory will be of prime importance.

References

[1] V. M. Abazov et al., The D0 Collaboration, arXiv:1110.3771, submitted to Phys. Rev. D. See also C. Schwanenberger, Hadron Collider Physics Summer School, Fermilab, August 20, 2011

[2] V. M. Abazov et al., The D0 Collaboration, Phys. Rev. D 80, 111107 (2009).

[3] V. M. Abazov et al., The D0 Collaboration, Phys. Rev. Lett. 80, 666 (1998). See also G. Hesketh, Fermilab Wine and Cheese seminar, July 24, 2009.

[4] T. Affolder et al., the CDF Collaboration, Phys. Rev. Lett. 85, 2062 (2000)

[5] T. Affolder et al., the CDF Collaboration, PhysRevD.79.112002

[6] M. Martinez, Proceedings of the Workshop on Spectroscopy with Hadron Jets, Pisa, April 2010. See also Jonathan Lewis, CDF Results: Winter 2011, Fermilab seminar, March 11, 2011.

[7] T. Aaltonen et al., The CDF Collaboration, Phys. Rev. D79, 052008 (2009). See also Ankus Mitra, 2011 CDF summer results, Fermilab seminar, June 22, 2011.

[8] T. Aaltonen et al., The CDF Collaboration, Phys. Rev. Lett. 108, 101801 (2012)

[9] T. Aaltonen et al., The CDF Collaboration, Phys. Rev. Lett. 103, 091803 (2009)

[10] T. Aaltonen et al., The CDF Collaboration, Phys. Rev. Lett. 104, 101801 (2010)

[11] T. Aaltonen et al., The CDF Collaboration, Phys. Rev. Lett. 106, 171801 (2011)

[12] T. Aaltonen et al., The CDF Collaboration, Phys. Rev. Lett. 106, 171801 (2011). See also V. Cavaliere, Joint Theoretical-Experimental Seminar, Fermilab, April 6, 2011

[13] V. M. Abazov et al., D0 Collaboration, Phys. Rev. Lett. 107, 011804 (2011). See also J. Haley, Fermilab Wine and Cheese seminar, June 10, 2011.

[14] A Annovi, Proceedings of the 2011 Lepton-Photon Conference. V. Cavaliere, Proceedings of the EPS-HEP2011 conference.

[15] F. Sforza, Proceedings of the EPS-HEP2011 Conference, FERMILAB-CONF-11-517-E, e-Print: *arXiv:1110.0143 [hep-ex]*. See also F. Sforza, Joint Theoretical-Experimental Seminar, Fermilab, August 5, 2011.

[16] T. Aaltonen et al., The CDF Collaboration, Phys. Rev. Lett. June 29, 2011. See also Raz Halon, Proceedings of the EPS-HEP2011 Conference.

Figures

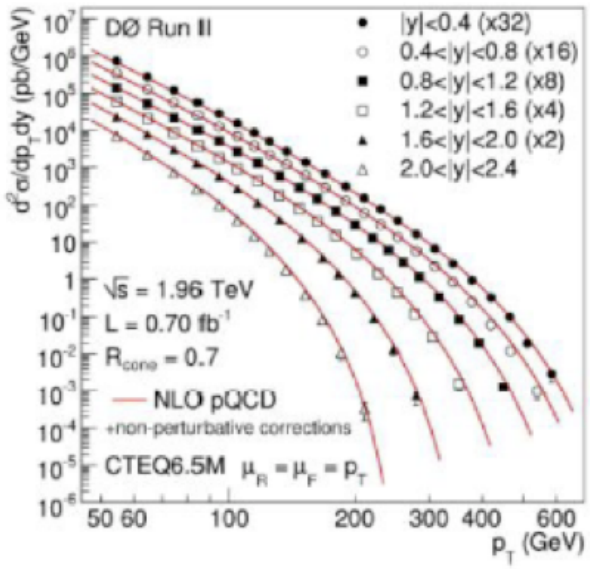

Figure 1: D0 inclusive jet cross-section as a function of transverse momentum and rapidity [1].

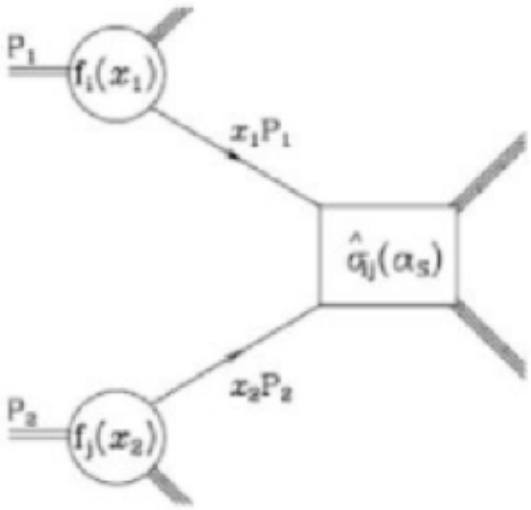

Figure 2: First order diagram illustrating the dependence of the parton scattering amplitudes on α_s in [1].

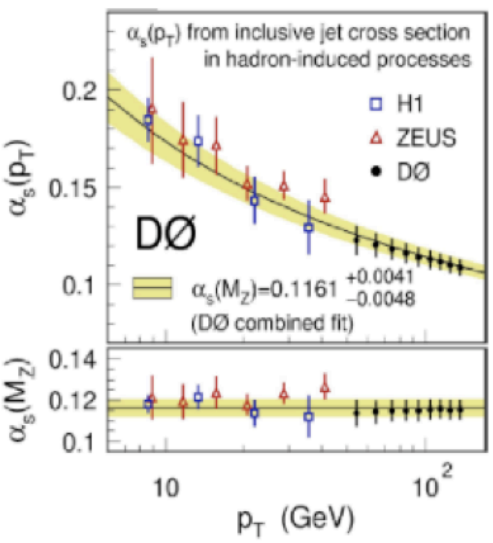

Figure 3: Running of α_s from HERA to Tevatron energies, including the run 2 D0 data [2].

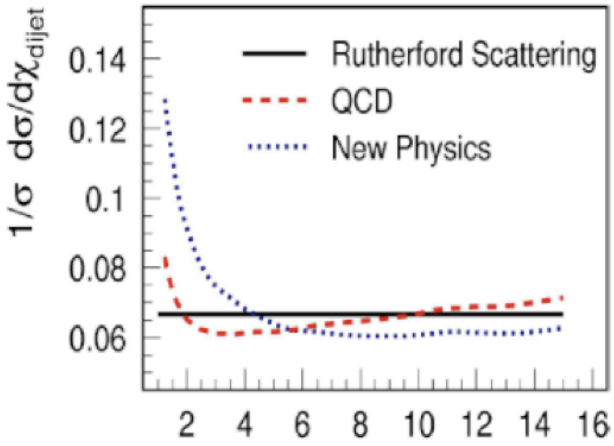

Figure 4: Expected difference from pure Rutherford and QCD scattering in the χ distribution of jet pairs due to the onset of a new point-like interaction between partons [3].

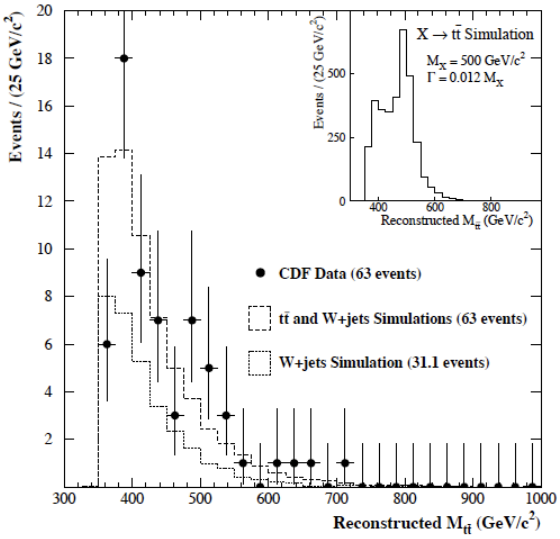

Figure 5: The $t\bar{t}$ spectrum observed by CDF at the end of run 1 (points) compared to the standard model predictions (thick dashes). The inset shows a simulation of a narrow, vector like resonance of mass 500 GeV/c^2 [4].

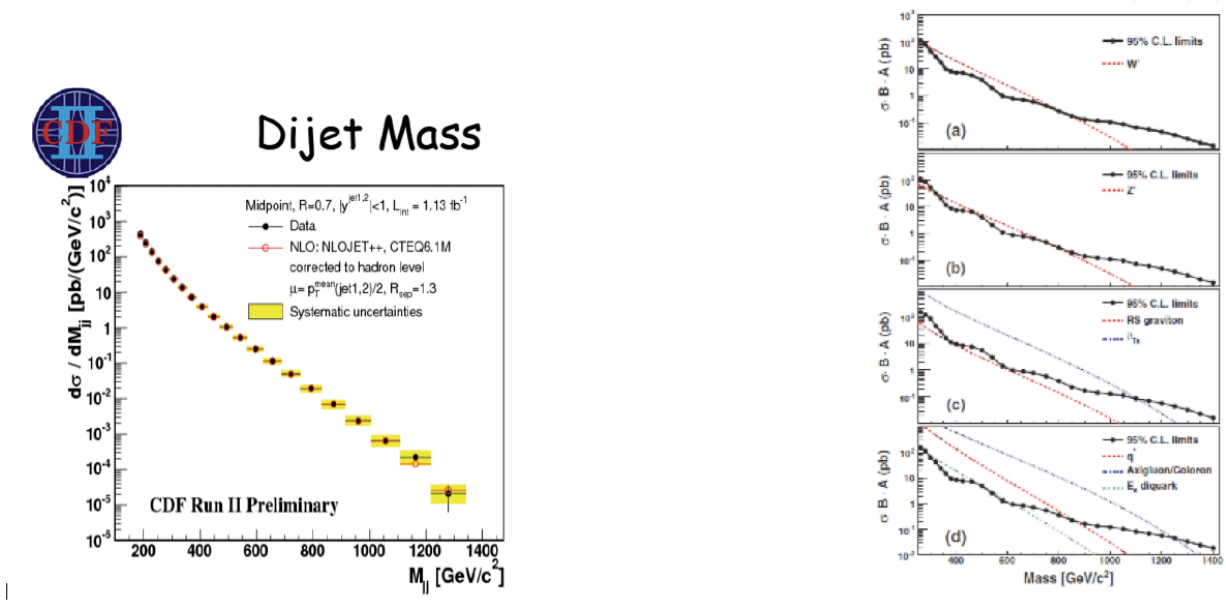

Figure 6: At left, inclusive dijet mass distribution measured by CDF in run 2 with $1.13 fb^{-1}$ integrated luminosity; at right, CDF limits on the production of exotic particles decaying into two jets [5].

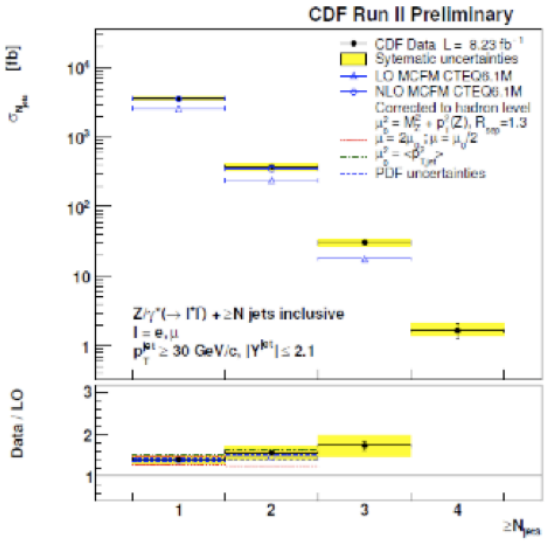

Figure 7: Jet multiplicity distribution in Z+jets events by CDF [6]. While the leading order calculation requires a normalization factor of 1.46 in order to fit the data, the NLO calculation fits well.

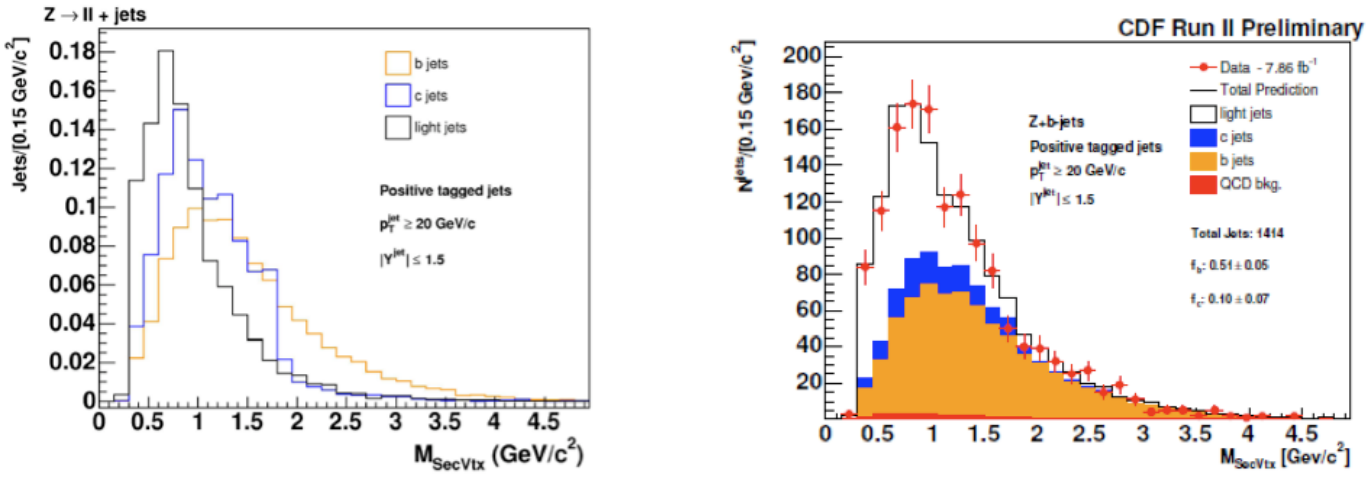

Figure 8: At left, simulated mass distribution of secondary vertices in b-jets, c-jets and light quark jets in CDF; at right, fit to the mass distribution of secondary vertices in Zjj events in terms of b jets and of various backgrounds [7].

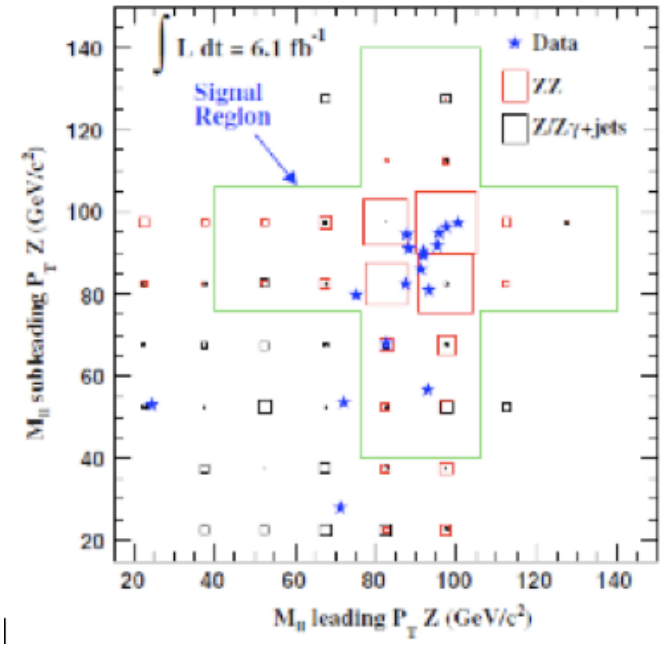

Figure 9: Two-by-two pairings of the 4 charged leptons in CDF ZZ search, showing dominance of the diboson process over background [8].

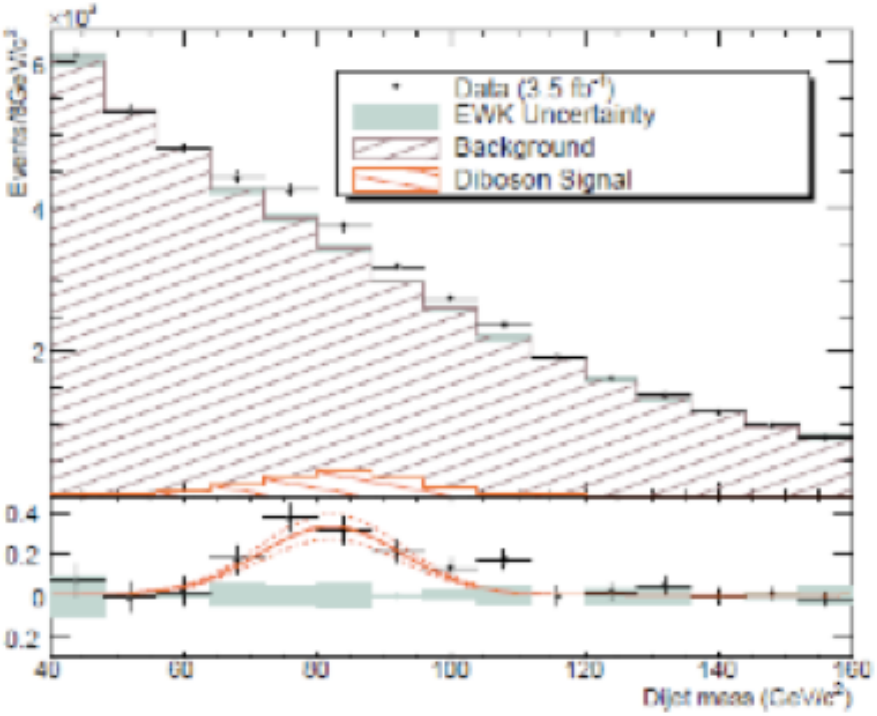

Figure 10: CDF observation of the diboson signal WW/WZ/ZZ in the sample of large invisible transverse energy and jets [9].

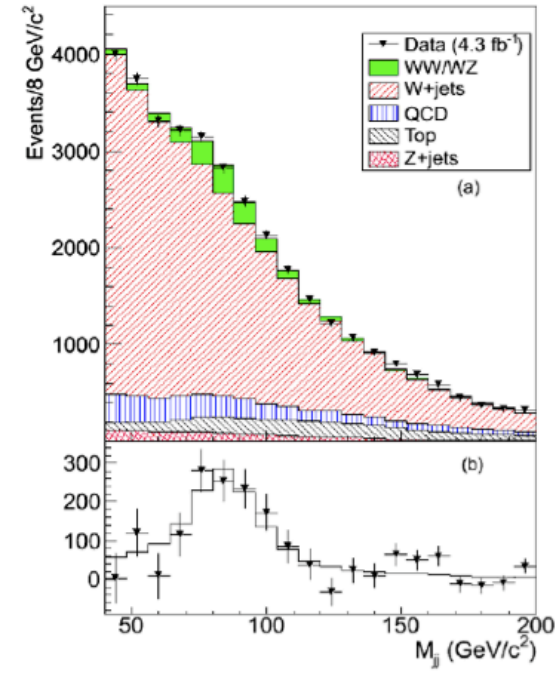

Figure 11: $W/Z \to jj$ signal observed by CDF in events with a charged lepton and $E_{t,miss}$ [10].

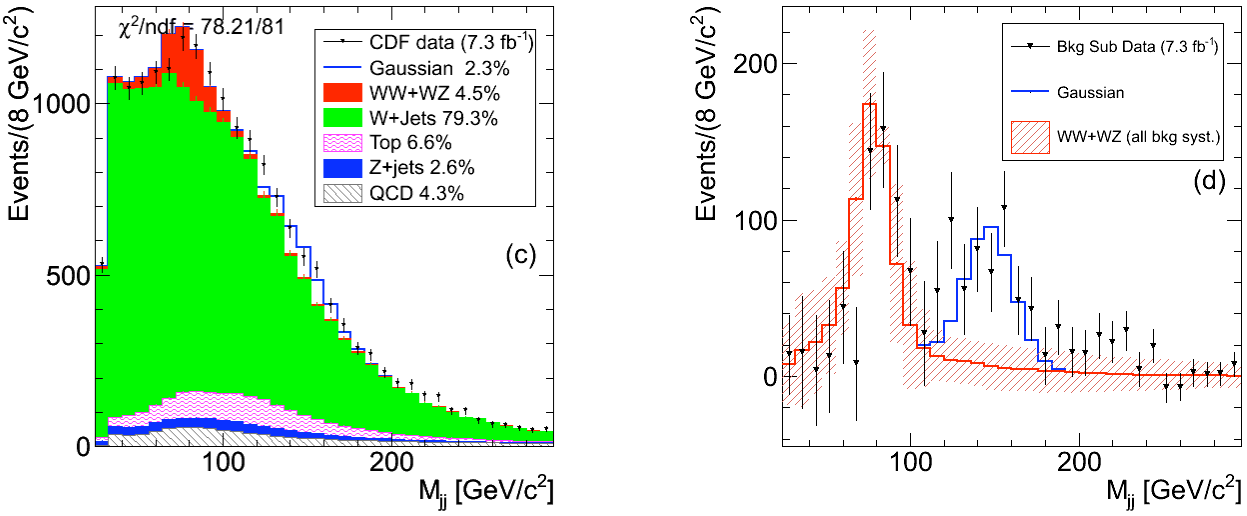

Figure 12: a), dijet mass distribution in lepton, missing E_t and exclusive two jets events up to 300 GeV. b) Distribution after subtracting the known SM contributions [11].

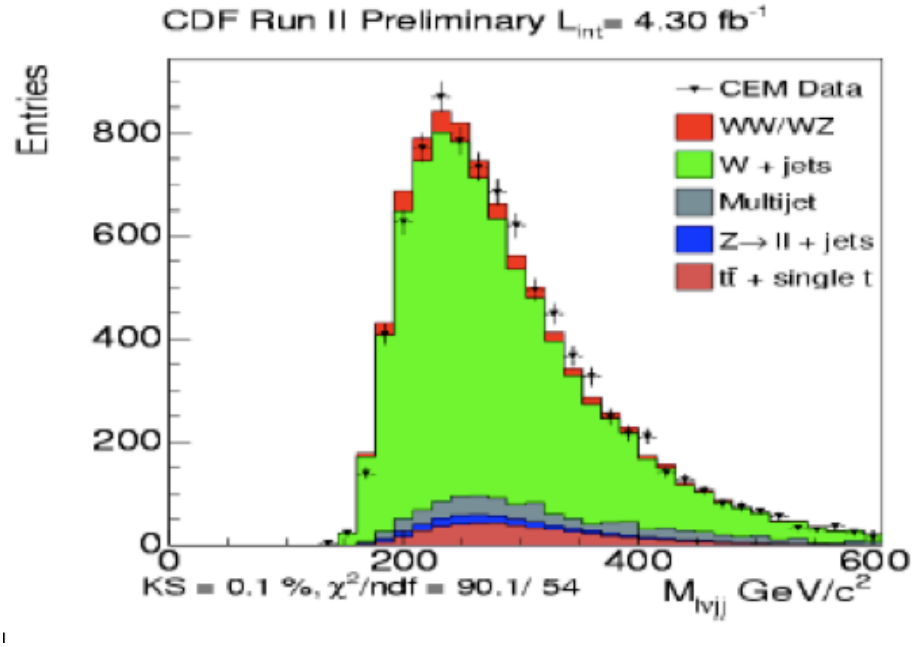

Figure 13: Distribution of the lepton + missing E_t + ij mass in the sample of [12].

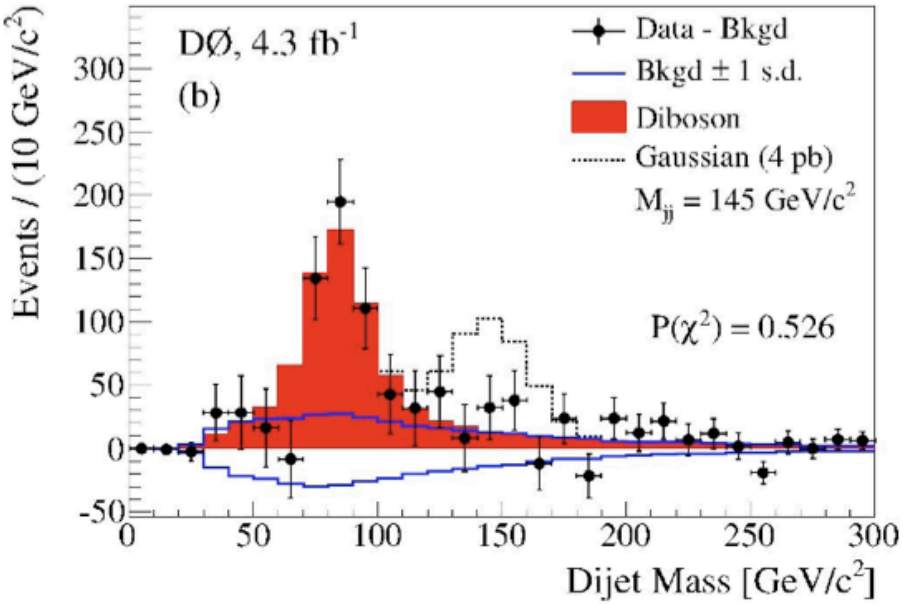

Figure 14: Dijet mass distribution by D0 in the lepton, missing Et and exclusive two jets events after subtracting all SM contributions except dibosons. The dotted histogram represents the expected signal from a resonance at 145 GeV with cross section as large as suggest by CDF [13].

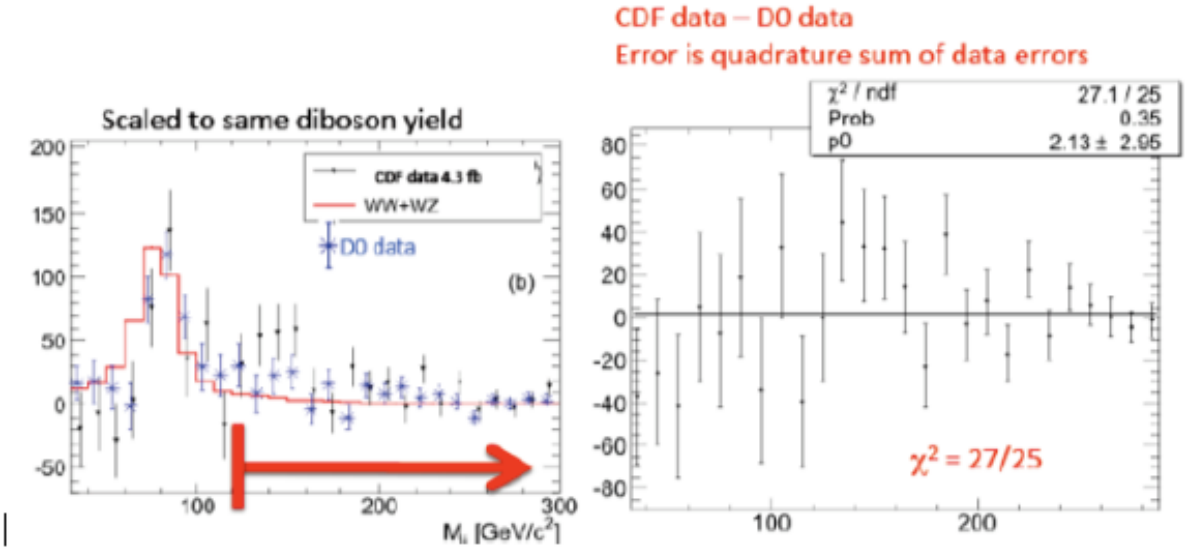

Figure 15: CDF comparison of the rates observed at mjj ¿ 120 GeV by their experiment and by D0 (left), and distribution of the rate difference (right) [14].

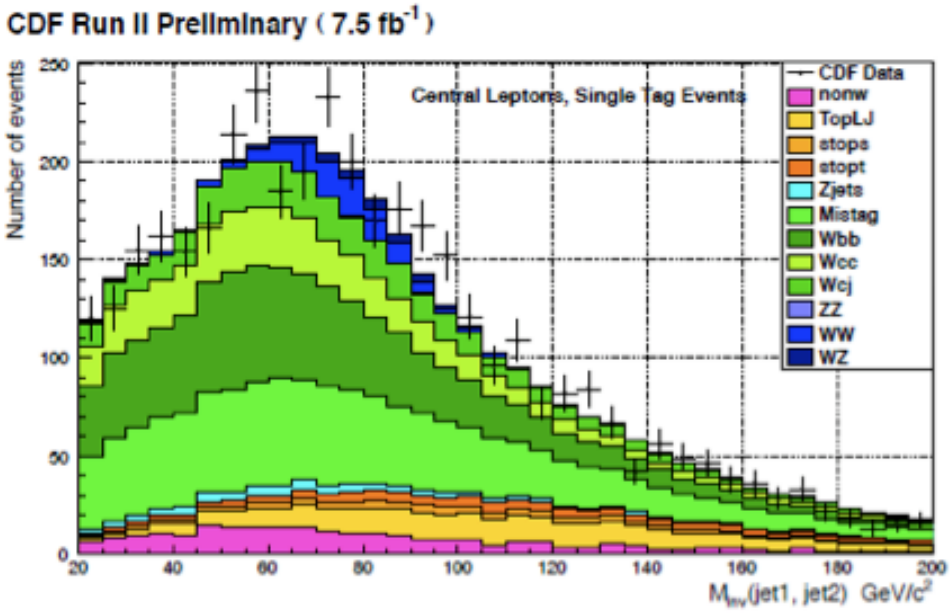

Figure 16: Mass distribution of heavy flavored dijets in W/Z events. Charm is tagged with a $\sim$ 6% efficiency, beauty with a $\sim$ 40% efficiency. The distribution is fitted with a WW + WZ contribution with a p-value of 0,12% (a 3σ evidence) [15].

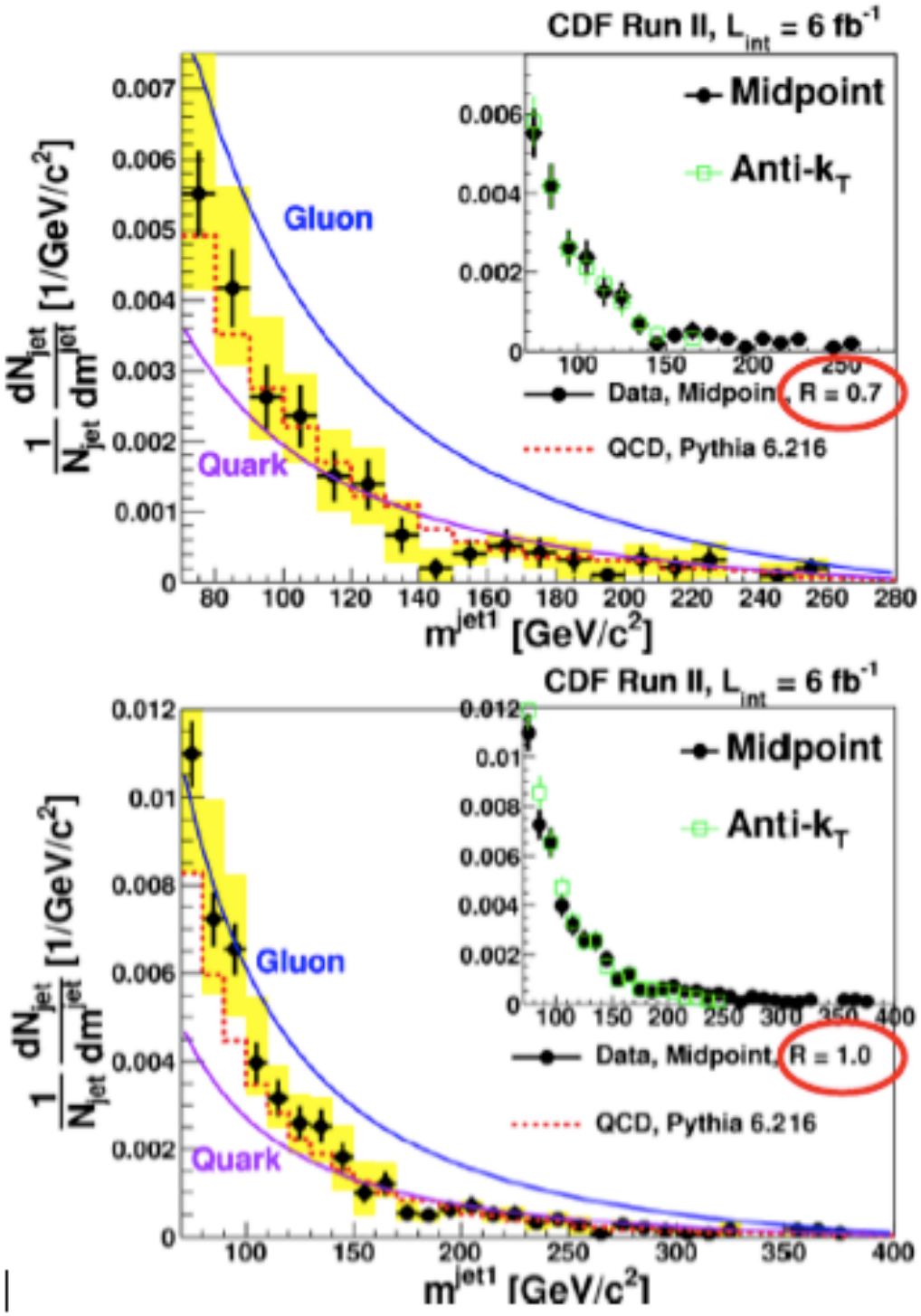

Figure 17: Inclusive jet distribution as a function of mass, indicating that quark jets dominate over gluon jets at large mass [16].

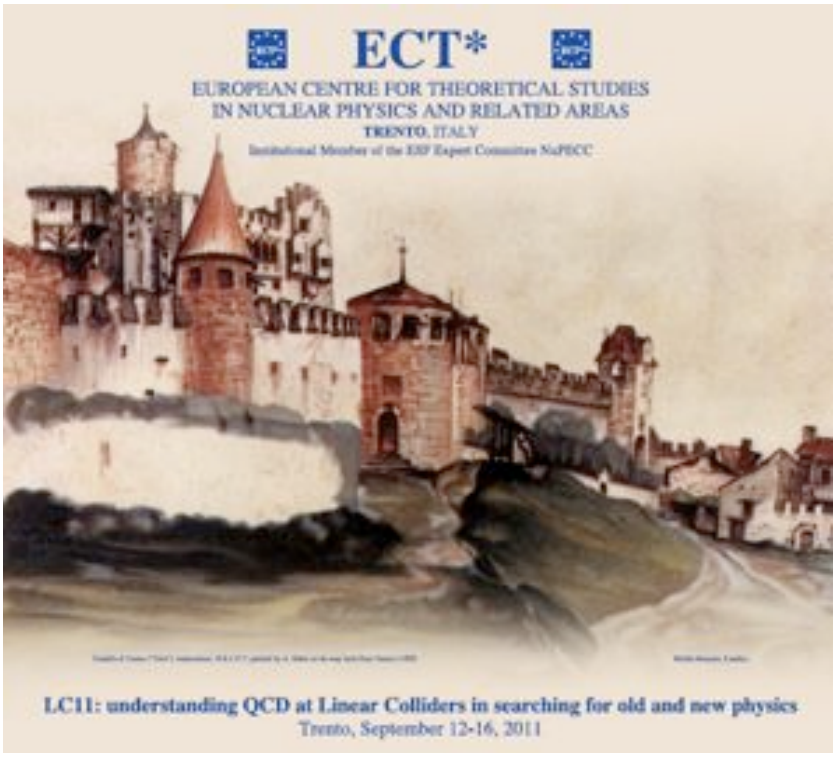

Castello di Trento painted by A. Dürer on his way back from Venice (1495).

5.2 A.D. Martin, E.G. de Oliveira and M.G. Ryskin - Parton distributions and the LHC

Parton distributions and the LHC

A.D. Martin [1]
Institute for Particle Physics Phenomenology, Durham University, DH1 3LE, UK
A.D.Martin@durham.ac.uk

E.G. de Oliveira and M.G. Ryskin
Instituto de Física, Universidade de São Paulo, Brazil and PNPI, St Petersburg, Russia

Abstract To date, observations at the LHC are in agreement with Standard Model expectations based on the known PDFs. Precise measurements of W, Z, $t\bar{t}$ and jet production at the LHC will, in turn, improve our knowledge of the PDFs. In addition, by studying forward-going relatively low-mass systems, the LHC has the possibility to probe the very low x domain at low scales, where BFKL, non-linear absorptive and saturation effects may be illuminated. In particular, we discuss the possibility of using forward-going $b\bar{b}$ production at the LHC to pin down the gluon PDF at very low x. We describe how the huge factorization scale uncertainty may be reduced, so that the shape of the x behaviour of the gluon can be measured down to $x \sim 10^{-5}$.

1 Introduction

The global analyses of HERA, Tevatron and low-energy fixed target data have reliably determined the parton distributions functions (PDFs) of the proton, at least in the kinematic domain $x \gtrsim 10^{-3}$ and $Q^2 \gtrsim 4$ GeV^2, see, for example, Refs. [1, 2, 3]. These PDFs are important ingredients in the predictions of reaction cross sections at the LHC. To date, many processes have been observed at the LHC, all of which appear to be in good agreement with Standard Model expectations. In particular, the expected rates for the central production of W, Z, and Higgs bosons, rely on PDFs in the domain where they are well known, see Fig. 1. As the observations of W, Z, $t\bar{t}$ and jet production at the LHC increase in precision, they will, in turn, increase our knowledge of the PDFs.

However existing accelerator data do not constrain the behaviour of the low x PDFs. Indeed, if $Q^2 \sim 4$ GeV^2, then already for $x \lesssim 10^{-3}$ there is a significant difference between the gluon distributions found in the different global PDF analyses. On the other hand, this is just the region sampled by the underlying events at the LHC, which becomes increasingly important with the "pile-up" of interactions in each bunch crossing as the LHC luminosity is raised.

[1] Speaker

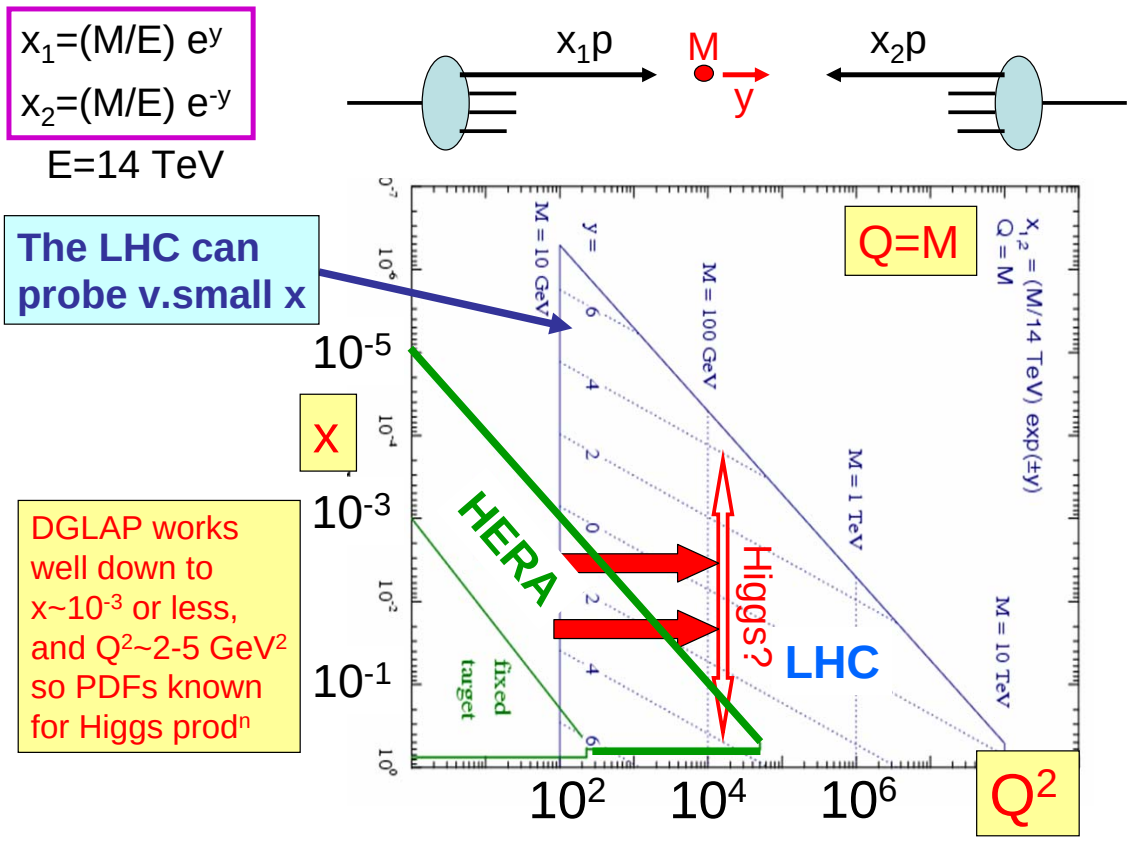

Figure 1: The LHC reach, at 14 TeV, for producing a system of mass M with rapidity y, which depends on PDFs with $x_{1,2} = (M/\sqrt{s})e^{\pm y}$ and $Q^2 \sim M^2$. The block arrows represent the DGLAP PDF evolution from HERA (Tevatron and fixed-target) data, relevant for the central production ($|y| < 1$) of a Higgs boson if it has a mass 130 GeV.

Here, we will concentrate on how observations at the LHC may illuminate knowledge of PDFs in the low x domain, see Fig. 1. Apart from the practical reason of improving knowledge of the underlying events, there is much theoretical interest in the very low x domain at low Q^2. The schematic plot of Fig. 1, shown in Fig. 2, illustrates the dominance of BFKL evolution in this LHC domain, with the onset of non-linear absorptive effects, leading perhaps to gluon saturation as smaller and smaller x values are probed at the LHC. This may prove to be a particularly reliable way to study these effects.

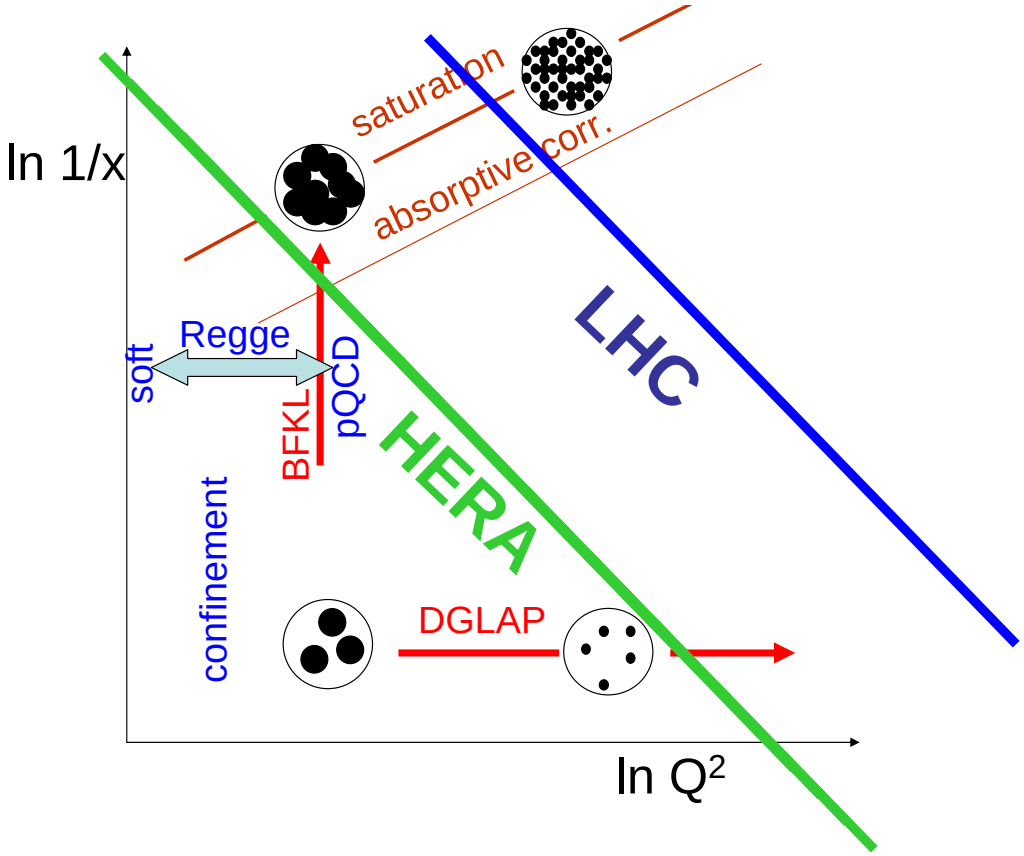

Figure 2: As compared to HERA, processes observed at the LHC can probe the very small x domain, where first BFKL dominates, then where absorptive effects may occur and finally where gluon saturation may set in.

2 LHC probes of the low x region

We see from Fig. 1 that W production in the very forward region can probe the PDFs for small x. For example, at the LHC energy of 7 TeV, a forward W with rapidity $y = 4$ depends on PDFs with $x_2 = 2 \times 10^{-4}$ and $x_1 = 0.6$. This region has already started to be probed by the LHCb experiment. However the data are sensitive to the u, d sea quark PDFs at small x, and, moreover, at high scales, $Q^2 \sim M_W^2$. Observation of forward going low-mass Drell-Yan pairs, $pp \to (\gamma^* \to \ell^+\ell^-) + X$, can sample very small x values at lower scales, $Q^2 \sim M_{\ell\ell}^2$. However, on the theoretical side, the convergence of the perturbative (LO, NLO, NNLO) expansion is slow in this domain [4]; see also the discussion in Section 3.1 for a related problem. However, these Drell-Yan processes do not probe the gluon PDF. For this, observation of forward going $b\bar{b}$ events looks promising, where the dominant subprocess is $gg \to b\bar{b} + X$.

3 $b\bar{b}$ production at the LHC

To study the behaviour of the gluon distribution in the very low-x region, at low scales, it appears attractive to use the inclusive $b\bar{b}$ production at the LHC. Due to the rather large mass of the b quark, the process may be described in the framework of perturbative QCD. The dominant contribution arises from the $gg \to b\bar{b}$ hard subprocess. The cross section resulting from this subprocess has the following structure

$$d\sigma/d^3p \;=\; \int dx_1 dx_2 \; g(x_1,\mu_F) \; |\mathcal{M}(p;\mu_F,\mu_R)|^2 \; g(x_2,\mu_F) \; , \tag{1}$$

where the gluon densities, $g(x_i,\mu_F)$, are taken at some factorization scale μ_F, and the matrix element squared, $|\mathcal{M}|^2$, describes the cross section of the elementary $gg \to b\bar{b}$ subprocess. The process samples gluons which carry momenta fractions of the initial protons are $x_{1,2} = (m_{\rm hard}/\sqrt{s})\exp(\pm y)$. At the LHC energy of $\sqrt{s} = 7$ TeV, and rather large rapidity[2], $y \sim 5$, of the whole system produced in hard subprocess, one can probe the gluon densities with $x \sim 10^{-5}$. For this estimate we have taken the mass created in 'hard subprocess' $m_{\rm hard} = 10$ GeV. Recall that at present there are no data in this small x domain and different global parton analysis predict quite different gluons, especially close to the input scale for parton evolution. It therefore appears that the LHC, and the LHCb experiment in particular, offers a golden opportunity to make a precise determination of the gluon in this important low x domain. However, first we must face the problem of the choice of factorization and renormalization scales.

3.1 Problems with choice of factorization and renormalization scales

A factorization scale μ_F is needed to separate the contributions hidden in the incoming PDFs from those that included in the hard matrix element $|\mathcal{M}|^2$. Contributions with low gluon virtuality $q^2 < \mu_F^2$ are included in the PDF, while those with $q^2 > \mu_F^2$ are assigned to the matrix element. The second scale, the renormalization scale μ_R, in (1) is necessary to fix the small value of QCD coupling, $\alpha_s(\mu_R)$, and to justify the perturbative QCD approach. In principle, if all contributions (NLO, NNLO, etc.) are included, then calculated cross section would not depend on the values chosen for both of the scales μ_R and μ_F.

However, one faces difficulties in the description of the new LHC data [5] for $b\bar{b}$ production. Following Ref. [6], we list these below.

- The NLO QCD prediction strongly depends on the choice of factorization scale, see Fig. 3. For example, the result obtained with the choice $\mu_F = 2m_\perp$ is more than twice larger than that for the case of $\mu_F = m_\perp/2$, where here $m_\perp \equiv \sqrt{p_T^2 + m_b^2}$).

[2]Rapidities in this range are optimal for the LHCb experiment [5].

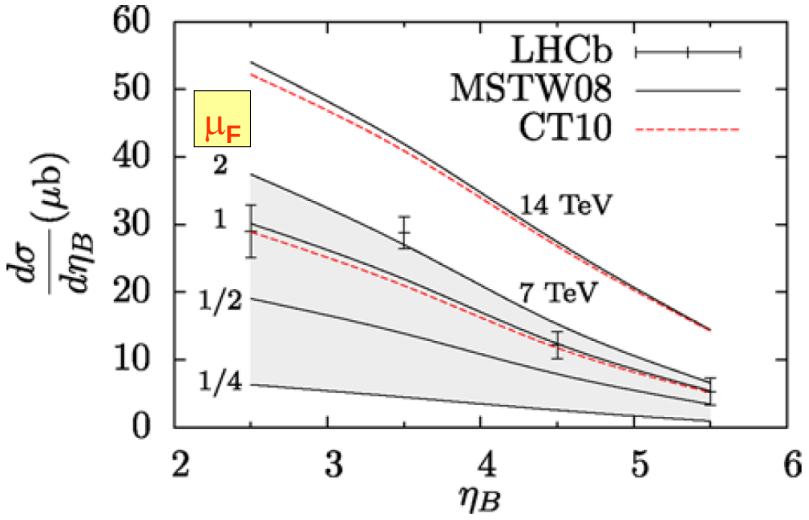

Figure 3: The NLO predictions for the cross section of $b\bar{b}$ production, obtained using the MSTW08 [1] (continuous curves) and CT10 [2] (dashed curves) parton sets, at the LHC energies of 7 TeV and 14 TeV, as a function of pseudo-rapidity η_B with scale $\mu_F = m_\perp$ and m_b=4.75 GeV; compared with LHCb data at 7 TeV [5]. The predictions using MSTW08 partons are also shown for four choices of factorization scale: $\mu_F = 2m_\perp,\ m_\perp,\ m_\perp/2,\ m_\perp/4$. The renormalization scale is set to $\mu_R = m_\perp$. The figure is taken from Ref. [6].

- Moreover, at the NLO, we have a sizeable contribution from the $2 \to 3$ ($gg \to b\bar{b}g$) subprocess, where one additional gluon is emitted in the hard collision. This leads to a considerable smearing of the x domain where we sample the incoming gluons. The smearing is especially strong if we adopt a low factorization scale, because then there is a large phase space allowed for gluon emission from the matrix element. Note that the probability of emission is enhanced by two large logarithms[3]: $\ln(m_\perp^2/\mu_F^2)$ and $\ln(1/x)$. The large longitudinal logarithm, $\ln(1/x)$, is due to the emission of gluons which carry

[3]The $\ln(1/x)$ enhancement is the main origin of the scale uncertainty observed in the collinear NLO approach at very small x. If we were to decrease the factorization scale μ_F, then we have to move gluons with $p_{gT} \sim \mu_F$ from the PDF to the matrix element. The problem is that, at very low x, there may be several gluons emitted in the PDF, while only one gluon emission is allowed in the NLO matrix element. This spoils the compensation between the variations of $|\mathcal{M}|^2$ and the PDF, which should provide (and, indeed, in the larger x region, does provide) the stability of the results under scale variations.

away almost all of the momentum of the incoming parton. As a result the momentum fraction, z, which goes to the $b\bar{b}$ pair is small. That is, the mass of pair becomes much less than the mass created in the NLO subprocess, and hence $M^2_{b\bar{b}}/m^2_{\rm hard} = z \ll 1$. In practice, the mass $M_{b\bar{b}} > 2m_b$ is fixed (and limited from below). As a consequence $m_{\rm hard} > 2m_b/\sqrt{z}$ and therefore we sample gluons with rather large values of x_2. In particular, Fig. 4 shows that if we choose a scale $\mu_F = m_\perp/4$ then the major contribution comes from $x \sim 10^{-2}$, and not from $x \sim 10^{-5}$ as we had hoped. From this viewpoint it would be better to take a large μ_F.

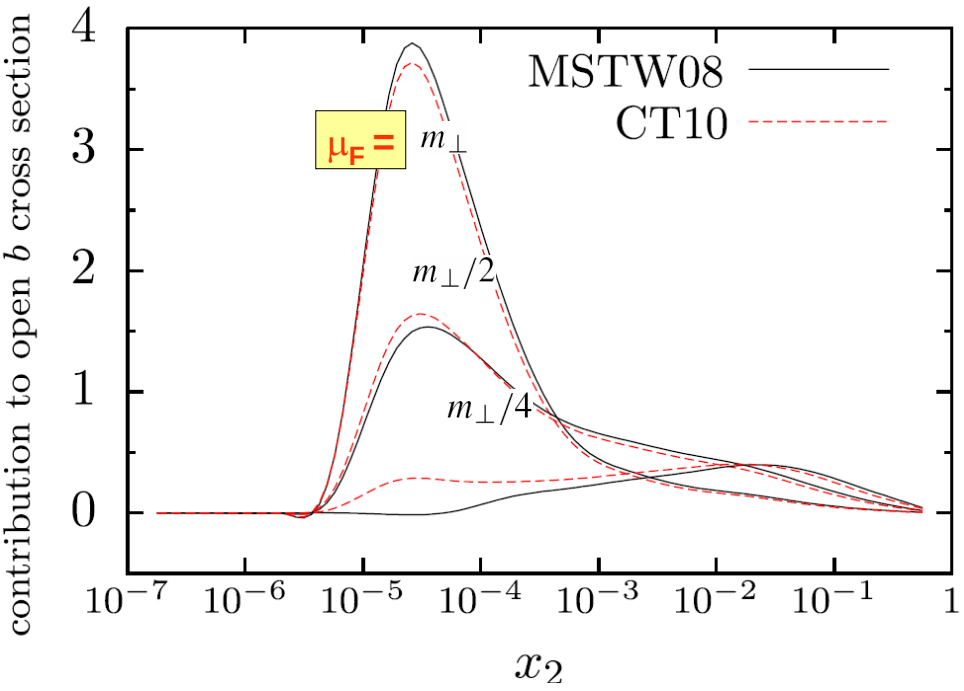

Figure 4: The distribution of the values of x_2 of the gluons sampled in NLO $b\bar{b}$ production with $\eta_b = 5.5$ at the LHC energy of 7 TeV, after the cross section has been integrated over x_1 and p_T. The renormalisation scale is taken to be $\mu_R = m_\perp$. The figure is taken from Ref. [6].

- On the other hand, to differentiate between the low x gluons it would be better to work with a relatively low μ_F, where the difference between the different global PDF analyses is larger. At high scales μ_F, a large fraction of low x gluons comes from a region of much larger x in input distribution, where the input distribution is already well constrained

by existing data. Therefore, at larger μ_F, predictions for LHCb $b\bar{b}$ production, based on different PDF sets, become close to each other.

- Moreover, recall that since for a large scale $\mu_F \sim 2m_\perp$ up to the half of the cross section originates from rather heavy virtual gluons, the original perturbative calculation, which assumes that the gluon virtuality q^2 is small in comparison with the quark mass (or $m_\perp$), becomes inconsistent.

- Finally, at NLO, we also have an unavoidable $\pm 30\%$ uncertainty in the prediction of $b\bar{b}$ production arising from the choice of the renormalization scale, μ_R.

However, despite these difficulties, it is still possible to use the LHC $b\bar{b}$ data to make a measurement of the shape of the gluon PDF in the interval $10^{-5} \lesssim x \lesssim 10^{-3}$.

3.2 Fixing the renormalization scale

To overcome the problems associated with the choice of renormalization scale, we may ask for the measurement of the cross section of $b\bar{b}$ events in which the two quarks balance each other in the transverse momentum plane to some accuracy; that is $\vec{p}_{1T} \simeq -\vec{p}_{2T}$. In other words, to seek events which satisfy a cut on the vector sum of the transverse momenta of the heavy quarks,

$$|\vec{p}_{1T} + \vec{p}_{2T}| < k_0 \ . \tag{2}$$

We cannot measure the quark momentum directly. However the momentum of the B-meson can be measured, and due to the strong leading effect in B-meson production, the event selection, proposed in (2), can be performed with sufficient accuracy for those events with reasonably small transverse momenta of the B-mesons, say, $|\vec{p}_{TB}| < 5$ GeV.

Note that, there are a few reasons which do not allow us to take the value of k_0 too small. First, there is an infrared divergency at $k_0 \to 0$ (see, for example, [7]). The collinear (single log) part of this divergency should be absorbed by the incoming parton distributions and the b-quark fragmentation function. Since the parton distributions are not known for a very low starting scale $Q_0 < 1$ GeV we have to take $k_0 > Q_0$. However, the main divergency is caused by the Sudakov-like double-logarithmic form factors. To ensure that the value of the corresponding double logarithm, $\ln^2(m_\perp/k_0)$, is not too large, we take $k_0 = 2$ GeV$\sim m_b/2$ and have introduced the additional cut on the transverse momenta of the b-quarks, $p_T < 5$ GeV.

Next, the value of the final B-meson momentum may be affected by the hadronization leading to some uncertainty $\delta p_T \sim 0.4$ GeV. This uncertainty should not be large in comparison with k_0. Moreover in order to better constrain the x values of the gluons in our selected events, we may put an additional cut on the pseudo-rapidities of the B-mesons, say,

$$\eta - 0.5 < \eta_1, \eta_2 < \eta + 0.5. \tag{3}$$

With the above kinematics it is natural to choose $\mu_F = k_0$. At first sight, in this way we appear to have excluded any gluon emission due to the NLO matrix element; a gluon with a transverse momentum, p_{gT}, less than μ_F should be included in the PDF, while one with $p_{gT} > \mu_F$ spoils the cut (2). However, this is not true at NLO. DGLAP evolution is written in terms of parton virtualities $q^2 = q_T^2/(1-z)$, where z is the fraction of parent parton momentum carried by the next (in this case, final) parton. So, a relatively soft gluon with $p_{gT} < \mu_F$ may correspond to $q^2 > \mu_F^2$, and thus be assigned to the matrix element. However, this will happen mainly for large z close to 1, that is, in a situation where the emission of an additional (and now *soft*) gluon does not change the mass $m_{\rm hard}$ created by the NLO subprocess too much; and thus does not smear out the low x of the gluon sampled by the process.

3.3 Scale sensitivity for $b\bar{b}$ production at small x

To illustrate the dependence of the predictions for $b\bar{b}$ production on the choice of the factorization scale, μ_F, we evaluate the cross section for the production of b and $\bar{b}$ quarks with both of their pseudo-rapidities in the interval $5 < \eta_{1,2} < 6$, first using $\mu_F = 2$ GeV, and then for $\mu_F = 4$ GeV. We repeat the exercise for the interval $2 < \eta_{1,2} < 3$. For both choices of rapidity intervals, the cross section calculated with the higher scale, $\mu_F = 4$ GeV, is about 3 - 4 times larger than that calculated with $\mu_F = 2$ GeV, see Fig. 5. Such a strong factorization scale dependence is due to the behaviour of the incoming parton densities. In the small x domain, relevant for the LHC, the summation of the double logarithmic terms,

$$\Sigma_n c_n (\alpha_s \ln(1/x) \ln(\mu_F^2/Q_0^2))^n, \tag{4}$$

in the DGLAP evolution, leads to an

$$\exp\left(\sqrt{(4N_c\alpha_s/\pi)\ln(1/x)\ln(\mu_F^2/Q_0^2)}\right) \tag{5}$$

growth of the gluon density with increasing μ_F. The exponential growth comes from the sum over the possibilities of emitting different numbers of gluons. The growth cannot be compensated by the 'hard' matrix element, which at NLO level, allows for the emission of only one gluon. This double-logarithmic effect is the main source of the strong factorization scale dependence of the predictions for the single b-quark inclusive cross section.

Note however, that if we choose a 'large' value of the scale, $\mu_F > k_0$, then we invalidate our proposed 'p_T' cut (2). Recall that an *integrated* parton density at a scale μ_F includes the effects of all partons with transverse momenta $k_t < \mu_F$; and the transverse momentum of an incoming parton with a 'large' k_t will spoil the p_T balance in (2). To control the transverse momenta of the incoming partons we may use the *unintegrated* gluon distributions, $f_g(x, k_t, \mu_F)$, and then integrate over all $k_t < k_0$.

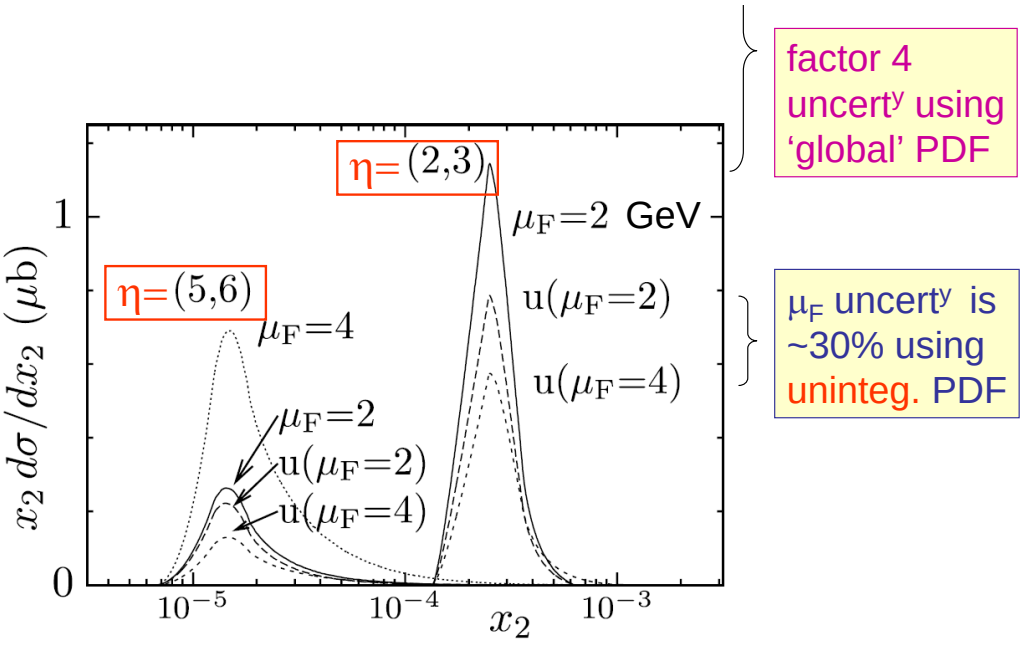

Figure 5: The $b\bar{b}$ cross sections at the 7 TeV LHC as a function of the momentum fraction carried by the slowest gluon, after cuts (2) and (3) have been imposed, predicted using integrated and unintegrated PDFs for two choices of factorization scale, $\mu_F = 2$ and 4 GeV. The prefix "u" indicates unintegrated PDFs are used. The left and right plots correspond to the rapidity intervals (5,6) and (2,3) specified by taking $\eta = 5.5$ and $\eta = 2.5$ in (3). The $\mu_F = 4$ GeV prediction obtained from integrated partons is not shown for the latter interval since it about 4 times higher than that for $\mu_F = 2$ GeV. CT10 NLO partons [2] are used for both the integrated and unintegrated PDFs, where the latter are calculated as in [8]. The figure is taken from Ref. [6].

Contrary to conventional integrated PDFs, where the scale μ_F fixes the maximum allowed value of the parton transverse momentum, k_t, now, in terms of unintegrated PDFs, the value of k_t, is known. In the latter case, the scale μ_F controls the angular ordering of emitted gluons [8]. Besides this, the unintegrated PDFs resum all the virtual DGLAP loop contributions up to the scale μ_F. This resummation produces the Sudakov factor $T(k, \mu_F)$ which accounts for the probability *not* to emit an extra parton and thus not to enlarge k_t during the evolution from k to μ_F. The virtual loop contribution does not depend on x and therefore in the low x region it is not enhanced by the large logarithm, $\ln(1/x)$. So, we expect a much better compensation between the hard matrix element and the unintegrated PDF under variations of

the factorization scale μ_F. Recall that the upper limit of k_t of the gluon is now *exactly* fixed by the value of k_0 of the cut proposed in (2).

As anticipated, the net effect of a procedure [6], based on NLO 'unintegrated gluons' [8], is a great reduction in the dependence on the choice of the factorization scale. For example, changing the scale μ_F from 2 to 4 GeV now leads to less than 30(40)% decrease in the prediction of the $b\bar{b}$ cross section in the intervals $2 < \eta < 3$ (and $5 < \eta < 6$), rather than the factor of 4 (3) increase, see Fig. 5.

Despite these uncertainties in the normalization, the expected *ratio* of the cross sections measured in different rapidity intervals is quite stable and is driven entirely by the x behaviour of the gluon. After imposing the cuts of (2) and (3), the variation of the mass, $m_{\rm hard}$, created in the hard subprocess, is strongly limited. The contribution of the $2 \to 3$ subprocess never exceeds 40% of the whole cross section; typically it only amounts to about 1/3. Moreover, this $2 \to 3$ contribution arises from relatively soft gluon emission, which does not change $m_{\rm hard}$ very much. An important consequence is that these $b\bar{b}$ events in different intervals of pseudo-rapidity, η, sample the gluon in rather narrow intervals of x (see Fig. 5), which allows a precise study of the shape of gluon x distribution.

4 Conclusion

The precision of LHC data requires the use of NNLO PDFs. The existing PDFs are sufficiently well known to describe the production of heavy-mass systems, such as W, Z and $t\bar{t}$ production, and to provide estimates of Higgs production. As the precision of the LHC measurements increases, they, in turn, will improve our knowledge of the PDFs.

Our main concern has been the possibility of the LHC making measurements of forward going, relatively low-mass, systems to probe PDFs at very low x and low scales. Here, we face the theoretical problem of the great sensitivity of the predictions to the choice of the factorization scale. Taking forward going $b\bar{b}$ production as an example, we have described a procedure that overcomes this problem, and which should allow the LHC to measure the shape of the gluon distribution at small values of x.

Acknowledgements

One of us (A.D.M) thanks the organizers of the Workshop and, in particular Giulia Pancheri, for their efforts in making the meeting such a success; and thanks both ECT* and INFN for support. E.G.O is supported by FAPESP (Brazil) under contract 2011/50597-8.

References

[1] A.D. Martin, W.J. Stirling, R.S. Thorne and G. Watt, Eur. Phys. J. C **63**, 189 (2009).

[2] H. L. Lai, M. Guzzi, J. Huston, Z. Li, P. M. Nadolsky, J. Pumplin and C. P. Yuan, Phy. Rev. **D82**, 074024 (2010).

[3] NNPDF, R.D. Ball *et al.*, Nucl. Phys. B **849**, 296 (2011).

[4] A.D. Martin, W.J. Stirling, R.S. Thorne and G. Watt, Proc. of DIS2008, London, 30; arXiv:0808.1847.

[5] R. Aaij *et al.* [LHCb Collaboration], Phys. Lett. **B694**, 209 (2010).

[6] E.G. de Oliveira, A,D. Martin and M.G. Ryskin, Eur. Phys. J. C **71**, 1727 (2011),

[7] S. Frixione and G. Ridolfi, Nucl. Phys. **B507**, 315 (1997).

[8] A.D. Martin, M.G. Ryskin and G. Watt, Eur. Phys. J **C66**, 163 (2010).

5.3 A.D. Martin, V.A. Khoze and M.G. Ryskin - Partonic description of soft high energy pp interactions

Partonic description of soft high energy pp interactions

A.D. Martin [1]
Institute for Particle Physics Phenomenology, Durham University, DH1 3LE, UK
A.D.Martin@durham.ac.uk

V.A. Khoze and M.G. Ryskin
IPPP, Durham University, UK and PNPI, Gatchina, St. Petersburg, Russia

Abstract We discuss how the main features of high-energy 'soft' and 'semihard' pp collisions may be described in terms of parton cascades and multi-Pomeron exchange. The interaction between Pomerons produces an effective infrared cutoff, $k_{\rm sat}$, by the absorption of low k_t partons. This provides the possibility of extending the parton approach, used for 'hard' processes, to also describe high-energy soft and semihard interactions. We outline a model which incorporates these features. Finally, we discuss what the most recent LHC measurements in the soft domain imply for the model.

1 A unified description?

'Soft' and 'hard' high-energy pp interactions are described in different ways. The appropriate formalism for high-energy soft interactions is based on Reggeon Field Theory with a phenomenological (soft) Pomeron, whereas for hard interactions we use a QCD partonic approach, where the (QCD) Pomeron is associated with the BFKL vacuum singularity [1]. However, the two approaches appear to merge naturally into one another. That is, the partonic approach seems to extend smoothly into the soft domain.

The BFKL equation describes the development of the gluon shower as the momentum fraction, x, of the proton carried by the gluon decreases. That is, the evolution parameter is $\ln(1/x)$, rather than the $\ln k_t^2$ evolution of the DGLAP equation. Formally, to justify the use of perturbative QCD, the BFKL equation should be written for gluons with sufficiently large k_t. However, it turns out that, after accounting for NLL$(1/x)$ corrections and performing an all-order resummation of the main higher-order contributions [2], the intercept of the BFKL Pomeron depends only weakly on the scale for reasonably small scales. The intercept is seen to be $\Delta \equiv \alpha_P(0) - 1 \sim 0.35$ over a large interval of smallish k_t, Fig. 1. Thus the BFKL Pomeron is a natural object to continue from the 'hard' domain into the 'soft' region.

[1] Speaker

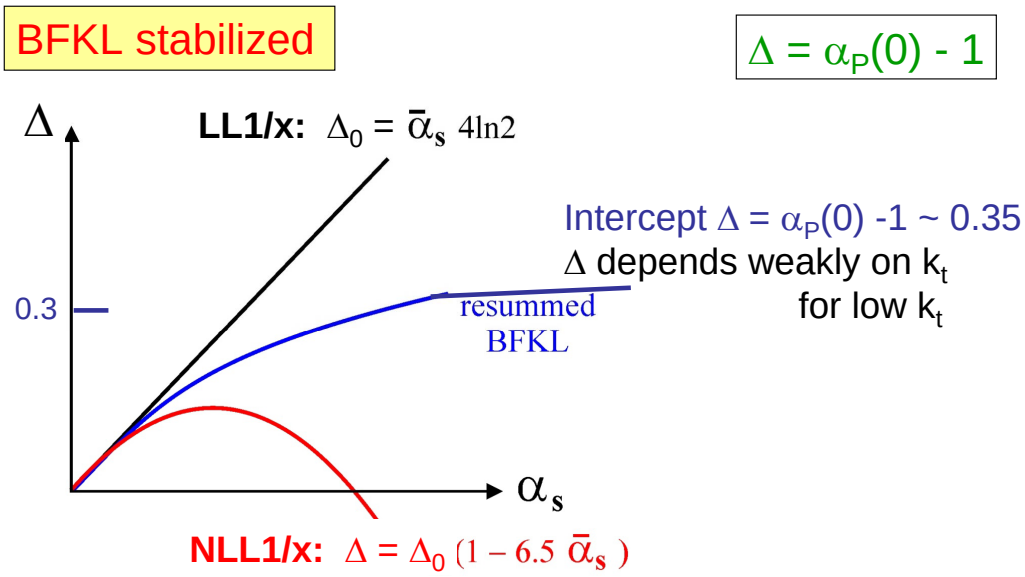

Figure 1: The behaviour found for the Pomeron intercept at leading and next-leading $\log(1/x)$ order, where $\bar{\alpha}_s \equiv \alpha_s/3\pi$. When an all-order resummation of the main high-order contributions is included, Δ tends to a value of about 0.35 for reasonably large values of α_s.

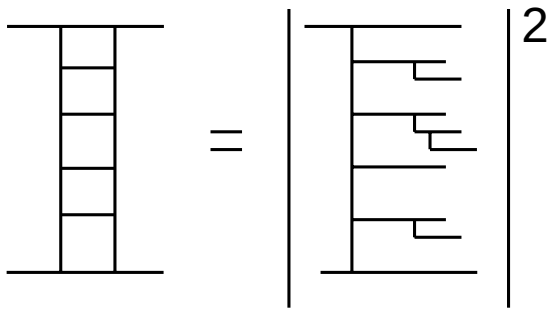

Figure 2: The cascade structure of a gluon ladder. The BFKL or QCD Pomeron is the sum of ladder diagrams, each with a different number of rungs.

The BFKL or QCD Pomeron may be viewed as a sum of ladders based on the exchange of two t-channel (Reggeized) gluons. Each ladder produces a gluon cascade which develops in $\ln(1/x)$ space, and which is not strongly ordered in k_t, see Fig. 2. There are phenomenological arguments (such as the small slope of the Pomeron trajectory[2], the success of the Additive Quark Model relations[3], etc.) which indicate that the size of an individual Pomeron is relatively

[2]Recall that $\alpha'_P \propto 1/\langle k_t^2 \rangle \propto R^2_{\rm Pom}$.

[3]The argument is best seen by analogy with nuclear physics. For light nuclei we have 'additive' cross sections, $\sigma = A_1 A_2 \sigma_{nn}$, since the nuclei radii $R \gg r_{nn}$. On the other hand for a heavy nucleus, where $r_{nn} \sim R$, large Glauber corrections break the additive result. Similarly, the experimental success of the AQM indicates that $r_{qq} \sim R_{\rm Pom} \ll R_p$.

small as compared to the size of a proton or pion etc. Thus we may regard the cascade as a small-size 'hot-spot' inside the colliding protons.

At LHC energies the interval of BFKL $\ln(1/x)$ evolution is much larger than that for DGLAP $\ln k_t^2$ evolution. Moreover, the data already give hints that we need contributions not ordered in k_t, *à la* BFKL, since typically DGLAP overestimates the observed $\langle k_t \rangle$ and underestimates the mean multiplicity [3, 4]. Further, it is not enough to have only one Pomeron ladder exchanged; we need to include multi-Pomeron exchanges.

Basically, the picture is as follows. In the perturbative domain we have a single bare 'hard' Pomeron exchanged with a trajectory $\alpha_P^{\rm bare} \simeq 1.35 + \alpha'_{\rm bare} t$, where $\alpha'_{\rm bare} \lesssim 0.05$ GeV^{-2}. The transition to the soft region is accompanied by absorptive multi-Pomeron effects, such that an *effective* 'soft' Pomeron may be approximated by a linear trajectory $\alpha_P^{\rm eff} \simeq 1.08 + 0.25t$ in the *limited* energy range up to Tevatron energies [5]. This smooth transition from hard to soft is well illustrated by Fig. 3, which shows the behaviour of the data for vector meson ($V = \rho, \omega, \phi, J/\psi$) production at HERA, $\gamma^* p \to V(M)p$, as $Q^2 + M^2$ decreases from about 50 GeV^2 towards zero.

2 Multi-Pomeron diagrams

The *eikonal* model accounts for the multiple rescattering of the incoming fast particles. We have[4]

$$\mathrm{Im}T \;=\; (1 - e^{-\Omega/2}) \;=\; (\Omega/2) - (\Omega^2/8) + ... \tag{1}$$

which displays the multi-Pomeron corrections to the bare Pomeron amplitude, $\Omega/2$, that tame the power growth of the cross section with energy. Simultaneously, these multi-Pomeron diagrams also explain the growth of the central plateau [3, 4]

$$\frac{dN}{d\eta} \;=\; n_P \frac{dN_{1-\rm Pom}}{d\eta}, \tag{2}$$

where $dN_{1-\rm Pom}/d\eta$ is the plateau due to the exchange of one Pomeron, which is independent of collider energy. The growth is due to the increasing number, n_P, of Pomerons exchanged as energy increases. These (eikonal) multi-Pomeron contributions are included in the present Monte Carlos to some extent, as a Multiple Interaction (MI) option, but Pomeron-Pomeron interactions are not allowed for.

Since the (small size) Pomeron cascades (hot spots) occur at different impact parameters, b, there is practically no interference between them. Moreover, at this 'eikonal' stage, the multi-Pomeron vertices, which account for the interaction between Pomerons, are not yet included in the formalism. These are interactions between partons within an individual hot spot

[4]To allow for low-mass proton dissociation, the amplitude (1) is written in matrix form, T_{ik}, between (Good-Walker [6]) diffractive eigenstates.

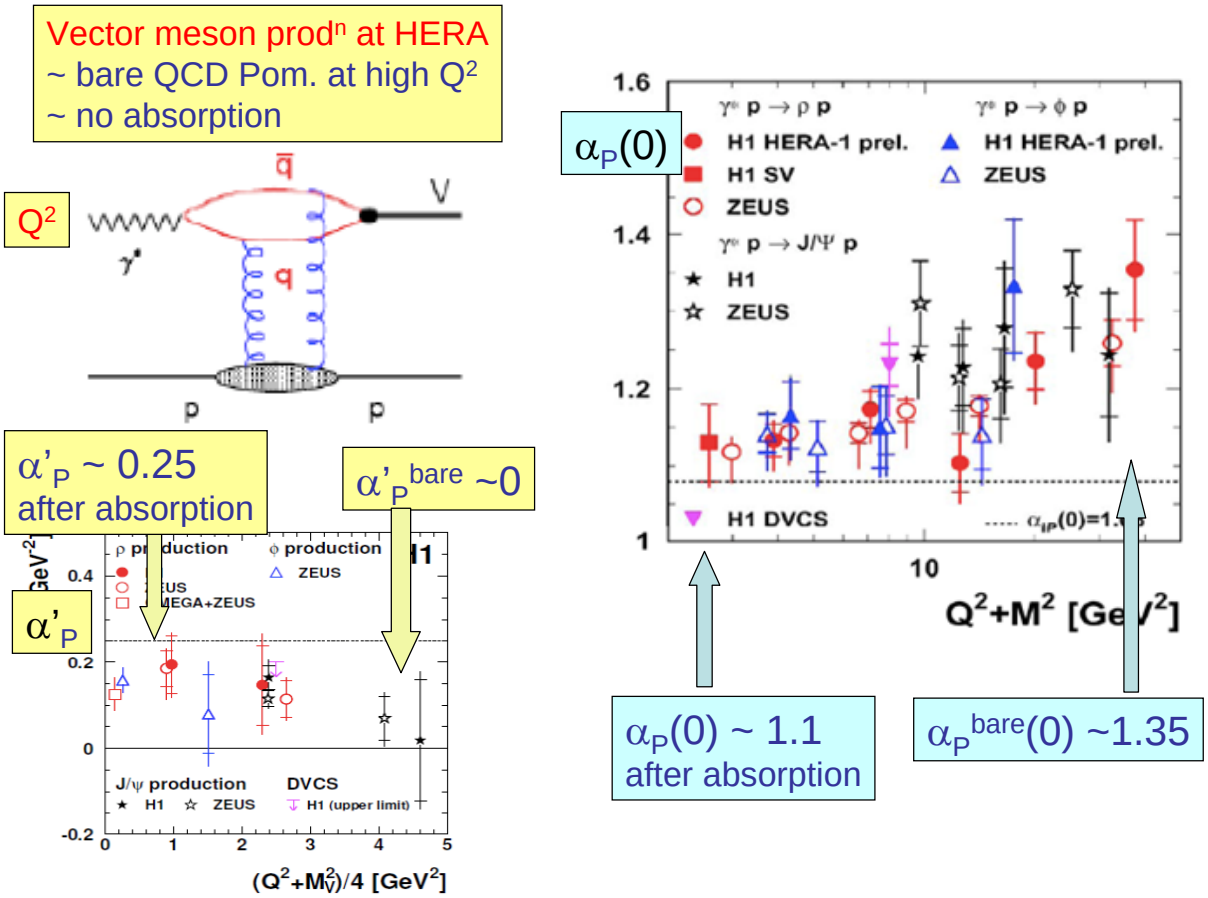

Figure 3: The parameters of the Pomeron trajectory, $\alpha_P(t) = \alpha_P(0) + \alpha'_P t$, determined from the energy and t behaviour of high energy HERA data for vector meson production, $\gamma^* p \to V(M)p$.

(Pomeron). Formally, these are NNLO interactions, but their contribution is *enhanced* by the large multiplicity of partons within a high-energy cascade. In terms of Reggeon Field Theory, the additional interactions are described by so-called *enhanced* multi-Pomeron diagrams, whose contributions are controlled by triple-Pomeron (and more complicated multi-Pomeron) couplings[5]. Recall that non-enhanced (eikonal) multi-Pomeron interactions are caused mainly by Pomerons occurring at different impact parameters, and well separated from each other in the b-plane. On the other hand, the enhanced contributions mainly correspond to additional interactions (absorption) within an *individual* hot spot, but with the partons well separated in rapidity.

The main effect of the enhanced contribution is the absorption of low k_t partons. Note that

[5]These diagrams are responsible for high-mass proton dissociation.

the probability of these additional interactions is proportional to $\sigma_{\rm abs} \sim 1/k_t^2$, and their main qualitative effect is to induce a splitting of low k_t partons into a pair of partons each with lower x, but larger k_t. Effectively this produces a dynamical infrared cut-off, $k_{\rm sat}$, on k_t, and partly restores a DGLAP-like k_t-ordering within the cascade at larger k_t.

3 Schematic sketches of the model

Qualitatively, the structure of soft interactions based on the 'BFKL' multi-Pomeron approach is as follows. The evolution produces a parton cascade which occupies a relatively small domain in b-space, as compared to the size of the proton. We have called this a hot spot. The multiplicity of partons grows as $x^{-\Delta}$, while the k_t's of the partons are not strongly ordered and depend weakly on $\ln s$. Recall $\Delta \equiv \alpha_P(0) - 1$. Allowing for the running of α_s, the partons tend to drift to lower k_t where the coupling is larger. This is shown schematically in Fig. 4(a).

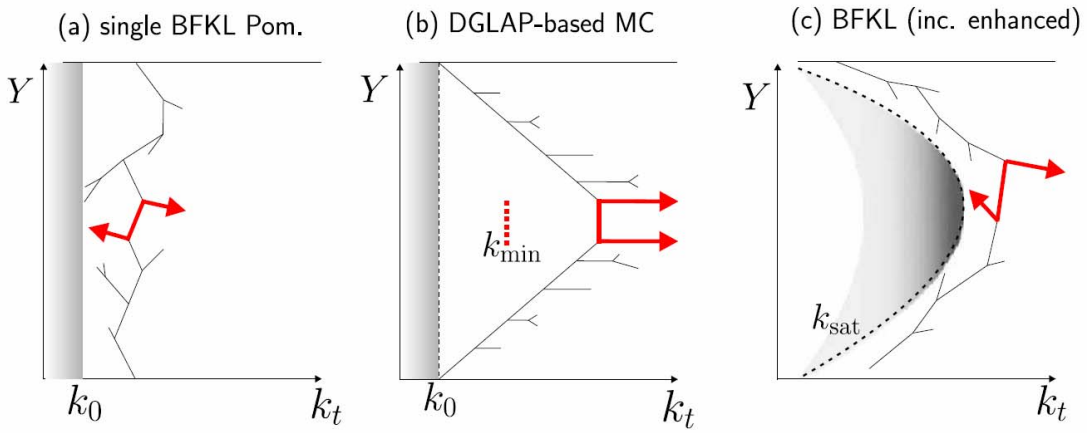

Figure 4: Sketches of the basic diagram for semi-hard particle production in pp collisions. The figure is taken from Ref. [7].

On the contrary, the DGLAP-based Monte Carlos generate parton cascades strongly ordered in k_t. That is, the parton k_t increases as we evolve from the input PDF of the proton to the matrix element of the hard subprocess, which occurs near the centre of the rapidity interval, Fig. 4(b). Since the cross section of the hard subprocess behaves as $d\hat{\sigma}/dk_t^2 \propto 1/k_t^4$, the dominant contributions come from near the lower limit $k_{\rm min}$, of the k_t integration. In fact, in order to describe the high-energy collider data, it is necessary to artificially introduce an energy dependent infrared cutoff; $k_{\rm min} \propto s^a$ with $a \sim 0.12$ [8]. This cutoff is only applied to the hard matrix element, whereas in the evolution of the parton cascade a constant cutoff k_0,

corresponding to the input PDFs, is used. Note that during the DGLAP evolution, the position of the partons in b-space is frozen. Thus such a cascade also forms a hot spot.

Accounting for the multiple interaction option, that is for contributions containing a few hot spots, we include the eikonal multi-Pomeron contributions, both for the DGLAP and BFKL based descriptions; that is the presence of a few small-size QCD Pomeron cascades.

Next, we include the enhanced multi-Pomeron diagrams introducing the absorption of the low k_t partons. The strength of absorption is driven by the parton density and therefore the effect grows with energy, that is with $\ln(1/x)$. We thus have an effective infrared cutoff, $k_{\rm sat}(x)$, which modifies the k_t distribution of the 'BFKL' cascade. The result is shown Fig. 4(c), which has some similarity to the DGLAP cascade of Fig. 4(b). However, now the cutoff $k_{\rm sat}$ is not a tuning parameter, but is generated dynamically by the enhanced multi-Pomeron diagrams. Recall that the same diagrams describe high-mass proton dissociation. That is, the value of the multi-Pomeron vertex simultaneously controls the cross sections of high-mass dissociation and the effective cutoff $k_{\rm sat}$ – two phenomena which, at first sight, appear to be quite different.

4 The Durham model

Main parameters:

$\Delta = \alpha_P(0)-1$, bare Pom. intercept (expect $\Delta \sim 0.35$) (s-dep.)

slope α'_P (taken zero in the 2011 KMR analysis)

d controls BFKL diffusion in log k_t

λ strength of triple (and multi) Pom. couplings (triple-Regge data)

γ specifies diff^{ve} estates (determined by low M diff^{ve} dissoc^{n})

N absolute value of initial gluon density

Figure 5: Some of the main parameters of the KMR model [9]; and how they are constrained.

How may the partonic model of the Pomeron be implemented in practice? To achieve this we note that the absorption of low k_t partons is driven by the opacity, Ω, which depends both on k_t and $y = \ln(1/x)$. The opacity, $\Omega_{ik}(y, k_t, b)$, is obtained [9] by solving the corresponding BFKL-type evolution equations in y with a simplified form of the kernel, but which incorporates the main features of BFKL: diffusion in $\ln k_t^2$ and $\Delta = \alpha_P^{\rm bare}(0) - 1 \simeq 0.35$. (A two-channel eikonal is used, $i, k = 1, 2$.) The inclusion of the k_t dependence is crucial for the transition from the hard to the soft domain. The absorptive factors in the equation embody the result

that there is less screening for larger k_t. The model [9] has only a small number of physically motivated parameters, see Fig. 5. whose values are tuned to reproduce the available high energy pp and $p\bar{p}$ data for $\sigma_{\rm tot}$, $d\sigma_{\rm el}/dt$, $\sigma_{\rm SD}^{{\rm low}M}$, $\sigma_{\rm SD}^{{\rm high}M}/dtdM^2$ etc. Given $\Omega_{ik}(y,k_t,b)$ we can, in principle, predict all soft and semi-hard inclusive phenomena, such as the survival factors of rapidity gaps, the PDFs and diffractive PDFs at low x and low scales, etc. The predictions for some of the cross sections are given in the left-half of Table 1, as their values will be relevant for the discussion in Section 5. It is important to note that hadronization can be incorporated

	KMR model				KMR 3-ch eikonal				
energy	$\sigma_{\rm tot}$	$\sigma_{\rm el}$	$\sigma_{{\rm low}M}^{\rm SD}$	$\sigma_{{\rm low}M}^{\rm DD}$	$\sigma_{\rm tot}$	$\sigma_{\rm el}$	$B_{\rm el}$	$\sigma_{{\rm low}M}^{\rm SD}$	$\sigma_{{\rm low}M}^{\rm DD}$
1.8	72.7	16.6	4.8	0.4	79.3	17.9	18.0	5.9	0.7
7	87.9	21.8	6.1	0.6	97.4	23.8	20.3	7.3	0.9
14	96.5	24.7	7.8	0.8	107.5	27.2	21.6	8.1	1.1
100	122.3	33.5	9.0	1.3	138.8	38.1	25.8	10.4	1.6

Table 1: Some results of the complete KMR model [9] prior to the LHC data (left-hand Table), and results obtained from a simpler approach, described in Section 5, based on a 3-channel eikonal description [10] of all elastic (and quasi-elastic) pp and $p\bar{p}$ data, including the TOTEM LHC data (right-half of the Table). $\sigma_{\rm tot}$, $\sigma_{\rm el}$ and $\sigma_{{\rm low}M}^{\rm SD,DD}$ are the total, elastic and low-mass single and double dissociation cross sections (in mb) respectively. The cross section $\sigma^{\rm SD}$ is the sum of the dissociations of both the 'beam' and 'target' protons. $B_{\rm el}$ is the mean elastic slope (in ${\rm GeV}^{-2}$), $d\sigma_{\rm el}/dt = e^{B_{\rm el}t}$, in the region $|t| < 0.2$ GeV^2. The collider energies are given in TeV. The former (latter) analysis fit to the CERN-ISR observations that $\sigma_{{\rm low}M}^{\rm SD}$=2(3) mb at $\sqrt{s} = 53$ GeV, with low mass defined to be $M < 2.5(3)$ GeV.

in this partonic description of the Pomeron, via Monte Carlo generators, which now would have the advantage of an effective dynamical cutoff $k_{\rm sat}$ to suppress low k_t parton emissions.

In summary, some of the main features of the model are:

(i) values of the high energy pp total cross section which are suppressed by absorptive corrections. Increasingly large values of $\sigma_{\rm SD}^{{\rm high}M}$ are found due to the increasing phase space with collider energy.

(ii) multi-Pomeron contributions arising from eikonal diagrams, that is the presence of a few small-size QCD Pomeron cascades (hot spots). This can be tested by measuring Bose-Einstein correlations, see Fig. 6. Specifically, identical pion correlations measure the size of their emission region.

(iii) multi-Pomeron contributions arising from enhanced diagrams, which lead to the absorption of low k_t partons and automatically introduce an effective cutoff $k_{\rm sat}$ which increases with energy. Due to the cutoff, $k_t > k_{\rm sat}$, the main inelastic process is *minijet* production. The

dominance of minijets can be tested by observing the two-particle correlations of secondaries at the LHC [7].

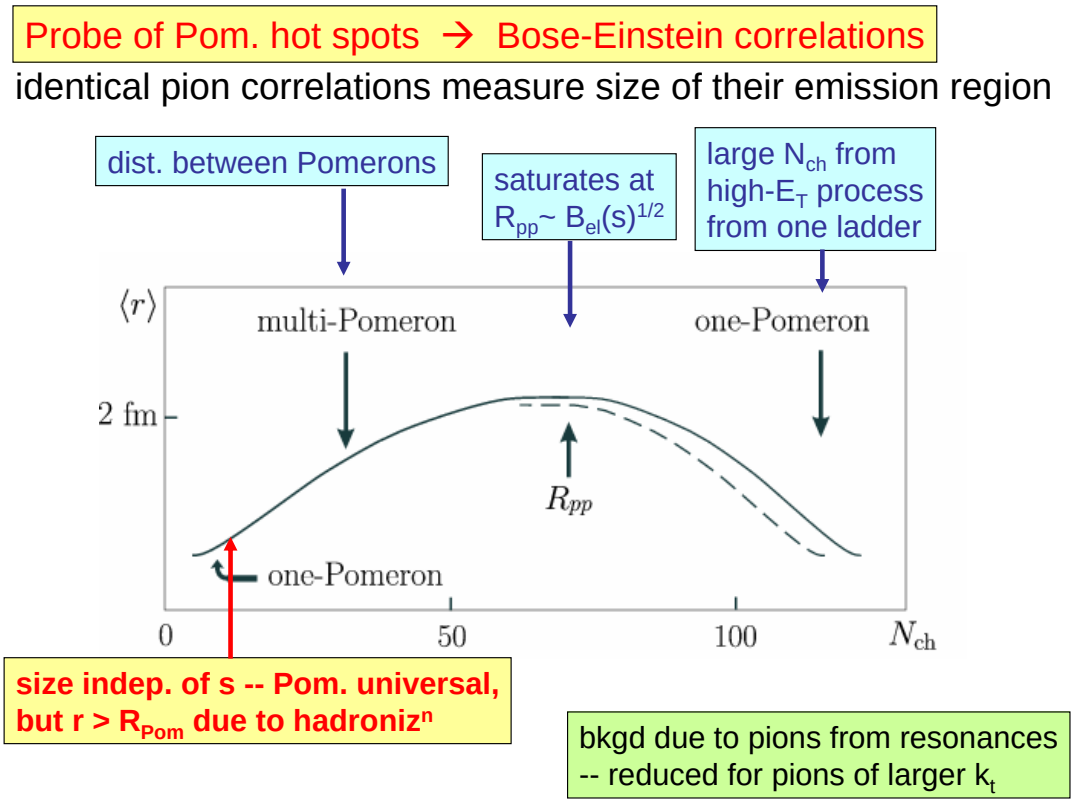

Figure 6: A sketch of the size $\langle r \rangle$ of the source of identical pions as a function of the multiplicity of charged particles in high-energy pp interactions [11]. The continuous and dashed curves correspond to, say, $\sqrt{s} = 7$ and 0.9 TeV respectively. At low $N_{\rm ch}$ we expect $\langle r \rangle$ to be independent of collider energy, $\sqrt{s}$, while for the plateau we expect $\langle r \rangle \sim R_{pp} \propto \sqrt{B_{\rm el}(s)}$ to increase very slowly with energy. Very high multiplicities are expected to arise from high-E_T events originating from a single ladder.

5 Implications of latest LHC 'soft' data

As a postscript to the Durham approach, we briefly discuss the implications of some recent LHC data on 'soft' diffractive processes which became available after the LC11 meeting.

First, we look at the implications of the recent TOTEM measurements, at 7 TeV, of $d\sigma_{\rm el}/dt$ down to $-t = 0.02$ GeV^{-2} [12]. From these data, TOTEM find

$$\sigma_{\rm tot} = 98.3 \text{ mb}, \qquad \sigma_{\rm el} = 24.8 \text{ mb}, \qquad \sigma_{\rm inel} = 73.5 \text{ mb}. \tag{3}$$

In the discussion below, we will ignore the (important) experimental errors, just to get some ideas of the trends of the data. The KMR model [9] predicts lower values of 88, 22 and 66 mb respectively, see the left-half of Table 1. The model was tuned to describe collider data for $\sigma_{\rm tot}$. At the Tevatron energy, where the CDF [13] and E710 [14] measurements disagree by some 10%, we were much closer to the lower E710 value.

To investigate this further, we performed a simpler study than that in [9]. The idea was to see if we can describe all the elastic pp and $p\bar{p}$ collider data in terms of a 3-channel eikonal model with only one Pomeron, with parameters that are naturally linked to the perturbative QCD (BFKL) framework, as discussed in the previous sections of this paper. However, for the simpler study [10], we used an effective Pomeron, rather than the bare QCD Pomeron with intercept $\Delta_{\rm bare} \equiv \alpha_P(0) - 1 = 0.32$ of [9]. With an economical parametrization of the three (Good-Walker) diffractive eigenstates, we are, indeed, able to obtain a good description of all these data for $|t| \lesssim 0.3$ GeV^2 with $\Delta_{\rm eff} = 0.14$, see Fig. 7. Since our eikonal model was devised to fit the data it is not surprising to have agreement with the TOTEM cross sections of (3). We call the Pomeron 'effective' since, although we accounted for eikonal rescattering of the incoming partons, unlike [9], we did not explicitly consider enhanced rescattering involving intermediate partons. The latter are included implicitly since their main effect is to renormalize the bare Pomeron trajectory.

However, some observations can be made. First, the eikonal description is close to the CDF total cross section value, and yet the description of the E710 $d\sigma_{\rm el}/dt$ measurements is good. Secondly, the insertion of the pion loop[6] into the Pomeron trajectory would decrease the total cross value in Table 1 by 1 mb, to 96.4 mb [10]. The conclusion is that there is quite a bit of uncertainty in the extrapolation of the $d\sigma_{\rm el}/dt$ data to the optical point, in addition to the 3-4% normalization uncertainty. Future precise elastic measurements[7] even closer to $t = 0$ will help reduce the uncertainty in the value of $\sigma_{\rm tot}$. If the values of $\sigma_{\rm tot}$ and $d\sigma_{\rm el}/dt$ at the LHC are confirmed to be significantly higher than those obtained in [9], then this full analysis should be repeated with these data included. It will result in a somewhat larger value of $\Delta_{\rm bare}$.

Let us now compare the results shown in Table 1 with the inelastic cross section obtained by CMS, ATLAS and ALICE at 7 TeV. The measured value is defined as the cross section with at least two particles in some central (but far from complete) rapidity, η, interval. For instance, ATLAS find $\sigma_{\rm inel} = 60.3$ mb for the cross section of processes with $M > 15.7$ GeV, that is $\xi = M^2/s > 5 \times 10^{-6}$ [20]. After a model dependent extrapolation to cover the entire rapidity interval they obtain $\sigma_{\rm inel} = 69.4$ mb. CMS find a very similar result, namely 68.0 mb

[6]Recall that the pion loop insertion modifies the Pomeron trajectory at very small t [18]. Indeed the presence of the 2π singularity at $t = 4m_\pi^2$ leads to some curvature in the t behaviour of $d\sigma_{\rm el}/dt$. That is, to some variation of the local elastic slope $B_{\rm el}(t)$. Including the pion loop gives an equally good description of the elastic data.

[7]Note also that the simultaneous measurement of bremsstrahlung photons, accompanying elastic proton-proton scattering in CMS will, with the help of the Zero Degree Calorimeter, allow an independent determination of $\sigma_{\rm el}/\langle B_{\rm el}\rangle$; see [19] for details.

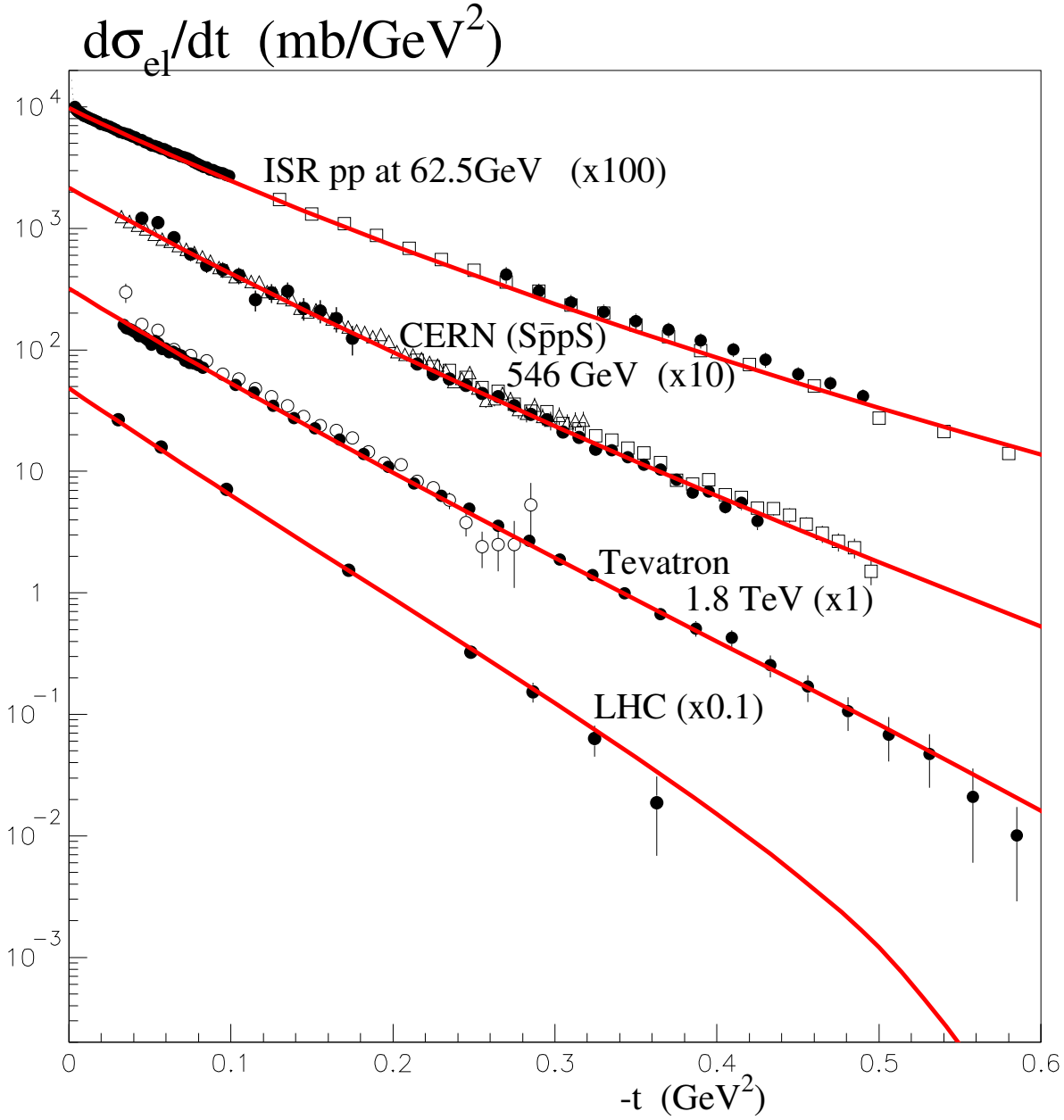

Figure 7: The description of the data for the differential cross sections for pp (or $p\bar{p}$) elastic scattering in the energy range 62.5 to 7000 GeV [12, 15, 13, 14, 16] using a 3-channel eikonal model. The Tevatron data with open and closed circles are those of the CDF and E710 collaborations respectively. Only very selected TOTEM points are shown, which have been read off their published plot. The excellent agreement of our model with the data for small $|t|$ is achieved with a very economical parametrization of the diffractive eigenstates. It is straightforward to describe the elastic data in the region of the diffractive LHC dip [17], but at the expense of a more complicated parametrization of the form factors of the three eigenstates.

[21]. ALICE also get a similar result [22]. These estimates are about 5 mb lower than the recent TOTEM value of 73.5 mb of (3). The difference may be attributed to the extrapolated values being 5 mb deficient for low-mass diffraction. (The extrapolation in the high-mass interval is confirmed by the ATLAS measurement $d\sigma/d\Delta\eta \simeq d\sigma/d\ln M^2 \simeq 1$ mb per unit of rapidity [23].) More specifically, if we define low mass to be $M < 3$ GeV, then, noting that the unmeasured interval from $M = 15.7$ to $M = 3$ GeV gives $\Delta\ln M^2 = 3.3$, it follows that the ATLAS, CMS results imply $\sigma_{\rm inel}^{{\rm high}M} \simeq 64$ mb. Then using the TOTEM result we find that low-mass diffractive dissociation is expected to have a rather large cross section

$$\sigma_{\rm inel}^{{\rm low}M} \simeq 73.5 - 64 \;=\; 9.5 \text{ mb}. \tag{4}$$

Note, however, that the low-mass diffractive dissociation given in Table 1,

$$\sigma_{{\rm low}M}^{\rm SD+DD} \;=\; 7.3 + 0.9 \;=\; 8.2 \text{ mb}, \tag{5}$$

in satisfactory agreement with (4).

Another valuable set of soft diffractive measurements have been made by the ATLAS collaboration. They measure $d\sigma/d\Delta\eta$ versus $\Delta\eta$ for events with large rapdity gaps [23]. For $\Delta\eta \gtrsim 5$, fluctuations in hadronization are greatly suppressed [24], and we cleanly probe high-mass diffractive dissociation. In Ref. [10] these data are shown to be well described by a triple-Pomeron approach, *provided* the sizeable absorptive or rescattering corrections are taken into account. These corrections are computed in a parameter-free way using the 3-channel eikonal model discussed above.

Acknowledgements

We thank Giulia Pancheri for arranging such an enjoyable Workshop.

References

[1] for a recent detailed review see V.S. Fadin,B.L. Ioffe and L.N. Lipatov, *in* Quantum Chromodynamics (Camb. Univ. Press, 2010).

[2] M. Ciafaloni, D. Colferai and G. Salam, Phys. Rev. **D60**, 114036 (1999);
V.A. Khoze, A.D. Martin, M.G. Ryskin and W.J. Stirling, Phys. Rev. **D70**, 074013 (2004).

[3] CMS Collaboration, Phys. Rev. Lett. **105**, 022002 (2010).

[4] ATLAS Collaboration, Phys. Rev. **D83**, 112001 (2011).

[5] A. Donnachie and P.V. Landshoff, Phys. Lett. **B296**, 227 (1992).

[6] M.L. Good and W.D. Walker, Phys. Rev. **120**, 1857 (1960).

[7] M.G. Ryskin, A.D. Martin and V.A. Khoze, J. Phys. G **38**, 085006 (2011).

[8] T. Sjostrand, S. Mrenna and P.Z. Skands, Comput. Phys. Commun. **178**, 852 (2008).

[9] M.G. Ryskin, A.D. Martin and V.A. Khoze, Eur. Phys. J. **C71**, 1617 (2011).

[10] M.G. Ryskin, A.D. Martin and V.A. Khoze, arXiv:1201.6298.

[11] V.A. Schegelsky, A.D. Martin, M.G. Ryskin and V.A. Khoze, Phys. Lett. **B703**, 288 (2011).

[12] TOTEM Collaboration, Europhys. Lett. **96**, 21002 (2011).

[13] CDF Collaboration, Phys. Rev. **D50**, 5518 (1994).

[14] E710 Collaboration, Phys. Lett. **B247**, 127 (1990).

[15] UA4 Collaboration, Phys. Lett. **B147**, 385 (1984);
UA4/2 Collaboration, Phys. Lett. **B316**, 448 (1993);
UA1 Collaboration, Phys. Lett. **B128**, 336 (1982).

[16] N. Kwak et al., Phys. Lett. **B58**, 233 (1975);
U. Amaldi et al., Phys. Lett. **B66**, 390 (1977);
L. Baksay et al., Nucl. Phys. **B141**, 1 (1978).

[17] TOTEM Collaboration, Europhys. Lett. **95**, 41001 (2011).

[18] A.A. Anselm and V.N. Gribov, Phys. Lett. **B40**, 487 (1972);
V.A. Khoze, A.D. Martin and M.G. Ryskin, Eur. Phys. J. **C18**, 167 (2000).

[19] V.A. Khoze, J.W. Lamsa, R. Orava and M.G. Ryskin, JINST **6**, P01005 (2011);
H. Gronqvist, V.A. Khoze, J.W. Lamsa, M. Murray and R. Orava, arXiv:1011.6141.

[20] ATLAS Collaboration, Nature Commun. **2**, 463 (2011); arXiv:1104.0326 [hep-ex].

[21] CMS Collaboration, Note CMS-PAS-FWD-11-001, (2011).

[22] M.G. Poghosyan, for the ALICE Collaboration, J. Phys. G **38**, 124044 (2011).

[23] ATLAS Collaboration, arXiv:1201.2808.

[24] V.A. Khoze et al., Eur. Phys. J. **C69**, 85 (2010).

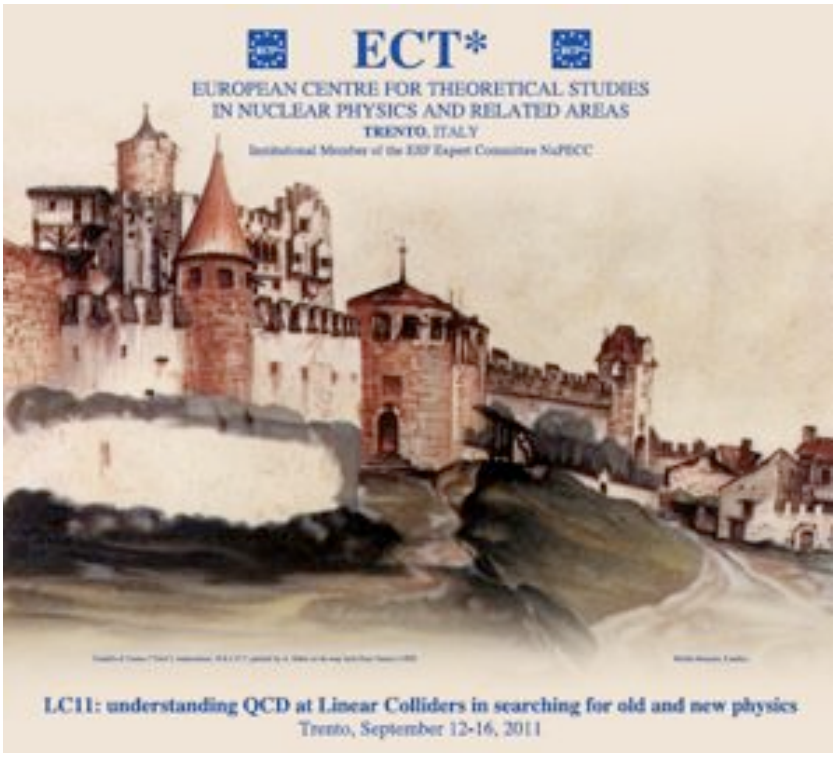

Castello di Trento painted by A. Dürer on his way back from Venice (1495).

5.4 N. Marinelli - QCD results at LHC

QCD results at the LHC

Nancy Marinelli High Energy Physics Departement, University of Notre Dame, IN, USA
nancy.marinelli@cern.ch

on behalf of the ATLAS and CMS Collaborations

Abstract A highlighted selection of the many QCD results obtained with the ATLAS and CMS detectors during the first year of data taking at the LHC is presented here, concentrating the emphasis on hard QCD related with jet and photon production.

1 Introduction

The Large Hadron Collider at CERN started producing pp interactions at $\sqrt{s} = 7$ TeV in 2010, delivering to each of ATLAS and CMS experiments an integrated luminosity of about 40 pb^{-1}. Although the amount of the first-year data was rather small, an incredibly large and varied set of physics results were already obtained. Special interest sits in QCD studies for a number of interconnected reasons; at the pp interaction energies reached at the LHC, QCD processes dominate above everything else and as a consequence they affect all other measurements, constituting in many cases the largest background. Precise measurements in the domain of QCD are hence necessary for a satisfactory interpretation of data, especially when searching for new physics.

The unprecedented centre-of-mass energy at the LHC gives access to yet unexplored kinematic regions of the hard-interaction processes, allowing to probe x and Q^2 well beyond the ranges tested at the Tevatron and HERA allowing for tests of the perturbative QCD (pQCD) in the multi-TeV region.

Furthermore, constraints can be derived from accurate understanding of QCD and imposed to the parton distribution functions (PDF) of the proton so to reduce their uncertainties, with great benefit, for example, in the search of the Higgs boson.

Last but not the least, the large majority of pp interactions are soft, i.e. there is no hard scattering between the proton partons, a regime which cannot be described in terms of pQCD. Simulation models exist, which describe phenomenologically such interactions and need new inputs to be better tuned to match the data.

The LHC low luminosity regime ($10^{32}\text{cm}^{-2}\text{s}^{-1}$) in the 2010 run brought as positive side-effects a low rate ($\sim$2.2) of superimposed pp interactions per LHC bunch-crossing (pile-up events) and the possibility to use low pre-scaling factors on the soft triggers used for QCD, hence putting ATLAS and CMS in the best conditions for such measurements.

2 Soft QCD

The charged hadron multiplicity, i.e. the number, n, of primary charged hadrons is a basic global observable characterizing final states in high-energy collision processes and provide insights in the strong interactions at low energy scales. The multiplicity distribution, $\mathcal{P}_n$, gives the probability of producing n charged hadrons in the event; the CMS Collaboration measured $\mathcal{P}_n$ in non-single-diffractive (NSD) pp collisions in Minimum Bias data [2] finding that $\mathcal{P}_n$ shows large tails at high values of n at $\sqrt{s} = 7$ TeV and that no simulated model available so far is able to describe 100% the data (Fig. 1), although PYTHIA 8 [1] seems to provide the best approximation. The charge particle multiplicity is studied also as a function of the pseudo-rapidity and both ATLAS [3] and CMS show that the average number of charged particle is higher in data than in any model available.

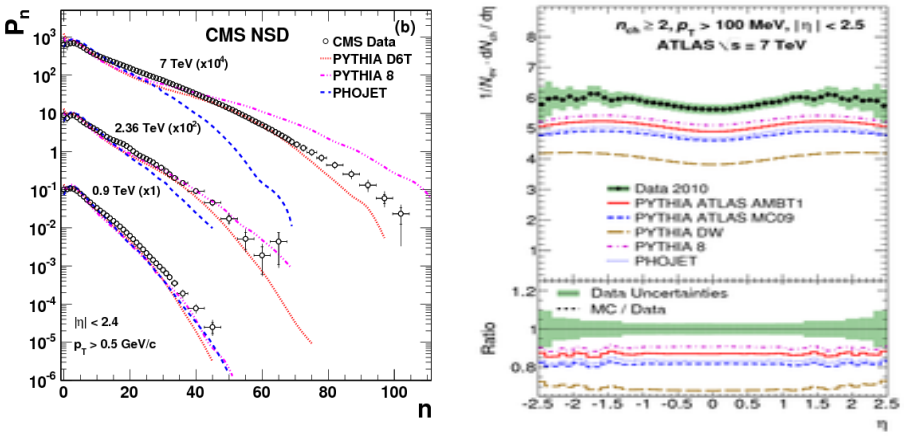

Figure 1: Charged hadron multiplicity. Left) For $|\eta|$ <2.4 and p_T >500 MeV/c at $\sqrt{s}$= 0.9, 2.36, and 7 TeV, compared to two different PYTHIA models and the PHOJET model. For clarity, results for different centre-of-mass energies are scaled by powers of 10 as given in the plots. Right) As a function of the pseudo-rapidity for events with nch>=2, p_T >100 MeV and $|\eta| < 2.5$ at $\sqrt{s} = 7$ TeV. The dots represent the data and the curves the predictions from different simulation models. The vertical bars represent the statistical uncertainties, while the shaded areas show statistical and systematic uncertainties added in quadrature.

3 Hard QCD

3.1 Jets

The measurement of the inclusive jet production cross section is a benchmark study at hadron colliders; at the LHC it allows for tests of the QCD at the smallest distance so far achievable and for constraining the PDF of the proton. Any significant deviation from predictions of the inclusive jet production cross section at high transverse momentum could also be an indication of new physics beyond the Standard Model. The inclusive jet cross section is defined as $d^2\sigma_{jet}/(dp_T dy) = N_{jet}/(\Delta p_T \Delta y)[1/\epsilon\mathcal{L}]$, where p_T is the transverse momentum and y the rapidity, N_{jet} is the number of jets per bin of the two variables, $\mathcal{L}$ is the integrated luminosity and ϵ is the product between the event and jet selection efficiency.

Jets are reconstructed with the "Anti-kT" jet clustering algorithm [4], usually with the size parameter ranging from 0.4 to 0.7. Both ATLAS and CMS reported this measurement on the first year of LHC data [5], [6] reaching the same kind of conclusions, i.e. that there is an excellent agreement between data and theoretical calculations up to about 1 TeV, as shown in Fig. 2. The measured value is compared with Next-To-Leading order pQCD calculations.

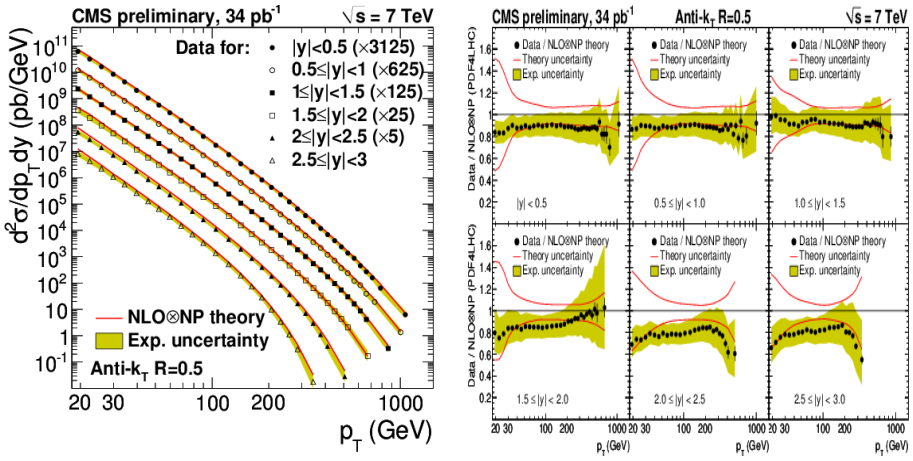

Figure 2: (Left) Unsmeared inclusive jet pt spectra for different y bins with the next-to-leading-order (NLO) theoretical prediction, corrected for non-perturbative (NP) effects, superimposed. (Right)The unsmeared measured spectra in data plotted as the ratio of data to theory prediction. The solid lines represent total theoretical systematic uncertainty. The shaded band about the data points represents the experimental systematic systematic uncertainty.

The di-jet production cross section is the next important item to study since it is sensitive to the possible presence of high energy di-jet resonances. Figure 3 shows the ATLAS measurement [6] for the di-jet double-differential cross section as a function of the di-jet invariant

mass for several bins of the variable y, which is the rapidity in the two-parton centre-of-mass frame. The cross section measurements extend from di-jet masses of 70 GeV to almost 5 TeV, covering two orders of magnitude in invariant mass and nine orders of magnitude in the cross section. The di-jet measurements are fully corrected for detector effects and are compared to NLOJET++ predictions. The di-jet data are also compared with NLOJET++ predictions obtained using the MSTW2008, NNPDF 2.1,and HERAPDF 1.5 PDF sets in Fig. 4.

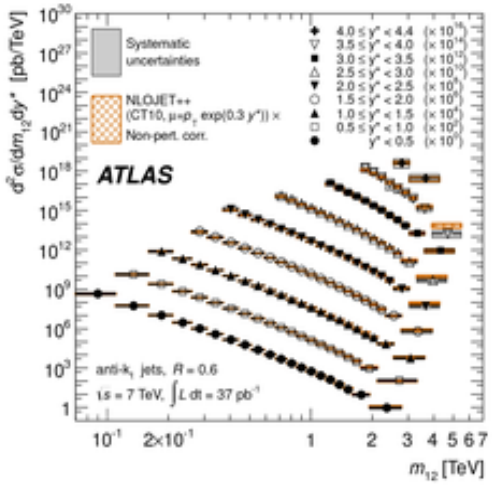

Figure 3: Di-Jet double-differential cross section as a function of di-jet mass, binned in half the rapidity separation between the two leading jets, $y^* = |y1 - y2|/2$. The results are shown for jets identified using the anti-kt algorithm with R=0.6. For convenience, the cross sections are multiplied by the factors indicated in the legend. The data are compared to NLO pQCD calculations using NLOJET++ to which non-perturbative corrections have been applied. Systematic and theoretical uncertainties are shown.

Overall the differences between the data and each PDF set lie well within the systematic and theory uncertainties, indicating a reasonable agreement with the di-jet data, particularly in the kinematic region at low y. The corresponding result for CMS is reported in [7].

At Born level, QCD predicts the decorrelation between the two most energetic jets, $\Delta\phi$, as a function of the number of partons produced. Events with only two high-p_T jets have small azimuthal decorrelations, $\Delta\phi \sim \pi$, while $\Delta\phi \ll \pi$ is evidence of events with several high-p_T jets. Di-jet azimuthal decorrelations can be used to study QCD radiation effects over a wide range of jet multiplicities without the need to measure all the additional jets present in the event. Such studies are important because an accurate description of multiple-parton radiation is still lacking in perturbative QCD (pQCD).

Figure 5 (left) shows ATLAS [8] $\Delta\phi$ distribution for jets with p_T >100 GeV; it illustrates that the decorrelation increases when a third high-p_T jet is also required. Events with addi-

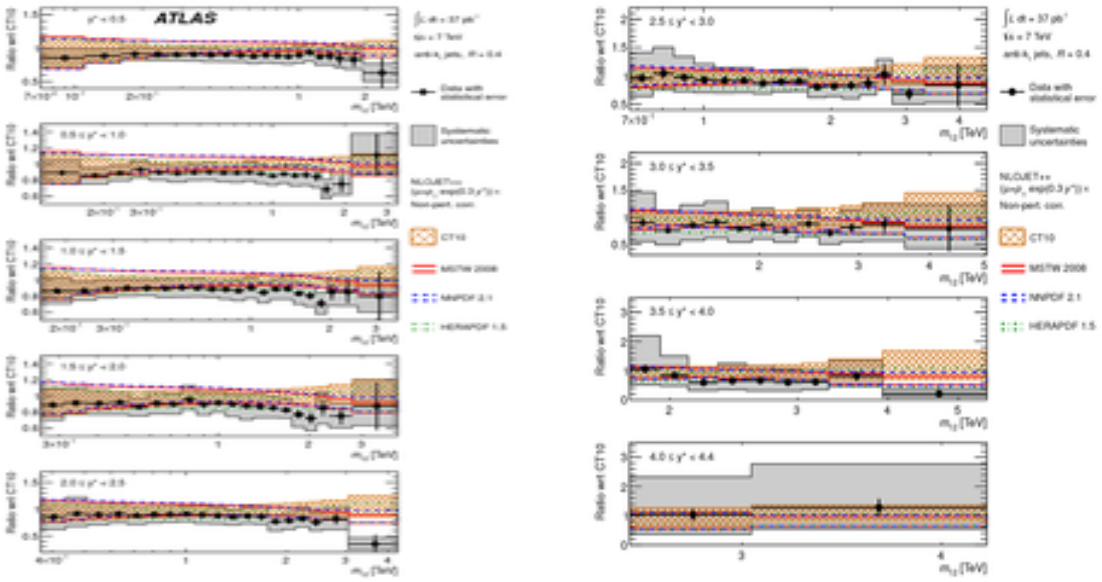

Figure 4: Ratios of di-jet double-differential cross section to the theoretical predictions. The ratios are shown as a function of di-jet mass, binned in half the rapidity separation between the two leading jets, $y^* = |y1 - y2|/2$. The results are shown for jets identified using the anti-kt algorithm with R=0.4. The theoretical error bands obtained by using NLOJET++ with different PDF sets (CT10, MSTW 2008, NNPDF 2.1, HERAPDF 1.5) are shown. The systematic and theoretical uncertainties are included.

tional high-p_T jets widen the overall distribution. The right plot of Fig. 5 is the CMS di-jet cross section [9] in $\Delta\phi_{dijet}$, normalized by the di-jet cross section integrated over the entire $\Delta\phi_{dijet}$ space. The distributions are scaled by multiplicative factors for presentation purposes. The simulated $\Delta\phi_{dijet}$ distributions from the PYTHIA6 (D6T and Z2 tunes), PYTHIA 8.135 (PYTHIA8), HERWIG, and MADGRAPH 4.4.32 event generators are presented for comparison. The NLO pQCD + non perturbative correction describe well the data for $\Delta\phi > 120$ deg (3jet topologies).

Finally di-jet angular distributions provide a way to search for quark compositeness. The CMS Collaboration [10] meaures the angular distribution in terms of the variable $\chi_{dijet} = exp(2y^*)$ which for collinear massless-parton scattering takes the form $\chi_{dijet} = (1+|cos\theta^*|)/(1-|cos\theta^*|)$. Quark compositeness would show up with excesses at very low values of χ_{dijet} (Fig. 6). The absence of an excess allows for setting a 95% CL lower limit on the contact interaction scale for a left-handed quark compositeness model, i.e Λ^+=5.6 TeV and Λ^-=6.7 TeV.

3.2 Photons

In high-energy pp collisions, prompt photons are produced directly in qg Compton scattering and $q\bar{q}$ annihilation, and in the fragmentation of partons with large transverse momentum.

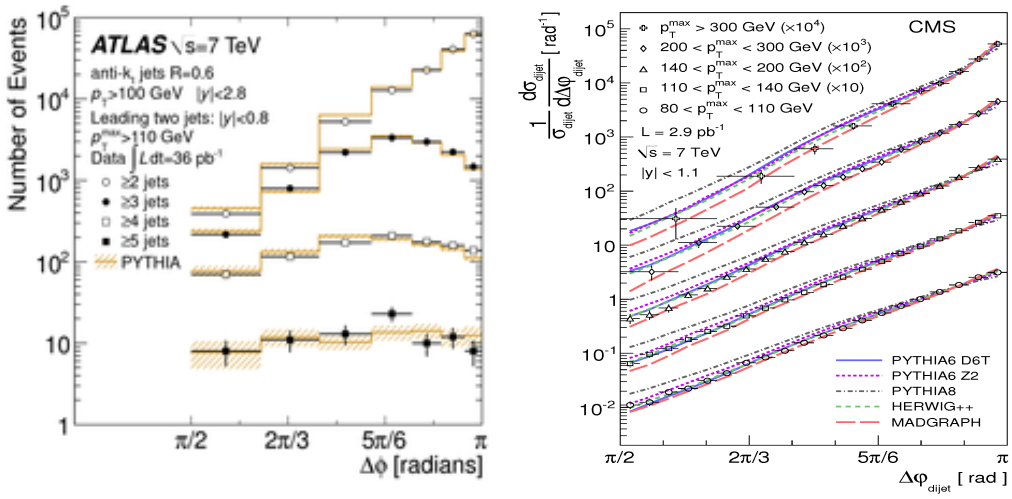

Figure 5: (Left) The $\Delta\phi$ distribution for >= 2, >= 3, >= 4, and >= 5 jets with p_T >100 GeV. Overlaid on the calibrated but otherwise uncorrected data (points) are results from PYTHIA processed through the detector simulation (lines). All uncertainties are statistical only. (Right) Normalized $\Delta\varphi_{dijet}$ distributions in several p_T^{max} regions, scaled by the multiplicative factors given in the figure for easier presentation. The curves represent predictions from PYTHIA6, PYTHIA8, HERWIG++, and MADGRAPH. The error bars on the data points include statistical and systematic uncertainties.

On the other hand, photons pairs are produced directly (Born and Box diagrams) or as a result of parton fragmentation. Measuring the inclusive photon production as well as the di-photon production cross sections is complementary to jet production measurements and provide an additional and very clean possibility to constrain the PDF of the proton by probing its gluon content. Also, a comprehensive understanding of photon production is important as it represents a major background in certain searches for rare or exotic processes, such as the production of a light Higgs boson, extra-dimension gravitons, and some super-symmetric states. Both ATLAS and CMS have performed these measurements [11], [12], [13], [14], showing that in general, there is good agreement between the data and the NLO pQCD prediction. In Fig. 7 the inclusive photon production cross section measured by CMS is shown. Over most of the extended kinematic range probed to measure the inclusive photon production cross section, the experimental accuracy already challenges the theoretical uncertainty, hence the discrimination between PDFs is not possible because of their large errors.

In the case of the di-photon production. the cross section is measured as a function of di-photon invariant mass and transverse momentum, the difference between the two photon azimuthal angles, and $|cos\theta^*|$. Whereas there is an overall agreement between theory and data in the di-photon mass spectrum, the theory underestimates the cross section in the low di-photon mass region (Fig. 8).

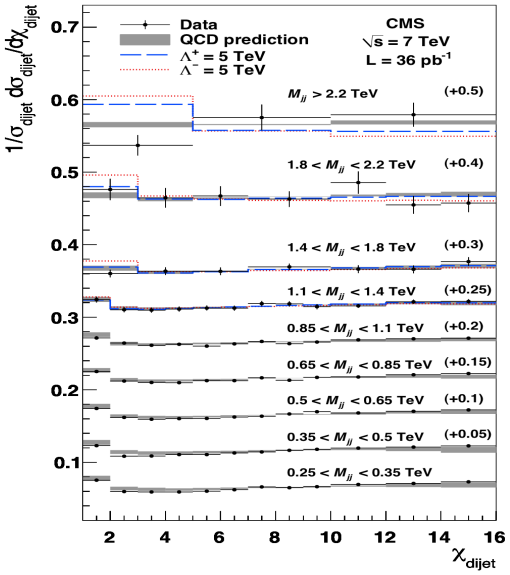

Figure 6: Normalized di-jet angular distributions in several M_{jj} ranges, shifted vertically by the additive amounts given in parentheses in the figure for clarity. The data points include statistical and systematic uncertainties. The results are compared with the predictions of pQCD at NLO (shaded band) and with the predictions including a contact interaction term of compositeness scale $\Lambda^+ = 5$ TeV (dashed histogram) and $\Lambda^-= 5$ TeV (dotted histogram).

4 Summary

The large number of high-quality QCD studies carried out by the ATLAS and CMS Collaborations on the data sets collected at the LHC during 2010 show overall good agreement with the theoretical predictions and already challange the PDF precision.

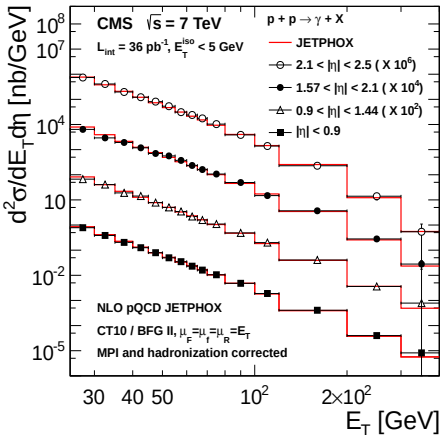

Figure 7: Measured isolated prompt photon differential cross sections (markers) as a function of transverse energy in the four pseudo-rapidity regions and the predictions from JETPHOX 1.3.0 using the CT10 PDFs (histograms). The error bars are the quadrature sums of statistical and systematic uncertainties on the measurements. The cross sections are scaled by the factors shown in the legend for easier viewing.

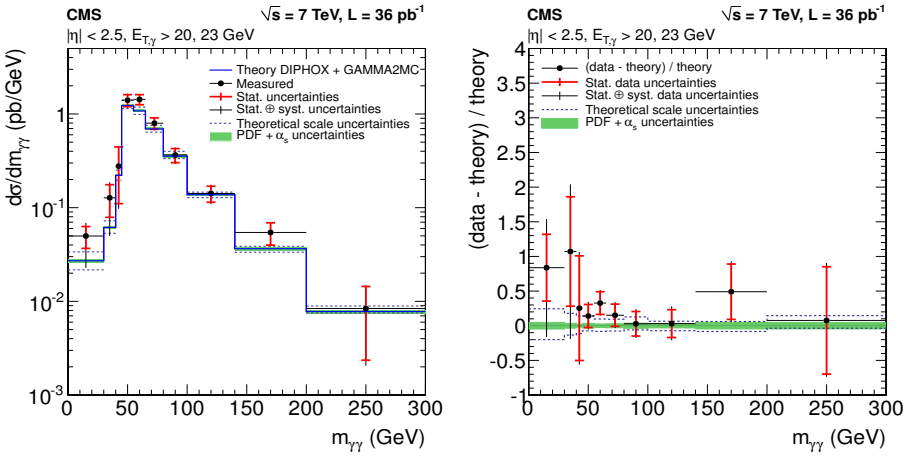

Figure 8: (Left) Di-photon differential cross section as a function of the photon pair invariant mass $m_{\gamma\gamma}$ from data (points) and from theory (solid line) for the photon pseudo-rapidity range $|\eta| < 2.5$. (Right) The difference between the measured and theoretically predicted di-photon cross sections, divided by the theory prediction, as a function of $m_{\gamma\gamma}$. In both plots, the inner and outer error bars on each point show the statistical and total experimental uncertainties. The 4% uncertainty on the integrated luminosity is not included in the error bars. The dotted line and shaded region represent the systematic uncertainties on the theoretical prediction from the theoretical scales and the PDFs, respectively.

References

[1] "Brief Introduction to PYTHIA 8.1", Sjostrand T., Mrenna S. and Skands P. Z., Comput. Phys. Commun. 178 852-67, arXiv:0710.3820;

[2] "Charged particle multiplicities in pp interactions $\sqrt{s}$= 0.9, 2.36, and 7 TeV", The CMS Collaboration, J. High Energy Phys. 01 (2011) 079;

[3] "Charged-particle multiplicities in pp interactions measured with the ATLAS detector at the LHC" , The ATLAS Collaboration, New J Phys 13 (2011) 053033;

[4] "The anti-kt jet clustering algorithm", M. Cacciari, G. P. Salam, G. Soyez, J. High Energy Phys. 94 (2008) 063;

[5] "Measurement of the Inclusive Jet Cross Section in pp Collisions at $\sqrt{s}$ = 7 TeV", The CMS Collaboration, Phys. Rev. Lett. 107, 132001 (2011);

[6] "Measurement of inclusive jet and dijet cross sections in proton-proton collisions at 7 TeV centre-of-mass energy using the ATLAS detector", The ATLAS Collaboration, arXiv:1112.6297v1 ;

[7] "Measurement of the differential dijet mass cross section in proton-proton collisions at $\sqrt{s}$ = 7 TeV ", The CMS Collbaoration, Phys. Lett. B 700 (2011) 187;

[8] "Measurement of Dijet Azimuthal Decorrelations in pp Collisions at $\sqrt{s}$ = 7 TeV", The ATLAS Collaboration, Phys. Rev. Lett. 106 (2011) 172002;

[9] "Dijet Azimuthal Decorrelations in pp Collisions at $\sqrt{s} = 7$ TeV", The CMS Collaboration, Phys. Rev. Lett. 106 (2011) 122003;

[10] "Measurement of Dijet Angular Distributions and Search for Quark Compositeness in pp Collisions at $\sqrt{s} = 7$ TeV ", The CMS Collaboration, Phys. Rev. Lett. 106 (2011) 201804;

[11] "Measurement of the inclusive isolated prompt photon cross-section in pp collisions at $\sqrt{s}$ = 7 TeV using 35 pb^{-1} of ATLAS data", The ATLAS Collaboration, Phys. Lett. B706 (2011), 150-167;

[12] "Measurement of the isolated di-photon cross-section in pp collisions at $\sqrt{s} = 7$ TeV with the ATLAS detector ", The ATLAS Collaboration, Phys. Rev. D 85, 012003 (2012);

[13] "Measurement of the isolated prompt photon production cross section in pp collisions at $\sqrt{s}$= 7 TeV", The CMS Collaboration, Phys. Rev. D 84 (2011) 052011;

[14] "Measurement of the Production Cross Section of Pairs of Isolated Photons in pp collisions at $\sqrt{s} = 7$ TeV ", The CMS Collaboration, arXiv:1110.6461, CERN-PH-EP-2011-171;

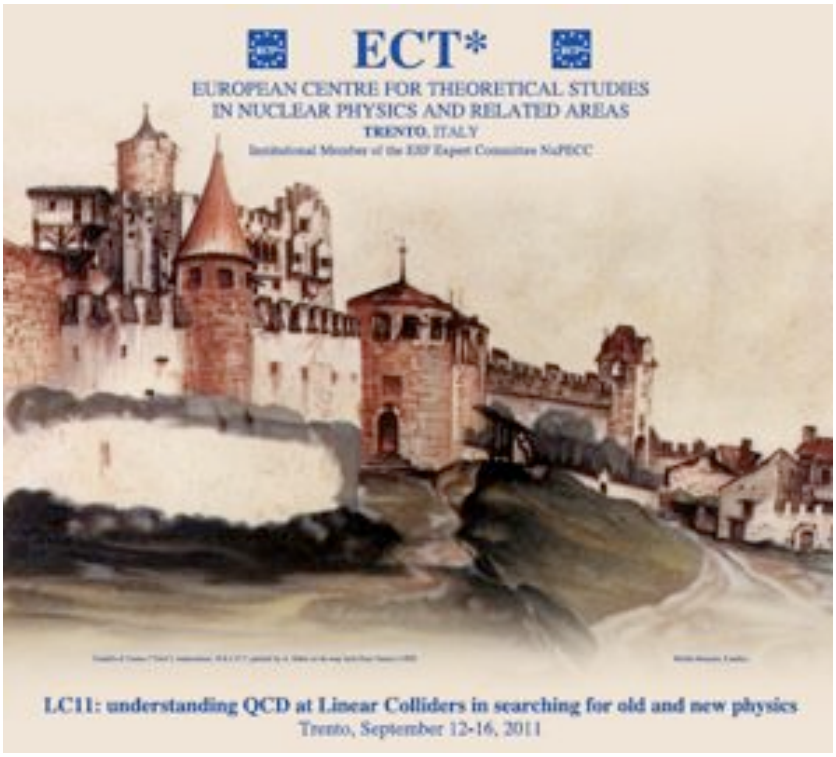

Castello di Trento painted by A. Dürer on his way back from Venice (1495).

Chapter 6

Higgs, Top and Flavour Physics

6.1 M. Mühlleitner, R.M. Godbole, C. Hangst, et al. - Analysis of Higgs Spin and CP properties in a model-independent way in $e^+e^- \to t\bar{t}\Phi$

Analysis of Higgs Spin and CP properties in a model-independent way in $e^+e^- \to t\bar{t}\Phi$

M. Mühlleitner [1]
Inst. for Theoretical Physics, Karlsruhe Institute of Technology, 76128 Karlsruhe, Germany
maggie@particle.uni-karlsruhe.de

R.M. Godbole
Center for High Energy Physics, Indian Institute of Science, Bangalore 560 012, India
rohini@cts.iisc.ernet.in

C. Hangst
Inst. for Theoretical Physics, Karlsruhe Institute of Technology, 76128 Karlsruhe, Germany
hangst@particle.uni-karlsruhe.de

S.D. Rindani
Theor. Physics Div., Physical Research Laboratory, Navrangpura, Ahmedabad 380 009, India
saurabh@prl.res.in

P. Sharma
Theor. Physics Div., Physical Research Laboratory, Navrangpura, Ahmedabad 380 009, India
pankajs@prl.res.in

Abstract We study the prospects of establishing the CP quantum numbers of the Higgs boson in the CP-conserving and CP-violating case in associated Higgs production with a top quark pair, by exploring the combined use of the total cross section and its energy dependence, the polarisation asymmetry of the top quark and the up-down asymmetry of the antitop with respect to the top-electron plane. The combination remarkably reduces the error on the determination of the CP properties of the Higgs Yukawa coupling. Furthermore, it is shown that the top polarisation asymmetry and the ratio of cross sections at different collider energies are sensitive to the spin of the particle produced in association with a $t\bar{t}$ pair.

1 Introduction

One of the major goals of the LHC is the search for the Higgs boson. Both ATLAS and CMS have presented results on the observation of an excess of events for a Standard Model (SM) Higgs boson mass hypothesis in the region 124-126 GeV [1]. While the statistical significance is

[1] Speaker

too low to claim discovery the run in 2012 may accumulate enough data to clarify the question if there exists a SM-like Higgs boson in the low-mass region. Once a Higgs boson has been discovered the clean environment of the International Linear Collider (ILC) will allow for the determination of the particle properties with sufficient precision. The measurements of the spin and CP quantum numbers, of the couplings to fermions and gauge bosons and finally the Higgs self-couplings are needed to clarify if the Higgs mechanism is at the origin of electroweak (EW) symmetry breaking. Whereas the SM Higgs boson is predicted to have spin zero and be CP-even, in extensions beyond the SM Higgs sectors with more than one spin zero particle are possible. These may be CP-even, CP-odd or even be states with indefinite CP quantum number.

Information on the Higgs spin and CP properties and on the amount of CP-mixing in case of CP violation can be obtained by studying the Higgs couplings to the heaviest fermions and to massive $V = W, Z$ gauge bosons either in Higgs production or decay. Also the couplings to a photon or a gluon pair, which proceed through loops of these particles, can be exploited [2]. While the coupling of a pseudoscalar Higgs boson to a VV pair is loop-induced and therefore suppressed with respect to the tree-level coupling of a scalar state, the top quark couples democratically to the CP-even and the CP-odd components of the Higgs boson. At an ILC Higgs production in association with a top quark pair $e^+e^- \to t\bar{t}\Phi$ [3, 4, 5, 6] yields sufficiently high rates [7] to be exploited to extract CP information [8, 9, 10] through angular correlations and/or the polarisation of heavy fermions. We discuss how a general CP-violating $t\bar{t}\Phi$ vertex can be probed in the combined study of three observables, given by the total cross section σ and its energy dependence, the top quark polarisation asymmetry P_t and the up-down asymmetry A_ϕ of the antitop quark with respect to the top-electron plane. The latter can directly probe CP violation. We also show that the energy dependence of the cross section and the top polarisation asymmetry are sensitive to the spin of the particle produced with a $t\bar{t}$ pair. For details see [10].

2 The observables

The total cross section: Fig. 1 shows the diagrams contributing to $t\bar{t}H$ SM Higgs boson pro-

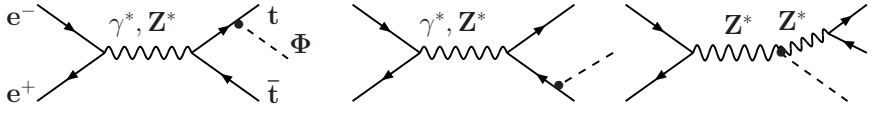

Figure 1: Feynman diagrams contributing to $t\bar{t}\Phi$ production.

duction. The process can be measured in the SM with 10% accuracy for $M_H \lesssim 200\,\text{GeV}$ [7]. The bulk of the cross section stems from the splitting of the virtual photon into $t\bar{t}$. In models with more than one Higgs boson there are additional diagrams with a CP-odd (even) Higgs

boson splitting into $t\bar{t}$ for (pseudo-)scalar Higgs production. In CP-violating models both Higgs bosons are CP-mixed states with one of them splitting into a $t\bar{t}$ pair. In the following, we will assume that by the time the CP quantum numbers of Higgs bosons will be tested, all Higgs bosons will have been discovered and their masses determined, so that the contribution of these additional diagrams can safely be neglected by applying appropriate cuts on the $t\bar{t}$ invariant mass. For the discussion of a general CP-mixed state Φ the $t\bar{t}\Phi$ coupling is parameterized as

$$C_{tt\Phi} = -i\frac{e}{\sin\theta_W}\frac{m_t}{2M_W}(a + ib\gamma_5) \equiv -ig_{ttH}(a + ib\gamma_5) \ , \tag{1}$$

where θ_W denotes the Weinberg angle, m_t the top quark mass and M_W the W boson mass. The coefficients a and b are assumed to be real and in the SM they are given by $(a, b) = (1, 0)$. A pure pseudoscalar coupling is provided by $a = 0, b \neq 0$, and a coupling to a Higgs state with indefinite CP quantum numbers corresponds to simultaneously $a \neq 0$ and $b \neq 0$. The values of a, b depend on the model under consideration and are constrained by the experiment. It has been shown [11] that in a general 2-Higgs doublet model (2HDM) with maximal CP violation values with $|ab| \lesssim 2$ are in accordance with low-energy constraints. The parameters a, b are varied between -1 and 1 in the following. The $ZZ\Phi$ coupling is parameterized in terms of the SM coupling g_{ZZH} by a parameter c,

$$g^{\mu\nu}_{ZZ\Phi} = -ic\,\frac{eM_Z}{\sin\theta_W\cos\theta_W}g^{\mu\nu} \equiv -ic\,g_{ZZH}\,g^{\mu\nu} \ . \tag{2}$$

With the $ZZ\Phi$ coupling and hence the parameter c being determined from other channels [12, 13] the analysis can be performed for a fixed value of c. To reduce the number of free parameters we will choose $c = -a$, ensuring the $ZZ\Phi$ coupling to take the SM form for $a = 1$, being zero in the CP-odd case and $|c| \leq 1$ in general. While the total cross section is a CP-even observable and not sensitive to possible CP violation, its threshold rise is strikingly different for the scalar and pseudoscalar case [10]. With ρ parameterizing the deviation from the threshold,

$$\rho = 1 - \frac{2m_t}{\sqrt{s}} - \frac{M_\Phi}{\sqrt{s}} \ , \tag{3}$$

in the scalar case we have a dependence $\sim \rho^2$ whereas in the pseudoscalar case $\sim \rho^3$. Taking into account only statistical fluctuations, an integrated luminosity of 500 fb^{-1} is sufficient for a 125 GeV Higgs boson to distinguish the purely pseudoscalar from the SM case at 5σ confidence level, *cf.* Fig. 2. The QCD corrections to the total cross section can be significant near the threshold, while in the continuum, for a $\sqrt{s} = 1$ TeV they are of moderate size for both the scalar and pseudoscalar Higgs boson [4, 5]. The EW corrections can reach about 10% [6]. In this analysis, higher-order corrections are neglected in a first approximation. The polarisation

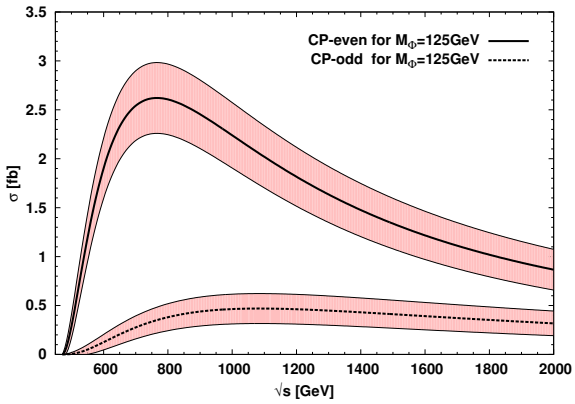

Figure 2: Total cross section in fb for SM (full) and purely CP-odd (dashed) Higgs production in association with a $t\bar{t}$ pair as function of the c.m. energy for $M_\Phi = 125\,\text{GeV}$ and unpolarised $e^\pm$ beams. The pink (grey) band indicates the statistical error at $\pm 5\sigma$ with $\int \mathcal{L} = 500\ \text{fb}^{-1}$.

asymmetry discussed below is expected to be less sensitive to such corrections.

For the sensitivity of an observable O to a, b we define a level of confidence f identifying the area in the (a, b) plane where the value of $O(a, b)$ cannot be distinguished from the reference value $O(a_0, b_0)$. Ignoring systematic errors, it is given by

$$|O(a, b) - O(a_0, b_0)| = f\Delta O(a_0, b_0)\ , \tag{4}$$

where $\Delta O(a_0, b_0)$ is the statistical fluctuation in O at an integrated luminosity $\mathcal{L}$ chosen to be 500 fb^{-1} in the following, if not stated otherwise. For the cross section we have $\Delta\sigma = \sqrt{\sigma/\mathcal{L}}$. The errors on a and b in (a_0, b_0) are given by the maximal extensions Δa^+ (Δa^-) in positive (negative) a direction and Δb^+ (Δb^-) in positive (negative) b direction, which are necessary to reach the area outside the range of insensitivity. The errors for a, b being extracted from the total cross section are shown in Fig. 3. While σ is very sensitive to a, the error on b is large in most of the parameter space. The total cross section can hence be exploited to determine the CP-even part of the $t\bar{t}\Phi$ coupling. The sensitivity to a will significantly improve if b can be constrained from other observables. Polarised $e^\pm$ beams[2] improve the sensitivity only marginally.

The top quark polarisation asymmetry: Due to its large decay width the top decays much before hadronization so that its spin information is translated to the distributions of the decay products and not contaminated by strong interaction effects. The top quark polarisation asymmetry is therefore another observable to probe the Higgs CP properties. Denoting by $t_{L,R}$ a left-, right-handed top quark, for (un)polarised $e^\pm$ beams it is defined as

$$P_t = \frac{\sigma(t_L) - \sigma(t_R)}{\sigma(t_L) + \sigma(t_R)}\ . \tag{5}$$

[2]The degree of polarisation is taken $P_{e^-} = -0.8$, $P_{e^+} = 0.6$, with positive P_{e^-,e^+} corresponding to right-handed polarisation.

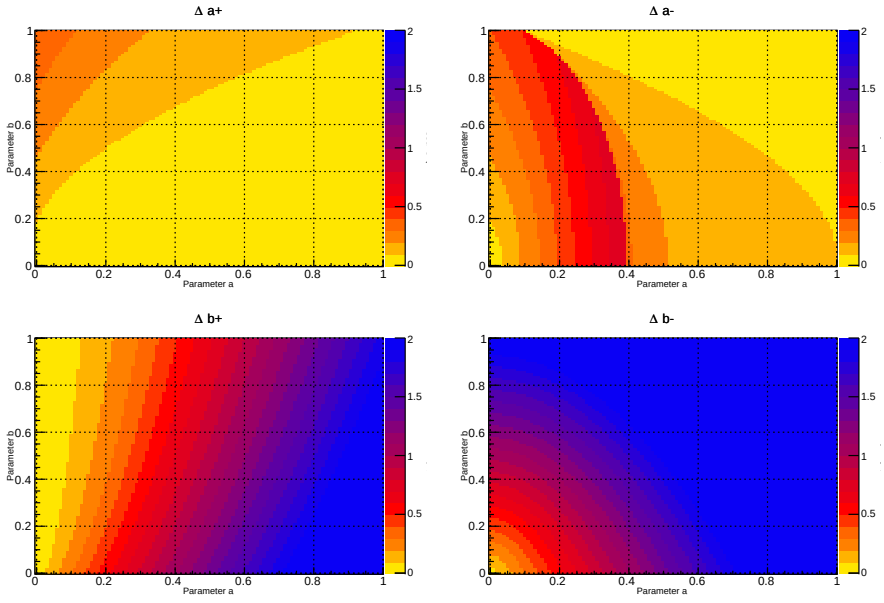

Figure 3: Errors Δa^+ (upper left) and Δa^- (upper right) on a as well as Δb^+ (lower left) and Δb^- (lower right) on b, extracted from the total cross section $\sigma(e^+e^- \to t\bar{t}\Phi)$ at 1σ confidence level for $M_\Phi = 125\,\text{GeV}$ at $\sqrt{s} = 800\,\text{GeV}$ with $\int \mathcal{L} = 500\ \text{fb}^{-1}$. The $e^\pm$ beams are unpolarised. The colour code indicates the magnitude of the respective error.

As P_t is CP-even, in case of an anti-top it simply changes sign. The threshold rise is approximately the same for the scalar and the pseudoscalar Higgs boson. The P_t values in the continuum, however, are very different for a CP-even and a CP-odd Higgs boson. The errors on a, b extracted from P_t turn out to be large, so that P_t alone cannot be used to determine a, b accurately.

The CP-violating up-down asymmetry: The up-down asymmetry A_ϕ of the antitop with respect to the top-electron plane is sensitive to CP-violation. With $q_{a,b}$ ($p_{1,2}$) the four-momenta of the incoming e^-, e^+ (of top, antitop), respectively, the angle ϕ between the antitop direction and the top-electron plane is given by

$$\sin\phi = \frac{\vec{p}_2 \cdot (\vec{q}_a \times \vec{p}_1)}{|\vec{p}_2||\vec{q}_a \times \vec{p}_1|} \sim \epsilon^{p_1 p_2 q_a q_b} \,, \tag{6}$$

with the totally antisymmetric Levi-Civita tensor ϵ. Denoting by 'up' ('down') the cross section value of the ϕ integration performed for $\phi \in [0, \pi)$ ($\phi \in [\pi, 2\pi)$), A_ϕ is defined as

$$A_\phi = \frac{\sigma(\text{up}) - \sigma(\text{down})}{\sigma(\text{up}) + \sigma(\text{down})} \,. \tag{7}$$

It turns out to be given by the interference of the diagram where the Higgs is radiated from the top-quark with the diagram where the Higgs is radiated from the Z boson [8] and can be expressed by the asymmetric interference term proportional to bc, $A_\phi \sim bc\,\sigma_{as}$. A non-vanishing

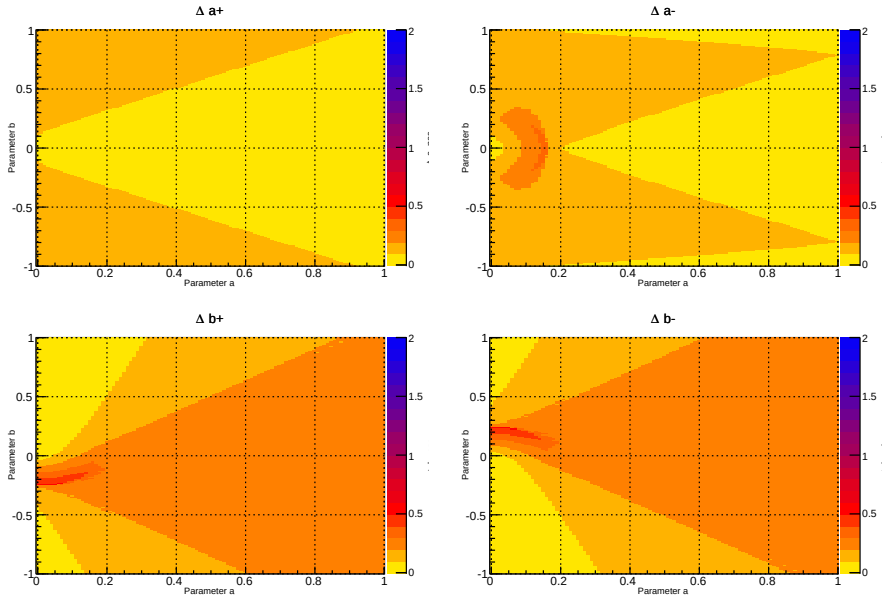

Figure 4: Errors Δa^+ (upper left) and Δa^- (upper right) on a as well as Δb^+ (lower left) and Δb^- (lower right) on b, by combining all 3 observables σ, P_t, A_ϕ, at 1σ confidence level for $M_\Phi = 125\,\text{GeV}$ and $\sqrt{s} = 3\,\text{TeV}$ with $\mathcal{L} = 3\ \text{ab}^{-1}$. The $e^\pm$ beams are polarised. The colour code indicates the magnitude of the respective error.

A_ϕ is hence an unambiguous indicator of CP violation. The errors on a, b determined from A_ϕ turn out to be larger than their absolute values.

3 The combined sensitivity

As the accuracy on a (b) substantially improves if b (a) has been extracted beforehand from some other measurement, all three observables O_i ($i = 1, 2, 3$) given by σ, P_t, A_ϕ are combined to derive new sensitivity areas for a, b by performing a χ^2 test, with

$$\chi^2 = \sum_{i=1,2,3} \frac{(O_i(a,b) - O_i(a_0,b_0))^2}{(\Delta O_i(a_0,b_0))^2} \ . \tag{8}$$

While for unpolarised $e^\pm$ beams essentially the errors on a, b extracted from σ alone are reproduced, they are remarkably reduced for polarised initial beams. The latter increasing σ (P_t) by roughly a factor 2 (3), it is the mutual interplay of σ and P_t which constrains the parameter ranges at $\sqrt{s} = 800\,\text{GeV}$. At higher c.m. energies σ decreases which is compensated by higher integrated luminosities. While P_t does not change a lot, A_ϕ increases with rising $\sqrt{s}$. At multi-TeV energies therefore all three observables contribute significantly to χ^2 resulting in remarkably small errors on a while the errors on b are larger, as can be inferred from Fig. 4.

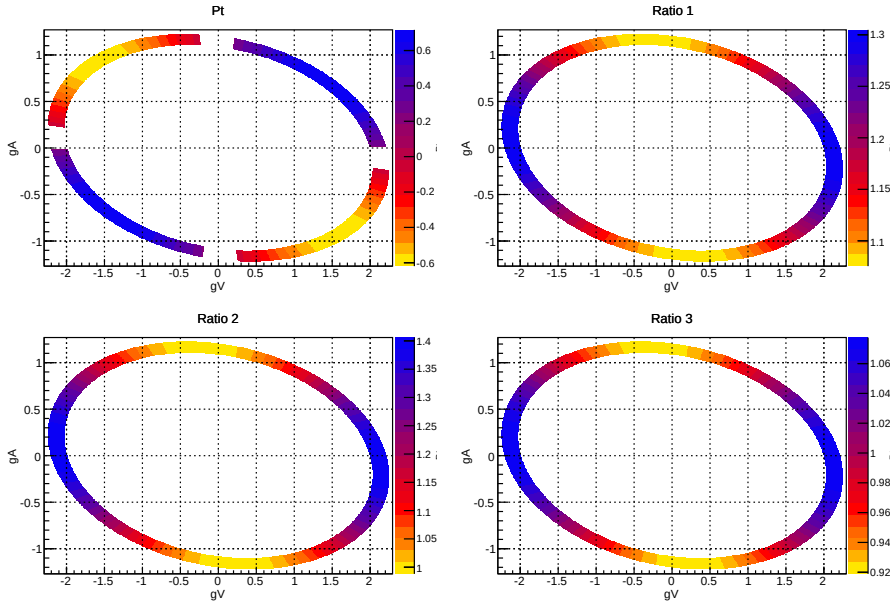

Figure 5: The P_t contours for $t\bar{t}Z'$ production with $M_{Z'} = 125\,\text{GeV}$ and $\sqrt{s} = 800\,\text{GeV}$ (upper left). The contours for the ratio of the cross sections at different c.m. energies are shown in the upper right plot for $\sigma(1000\text{ GeV})/\sigma(800\text{ GeV})$, the lower left plot for $\sigma(1300\text{ GeV})/\sigma(800\text{ GeV})$ and the lower right plot for $\sigma(1300\text{ GeV})/\sigma(1000\text{ GeV})$. The colour code indicates the magnitude of P_t and of the ratios, respectively. The couplings g_A and g_V have been chosen as described in the text.

4 Radiation of a spin 1 particle

To investigate the question to what extent the spin of the radiated particle affects σ and P_t we consider the associated production of a particle Z' with spin $J = 1$ demanded to couple only to top quarks but not $e^{\pm}$, like the SM Higgs boson H. In a first approach we do not take into account anomalous $t\bar{t}Z'$ couplings of dimension higher than 4 [14], and parameterize the coupling as

$$C_{ttZ'} = -ie\gamma_\mu(g_V - g_A\gamma_5)\,, \tag{9}$$

with the vector and axial-vector couplings g_V and g_A chosen to be of $\mathcal{O}(1)$. We consider $t\bar{t}Z'$ production with $M_{Z'} = M_H = 125\,\text{GeV}$ and assume the cross section to have the same magnitude as for SM Higgs $t\bar{t}H$ production at $\sqrt{s} = 800\,\text{GeV}$ within 10%, which is the expected error on σ. This leads to a range $\mathcal{P}$ of values g_V, g_A,

$$g_V, g_A \in \mathcal{P} \quad \Longleftrightarrow \quad \sigma_{t\bar{t}Z'}(g_V, g_A) = \sigma_{t\bar{t}H} \pm 10\%\,, \tag{10}$$

for which P_t is calculated and compared to $P_t(t\bar{t}H) = 0.10$, *cf.* Fig. 5 (upper left). The small white strips in the coloured area appear where $P_t(t\bar{t}Z')$ differs from $P_t(t\bar{t}H)$ by less than 5σ.

Moreover, the ratio of cross sections at different c.m. energies can be exploited to distinguish a spin 0 from a spin 1 state, as is shown in Figs. 5 upper right, lower left and lower right, where the ratio of the $t\bar{t}Z'$ cross section at two different c.m. energies for three energy combinations, respectively, is plotted. Each of them is larger than its corresponding SM value and differs from it by more than 5σ. The top polarisation asymmetry and/or ratios of cross sections are therefore sensitive to the spin of the particle produced in association with $t\bar{t}$.

5 Summary

It has been shown that the top sector allows to test the Higgs boson CP properties once it has been discovered at the LHC. The combination of the three observables total cross section and its energy dependence, top polarisation asymmetry and up-down asymmetry, due to their mutual interplay at high c.m. energies and for polarised $e^{\pm}$ beams, remarkably constrains the range of a and b, which parameterize in a model-independent way the CP properties of the Higgs coupling to a top quark pair. Furthermore, the top polarisation asymmetry and ratios of cross sections at different collider energies have been shown to be good observables to tell a spin 0 from a spin 1 particle.

Acknowledgements

I would like to thank the organizers of LC11 for the invitation to present our results and the kind atmosphere. RG and SDR wish to acknowledge support from the Department of Science and Technology, India under the J.C. Bose Fellowship scheme under grant nos. SR/S2/JCB-64/2007 and SR/S2/JCB- 42/2009, respectively. CH and MM are supported by the DFG SFB/TR9 Computational Particle Physics.

References

[1] G. Aad *et al.* [ATLAS Collaboration], arXiv:1202.1408 [hep-ex]; S. Chatrchyan *et al.* [CMS Collaboration], arXiv:1202.1488 [hep-ex].

[2] For a review, see, E. Accomando et al., Workshop on CP studies and non-standard Higgs physics, CERN-2006-009 [hep-ph/0608079] and references therein.

[3] K. J. F. Gaemers, G. J. Gounaris, Phys. Lett. **B77** (1978) 379; A. Djouadi *et al.*, Mod. Phys. Lett. **A7** (1992) 1765; A. Djouadi *et al.*, Z. Phys. **C54** (1992) 255; B. Grzadkowski *et al.*, Phys. Rev. **D60** (1999) 075011 [hep-ph/9902308].

[4] S. Dawson, L. Reina, Phys. Rev. **D57** (1998) 5851 [hep-ph/9712400] and **D59** (1999) 054012 [hep-ph/9808443]; S. Dittmaier *et al.*, Phys. Lett. **B441** (1998) 383 [hep-ph/9808433]; S. Dawson, L. Reina, Phys. Rev. **D60** (1999) 015003 [hep-ph/9812488]; S. Dittmaier *et al.*, Phys. Lett. **B478** (2000) 247 [hep-ph/0002035].

[5] S. -h. Zhu, [hep-ph/0212273].

[6] Y. You *et al.*, Phys. Lett. **B571** (2003) 85 [hep-ph/0306036]; G. Belanger *et al.*, Phys. Lett. **B571** (2003) 163 [hep-ph/0307029]; A. Denner *et al.*, Phys. Lett. **B575** (2003) 290 [hep-ph/0307193] and Nucl. Phys. **B680** (2004) 85 [hep-ph/0309274].

[7] S. Moretti, Phys. Lett. **B452** (1999) 338 [hep-ph/9902214]; A. Juste, G. Merino, [hep-ph/9910301]; M. Martinez, R. Miquel, Eur. Phys. J. **C27** (2003) 49 [hep-ph/0207315]; A. Gay, LCNote 2004; K. Desch and M. Schumacher in G. Weiglein et al., Phys. Rept. **426** (2006) 47.

[8] S. Bar-Shalom *et al.*, Phys. Rev. **D53** (1996) 1162 [hep-ph/9508314]; S. Bar-Shalom, [hep-ph/9710355]; D. Atwood *et al.* Phys. Rept. **347** (2001) 1 [hep-ph/0006032].

[9] J. F. Gunion *et al.*, Phys. Rev. Lett. **77** (1996) 5172 [hep-ph/9605326]; C. -S. Huang, S. -h. Zhu, Phys. Rev. **D65** (2002) 077702 [hep-ph/0111280].

[10] P. S. Bhupal Dev *et al.*, Phys. Rev. Lett. **100** (2008) 051801 [arXiv:0707.2878 [hep-ph]]; R. M. Godbole *et al.*, [arXiv:0710.2669 [hep-ph]]; R. M. Godbole *et al.*, Eur. Phys. J. C **71** (2011) 1681 [arXiv:1103.5404 [hep-ph]].

[11] T. Hayashi *et al.*, Phys. Lett. **B348** (1995) 489 [hep-ph/9410413]; W. Bernreuther *et al.*, [hep-ph/9812387].

[12] ATLAS Collaboration, Technical Design Report, CERN-LHCC-14 and CERN-LHCC-15; CMS Collaboration, Technical Design Report, CMS-LHCC-2006-21; D. Zeppenfeld *et al.*, Phys. Rev. **D62** (2000) 013009 [hep-ph/0002036]; M. Duhrssen *et al.*, Phys. Rev. **D70** (2004) 113009 [hep-ph/0406323]; M. Duhrssen *et al.*, [hep-ph/0407190].

[13] E. Accomando *et al.* [ECFA/DESY LC Physics Working Group Coll.], Phys. Rept. **299** (1998) 1 [hep-ph/9705442]; J. A. Aguilar-Saavedra *et al.* [ECFA/DESY LC Physics WG Coll.], [hep-ph/0106315]; T. Abe *et al.* [American Linear Collider WG Coll.], [hep-ex/0106055-58]; K. Abe *et al.* [ACFA LC WG Coll.], [hep-ph/0109166]; G. Aarons *et al.* [ILC Coll.], [arXiv:0709.1893 [hep-ph]]; P. Garcia-Abia, W. Lohmann, Eur. Phys. J. direct **C2** (2000) 2 [hep-ex/9908065]; M. Battaglia, [hep-ph/9910271].

[14] F. Larios, C. P. Yuan, Phys. Rev. **D55** (1997) 7218 [hep-ph/9606397]; W. Hollik *et al.*, Nucl. Phys. **B551** (1999) 3 [hep-ph/9812298].

6.2 R. Di Sipio - Top quark physics at the LHC

Top Quark Physics at the LHC

Riccardo Di Sipio University of Bologna and INFN, Italy
On behalf of the ATLAS and CMS collaborations
disipio@cern.ch

Abstract In this contribution we shall present the results about the physics of the top quark by CERN's ATLAS and CMS experiments. After a brief motivation of why it is important to study the top quark at the LHC, we shall discuss the measurement of the production cross sections of top pairs ($t\bar{t}$) and single tops. Then, we shall present an overview its properties: mass, flavour-changing neutral currents (FCNC), anomalous $\not\!\!E_T$, resonances and charge asymmetry. The overall agreement with the Standard Model predictions is very good.

1 Introduction

The top quark is the heaviest elementary particle discovered so far. Its large mass, in the order of the electroweak breaking scale, forces this particle to decay in about 10^{-33} s, a time much shorter of the hadronization time. No top bound states exist: it is the only "bare" quark. Most of its properties are not washed out by the hadronization and are thus experimentally accessible as they are. Top quark events are often a large background in many Beyond the Standard Model scenarios. For this reason, a deep knowledge of its properties and behaviour is of crucial importance in searches for New Physics at the LHC.

2 The LHC as a top factory

In a typical event in which top quarks are produced, a large number of particles are present in the final state: charged leptons, a neutrino and at least four jets of hadrons, two of which originated from a bottom quark. Experimental apparatuses like ATLAS[1] and CMS[2] are required to reconstruct them with a high resolution in order to select a pure sample of events containing top quarks. According to the Standard Model prediction, in such conditions a top pairs is produced in only one interaction per billion. With a center-of-mass energy of 7 TeV and an average luminosity[3] of 10^{33} $cm^{-2}s^{-1}$, during the first half the 2011 data taking the LHC delivered an integrated luminosity of about 1200 pb^{-1}: the LHC produced about 100 top pairs per minute. This consideration makes the LHC a real top quark factory.

3 Production cross-section

The first test for the Standard Model at 7 TeV is represented by the production rate. Top quarks can be produced either in pairs via strong interaction, or alone via electroweak interaction. The latter can be obtained in three different ways: the leading production is the t-channel, followed by the associated production Wt, and finally the s-channel. Theory predicts a cross-section at next-to-leading order (NLO) of $\sigma_{t\bar{t}} = 165^{+11}_{-16}$ pb for top pairs[4], with an uncertainty in the order of 10%. As for the single top production, the theoretical predictions are $\sigma_t^{t-ch} = 64.57^{+3.32}_{-2.62}$ pb, $\sigma_t^{Wt-ch} = 15.74^{+1.34}_{-1.36}$ pb and $\sigma_t^{s-ch} = 4.63^{+0.29}_{-0.27}$ pb.

Both ATLAS and CMS experiments measured the top pairs production cross-section combining different channels and different techniques. For both experiments, the most precise result is obtained in the lepton+jets channels using multivariate analysis and b-tagging. ATLAS[5] [6][7][8][9] measured a $\sigma_{t\bar{t}} = 176 \pm 5(stat)^{+13}_{-10}(syst) \pm 7(lumi)$ pb, CMS [10][11][12][13][14][37] obtained $\sigma_{t\bar{t}} = 154 \pm 17(stat + syst) \pm 6(lumi)$ pb. The two results are compatible with each other and with the Standard Model prediction (see Fig. 1, left) assuming a top mass of 172.5 GeV. In both cases the uncertainty is of the same order of the theoretical one.

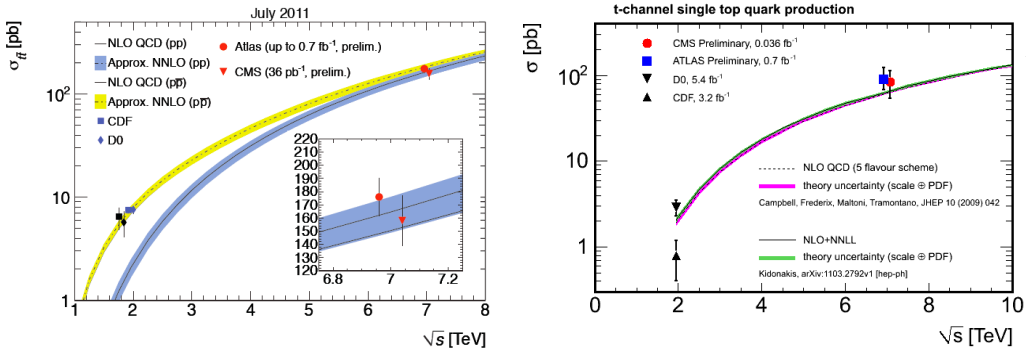

Figure 1: Top quark pairs (left) and single top t-channel (right) production cross-sections measured by ATLAS and CMS

Both the experiments measured the single top production cross-section in the t-channel as well. CMS[20] measured a value of $\sigma_t^{t-ch} = 83.6 \pm 29.8(stat + syst) \pm 3.3(lumi)$ pb, ATLAS[17] obtained $\sigma_t^{t-ch} = 90 \pm 9(stat)^{+31}_{-20}(syst)$ pb. Both values are compatible with each other and with the Standard Model prediction[16] (see Fig. 1, right). ATLAS set limits to Wt- and s-channels as well[18][19].

4 Mass

The mass of the top quark has been measured by both the experiments using various techniques. ATLAS made use of a template fit for signal and background. This results was cross-checked using a simultaneous fit of m_t and the jet energy scale (JES), which is the largest source of systematic uncertainty. Combining these results with the 2010 data, ATLAS[22] measured $m_t = 175.9 \pm 0.9(stat) \pm 2.7(syst)$ GeV. CMS[24] performed a kinematic fit, cross-checked by a simultaneous fit of m_t and the JES. Combining this measurement with a kinematic fit in di-leptonic events, the final value is $m_t = 173.4 \pm 1.9(stat) \pm 2.7(syst)$ GeV (see Fig. 2). The two results are compatible with each other and with the combined Tevatron result[21], although with a larger uncertainty.

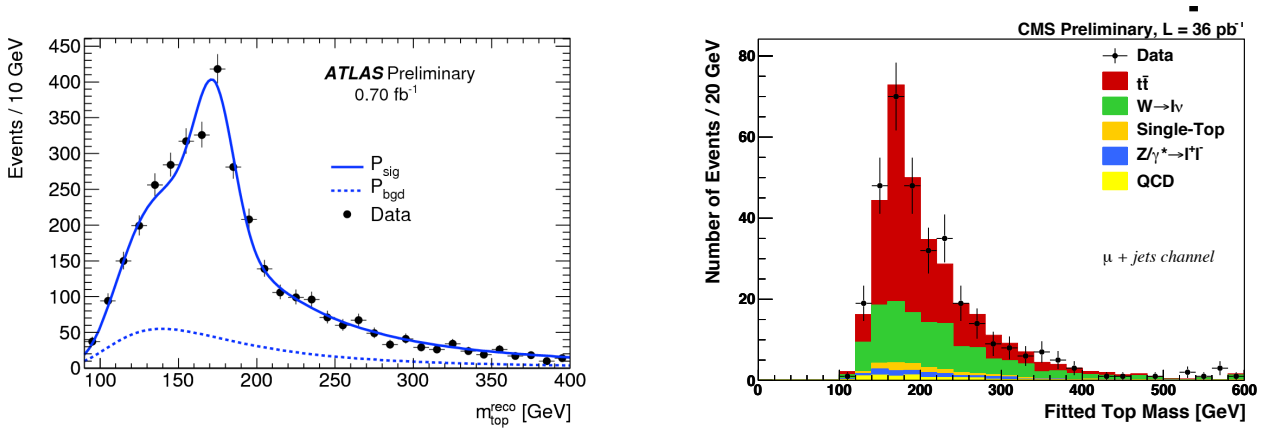

Figure 2: Top quark mass measured by ATLAS (left) and CMS in the μ+jets channel.

The large mass of the top quark can be interpreted as a large coupling to the Higgs boson. A very precise determination of this attribute is not only important *per se*, but it turns out to constrain very tightly the Higgs mass global fit. At present, Tevatron's measurement is still the world's best, with a precision of about 1 GeV.

It should be pointed out that beyond leading-order Quantum Chromodynamics (QCD) predictions, the top-quark mass value depends on the renormalization scheme. The measurements illustrated so far aim to quantify the parameter that enters into the Monte Carlo simulations. The top-quark mass in these MC generators (m_{MC}) does not correspond to a well-defined renormalization scheme leading to an uncertainty in its definition.

However, it is possible to express the production cross-section as a function of the pole mass of the particle. In the case of interest, the top quark is treated as it was a free particle. Using the 36 pb^{-1} acquired during the 2010 run, ATLAS[23] extracted the top quark pole

mass from the measurement of $\sigma_{t\bar{t}}$ with three different parametrizations[25][26][27], obtaining a set of values compatible with previous measurements performed by the D0 experiment[28]. A similar analysis has been performed by CMS[29] using 1.14 fb^{-1} yielding results compatible with previous measurements and with Tevatron's direct measurement.

5 Flavour-Changing Neutral Currents (FCNC)

In the Standard Model, the top quark decays almost exclusively to a W boson and a b quark. However, many extensions of the SM predicts the existence of vertices in which the flavour is not conserved[30]. In the SM, such vertices are forbidden at tree level and higher-order corrections are very small. ATLAS searched for $t \to qZ$ decay in the $t\bar{t}$ di-leptonic channel and for $qg \to t$ in single top lepton+jets channel.

Due to the limited statistics, ATLAS[31] could only set limits to FCNC. Top tri-leptonic decay, if it existed, has a branching ratio $\mathcal{B}(t \to qZ) < 17\%$ at 95% C.L. Anomalous single top production via FCNC must have a $\sigma(qg \to t) \times BR(t \to Wb) < 17.3$ pb at 95% C.L. In both cases, the measured value is compatible with the SM prediction.

6 Anomalous $\not{E}_T$ production

In some extensions of the Standard Model a top-like particle (T) can decay to top quarks and weakly interactive massive particles (WIMP A^0) such as the supersymmetric neutralino, that leaves no traces in the detector[32]. For this reason, it is interesting to investigate the $\not{E}_T$ spectrum to search for anomalous enhancements in the high-end tail of the distribution.

ATLAS[33] set limits to the mass of such new particles: the mass of the top-like particle must be higher than 300 GeV if the mass of the WIMP is less than 10 GeV at 95% C.L., or higher than 275 GeV if the WIMP is lighter than 50 GeV at 95% C.L.

7 Resonances

Many extensions of the Standard Model predict the existence of high-mass (~ 1 TeV) particles that decay directly to $t\bar{t}$ pairs, such as leptophobic topcolor (Z'), Kaluza-Klein gluons (g_{KK}), gravitons and black holes.

The general experimental strategy is to reconstruct the kinematic of the $t\bar{t}$ decay and search for resonances in the invariant mass spectrum. Not all the models have been taken in consideration: for instance, Z' is used to model narrow peaks[34] (1% of the mass of the resonance) and g_{KK} for broad peaks[35] (10% of the mass of the resonance). The most stringent limit set by ATLAS[36] was obtained using the sum of $\not{E}_T$ and the transverse energies of final

state particles in the di-leptonic channel (see Fig. 3, left). If g_{KK} exist, their mass must be higher than 840 GeV. An analogous search in the lepton+jets channel resulted to be less sensitive.

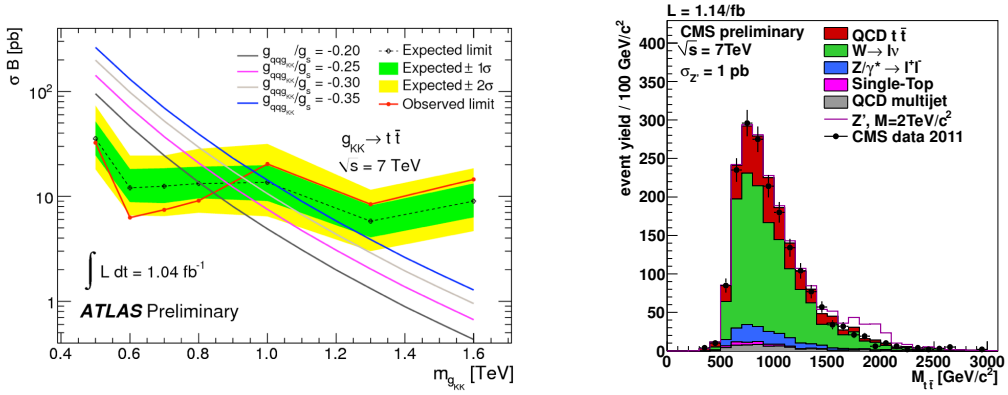

Figure 3: Search for top pairs resonances: Kaluza-Klein gluons (ATLAS, left) and Z' (CMS, right).

For masses higher than about 1 TeV, the top quarks gain a higher Lorentz boost and thus the angular separation among final state particles becomes narrower. CMS[37] optimized its search strategies to cope with such change of event topology. For intermediate ($\sim$1 TeV) masses, the charged lepton is close to the b-jet and cannot be considered isolated. The limit on the production of leptophobic topcolor Z' is $\sigma(Z' \to t\bar{t}) < 1$ pb for $m_{Z'} > 1.35$ TeV (see Fig. 3, right).

For even higher masses (>1 TeV) the jets become collimated and a completely different strategy has been devised. Making use of jet clustering algorithm with broader aperture parameter (*e.g.* the Cambridge-Aachen algorithm with $R = 1.0$), a pattern is searched in the cluster distribution *inside* the jet. Such W- and t-tagging algorithms are applied to 2- and 3-jets events to look for boosted $t\bar{t}$ full-hadronic decays. In this case the production limit set by CMS[38] is $\sigma(Z' \to t\bar{t}) < 1$ pb for $m_{Z'} > 1.5$ TeV.

8 Charge Asymmetry

The Standard Model predicts a very small (1%) charge-asymmetric production of top pairs due to interference among quark-antiquark vertices at NLO[39]. Recently, Tevatron's CDF and D0 experiments reported a remarkably high (40%) asymmetric production[40][41], with a dependence on the invariant mass of the $t\bar{t}$ system, more than 3σ away from the SM prediction[42]. Unfortunately, ATLAS and CMS are not able to measure the same observables: the LHC is a

symmetric pp collider, and the main production channel is gluon-gluon fusion instead of quark-antiquark annihilation. New variables sensible to the charge asymmetry have been worked out, namely $\Delta\eta = |\eta_t| - |\eta_{\bar{t}}$ deployed by CMS and $\Delta Y = |Y_t| - |Y_{\bar{t}}$ used by both experiments. They ultimately aim to measure the asymmetry $A(\Delta) = \frac{N(\Delta>0)-N(\Delta<0)}{N(\Delta>0)+N(\Delta<0)}$. In order to compare the two results, the resulting distributions are unfolded to the parton level using different inversion techniques.

ATLAS[43] found $A^Y = -0.024 \pm 0.016(stat) \pm 0.023(syst)$ while CMS[44] measured $A^Y = -0.013 \pm 0.026(stat)^{+0.026}_{-0.021}(syst)$ (see Fig. 4, left) and $A^\eta = -0.016 \pm 0.030(stat)^{+0.010}_{-0.019}(syst)$. The two results are compatible with each other and with the Standard Model prediction. CMS searched for a dependence of A^η on the invariant mass of the $t\bar{t}$ system, not finding any deviation from the SM (see Fig. 4, right).

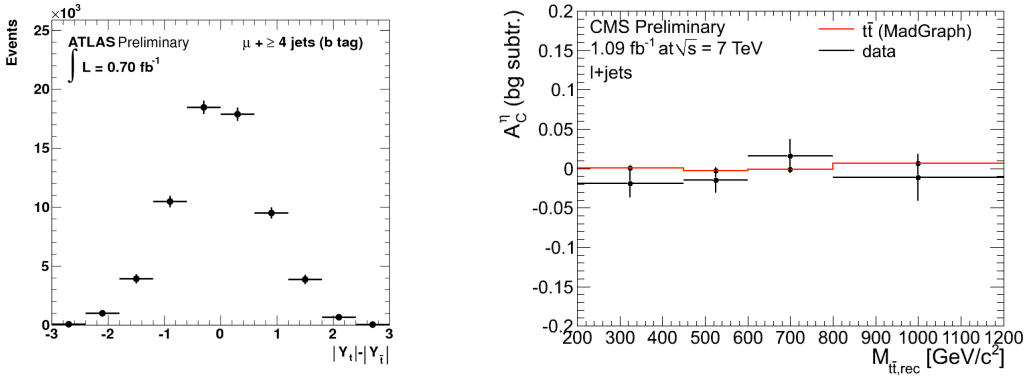

Figure 4: Charge asymmetry A^Y after unfolding (ATLAS, left) and A^η as a function of the $t\bar{t}$ invariant mass (CMS, right).

9 Conclusions

The LHC proved to be an extraordinary top quark factory, delivering more than 1200 pb^{-1} of data during the first half of the 2011 pp run. Top quark physics finally entered the precision era at the LHC. Lots of measurements have been performed looking for deviations from the Standard Model predictions, finding none. Using the larger data sample that has been acquired in the second half of 2011 it will be possible to obtain more precise results and set tighter limits to New Physics beyond the Standard Model.

References

[1] The ATLAS Collaboration et al, The ATLAS Experiment at the CERN Large Hadron Collider, JINST 3 S08003 (2008)

[2] The CMS Collaboration et al, The CMS experiment at the CERN LHC, JINST 3 S08004 (2008)

[3] The ATLAS Collaboration, ATLAS-CONF-2011-116 (2011)

[4] S. Moch and P. Uwer, Nucl. Phys. Proc. Suppl. 183 (2008) 7580, arXiv:0807.2794.

[5] The ATLAS Collaboration, ATLAS-CONF-2011-100 (2011)

[6] The ATLAS Collaboration, ATLAS-CONF-2011-121 (2011)

[7] The ATLAS Collaboration, ATLAS-CONF-2011-035 (2011)

[8] The ATLAS Collaboration, ATLAS-CONF-2011-023 (2011)

[9] The ATLAS Collaboration, ATLAS-CONF-2011-119 (2011)

[10] The CMS Collaboration, TOP-10-005 (2010)

[11] The CMS Collaboration, arXiv:1105.5661 (2011)

[12] The CMS Collaboration, arXiv:1108.3773 (2011)

[13] The CMS Collaboration, arXiv:1106.0902 (2011)

[14] The CMS Collaboration, TOP-11-006 (2011)

[15] The CMS Collaboration, TOP-11-007 (2011)

[16] N. Kidonakis, Phys. Rev. D83 (2011) 091503, arXiv:1103.2792

[17] The ATLAS Collaboration, ATLAS-CONF-2011-118 (2011)

[18] The ATLAS Collaboration, ATLAS-CONF-2011-104 (2011)

[19] The ATLAS Collaboration, ATLAS-CONF-2011-101 (2011)

[20] The CMS Collaboration, TOP-10-008 (2010)

[21] The CDF and D0 Collaborations and the Tevatron Electroweak Working Group (2010) , arXiv:1007.3178

[22] The ATLAS Collaboration, ATLAS-CONF-2011-120 (2011)

[23] The ATLAS Collaboration, ATLAS-CONF-2011-054 (2011)

[24] The CMS Collaboration, TOP-11-019 TOP-10-009 (2011)

[25] U. Langenfeld, S. Moch and P. Uwer, Phys. Rev. D80 (2009), arxiv:0906.5273

[26] N. Kidonakis, Phys. Rev. D82 (2010) 114030, arxiv:1009.4935

[27] V. Ahrens et al., JHEP 09 (2010) 097, arxiv:1003.5827

[28] The D0 Collaboration, Phys. Rev. D80 (2009) 071102, arXiv:0903.5525

[29] The CMS Collaboration, TOP-11-008 (2011)

[30] G. Lu, F. Yin, X. Wang, and L. Wan, Phys. Rev. D68 (2003) 015002, arXiv:hep-ph/0303122.

[31] The ATLAS Collaboration, ATLAS-CONF-2011-061 (2011)

[32] J. Alwall, J. L. Feng, J. Kumar et al., Phys. Rev. D81, 114027 (2010)

[33] The ATLAS Collaboration, ATLAS-CONF-2011-070 (2011)

[34] R. M. Harris, C. T. Hill, and S. J. Parke (1999), arXiv:hep-ph/9911288

[35] B. Lillie, L. Randall, and L.-T. Wang, JHEP 09 (2007) 074, arXiv:hep-ph/0701166

[36] The ATLAS Collaboration, ATLAS-CONF-2011-123 (2011)

[37] The CMS Collaboration, TOP-11-007 (2011)

[38] The CMS Collaboration, EXO-11-006 (2011)

[39] J.H.Kühn and G.Rodrigo, Phys. Rev. Lett. 81 (1998) 4952, arXiv:hep-ph/9802268.

[40] The CDF Collaboration, Phys. Rev. Lett. 101 (2008) 202001

[41] The D0 Collaboration, DO note 6062-CONF (2010)

[42] The CDF Collaboration (2011), arXiv:1101.0034

[43] The ATLAS Collaboration, ATLAS-CONF-2011-106 (2011)

[44] The CMS Collaboration, TOP-11-014 (2011)

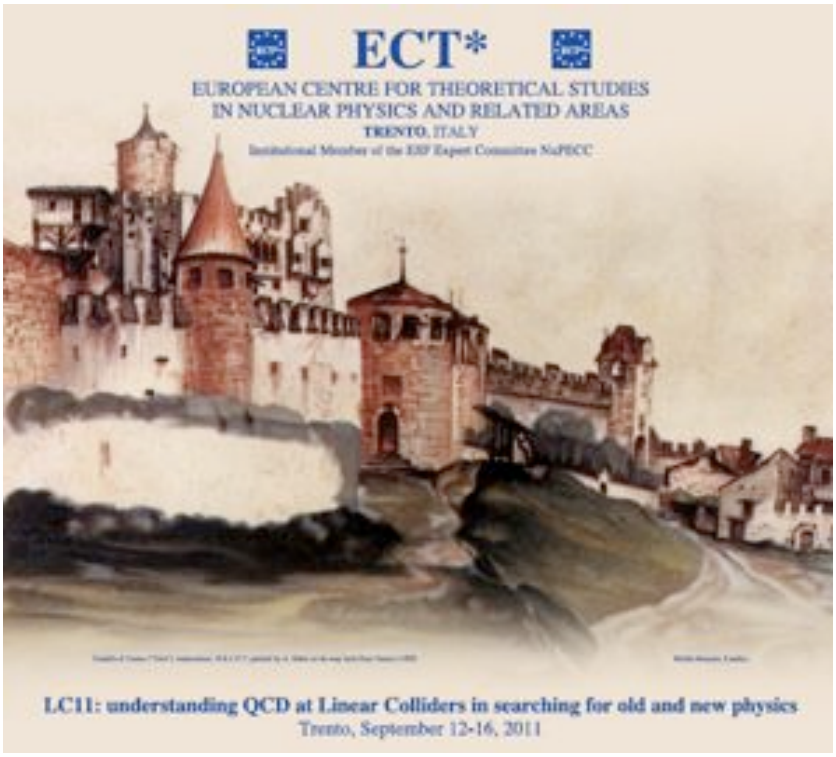

Castello di Trento painted by A. Dürer on his way back from Venice (1495).

6.3 A. Crivellin - Flavour violation in the MSSM and implications for top and squark searches at colliders

Flavor violation in the MSSM and implications for top and squark searches at colliders

Andreas Crivellin
ITP, University of Bern, Switzerland
crivellin@itp.unibe.ch

Abstract In this article I review some connections between flavor physics and collider physics. The first part discusses the effect of right-handed charged currents on the determination of the CKM elements V_{ub} based on Ref. [1]. It is shown that such an effective right-handed W-coupling can be generated in the MSSM which would lead to a sizable enhancement of single-top production at the LHC. The second part of this article focuses on the constraints on the mass splitting between left-handed squarks from Kaon and D mixing based on Ref. [2]. Such a mass splitting has interesting consequences for squark decay chains at colliders.

1 Right-handed W-coupling

In the standard model (SM) the tree-level W coupling has a pure $V-A$ structure meaning that all charged currents are left-handed. Right-handed charged currents were first studied in the context of left-right symmetric models [3] which enlarge the gauge group by an additional $SU(2)_R$ symmetry between right-handed doublets. In these models new right-handed gauge bosons W_R, Z_R appear and the physical SM-like W-boson has a dominant left-handed component with a small admixture of W_R. The latter will generically lead to small right-handed couplings to both quarks and leptons. The right-handed mass scale inferred from today's knowledge on neutrino masses is so large that all right-handed gauge couplings are undetectable. Most of these couplings are further experimentally strongly constrained [4]. A different source of right-handed couplings of quarks to the W-boson can be loop effects, which generate a dimension-6 quark-quark-W vertex. In this case no right-handed lepton couplings occur, as long as the neutrinos are assumed left-handed.

1.1 Right-handed W couplings

An appropriate framework for our analysis is an effective Lagrangian. Following the notation of Ref. [5], we write

$$\mathcal{L} = \mathcal{L}_{\rm SM} + \frac{1}{\Lambda}\sum_i C_i^{(5)} Q_i^{(5)} + \frac{1}{\Lambda^2}\sum_i C_i^{(6)} Q_i^{(6)} + \mathcal{O}\left(\frac{1}{\Lambda^3}\right), \tag{1}$$

here $\mathcal{L}_{\rm SM}$ is the standard model (SM) Lagrangian, while $Q_i^{(n)}$ stand for dimension-n operators built out of the SM fields and being invariant under the SM gauge symmetries. Such an effective theory approach is appropriate for any SM extension in which all new particles are sufficiently heavy ($M_{\rm new} \sim \Lambda \gg m_t$). As long as only processes with momentum scales $\mu \ll \Lambda$ are considered, all heavy degrees of freedom can be eliminated [6], leading to the effective theory defined in (1). The operators $Q_i^{(5)}$ and $Q_i^{(6)}$ have been completely classified in Ref. [7]. Here, we need the following dimension-six operator describing anomalous (not present in the SM) right-handed W-couplings to quarks:

$$Q_{RR} = \bar{u}_f \gamma^\mu P_R d_i \left(\tilde{\phi}^\dagger i D_\mu \phi\right) + h.c. \tag{2}$$

where ϕ denotes the Higgs doublet D_μ is the covariant derivative and $\widetilde{\phi} = i\tau^2\phi^*$. The Feynman rule for the W-u_f-d_i interaction vertex,

$$\frac{-ig_2\gamma^\mu}{\sqrt{2}}\left(V_{fi}^L P_L + V_{fi}^R P_R\right), \tag{3}$$

is found by combining the usual SM interaction with the extra contributions that are obtained by setting the Higgs field in Eq. (2) to its vacuum expectation value. In Eq. (3) V_{fi}^L and V_{fi}^R denote elements of the effective CKM matrices, which are not necessarily unitary. V_{fi}^R is related to the Wilson coefficient in Eq. (1) via $V_{fi}^R = C_{RR}/2\sqrt{2}G_F\Lambda^2$. V_{fi}^L receives contributions from the tree-level CKM matrix and the LL analogue of Q_{RR} in Eq. (2).

In Ref. [5] it was pointed out that very strong constraints can be obtained on V_{tb}^R from $b \to s\gamma$, because the usual helicity suppression factor of m_b/M_W is absent in the right-handed contribution. By the same argument V_{td}^R is tightly constrained. Large effects concerning transitions between the first two generations are unlikely, because $V_{us,cd}^L$ are larger than other off-diagonal CKM elements. Thus, we focus our attention on the remaining element V_{ub}^R (similar effects are possible for V_{cb}^R but the signature is less significant).

The experimental determination of $|V_{ub}|$ from both inclusive and exclusive B decays is a mature field by now [4]. To discuss the impact of right-handed currents we denote the CKM element extracted from data with SM formula by V_{ub}. If the matrix element of a considered exclusive process is proportional to the vector current, V_{ub}^L and V_{ub}^R enter with the same sign and the true" value of V_{ub}^L in the presence of V_{ub}^R is given by:

$$V_{ub}^L = V_{ub} - V_{ub}^R \tag{4}$$

For processes proportional to the axial-vector current V_{ub}^R enters with the opposite sign as V_{ub}^L, so that

$$V_{ub}^L = V_{ub} + V_{ub}^R. \tag{5}$$

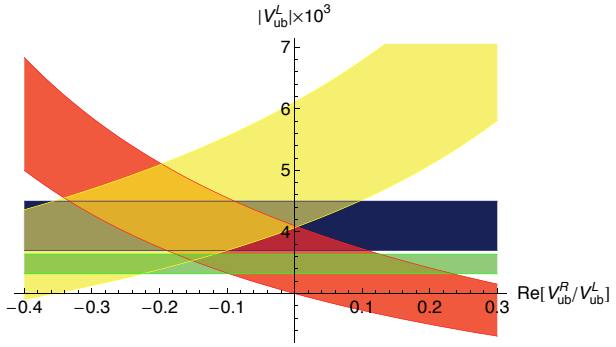

Figure 1: $\left|V_{ub}^L\right|$ as a function of $\mathrm{Re}\left[\mathrm{V_{ub}^R/V_{ub}^L}\right]$ extracted from different processes. Blue(darkest): inclusive decays. Red(gray): $B \to \pi l\nu$. Yellow(lightest gray): $B \to \tau\nu$. Green(light gray): V_{ub}^L determined from CKM unitarity.

In inclusive decays the interference term between the left-handed and right-handed contributions is suppressed by a factor of m_u/m_b so that it is irrelevant for V_{ub}. The remaining dependence on V_{ub}^R is quadratic and therefore negligible. Note that the determinations from inclusive and exclusive semileptonic decays agree within their errors, but the agreement is not perfect [4, 8]. The analysis of $B \to \tau\nu$ is affected by the uncertainty in the decay constant f_B. Within errors the three determinations of $|V_{ub}|$ are compatible for $V_{ub}^R = 0$, as one can read off from Fig. 1. The picture looks very different once the information from a global fit to the unitarity triangle (UT) is included: As pointed out first by the CKMFitter group, the measured value of $B \to \tau\nu$ suffers from a tension with the SM of 2.4–2.7σ [8]. First, the global UT fit gives a much smaller error on $|V_{ub}|$ (as a consequence of the well-measured UT angle β); the corresponding value is also shown in Fig. 1. Second, the data on $B_d - \overline{B}_d$ mixing exclude very large values for f_B, which in turn cuts out the lower part of the yellow (light gray) region in Fig. 1. Essentially we realize from Fig. 1 that we can remove this tension while simultaneously bringing the determinations of $|V_{ub}|$ from inclusive and exclusive semileptonic decays into even better agreement. For this the right-handed component must be around $\mathrm{Re}\,(V_{ub}^R/V_{ub}^L) \approx -0.15$.

1.2 MSSM renormalization of the quark-quark-W vertex

In Ref. [9] the renormalization of the quark-quark-W vertex by non-decoupling chirally enhanced supersymmetric self-energies has been computed. Here, we extend this analysis and calculate the leading contributions to the quark-quark-W vertex which decouple for $M_{\mathrm{SUSY}} \to \infty$. Using the conventions of Ref. [9] we expand to first order in the external momenta and decompose the self-energies as

$$\Sigma_{fi}^q = \left(\Sigma_{fi}^{q\,LR} + \not{p}\Sigma_{fi}^{q\,RR}\right) P_R + \left(\Sigma_{fi}^{q\,RL} + \not{p}\Sigma_{fi}^{q\,LL}\right) P_L. \tag{6}$$

These self-energies lead to a flavor-valued wave-function renormalization $\Delta U_{fi}^{q\,L,R}$ for all external left- and right-handed fields. It is useful to decompose these factors further in to an unphysical

anti-Hermitian part $\Delta U_{fi}^{q\,L\,A}$, which can be absorbed into the renormalization of the CKM matrix, and a Hermitian part $\Delta U_{fi}^{q\,L\,H}$, which can constitute a physical effect appearing as a deviation from CKM unitarity: $\Delta U_{fi}^{q\,L,R\,H} = \Sigma_{fi}^{q\,LL,RR}/2$. Neglecting external momenta, the genuine vertex-correction originating from a squark-gluino loop is given by

$$-i\Lambda_{u_f d_i}^{W\,\tilde{g}} = \tag{7}$$
$$\frac{g_2}{\sqrt{2}}\frac{i\alpha_s}{3\pi}\gamma^\mu \sum_{s,t=1}^{6}\sum_{j,k=1}^{3}\Big(W_{fs}^{\tilde{u}} W_{ks}^{\tilde{u}*} V_{kj}^L W_{jt}^{\tilde{d}} W_{it}^{\tilde{d}*} P_L + W_{f+3,s}^{\tilde{u}} W_{ks}^{\tilde{u}*} V_{kj}^L W_{jt}^{\tilde{d}} W_{i+3,t}^{\tilde{d}*} P_R\Big) C_2\left(m_{\tilde{u}_s}, m_{\tilde{d}_t}, m_{\tilde{g}}\right).$$

The matrices $W_{st}^{\tilde{q}}$ diagonalize the squark mass matrices [9]. The part proportional to P_L in Eq. (7) cancels with the anti-Hermitian part of the wave-function renormalization due to the SU(2) relation between the left-handed up and down squarks for $M_{\rm SUSY} \to \infty$ according to the decoupling theorem [6]. Since the loop function C_2 depends only weakly on $M_{\rm SUSY}$, the cancellation is very efficient, even for light squarks around 300 GeV. Therefore, the unitarity of the CKM matrix is conserved with very high accuracy. A right-handed coupling of quarks to the W boson is induced by the diagram in Fig. 2 if left-right mixing of squarks is present. The effective coupling corresponds to Q_{RR} in Eq. (2) and vanishes in the decoupling limit $M_{\rm SUSY} \to \infty$. There is no wave-function renormalization of right-handed quarks which can be applied to the W vertex, therefore no gauge cancellations occur.

We show the relative size of the right-handed coupling involving u,c and b in Fig. 2. Note that the mass insertion $\delta_{13}^{u\,RL}$ is not affected by the fine-tuning argument imposed in [9] nor severely restricted by flavor-changing neutral current (FCNC) processes. Therefore, the size of the induced couplings V_{ub}^R can be large enough to explain (attenuate) the apparent discrepancies among the various determinations of $|V_{ub}|$.

1.3 Right-handed W coupling and single-top production

We have seen that the disturbing problem with $B \to \tau\nu_\tau$ [8] can be removed and the inclusive and exclusive determinations of $|V_{ub}|$ can be brought into agreement. If one wants to achieve this in the MSSM a large left-right mixing between sbottom squarks (as present in e.g. the popular large-tan β scenarios) and a large A_{31}^u-term is needed. Large values for A_{31}^u enhance single-top production, making it observable at the LHC. If $\delta_{13}^{u\,RL} \approx 0.6$ a 95% CL signal can already be detected with 50 inverse femtobarn [10].

2 Non-degenerate squark masses

Already in the early stages of minimal supersymmetric standard model (MSSM) analyses it was immediately noted, that a super GIM mechanism is needed in order to satisfy the bounds from

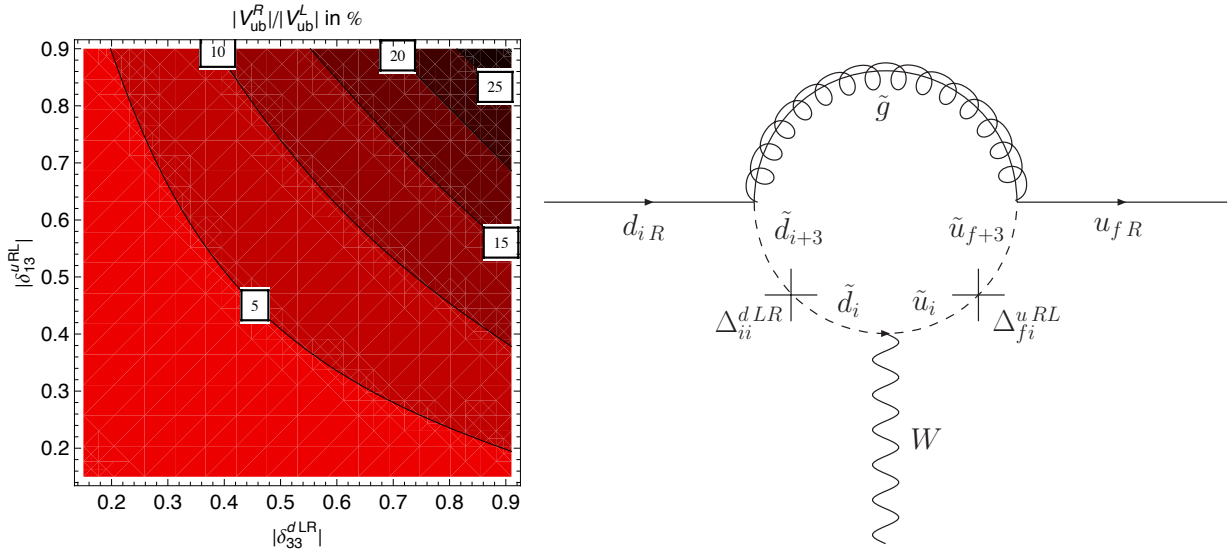

Figure 2: Right: Feynman diagram which induces the effective right-handed W coupling of a down-type quark of flavor i to an up-type quark of flavor f. The crosses stand for the flavor and chirality changes needed to generate the coupling.
Left: Relative strength of the induced right-handed coupling $|V_{ub}^R|$ with respect to $|V_{ub}^L|$ for $M_{\rm SUSY} = 1\,\text{TeV}$. $|V_{ub}^L|$ is determined from CKM unitarity.

flavor changing neutral currents (FCNCs) [11]. Therefore, the mass matrix of the left-handed squarks should be (at least approximately) proportional to the unit matrix, since otherwise flavor off-diagonal entries arise inevitably either in the up or in the down sector due to the SU(2) relation between the left-handed squark mass terms (i. e. left-handed up squark and down squark mass matrices differ only by a CKM rotation). The idea that nondegenerate squarks can still satisfy the FCNC constraints (K and D mixing) was first discussed in Ref. [12] in the context of Abelian flavor symmetries.

The squark spectrum is also a hot topic concerning bench-mark scenarios for the LHC. It is commonly assumed that the squarks are degenerate at some high scale and that non-degeneracies are introduced via the renormalization group [13, 14]. In such scenarios, the non-degeneracies are proportional to Yukawa couplings and therefore only sizable for the third generation. In principle, there remains the possibility that squarks have already different masses at some high scale. The question to be clarified is which regions in parameter space with non-degenerate squarks are compatible with $D-\overline{D}$ and $K-\overline{K}$ mixing.

2.1 Meson mixing between the first two generations

Measurements of FCNC processes put strong constraints on new physics at the TeV scale and provide an important guide for model building. In particular $D-\overline{D}$ and $K-\overline{K}$ mixing strongly constrain transitions between the first two generations and combining both is especially

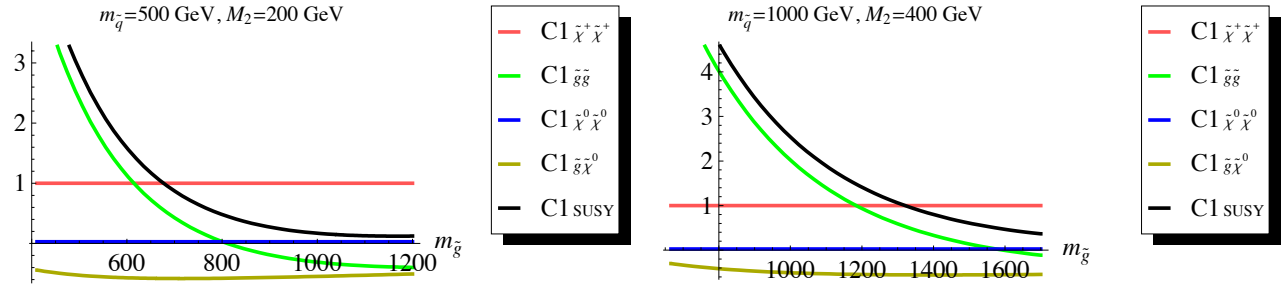

Figure 3: Size of the real part of Wilson coefficients [see Eqs. (12) and (13)] contributing to $D-\overline{D}$ or $K-\overline{K}$ mixing normalized to the chargino contribution as a function of $m_{\tilde{g}}$ for different values of $m_{\tilde{q}}$ and M_2 assuming a small nonzero (real) off-diagonal element $\delta_{12}^{q\,LL}$. $C_{1\mathrm{SUSY}}$ is the sum of all Wilson coefficients contributing in addition to the SM one. The relative size of the coefficients remains unchanged also in the case of complex elements $\delta_{12}^{q\,LL}$.

powerful to place bounds on new physics [15]. In the down sector FCNCs between the first two generations are probed by the neutral Kaon system. Here the experimental values for the mass difference and the CP violating quantity ϵ_K are [4]:

$$\begin{aligned}\Delta m_K/m_K &= (7.01 \pm 0.01) \times 10^{-15} \\ \epsilon_K &= (2.23 \pm 0.01) \times 10^{-3}\end{aligned} \tag{8}$$

As we see from Eq. (8) both the mass difference and the size of the indirect CP violation are tiny and the numbers are in agreement with the standard model (SM) prediction: The SM contribution to the mass difference is small due to a rather precise GIM suppression (the top contribution is suppressed by small CKM elements) and also the CP asymmetry is strongly suppressed because CP violation necessarily involves the tiny CKM combination $V_{td}V_{ts}^*$ related to the third fermion generation. Therefore, Kaon mixing puts very strong bounds on NP scenarios like the MSSM. According to the analysis of Ref. [16] the allowed range in the $C_{M_K} - C_{\epsilon_K}$ plane is rather limited. At 95% confidence level on can roughly expect the NP contribution to the mass difference ΔM_K to be at most of the order of the SM contribution. The NP contribution to ϵ_K is even more restricted.

In the up sector FCNCs are probed by $D-\overline{D}$ mixing. In contrast to the well-established Kaon mixing, it was only discovered recently in 2007 by the BABAR and BELLE collaborations. The current experimental values are [4]:

$$\begin{aligned}\Delta m_D/m_D &= (8.6 \pm 2.1) \times 10^{-15} \\ A_\Gamma &= (1.2 \pm 2.5) \times 10^{-3}\end{aligned} \tag{9}$$

Short-distance SM effects are strongly CKM suppressed and the long-distance contributions can only be estimated. Therefore, conservative estimates assume for the SM contribution a range up to the absolute measured value of the mass difference. However, due to the small measured

mass difference D mixing still limits NP contributions in a stringent way. Furthermore, a CP violating phase in the neutral D system can directly be attributed to NP.

In summary, $D-\overline{D}$ and $K-\overline{K}$ mixing restrict FCNC interactions between the first two generations in a stringent way and one should expect the NP contributions to the mass difference to be smaller than the experimental value [15]:

$$\Delta m_{D,K}^{\rm NP} \leq \Delta m_{D,K}^{\rm exp} \tag{10}$$

CP violation associated with new physics is even more restricted, especially in the d sector:

$$\epsilon_K^{\rm NP} \leq 0.6 \epsilon_K^{\rm exp} \tag{11}$$

Equations (10) and (11) summarize in a concise way the allowed range for NP and we will use them to constrain the NP contributions to K and D mixing in Sec. 2.2.

2.2 Constraints on the mass splitting from Kaon and D mixing.

In the common definition of MFV [17] flavor-violation due to NP is postulated to stem solely from the Yukawa sector, resulting in FCNC transitions proportional to products of CKM elements and Yukawa couplings. Therefore, such scenarios allow only sizable deviations from degeneracy with respect to the third generation. A more general notion of MFV could be defined by stating that all flavor changes should be induced by CKM elements. This definition would also cover the case with a diagonal squark mass matrix in one sector (either the up or the down sector) but with off-diagonal elements, introduced by the $SU(2)$ relation, in the other sector. This setup corresponds to an exact alignment of the squark mass term $m_{\tilde{q}}^2$ with the product of Yukawa matrices $Y_u^\dagger Y_u$ (or with $Y_d^\dagger Y_d$ in the case of a diagonal down squark mass matrix).

The obvious way how off-diagonal elements of the squark mass matrices enter meson mixing is via squark-gluino diagrams. These contributions to $O_1 = \bar{s}\gamma^\mu P_L d \otimes \bar{s}\gamma_\mu P_L d$ are commonly expected to be dominant since they involve the strong coupling constant:

$$C_1^{\tilde{g}\tilde{g}} = -\frac{g_s^4}{16\pi^2}\sum_{s,t=1}^{6}\left[\frac{11}{36}D_2\left(m_{\tilde{q}_s}^2, m_{\tilde{q}_t}^2, m_{\tilde{g}}^2, m_{\tilde{g}}^2\right) + \frac{1}{9}m_{\tilde{g}}^2 D_0\left(m_{\tilde{q}_s}^2, m_{\tilde{q}_t}^2, m_{\tilde{g}}^2, m_{\tilde{g}}^2\right)\right] V_{s\,12}^{q\,LL} V_{t\,12}^{q\,LL} \tag{12}$$

Our conventions for the loop-functions and the matrices in flavor space $V_{s\,12}^{q\,LL}$ are given in the appendix of Ref. [9]. However, if we have flavor-changing LL elements it is no longer possible to concentrate on the gluino contributions for four reasons:

- The gluino contributions suffer from cancellations between the boxes with crossed and uncrossed gluino lines corresponding to the two terms in the square brackets in Eq. (12). The crossed box diagrams occur since the gluino is a Majorana particle. This cancellation occurs approximately in the region where $m_{\tilde{g}} \approx 1.5\, m_{\tilde{q}}$.

- In the SU(2) limit with unbroken SUSY the winos couple directly to left-handed particles with the weak coupling constant g_2. Therefore, flavor-changing LL elements can contribute without involving small left-right or gaugino mixing angles.
- Since charginos are Dirac fermions, there are no cancellations between different diagrams at the one-loop order.
- The wino mass M_2 is often assumed to be much lighter than the gluino mass. In most GUT models the relation $M_2 \approx m_{\tilde{g}}\alpha_2/\alpha_3$ holds. Since the loop function is always dominated by the heaviest mass, one can expect large chargino and neutralino contributions if the squarks masses are similar to the lighter chargino masses.

Therefore, we have to take into account the weak (and the mixed weak-strong) contributions to C_1:

$$\begin{aligned}
C_1^{\tilde{\chi}^0\tilde{\chi}^0} &= -\tfrac{1}{128\pi^2}\tfrac{g_2^4}{4}\sum_{s,t=1}^{6}\left(D_2\left(m^2_{\tilde{q}_s},m^2_{\tilde{q}_t},M_2^2,M_2^2\right)+2M_2^2D_0\left(m^2_{\tilde{q}_s},m^2_{\tilde{q}_t},M_2^2,M_2^2\right)\right)V_{s\,12}^{q\,LL}V_{t\,12}^{q\,LL}\\
C_1^{\tilde{g}\tilde{\chi}^0} &= -\tfrac{1}{16\pi^2}\tfrac{g_s^2g_2^2}{2}\sum_{s,t=1}^{6}\left(\tfrac{1}{6}D_2\left(m^2_{\tilde{q}_s},m^2_{\tilde{q}_t},m^2_{\tilde{g}},M_2^2\right)+\tfrac{1}{3}m_{\tilde{g}}M_2D_0\left(m^2_{\tilde{q}_s},m^2_{\tilde{q}_t},m^2_{\tilde{g}},M_2^2\right)\right)V_{s\,12}^{q\,LL}V_{t\,12}^{q\,LL}\\
C_1^{\tilde{\chi}^+\tilde{\chi}^+} &= -\tfrac{g_2^4}{128\pi^2}\sum_{s,t=1}^{6}D_2\left(m^2_{\tilde{q}_s},m^2_{\tilde{q}_t},M_2^2,M_2^2\right)V_{s\,12}^{q\,LL}V_{t\,12}^{q\,LL}
\end{aligned} \tag{13}$$

In Eq. (13) we have set all Yukawa couplings to zero and neglected small chargino and neutralino mixing. Because of the small Yukawa couplings of the first two generations and the suppressed bino-wino mixing the only sizable contribution of both the gluino and the electroweak diagrams is to the same operator $O_1 = \bar{s}\gamma^\mu P_L d \otimes \bar{s}\gamma_\mu P_L d$ as the SM contribution. Note that in all contribution the same combination of mixing matrices enters, since the CKM matrices in the chargino vertex cancels with the ones in the squark mass matrix.

In Fig. 3 we show the size of the different contributions to C_1 as a function of the gluino mass. We have normalized all coefficients to $C_1^{\tilde{\chi}^+\tilde{\chi}^+}$ since only one box diagram contributes to it and therefore the coefficient depends only on one loop-function which is strictly negative.

As stated before, SU(2) symmetry links a mass splitting in the up (down) sector to flavor-changing LL elements in the down (up) sector. So, if one assumes a next-to minimal" setup in which one mass matrix is diagonal, one has to specify if this is the up or the down squark mass matrix. If the down (up) squark mass matrix is diagonal, which implies that it is aligned to $Y_d^\dagger Y_d$ ($Y_u^\dagger Y_u$), one has contributions to $D-\overline{D}$ ($K-\overline{K}$) mixing. Assuming a diagonal up-squark (down-squark) mass matrix, the allowed regions compatible with $K-\overline{K}$ mixing ($D-\overline{D}$ mixing) are shown in Fig. 4. Note that there are large regions in parameter space with nondegenerate squark still allowed by $K-\overline{K}$ ($D-\overline{D}$) mixing due to the cancellations between the different contributions shown in Fig. 3. However, departing from an exact alignment with either $Y_u^\dagger Y_u$ or $Y_d^\dagger Y_d$ there are points in parameter space which allow for an even larger mass splitting [15]

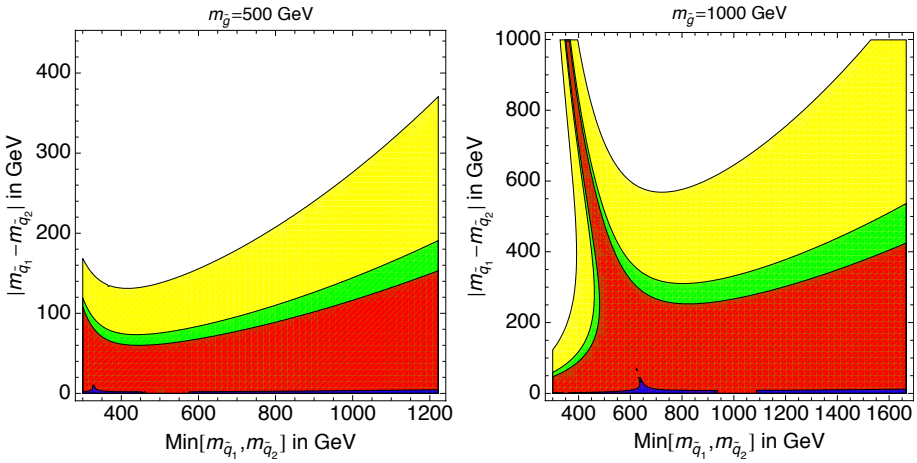

Figure 4: Allowed mass splitting between the first two generations of left-handed squarks for different gluino masses. We assume the approximate GUT relation $M_2 = (\alpha_2/\alpha_s)m_{\tilde{g}} \cong 0.35$. Yellow (lightest) corresponds to the maximally allowed mass splitting assuming an intermediate alignment of $m^2_{\tilde{q}}$ with $Y_u^\dagger Y_u$ and $Y_d^\dagger Y_d$ [15]. The green (red) region is the allowed range assuming an diagonal up (down) squark mass matrix. The blue (darkest) area is the minimal region allowed for the mass splitting between the left-handed squarks, which corresponds to a scenario with equal diagonal entries in the down squark mass matrix but with an off-diagonal element carrying a maximal phase. Note that the allowed mass splittings are large enough to permit the decay of the heavier squark into the lighter one plus a W boson.

due to an additional off-diagonal element in the squark mass matrix. If this element is real one can choose an appropriate value which maximizes the allowed mass splitting [1]. Nevertheless, this additional off-diagonal element now present in both sectors due to the SU(2) relation could also carry a phase additional to the CKM matrix. If this phase is maximal one obtains the minimally allowed range for the mass splitting due to the severe constraint from ϵ_K. These minimally and maximally allowed regions for the mass splittings are also shown in Fig. 4.

This has interesting consequences both for LHC benchmark scenarios (which usually assume degenerate squarks for the first two generations) and for models with Abelian flavor symmetries (which predict non-degenerate squark masses for the first two generation) because $K-\overline{K}$ and $D-\overline{D}$ mixing cannot exclude non-degenerate squark masses of the first two generations. This allows for different decay chains of squarks. For example if the mass difference is larger than 80 GeV an additional W can be emitted leading to an additional jet or a charged lepton in the final state.

[1] We thank Gilad Perez for bringing this to our attention.

Acknowledgments

I thank the organizers, especially Francesca Borzumati, for the invitation and the opportunity to participate in this very interesting workshop. I also thank Daniel Arnold for a careful proofreading of the article. A.C. is supported by the Swiss National Science Foundation. The Albert Einstein Center for Fundamental Physics is supported by the "Innovations- und Kooperationsprojekt C-13 of the Schweizerische Universitätskonferenz SUK/CRUS".

References

[1] A. Crivellin, Phys. Rev. D **81** (2010) 031301 [arXiv:0907.2461 [hep-ph]].

[2] A. Crivellin and M. Davidkov, Phys. Rev. D **81** (2010) 095004 [arXiv:1002.2653 [hep-ph]].

[3] G. Senjanovic and R. N. Mohapatra, Phys. Rev. D **12** (1975) 1502.

[4] C. Amsler *et al.* [Particle Data Group Collaboration], Phys. Lett. B **667** (2008) 1.

[5] B. Grzadkowski and M. Misiak, Phys. Rev. D **78** (2008) 077501 [Erratum-ibid. D **84** (2011) 059903] [arXiv:0802.1413 [hep-ph]].

[6] T. Appelquist and J. Carazzone, Phys. Rev. D **11** (1975) 2856.

[7] W. Buchmuller and D. Wyler, Nucl. Phys. B **268** (1986) 621.

[8] J. Charles *et al.* [CKMfitter Group Collaboration], Eur. Phys. J. C **41** (2005) 1 [hep-ph/0406184].

[9] A. Crivellin and U. Nierste, Phys. Rev. D **79** (2009) 035018 [arXiv:0810.1613 [hep-ph]].

[10] T. Plehn, M. Rauch and M. Spannowsky, Phys. Rev. D **80** (2009) 114027 [arXiv:0906.1803 [hep-ph]].

[11] S. Dimopoulos and H. Georgi, Nucl. Phys. B **193** (1981) 150.

[12] Y. Nir and N. Seiberg, Phys. Lett. B **309** (1993) 337 [hep-ph/9304307].

[13] J. A. Aguilar-Saavedra *et al.*, Eur. Phys. J. C **46** (2006) 43 [hep-ph/0511344].

[14] A. De Roeck *et al.*, Eur. Phys. J. C **49** (2007) 1041 [hep-ph/0508198].

[15] K. Blum, Y. Grossman, Y. Nir and G. Perez, Phys. Rev. Lett. **102** (2009) 211802 [arXiv:0903.2118 [hep-ph]].

[16] M. Ciuchini *et al.*, JHEP **0107** (2001) 013 [hep-ph/0012308].

[17] G. D'Ambrosio, G. F. Giudice, G. Isidori and A. Strumia, Nucl. Phys. B **645** (2002) 155

6.4 S. Barsuk - Heavy flavours and QCD: selected LHCb results

Heavy flavours and QCD: selected LHCb results

Sergey Barsuk for the LHCb Collaboration LAL, Paris XI University and IN2P3/CNRS, France
barsuk@lal.in2p3.fr

Abstract The LHCb experiment accumulates and analyzes data from pp collisions at the LHC. Selected results and prospects on heavy flavours and QCD are reported below, focusing on heavy flavour production and decays, lifetime-based studies and CP violation studies.

1 Introduction

Despite numerous attempts to disqualify it, the Standard Model (SM) proved to describe successfully all experimental measurements for decades. The experimental tests have reached now unprecedented precision with the contributions from the B-factories, Tevatron and since recently LHC data. Heavy flavours provide a powerful tool for precision measurements of the SM parameters and the search for effects beyond SM [1]. Prolific heavy flavour production at the LHC, together with a detector optimized for heavy flavour studies, place the LHCb experiment in the leading position for further precision tests. Below, after the LHCb experiment is briefly described, selected heavy flavour results are outlined. Production measurements, search for CP violation (CPV) in lifetime based charm studies, the angle γ and $B_s\bar{B}_s$ mixing phase ϕ_s, new results on b-baryons, radiative penguins $b \to s\gamma$, and search for $B_s \to \mu^+\mu^-$ are chosen to illustrate the LHCb physics reach.

2 LHCb detector overview

The LHCb detector [2] is a single-arm forward spectrometer covering the pseudorapidity range $2 < \eta < 5$ (Fig. 1), designed for studies of rare phenomena in b and c decays in order to precisely constrain the SM parameters and search for effects beyond. At the LHC energies, the production of b and $\bar{b}$ quarks is highly correlated with respect to the boost, so that if a b quark goes into the detector acceptance, the corresponding $\bar{b}$ quark products are also captured with high probability. With only about 4% solid angle instrumented, LHCb captures about 40% of the heavy flavour production cross section. Owing to a better acceptance in the forward direction, a factor 2 higher $b\bar{b}$ cross section is expected at LHCb compared to the ATLAS or CMS experiments. The acceptance is unique amongst the LHC experiments, and gives access to valuable QCD studies in the forward region.

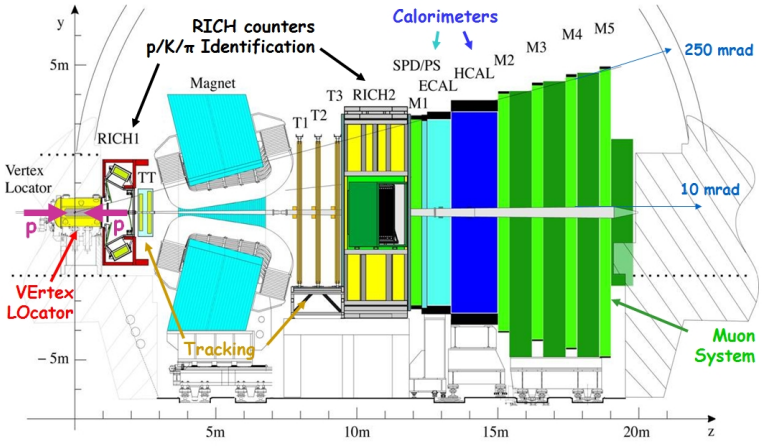

Figure 1: The LHCb detector

The detector includes a high precision tracking system consisting of a silicon-strip vertex detector surrounding the pp interaction region, a large-area silicon-strip detector located upstream of a dipole magnet with a bending power of about 4 Tm, and three stations of silicon-strip detectors and straw drift-tubes placed downstream. The combined tracking system has a momentum resolution $\Delta p/p$ that varies from 0.4% at 5 GeV/c to 0.6% at 100 GeV/c, and an impact parameter resolution of 20 μm for tracks with high transverse momentum. Charged hadrons are identified using two ring-imaging Cherenkov detectors. Photon, electron and hadron candidates are identified by a calorimeter system consisting of scintillating-pad and pre-shower detectors, an electromagnetic calorimeter and a hadronic calorimeter. Muons are identified by a muon system composed of alternating layers of iron and multiwire proportional chambers. The trigger consists of a hardware stage, based on information from the calorimeter and muon systems, followed by a software stage which applies a full event reconstruction.

For the results discussed below, precision vertex reconstruction and particle identification (ID) are very important. The VELO system comprises 21 stations of two semicircular silicon sensors each yielding a polar coordinates measurement. The sensors are retractable in order to provide safe conditions during injection and until stable beams are achieved. At closed position, the sensitive area is as close as 8 mm to the beam axis. VELO provides excellent proper time resolution of about 50 fs, as determined for the early B-lifetime measurements [3].

A system of two Cherenkov detectors is used for charged hadron separation. Aiming at lower momenta particles' ID, the RICH1 detector is installed upstream of the magnet. It covers a momentum range from 1 to about 70 GeV/c in the 25 to 250 (300) mrad vertical (horizontal) acceptance, and uses silica aerogel and C_4F_{10} as radiators. RICH2 employs CF_4 radiator and

provides ID for particles of 15 to about 100 GeV/c momenta in the 15 to 100 (120) mrad vertical (horizontal) acceptance, and is positioned downstream of the magnet. Presently achieved ID performance using RICH is extracted from data and yields the rate of pions erroneously identified as kaons of ∼7%, while maintaining kaon ID efficiency at ∼95% for typical charged hadron spectra from b decays.

In 2010 and 2011 the LHC machine operated at the reduced energy of $E_{CM} = 7$ TeV, which then will be progressively increased to the design value of 14 TeV. The LHCb runs at a reduced LHC luminosity, tuneable by defocusing beams, close to a maximum contribution of single interaction probability per beam crossing, in order to maximize the physics reach. A nominal LHCb operation assumes 10^7 s effective annual operation time and instantaneous luminosity of 2×10^{32} cm^{-2}s^{-1}, corresponding to the integrated luminosity of 2 fb^{-1}.

Assuming $\sigma_{b\bar{b}} \approx 0.6$ mb and $\sigma_{c\bar{c}} \approx 8.3$ mb cross sections, samples of 10^{12} $b\bar{b}$ pairs and 6×10^{12} $c\bar{c}$ pairs are expected in one year of nominal running. Reduced heavy flavour production at $E_{CM} = 7$ TeV together with the integrated luminosity of 1 fb^{-1} in 2011, correspond to 3×10^{11} $b\bar{b}$ pairs and 2×10^{12} $c\bar{c}$ pairs. Note that all the heavy flavour species are produced.

LHCb collected 37 pb^{-1} of data in 2010, and more than 700 pb^{-1} by the time of the conference, the goal of 1 fb^{-1} in 2011 has been reached thereafter. This was possible thanks to the excellent performance of the LHC machine, with a peak luminosity of 2×10^{33} cm^{-2}s^{-1} achieved with about 1300 bunches. In 2011 LHCb recorded data with an efficiency above 90%, being able to accumulate more than 1 pb^{-1}/hour under instantaneous luminosity of up to 4×10^{32} cm^{-2}s^{-1}, achieved in 2011, in auto-levelling mode. The LHCb luminosity levelling allowed the operation at effectively constant instantaneous luminosity over almost all the LHC fill. Exceeding nominal luminosity of 2×10^{32} cm^{-2}s^{-1} assumes higher track multiplicity with one primary vertex corresponding to an average of 30 tracks per rapidity range, and is dangerous for reconstruction. In particular, additional background for c- and b- decay vertex reconstruction has to be considered, since e.g. the average minimum distance between four primary vertices amounts to about 12 mm, and is comparable to the average B travel distance of about 10 mm.

3 Heavy flavour production

LHCb exploits prolific production of heavy flavours at the LHC. Below production studies for prompt and secondary quarkonia, exotic states, and open beauty are addressed.

Already the very first data, corresponding to 5.2 pb^{-1} integrated luminosity, yielded a sample of 565000 reconstructed $J/\psi \to \mu^+\mu^-$ decays [4]. The differential cross-section for J/ψ production was measured separately for prompt J/ψ and J/ψ from b-hadron decays, as a function of the J/ψ transverse momentum and rapidity in the forward region, $2.0 < y < 4.5$. This measurement is the first measurement of prompt J/ψ and J/ψ from b production in the forward region at $\sqrt{s} = 7$ TeV. The results obtained are in good agreement with the CMS

analysis [5] at the same centre-of-mass energy, in a region corresponding to the low rapidity part of the LHCb acceptance. The results are also in good general agreement with the theoretical calculations of J/ψ hadroproduction [6], even if the uncertainties on the predictions are still large. In order to efficiently discriminate amongst various models, studies of other observables such as the J/ψ polarisation measurement will be necessary. The measurement of the cross-section for J/ψ from b-hadron decays agrees very well with FONLL predictions. In addition, this measurement yields an estimate of the $b\bar{b}$ cross-section in pp collisions at $\sqrt{s} = 7$ TeV, which is in excellent agreement with measurements performed analysing different b decay modes [7].

The di-muon final state was also used for bottomonium production studies [8]. After taking into consideration NNLO, the colour singlet model (CSM) agrees with the LHCb data, though the theoretical uncertainty is still large.

Higher quarkonium states, χ_c and χ_b, have been reconstructed via their radiative transitions to J/ψ and $\Upsilon(1S)$ respectively using about 35 pb^{-1} of 2010 data. Experimental precision reasonably allows to resolve χ_{c2} and χ_{c1} signals, yielding their production ratio, depending on charmonium transverse momentum. The resulting distribution exceeds systematically theory curves for LO CSM and NLO NRQCD, though errors on both theoretical and experimental results are still large [9]. The $\chi_{b0,1,2}$ states cannot be resolved in the current analysis, a signal of 350 ± 59 χ_b candidates is observed, see Fig. 2.

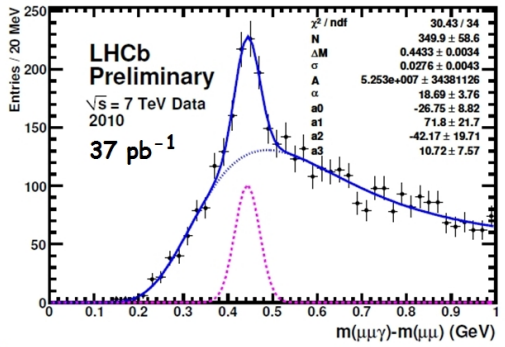

Figure 2: Search for χ_b states via their radiative transition to $\Upsilon(1S)$

New data on the $X(3872)$ exotic state production, as well as an improvement of the precision of its mass measurement, are needed for its internal structure interpretation. The LHCb studies rely on the $X(3872)$ state reconstruction via $X(3872) \to J/\psi\pi^+\pi^-$ decay mode. The inclusive studies are based on 35 pb^{-1} of 2010 data. Mass calibration was performed by scaling track momenta and constraining $\Upsilon(1S)$ and $\psi(2S)$ masses using the dimuon channel, and D^0 and K^0_s masses using h^+h^- final state. Topologically identical $\psi(2S) \to J/\psi\pi\pi$ channel was used as a control channel. The $X(3872)$ mass was measured to be [10] $M = 3871.96 \pm 0.46 \pm 0.10$

MeV/c^2, and the production to be [11] $\sigma \times BR(X(3872) \to J/\psi\pi^+\pi^-) = 4.74 \pm 1.10 \pm 1.01$ for 5 GeV/c $< p_T <$ 20 GeV/c and $2.5 < \eta < 4.5$, with the precision expected to improve with statistics. Secondary $X(3872)$ from $B^+ \to X(3872)K^+$ decays were observed with statistics of 376 pb^{-1}, see Fig. 3. This sample will allow better precision for mass determination, and the

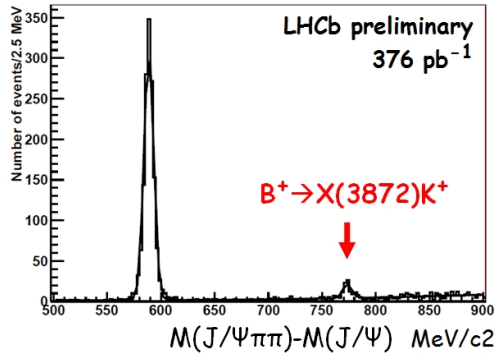

Figure 3: Secondary $X(3872)$ from $B^+ \to X(3872)K^+$ decays

angular studies to probe quantum numbers of $X(3872)$.

LHCb did not confirm another state $X(4140)$, observed by CDF in $B^+ \to J/\psi\phi K^+$ decays with $X(4140) \to J/\psi\phi$ [12]. Using 376 pb^{-1} of data, LHCb reports 2.4σ tension [13] with the CDF result.

LHCb studied b-hadron production using detached J/ψ, $D\mu$ tags or fully reconstructed $J/\psi X$ final states, with all approaches giving consistent results. The observed transverse momentum dependence of the production cross section is well described by theory, FONLL, MC@NLO. In order to quantify the relative rates of various b-hadrons, fragmentation functions were determined by measuring the ratio of related hadronic decays [14], e.g. $B^0 \to D^-K^+$ and $B_s^0 \to D_s^-\pi^+$, or by the semi-leptonic analysis with $D^0\mu X$, $D^+\mu X$, $D_s^+\mu X$ and $\Lambda_c\mu X$, accounting also for cross-feeds [15]. Both approaches are complementary, being employed on 35 pb^{-1} of 2010 data, give consistent results for the B_s^0/B^0 fragmentation ratio f_s/f_d, and are combined: $< f_s/f_d >= 0.267^{+0.021}_{-0.020}$. Though f_s/f_d is not a priori a "universal" number, the LHCb result is similar to those from LEP and Tevatron. The ratio f_s/f_d provides an important input for the $B_s \to \mu^+\mu^-$ studies (sec. 5). The corresponding ratio $f_{\Lambda_b}/(f_u + f_d)$ is found to be dependent upon the transverse momentum of the charmed hadron-muon pair.

The B_c^+ production rate was measured relative to that for B^+ in the fiducial region $p_T > 4$ GeV/c, $2.5 < \eta < 4.5$ with 33 pb^{-1} of 2010 data [16]. The B_c^+ signal comprises 43 ± 13 $B_c^+ \to J/\psi\pi^+$ candidates, and yields the production measurement:

$$\frac{\sigma(B_c^+) \times BR(B_c^+ \to J/\psi\pi^+)}{\sigma(B^+) \times BR(B^+ \to J/\psi K^+)} = (2.2 \pm 0.8 \pm 0.2)\% \ .$$

Note, that precision is dominated by the available statistics, and the systematic uncertainty comes mainly from the B_c^+ lifetime measurement, so that already the 2011 data are expected to significantly improve the measurement.

Exclusive particle production in pp collisions are elastic processes, when the protons remain intact, and new particles are created through photon and/or gluon propagators. While purely photon propagators assume well understood electromagnetic processes, processes involving gluons provide important tests of QCD [17]. Since the object that couples to the proton must be colourless, potential pomeron (two gluon states) or odderon (three gluons), predicted in QCD but never unambiguously observed, can be studied in a clean experimental environment. The J/ψ or ψ' exclusive production is interpreted as photon-pomeron fusion or odderon-pomeron fusion, and χ_c exclusive production is interpreted as double pomeron exchange.

The LHCb analysis is based on 2010 data equivalent to an integrated luminosity of 3.1 ± 0.6 pb^{-1}. Exclusive charmonia at LHCb [18] provides clean experimental signature with precisely two forward muon tracks and no backward tracks, with no photon for J/ψ or ψ' analysis and precisely one photon for χ_c production. The effect is then observed by counting the number of reconstructed ψ' and J/ψ depending on the number of forward tracks, with the smooth background behaviour after having subtracted the $\psi' \to J/\psi\pi^+\pi^-$ feeddown from the J/ψ distribution (Fig. 4). Purity from forward track counting was estimated to be about 85%.

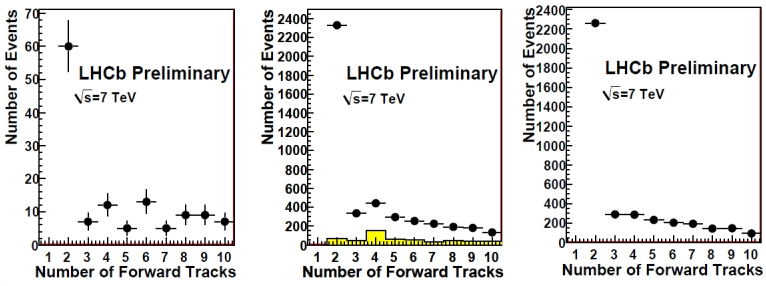

Figure 4: Number of forward tracks with no backward tracks in events where the invariant mass of the muons is consistent with the $\psi(2S)$ (left plot) or J/ψ (central and right plots). The shaded histogram is the estimated component from $\psi(2S)$ decays having a J/ψ in the final state. The data points in the right plot have this background subtracted

Because of the rapidity coverage gap of 2 units in the backward direction, p_T spectrum was used in addition to simple track counting to prove exclusivity, and yielded a consistent purity of $(80 \pm 3)\%$ for J/ψ with p_T <900 MeV/c, in agreement with the track counting.

Exclusive χ_c family resonances can also produce J/ψ in the final state via the decay $\chi_c \to J/\psi\gamma$. There is no corresponding resonance above the $\psi(2S)$. Fig. 5 shows photon counting in events with no backwards tracks, and precisely two forward tracks consistent with the J/ψ or

$\psi(2S)$ resonances. As expected, additional photons are observed to accompany J/ψ but not

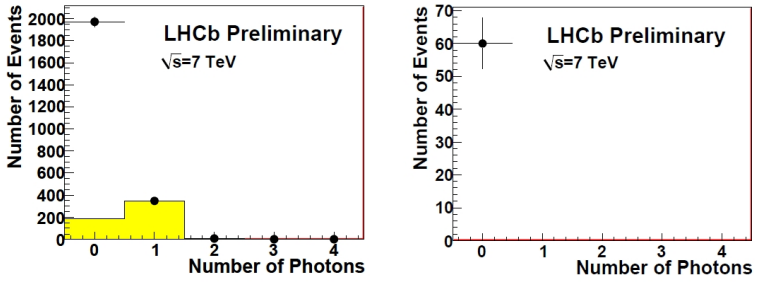

Figure 5: Number of photons in events with no backward tracks and two forward tracks whose invariant mass is consistent with a J/ψ (left) or $\psi(2S)$ (right). The points are data. The shaded histogram is the esimated feed-down from the decay of χ_c

$\psi(2S)$. The events with one additional photon are χ_c candidates. Note, that despite looking at prompt production in pp-collisions, clean mass peaks of J/ψ and $\psi(2S)$ resonances are observed (Fig. 6a,b). Contribution from non-resonant background and misID is small. An even cleaner

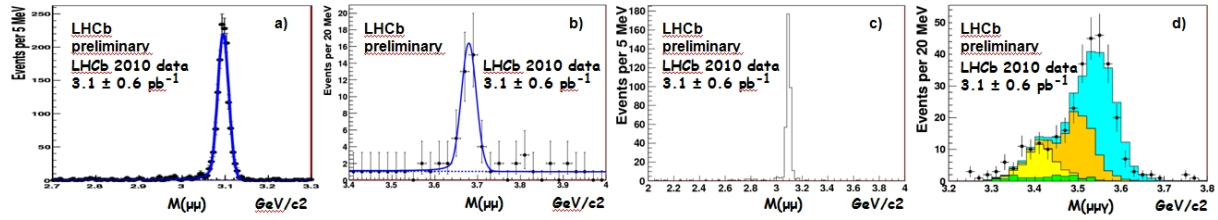

Figure 6: Invariant mass distribution for events with no backward tracks, two forward tracks and no (a,b) or exactly one (c,d) identified photon for J/ψ (a,c), $\psi(2S)$ (b) and χ_c (d) signals. The fit is to the sum of a Crystal Ball Function and an exponential (a-c) and from bottom to top $\psi(2S)$ with a single identified photon and $\chi_{c0,1,2}$ shapes taken from simulation (d)

J/ψ sample is observed, when requiring exactly one photon in addition in the search for χ_c candidates. Events with two muons and a single photon are more often associated with a J/ψ than events without a photon since there is no process with photons corresponding to the QED production of two muons. Fig. 6d shows the invariant mass of the photon plus dimuon system. A clear resonance structure is apparent around the χ_c masses. It was shown, that all three χ_c states are needed to describe the observed spectrum.

Contributions from all five charmonium states, J/ψ, $\psi(2S)$, $\chi_{c0,1,2}$, is seen. The theory-experiment comparison requires major efforts from both parts. Large theoretical uncertainties

come e.g. from rescattering corrections which can alter the cross-section by about 20%. Reasonable precision for J/ψ and $\psi(2S)$ is achieved. The result is consistent with refs. [19, 20]. More statistics is required to achieve precise determination of individual χ_c states production. The results are consistent with ref. [21] and do not agree with ref. [22]. In the ratio of $\psi(2S)$ production to that for J/ψ, most of the trigger, tracking, and muon ID systematics cancel as does the luminosity uncertainty. The uncertainty is therefore dominated by the number of $\psi(2S)$ candidates. Correcting for the branching ratios to muon pairs [23], the ratio of the cross-section of $\psi(2S)$ to J/ψ was measured to be 0.20 ± 0.03. The result is consistent with HERA and Tevatron results and with ref. [20]. Due to a new dedicated trigger line implemented now and a 30 times increased statistics in 2011, significant improvement is expected.

4 Studies of open charm

LHCb functions also as a charm factory due to the abundant charm production at LHC energies, precise vertex reconstruction and hadron ID capability. However low transverse momentum decays have to be reconstructed. Large clean samples of about 1.0M $D^+ \to K^+K^-\pi^+$, 1.3M $D_s^+ \to K^+K^-\pi^+$, and 0.4M $D^{*+} \to D^0(K^+K^-)\pi^+$ are reconstructed at LHCb per 100 pb^{-1}. Mixing in the charm sector is non-zero at more than 5σ [26], however no single measurement excludes zero. CPV in mixing, in the framework of the SM or new physics (NP), is driven by the mixing parameters $x = \Delta m/\Gamma$ and $y = \Delta\Gamma/2\Gamma$, both of the order of 1%. CPV in $D^0\bar{D}^0$ mixing is negligible in the SM, but may be enhanced in many other models [24], while existing constraints are weak [26]. The best place to look for direct CPV is Cabibbo suppressed decays, where gluonic penguins are significant. Mixing parameter y_{CP} studies were performed using effective lifetimes in the D^0 decays to CP eigenstate K^+K^- and to the $K^-\pi^+$ state without defined CP parity,

$$y_{CP} = \frac{\tau(D^0 \to K^-\pi^+)}{\tau(D^0 \to K^-K^+)} - 1 \ .$$

Flavour tagging was achieved by using the D^0 sample from $D^{*+} \to D^0\pi^+$ decays. Reconstruction of the $D \to K^-K^+$ decay together with flavour tagging, allows also to probe CPV in charm mixing via the A_Γ parameter:

$$A_\Gamma = \frac{\tau(\bar{D}^0 \to K^-K^+) - \tau(D^0 \to K^-K^+)}{\tau(\bar{D}^0 \to K^-K^+) + \tau(D^0 \to K^-K^+)} \ .$$

Both studies [25] rely on 28 pb^{-1} of 2010 data. The main challenges in time-dependent charm studies at LHCb are to properly describe the contribution from $B \to DX$ decays to the prompt charm sample, which is done using the χ^2 of the D impact parameter (Fig. 7), and to correct for lifetime bias, which is done on an event-by-event basis, see e.g. Fig. 8. The obtained

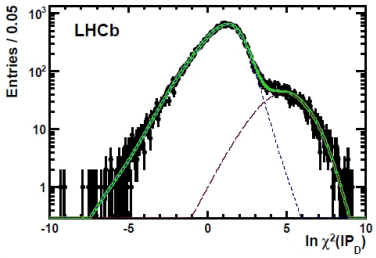

Figure 7: $\ln \chi^2(IP_D)$ fit projection of $D^0 \to K^+K^-$ candidates. Shown are data (points), the total fit (green, solid), the prompt signal (blue, short-dashed), and the secondary signal (purple, long-dashed)

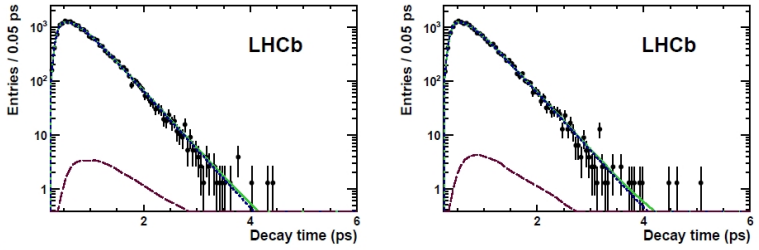

Figure 8: Proper-time fit projections of (left) $D^0 \to K^-K^+$ and (right) $\bar{D}^0 \to K^-K^+$ candidates after applying of the $\ln \chi^2(IP_D) < 2$ cut. Shown are data (points), the total fit (green, solid), the prompt signal (blue, short-dashed), and the secondary signal (purple, long-dashed)

result for the mixing parameter $y_{CP} = (5.5 \pm 6.3 \pm 4.1) \times 10^{-3}$ will improve with statistics increased by a factor 30 with the 2011 data, and with reduced systematic uncertainty due to an improved treatment of background events, so that it will improve the present HFAG value [26] of $(11.1 \pm 2.2) \times 10^{-3}$ without including the LHCb result. The precision on the result for the CPV parameter $A_\Gamma = (-0.59 \pm 0.59 \pm 0.21) \times 10^{-2}$ will similarly improve the present HFAG value [26], $(0.12 \pm 0.25) \times 10^{-2}$, which does not include the LHCb result.

5 Beauty studies

This section focuses on rare effects and mostly $b \to s$ transitions, described by penguin or box diagrams, where potential NP contributions can compete. In the framework of the angle γ studies, evidence of the suppressed ADS mode $B \to DK$, direct CPV in charmless B decays, and new results on b baryons, $\Lambda_b \to D^0 p K^-$, are addressed. The first measurement of the $B_s^0 \bar{B}_s^0$

mixing parameter ϕ_s from $B_s \to J/\psi\phi$ and $B_s \to J/\psi f_0(980)$ is then explained. Finally, rare decays are illustrated by radiative penguins studies and the search for $B_s \to \mu^+\mu^-$.

One of the important consistency checks of the unitarity triangle relies on the constraint from the "mixing" ($\Delta m_d/\Delta m_s$) side against the constraint from the opposite angle γ. While the "mixing" side precision is limited by lattice calculations, the precision of γ is limited by experiment. Thus improving γ precision directly means improving the unitarity triangle closure check. The γ measurements are also important in the search for NP by comparing e.g. tree-mediated processes (γ angle, "V_{ub}" side) to those involving loop diagrams (γ and β angles, "mixing" side) and thus more sensitive to potential NP contribution.

The $B^\pm \to DK^\pm$ decays using a common mode for D^0 and $\bar{D}^0$ provide γ sensitive interference and different B^+ versus B^- rates will mean CP asymmetry. The interference can be maximized by choosing a mode, which is suppressed for D^0, while favoured for $\bar{D}^0$, for example the doubly Cabibbo suppressed $D^0 \to K^+\pi^-$ mode for D^0, is Cabibbo favoured $\bar{D}^0 \to K^+\pi^-$ for $\bar{D}^0$ [27]. Note, that the total visible branching fraction is very small $\sim 10^{-7}$. Using 343 pb^{-1} of data, LHCb has obtained [28] 4.0σ significant signal for the suppressed ADS mode $B^+ \to (K^-\pi^+)K^+$, yielding the ratio to favoured mode $R^{DK}_{ADS} = (1.66 \pm 0.39 \pm 0.24) \times 10^{-2}$, consistent with the HFAG average [26] of $(1.6 \pm 0.3) \times 10^{-2}$, which does not include the LHCb result. The CP asymmetry, visible already on the raw data plots (Fig. 9), $A^{DK}_{ADS} = -0.39 \pm 0.17 \pm 0.02$,

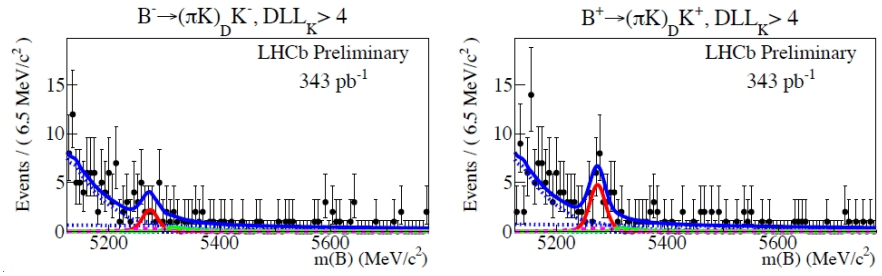

Figure 9: Invariant mass distributions of suppressed $B^- \to (K^+\pi^-)K^-$ (left) and $B^+ \to (K^-\pi^+)K^+$ (right) candidates. The solid red curve is the $B^\pm \to DK^\pm$ signal. Sensitivity to charge asymmetries is obtained by comparing left to right signal components. The charmless components are shown as dashed lines. The combinatoric, partially-reconstructed and semi-leptonic backgrounds are shown by dotted lines. The solid line is the total PDF

is also consistent with the HFAG average [26] of -0.58 ± 0.21 which does not include the LHCb result, while the precision is dominated by available statistics and will progressively improve.

Two-body charmless B decays contain a significant contribution of penguin diagrams and are important for NP searches. Powerful charged hadron particle ID allows to disentangle different components from a clear b-hadron signal on the two charged hadrons invariant mass

spectrum. Clean samples are thus obtained for $B^0 \to K\pi$, $B^0 \to \pi\pi$, $B_s^0 \to KK$, $\Lambda_b \to pK$ and $\Lambda_b \to p\pi$ [29]. Direct CPV can be probed using the $B \to K\pi$ mode. Comparing the B^0 and $\bar{B}^0$ signals from $B_d \to K\pi$, using the 320 pb^{-1} data sample, LHCb obtained the most precise single measurement and the first 5σ observation of CPV at a hadron machine, $A_{CP}(B^0 \to K^+\pi^-) = -0.088 \pm 0.011 \pm 0.008$, consistent with the HFAG average [26] of $-0.098^{+0.012}_{-0.011}$, which does not include the LHCb result. Fig. 10 shows the direct CP asymmetry to be clearly visible from raw data. From the same $K\pi$ invariant mass spectrum (Fig. 11), a first evidence of CPV in B_s^0

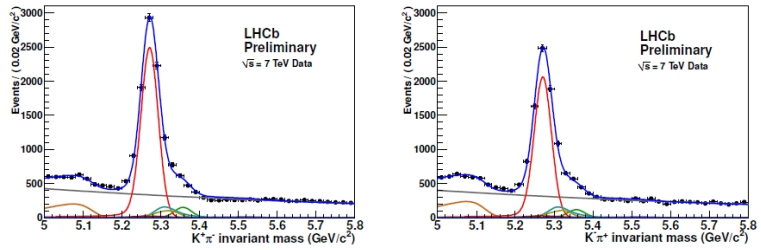

Figure 10: $K^+\pi^-$ (left) and $K^-\pi^+$ (right) invariant mass spectra. The result of an unbinned maximum likelihood fit is superimposed. The main components contributing to the fit model are $B^0 \to K\pi$ (red), wrong sign $B^0 \to K\pi$ combination (dark red), $B^0 \to \pi^+\pi^-$ (light blue), $B_s^0 \to K^+K^-$ (dark yellow), $B_s^0 \to K\pi$ (green), combinatorial background (grey), 3-body partially reconstructed decays (orange)

decays is seen, $A_{CP}(B_s^0 \to K^-\pi^+) = 0.27 \pm 0.08 \pm 0.02$. This measurement can be compared

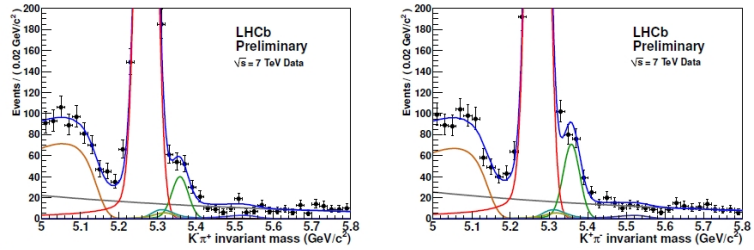

Figure 11: $K^-\pi^+$ (left) and $K^+\pi^-$ (right) invariant mass spectra, magnified to focus on the B_s^0 signal peaks. The result of an unbinned maximum likelihood fit is superimposed. The main components contributing to the fit model are the same as in Fig. 10

to the CDF result [30] $A_{CP}(B_s^0 \to K^-\pi^+) = 0.39 \pm 0.15 \pm 0.08$. Future LHCb time-dependent studies, in particular using $B_s^0 \to KK$ [31], should yield a NP sensitive measurement of γ [32].

LHCb observed for the first time, the $\Lambda_b \to D^0 p K^-$ decay [33] (Fig. 12), which is another potentially powerful tool for measuring γ. Using the normalization channel $\Lambda_b \to D^0 p \pi^-$, the

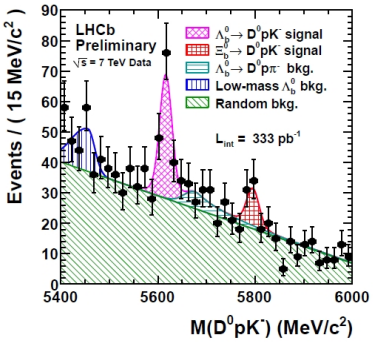

Figure 12: $D^0 p K^-$ invariant mass spectrum. Points with error bars are the data, hatched areas are the different components in the fit model as detailed in the legend

branching fraction was determined as:

$$\frac{BR(\Lambda_b \to D^0 p K^-)}{BR(\Lambda_b \to D^0 p \pi^-)} = 0.112 \pm 0.019^{+0.011}_{-0.014} \ .$$

The same $D^0 p K^-$ invariant mass spectrum also shows a 2.6σ (both statistical and systematic uncertainty taken into account) significant signal, consistent with the $\Xi_b^0 \to D^0 p K^-$ decay. The relative production times the branching ratio was determined:

$$\frac{f_{b\to\Xi_b^0} \times BR(\Xi_b^0 \to D^0 p K^-)}{f_{b\to\Lambda_b^0} \times BR(\Lambda_b^0 \to D^0 p K^-)} = 0.29 \pm 0.12 \pm 0.08 \ .$$

The Ξ_b^0 mass, measured relative to that of Λ_b^0, $M(\Xi_b^0) - M(\Lambda_b^0) = (181.8 \pm 5.5 \pm 0.5)$ MeV/c^2, is consistent with the CDF result [34], obtained with the $\Xi_b^0 \to \Xi_c^+ \pi^-$ mode.

LHCb studied the $B_s^0 \bar{B}_s^0$ mixing phase ϕ_s using $B_s \to J/\psi\phi$ decays, with 337 pb^{-1} of data [36]. In the SM, ϕ_s is small, $\phi_s = 0.0363 \pm 0.0017$ rad [35], but NP can produce large deviations from this value. Time dependent analysis requires good proper time resolution. It was determined to be 50 fs, using prompt J/ψ background. Tagging of the initial B_s flavour is required: the per event mis-tagging function was calibrated using $B^+ \to J/\psi K^+$ and $B_d \to D^* \mu \nu_\mu$ modes. Since $B_s \to J/\psi\phi$ is a decay of a pseudoscalar to two vector particles, angular analysis is needed to resolve CP-even and CP-odd components. The angular acceptance was determined from Monte Carlo (MC) studies with 5% maximum deviation from uniform distribution. Fig. 13 shows the result in $\Delta\Gamma_s$ and ϕ_s coordinates, with the two solutions well distinguished,

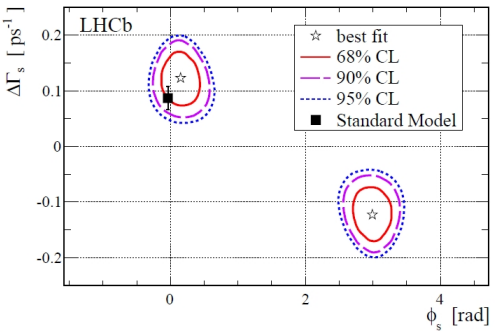

Figure 13: Likelihood confidence regions in the $\Delta\Gamma_s$ - ϕ_s plane. The black square and error bar corresponds to the SM prediction

which translates into $\phi_s = 0.15 \pm 0.18 \pm 0.06$ rad and $\Delta\Gamma_s = 0.123 \pm 0.029 \pm 0.011$ ps^{-1}. Note the first 4σ evidence of $\Delta\Gamma_s > 0$. This analysis can be complemented by including the $B_s \to J/\psi f_0(980)$ decay mode, observed by LHCb with the first data [37] and confirmed by Belle [38] and CDF [39]. The $f_0(980)$ is a scalar, so that no angular analysis is needed.

Radiative penguins, $B \to K^*\gamma$ and $B_s \to \phi\gamma$ were studied using 340 pb^{-1} of data. A ratio between the $B \to K^*\gamma$ and $B_s \to \phi\gamma$ branching fractions provides an important test for NNLO QCD predictions [40]. The largest so far sample of 210 ± 21 $B_s \to \phi\gamma$ decays accumulated by LHCb yields a ratio [41]:

$$\frac{BR(B^0 \to K^{*0}\gamma)}{BR(B_s^0 \to \phi\gamma)} = 1.52 \pm 0.14_{stat} \pm 0.10_{syst} \pm 0.12_{f_s/f_d} \ ,$$

which should be compared to the SM prediction of 1.0 ± 0.2. The eventual goal is to study the time evolution and CP asymmetries.

Flavour Changing Neutral Current (FCNC) processes are highly suppressed in the SM and can only occur through higher-order diagrams. The FCNC processes can provide indirect constraints on particles, that are too heavy to be produced directly. The SM predicts $BR(B_s^0 \to \mu^+\mu^-) = (3.2 \pm 0.2) \times 10^{-9}$ [42], while contributions from new processes or new heavy particles can significantly enhance this value. For example, within Minimal Supersymmetric extensions of the SM, in the large $\tan\beta$ regime, $BR(B_s^0 \to \mu^+\mu^-)$ is nearly proportional to $\tan^6\beta$ [43], where $\tan\beta$ is the ratio of vacuum expectation values of the two neutral CP-even Higgs fields.

Using statistics of 300 pb^{-1}, LHCb has searched for $B_s^0 \to \mu^+\mu^-$, using a boosted decision tree (BDT) constructed out of nine kinematical and topological variables [46]. The BDT was tuned on MC, but calibrated using $B \to hh$ data triggered by the other B, and the sidebands. The invariant mass resolution was calibrated on data, using di-muon resonance decays and $B \to hh$. Normalization to the $B^+ \to J/\psi K^+$, $B_s^0 \to J/\psi\phi$ and $B^0 \to K^+\pi^-$ channels

was used with all channels giving consistent results. Expected combinatorial background and expected SM signal with respect to the number of observed candidates were analyzed looking on the 6×4 grid of di-muon invariant mass versus BDT output. The BDT PDF for signal events is determined using an inclusive $B^0_s \to h^+h'^-$ sample. Only the events triggered independently of the signal candidates have been considered.

The distribution of the invariant mass in the four BDT bins is shown in Fig. 14. The

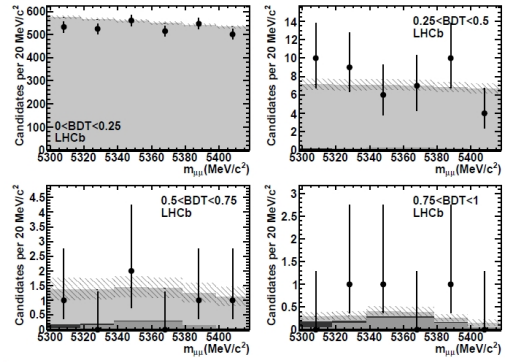

Figure 14: Distribution of selected di-muon events in the $B^0_s \to \mu^+\mu^-$ mass window for the four BDT output bins. The black dots are data, the light grey histogram shows the contribution of the combinatorial background, the black filled histogram the contribution of the $B^0_{(s)} \to h^+h'^-$ background and the dark grey filled histogram the contribution of $B^0_s \to \mu^+\mu^-$ signal according to the SM rate. The hatched area depicts the uncertainty on the sum of the expected contributions

limits were computed using frequentist CLs method and the LHCb combined result for f_s/f_d. The expected CLs values are shown in Fig. 15 as dashed black lines under the hypothesis that background and SM events are observed. The shaded areas cover the region of $\pm1\sigma$ of compatible observations. The obtained result, $BR(B^0_s \to \mu^+\mu^-) < 1.5 \times 10^{-8}$@95% confidence level (CL), improves the CDF limit [44] obtained with 7 fb^{-1} data of 4.0×10^{-8}@95%CL, and replaces the previous LHCb limit [45] obtained with 0.037 fb^{-1} data of 5.6×10^{-8}@95%CL.

6 Conclusions

With the detector optimized for heavy flavour studies together with the prolific production of charm and beauty hadrons at the LHC, LHCb provides a heavy flavour factory, capable of yielding new stringent tests of the SM already with the first data. Production of quarkonia and open heavy flavour hadrons is being systematically studied to provide an important test

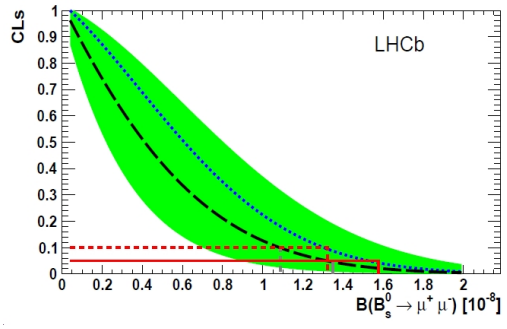

Figure 15: CLs as a function of the assumed $BR(B_s^0 \to \mu^+\mu^-)$. Expected (observed) values are shown by dashed black (dotted blue) lines. The expected CLs values assume a signal yield corresponding to the SM branching fractions. The green shaded area covers the region of $\pm 1\sigma$ of compatible observations. The measured upper limits at 90% and 95% CL are also shown

for QCD approaches that describe production mechanisms. Observation of the CP asymmetry in D mesons could be a sign of effects beyond the SM. The technique to search for such effects in LHCb has been validated on data. Precision studies on the CKM angle γ are launched, a hint of the ADS asymmetry in $B \to DK$ is observed. The most precise measurement of direct CPV in the $B \to K\pi$ is achieved, and the first evidence of direct CPV for B_s is observed in $B_s \to K\pi$. New data on the b baryons have been discussed. Finally the best-to-date upper limit for BR($B_s \to \mu^+\mu^-$) was obtained. Many analyses are ongoing, and the results based on more than 1 fb^{-1} data collected by LHCb in 2011, will set the scene for further precision rare effects studies.

Acknowledgements

It is my pleasure to acknowledge the excellent level of the Workshop and the hospitality of the organizers. I would like to thank M.-N. Minard for the help in preparing the talk.

References

[1] See e.g. A. Masiero, *talk at this workshop*; M. Ciuchini, *talk at this workshop*.

[2] A. A. Alves Jr. *et al.*, *LHCb collaboration*, *JINST* **3** (2008) S08005.

[3] *LHCb-CONF-2011-001*.

[4] R. Aaij *et al.*, *LHCb collaboration*, *Eur. Phys. J.* **C71** (2011) 1645.

[5] V. Khachatryan *et al.*, *CMS collaboration*, *Eur. Phys. J.* **C71** (2011) 1575.

[6] M. Butenschn, B. A. Kniehl, *Phys. Rev. Lett.* **106** (2011) 022301; P. Artoisenet, J. M. Campbell, J.-P. Lansberg, F. Maltoni, F. Tramontano, *Phys. Rev. Lett.* **101** (2008) 152001; J.-P. Lansberg, *Eur. Phys. J.* **C61** (2009) 693; Y. Q. Ma, K.Wang, K. T. Chao, *Phys. Rev. Lett.* **106** (2011) 042002; A. D. Frawley, T. Ullrich, R. Vogt, *Phys. Rep.* **462** (2008) 125.

[7] R. Aaij *et al.*, *LHCb collaboration*, *Phys. Lett.* **B694** (2010) 209.

[8] *LHCb-CONF-2011-016*.

[9] *LHCb-CONF-2011-020*.

[10] *LHCb-CONF-2011-021*.

[11] *LHCb-CONF-2011-043*.

[12] e-Print: arXiv:1101.6058 [hep-ex].

[13] *LHCb-CONF-2011-045*.

[14] R. Aaij *et al.*, *LHCb collaboration*, *Phys. Rev. Lett.* **107** (2011) 211801.

[15] R. Aaij *et al.*, *LHCb collaboration*, *Phys. Rev.* **D85** (2012) 032008.

[16] *LHCb-CONF-2011-017*.

[17] A. Martin, *talk at this workshop*.

[18] *LHCb-CONF-2011-022*.

[19] L. Motyka, G. Watt, *Phys. Rev.* **D78** (2008) 014023.

[20] W. Schaefer, A. Szczurek, *Phys. Rev.* **D76** (2007) 094014.

[21] e-Print: arXiv:0909.4748 [hep-ph].

[22] T. Aaltonen *et al.*, *CDF collaboration*, *Phys. Rev. Lett.* **102** (2009) 242001.

[23] K. Nakamura *et al.* (Particle Data Group), *J. Phys.* **G37** (2010) 075021.

[24] Y. Grossman, A. L. Kagan, Y. Nir, *Phys. Rev.* **D75** (2007) 036008; I. I. Bigi, M. Blanke, A. J. Buras, S. Recksiegel, *JHEP* **0907** (2009) 097.

[25] e-Print: arXiv:1112.4698 [hep-ex].

[26] http://www.slac.stanford.edu/xorg/hfag/.

[27] D. Atwood, I. Dunietz, A. Soni, *Phys. Rev. Lett.* **78** (1997) 3257.

[28] *LHCb-CONF-2011-044*.

[29] *LHCb-CONF-2011-042*.

[30] T. Aaltonen *et al.*, *CDF collaboration*, *Phys. Rev. Lett.* **106** (2011) 181802.

[31] R. Aaij *et al.*, *LHCb collaboration*, *Phys. Lett.* **B707** (2012) 349.

[32] R. Fleischer, *Phys. Lett.* **B459** (1999) 306.

[33] *LHCb-CONF-2011-036*.

[34] T. Aaltonen *et al.*, *CDF collaboration*, *Phys. Rev. Lett.* **107** (2011) 102001.

[35] http://ckmfitter.in2p3.fr/.

[36] e-Print: arXiv:1112.3183 [hep-ex].

[37] R. Aaij *et al.*, *LHCb collaboration*, *Phys. Lett.* **B698** (2011) 115.

[38] J. Li *et al.*, *BELLE collaboration*, *Phys. Rev. Lett.* **106** (2011) 121802.

[39] T. Aaltonen *et al.*, *CDF collaboration*, *Phys. Rev.* **D84** (2011) 052012.

[40] A. Ali, B.D. Pecjak, C. Greub, *Eur. Phys. J.* **C55** (2008) 577.

[41] *LHCb-CONF-2011-055*.

[42] e-Print: arXiv:1005.5310 [hep-ph]; e-Print: arXiv:1012.1447 [hep-ph].

[43] S. Choudhury, N. Gaur, *Phys. Lett.* **B451** (1999) 86; C. Hamzaoui, M. Pospelov, M. Toharia, *Phys. Rev.* **D59** (1999) 095005; K. Babu, C.F. Kolda, *Phys. Rev. Lett.* **84** (2000) 228; L.J. Hall, R. Rattazzi, U. Sarid, *Phys. Rev.* **D50** (1994) 7048; C.-S. Huang, W. Liao, Q.-S. Yan, *Phys. Rev.* **D59** (1999) 011701.

[44] T. Aaltonen *et al.*, *CDF collaboration*, *Phys. Rev. Lett.* **107** (2011) 191801.

[45] R. Aaij *et al.*, *LHCb collaboration*, *Phys. Lett.* **B699** (2011) 330.

[46] R. Aaij *et al.*, *LHCb collaboration*, *Phys. Lett.* **B708** (2012) 55.

Chapter 7

Beyond the Standard Model

7.1 S. Bianco - Searches for Supersymmetry and Beyond the Standard Model Physics in ATLAS and CMS

Searches for Supersymmetry and Beyond the Standard Model Physics in ATLAS and CMS

Stefano Bianco
Laboratori Nazionali di Frascati dell'INFN
Frascati, I-00044 Italy
stefano.bianco@lnf.infn.it
on behalf of the ATLAS and CMS Collaborations

Abstract The Large Hadron Collider has successfully made possible for both ATLAS and CMS experiment to record more than 2 fb^{-1} of data during the first half of year 2011. A review of the search results on supersymmetry and beyond the standard model processes on 1 fb^{-1} of data analyzed by Summer 2011 is presented.

1 Introduction

This paper reports on results of searches for supersymmetry (SUSY) and beyond the standard model (BSM) particles carried out by the ATLAS and CMS experiments at the Large Hadron Collider (LHC) at CERN, Geneva (Switzerland). The LHC is providing proton-proton (pp) collisions at the unprecedented 7 TeV center-of-mass energy. The LHC performed splendidly in 2011 providing about 80 pb^{-1} of data per day at a 2.5 10^{33} cm^{-2} s^{-1} peak luminosity, corresponding to a total of 2.5 fb^{-1} of data delivered by Summer 2011. Results shown in this paper refer to about 1 fb^{-1} of data analyzed.

The ATLAS and CMS detectors are described in [1, 2], while a full list of public results can be found in [3, 4]. For extensive, detailed, excellent reviews see [5, 6, 7, 8].

2 SUSY Searches

Several theories address the gauge hierarchy problem by introducing new particles that are partners of the SM particles. These new particles may include neutral, stable, and weakly interacting particles that are good dark-matter candidates. SUSY predicts a new symmetry between bosons and fermions such that, for every Standard Model (SM) particle, a superpartner should exist with a spin value differing by one half unit [9, 10, 11, 12]. SUSY models define the quantity R-parity [13] $R \equiv (-1)^{2S+3(B-L)}$ where S is the spin, B and L the baryonic and the leptonic number respectively). SUSY searches are classified in R-parity conserving (RPC) and

violating (RPV). In RPC searches, dark matter candidates are stable as a result of R-parity conservation, which requires all SUSY particles to be produced in pairs and the Lightest SUSY Particle (LSP) - good dark matter candidate - to be stable. Conversely, RPV signatures are mostly characterized by the possibility of producing mass resonances from the decay of SUSY particles into SM particles.

Coloured SUSY particles can be pair-produced copiously at the LHC, where the pp production is dominated by production of squark and gluino. These particles will either decay directly into SM particles and an LSP, or via intermediate colour-singlet states that ultimately decay into an LSP. The LSP will pass through the detector without interacting, carrying away a substantial amount of energy and creating an imbalance in the measured transverse momentum (p_T) and/or transverse energy (E_T). Fundamental variable for the identification of SUSY decays is, therefore, the Missing Transverse Energy (MET), as well as of paramount importance is the jet (j) reconstruction. All SUSY searches are topology-based, therefore independent of models. Most search strategies are based on the study of tails of MET distributions, while the possibility of applying very low p_T cuts is crucial to probe as large as possible a phase space, and the background estimate proceeds via data driven methods to minimize dependence on montecarlo estimates.

The j+MET is the most model-independent search channel, and it avails of the dominant squark-gluino production in pp collisions at LHC. It also suffers from large backgrounds, such as $Z \to \nu\bar{\nu}$, $W \to \ell\bar{\nu} + j$ with missing lepton ℓ, and QCD events with large MET. Both ATLAS and CMS have published a variety [14, 15, 16, 17, 18, 19, 20] of results on leptonless searches. Figure 1 and Figure 2 show limits on universal gaugino mass $m_{1/2}$ and universal scalar mass m_0 parameters of the Constrained Minimal Supersymmetric Standard Model (CMSSM) [21], for ATLAS and CMS respectively.

The lepton(s)+j+MET search relies on a lesser background level such as the QCD multi-j production, and makes the analysis sensitive to SUSY cascade decays involving leptons, with leptons coming from slepton/chargino/W/Z decays. However, the branching ratios are smaller than j+MET, thus providing weaker limits, but a complementary search. The event selection can profit of W/Z invariant mass cuts. Both ATLAS and CMS have published limits with both electrons and muons [22, 23, 24, 25, 26, 27, 28, 29]

Searches for b-jets + lepton(s) + MET are aimed to the detection of sbottom and stop. Production of uncoloured particles as chargino or neutralino is disfavoured in pp compared to $p\bar{p}$ collisions, and the LHC at 1 fb^{-1} is not as yet competitive with searches at the Tevatron. Nevertheless, ATLAS has searched for gluino-mediated production of sbottom in the four b-jets and MET, with gluino assumed to decay via sbottom to the LSP [30]. ATLAS also searched for gluino-mediated stop decay to the LSP with the signature of four jets (at least one b-jet) + lepton + MET [31].

The search for photon(s)+jets+MET is particularly sensitive to models such as Gauge Mediated Supersymmetry Breaking (GMSB) [32] which postulates the SUSY particles masses

to generate via gauge interactions, and the LSP to be always a gravitino with a diphoton + MET experimental signature. Backgrounds come from QCD (diphoton, photon + jet and dijet production) and electroweak (W and Z decays with escaping neutrinos) [33, 34].

Finally, RPV scenarios (which, however, are strongly constrained by experimental limits such as proton lifetime) are probed by searching for a resonance state produced by the decay of SUSY particles to SM particles. ATLAS searched for scalar neutrino decays $\tilde{\nu}_\tau \to e^- \mu^+$, while CMS searched for gluino pair production decaying to three jets [35, 36].

All analyses performed out of 1 fb^{-1} of data show no significant deviation from SM expectations (Figures 2 3 4).

3 BSM Searches

The cross section of rare processes increases sensibly with the higher center of mass energy, thus making the very first searches with $\sqrt{s} = 7$ TeV at the LHC with just 35 pb^{-1} of data collected in 2010 already competitive with the results obtained with $\sqrt{s} = 1.96$ TeV at the Tevatron. Results shown here from the 1 fb^{-1} data set collected before Summer 2011 led to a flood of new results from both ATLAS and CMS. Differently from the SUSY searches section, in the following a topic-driven discussion will be preferred to the signature-driven discussion.

3.1 Heavy Resonances

The decays of heavy resonances to a pair of leptons are predicted by many extensions of the SM with no precise hint of mass: the sequential SM Z'_{SSM} with SM-like couplings; the Z'_ψ predicted by grand unified theories; Kaluza-Klein graviton excitations arising in the Randall-Sundrum (RS) model of extra dimensions [37, 38, 39, 40]. Experimentally challenging, these analyses search for signals in high-end invariant mass distributions over SM backgrounds and need detectors with great momentum/energy resolution, accurate momentum/energy scale over 1 TeV. Backgrounds to be tamed are the high-end tails of SM processes. In the dileptons channel [41, 42] limits are now close to 2 TeV.

Heavy W-like resonances [43] are searched with a W-like experimental signatures in the lepton+MET channel, i.e., a high mass jacobian peak in transverse mass, with main background the SM W production [44, 45, 46]. Other heavy resonances searches performed are for diphotons [47, 48], dijets [49, 50], $t\bar{t}$ pairs in both all-hadronic [51] and muons + jets [52], WZ resonances in $\ell + \ell + \ell$+MET final state [45], heavy neutrinos [53, 54, 55] in lepton+lepton+jet+jet final state [56, 57], same-sign dileptons to look for exotic doubly-charged Higgs [58].

Finally, ATLAS searched for and did not confirm [59] the W+jet+jet structure reported by CDF at 145 GeV [60, 61] and not confirmed by D0 [62].

3.2 Extra Dimensions

The existence of extra spatial dimensions is a scenario that may solve the hierarchy problem [63] of the SM, i.e., the puzzling fact that the fundamental scale of gravity 10^{19} GeV is so much higher than the electroweak symmetry breaking scale 10^3 GeV. More than ten years ago Arkani-Hamed, Dimopoulos, and Dvali [64, 65, 66] suggested the SM to be constrained to the common 3+1 space-time dimensions (brane), while gravity being free to propagate through the entire multidimensional space (bulk). The gravitational flux on the brane is therefore diluted by virtue of Gauss' law in the bulk, which relates the fundamental Planck scale M_D to the apparent reduced scale $\bar{M}_{Planck} \sim 2 \times 10^{18}$ GeV according to the formula $M_D^{n_{ED}+2} = \frac{\bar{M}_{Planck}^2}{r^{n_{ED}}}$ where r and n_{ED} are the size and number of the extra dimensions (ED), respectively. The main phenomenological consequence tested by searches is the production of gravitons coupled to high-mass diphoton and dilepton pairs + MET [48, 67] and high-energy single jet + MET [68, 69, 70] and single photons + MET [69] , where the MET signals the graviton escaping detection.

Finally, extra-dimensions theories allow microscopic, quantum black holes to be formed and decay due to Hawking radiation. Signature is an isotropic decay to all SM species, therefore resulting in high multiplicity final states. The total transverse energy is used to separate black hole candidate events from backgrounds. [71, 72, 73, 74]

3.3 Leptoquarks

The intriguing symmetry in the SM between quarks and leptons suggested several theories to predict the existence of new bosons called leptoquark (LQ). A LQ carries colour, has fractional electric charge, can have spin 0 or spin 1, and couples to a lepton and a quark with coupling strength λ. A LQ would decay to a charged lepton and a quark, with an unknown branching fraction β, or a neutrino and a quark, with branching fraction $(1 - \beta)$. Suggested observables are the LQ invariant mass and the MET. A new search performed by ATLAS [75] yields no significant evidence above the SM backgrounds.

3.4 Fourth generation b' t'

Excluded in the nineties by electroweak results on the number of neutrino species, fourth generation models [76, 77, 78, 79] have found recently renewed interest since it has been shown that the electroweak bounds are less constraining for a non-degenerate fourth generation. With a fourth generation, indirect bounds on the Higgs boson mass can be relaxed, and an additional generation of quarks may possess enough intrinsic matter and anti-matter asymmetry to be relevant for the baryon asymmetry of the Universe.

Both ATLAS and CMS searched for t' and b' decays $t'/b' \to t/b + W/Z$ in the dilepton and lepton+jets channels, exploiting a MET selection as well. Backgrounds are $t\bar{t}$ and W/Z+jets events, the dominant systematic uncertainties are b-tagging and lepton efficiency [80, 81, 82, 83, 84, 85].

3.5 Long-Lived Particles

Heavy Stable (or long-lived) Charged Particles (HSCP) appear in various extensions of the SM [86, 87, 88, 89, 90, 91] . If the lifetime of an HSCP produced at the LHC is longer than a few nanoseconds, the particle will travel over distances that are comparable or larger than the size of a typical particle detector. In addition, if the HSCP mass is greater than 100 GeV/c^2, a significant fraction of these particles will have a velocity $\beta < 0.9$. These HSCP will be directly observable: a high momentum particle with an anomalously large rate of energy loss through ionization (dE/dx) and an anomalously long time-of-flight (TOF). The production of HSCP is peculiar signature of split supersymmetry, where the gluino decay is suppressed because of the large gluino-squark mass splitting. The search for HSCP showed no significant excess above background [92, 93, 94, 95] .

4 Conclusions and Outlook

A grand summary of ATLAS and CMS limits is shown in Figures 2 3 4 5. Thanks to the outstanding performance of LHC, to the excellent reliability and consistent performances of ATLAS and CMS detectors, and the efficient computing and data analysis, more than 1 fb^{-1} of data out of the more than 2 fb^{-1} collected was analyzed by Summer 2011, thus providing a flood of new results and limits which vastly improved — sometimes outclassed - the previous limits. From a global look to the limits published, a scenario emerges in Summer 2011 where SUSY is explored up to about 1 TeV, the fourth generation is excluded up to about 0.5 TeV and the search for new resonances is explored up to about 2 TeV. Prospects for the 2012 data taking period look very promising [1].

Acknowledgments

I thank the organizers for invitation and patience, the Atlas collaboration and all my CMS colleagues, particularly SUSY and EXOTICA conveners from ATLAS and CMS names, my fellow

[1] Note added in proofs: the Chamonix workshop produced the decision of increasing the LHC energy to $\sqrt{s} = 8$ TeV.

speakers Shahram Rahatlou (PIC11), Henri Bachacou (LP11), Xavier Portell-Bueso (PIC11), Isabell-A. Melzer-Pellmann (SUSY11).

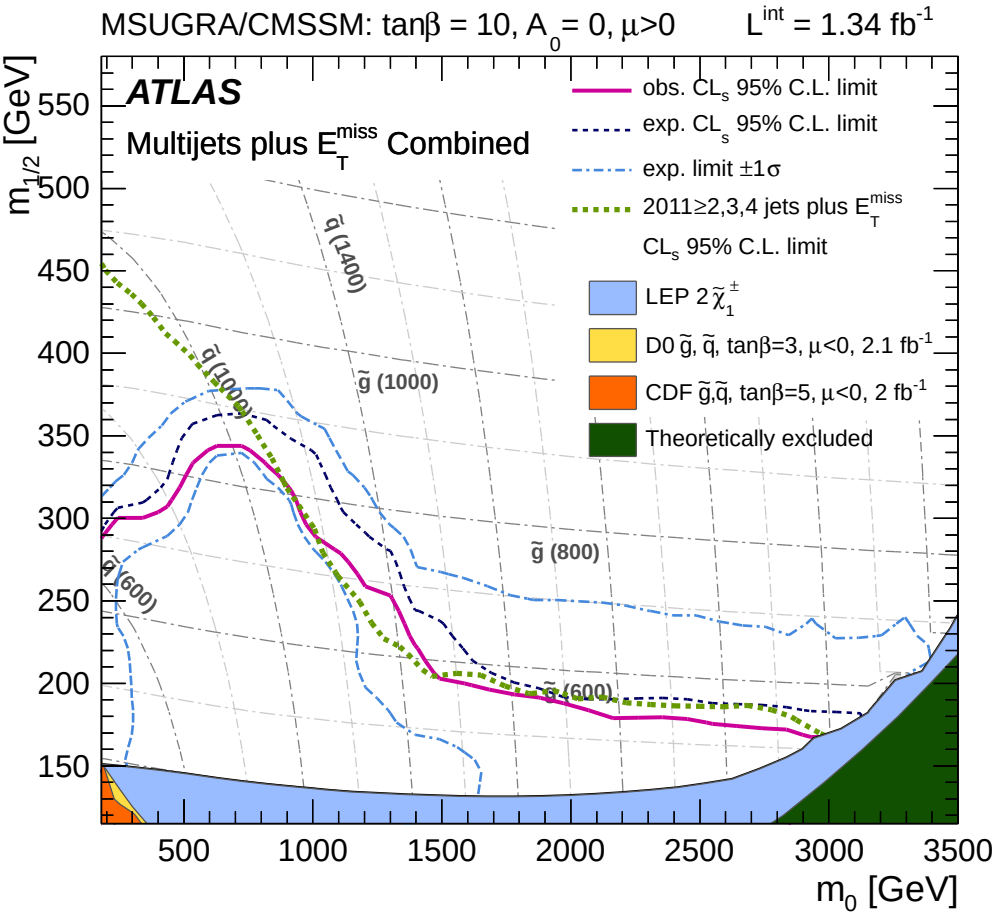

Figure 1: ATLAS combined exclusion bounds in the $\tan\beta = 10, A_0 = 0, \mu > 0$ slice of the MSUGRA/CMSSM space (from [15]) .

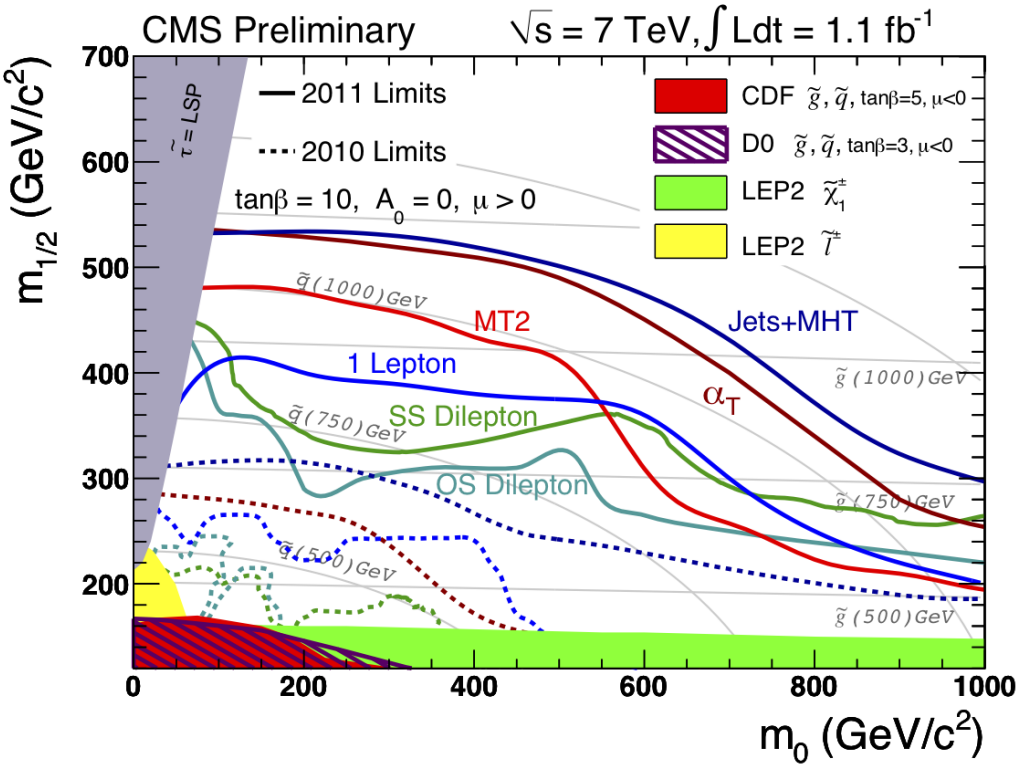

Figure 2: Observed limits from several 2011 CMS SUSY searches plotted in the CMSSM $(m_0, m_{1/2})$ plane.

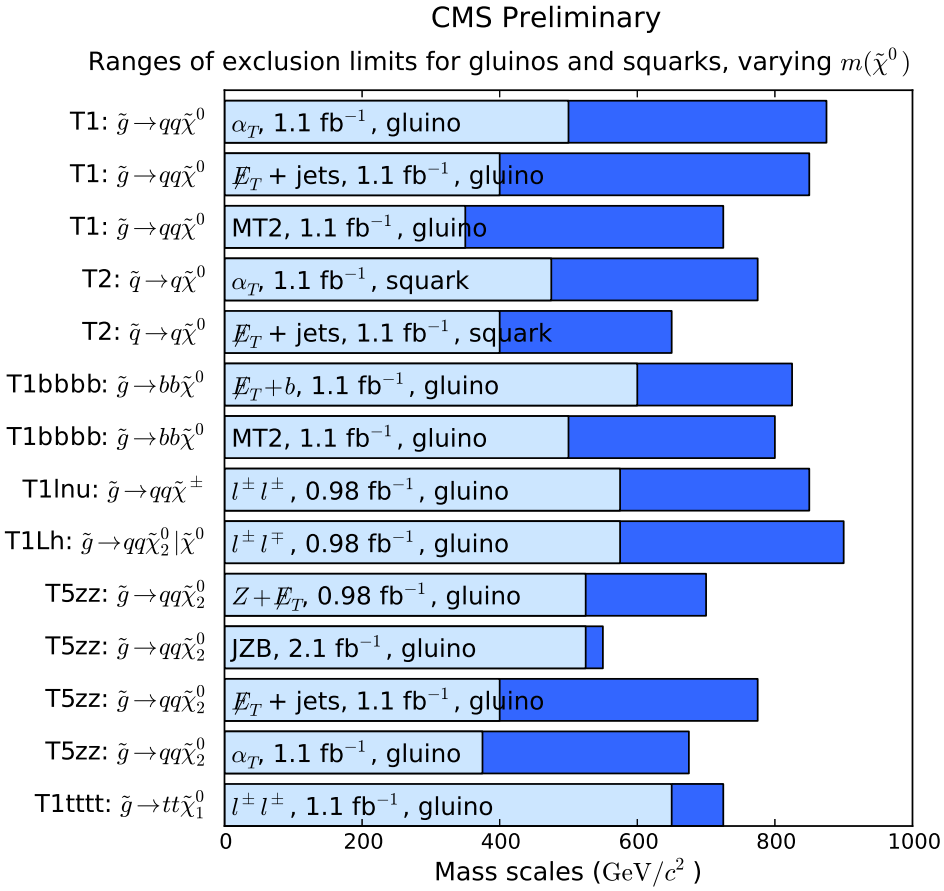

Figure 3: Range of excluded mass scale in Simplified Model Spectra from several 2011 CMS SUSY searches .

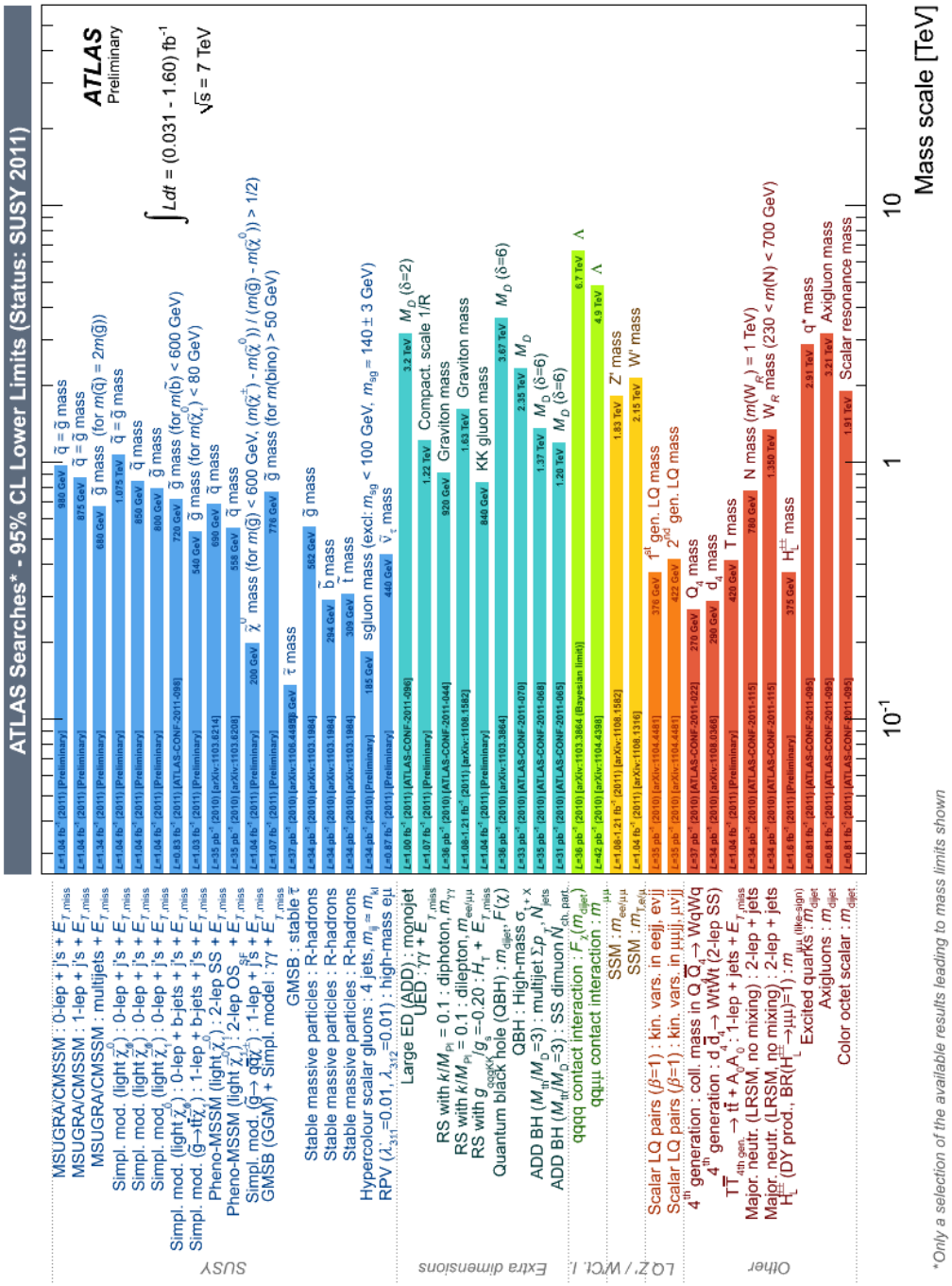

Figure 4: ATLAS SUSY and BSM grand summary limits.

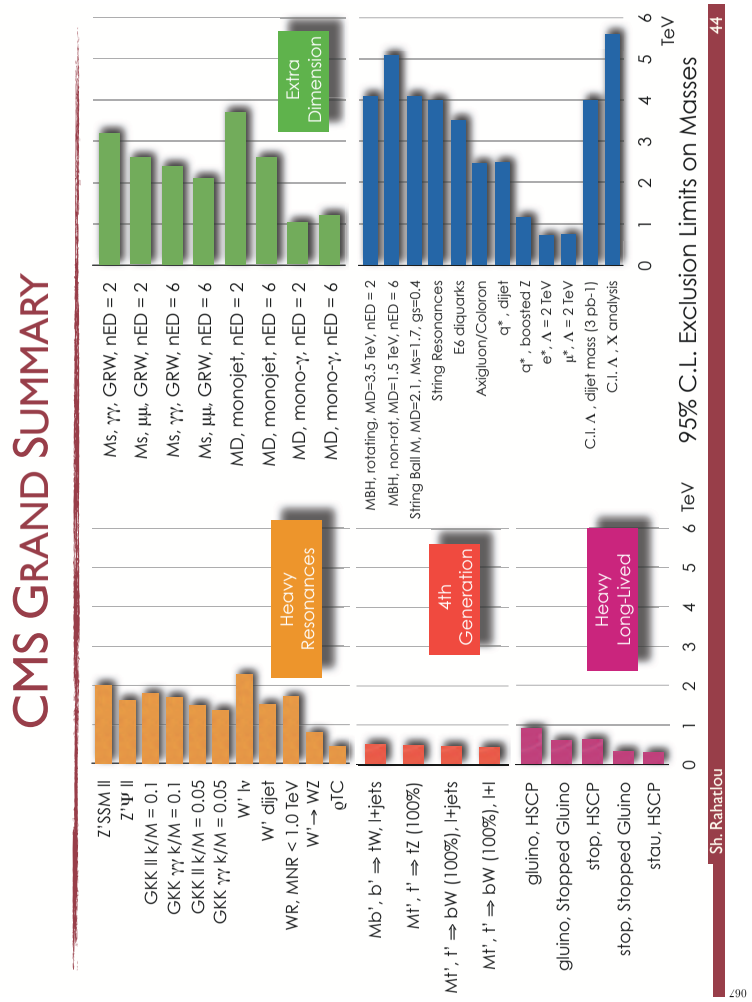

Figure 5: CMS BSM grand summary limits (from [6]).

References

[1] ATLAS Collaboration, J. of Instr. **3**, S08003 (2008).

[2] CMS Collaboration, J. of Instr. **3**, S08004 (2008).

[3] `https://twiki.cern.ch/twiki/bin/view/AtlasPublic`

[4] `https://twiki.cern.ch/twiki/bin/view/CMSPublic/PhysicsResults`

[5] X. Portell Bueso, arXiv:1112.1723v1 (2011).

[6] S. Rahatlou, CMS Conference report CR-2011/306.

[7] H. Bachacou for the ATLAS Coll., Lepton Photon 2011, Mumbai (India).

[8] Isabell-A. Melzer-Pellmann for the CMS Coll., SUSY 2011, Fermilab, Batavia (IL) USA.

[9] H.P. Nilles, Phys. Rep. 110, 1 (1984), and references therein.

[10] S. Weinberg, Phys. Rev. D 13, 974 (1976), Phys. Rev. D 19, 1277 (1979); E. Gildener, Phys. Rev. D 14, 1667 (1976); L. Susskind, Phys. Rev. D 20, 2619 (1979); G.'t Hooft, in Recent developments in gauge theories, Proceedings of the NATO Advanced Summer Institute, Cargese 1979, (Plenum, 1980)

[11] U. Amaldi, W. de Boer, and H. Furstenau, Phys. Lett. B 260, 447 (1991)

[12] S.P. Martin, arXiv:hep-ph/9709356v6.

[13] R. Barbier et al., Phys. Rept. 420, 1 (2005) arXiv:hep-ph/0406039

[14] ATLAS Collab., arXiv:1109.6572 [hep-ex]

[15] ATLAS Collab., arXiv:1110.2299 [hep-ex]

[16] CMS Collab., PAS-SUS-11-004

[17] CMS Collab., PAS-SUS-11-001

[18] CMS Collab., arXiv:1109.2352 [hep-ex]

[19] CMS Collab., arXiv:1107.1279 [hep-ex]

[20] CMS Collab., arXiv:1101.1628 [hep-ex]

[21] G. L. Kane et al., Phys. Rev. D 49, 6173-6210 (1994), arXiv:hep-ph/9312272.

[22] ATLAS Collab., arXiv:1109.6606 [hep-ex]

[23] ATLAS Collab., Eur. Phys. J. C 71 1577 (2011), arXiv:1012.1792 [hep-ex]

[24] CMS Collab., PAS-SUS-11-015

[25] CMS Collab., PAS-SUS-11-010

[26] CMS Collab., PAS-SUS-11-011

[27] ATLAS Collab., arXiv:1110.6189 [hep-ex]

[28] CMS Collab., arXiv:1104.3168 [hep-ex]

[29] CMS Collab., arXiv:1106.0933 [hep-ex]

[30] ATLAS Collab., ATLAS-CONF-2011-098

[31] ATLAS Collab., ATLAS-CONF-2011-130

[32] M. Dine et al., Nucl.Phys. B 189, 575 (1981).

[33] ATLAS Collab., arXiv:1111.4116 [hep-ex]

[34] CMS Collab., PAS-SUS-11-009

[35] ATLAS Collab., arXiv:1109.3089 [hep-ex]

[36] CMS Collab., Phys. Rev. Lett. 107, 101801 (2011), arXiv:1107.3084 [hep-ex]

[37] Francesco Spano, arXiv:1112.3906v1

[38] A. Leike, Phys. Rept. 317 (1999) 143, arXiv:hep-ph/9805494.

[39] L. Randall and R. Sundrum, Phys. Rev. Lett. 83 (1999) 4690, arXiv:hep-th/9906064.

[40] L. Randall and R. Sundrum, Phys. Rev. Lett. 83 (1999) 3370, arXiv:hep-ph/9905221.

[41] ATLAS Collaboration, arXiv:1108.1582.

[42] CMS Collaboration, CMS PAS EXO-11-019(2011).

[43] G. Altarelli, B. Mele, and M. Ruiz-Altaba, Z. Phys. C45 (1989) 109.

[44] ATLAS Collaboration, arXiv:1108.1316.

[45] CMS Collaboration, CMS PAS EXO-11-024.

[46] CMS Collaboration, CMS PAS EXO-11-041.

[47] ATLAS Collaboration, ATLAS-CONF-2011-044(2011).

[48] CMS Collaboration, CMS PAS EXO-11- 038(2011).

[49] ATLAS Collaboration, arXiv:1108.6311v1.

[50] CMS Collaboration, arXiv:1107.4771v1.

[51] CMS Collaboration, CMS PAS-EXO-2011-006.

[52] CMS Collaboration, CMS PAS-EXO-2011-055.

[53] J. C. Pati and A. Salam, Phys. Rev. D 10 (1974) 275.

[54] R. N. Mohapatra and J. C. Pati, Phys. Rev. D 11 (1975) 366.

[55] G.Senjanovic and R.N.Mohapatra, Phys. Rev. D12 (1975) 1502.

[56] ATLAS Collaboration, ATLAS-CONF-2011-115.

[57] CMS Collaboration, CMS PAS EXO-11-002.

[58] ATLAS Collaboration, ATLAS-CONF-2011-127.

[59] ATLAS Collaboration, ATLAS-CONF-2011-097.

[60] T. Aaltonen et al. (CDF Collaboration), Phys. Rev. Lett. 106, 171801 (2011).

[61] `http://www-cdf.fnal.gov/physics/ewk/2011/wjj/`

[62] D0 Collaboration, Phys. Rev. Lett. 107 (2011) 011801.

[63] E. Witten, Phys. Lett. B 105 (1981) 267.

[64] N. Arkani-Hamed, S. Dimopoulos, and G. Dvali, Phys. Lett. B 429 (1998) 263.

[65] G. Giudice, R. Rattazzi, and J. Wells, Nucl. Phys. B 544 (1999) 3.

[66] T. Han, J. Lykken, and R.-J. Zhang, Phys. Rev. D59 (1999) 105006.

[67] CMS Collaboration, CMS PAS EXO-11-039.

[68] ATLAS Collaboration, ATLAS-CONF-2011-096.

[69] CMS Collaboration, CMS PAS EXO-11-058.

[70] CMS Collaboration, CMS PAS EXO-11-059.

[71] ATLAS Collaboration, ATLAS-CONF-2011-065.

[72] ATLAS Collaboration, ATLAS-CONF-2011-068.

[73] ATLAS Collaboration, New J. Phys. 13 (2011) 053044.

[74] CMS Collaboration, CMS PAS EXO-11-071.

[75] ATLAS Collaboration, arxiv:1104.4481.

[76] P. Q. Hung and M. Sher, Phys. Rev. D 77 (Feb, 2008) 037302.

[77] G. D. Kribs, T. Plehn, M. Spannowsky et al., Phys. Rev. D 76 (Oct, 2007) 075016.

[78] W.-S. Hou, Chin. J. Phys. 47 (2009) 134, arXiv:0803.1234.

[79] B. Holdom et al., PMC Phys. A3 (2009) 4, arXiv:0904.4698.

[80] CMS Collaboration, CMS PAS EXO-11-036.

[81] CMS Collaboration, CMS PAS EXO-11-051.

[82] CMS Collaboration, CMS PAS EXO-11-050.

[83] CMS Collaboration, CMS PAS EXO-11-005.

[84] ATLAS Collaboration, ATLAS-CONF-2011-022.

[85] ATLAS Collaboration, I JHEP 10 (2011) 107.

[86] M. Fairbairn et al., Phys. Rept. 438 (2007) 163.

[87] S. Dimopoulos, M. Dine, S. Raby et al., Phys. Rev. Lett. 76 (1996) 34943497.

[88] H. Baer, K.-m. Cheung, and J. F. Gunion, Phys. Rev. D59 (1999) 075002.

[89] T. Jittoh, J. Sato, T. Shimomura et al., Phys. Rev. D73 (2006) 055009, arXiv:hep-ph/0512197.

[90] N. Arkani-Hamed and S. Dimopoulos, JHEP 06 (2005) 073, arXiv:hep-th/0405159.

[91] A. Arvanitaki, et al., Phys. Rev. D76 (2007) 055007, arXiv:hep-ph/0506242.

[92] CMS Collaboration, CMS PAS EXO-11-020.

[93] CMS Collaboration, CMS PAS EXO-11-022.

[94] ATLAS Collaboration, Phys. Lett. B 701 (2011) 1-19.

[95] CMS Collaboration, JHEP 3 (2011) 24,

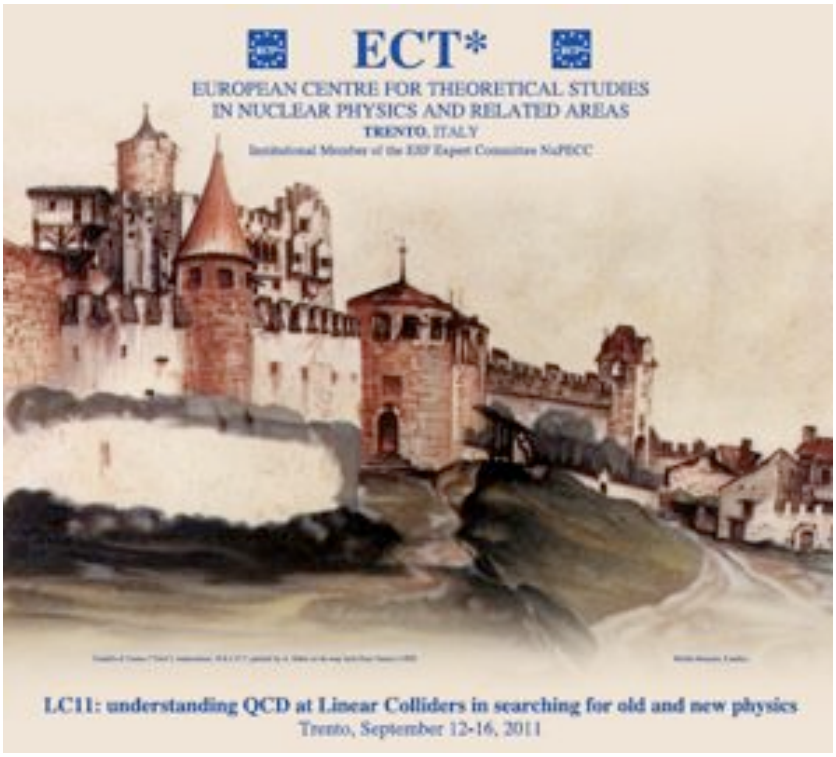

Castello di Trento painted by A. Dürer on his way back from Venice (1495).

7.2 M. Kraemer, P. Bechtle, K. Desch, et al. - Constrained supersymmetric models in the light of LHC exclusions, precision measurements and astroparticle physics

Constrained supersymmetric models in the light of LHC exclusions, precision measurements and astroparticle physics

Michael Krämer [1]
Institute for Theoretical Particle Physics and Cosmology, RWTH Aachen University, Aachen, Germany
mkraemer@physik.rwth-aachen.de

Philip Bechtle, Klaus Desch, Herbi K. Dreiner
Physikalisches Institut, University of Bonn, Bonn, Germany

Ben O'Leary
Institute for Theoretical Physics and Astrophysics, Würzburg University, Würzburg, Germany

Carsten Robens
Institute for Theoretical Particle Physics and Cosmology, RWTH Aachen University, Aachen, Germany

Björn Sarrazin
Deutsches Elektronen-Synchrotron DESY, Hamburg, Germany

Peter Wienemann
Physikalisches Institut, University of Bonn, Bonn, Germany

Abstract We have investigated the implications for the constrained minimal supersymmetric model (CMSSM) from the absence of any signal in the first period of LHC data taking at 7 TeV center-of-mass energy with $2\,\mathrm{fb}^{-1}$ integrated luminosity. We have considered the zero-lepton plus four jets and missing transverse energy signature, and performed a combined fit of low-energy measurements, the dark matter relic density constraint and LHC exclusions. The non-observation of supersymmetry in the first period of LHC data taking stills allow for a reasonable description of low-energy data and the dark matter relic density even within the CMSSM, but excludes squarks and gluinos with masses below 1 TeV.

1 Introduction

Extending the Standard Model (SM) through supersymmetry (SUSY) is a very promising solution to the hierarchy problem between the weak scale and the Planck scale [1] if the SUSY

[1] Speaker

particle masses are of order 1,TeV. Supersymmetric particles can contribute to low-energy observables via radiative quantum corrections. In fact, SUSY models provide an excellent fit to the extensive low-energy data, see for example Refs. [2, 3]. The fits generically prefer a light SUSY spectrum, typically below 1 TeV, thus providing further motivation for low-energy supersymmetry.

The minimal supersymmetric SM has 124 free parameters. However, current precision observables and direct search limits only provide sensitivity to very restricted SUSY models with a small number of parameters, like the constrained minimal supersymmetric model (CMSSM) [1] which only has 5 free parameters beyond those of the SM. Specifically, they are characterized by a common supersymmetric scalar mass M_0, a common gaugino mass $M_{1/2}$, a universal trilinear coupling A_0, the ratio of the two Higgs vacuum expectation values, $\tan\beta$, and the sign of the Higgs mixing mass parameter, $\text{sign}(\mu)$. In the following, we focus on the CMSSM.

The ATLAS and CMS experiments at the Large Hadron Collider (LHC) at CERN have searched for supersymmetry based on approximately $1\,\text{fb}^{-1}$ of integrated luminosity at 7 TeV center-of-mass energy [4]. So far, unfortunately, no sign of supersymmetry has been found, and squarks and gluinos with masses close to 1 TeV have been excluded within the CMSSM. The search will continue with the $5\,\text{fb}^{-1}$ of data accumulated in 2011, and with data collected at 8 TeV in 2012.

To obtain consistent limits on the SUSY parameter space and the resulting mass spectrum in the absence of a SUSY signal at the LHC, one needs to combine the LHC exclusion limits and current low energy precision observables in a global fit. We have employed the FITTINO framework [3, 5] to study such a scenario, and present work obtained in Refs. [6]

2 Fit Observables

We have followed the FITTINO analysis in Ref. [3] and considered the following set of low-energy observables and existing collider limits: *(i)* rare decays of B- and K-mesons; *(ii)* the anomalous magnetic moment of the muon, a_μ; *(iii)* electroweak precision measurements from LEP, SLC and the Tevatron and the Higgs boson mass limit from LEP; and *(iv)* the relic density of cold dark matter in the universe, Ω_χ. In contrast to Ref. [3], we have employed the program HIGGSBOUNDS [7] and not a rigid Higgs mass limit. We refer to Ref. [3] for a detailed discussion of the low-energy inputs and the collider limits.

At the LHC, the most stringent limits on supersymmetric models with R-parity conservation can be expected from searches in channels with jets, leptons and missing transverse energy, E_T^{miss}. We have followed the ATLAS analysis presented in Ref. [8] and considered the search channel with four jets, zero leptons and E_T^{miss}. This channel drives the sensitivity, in particular for large $M_{1/2}$. The selection cuts are

– four or more central jets with the pseudorapidity $|\eta(\text{jet})| < 2.5$, and with the transverse

momentum $p_T > 100\,\text{GeV}$ for the leading jet, and $p_T > 40\,\text{GeV}$ for the other jets;
- an opening angle between the transverse momentum of the three leading jets and $\vec{p}_T^{\,\text{miss}}$ satisfying $\Delta\phi(\vec{p}_T^{\,\text{jet},i}, \vec{p}_T^{\,\text{miss}}) > 0.2$;
- the missing transverse energy $E_T^{\text{miss}} > 80\,\text{GeV}$;
- the ratio of the missing transverse energy and the effective mass satisfying $E_T^{\text{miss}}/M_{\text{eff}} > 0.2$;
- the transverse sphericity $S_T > 0.2$;
- no leptons with $p_T > 20\,\text{GeV}$.

The effective mass is defined as the scalar sum of the transverse momenta of all main objects, *i.e.*

$$M_{\text{eff}} = \sum_{i=1}^{N_{\text{jets}}=4} p_T^{\text{jet},i} + E_T^{\text{miss}}. \tag{1}$$

The SM background processes have been described in detail in Ref. [8]. After the cuts listed above, the combined SM cross section has been estimated to $\sigma_{\text{SM}} = 2.42\,\text{pb}$ at 7 TeV. We have used the estimate of the background contribution to the M_{eff} distribution from the ATLAS analysis, including a systematic uncertainty of 20% [8]. The signal cross section is dominated by squark and gluino pair production, $pp \to \tilde{q}\tilde{q}^*, \tilde{q}\tilde{q}, \tilde{q}\tilde{g}$ and $\tilde{g}\tilde{g}$, but all SUSY pair production processes are included in our numerical analysis. We use Herwig++ [9] in combination with the parametrized fast detector simulation Delphes [10] to obtain the detector response and, in particular, the shape of the M_{eff} distribution for a given point in the supersymmetric parameter space. The signal estimate is normalized to the NLO+NLL QCD prediction for the inclusive squark and gluino cross sections [11]. We have assigned a systematic uncertainty of 30% on our signal estimate.

The fit presented in Section 3 is based on a grid spanned in M_0 and $M_{1/2}$ for the prediction of the M_{eff} spectrum. In between the grid points, a bi-linear interpolation is used. The variation of the M_{eff} distribution with the remaining CMSSM parameters $\tan\beta$ and A_0 has been studied carefully. We found that the variations are always within the systematic uncertainty, as exemplified in Fig. 1 for two points in the $(M_0, M_{1/2})$ parameter space.

To obtain good sensitivity to a SUSY signal, the full distribution of M_{eff} is included in the statistical analysis. We consider ten bins in the range $0 < M_{\text{eff}} < 4\,\text{TeV}$ and calculate the χ^2 contribution to the SUSY parameter fit from the number of signal and background events in each bin of the M_{eff} distribution. We define a test statistic $t = -2\ln Q$ with Q being the likelihood ratio

$$Q = \prod_{i=1}^{N_{\text{bins}}} \frac{\mathcal{L}(\mu_i = s_i + b_i; n_i)}{\mathcal{L}(\mu_i = b_i; n_i)}. \tag{2}$$

Here $\mathcal{L}(\mu; n) = \mu^n e^{-\mu}/n!$ is the Poisson probability to observe n events if μ are expected. s_i and b_i are the expected number of signal and background events in bin i, and n_i is the observed

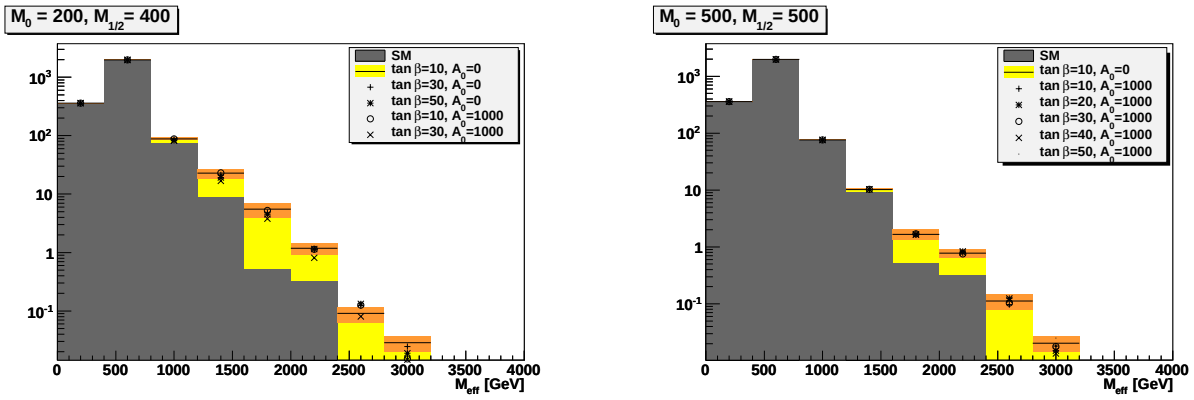

Figure 1: $M_{\rm eff}$ distribution for two points in the $(M_0, M_{1/2})$ parameter space. Shown are the SM background (gray), the CMSSM signal expectation for $\tan\beta = 10$ and $A_0 = 0$ (yellow) together with the systematic uncertainty of 30% (orange), and various other signal estimates based on different values of $\tan\beta$ and A_0. The variation of the $M_{\rm eff}$ distribution with $\tan\beta$ and A_0 is within the uncertainty assigned to the default prediction.

event count in this bin. s_i is a function of the SUSY parameters, whereas b_i is fixed. We consider a signal excluded with 95% confidence level (CL) if

$$\mathrm{CL}_{s+b} = \int_{t_{\rm obs}}^{\infty} P_{s+b}(t)\, dt < 0.05\,. \tag{3}$$

Here $P_{s+b}(t)$ is the probability density function of t assuming the presence of a signal and $t_{\rm obs}$ the actually observed value of t. Uncertainties on the cross-sections are taken into account by a correlated smearing of the expected event numbers. A given CL_{s+b} value can be approximately translated into a χ^2 contribution using the formula [12]

$$\chi^2 = 2[\,\mathrm{erf}^{-1}(1 - 2\,\mathrm{CL}_{s+b})]^2\,. \tag{4}$$

To obtain expected exclusion limits we use the Asimov data set $n_i = b_i$, $i = 1, \ldots, N_{\rm bins}$.

3 Numerical results

We present results from a global fit of the CMSSM to low-energy precision observables, the dark matter relic density, existing collider data from LEP, SLC and the Tevatron, and the current LHC exclusion limit corresponding to $2\,\mathrm{fb}^{-1}$ integrated luminosity.

In Fig. 2 (left panel) we show the CMSSM parameter region in M_0 and $M_{1/2}$ compatible with the existing low energy observables, the existing collider limits from LEP, SLC and the

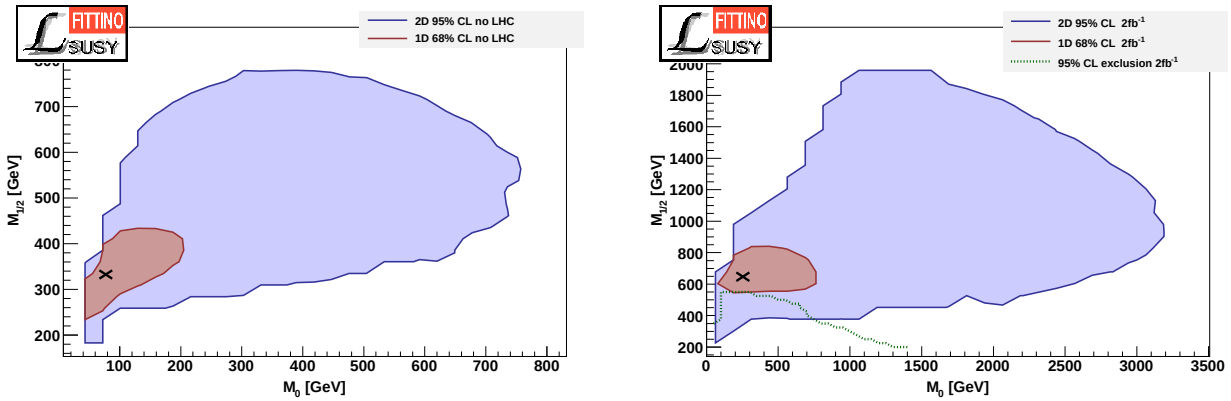

Figure 2: CMSSM parameter region in M_0 and $M_{1/2}$ compatible with low-energy observables, current collider data from LEP, SLC and the Tevatron, and the dark matter relic density. Left panel: without LHC exclusions; right panel: including the LHC exclusion limit in the four-jet, zero-lepton and $E_T^{\rm miss}$ channel for $2\,{\rm fb}^{-1}$ integrated luminosity. Shown are the two-dimensional 95% and one-dimensional 68% CL regions. Also shown in the right panel is the LHC 95% CL exclusion limit.

Tevatron, and the cold dark matter relic density, but no LHC exclusions imposed. Note that a positive sign of μ is preferred to describe the anomalous magnetic moment of the muon, so we have fixed ${\rm sign}(\mu) = +$ and determined M_0, $M_{1/2}$, A_0, and $\tan\beta$ from the fit. Including the 1σ uncertainty, we find $M_0 = 75\,^{+115}_{-29}\,{\rm GeV}$, $M_{1/2} = 329\,^{+92}_{-83}\,{\rm GeV}$, $A_0 = 417\,^{+715}_{-725}\,{\rm GeV}$ and $\tan\beta = 13\,^{+10}_{-7}$, in good agreement with Ref. [3]. The minimum χ^2 value is 19 for 20 degrees of freedom. Note that in regions with small M_0 and large $M_{1/2}$ the $\tilde{\tau}$ may be the lightest supersymmetric particle; such regions are thus excluded from the fit.

In Fig. 2 (right panel) we show the result of the global fit where we have combined the current LHC exclusion limit corresponding to $2\,{\rm fb}^{-1}$ integrated luminosity, the low-energy precision and collider observables, and the dark matter relic density constraint. The best fit now corresponds to $M_0 = 270\,^{+423}_{-143}\,{\rm GeV}$, $M_{1/2} = 655\,^{+150}_{-81}\,{\rm GeV}$, $A_0 = 763\,^{+1238}_{-879}\,{\rm GeV}$ and $\tan\beta = 32\,^{+18}_{-21}$, with a minimum χ^2 value of 24 for 21 degrees of freedom. It is noteworthy that the global fit allows areas in the SUSY parameter space at 95% CL, which are located in the region of 95% CL exclusion of the LHC, see Fig. 2, right panel. This is due to the weak dependence of the LHC contribution to the χ^2 on $M_{1/2}$.

The sparticle mass spectra corresponding to the CMSSM fits without and with LHC exclusions are presented in Fig. 3, left and right panels, respectively. The LHC exclusion in the zero-lepton, four-jet plus $E_T^{\rm miss}$ channel is mainly sensitive to the squark and gluino masses and drives M_0 and $M_{1/2}$ to larger values. The low-energy precision observables and the relic density, on the other hand, are mainly constraining the masses of colour-neutral sparticles. Supersym-

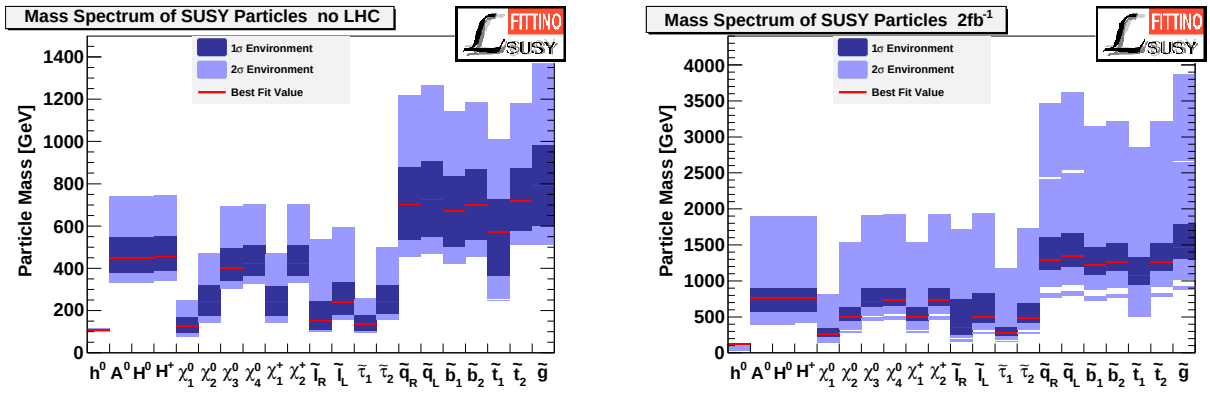

Figure 3: SUSY mass spectrum as predicted by a CMSSM fit of low-energy observables, current collider data from LEP, SLC and the Tevatron, and the dark matter relic density (left), and including the LHC exclusion limit in the four-jet, zero-lepton and $E_T^{\rm miss}$ channel for $2\,{\rm fb}^{-1}$ integrated luminosity (right).

metric models with common scalar and gaugino masses like the CMSSM connect these two, leading to a tension between the two sets of observables. In addition, for larger M_0 and $M_{1/2}$ both a_μ and Ω_χ require an increased $\tan\beta$. Furthermore values of M_0 and $M_{1/2}$ below the direct LHC limit allow for a significantly better χ^2 from the low energy data, compensating the contribution from the LHC. Thus the lower limits on the SUSY masses from the global fit including the LHC are significantly lower than the direct exclusion limits.

We note that after the completion of the work presented in Refs. [6] a number of other analyses appeared [13], which have addressed the impact of LHC exclusions on global CMSSM fits. The analyses differ in the way the LHC exclusions have been implemented and thus do not necessarily agree on their best fit results, see [14].

4 Conclusions

We have presented a global CMSSM analysis of supersymmetric models which includes low-energy precision measurements, the dark matter relic density as well as current LHC exclusion limits from direct SUSY searches in the zero-lepton plus jets and missing transverse energy channel.

We conclude that it is, in principle, possible to reconcile the supersymmetric description of low-energy observables and the dark matter relic density with a non-observation of supersymmetry in the first phase of the LHC, despite some tension building up in a combined fit within the CMSSM framework. Moreover, we find that a global CMSSM fit including LHC

exclusion limits yields lower bounds on squark and gluino masses of about 1 TeV already with $2\,\mathrm{fb}^{-1}$ integrated LHC luminosity.

While our study has been exploratory in the sense that it was based on one search channel only, and on a simplified description of the LHC detectors, it clearly demonstrates the potential of the first phase of LHC running at 7 TeV in 2011 to constrain supersymmetric models and the sparticle mass spectrum.

Acknowledgements

This work has been supported in part by the Helmholtz Alliance "Physics at the Terascale", the DFG SFB/TR9 "Computational Particle Physics", the DFG SFB 676 "Particles, Strings and the Early Universe", the European Community's Marie-Curie Research Training Network under contract MRTN-CT-2006-035505 "Tools and Precision Calculations for Physics Discoveries at Colliders" and the Helmholtz Young Investigator Grant VH-NG-303. MK thanks the CERN TH unit for hospitality and the organizers for the invitation to such an interesting and enjoyable workshop.

References

[1] H.P. Nilles, *Phys. Rep.* **110** (1984) 1; H.E. Haber and G.L. Kane, *Phys. Rep.* **117** (1985) 75; R. Barbieri, *Riv. Nuovo Cim.* **11** (1988) 1; S. P. Martin, arXiv:hep-ph/9709356.

[2] R. R. de Austri, R. Trotta, L. Roszkowski, JHEP **0605** (2006) 002; B. C. Allanach, K. Cranmer, C. G. Lester *et al.*, JHEP **0708** (2007) 023; R. Lafaye, T. Plehn, M. Rauch *et al.*, Eur. Phys. J. **C54** (2008) 617-644; O. Buchmueller *et al.*, JHEP **0809** (2008) 117.

[3] P. Bechtle, K. Desch, M. Uhlenbrock and P. Wienemann, Eur. Phys. J. C **66** (2010) 215.

[4] G. Aad *et al.* [ATLAS Collaboration], arXiv:1107.0561 [hep-ex]; Eur. Phys. J. C **71** (2011) 1682; Eur. Phys. J. C **71** (2011) 1647; Phys. Lett. B **701** (2011) 398; Phys. Lett. B **701** (2011) 1; Phys. Rev. Lett. **106** (2011) 131802; J. B. G. da Costa *et al.* [ATLAS Collaboration], Phys. Lett. B **701** (2011) 186; S. Chatrchyan *et al.* [CMS Collaboration], CERN-PH-EP-2011-138; JHEP **1108** (2011) 156; arXiv:1107.1279 [hep-ex]; JHEP **1108** (2011) 155; JHEP **1107** (2011) 113; arXiv:1106.0933 [hep-ex]; JHEP **1106** (2011) 093; JHEP **1106** (2011) 077; JHEP **1106** (2011) 026; Phys. Rev. Lett. **106** (2011) 211802; V. Khachatryan *et al.* [CMS Collaboration], Phys. Lett. B **698** (2011) 196; Phys. Rev. Lett. **106** (2011) 011801.

[5] P. Bechtle, K. Desch and P. Wienemann, Comput. Phys. Commun. **174** (2006) 47.

[6] P. Bechtle, B. Sarrazin, K. Desch, H. K. Dreiner, P. Wienemann, M. Krämer, C. Robens and B. O'Leary, Phys. Rev. D **84** (2011) 011701; arXiv:1105.5398 [hep-ph].

[7] P. Bechtle, O. Brein, S. Heinemeyer, G. Weiglein and K. E. Williams, Comput. Phys. Commun. **181** (2010) 138.

[8] The ATLAS collaboration, "Prospects for Supersymmetry discovery based on inclusive searches at a 7 TeV centre-of-mass energy with the ATLAS detector," ATL-PHYS-PUB-2010-010.

[9] M. Bähr *et al.*, Eur. Phys. J. C **58** (2008) 639.

[10] S. Ovyn, X. Rouby and V. Lemaitre, arXiv:0903.2225 [hep-ph].

[11] W. Beenakker, R. Höpker, M. Spira *et al.*, Nucl. Phys. **B492** (1997) 51-103; W. Beenakker, M. Krämer, T. Plehn *et al.*, Nucl. Phys. **B515**, 3-14 (1998); A. Kulesza, L. Motyka, Phys. Rev. Lett. **102** (2009) 111802 and Phys. Rev. **D80** (2009) 095004; W. Beenakker, S. Brensing, M. Krämer *et al.*, JHEP **0912** (2009) 041, JHEP **1008** (2010) 098 and Int. J. Mod. Phys. A **26** (2011) 2637.

[12] J. R. Ellis, S. Heinemeyer, K. A. Olive, A. M. Weber, G. Weiglein, JHEP **0708** (2007) 083.

[13] B. C. Allanach, T. J. Khoo, C. G. Lester, S. L. Williams, JHEP **1106** (2011) 035; G. Bertone *et al.* [arXiv:1107.1715 [hep-ph]]; O. Buchmueller *et al.*, Eur. Phys. J. **C71** (2011) 1722; A. Strumia, JHEP **1104** (2011) 073; D. Feldman *et al.*, Phys. Rev. **D84** (2011) 015007; S. Scopel, S. Choi, N. Fornengo and A. Bottino, Phys. Rev. **D83** (2011) 095016; S. Akula *et al.*, Phys. Lett. **B699** (2011) 377-382; S. Akula *et al.*, Phys. Lett. **B699** (2011) 377-382; M. J. Dolan *et al.*, JHEP **1106** (2011) 095; A. Strumia, arXiv:1107.1259 [hep-ph]; M. Farina *et al.*, [arXiv:1104.3572 [hep-ph]].

[14] S. S. AbdusSalam *et al.*, Eur. Phys. J. C **71** (2011) 1835.

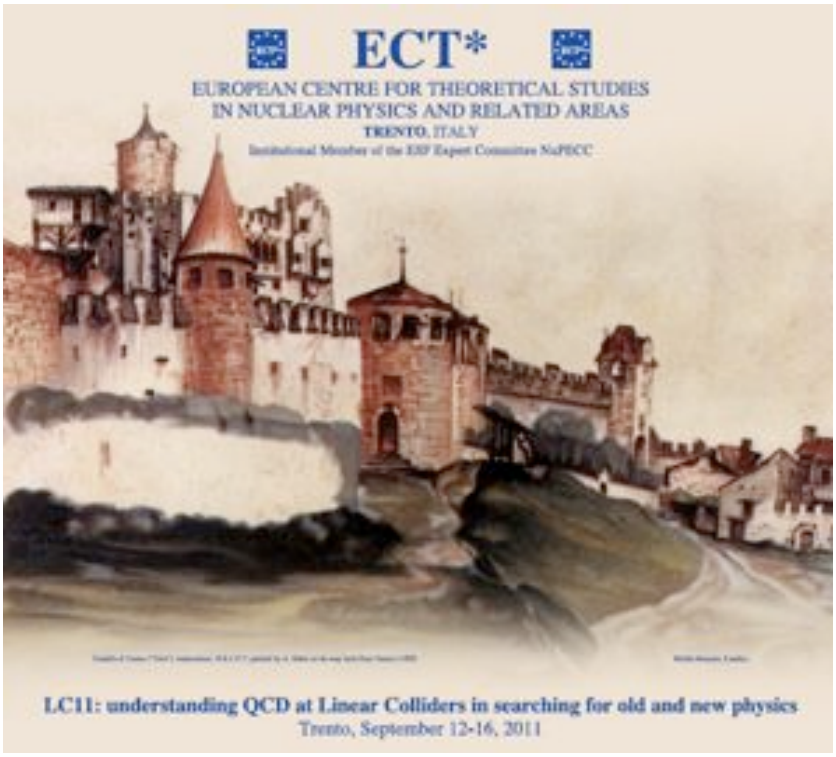

Castello di Trento painted by A. Dürer on his way back from Venice (1495).

7.3 R. Ferrari - Metamorphosis in the Electroweak Model

Metamorphosis in the Electroweak Model

Ruggero Ferrari
Università degli Studi di Milano and INFN, Sez. di Milano, Italy
ruggero.ferrari@mi.infn.it

Abstract The high energy behavior of massive nonabelian gauge theories (e.g. in the Electroweak Model) is compared in the two cases of Higgs Mechanism (HM) and of Non Linear Realization (NLR) of the gauge group (Stückelberg mass). In most extreme cases this problem can be translated into the study of the zero-mass limit (single scale processes). In this way the question becomes a fundamental issue since a massless vector meson has two degrees of freedom while a massive one has three.
The two scenarios (HM and NLR) have strikingly different behavior: in the HM there is a metamorphosis of the longitudinal state into the Goldstone scalars, while in the NLR a phase transition line separates the massive theory from the pure massless case (i.e. no Goldstone modes and no longitudinal states).
There are phenomenological consequences of this differences, in particular in the case of HM all the Higgs fields become physical modes. This signature might be detected in a linear collider at high energy.
From a theoretical point of view, the aim of this work is to show that the problem of unitarity at high energy in nonabelian gauge theory with no Higgs boson can open new perspectives in quantum field theory.

1 Introduction

We are going to compare the usual HM generated mass term in a $SU(2)$ Yang-Mills

$$S_{YM} + \Lambda^{D-4} \int d^D x \, \Big[(\partial_\mu - igA_\mu)\Phi\Big]^\dagger (\partial_\mu - igA_\mu)\Phi$$

with the Stückelberg mass

$$S_{YM} + \Lambda^{D-4} M^2 \int d^D x \; Tr\Big\{ \Big[gA_\mu - i\Omega\partial_\mu\Omega^\dagger\Big]^2 \Big\},$$

where S_{YM} is the pure gauge action.

In HM we have

$$\Phi = \begin{pmatrix} i\phi_1 + \phi_2 \\ \phi_0 - i\phi_3 \end{pmatrix}$$

and ϕ_0 is the field of the Higgs boson.

In the NLR gauge theory

$$\Omega = \phi_0 + i\phi_a\tau_a = \begin{pmatrix} \phi_0 + i\phi_3 & i\phi_1 + \phi_2 \\ i\phi_1 - \phi_2 & \phi_0 - i\phi_3 \end{pmatrix}, \qquad \Omega \in SU(2).$$

Since Ω is a unitary matrix, there is a constraint, here given by

$$\phi_0 = \sqrt{1 - \vec{\phi}^{\,2}}.$$

Thus the NLR gauge theory is nonrenormalizable due to the constraint on ϕ_0. The subtraction procedure presented in Refs. [1] and [2] does not introduce new parameters in the action. Therefore the resulting theory is considered fundamental (not an effective one).

Two questions are discussed here about this novel approach:
A) The suggested subtraction procedure is based on dimensional regularization. The strategy would be better founded if other regularization procedures could be employed.
B) Although perturbative unitarity is valid, the behavior of some cross sections at high energy, evaluated at fixed order, is untenable (e.g. the celebrated case of W_LW_L elastic scattering [3]-[8]). It is important to understand what is the fate of NLR gauge theories at very high energy [9].

2 The Unitarity Conundrum

In their seminal paper Lee, Quigg and Thacker [4] correctly remark that, at very high energies, the vanishing of the most divergent terms proceeds through the cancellation of various contributions, which includes the one of the Higgs boson [1]. Many physicists have shortcutted this correct statement by concluding that *by removing the Higgs boson, unitarity is violated*. To our opinion this conclusion has to be carefully reconsidered.

2.1 Higgs mechanism

Lets us recall briefly the argument for the case of $SU(2)$, with Higgs Mechanism. For longitudinally polarized vector bosons

$$\epsilon_L = \frac{1}{M}\left(|\vec{p}|, \frac{\vec{p}}{|\vec{p}|}E\right)$$

[1] See the comment after their eq. (2.3)

the sum of the gauge **tree** graphs for $W_L^+W_L^-$ elastic amplitude in the center of mass behaves like

$$M_{gauge} = g^2 \frac{s}{8M_W^2}(\cos\theta + 1) + \mathcal{O}(s^0).$$

The Higgs $s,t-$channels contribution cancels this bad behavior and

$$M_{gauge} + M_H = g^2[\frac{3+\cos^2\theta}{4\cos^2\theta_W(\cos\theta - 1)} - \frac{M_H^2}{2M_W^2} + \mathcal{O}(s^{-1})].$$

2.2 Very High Energy with Stückelberg: Problems

The behavior of a NLR nonabelian gauge theory is very singular for $M \to 0$. The self-coupling vertex has a coupling $\simeq M^2$ but the ϕ - propagator has a factor $\simeq M^{-2}$. Thus a graph with a vertex, with many ϕ-propagators attached, has a singular behavior. If the $M \sim 0$ behavior is dominated by the nonlinear sigma model features, then the forward scattering amplitude at high energy (neglecting infrared divergences!) behaves like

$$T_{\phi\phi}^{(n)}(s) \sim \left(\frac{s}{M^2}\right)^{(n+1)},$$

where n is the number of loops.
Although perturbative unitarity is preserved, the perturbative series cannot account for high energy behavior.

3 Some other troublesome questions

In extreme processes we can translate the limit of high energy to the more fundamental one $M \to 0$. In the limit we face a problem connected to the number of physical modes:

- For $M = 0$ only two polarizations are physical while for $M \neq 0$ they are three: problems with the matching among unphysical vector meson modes, Goldstone bosons and Faddeev-Popov ghosts in order to provide Physical Unitarity.
- Do longitudinal polarizations decouple from physical states like in QED?
- Or else?

4 Scenario at very High Energy (Higgs): a prologue

At very high energy the longitudinal polarization of a vector boson

$$\epsilon_L = \frac{1}{M}\,(|\vec{p}|, \hat{p}E)$$

becomes indistinguishable from a spin zero particle described by a scalar boson $\partial_\mu \phi$

$$\epsilon_{J=0} = \frac{1}{M}\,(E, \vec{p}).$$

Thus the experimental setup provides a cut-off energy E_c. Only for $E < E_c$ one can distinguish the two polarization states. E_c depends on the precision of the momentum and energy measurements. Thus it is tempting to affirm that in the limit $v \to 0$ the symmetry is restored and the longitudinal polarization modes transform into the (former, $v \neq 0$) Goldstone bosons. The metamorphosis is abrupt: for $v \neq 0$ the Goldstone bosons are unphysical modes and they become physical modes for $v = 0$. At the same time the vector mesons carry two physical- and two unphysical modes.
In the limit the Higgs fields are physical modes, therefore the nonabelian gauge theory is not asymptotically free.
A small value of v provides a very good infrared regulator for the otherwise ill-defined massless theory, since all the requirements are met: physical unitarity, BRST, locality, etc.

5 Equivalence Theorem (ET)

For a quantitative description of the metamorphosis process some help is provided by the ET [3], [6], [10]- [16]. We use

$$\epsilon_L = \frac{1}{M}\,(|\vec{p}|, \hat{p}E) = \frac{p_\mu}{M} + \frac{1}{M}\left(-\frac{M_G^2}{|\vec{p}| + E_G}, \hat{p}\frac{M^2}{|\vec{p}| + E}\right) = \frac{p_\mu}{M} + \mathcal{O}(M),$$

where $M_G^2 = \text{mass}^2$ of the Goldstone boson equal to $\xi^{-1}M^2$ at the tree level. Then for very large energy processes ($s, t >> M^2$) we can consider the limit $M \to 0$. ET theorem says that for $M \to 0$

$$\epsilon_L^{\mu_1} \cdots \epsilon_L^{\mu_k} W_{\widehat{A^{\mu_1}(p_1)}\cdots\widehat{A^{\mu_k}(p_k)}***}\Big|_{p^2=M^2} \simeq [iR]^k W_{\widehat{\phi(p_1)}\cdots\widehat{\phi(p_k)}***}\Big|_{p^2=M_G^2},$$

$$R \equiv i\frac{p^\nu \Gamma_{\phi A^\nu}}{M\Gamma_{\phi\phi}}\Big|_{p^2=M_\alpha^2} = \xi\frac{M_G^2}{M^2}.$$

The $\widehat{\ }$ on a subscript field indicates that the line has been removed. This is the required relation for a quantitative fixing of the metamorphosis.

6 Summary of the limit $M = 0$ in the Higgs case

- The longitudinal modes transforms into the Goldstone bosons
- The Goldstone bosons become physical, like the Higgs singlet.
- The vector gauge field (massless) describe two transverse and physical modes and two unphysical.
- The theory is not asymptotically free, even if the mass of the gauge field is zero.

7 Scenario at very High Energy (Stückelberg): Asymptotic Freedom?

The ET is based on the Slavnov-Taylor identities, thus it works also in the nonlinear case. However a metamorphosis of the longitudinal modes is not allowed, because the Goldstone bosons remain unphysical, if not decoupled form physical states (due to BRST).

We dare an educated guess on the limit $M = 0$: the limit is not permitted by the presence of a phase transition line. The line is supposed to separate the particle phase from the confinement (asymptotic freedom). This guess is pertinent only for extreme processes, where kinematically the $M = 0$ limit reproduces the large energy regime.

The guess is supported by the lattice simulation of the *massive* Yang-Mills theory. The lattice action is [17]

$$S_E = -\frac{\beta}{2}\,\mathfrak{Re}\sum_{\Box} Tr(U_{\Box})$$
$$-\frac{\beta}{2}m^2\mathfrak{Re}\sum_{x\mu} Tr\Big\{\Omega(x)^{\dagger}U(x,\mu)\Omega(x+\mu)\Big\},$$

where $\beta = \frac{4}{g^2}$ and $m^2 \equiv M^2a^2$. Thanks to the limit (classical)

$$-\lim_{a=0}\frac{\beta}{2}M^2a^2\mathfrak{Re}\sum_{x\mu} Tr\Big\{\Omega(x)^{\dagger}U(x,\mu)\Omega(x+\mu) - 1\Big\}$$
$$= \frac{M^2}{g^2}\int d^4x Tr\,\Big\{(A_\mu - i\Omega\partial_\mu\Omega^{\dagger})^2\Big\}$$
$$= \frac{M^2}{g^2}\int d^4x Tr\,\Big\{[(i\partial_\mu + A_\mu)\Omega]^{\dagger}(i\partial_\mu + A_\mu)\Omega\Big\}. \qquad (1)$$

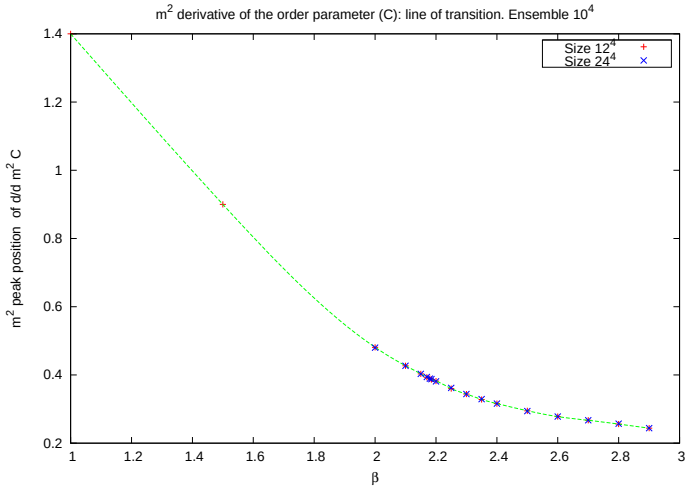

Figure 1: Phase transition line

8 Lattice simulation: the phase diagram [18]

The simulation is on the partition function (N is the number of sites and $D = 4$ the dimension of the lattice)

$$Z[\beta, m^2, N] = \sum_{\{U,\Omega\}} e^{-S_E}.$$

Moreover we introduce the order parameter

$$\mathfrak{C} = \frac{1}{DN\beta}\frac{\partial}{\partial m^2}\ln Z = \frac{1}{2ND}\Big\langle \mathfrak{Re}\sum_{x\mu} Tr\{\Omega^\dagger(x)U(x,\mu)\Omega(x+\mu)\}\Big\rangle. \tag{2}$$

and study the behavior of Energy, Order Parameter and their derivatives with respect to β and m^2. The model has been studied since long as a Higgs mechanism where the boson field is frozen in length [19]. Our results are numerically consistent with previous findings. A line is found where the order parameter and energy have an inflection point as shown in Figure 1. The end point is around $\beta = 2.2$ and $m^2 = 0.381$.
This is a very important result that supports our guess on the zero mass limit. On the line both the energy E and the order parameter $\mathfrak{C}$ have inflection points in their dependence on β

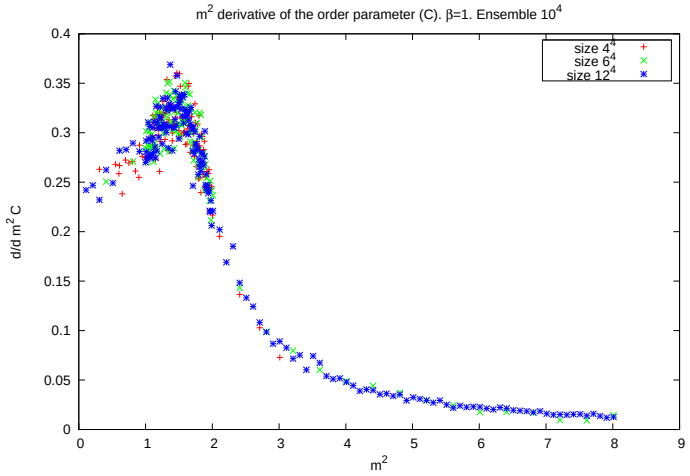

Figure 2: The derivative of $\mathfrak{C}$ with respect to m^2 at $\beta = 1$

and m^2. Figure 2 is showing this behavior for β lower than the endpoint ($\beta = 1$). There is no size effect. Figure 3 is showing this behavior for β larger than the endpoint value ($\beta = 3$). Here the size effect looks relevant.

On the transition line both the energy E and the order parameter $\mathfrak{C}$ seem to be continuous. For small β they have a moderate increase on the line, while for high β their increase is very sharp, as exemplified by the Figure 4. In the two regions (above and below the line) the two-point functions of the *gauge invariant* fields

$$C(x,\mu) \equiv \Omega^\dagger(x) U(x,\mu) \Omega(x+\mu) = C_0(x,\mu) + i\tau_a C_a(x,\mu) \tag{3}$$

have different behavior. Above they show the presence of an energy gap. By crossing the line the deconfined phase disappears. Notice that in the continuum limit we recover the gauge invariant fields introduced in the Stückelberg mass: for C_1, C_2, C_3 we have

$$C(x,\mu) = -ia\Omega^\dagger \Big(A_\mu(x) - i\Omega\partial_\mu\Omega^\dagger \Big)\Omega + \mathcal{O}(a^2);$$

while for C_0 we have

$$C_0(x,\mu) = 1 - \frac{a^2}{4} Tr\, \Big\{ (A_\mu - i\Omega\partial_\mu\Omega^\dagger)^2 \Big\} + \mathcal{O}(a^4).$$

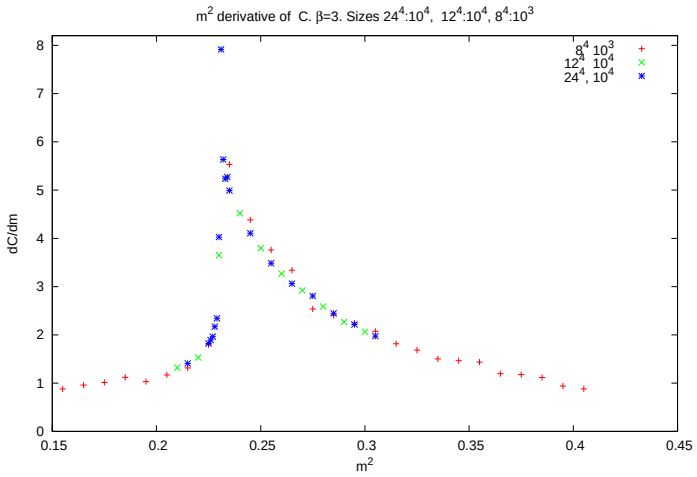

Figure 3: The derivative of $\mathfrak{C}$ with respect to m^2 at $\beta = 3$

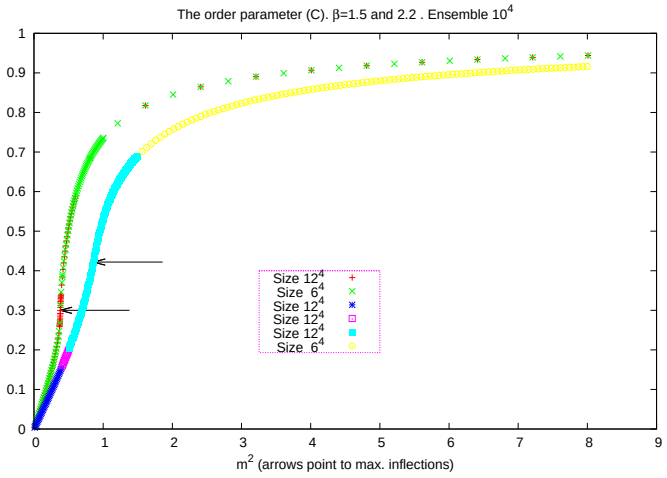

Figure 4: The order parameter $\mathfrak{C}$ as function of m^2 at $\beta = 1.5$ and $\beta = 2.2$

We study the operators

$$C_{a,\mu}(t) := \frac{1}{\sqrt{N^{\frac{3}{4}}}} \sum_{\vec{x}} C_a(\vec{x}, x_4, \mu)\Big|_{x_4=t}, \ a = 0, 1, 2, 3, \ \mu, \nu = 1, 2, 3, 4. \tag{4}$$

We consider the two-point correlators

$$C_{ab,\mu\nu}(t) := \Big\langle C_{a,\mu}(t + t_0) C_{b,\nu}(t_0) \Big\rangle_C. \tag{5}$$

Numerical simulations support the selection rules

$$\begin{aligned} &C_{0b,\mu\nu}(t) = 0 \\ &C_{ab,\mu\nu}(t)\Big|_{a\neq b} = 0, \quad a, b = 1, 2, 3. \end{aligned} \tag{6}$$

The spin analysis is done by decomposing the correlators into a spin one and spin zero parts (dots stand for 00 or 11,22,33)

$$C_{\cdots,\mu\nu}(t) = V_{\cdots}(t)(\delta_{\mu\nu} - \delta_{4\mu}\delta_{4\nu}) + S_{\cdots}(t)\delta_{4\mu}\delta_{4\nu}. \tag{7}$$

We fit the amplitudes by a single exponential form

$$F(t) = a + be^{-t\Delta}. \tag{8}$$

Figures 5 and 6 show the correlators for $\beta = 3.0$, i.e. in the region where a phase transition is present. Figure 7 is showing the energy gaps for various values of m^2. The data are consistent with the presence of a deconfined phase for $m^2 >> 0.231$ (energy gap) and a confined phase for $m^2 << 0.231$ (null correlators for $t > 0$) [20], [21], [22].

Thus the lattice simulation gives a strong support to the conjecture on the $M = 0$ limit of the NLR of nonabelian gauge theory: the presence of the phase transition line forbids the use of the perturbative expansion for the limit. Moreover across the line the model behaves as a massless nonabelian theory (asymptotically free theory). Let us stress that the range of the validity of the result is confined to kinematically extreme high energy processes with a single scale.

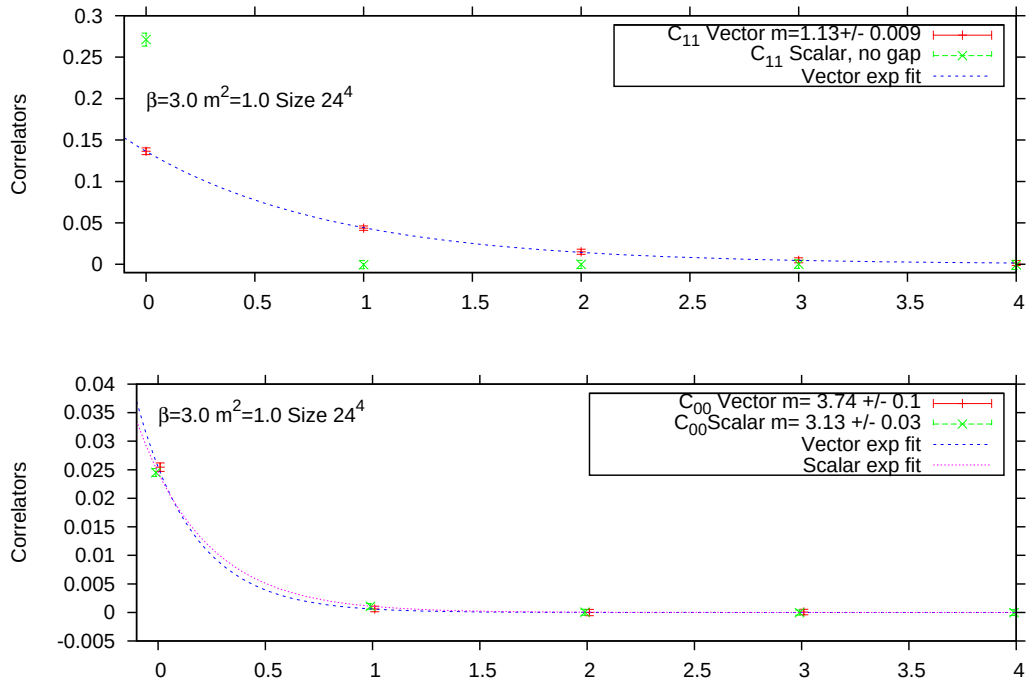

Figure 5: The time dependence of the correlators for $\beta = 3$ and $m^2 = 1.0$

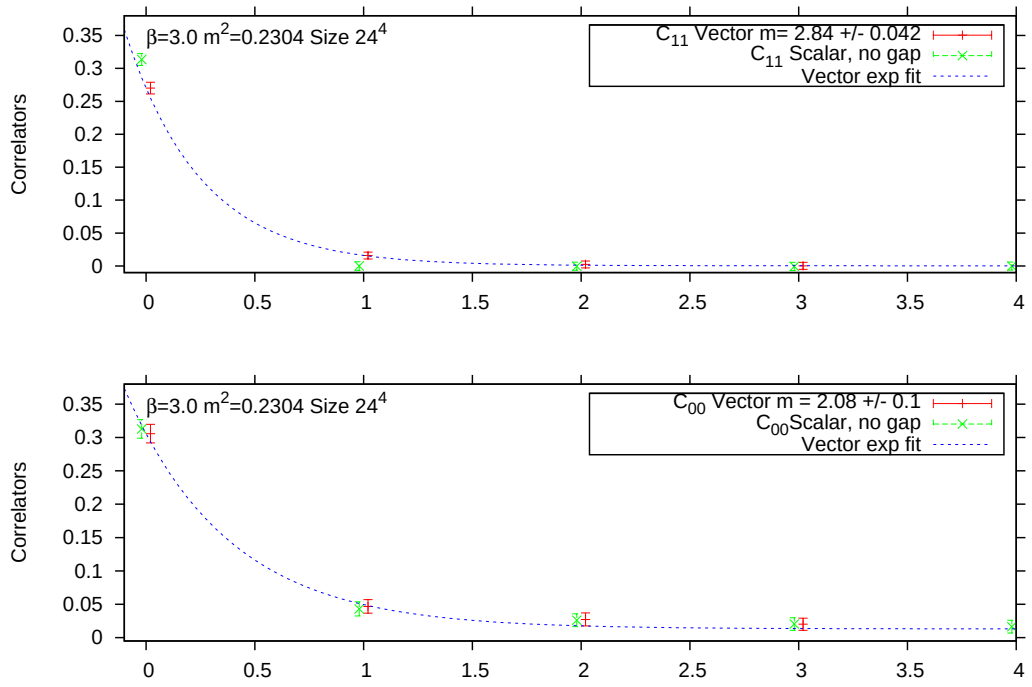

Figure 6: The time dependence of the correlators for $\beta = 3$ and $m^2 = 0.2304$

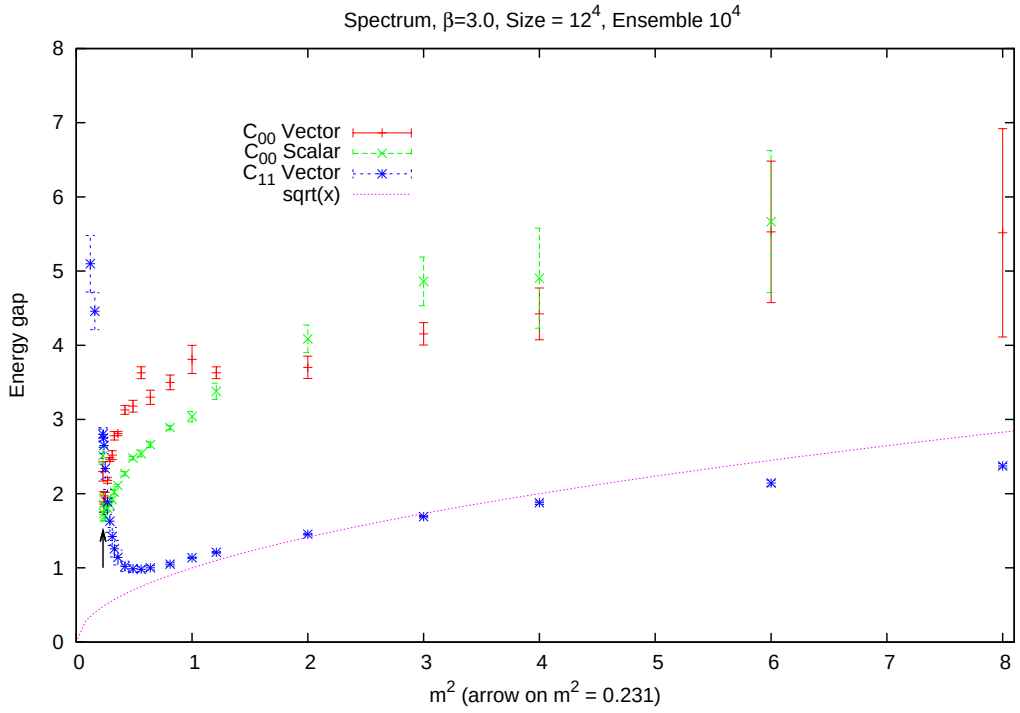

Figure 7: Energy gaps in correlators C_{00} Spin 1, C_{00} Spin 0 and C_{11} Spin 1 for $\beta = 3$. Critical mass at $m^2 = 0.231$.

9 An Example

The difference between HM and NLR nonabelian massive gauge theories can be shown in many realms. The loop corrections in the two theories have been discussed and analytically evaluated in Ref. [23]. HM and NLR nonabelian gauge theories show marked differences in the celebrated processes WW, WZ and ZZ elastic scattering. In fact the limit $M = 0$ of the NLR theory, according to the previously presented arguments, is a pure nonabelian gauge model without Higgs scalars. Moreover the longitudinal polarization of the vector mesons does not enter in the game in the limit.

In the present Section we consider a process involving quarks or leptons in order to illustrate the metamorphosis and its consequences.

$$d + \bar{u} \to b + \bar{t}.$$

In case of Higgs mechanism we have a Drell-Yan process mediated by W^- and ϕ^-. In the Landau gauge we have (we consider only the $s-$channel graph)

$$\begin{aligned}\mathfrak{M}(M) = &\frac{g^2 V_{ud} V_{tb}^*}{2} \bar{v}_u \gamma_\mu \frac{1-\gamma_5}{2} u_d \frac{g^{\mu\nu} - \frac{q^\mu q^\nu}{q^2}}{q^2 - M^2} \bar{u}_b \gamma_\nu \frac{1-\gamma_5}{2} v_t \\ &+ V_{ud} V_{tb}^* \bar{v}_u \Big[f_u \frac{1-\gamma_5}{2} - f_d \frac{1+\gamma_5}{2} \Big] u_d \frac{1}{q^2} \bar{u}_b \Big[f_t \frac{1-\gamma_5}{2} - f_b \frac{1+\gamma_5}{2} \Big] v_t \end{aligned} \tag{9}$$

with $M = gv$ and $\sqrt{2} f_x v = m_x$. Unitarity is preserved on-shell; in fact at $q^2 = M^2$ the only pole is in the propagator. Its residuum projects on the physical polarizations. Moreover there is no pole at $q^2 = 0$, since the Goldstone boson cancels the spin zero part of the vector meson.

Eq. (9) shows in detail what happens in the limit $v = 0$: the $q^\mu q^\nu$ term in the W-propagator vanishes via Dirac equation, while the "Goldstone" field contribution survives, as in the mechanism described by the Equivalence Theorem. This exemplifies the metamorphosis of the longitudinal polarization into the physical massless scalar mode, originally associated to the unphysical Goldstone boson for $v \neq 0$.
For every value of M the two terms add to

$$\mathfrak{M}(M) = \frac{g^2 V_{ud} V_{tb}^*}{2} \bar{v}_u \gamma_\mu \frac{1-\gamma_5}{2} u_d \frac{g^{\mu\nu} - \frac{q^\mu q^\nu}{M^2}}{q^2 - M^2} \bar{u}_b \gamma_\nu \frac{1-\gamma_5}{2} v_t. \tag{10}$$

The M^{-2} term does survive in the limit of zero mass, since the $q^\mu q^\nu$ produce a quadratic term in the quark or lepton masses and therefore the v^2 dependence disappears in the ratio. In the nonlinear theory, according to our guess, such terms are not present and the W-propagator in the Landau gauge is as usual

$$-i \frac{g^{\mu\nu} - \frac{q^\mu q^\nu}{q^2}}{q^2},$$

where the $\frac{q^\mu q^\nu}{q^2}$ vanishes on the quark and lepton chiral currents, since the $M = 0$ limit has been already taken. Finally, the difference between the two scenarios (linear versus nonlinear) are traced simply by the presence of a $\frac{1}{M^2}$ factor.

Now we look whether the difference is of some phenomenological relevance. The square modulus of the amplitude (10) summed over the polarizations of the incoming and outgoing particles yields

$$\sum_{\rm POL} |\mathfrak{M}(M)|^2 = \frac{1}{(q^2 - M^2)^2}\Bigg\{ 16(p_b p_u)(p_t p_d) \\ -\frac{8}{M^2}\Big[m_t^2 m_u^2 (p_b p_d) + m_t^2 m_d^2 (p_b p_u) + m_b^2 m_u^2 (p_t p_d) + m_b^2 m_d^2 (p_t p_u)\Big] \\ +\frac{4}{M^4}\Big[2m_t^2 m_b^2 + (m_b^2 + m_t^2)(p_b p_t)\Big]\Big[2m_u^2 m_d^2 + (m_u^2 + m_d^2)(p_u p_d)\Big]\Bigg\}. \qquad (11)$$

It is clear that the M^{-2} and M^{-4} terms are negligible and therefore one cannot discriminate the linear model (with Higgs boson) from the nonlinear one (without Higgs boson) in this process.

10 Conclusions

We have compared the high energy behavior of HM- and NLR-nonabelian massive gauge theory. We have used arguments based on unitarity, ET, BRST invariance and lattice simulations. The result of the investigation can be summarized by the following items.

- In the Higgs Mechanism the $M = 0$ limit is consistent via a metamorphosis of the longitudinal modes into the Goldstone bosons: a massless gauge theory coupled to massless scalars. The theory is not asymptotically free.
- In the nonlinear case we envisage a transition to a phase where longitudinal modes and Goldstone bosons are decoupled (asymptotic freedom).
- Lattice simulations support the conjecture that $M^2 \neq 0$ and $M^2 = 0$ are different phases.
- In lattice gauge theory the evaluation of amplitudes near the transition line is at reach.

Acknowledgments

It is a pleasure to thank the organizers for the opportunity to participate to the Workshop.

References

[1] R. Ferrari, JHEP **0508**, 048 (2005) [arXiv:hep-th/0504023].

[2] D. Bettinelli, R. Ferrari and A. Quadri, Phys. Rev. D **77** (2008) 045021 [arXiv:0705.2339 [hep-th]].

[3] J. M. Cornwall, D. N. Levin and G. Tiktopoulos, Phys. Rev. D **10**, 1145 (1974) [Erratum-ibid. D **11**, 972 (1975)].

[4] B. W. Lee, C. Quigg and H. B. Thacker, Phys. Rev. D **16**, 1519 (1977).

[5] H. A. Weldon, Phys. Rev. D **30**, 1547 (1984).

[6] M. S. Chanowitz and M. K. Gaillard, Nucl. Phys. B **261**, 379 (1985).

[7] A. Denner, S. Dittmaier and T. Hahn, Phys. Rev. D **56**, 117 (1997) [arXiv:hep-ph/9612390].

[8] A. Denner and T. Hahn, Nucl. Phys. B **525**, 27 (1998) [arXiv:hep-ph/9711302].

[9] R. Ferrari, "Metamorphosis versus Decoupling in Nonabelian Gauge Theories at Very High Energies," arXiv:1106.5537 [hep-ph].

[10] G. J. Gounaris, R. Kogerler and H. Neufeld, Phys. Rev. D **34**, 3257 (1986).

[11] Y. P. Yao and C. P. Yuan, Phys. Rev. D **38**, 2237 (1988).

[12] J. Bagger and C. Schmidt, Phys. Rev. D **41**, 264 (1990).

[13] H. J. He, Y. P. Kuang and X. y. Li, Phys. Rev. Lett. **69**, 2619 (1992).

[14] H. J. He, Y. P. Kuang and X. y. Li, Phys. Lett. B **329**, 278 (1994) [arXiv:hep-ph/9403283].

[15] H. J. He, Y. P. Kuang and X. y. Li, Phys. Rev. D **49**, 4842 (1994).

[16] A. Denner and S. Dittmaier, Phys. Rev. D **54**, 4499 (1996) [arXiv:hep-ph/9603341].

[17] K. G. Wilson, Phys. Rev. D **10**, 2445 (1974).

[18] R. Ferrari, "On the Phase Diagram of Massive Yang-Mills," arXiv:1112.2982 [hep-lat].

[19] E. H. Fradkin and S. H. Shenker, Phys. Rev. D **19**, 3682 (1979).

J. Greensite and S. Olejnik, Phys. Rev. D **74**, 014502 (2006) [arXiv:hep-lat/0603024].

W. Caudy and J. Greensite, Phys. Rev. D **78**, 025018 (2008) [arXiv:0712.0999 [hep-lat]].

C. Bonati, G. Cossu, M. D'Elia and A. Di Giacomo, Nucl. Phys. B **828**, 390 (2010) [arXiv:0911.1721 [hep-lat]].

[20] M. Creutz, Phys. Rev. Lett. **43**, 553 (1979) [Erratum-ibid. **43**, 890 (1979)].

[21] B. E. Lautrup and M. Nauenberg, Phys. Rev. Lett. **45**, 1755 (1980).

[22] J. Engels, J. Jersak, K. Kanaya, E. Laermann, C. B. Lang, T. Neuhaus and H. Satz, Nucl. Phys. B **280**, 577 (1987).

[23] D. Bettinelli, R. Ferrari and A. Quadri, Phys. Rev. D **77**, 105012 (2008) [arXiv:0709.0644 [hep-th]].

Chapter 8

The future of QCD in e^+e^- physics

8.1 A. Banfi - QCD at work, from lepton to hadron colliders and back

QCD at work: from lepton to hadron colliders and back

Andrea Banfi
Department of Physics, University of Freiburg, Germany
andrea.banfi@physik.uni-freiburg.de

Abstract The astounding Physics results obtained with high-energy colliders in the last two decades owe much to an impressive progress in the understanding of the dynamics of strong interactions. I give here a personal overview of how the advance in QCD triggered by the Physics of hadronic final states at LEP has been exploited for New Physics searches at the LHC. Conversely, the need for precision calculations for LHC experiments has stimulated a huge progress in the understanding of the all-order structure of gauge theories. These results raise high expectations on the status of QCD at the start of a linear collider.

1 Introduction

With the start of the LHC Particle Physics has entered a new era. Not only will we probably have a final answer on the mechanism of spontaneous breaking of electroweak symmetry, but we could also observe novel phenomena like dark-matter or black-hole production. The LHC, being a hadron collider, can access a wide range of scales for Physics beyond the (known) Standard Model, from the LEP boundary of about 100 GeV up to the TeV scale. The price we have to pay is that events appear contaminated by the presence of a large number of hadrons. Among those, only a small fraction is related to the short-distance processes we are interested in, the rest comes either from secondary collisions of the remnants of the two broken protons (underlying event), or even from further soft collisions occurring within the same proton bunch, the so-called pile-up. This is in sharp contrast with the situation at LEP, where only a few tens of hadrons were produced. A further important difference between e^+e^- and hadronic colliders is the possibility of detection of individual hadrons. In the e^+e^- case, the tracker has basically full solid-angle acceptance, so that information on charged hadrons is available everywhere in rapidity. At hadron colliders the tracker extends only inside a central region spanning a few units in rapidity, whilst outside the only available information comes from the calorimetric towers. Therefore, although both LHC experiments are able to combine detector information into objects like "topo-clusters" [1] or "particle flows" [2] which should be quite close to individual particles, at the moment the preferred objects for studies of hadronic final states are just jets. This experimental issue has also theoretical implications, as we will describe in the following.

QCD at LEP is a "theory of hadrons", whose dynamics can be investigated from high momentum scales where quarks and gluons are produced, to the low momentum scales where the hadronisation mechanism is effective. This is done through final-state observables, like event-shape distributions or jet rates, which combine in various ways hadron momenta in numbers that provide an insight on the jet structure or the geometry of each event. The typical situation at LEP is that the hard scale of the process, the centre-of-mass energy Q, is much larger than the hadronisation scale Q_0, which is of the order of the mass of the proton. It is therefore possible to find values Q_V for final-state variables such that $Q_0 \ll Q_V$, so that the corresponding distributions can be reliably computed in perturbative QCD. Furthermore, due to the fact that most e^+e^- observables are global, i.e. sensitive to emissions everywhere in the phase space, and that in e^+e^- annihilation one can safely rely on QCD coherence, it is always possible to approximate multiple soft-collinear parton matrix elements with a probabilistic angular ordered branching [3]. This feature is the key of the success in the description of QCD final states in e^+e^- annihilation with both Monte Carlo event generators and analytical calculations (for a review see [4], and references therein). Just to recall the impressive accuracy reached by QCD calculations for hadronic final states in e^+e^- annihilation, a fully differential code for e^+e^- into three jets is available to order α_s^3 (next-to-next-to leading order, NNLO) [5, 6], all-order resummation of large logarithms has been computed for selected event shapes (thrust, heavy-jet mass) at next-to-next-to leading logarithmic accuracy (NNLL) [7, 8, 9],[1] and there exist also QCD inspired analytical models for (leading) hadronisation corrections [10, 11, 12, 13].

At the LHC QCD has to be the "theory of jets", since resolving single hadrons is in general a difficult task. Although jet cross sections are generally within the domain of perturbative QCD, there are a number of features that make an all-order perturbative description of jet observables problematic. First of all, jets themselves are non-inclusive objects, there is no closed mathematical expression that relates the momentum of a jet to the momenta of final-state hadrons, not even approximately as happens for instance for the thrust in e^+e^- in the two-jet limit. This makes it impossible to write jet cross sections in terms of operator matrix elements, as is done for many inclusive observables [14, 15, 16, 17], and sometimes also for event-shape distributions [7, 8, 18]. Another traditional worry expressed by all-order QCD practitioners is that jet cross sections are generally non-global observables [19, 20, 21]. Non-globalness, together with the fact that the presence of two hadrons in the initial state might spoil collinear factorisation [22, 23], cast serious doubts on the applicability of coherent branching to jet observables in hadronic collisions. At hadron colliders, especially at the LHC, there is also a major concern about the separation of scales between perturbative and non-perturbative Physics. Poorly understood phenomena like underlying event of pile-up can add several tens of GeV's of extra transverse momentum to QCD jets, causing huge distortions in many commonly studied hadronic final-state observables (e.g. event-shape distributions) [24].

[1] For the special case of the thrust even NNNLL accuracy is claimed in Refs. [7, 10]

Given this situation, it might seem that the knowledge of QCD we have inherited from LEP is of little use for LHC Physics. While this consideration might be true for precision studies (e.g. measurements of α_s), the insight on hadron dynamics we have at present can be largely exploited for LHC phenomenology. This will be the subject of the first part of my contribution (Section 2). In the second part (Section 3) I will shortly review the progress in QCD triggered by the quest for precision calculations in a multi-jet environment such as the LHC, and how these results have already influenced e^+e^- phenomenology. I will conclude with my personal view on the challenges that we will have to face at the start of the Linear Collider (LC), and on what theoretical tools should be needed to tackle them.

2 LEP wisdom for LHC Physics

Before discussing how QCD results from LEP can be exploited at the LHC, it is worth asking ourselves whether at the LHC precision Physics has to be limited only to inclusive quantities like Z or W differential cross sections, or can also involve direct measurements of the hadronic energy-momentum flow. As already stated in the introduction, for precision purposes it is very difficult to exploit final-state observables, like event shapes, that are defined in terms of individual hadrons, since they get huge contributions from poorly understood phenomena like underlying event or pile-up. However, jets constructed with modern algorithms are less sensitive to these effects, and their cross sections can be computed in perturbative QCD and directly compared to data. In particular, for well separated jets, fixed order perturbation theory is enough to obtain a reliable description of data, allowing for measurements of the strong coupling constant (see for instance [25]). Furthermore, if the rapidity range in which jets are observed covers the full detector acceptance, observables like jet rates become global, and hence can be studied in the whole range of values of the jet resolution parameters with all-order resummation techniques [24]. Resummed jet rates are known from LEP to have small theoretical uncertainties, and therefore seem the best candidates for precision QCD studies. A close relative of jet rates is the jet-veto efficiency, for which one can obtain accurate QCD predictions, which can in turn be exploited in several New Physics contexts, for instance in Higgs or dark-matter searches.

Most observables at the LHC however are not suitable for precision studies, but, like jet masses, are relevant for New Physics searches. In this case LEP wisdom can be exploited in various ways, for instance one can try to answer the following questions:

- Can one reduce contamination from non-perturbative effects in jets?
- Is there an optimal procedure to filter jets originating from boosted object decays?
- Can we distinguish jets originating from colour singlet decays from pure QCD jets?

In the following I give examples on how the theoretical methods developed at LEP have been already exploited to gain some analytical insight on these issues.

2.1 Non-perturbative effects in jets

One of the major theoretical achievements inherited from LEP is analytical models for hadronisation corrections. Within these approaches, leading hadronisation corrections to event-shape distributions and means are given as the product of a perturbatively calculable coefficient and a single universal non-perturbative parameter α_0, which is extracted from experimental data [13]. The universality of α_0 has been thoroughly tested at LEP, and is found to hold within 20% [4]. Since analytical hadronisation models rely basically on the universality of QCD soft radiation, they could be in principle equally applied to hadronisation corrections in hadronic collisions. This is what is done for instance in Ref. [26], where one finds the calculation of the transverse momentum loss of the leading jet due to hadronisation $\delta p_{\mathrm{t,had}}$, which appears in a variety of jet studies at the LHC. This quantity is indeed related to the universal parameter α_0, with a coefficient that scales as $1/R$, where R is the jet radius. Furthermore, since $\delta p_{\mathrm{t,UE}}$, the change in jet p_t due to a hadron background approximately uniform in rapidity and azimuth (like underlying event or pile-up), is found to scale as R^2, one can compute the radius that minimises the two effects, which should be then used for precision studies, e.g. inclusive jet transverse momentum spectra. For New Physics searches however, where one wishes for instance to identify a peak in a jet-mass distribution, it is also important to minimise the amount of perturbative QCD radiation that escapes the jet $\delta p_{\mathrm{t,pert}}$, which is found to scale as $\ln(1/R)$. The combined effect of the three sources of p_t loss is illustrated in Fig. 1 (left), from which it is evident that there exists an optimal radius for which the total $\langle \delta p_t \rangle^2$ (computed neglecting interference among its different contributions) is minimised. Since both $\delta p_{\mathrm{t,pert}}$ and $\delta p_{\mathrm{t,had}}$ are triggered by QCD radiation, they depend on the total colour charge of the parton initiating the jet, whilst $\delta p_{\mathrm{t,UE}}$ depends mainly on the centre of mass energy of the collider. Therefore we expect the optimal radius to change according to whether we consider quark or gluon jets, and whether we are at Tevatron or at LHC energies. This is confirmed by actual studies performed with parton shower event generators, and the resulting optimal radius as a function of the jet p_t is shown in Fig. 1 (right).

2.2 Non-global observables and jet filtering

A relevant topic for New Physics searches at the LHC is the exploitation of boosted kinematics and jet substructure to detect high-p_t heavy objects whose decay products fall inside the same jet (see [27] for a recent update). The basic search strategy consists in clustering each event into "fat" jets with a large radius, and then selecting a candidate jet which should contain the decay products of the heavy particle one is looking for. The best known example is a boosted

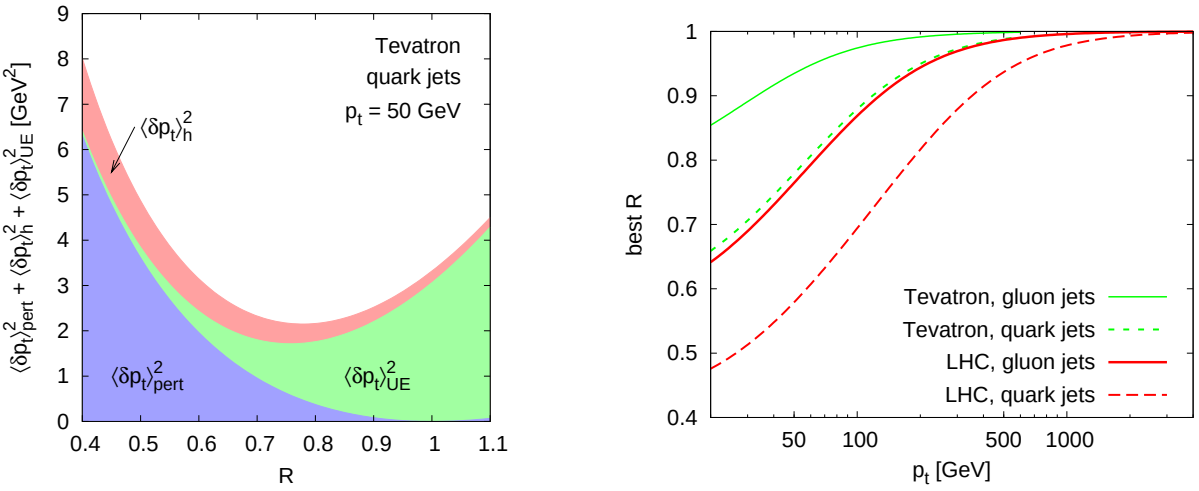

Figure 1: The average (squared) change in p_t of the leading jet as a function of the jet radius (left). The optimal radius given by the minimum of $\langle \delta p_t \rangle^2$ as a function of the jet p_t for quark and gluon jets at the Tevatron and at the LHC (right). Both plots are taken from Ref. [26].

Higgs decaying into a $b\bar{b}$ pair, where the candidate Higgs jet must contain at least two separated b-tagged subjets [28]. Once the candidate jet has been selected, the problem is how to clean it so that is contains as much as the Higgs decay products plus QCD radiation originated from them, and it is least contaminated by initial-state radiation or underlying event. This is the aim of the filtering procedure, which consists in reclustering the fat jet with a smaller radius $R_{\rm filt}$ and reconstructing the candidate Higgs using only the hardest $n_{\rm filt}$ subjets. The determination of the best $R_{\rm filt}$ and $n_{\rm filt}$ relies on the calculation of $\Sigma(\delta M)$, the fraction of events such that the difference between the Higgs mass and the jet mass is less than a given δM. Then one looks for the value of δM for which $\Sigma(\delta M) = f$, with f a given fraction of events, for instance 68%: clearly, the smaller δM, the better the mass resolution. The quantity $\Sigma(\delta M)$ is basically an event-shape fraction and, due to the fact that the Higgs is a colour singlet, can be computed with the theoretical tools developed for e^+e^- (non-global) event shapes. It is then possible to determine analytically the values of $R_{\rm filt}$ and $n_{\rm filt}$ that minimise δM (Fig. 2, left), and the dedicated study of Ref. [29] indicates as optimal values $n_{\rm filt} = 3$ and $R_{\rm filt} = \min\{R_{b\bar{b}}/2, 0.3\}$ (where $R_{b\bar{b}}$ is the usual η-ϕ distance between the two b-subjets). These values give a good resolution for the Higgs mass peak also after a full event simulation with parton shower Monte Carlo's (Fig. 2, right) [28].

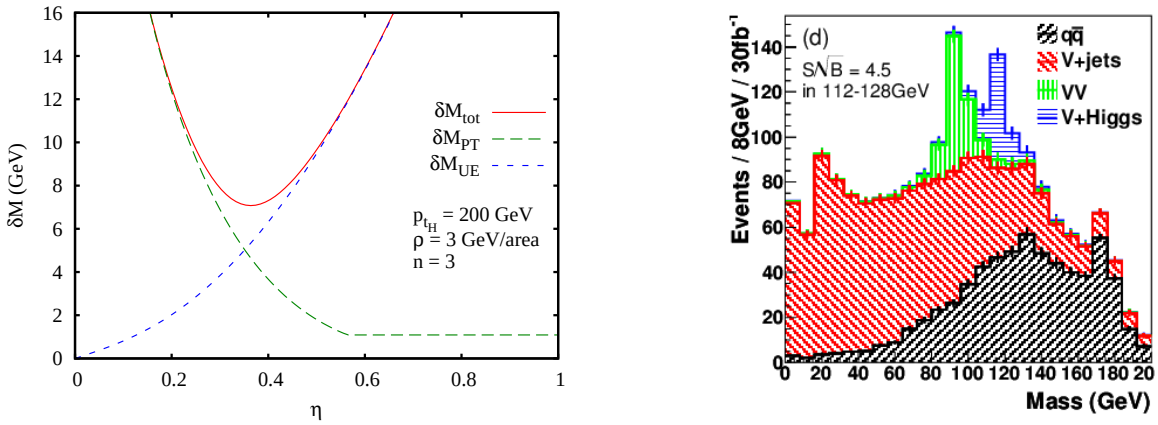

Figure 2: The width of the Higgs mass peak δM [29] for $n_{\rm filt} = 3$ as a function of $\eta = R_{\rm filt}/R$ (left), and the distribution in the invariant mass of the Higgs candidate jet corresponding to the selection cuts of Ref. [28] (right).

2.3 Colour connections and the "pull"

Many of the heavy objects we wish to observe at the LHC are colour singlets. This raises the question on whether we can distinguish jets originating from hadronic decays of colour singlets from pure QCD jets. Although there is no definitive answer to this question so far, hints might be gained by studying the QCD radiation pattern in the interjet region, which is expected to be determined by the colour flow of each event. Reconstruction of colour connections between jets was extensively studied at LEP, for instance by counting the number of hadrons in the interjet region in three-jet events. There one observed that the hadron multiplicity was different in QCD three-jet events rather than in $q\bar{q}\gamma$ events, and the observed difference could be simply accounted for by considering the colour connections between the hard emitting partons, the so-called string/drag effect [30, 31, 32, 33]. An analogous analysis for hadron colliders has been recently proposed [34]. It is based on the so-called "pull" vector of a jet, defined as

$$\vec{t} = \sum_{i \in \rm jet} \frac{p_{t,i}|\vec{r}_i|}{p_{t,jet}} \vec{r}_i, \qquad \vec{r}_i = (\Delta y_{i,\rm jet}, \Delta\phi_{i,\rm jet})\,. \tag{1}$$

The pull distribution "points" towards the jet to which the triggered jet is colour connected. For instance, following again Ref. [34], if one considers Higgs production in association with a Z boson, the distribution in the pull angle $\Delta\theta_t$ of the higher p_t is peaked around $\Delta\theta_t = 0$, corresponding to the "position" of the other jet, whilst that for the background $Zb\bar{b}$ is peaked around $\Delta\theta_t = \pm\pi$, corresponding to the beam (see Fig. 3 left).[2] Experimental studies in $t\bar{t}$ events at the Tevatron confirm this difference [35]. Indeed, the plot on the right-hand side of Fig. 3 shows the measured distribution in $\Delta\theta_t$ (labelled $\theta^{\rm rel}_{\rm pull}$ in Ref. [35]) for any of the

[2]Notice however that a definition of the pull vector as in eq. (1) raises a theoretical problem, since at tree level, when a jet consists of a single parton, the pull angle is undefined.

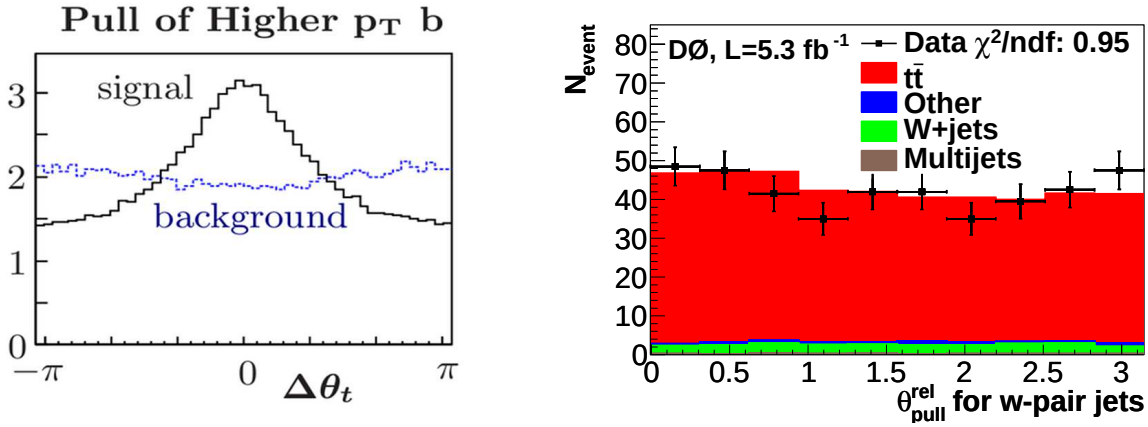

Figure 3: The distribution in the pull angle $\Delta\theta_t$ for the higher p_t b-jet in $Zb\bar{b}$ events, taken from Ref. [34] (left), and an analogous measurement performed at the Tevatron for a pair of jets coming from the decay of a W boson in $t\bar{t}$ events [35] (right).

two jets coming from the decay of a W boson. The distribution is peaked around $\theta^{\rm rel}_{\rm pull} = 0$, corresponding to the "position" of the other jet from W decay. Ref. [35] shows also plots for the pull angle distribution for the two colour disconnected b-jets from top decay, which is instead peaked towards larger values of $\theta^{\rm rel}_{\rm pull}$.

3 QCD predictions for multi-jet events

At LEP the majority of QCD precision studies has been performed for two-jet events. However, LEP produced many multi-jet events [36, 37, 38, 39], so that at present we have measurements that extend up to the inclusive six-jet rate [36]. However, these multi-jet events have not been fully exploited for QCD precision studies, the most notable exception being the three- and four-jet rates [40, 41, 42]. The main reason for this was the lack of fixed order calculations involving many legs in the final state. While at LEP one could restrict experimental analyses to low jet multiplicities, at the LHC many interesting phenomena, for instance production of top quarks or supersymmetric particles, involve a large number of jets in the final state. Notably, already now, there exists data for events Z or W boson production with six additional jets [43, 44, 45], whose e^+e^- counterpart is the eight-jet rate! It is therefore clear that one of the main problem theorists had to face in view of the LHC was how to perform precision calculations (especially NLO) for multi-leg processes. The traditional approach based on Feynman diagram looks prohibitive due to the large number of diagrams (e.g. tens of thousands for processes like $t\bar{t}b\bar{b}$, involving four QCD hard emitters in the final state) which have to be computed. Although, as the calculation of Ref. [46] shows, it is still possible to perform multi-leg NLO calculations using Feynman diagrams, in recent years a number of revolutionary ideas changed our way of looking at one-loop diagrams. The main observation, based on the pioneering work of Ref. [47],

is that the coefficients of the one-loop master integrals into which any one-loop amplitude can be decomposed are actually tree-level matrix elements [48, 49, 50]! This was the starting point of the so-called "unitarity-cut" techniques, through which it is possible to compute one-loop amplitudes as a whole instead of the individual Feynman diagrams (for a review see [51], and references therein). With these methods NLO predictions are nowadays produced at an industrial rate by various collaborations, such as BLACKHAT [52, 53], HELAC-NLO [54], ROCKET [55, 56], GOSAM [57]. In the meantime many methods have been developed to efficiently compute tree-level matrix elements, like MADGRAPH [58] or COMIX [59]. There are also programs, like ALPGEN [60] or SHERPA [61], that implement algorithms to coherently combine tree-level matrix elements to parton showers. Last but not least, in recent years new methods have been developed to match even NLO calculations to parton showers [62, 63], nowadays automated in the aMC@NLO [64] and POWHEG-BOX [65] frameworks.

Such enormous progress had consequences also for e^+e^- precision studies. For instance, for the first time it was possible to tackle the NLO calculation of the five-jet rate by crossing matrix elements used for Z plus three jets at NLO [66]. The resulting theoretical analysis, in particular the extraction of a value of $\alpha_s(M_Z)$, took also advantage of the matching between tree-level five-jet matrix elements and parton shower implemented in the SHERPA Monte Carlo. Indeed, only using SHERPA was it possible to obtain a reliable estimate of hadronisation corrections, and hence a precise measurement of $\alpha_s(M_Z)$ (see Fig. 4). The limit on the jet multiplicity is nowadays being pushed further and further, and at the moment there exist (leading colour) NLO calculations for e^+e^- up to seven jets [67]. It would be great to compare these predictions to LEP data, so as to have consistent extractions of $\alpha_s(M_Z)$ from all measured jet rates.

4 Outlook

The NLO revolution is just one example of the theoretical progress that has been triggered by LHC Physics in recent years. For processes like the production of colour singlets NNLO calculations are already available [68, 69, 70, 71, 72, 73] while considerable progress has been made towards NNLO predictions for top-antitop [74] or dijet production [75]. Given the complexity of two-loop calculations, many people have also tried to investigate whether the structure of QCD amplitudes could be deduced from general principles rather than obtained only through explicit calculations. This research stream involved on one hand the use of factorisation properties of gauge theories to arrive at a general formula for the infrared structure of gauge theories [76, 77]. On the other hand, also hard non singular contributions were investigated in theories with a high degree of symmetry, like $\mathcal{N} = 4$ Super Yang-Mills, hoping to be able to solve them at the quantum level (see for instance [78]). The latter studies have lead to the discovery of the simpler representation of multi-loop amplitudes in terms of mathematical objects called symbols [79]. The hope is to be able to associate to each amplitude its symbol content, so as to

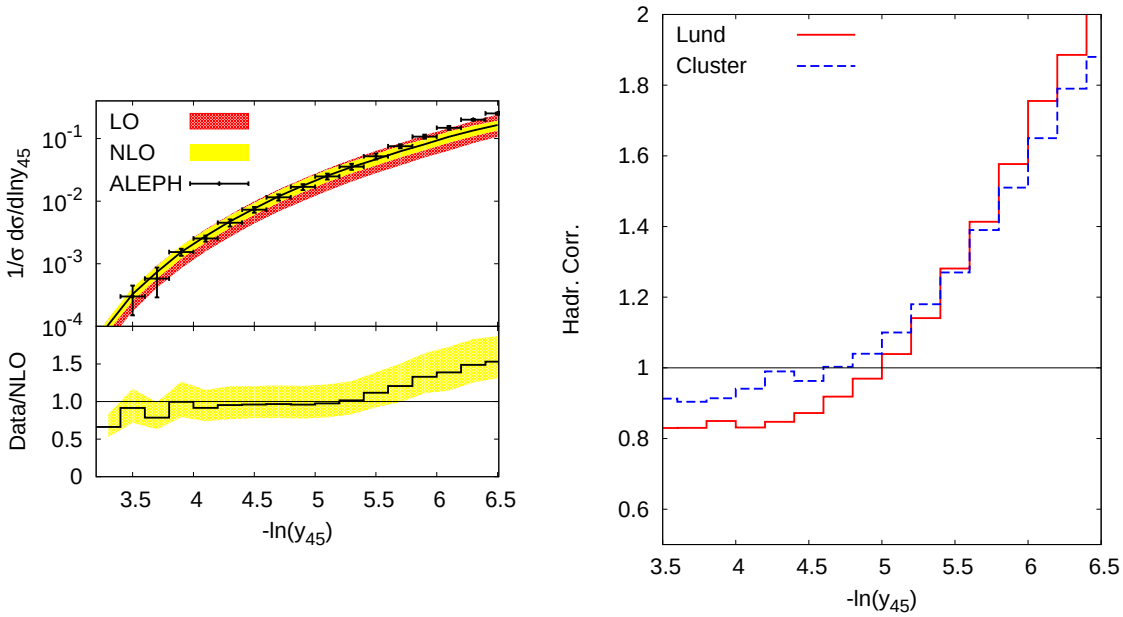

Figure 4: The NLO distribution in (log of) the 5-jet resolution y_{45} compared to ALEPH data (left), and the corresponding hadronisation corrections obtained with SHERPA (right).

avoid completely the explicit calculation of loop integrals.

Given the theoretical advances I have described so far, how can we imagine the state of the art of precision calculations at the start of the linear collider? Let us consider for instance the Higgsstrahlung process, the most widely used for Higgs searches at LEP, with both the Higgs and the recoiling vector boson decaying hadronically. The theoretical description of both signal and backgrounds (e.g. e^+e^- to four jets) will be very different from that of LEP days. Definitely higher order corrections, both QCD and electro-weak, will be available at NNLO, and probably we will know the all-order structure of the dominant virtual corrections. Sophisticated methods based on jet substructure will be able to discriminate the signal from the backgrounds. Experimental analyses will also take advantage of the fact that all parton shower event generators will be matched to NLO matrix elements.

Concerning precision Physics, for two-jet event shapes hadronisation corrections will be very small, so that, just using the already available NNLO+NNLL predictions, we could have a measurement of $\alpha_s(M_Z)$ at the permille accuracy. Jet rates had already very small hadronisation corrections at LEP, at LC they will have basically none. In this case we already have NNLO predictions for three-jet production, and probably we will have them for four-jet production as well. Unfortunately no resummation beyond NLL accuracy is available for jet rates so far. An improvement in this direction would probably allow for the most precise determination of $\alpha_s(M_Z)$ ever.

I would like to conclude with a couple of remarks on non-perturbative effects, which are in

fact the everlasting unknown in all collider experiments. The LC will not only be a precision machine, but also a means of investigation of those effects, especially in multi-jet events. For instance, when considering three-jet events, due to the extra radiation from a gluon, leading hadronisation corrections are expected to be roughly twice as large as in two-jet events. This feature, at LEP energies, made them too large to be allowed to neglect the contribution of subleading corrections, as was done for two-jet events. At the LC instead, non-perturbative corrections to three-jet event shapes like the D-parameter are of the same order of magnitude of the corresponding ones to two-jet event shapes at LEP. Therefore, more studies of the universality of the non-perturbative parameter α_0 could be performed, opening for the first time the possibility of making quantitative statements about hadronisation from a gluon in a multi-jet environment. Last but not least, there might be experimental high-luminosity setups for the LC which imply contamination of signal events from pile-up. We hope that the LHC will teach us how to model this effect better and better, so as to be able to properly deal with it before the start of the LC.

Acknowledgments

I am deeply grateful to the organisers of the workshop for the invitation and for the pleasant and stimulating atmosphere they were able to create. I also would like to thank Stephen Kluth, Gavin Salam and Giulia Zanderighi for helpful comments and suggestions during the preparation of my talk.

References

[1] G. Aad *et al.* [The ATLAS Collaboration], 0901.0512 [hep-ex].

[2] G. L. Bayatian *et al.* [CMS Collaboration], J. Phys. G **34** (2007) 995.

[3] A. Banfi, G. P. Salam and G. Zanderighi, JHEP **0503** (2005) 073 [hep-ph/0407286].

[4] M. Dasgupta and G. P. Salam, J. Phys. G **30** (2004) R143 [hep-ph/0312283].

[5] A. Gehrmann-De Ridder, T. Gehrmann, E. W. N. Glover and G. Heinrich, JHEP **0712** (2007) 094 [0711.4711 [hep-ph]].

[6] S. Weinzierl, JHEP **0906** (2009) 041 [0904.1077 [hep-ph]].

[7] T. Becher and M. D. Schwartz, JHEP **0807** (2008) 034 [0803.0342 [hep-ph]].

[8] Y. -T. Chien and M. D. Schwartz, JHEP **1008** (2010) 058 [1005.1644 [hep-ph]].

[9] P. F. Monni, T. Gehrmann and G. Luisoni, JHEP **1108** (2011) 010 [1105.4560 [hep-ph]].

[10] R. Abbate, M. Fickinger, A. H. Hoang, V. Mateu and I. W. Stewart, Phys. Rev. D **83** (2011) 074021 [1006.3080 [hep-ph]].

[11] Y. L. Dokshitzer, G. Marchesini and B. R. Webber, Nucl. Phys. B **469** (1996) 93 [hep-ph/9512336].

[12] G. P. Korchemsky and G. F. Sterman, Nucl. Phys. B **555** (1999) 335 [hep-ph/9902341].

[13] Y. L. Dokshitzer, A. Lucenti, G. Marchesini and G. P. Salam, JHEP **9805** (1998) 003 [hep-ph/9802381].

[14] J. C. Collins, D. E. Soper and G. F. Sterman, Nucl. Phys. B **250** (1985) 199.

[15] G. F. Sterman, Nucl. Phys. B **281** (1987) 310.

[16] T. Becher and M. Neubert, Eur. Phys. J. C **71** (2011) 1665 [1007.4005 [hep-ph]].

[17] V. Ahrens, T. Becher, M. Neubert and L. L. Yang, Eur. Phys. J. C **62** (2009) 333 [0809.4283 [hep-ph]].

[18] I. W. Stewart, F. J. Tackmann and W. J. Waalewijn, Phys. Rev. D **81** (2010) 094035 [0910.0467 [hep-ph]].

[19] M. Dasgupta and G. P. Salam, Phys. Lett. B **512** (2001) 323 [hep-ph/0104277].

[20] M. Dasgupta and G. P. Salam, JHEP **0203** (2002) 017 [hep-ph/0203009].

[21] A. Banfi, G. Marchesini and G. Smye, JHEP **0208** (2002) 006 [hep-ph/0206076].

[22] J. R. Forshaw, A. Kyrieleis and M. H. Seymour, JHEP **0608** (2006) 059 [hep-ph/0604094].

[23] S. Catani, D. de Florian and G. Rodrigo, 1112.4405 [hep-ph].

[24] A. Banfi, G. P. Salam and G. Zanderighi, JHEP **1006** (2010) 038 [1001.4082 [hep-ph]].

[25] S. Chatrchyan *et al.* [CMS Collaboration], Phys. Lett. B **702** (2011) 336 [1106.0647 [hep-ex]].

[26] M. Dasgupta, L. Magnea and G. P. Salam, JHEP **0802** (2008) 055 [0712.3014 [hep-ph]].

[27] A. Altheimer, S. Arora, L. Asquith, G. Brooijmans, J. Butterworth, M. Campanelli, B. Chapleau and A. E. Cholakian *et al.*, 1201.0008 [hep-ph], and references therein.

[28] J. M. Butterworth, A. R. Davison, M. Rubin and G. P. Salam, Phys. Rev. Lett. **100** (2008) 242001 [0802.2470 [hep-ph]].

[29] M. Rubin, JHEP **1005** (2010) 005 [1002.4557 [hep-ph]].

[30] W. Bartel *et al.* [JADE Collaboration], Phys. Lett. B **134** (1984) 275.

[31] H. Aihara *et al.* [TPC/Two Gamma Collaboration], Phys. Rev. Lett. **57** (1986) 945.

[32] P. Abreu *et al.* [DELPHI Collaboration], Z. Phys. C **70** (1996) 179.

[33] R. Akers *et al.* [OPAL Collaboration], Z. Phys. C **68** (1995) 531.

[34] J. Gallicchio and M. D. Schwartz, Phys. Rev. Lett. **105** (2010) 022001 [1001.5027 [hep-ph]].

[35] V. M. Abazov *et al.* [D0 Collaboration], Phys. Rev. D **83** (2011) 092002 [1101.0648 [hep-ex]].

[36] A. Heister *et al.* [ALEPH Collaboration], Eur. Phys. J. C **35** (2004) 457.

[37] J. Abdallah *et al.* [DELPHI Collaboration], Eur. Phys. J. C **29** (2003) 285 [hep-ex/0307048].

[38] P. Achard *et al.* [L3 Collaboration], Phys. Rept. **399** (2004) 71 [hep-ex/0406049].

[39] G. Abbiendi *et al.* [OPAL Collaboration], Eur. Phys. J. C **40** (2005) 287 [hep-ex/0503051].

[40] G. Dissertori, A. Gehrmann-De Ridder, T. Gehrmann, E. W. N. Glover, G. Heinrich and H. Stenzel, Phys. Rev. Lett. **104** (2010) 072002 [0910.4283 [hep-ph]].

[41] L. J. Dixon and A. Signer, Phys. Rev. D **56** (1997) 4031 [hep-ph/9706285].

[42] Z. Nagy and Z. Trocsanyi, Phys. Lett. B **634** (2006) 498 [hep-ph/0511328].

[43] G. Aad *et al.* [ATLAS Collaboration], 1201.1276 [hep-ex].

[44] G. Aad *et al.* [ATLAS Collaboration], 1111.2690 [hep-ex].

[45] S. Chatrchyan *et al.* [CMS Collaboration], 1110.3226 [hep-ex].

[46] A. Denner, S. Dittmaier, S. Kallweit and S. Pozzorini, Phys. Rev. Lett. **106** (2011) 052001 [1012.3975 [hep-ph]].

[47] Z. Bern, L. J. Dixon, D. C. Dunbar and D. A. Kosower, Nucl. Phys. B **425** (1994) 217 [hep-ph/9403226].

[48] R. Britto, F. Cachazo and B. Feng, Nucl. Phys. B **725** (2005) 275 [hep-th/0412103].

[49] G. Ossola, C. G. Papadopoulos and R. Pittau, Nucl. Phys. B **763** (2007) 147 [hep-ph/0609007].

[50] W. T. Giele, Z. Kunszt and K. Melnikov, JHEP **0804** (2008) 049 [0801.2237 [hep-ph]].

[51] R. K. Ellis, Z. Kunszt, K. Melnikov and G. Zanderighi, 1105.4319 [hep-ph].

[52] H. Ita, Z. Bern, L. J. Dixon, F. Febres Cordero, D. A. Kosower and D. Maitre, Phys. Rev. D **85** (2012) 031501 [1108.2229 [hep-ph]].

[53] Z. Bern, G. Diana, L. J. Dixon, F. Febres Cordero, S. Hoeche, D. A. Kosower, H. Ita and D. Maitre *et al.*, 1112.3940 [hep-ph].

[54] G. Bevilacqua, M. Czakon, M. V. Garzelli, A. van Hameren, A. Kardos, C. G. Papadopoulos, R. Pittau and M. Worek, 1110.1499 [hep-ph].

[55] T. Melia, K. Melnikov, R. Rontsch and G. Zanderighi, JHEP **1012** (2010) 053 [1007.5313 [hep-ph]].

[56] R. K. Ellis, K. Melnikov and G. Zanderighi, Phys. Rev. D **80** (2009) 094002 [0906.1445 [hep-ph]].

[57] G. Cullen, N. Greiner, G. Heinrich, G. Luisoni, P. Mastrolia, G. Ossola, T. Reiter and F. Tramontano, 1111.6534 [hep-ph].

[58] J. Alwall, M. Herquet, F. Maltoni, O. Mattelaer and T. Stelzer, JHEP **1106** (2011) 128 [1106.0522 [hep-ph]].

[59] T. Gleisberg and S. Hoeche, JHEP **0812** (2008) 039 [0808.3674 [hep-ph]].

[60] M. L. Mangano, M. Moretti, F. Piccinini, R. Pittau and A. D. Polosa, JHEP **0307** (2003) 001 [hep-ph/0206293].

[61] T. Gleisberg, S. .Hoeche, F. Krauss, M. Schonherr, S. Schumann, F. Siegert and J. Winter, JHEP **0902** (2009) 007 [0811.4622 [hep-ph]].

[62] S. Frixione and B. R. Webber, JHEP **0206** (2002) 029 [hep-ph/0204244].

[63] P. Nason, JHEP **0411** (2004) 040 [hep-ph/0409146].

[64] R. Frederix, S. Frixione, V. Hirschi, F. Maltoni, R. Pittau and P. Torrielli, 1110.4738 [hep-ph].

[65] S. Alioli, P. Nason, C. Oleari and E. Re, JHEP **1006** (2010) 043 [1002.2581 [hep-ph]].

[66] R. Frederix, S. Frixione, K. Melnikov and G. Zanderighi, JHEP **1011** (2010) 050 [1008.5313 [hep-ph]].

[67] S. Becker, D. Goetz, C. Reuschle, C. Schwan and S. Weinzierl, Phys. Rev. Lett. **108** (2012) 032005 [1111.1733 [hep-ph]].

[68] S. Catani, L. Cieri, D. de Florian, G. Ferrera and M. Grazzini, 1110.2375 [hep-ph].

[69] G. Ferrera, M. Grazzini and F. Tramontano, Phys. Rev. Lett. **107** (2011) 152003 [1107.1164 [hep-ph]].

[70] S. Catani, L. Cieri, G. Ferrera, D. de Florian and M. Grazzini, Phys. Rev. Lett. **103** (2009) 082001 [0903.2120 [hep-ph]].

[71] S. Catani and M. Grazzini, Phys. Rev. Lett. **98** (2007) 222002 [hep-ph/0703012].

[72] C. Anastasiou, K. Melnikov and F. Petriello, Phys. Rev. Lett. **93** (2004) 262002 [hep-ph/0409088].

[73] C. Anastasiou, L. J. Dixon, K. Melnikov and F. Petriello, Phys. Rev. Lett. **91** (2003) 182002 [hep-ph/0306192].

[74] M. Czakon, Nucl. Phys. B **849** (2011) 250 [1101.0642 [hep-ph]].

[75] A. Gehrmann-De Ridder, E. W. N. Glover and J. Pires, 1112.3613 [hep-ph], and references therein.

[76] E. Gardi and L. Magnea, JHEP **0903** (2009) 079 [0901.1091 [hep-ph]].

[77] T. Becher and M. Neubert, JHEP **0906** (2009) 081 [0903.1126 [hep-ph]].

[78] N. Beisert, C. Ahn, L. F. Alday, Z. Bajnok, J. M. Drummond, L. Freyhult, N. Gromov and R. A. Janik *et al.*, Lett. Math. Phys. **99** (2012) 3 [1012.3982 [hep-th]], and references therein.

[79] A. B. Goncharov, M. Spradlin, C. Vergu and A. Volovich, Phys. Rev. Lett. **105** (2010) 151605 [1006.5703 [hep-th]].

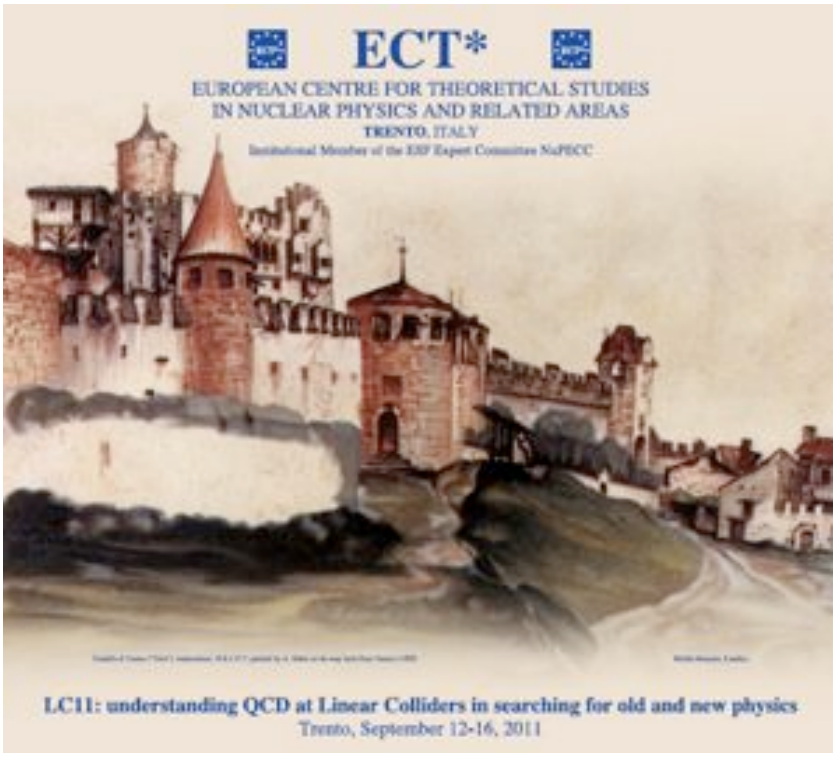

Castello di Trento painted by A. Dürer on his way back from Venice (1495).

8.2 S. Kluth - QCD tests from GeV to TeV scale

QCD Tests from GeV to TeV scales

Stefan Kluth
Max-Planck-Institut für Physik, Föhringer Ring 6, 80805 Munich, Germany
skluth@mpp.mpg.de

Abstract We report on experimental tests of QCD from low to high energy scales.

1 Introduction

The theory of strong interactions, Quantum Chromo Dynamics (QCD) [1, 2, 3] is well tested at colliders from low, i.e. GeV, to high, i.e. TeV, energy scales.

Tests of hard QCD processes can be broadly categorised into tests involving (almost) all final state particles, or tests with more exclusively selected final state particles. Examples of the first category are event shape observables using all particles, or all particles in a event hemisphere, while an example for more exclusive observables are jet clustering algorithms where e.g. only particles in the vicinity of an energetic jet are considered.

Tests of soft QCD processes are concerned with improving our understanding of the transition between the partons (quarks and gluons) of the theory and the observed final state hadrons and leptons. For this so-called hadronisation process no fundamental theory exists. Instead there are models of hadronisation implemented in Monte Carlo generator programs or analytically. The success of these models and the estimation of their uncertainties is a crucial ingredient in essentially all quantitative tests of QCD.

This short review will first discuss event shape observables, then jet based observables and finally tests of soft QCD in all hard production processes available at colliders: e^+e^- collisions, ep collisions, $p\bar{p}$ and pp collisions. We present illustrative examples of important studies while trying to give more complete coverage in the references, and apologise in advance for the huge amount of work left out, among them jet substructure studies [4] or reviews and average of measurements of α_S [5].

2 Event shapes

Event shape observables have been studied intensively in hadron production in e^+e^- collisions, see e.g. [6, 7]. Data set sizes from past e^+e^- experiments range from O(100) to O(10000) at

PETRA [1] energies 14 to 44 GeV and the LEP 2 energies 130 to 209 GeV to O(10^6) events collected by the LEP experiments near the Z^0 peak. Background processes to hadron production via a virtual Z boson or photon off the Z^0 peak region are two photon interactions with hadronic final states, hard initial state photon radiation from the incoming beam electrons, and production of τ lepton pairs decaying to hadrons. At the high LEP 2 energies production of W^+W^- pairs with hadronic decays are an additional background source. Below the W^+W^- production threshold of $\sqrt{s} = 161$ GeV backgrounds and especially near the Z^0 peak background processes are suppressed to negligible levels after event selections while above residual backgrounds of about 10% have to be subtracted [5].

A typical event shape observable is the thrust [8, 9] defined by

$$T = \max_{\vec{n}} \frac{\sum_i \vec{p}_i \cdot \vec{n}}{\sum_i |\vec{p}_i|} \tag{1}$$

where the $\vec{p}_i$ are the particle momenta and $\vec{n}$ is a normal vector in the direction of the thrust axis after the maximum has been found. Many other definitions of event shape observables exist, see e.g. [10]. For the quantity $1 - T$ the usual behaviour of event shape observables to be small for pencil-like collimated 2-jet events and to grow larger for events with more jet activity is found.

The QCD prediction for the distribution of a generic event shape observable y as a function of the hard scale Q is

$$\frac{1}{\sigma_0}\frac{d\sigma}{dy}(Q) = \frac{dA}{dy}\hat{\alpha}_S(Q) + \frac{dB}{dy}\hat{\alpha}_S^2(Q) + \frac{dC}{dy}\hat{\alpha}_S^3(Q) \tag{2}$$

where $\hat{\alpha}_S = \alpha_S/(2\pi)$. The coefficient functions dA/dy etc. are obtained by integrating the QCD matrix elements in leading order (LO), next-to-leading order (NLO) or next-to-next-leading order (NNLO) calculations over the phase space contours defined by the observable y. The availability of NNLO results [11, 12] and of matching to resummed next-to-leading log approximation (NLLA) calculations [13] led to several new analyses of the LEP and PETRA/JADE event shape data [14, 15, 16, 17].

Figure 1 (left) shows QCD predictions for $1 - T$ compared with ALEPH data corrected for experimental effects. The higher order predictions come closer to the data and have smaller theoretical uncertainties. However, even the NNLO prediction does not match the data since hadronisation corrections are not part of the prediction.

Hadronisation corrections in event shape analyses are usually evaluated using the Monte Carlo generators PYTHIA, HERWIG or ARIADNE by comparing event shape distributions from final states after the parton shower has stopped (parton level) and after hadronisation and decays (hadron or particle level). Since the Monte Carlo programs implement QCD processes

[1] Positron-Elektron-Tandem-Ring-Anlage at DESY from 1979 to 1986

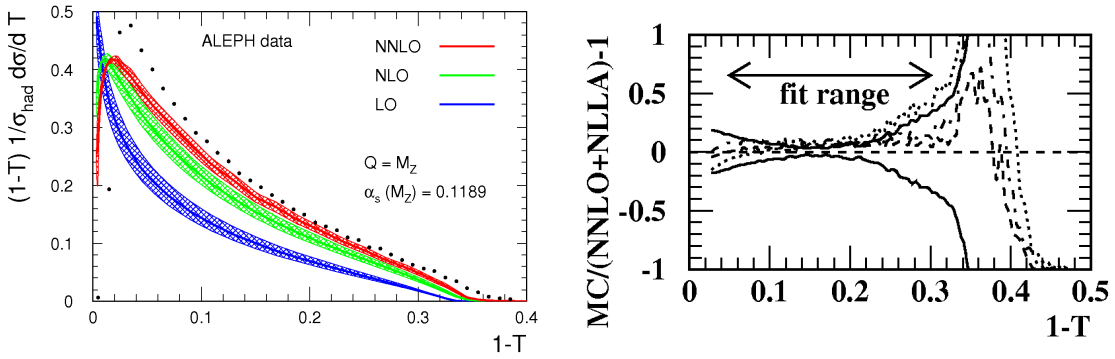

Figure 1: The figure on the left [11] shows a comparison of QCD predictions for $1-T$ up to NNLO with ALEPH data at $\sqrt{s} = m_{Z^0}$. The bands indicate the variation of the prediction for a change in the renormalisation scale by a factor of 0.5 or 2.0. The figure on the right from OPAL [16] shows the ratios of Monte Carlo parton level predictions (PYTHIA 6.1 dashed, HERWIG 6.2 dotted, ARIADNE 4.11 dash-dotted) to NNLO+NLLA QCD predictions for $1-T$ at $\sqrt{s} = m_{Z^0}$. The solid lines show the maximum difference of any pair of Monte Carlo prediction.

in LO only matched to parton showers in the leading-log (LL) approximation the hadronisation corrections could be inappropriate for NNLO calculations. This problem is studied by OPAL in figure 1 (right) showing the ratios of Monte Carlo parton level predictions to NNLO+NLLA predictions at $\sqrt{s} = m_{Z^0}$, and as solid lines the maximum difference of any pair of Monte Carlo predictions [16]. One finds that the differences between the Monte Carlo predictions are of similar size compared to the difference between the NNLO+NLLA QCD prediction and the Monte Carlo predictions. The systematic uncertainties of hadronisation corrections evaluated as the difference between the Monte Carlo generators thus also cover the uncertainty due to a mismatch between Monte Carlo parton level and the QCD prediction.

Figure 2 (left) shows a comparison of measurements of $\alpha_S(m_{Z^0})$ from OPAL event shape data [16]. The results from NLO, NLO+NLLA, NNLO and NNLO+NLLA are consistent and show how adding higher order corrections generally decreases total uncertainties. The total errors of the NNLO+NLLA result $\alpha_S(m_{Z^0}) = 0.1189 \pm 0.0008(\text{stat.}) \pm 0.0016(\text{exp.}) \pm 0.0010(\text{had.}) \pm 0.0036(\text{theo.})$ are not smaller than those of the NNLO results, because the NLLA involves running of α_S at leading order causing larger renormalisation scale uncertainties. Figure 2 (right) shows results from JADE [15] and OPAL as function of $\sqrt{s}$. The running of α_S is clearly demonstrated using e^+e^- event shape data alone. The relative precision of the OPAL result shown on the figure is 3.4% and thus among the best measurements available [5].

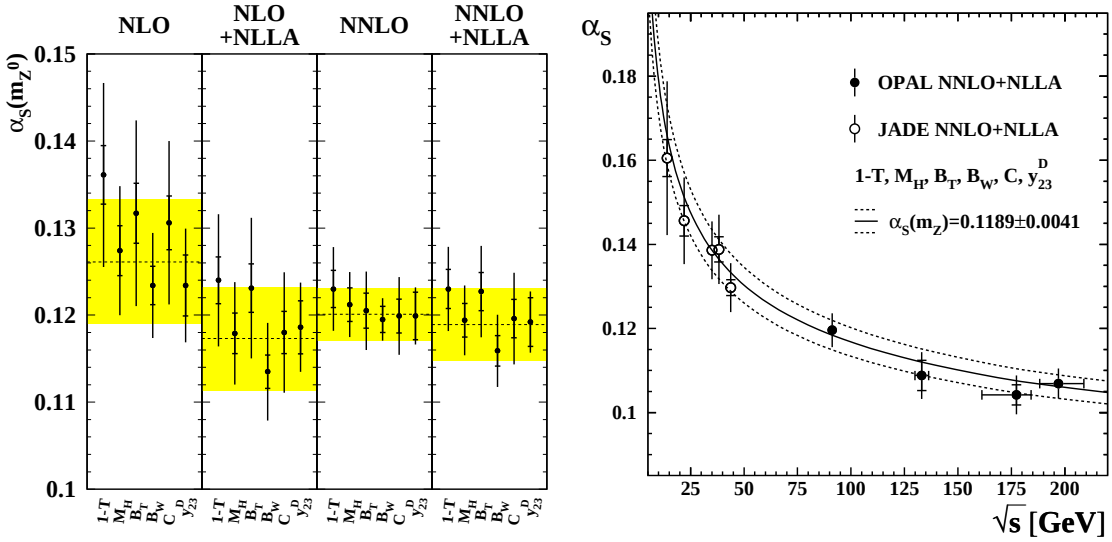

Figure 2: The figure on the left shows a comparison of different QCD predictions for the extraction of $\alpha_S(m_{Z^0})$ from OPAL event shape data. The inner error bars show combined statistical and experimental errors while the outer error bars show hadronisation and theory uncertainties. The figure on the right presents results for $\alpha_S(m_{Z^0})$ in NLLO+NLLA from OPAL and JADE as a function of $\sqrt{s}$ and compared with the result of the OPAL measurement [16].

Different approaches to the problem of modelling hadronisation have been tested intensively with event shape data, since these provide a way to separate soft and hard QCD effects due to their different scaling properties. Hard QCD effects scale like $1/\log(Q)$ via the running of the strong coupling while for most event shapes soft QCD effects scale like $1/Q$. Simultaneous analysis of event shapes at various $\sqrt{s}$ thus allows to disentangle the two effects. The dispersive or DMW model for power corrections [18] assumes that the strong coupling stays finite in the region around the Landau pole and introduces a new parameter α_0 corresponding to the integral over the coupling up to a matching scale μ_I. Analysis of renormalon ambiguities reveals the structure of power corrections for a range of event shapes, see e.g. [6, 7, 10] for reviews. The latest analysis [19] of this kind performed a global fit of the DMW model combined with NNLO+NLLA QCD to $1-T$ distributions for $14 < \sqrt{s} < 200$ GeV. The result $\alpha_S(m_{Z^0}) = 0.1164 \pm 0.0027$ is consistent and its relative error of 2.3% is smaller than e.g. the error from the OPAL analysis. The value of $\alpha_S(m_{Z^0})$ is found to be lower by about 0.003 compared with Monte Carlo based analyses of $1-T$ data.

Analyses of moments of event shape distributions have also been used to study power

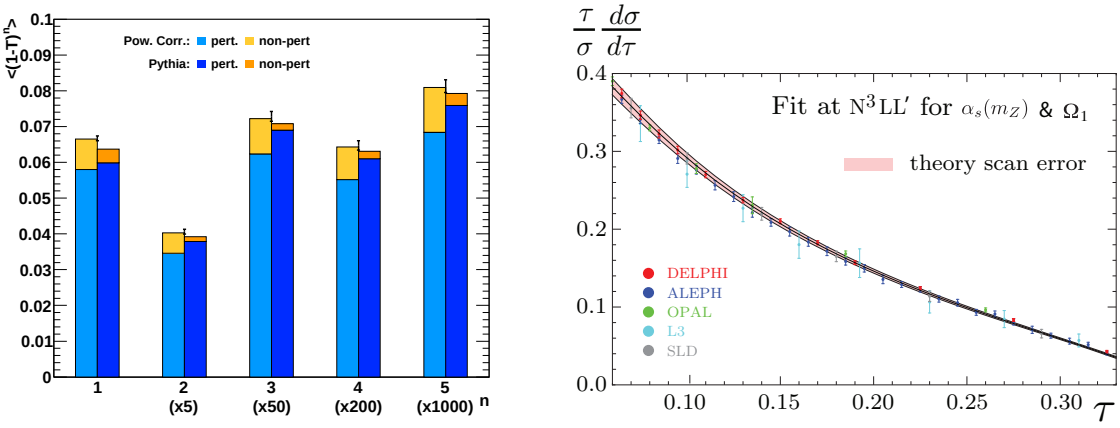

Figure 3: The figure on the left [20] shows contributions of perturbative and non-perturbative QCD to fits of the first five moments of $1-T$ for Monte Carlo and power correction based non-perturbative models. The figure on the right [21] shows data for $1-T=\tau$ together with the result of a fit to the data.

corrections [22, 20]. In these studies NLO or NNLO QCD predictions are combined with power corrections in the DMW model. Figure 3 (left) [20] compares the contributions of NNLO hard (perturbative) QCD and soft (non-perturbative) QCD on fits of the first five moments of $1-T$ in power correction and Monte Carlo based fits. In all cases fits with Monte Carlo hadronisation corrections have a larger perturbative and smaller non-perturbative part compared with the power correction results. Therefore values of $\alpha_S(m_{Z^0})$ are larger with Monte Carlo based analysis compared with power correction based analyses. The difference in $\alpha_S(m_{Z^0})$ is again about 0.003 for the mean value (first moment) of the $1-T$ distribution.

The subleading logarithmic contributions to the QCD prediction for the $1-T$ distribution have been calculated recently [21, 23]. In [21] this calculation was combined with a so-called shape function model for the soft QCD effects and a global fit of $1-T$ data was made. The result is a measurement $\alpha_S(m_{Z^0}) = 0.1135 \pm 0.0002(\text{exp.}) \pm 0.0005(\text{had.}) \pm 0.0009(\text{theo.})$ with a relative error of 1%. The result of the fit at $\sqrt{s} = m_{Z^0}$ is shown in figure 3 (right) [21]. The fitted prediction describes the $1-T=\tau$ data well over the whole distribution.

Event shape observables have also been studied in deep inelastic ep neutral current collisions by the HERA experiments [24, 25]. Their definition is based on the so-called Breit frame given by $E_{(Z^0/\gamma)^*} = 0$, where the scattering is head-on and elastic. Hemispheres defined by a plane orthogonal to the virtual $(Z^0/\gamma)^*$ direction separate the scattered proton constituent (H_γ) and

the proton remnant. As an example the two DIS thrust variants are then defined as

$$T = \frac{\sum_{i \in H_\gamma} |\vec{p}_i| \cdot \vec{n}}{\sum_{i \in H_\gamma} |\vec{p}_i|} \tag{3}$$

where $\vec{n} = \vec{n}_\gamma$ or $\vec{n} = \vec{n}_T$ after maximisation [24]. The H1 DIS selection collects events with $14 < Q < 200$ GeV and the data are analysed in bins of Q with $\langle Q \rangle = 15, 18, 24, 37, 58, 81, 116$ GeV. The H1 data are shown in figure 4 (left) as $1 - T = \tau$ and compared with fitted NLO+NLLA QCD calculations combined with the DMW power correction model for hadronisation effects. The fits yield measurements of α_S consistent with the running of the strong coupling. The final averaged result using several event shapes is $\alpha_S(m_{Z^0}) = 0.1198 \pm 0.0013(\text{exp.}) \pm 0.0050(\text{theo.})$ where the theory error contains hadronisation and parton density function (pdf) uncertainties.

The first study of event shape observables in pp collisions was shown by CMS [26]. The definition of the event shape observables follows [27, 28]. The event selection requires after jet finding with the anti-k_t algorithm [29] with $R = 0.5$ at least two jets with transverse momentum $p_t > 30$ GeV and pseudorapidity $|\eta| < 1.3$. Then for all selected jets within $|\eta| < 1.3$ the central transverse thrust is calculated as

$$\tau_{\perp,C} = 1 - \min_{\vec{n}} \frac{\sum_{i \in jets} |\vec{p}_{t,i} \cdot \vec{n}|}{\sum_{i \in jets} p_{t,i}} \tag{4}$$

This quantity behaves in a similar way to e^+e^- or ep event shapes: $\tau_{\perp,C} \ll 1$ for dijet events while $\tau_{\perp,C}$ grows with increasing jet multiplicity,

Figure 4 (right) [26] shows the CMS data for the distribution of $\log \tau_{\perp,C}$ from the sample with $125 < p_t < 200$ GeV for the p_t of the leading jet. The data are compared with predictions by various Monte Carlo generators. The generators PYTHIA6, PYTHIA8 and HERWIG++ describe the data reasonably well while the predictions by MadGraph or Alpgen combined with PYTHIA6 do not give a good description. This shows that hadron collider event shapes are sensitive to differences between generators which makes them potentially useful for generator tuning.

3 Jets

The clustering of particles in hadronic final states of e^+e^-, ep or pp ($p\bar{p}$) collisions into jets is a robust and intuitive way of analysing hadronic final states. In e^+e^- collisions many variants of iterative clustering algorithms have been developed, see e.g. [7, 30]. A popular example is the so-called Durham algorithm [31], where for each pair of particles i and j the distance metric

$$y_{ij} = \frac{2 \min(E_i, E_j)^2}{s} \tag{5}$$

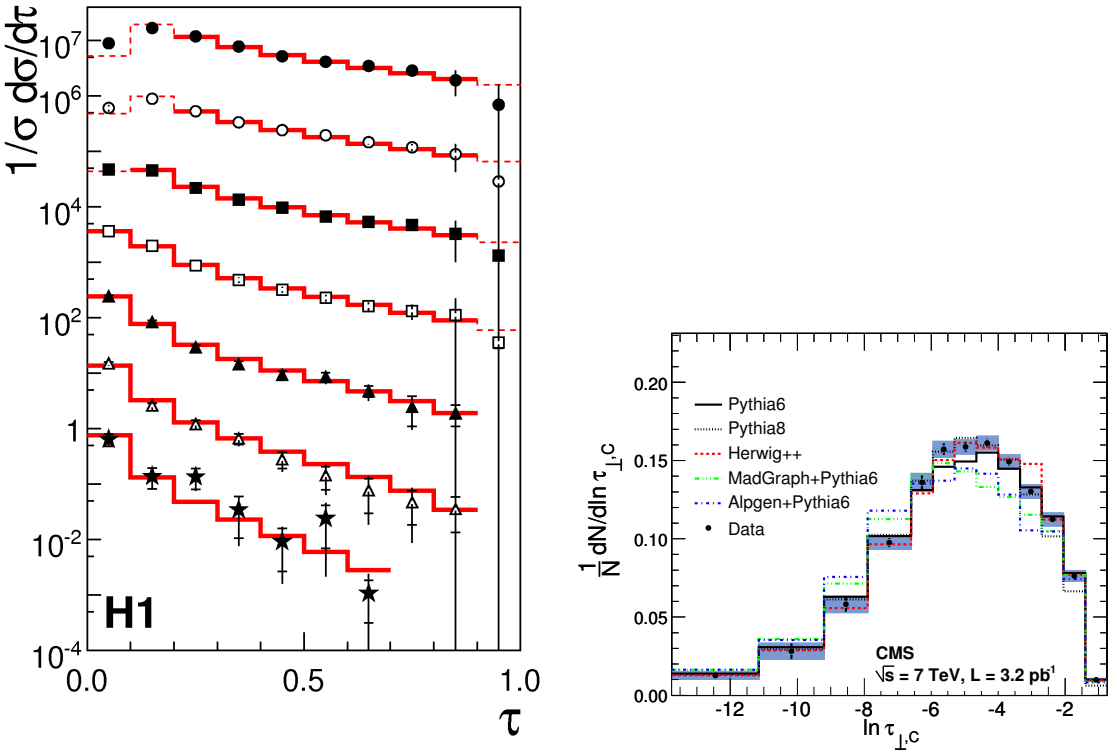

Figure 4: The figure on the left [24] shows data for the DIS thrust $1 - T = \tau$ measured by H1. The data are scaled such that from top to bottom data for $\langle Q \rangle = 15, 18, 24, 37, 58, 81, 116$ GeV are shown. The histograms give the result of fits (solid) and extrapolations (dotted) of NLO+NLLA QCD combined with power corrections to the data. The figure on the right [26] shows the distribution of central transverse thrust $\tau_{\perp,C}$ in pp collisions measured by CMS for $125 < p_{t,jet} < 200$ GeV. The lines show QCD predictions as indicated on the figure.

is calculated. The pair with the smallest y_{ij} is combined by adding their 4-vectors $p_{ij} = p_i + p_j$, the particles i and j are removed from the set of particles and their combination is added to the set. This procedure is repeated until a given number of entries called jets is left in the set, or the $y_{ij} > y_{\rm cut}$ for all i, j. For the Durham algorithm fixed order as well as resummed calculations are possible. Experimental and hadronisation corrections are found to be small compared with other algorithms.

Figure 5 (left) shows data from ALEPH [32] for n-jet ($n = 1, \ldots, 5$) fractions measured with the Durham algorithm at $\sqrt{s} = 206$ GeV. The data are compared with predictions by

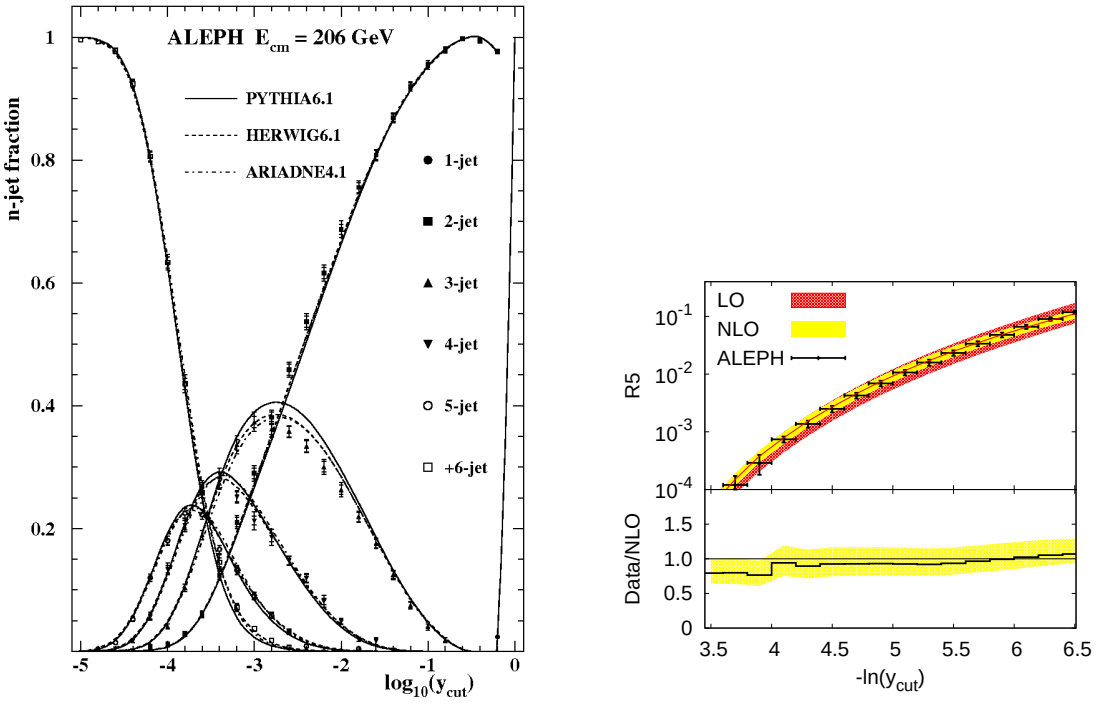

Figure 5: The figure on the left [32] shows data from ALEPH for the $1,\ldots,5$-jet rates and the inclusive 6-jet rate. The data are compared with predictions by Monte Carlo generators as indicated on the figure. The figure on the right [33] presents the result of a fit of the NLO QCD prediction for the 5-jet rate to the ALEPH data at $\sqrt{s} = m_{Z^0}$. The bands show the fitted predictions at LO and NLO combined with hadronisation corrections with theoretical uncertainties.

Monte Carlo generators which describe the data reasonably well. The ALEPH data for the 3-jet rate have been used in [34] to extract a precise measurement of $\alpha_S(m_{Z^0})$ with NNLO QCD predictions [35, 36]. The result from comparing the prediction to a single point $y_{\rm cut} = 0.02$ is $\alpha_S(m_{Z^0}) = 0.1175 \pm 0.0004(\text{stat.}) \pm 0.0019(\text{exp.}) \pm 0.0006(\text{had.}) \pm 0.0014(\text{theo.})$ with a total relative error of 2%. The experimental errors are larger than the combined hadronisation and theory uncertainties.

The 4-jet jet fractions with the Durham algorithm can be predicted in NLO+NLLA QCD [37, 38] and have been used to measure the strong coupling with PETRA/JADE and LEP data [39, 40, 41]. The result from OPAL combines measurements of α_S from $\sqrt{s} = m_{Z^0}$ to 197 GeV giving $\alpha_S(m_{Z^0}) = 0.1182 \pm 0.0003(\text{stat.}) \pm 0.0015(\text{exp.}) \pm 0.0011(\text{had.}) \pm 0.0018(\text{theo.})$ with a

total relative error 2%.

Recent advances in automation of NLO corrections made the calculation of processes with high multiplicity final states possible. The NLO calculation for the 5-jet fraction with the Durham algorithm in e^+e^- annihilation was reported in [33]. The extraction of $\alpha_S(m_{Z^0})$ depends on using a model for hadronisation effects. The analysis [33] compared traditional LO combined with LL parton shower Monte Carlo programs and the more recent treelevel multileg combined with LL parton shower Monte Carlo Program SHERPA [42]. It is found that for the 5-jet rate the predictions for the hadronisation corrections differ by about a factor of two between the different classes of Monte Carlo generators. Only with SHERPA based corrections are the results for $\alpha_S(m_{Z^0})$ from the analysis of ALEPH 5-jet rate data consistent with other results and recent world average values. The final result is $\alpha_S(m_{Z^0}) = 0.1156 \pm 0.0038$ combining values from all ALEPH data sets.

In neutral current ep DIS jets have been studied mostly using the longitudinally boost invariant formulation of the Durham algorithm [43], for a review see e.g. [44]. This algorithm is applied to final states in the Breit frame and generally clusters the proton remnant into the so-called beam jet and the final state from the scattered proton constituent into further jets. The experimental analysis [45] defines inclusive jet, 2-jet and 3-jet cross sections, where at least one, two or three jets are present in the event after the neutral current DIS event selection. The cross sections are measured as functions of four-momentum transfer Q^2 or p_t of the leading jet. The jets are clustered with radius $R = 1$, and have to pass $E_t > 5$ GeV in the Breit frame and $-1 < \eta < 2.5$ for pseudorapidity η. The jet cross sections are compared with NLO QCD predictions combined with hadronisation corrections using Monte Carlo generators. The combined measurement at $5 < Q^2 < 100$ GeV^2 is $\alpha_S(m_{Z^0}) = 0.1160 \pm 0.0014(\text{exp.}) \pm 0.0085(\text{theo.}) \pm 0.0016(\text{pdf})$. The analysis of measurements of α_S over the range of Q^2 values confirms the running of α_S with DIS jets data only. The results for α_S are shown in figure 6 (left) [45] as function of the scale $\mu_R = \sqrt{(Q^2 + p_t^2)/2}$ of the DIS.

The ZEUS collaboration has made in [46] a direct comparison of the longitudinally boost invariant Durham algorithm (k_t) with two new algorithms originally developed for pp collisions at LHC, namely the anti-k_t algorithm [29] and the SIScone algorithm [47]. In the neutral current ep DIS sample inclusive jet cross sections using the three algorithms are measured as a function of the momentum transfer Q^2 of the scattering. The results are shown in figure 6 (right). The jet requirements are shown on the figure. The data are compared with NLO QCD predictions combined with hadronisation corrections and a correction for Z^0 exchange. The three jet clustering algorithms show similar behaviour and all are well described by the NLO QCD predictions. The hadronisation corrections are also of similar size. Extracted values of the strong coupling from fits to the cross section data are $\alpha_S(m_{Z^0}) = 0.1207 \pm 0.0014(\text{stat.}) \pm 0.0033(\text{exp.}) \pm 0.0022(\text{theo.})$ (k_t), $\alpha_S(m_{Z^0}) = 0.1188 \pm 0.0014(\text{stat.}) \pm 0.0033(\text{exp.}) \pm 0.0022(\text{theo.})$ (anti-k_t) and $\alpha_S(m_{Z^0}) = 0.1186 \pm 0.0013(\text{stat.}) \pm 0.0033(\text{exp.}) \pm 0.0025(\text{theo.})$ (SIScone). The

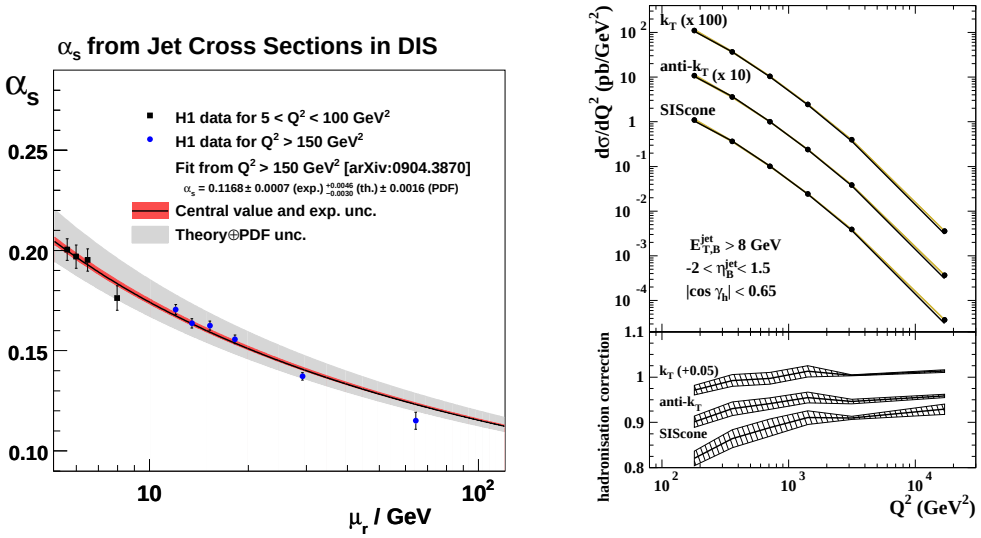

Figure 6: The figure on the left [45] shows measurements of α_S from fits to the inclusive, 2- and 3-jet cross sections in bins of Q^2 as function of $\mu_r = \sqrt{(Q^2 + p_t^2)/2}$. The bands present the prediction for the running of α_S as explained on the figure. The figure on the right [46] shows the inclusive jet cross section data measured by ZEUS using the k_t, anti-k_t and SIScone algorithm as functions Q^2. The data are compared with NLO QCD calculations (lines) corrected for effects of hadronisation and Z^0 exchange. The bands in the lower part show the hadronisation corrections with uncertainties for each jet clustering algorithm.

differences between the results are consistent with the theory uncertainty. This important cross check justifies the procedures used to evaluate the theory uncertainty.

Jets at the highest energies are now produced in pp collisions at the LHC. A recent survey of hard processes at LHC is [48]. The inclusive jet cross section with anti-k_t jets with rapidity satisfying $|y| < 2.8$ was measured by ATLAS [49] for $60 < p_t < 600$ GeV to and compared to NLO QCD calculations combined with hadronisation corrections. Within the errors of the data the QCD predictions describe the data over five orders of magnitude of the cross section. A similar measurement from CMS is [50].

Figure 7 (left) shows the angular correlation $\chi = e^{|y_1 - y_2|}$ measured by ATLAS [51] for dijet events with large invariant masses of the dijet system with jet rapidities y_1 and y_2. The leading and next-to-leading jet fulfil $p_{t,1} > 60$ GeV, $p_{t,2} > 30$ GeV and for their pseodorapidities $|\eta| < 2.8$. The data are compared successfully within the errors with NLO QCD predictions (bands). An alternative model where an additional contact interaction term with scale Λ is

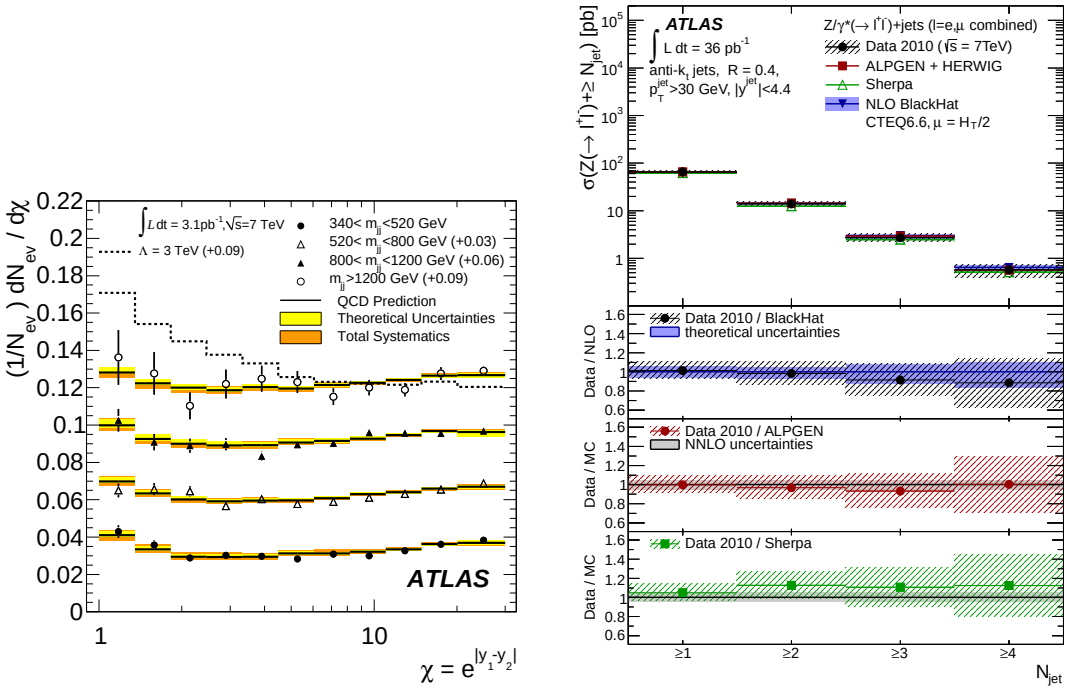

Figure 7: The figure on the left [51] shows the dijet angular correlation in bins of dijet invariant mass. The bands give the QCD prediction with uncertainties as indicated on the figure. The dashed line shows the prediction of QCD with an additional contact interaction term at scale Λ. The data points and bands are separated vertically for clarity. The figure on the right [52] shows the ATLAS measurement of Z^0 production in association with jets as indicated on the figure. The data are compared with NLO QCD and multileg treelevel Monte Carlo predictions.

added to the QCD Lagrangian is shown by the dashed line. This model is inconsistent with the data ruling out quark compositeness up to this scale. The analogous measurement from CMS is [53].

The measurement of the cross section for production of a Z^0 boson in association with jets in pp collisions is another important test of QCD, since the Z^0 with decays into lepton pairs allows efficient triggering and event selection and since NLO QCD predictions are available for jet multiplicities of up to four. These predictions are related by crossing to calculations for high jet multiplicity final states in e^+e^- annihilation, e.g. [33, 54]. Figure 7 (right) shows the ATLAS measurement [52] using Z^0 decays to electron or muon pairs. Z^0 bosons decaying to a lepton pair $\ell\ell$ are identified by $66 < m_{\ell\ell} < 116$ GeV. Jets are reconstructed using the anti-k_t

algorithm with $R = 0.4$ and selected by demanding $p_t > 30$ GeV and rapidity $|y| < 4.4$. The data points show the inclusive cross section for Z^0 production in association with at least one, two, three or four jets. The data are compared with predictions by NLO QCD and multileg tree level matrix element generators ALPGEN and SHERPA. Within the errors the predictions describe the data well. The corresponding CMS analysis is shown in [55].

4 Soft QCD

The study of low energy (soft) effects in QCD is a wide field and we can only give examples of interesting and important studies. Reviews of different aspects of soft QCD physics are e.g. [56, 57, 58].

An interesting quantity for studies of soft QCD effects is $\xi = \log(1/x)$. The variable $x = 2p/\sqrt{s}$ in e^+e^- collisions, $x = 2p/Q$ for ep DIS events in the Breit frame, and $x = p/E_{jet}$ for particles associated with jets in $p\bar{p}$ or pp collisions, where p is always the momentum of a final state charged hadron. Only charged hadrons are considered, because these can be measured well at low particle momenta in tracking detectors while this is difficult for neutral hadrons. The distribution of ξ is expected to vanish for $\xi \to 0$, corresponding to large x as well as for increasing ξ corresponding to small x, since finite hadron masses impose a non-zero Q-dependent lower limit on x.

The kinematic limit $x \sim m_h/Q$ translates into the expectation for the position of the peak ξ_0 to scale like $\xi_0 \sim \log(Q)$. The QCD prediction in the modified leading-log-approximation (MLLA) is $\xi_0 = 1/2\log(Q/\Lambda)(1 + h.o.)$ [59], i.e. the slope of $\xi_0(Q)$ is lower by a factor 1/2 due to destructive soft gluon interference compared with the expectation from pure kinematics. The MLLA prediction invokes local parton hadron duality (LPHD), i.e. that on average parton spectra correspond to hadron spectra except for a normalisation constant [60, 61], because hadronisation is a local process. Measurements of distributions of ξ in e^+e^- and ep collisions are summarised in [58] confirming the MLLA prediction.

CDF has measured momentum spectra of charged particles associated with jets using a cone centred on the jet axis [62]. Events with two energetic and central jets with balanced momenta in the transverse plane are selected. The events are analysed in bins of dijet invariant mass with mean values $80 < m_{jj} < 560$ GeV. Tracks from primary particles within cones of sizes $\theta_C = 0.28$, 0.36 and 0.47 around the jet axis are considered. The measured ξ distributions are shown in figure 8 (left) in bins of m_{jj}. The evolution of the peak ξ_0 with m_{jj} is clearly visible. The plot in figure 8 (right) shows the evolution of ξ_0 measured by CDF as function of the scaling variable $m_{jj} \sin\theta_C$. The CDF data for different cone sizes are compared with e^+e^- and ep data and a QCD MLLA prediction. Within the uncertainties the CDF $p\bar{p}$ data and the e^+e^- and ep data are consistent with a universal description by MLLA QCD with LPHD. More fragmentation studies using $p\bar{p}$ data are summarised e.g. in [63].

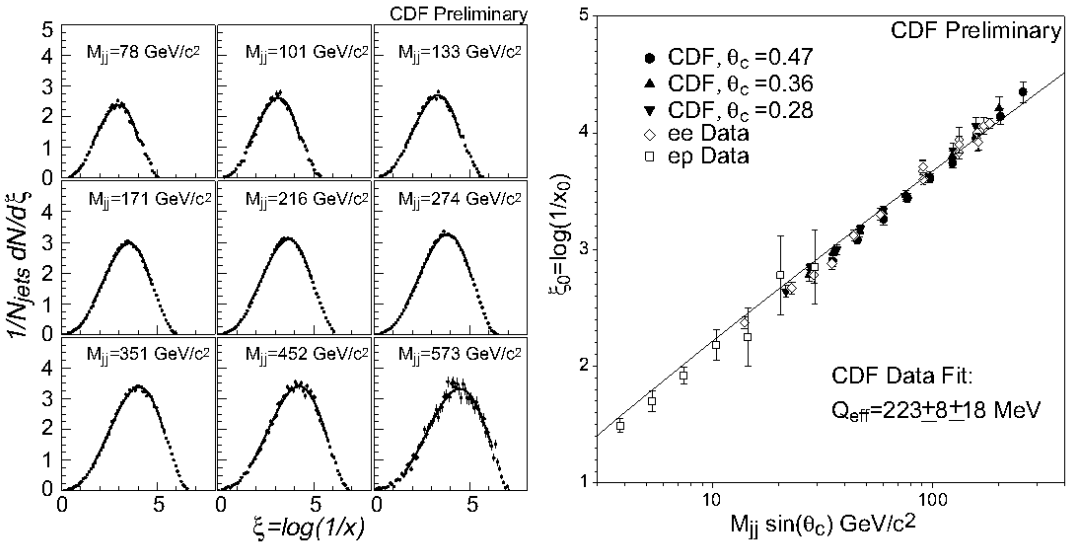

Figure 8: The figure [62] shows on the left distributions of ξ measured by CDF in bins of dijet invariant mass m_{jj}. The mean values of m_{jj} are given on the plots. The figure on the right shows the evolution of the peak position ξ_0 as function of $m_{jj} \sin\theta_C$ for three different values of θ_C as indicated on the figure. The data are compared with e^+e^- and ep data and with a MLLA QCD prediction.

5 Conclusions

We have shown important and illustrative examples of QCD tests at low and high energy scales. These tests use event shape observables or jet based observables to investigate properties of hadronic final states in e^+e^-, ep, pp or $p\bar{p}$ collisions.

In e^+e^- the theory has advanced to NNLO calculations combined with resummation of logarithmic term up to subleading level. This allows extractions of the value of the strong coupling constant $\alpha_S(m_{Z^0})$ with a precision reaching 1%. Comparisons of hadronisation models in Monte Carlo generators or in analytic form for the event shape $1-T$ shows that a residual uncertainty in hadronisation modelling of about 2-3% remains. Several analyses using only one model (or class of models) quote significantly smaller hadronisation uncertainties.

In ep DIS NLO QCD calculations are available together with a large amount of well measured data. Analyses using event shapes or jets confirm QCD with high precision and consistent with e^+e^- results.

The LHC experiments have shown their first results on jets in pp collisions. With jet transverse momenta reaching the TeV scale QCD is now tested at unexplored energy scales. NLO QCD predictions are available for many processes including some with many jets in the final state such a Z^0 production with up to four jets. The theory generally gives a satisfactory description of the data.

Studies of soft QCD in the GeV range or below are sensitive to the transition from the partons of the theory to the observed hadrons. For some well defined observables such as the momentum spectra of charged particles precise measurements and solid QCD predictions are possible. These confirm the applicability of QCD, in appropriate approximations, at low energy scales and give insight into some of the underlying mechanisms of hadronisation. In particular the success of MLLA QCD predictions together with LPHD imply that hadronisation is a local process.

We are looking forward with excitement to more measurements from LHC and more advances in the theory, and thus to a more complete understanding of processes at large and small energy scales.

Acknowledgments

The author would like to thank the organisers of the LC11 conference for the invitation and the interesting and stimulating meeting in a beautiful location.

References

[1] Fritzsch H, Gell-Mann M and Leutwyler H 1973 *Phys. Lett.* B **47** 365–368

[2] Gross D J and Wilczek F 1973 *Phys. Rev. Lett.* **30** 1343–1346

[3] Gross D J and Wilczek F 1973 *Phys. Rev.* D **8** 3633–3652

[4] Altheimer A *et al* e-print 1201.0008

[5] Bethke S, Hoang A H, Kluth S, Schieck J, Stewart I W *et al* 2011 FERMILAB-CONF-11-611-T, MIT-CTP-4301 e-print 1110.0016

[6] Biebel O 2001 *Phys. Rep.* **340** 165–289

[7] Kluth S 2006 *Rept. Prog. Phys.* **69** 1771–1846

[8] Brandt S, Peyrou C, Sosnowski R and Wroblewski A 1964 *Phys. Lett.* **12** 57–61

[9] Fahri E 1977 *Phys. Rev. Lett.* **39** 1587–1588

[10] Dasgupta M and Salam G P 2004 *J. Phys.* G **30** R143

[11] Gehrmann-De Ridder A, Gehrmann T, Glover E W N and Heinrich G 2007 *J. High Energy Phys.* **12** 094

[12] Weinzierl S 2009 *J. High Energy Phys.* **0906** 041

[13] Gehrmann T, Luisoni G and Stenzel H 2008 *Phys. Lett.* B **664** 265–273

[14] Dissertori G *et al* 2008 *J. High Energy Phys.* **02** 040

[15] JADE Coll. Bethke S, Kluth S, Pahl C and Schieck J 2009 *Eur. Phys. J.* C **64** 351–360

[16] OPAL Collaboration Coll. Abbiendi G *et al* 2011 *Eur. Phys. J.* C **71** 1733

[17] Dissertori G, Gehrmann-De Ridder A, Gehrmann T, Glover E, Heinrich G *et al* 2009 *J. High Energy Phys.* **0908** 036

[18] Dokshitzer Y, Marchesini G and Webber B 1996 *Nucl. Phys.* B **469** 93–142

[19] Davison R A and Webber B R 2009 *Eur. Phys. J.* C **59** 13–25

[20] Gehrmann T, Jaquier M and Luisoni G 2010 *Eur. Phys. J.* C **67** 57–72

[21] Abbate R, Fickinger M, Hoang A H, Mateu V and Stewart I W 2011 *Phys. Rev.* D **83** 074021

[22] Pahl C, Bethke S, Biebel O, Kluth S and Schieck J 2009 *Eur. Phys. J.* C **64** 533–547

[23] Monni P F, Gehrmann T and Luisoni G 2011 *J. High Energy Phys.* **1108** 010

[24] H1 Coll. Aktas A *et al* 2006 *Eur. Phys. J.* C **46** 343–356

[25] ZEUS Coll. Chekanov S *et al* 2007 *Nucl. Phys.* B **767** 1–28

[26] CMS Coll. Khachatryan V *et al* 2011 *Phys. Lett.* B **699** 48–67

[27] Banfi A, Salam G P and Zanderighi G 2004 *J. High Energy Phys.* **0408** 062 Erratum added online, nov/29/2004

[28] Banfi A, Salam G P and Zanderighi G 2010 *J. High Energy Phys.* **1006** 038

[29] Cacciari M, Salam G P and Soyez G 2008 *J. High Energy Phys.* **04** 063

[30] Bethke S, Kunszt Z, Soper D and Stirling W 1992 *Nucl. Phys.* B **370** 310–334

[31] Catani S *et al* 1991 *Phys. Lett.* B **269** 432

[32] ALEPH Coll. Heister A *et al* 2004 *Eur. Phys. J.* C **35** 457–486

[33] Frederix R, Frixione S, Melnikov K and Zanderighi G 2010 *J. High Energy Phys.* **1011** 050

[34] Dissertori G, Gehrmann-De Ridder A, Gehrmann T, Glover E, Heinrich G *et al* 2010 *Phys. Rev. Lett.* **104** 072002

[35] Gehrmann-De Ridder A, Gehrmann T, Glover E and Heinrich G 2008 *Phys. Rev. Lett.* **100** 172001

[36] Weinzierl S 2011 *Eur. Phys. J.* C **71** 1565

[37] Dixon L J and Signer A 1997 *Phys. Rev.* D **56** 4031–4038

[38] Nagy Z and Trocsanyi Z 1998 *Phys. Rev.* D **59** 014020 Erratum-ibid.D62:099902,2000

[39] ALEPH Coll. Heister A *et al* 2003 *Eur. Phys. J.* C **27** 1–17

[40] JADE Coll. Schieck J *et al* 2006 *Eur. Phys. J.* C **48** 3–13 Erratum-ibid.C50:769,2007

[41] OPAL Coll. Abbiendi G *et al* 2006 *Eur. Phys. J.* C **47** 295–307

[42] Gleisberg T, Hoeche S, Krauss F, Schonherr M, Schumann S *et al* 2009 *J. High Energy Phys.* **0902** 007

[43] Catani S, Dokshitzer Y L, Seymour M H and Webber B R 1993 *Nucl. Phys.* B **406** 187–224

[44] Klein M and Yoshida R 2008 *Prog. Part. Nucl. Phys.* **61** 343–393

[45] H1 Coll. Aaron F *et al* 2010 *Eur. Phys. J.* C **67** 1–24

[46] ZEUS Coll. Abramowicz H *et al* 2010 *Phys. Lett.* B **691** 127–137

[47] Salam G P and Soyez G 2007 *J. High Energy Phys.* **05** 086

[48] Butterworth J M, Dissertori G and Salam G P e-print 1202.0583 sub. toAnnu. Rev. Nucl. Part. Sci.

[49] ATLAS Coll. Aad G *et al* 2011 *Eur. Phys. J.* C **71** 1512

[50] CMS Coll. Chatrchyan S *et al* 2011 *Phys. Rev. Lett.* **107** 132001

[51] ATLAS Coll. Aad G *et al* 2011 *Phys. Lett.* B **694** 327–345

[52] ATLAS Coll. Aad G *et al* 2011 CERN-PH-EP-2011-162 e-print 1111.2690 acc. byPhys. Rev.D

[53] CMS Coll. Khachatryan V *et al* 2011 *Phys. Rev. Lett.* **106** 201804

[54] Becker S, Goetz D, Reuschle C, Schwan C and Weinzierl S 2012 *Phys. Rev. Lett.* **108** 032005

[55] CMS Coll. Chatrchyan S *et al* 2011 CERN-PH-EP-2011-125 e-print 1110.3226 acc. byJ. High Energy Phys.

[56] Albino S 2010 *Rev. Mod. Phys.* **82** 2489–2556

[57] Ryskin M, Martin A, Khoze V and Shuvaev A 2009 *J. Phys.* G **36** 093001

[58] PDG Coll. Nakamura K *et al* 2010 *J. Phys.* G **37** 075021

[59] Dokshitzer Y, Khoze V, Mueller A and Troyan S 1991 *Basics of perturbative QCD* (Editions Frontieres)

[60] Azimov Y I, Dokshitzer Y L, Khoze V A and Troian S I 1985 *Z. Phys.* C **27** 65–72

[61] Azimov Y I, Dokshitzer Y L, Khoze V A and Troian S I 1986 *Z. Phys.* C **31** 213–218

[62] CDF Coll. Safonov A 2002 FERMILAB-CONF-02-082-E, CDF-PUB-JET-CDFR-5941

[63] CDF Coll. Pronko A 2005 *Int. J. Mod. Phys.* A **20** 3723–3725

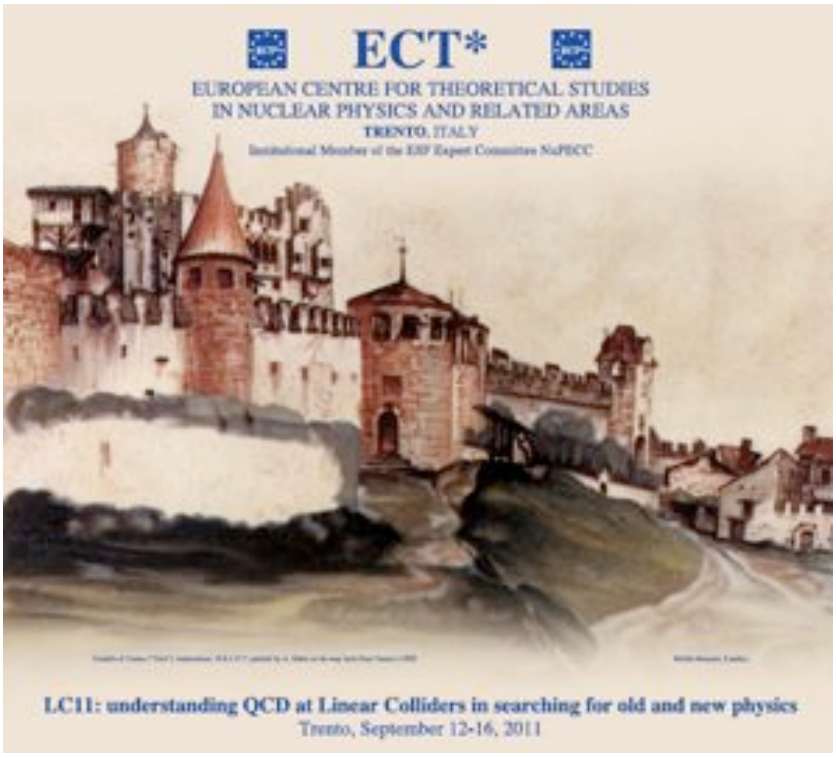

Castello di Trento painted by A. Dürer on his way back from Venice (1495).

8.3 N. Kauer - NLO automated tools for QCD and Beyond

NLO automated tools for QCD and beyond

Nikolas Kauer
Department of Physics, Royal Holloway, University of London, Egham TW20 0EX, UK
n.kauer@rhul.ac.uk

Abstract Theoretical predictions for scattering processes with multi-particle final states at next-to-leading order (NLO) in perturbative QCD are essential to fully exploit the physics potential of present and future high-energy colliders. The status of NLO QCD calculations and tools is reviewed.

1 Introduction

The study of hard scattering processes at the Large Hadron Collider (LHC) [1] and a future TeV-scale linear collider is our primary means to probe and extend the Standard Model of particle physics. It is driven by the comparison of experimental measurements with theoretical predictions, which depends on our ability to compute collider cross sections in perturbative QCD with adequate accuracy [2, 3]. This can only be achieved by going beyond leading order (LO) in QCD. When using conventional measures, LO scale uncertainties are typically large compared to experimental uncertainties. Moreover, for theoretical reasons a reliable estimation of the scale uncertainty is not feasible at LO. Consequently, an assessment of different scale choices, which is particularly important for many-particle/jet processes, is not possible. Furthermore, the convergence of the perturbative series cannot be assessed at LO. When going beyond LO by including NLO corrections, the situation improves significantly.[1] At NLO, scale uncertainties can be assessed more reliably, and the residual uncertainties are often comparable to experimental uncertainties.[2] NLO calculations thus deliver accurate predictions not only for the overall normalisation, but also for kinematic distributions including peripheral phase space regions. This is in part due to the fact that new subprocesses often become active at NLO, which modify the normalisation and kinematic distributions. Our ability to determine the uncertainty of parton distribution functions (PDF) and to model the structure of jets is also greatly enhanced at NLO.

[1] For processes with vastly differing scales, the resummation of large logarithms of ratios of scales may also be necessary.

[2] Notable exceptions are the hadroproduction of Higgs and $Wb\bar{b}$ with $\sigma_{\rm NLO}/\sigma_{\rm LO} \approx 2$.

In Section 2, the state-of-the-art methods, implementations and tools for parton-level NLO calculations are briefly reviewed. In Section 3, the status of collider physics applications is described. The review ends with a summary.[3]

2 Methods, implementations and tools

The structure and implied modularity of NLO calculations is illustrated in Eqs. (1)–(3):

$$\sigma_{\rm NLO} = \sigma_{\rm Born} + \sigma_{corr} \tag{1}$$

$$\sigma_{\rm Born} = \int d\phi_n \, \frac{1}{2\hat{s}} \quad |\mathcal{A}_{\rm LO}|^2 \tag{2}$$

$$\begin{aligned} \sigma_{corr} = & \int d\phi_n \, \frac{\alpha_s}{2\hat{s}} \quad \Big[\sum_j \int d\phi_j \mathcal{D}_j + \mathcal{A}_{\rm LO}\mathcal{A}^*_{\rm NLO,V} + \mathcal{A}^*_{\rm LO}\mathcal{A}_{\rm NLO,V} \Big] \\ & + \int d\phi_{n+1} \, \frac{\alpha_s}{2\hat{s}} \quad \Big[|\mathcal{M}_{\rm NLO,R}|^2 - \sum_j \mathcal{D}_j \Big] \end{aligned} \tag{3}$$

The new components of the NLO correction σ_{corr} are:[4] the virtual corrections (involving one-loop amplitudes), the real corrections (involving tree amplitudes) and the infrared subtraction terms.[5] The resulting procedure for NLO calculations is given in Table 1. The Binoth Les Houches Accord, a standard interface for combining the tree-level and loop-level contributions, has been defined in Ref. [6] and is implemented in many automated tools (see below).

Until circa 2005, the limiting factor of NLO calculations was the computation of the virtual corrections, which typically applied Passarino-Veltman (PV) [7] or PV-inspired [8] tensor integral reduction methods to evaluate the form factors of a Feynman-diagram-based amplitude representation. Several one-loop integral libraries are available as public codes: LoopTools [9, 10], QCDLoop [11], Golem95 [12], OneLOop [13] and PJFry [14]. The PV approach is general, but practical limitations arise due to the factorial growth of the number of Feynman graphs with $N = n + 2$, the strong growth of the number of reduction terms with N and due to numerical instabilities for exceptional kinematic configurations, which are caused by vanishing Gram determinants. It has nevertheless been used successfully to create collections of NLO calculations based on analytic formulae and semi-automated methods, such as MCFM [15, 16], MC@NLO [17] and VBFNLO [18, 19, 20, 21].[6] Since 2004, tremendous improvements have been achieved for the calculation of multi-leg one-loop amplitudes due to the exploitation of on-shell

[3] The important topics of next-to-next-to-leading order (NNLO) calculations and combining parton-level fixed-order calculations and parton-shower event generators are beyond the scope of this review.

[4] The Born amplitude is assumed to be at tree level.

[5] An alternative to the widely used subtraction formalism [4] is the phase space slicing method [5].

[6] The POWHEG BOX [22] library project [23, 24] was inspired by these collections.

1. Real correction: generate and evaluate $2 \to n+1$ tree-level amplitudes
2. Subtract soft and collinear singularities due to single unresolved real radiation to obtain finite result
3. Integrate over $(n+1)$-particle phase space
4. Virtual correction: generate and evaluate UV-renormalised $2 \to n$ one-loop amplitude after extraction of soft and collinear singularities to obtain finite result
5. Confirm cancellation of soft/collinear singularities (absorb initial state collinear singularities into PDF)
6. Integrate over n-particle phase space
7. Combine $2 \to n+1$ and $2 \to n$ contributions
8. Convolve with NLO PDF
9. Repeat for all contributing subprocesses

Table 1: Steps to calculate the NLO QCD corrections for a $2 \to n$ process. n excludes electroweak decays.

recursion relations and generalized-unitarity-cut constructibility as well as the possibility to even reconstruct the full rational terms [25, 26]. On-shell reduction related tools are CutTools [27], Rocket [28] and Samurai [29]. Further innovative, complementary methods are also being developed [30]. A comprehensive review of methods for multi-leg one-loop calculations can be found in Ref. [31].

Three widely-used algorithms for the generation of process-independent infrared subtraction terms are Catani-Seymour dipole subtraction [32], Frixione-Kunszt-Signer (FKS) subtraction [33] and antenna subtraction [34].[7] Several implementations for these standard schemes are available: Sherpa-Dipoles [36], MadDipole [37], HELAC-Dipoles [38], MadFKS [39], TeVJet [40] and AutoDipole [41].

The following programs aim to provide a comprehensive, automated solution for NLO calculations: aMC@NLO [27, 39, 42], BlackHat/Sherpa [26, 36, 43], HELAC-NLO [13, 27, 38, 44], GoSam [45], FeynArts/FormCalc/LoopTools [10, 46] and MadGolem [47].

3 Collider physics applications

Discussions at the Les Houches 2005 Physics at TeV Colliders Workshop resulted in a list of processes for which the knowledge of NLO corrections was considered of particular importance

[7] Research on alternative subtraction schemes is also being carried out [35].

for the LHC physics programme [48]. This experimenter's NLO "wish list" has guided theoretical efforts and was subsequently revised and updated in 2007 [49] as well as 2009 [50]. The most recent version is displayed in Table 2.

Due to the groundbreaking advances outlined in Section 2, since 2009 the frontier for collider physics applications of NLO techniques has also advanced considerably. The following $2 \to 4$ processes – most are on the wish list – have now been calculated at NLO QCD:[8] $pp \to W\gamma\gamma$+jet [21], $pp \to W$+3 jets [62, 63, 66, 67], $pp \to Z, \gamma^*$+3 jets [68], $pp \to t\bar{t}b\bar{b}$ [59, 60, 61, 69], $pp \to t\bar{t}jj$ [64, 70], $pp \to b\bar{b}b\bar{b}$ [71], $pp \to W^+W^-b\bar{b}$ [72], $pp \to W^\pm W^\pm jj$ [24, 73], $pp \to W^+W^-jj$ [74] and most recently $pp \to 4$ jets [75]. Leptonic decays of weak bosons can be included trivially. At the same level of complexity, complete off-shell effects for $pp \to t\bar{t}$ with dileptonic decay, i.e. $pp \to e^+\nu_e b\mu^-\bar{\nu}_\mu\bar{b}$, have been calculated at NLO QCD in Ref. [76], which allowed to explicitly confirm the $\mathcal{O}(\alpha_s\Gamma/M)$ effect predicted by Ref. [77]. Advancing the frontier for linear collider physics, the process $e^+e^- \to 5$ jets has recently been calculated at NLO [78], which allowed to extract a competitive value of $\alpha_s(M_Z)$ from 5-jet LEP data. Going beyond 4-particle final states in general requires the computation of 7-point one-loop amplitudes or higher. This is the current complexity frontier. At this level, NLO cross sections in leading-colour approximation have been calculated for $V + 4$ jets by the BlackHat/Sherpa collaboration ($pp \to W + 4$ jets [79] and $pp \to Z + 4$ jets [80]) and for $e^+e^- \to n$ jets up to $n = 7$ [81].[9] The $n = 7$ case required the computation of a one-loop 8-point function.

4 Summary

NLO QCD predictions for multi-particle processes are essential to fully exploit the physics potential of the LHC and a future linear collider. In recent years, tremendous progress has been made in developing the calculational methods and tools that are required to compute NLO corrections for hard scattering processes with 6, 7 or more external particles. At this level a (semi-)manual approach is no longer feasible, and the transition from collections of codes for specific processes to automated code generation for any process up to a maximum complexity has now been achieved. Several such automated tools are available or will become public in the near future. The modularity of NLO calculations allows to interface many tool components on the basis of the Binoth Les Houches Accord.

[8] pp is given as initial state, but $p\bar{p}$ is also implied.

[9] Recently, the full-colour virtual contribution to $pp \to W + 4$ jets has been calculated [82].

Process ($V \in \{Z, W, \gamma\}$)	Comments
Calculations completed since Les Houches 2005	
1. $pp \to VV$+jet	WW+jet completed by Dittmaier/Kallweit/Uwer [51, 52]; Campbell/Ellis/Zanderighi [53]. ZZ+jet completed by Binoth/Gleisberg/Karg/Kauer/Sanguinetti [54]
2. $pp \to$ Higgs+2jets	NLO QCD to the gg channel completed by Campbell/Ellis/Zanderighi [16]; NLO QCD+EW to the VBF channel completed by Ciccolini/Denner/Dittmaier [55, 56]
3. $pp \to VVV$	ZZZ completed by Lazopoulos/Melnikov/Petriello [57] and WWZ by Hankele/Zeppenfeld [19] (see also Binoth/Ossola/Papadopoulos/Pittau [58])
4. $pp \to t\bar{t}\,b\bar{b}$	relevant for $t\bar{t}H$ computed by Bredenstein/Denner/Dittmaier/Pozzorini [59, 60] and Bevilacqua/Czakon/Papadopoulos/Pittau/Worek [61]
5. $pp \to V$+3jets	calculated by the Blackhat/Sherpa [62] and Rocket [63] collaborations
Calculations remaining from Les Houches 2005	
6. $pp \to t\bar{t}$+2jets	relevant for $t\bar{t}H$ computed by Bevilacqua/Czakon/Papadopoulos/Worek [64]
7. $pp \to VV\,b\bar{b}$,	relevant for VBF $\to H \to VV$, $t\bar{t}H$
8. $pp \to VV$+2jets	relevant for VBF $\to H \to VV$ VBF contributions calculated by (Bozzi/)Jäger/Oleari/Zeppenfeld [20]
NLO calculations added to list in 2007	
9. $pp \to b\bar{b}b\bar{b}$	$q\bar{q}$ channel calculated by Golem collaboration [65]
NLO calculations added to list in 2009	
10. $pp \to V$+4jets	top pair production, various new physics signatures
11. $pp \to Wb\bar{b}j$	top, new physics signatures
12. $pp \to t\bar{t}t\bar{t}$	various new physics signatures
Calculations beyond NLO added in 2007	
13. $gg \to W^*W^*$ $\mathcal{O}(\alpha^2\alpha_s^3)$	backgrounds to Higgs
14. NNLO $pp \to t\bar{t}$	normalisation of a benchmark process
15. NNLO to VBF and Z/γ+jet	Higgs couplings and SM benchmark
Calculations including electroweak effects	
16. NNLO QCD+NLO EW for W/Z	precision calculation of a SM benchmark

Table 2: The experimenter's wish list for LHC processes in early 2010 (from [50]).

Acknowledgments

I would like to thank the organisers for the invitation to speak at Linear Collider 2011 and commend G. Pancheri and her team for hosting this well-organised and thoroughly enjoyable meeting. The hospitality of the European Centre for Theoretical Studies in Nuclear Physics and Related Areas (ECT*) as well as partial support from ECT* and INFN are gratefully acknowledged. This work was carried out as part of the research programme of the Royal Holloway and Sussex Particle Physics Theory Consortium and the NExT Institute. Financial support under the SEPnet Initiative from the Higher Education Funding Council for England and the Science and Technology Facilities Council (STFC) is gratefully acknowledged. This work was supported by STFC grant ST/J000485/1.

References

[1] J. M. Butterworth, G. Dissertori and G. P. Salam, arXiv:1202.0583 [hep-ex].

[2] G. P. Salam, PoS ICHEP **2010** (2010) 556 [arXiv:1103.1318 [hep-ph]].

[3] G. Zanderighi, arXiv:1201.3905 [hep-ph].

[4] R. K. Ellis, D. A. Ross and A. E. Terrano, Nucl. Phys. B **178** (1981) 421.

[5] K. Fabricius, G. Kramer, G. Schierholz and I. Schmitt, Z. Phys. C **11** (1981) 315; G. Kramer and B. Lampe, Fortsch. Phys. **37** (1989) 161; B. W. Harris and J. F. Owens, Phys. Rev. D **65** (2002) 094032 [hep-ph/0102128].

[6] T. Binoth *et al.*, Comput. Phys. Commun. **181** (2010) 1612 [arXiv:1001.1307 [hep-ph]].

[7] G. 't Hooft and M. J. G. Veltman, Nucl. Phys. B **153** (1979) 365; G. Passarino and M. J. G. Veltman, Nucl. Phys. B **160** (1979) 151.

[8] A. Denner and S. Dittmaier, Nucl. Phys. B **658** (2003) 175 [hep-ph/0212259]; T. Binoth, J. P. Guillet, G. Heinrich, E. Pilon and C. Schubert, JHEP **0510** (2005) 015 [hep-ph/0504267]; A. Denner and S. Dittmaier, Nucl. Phys. B **734** (2006) 62 [hep-ph/0509141].

[9] G. J. van Oldenborgh and J. A. M. Vermaseren, Z. Phys. C **46** (1990) 425.

[10] T. Hahn and M. Perez-Victoria, Comput. Phys. Commun. **118** (1999) 153 [hep-ph/9807565].

[11] R. K. Ellis and G. Zanderighi, JHEP **0802** (2008) 002 [arXiv:0712.1851 [hep-ph]].

[12] T. Binoth, J. -P. Guillet, G. Heinrich, E. Pilon and T. Reiter, Comput. Phys. Commun. **180** (2009) 2317 [arXiv:0810.0992 [hep-ph]]; G. Cullen, J. P. Guillet, G. Heinrich, T. Kleinschmidt, E. Pilon, T. Reiter and M. Rodgers, Comput. Phys. Commun. **182** (2011) 2276 [arXiv:1101.5595 [hep-ph]].

[13] A. van Hameren, Comput. Phys. Commun. **182** (2011) 2427 [arXiv:1007.4716 [hep-ph]].

[14] J. Fleischer and T. Riemann, Phys. Rev. D **83** (2011) 073004 [arXiv:1009.4436 [hep-ph]].

[15] R. K. Ellis and S. Veseli, Phys. Rev. D **60** (1999) 011501 [hep-ph/9810489]; J. M. Campbell and R. K. Ellis, Phys. Rev. D **60** (1999) 113006 [hep-ph/9905386]; J. M. Campbell and R. K. Ellis, Phys. Rev. D **62** (2000) 114012 [hep-ph/0006304]; J. M. Campbell and R. K. Ellis, Phys. Rev. D **65** (2002) 113007 [hep-ph/0202176]; J. M. Campbell, R. K. Ellis, F. Maltoni and S. Willenbrock, Phys. Rev. D **67** (2003) 095002 [hep-ph/0204093]; J. M. Campbell, R. K. Ellis and D. L. Rainwater, Phys. Rev. D **68** (2003) 094021 [hep-ph/0308195]; J. M. Campbell, R. K. Ellis, F. Maltoni and S. Willenbrock, Phys. Rev. D **69** (2004) 074021 [hep-ph/0312024]; J. M. Campbell, R. K. Ellis and F. Tramontano, Phys. Rev. D **70** (2004) 094012 [hep-ph/0408158]; J. M. Campbell and F. Tramontano, Nucl. Phys. B **726** (2005) 109 [hep-ph/0506289]; J. M. Campbell, R. K. Ellis, F. Maltoni and S. Willenbrock, Phys. Rev. D **73** (2006) 054007 [Erratum-ibid. D **77** (2008) 019903] [hep-ph/0510362]; J. M. Campbell, R. Frederix, F. Maltoni and F. Tramontano, Phys. Rev. Lett. **102** (2009) 182003 [arXiv:0903.0005 [hep-ph]]; J. M. Campbell, R. K. Ellis and C. Williams, Phys. Rev. D **81** (2010) 074023 [arXiv:1001.4495 [hep-ph]]; S. Badger, J. M. Campbell and R. K. Ellis, JHEP **1103** (2011) 027 [arXiv:1011.6647 [hep-ph]]; J. M. Campbell, R. K. Ellis and C. Williams, JHEP **1107** (2011) 018 [arXiv:1105.0020 [hep-ph]]; J. M. Campbell, R. K. Ellis and C. Williams, JHEP **1110** (2011) 005 [arXiv:1107.5569 [hep-ph]].

[16] J. M. Campbell, R. K. Ellis and G. Zanderighi, JHEP **0610** (2006) 028 [hep-ph/0608194].

[17] S. Frixione and B. R. Webber, JHEP **0206** (2002) 029 [hep-ph/0204244]; S. Frixione, P. Nason and B. R. Webber, JHEP **0308** (2003) 007 [hep-ph/0305252]; S. Frixione, E. Laenen, P. Motylinski and B. R. Webber, JHEP **0603** (2006) 092 [hep-ph/0512250]; S. Frixione, E. Laenen, P. Motylinski, B. R. Webber and C. D. White, JHEP **0807** (2008) 029 [arXiv:0805.3067 [hep-ph]]; S. Frixione, F. Stoeckli, P. Torrielli and B. R. Webber, JHEP **1101** (2011) 053 [arXiv:1010.0568 [hep-ph]]; B. Fuks, M. Klasen, F. Ledroit, Q. Li and J. Morel, Nucl. Phys. B **797** (2008) 322 [arXiv:0711.0749 [hep-ph]].

[18] T. Figy, C. Oleari and D. Zeppenfeld, Phys. Rev. D **68** (2003) 073005 [hep-ph/0306109]; T. Figy, S. Palmer and G. Weiglein, arXiv:1012.4789 [hep-ph]; T. Figy, V. Hankele and D. Zeppenfeld, JHEP **0802** (2008) 076 [arXiv:0710.5621 [hep-ph]]; C. Oleari and D. Zeppenfeld, Phys. Rev. D **69** (2004) 093004 [hep-ph/0310156]; C. Englert, B. Jager, M. Worek

and D. Zeppenfeld, Phys. Rev. D **80** (2009) 035027 [arXiv:0810.4861 [hep-ph]]; C. Englert, B. Jager and D. Zeppenfeld, JHEP **0903** (2009) 060 [arXiv:0812.2564 [hep-ph]]; K. Arnold, T. Figy, B. Jager and D. Zeppenfeld, JHEP **1008** (2010) 088 [arXiv:1006.4237 [hep-ph]]; F. Campanario, V. Hankele, C. Oleari, S. Prestel and D. Zeppenfeld, Phys. Rev. D **78** (2008) 094012 [arXiv:0809.0790 [hep-ph]]; G. Bozzi, F. Campanario, V. Hankele and D. Zeppenfeld, Phys. Rev. D **81** (2010) 094030 [arXiv:0911.0438 [hep-ph]]; G. Bozzi, F. Campanario, M. Rauch, H. Rzehak and D. Zeppenfeld, Phys. Lett. B **696** (2011) 380 [arXiv:1011.2206 [hep-ph]]; G. Bozzi, F. Campanario, M. Rauch and D. Zeppenfeld, Phys. Rev. D **83** (2011) 114035 [arXiv:1103.4613 [hep-ph]]; G. Bozzi, F. Campanario, M. Rauch and D. Zeppenfeld, Phys. Rev. D **84** (2011) 074028 [arXiv:1107.3149 [hep-ph]]; F. Campanario, C. Englert, M. Spannowsky and D. Zeppenfeld, Europhys. Lett. **88** (2009) 11001 [arXiv:0908.1638 [hep-ph]]; F. Campanario, C. Englert and M. Spannowsky, Phys. Rev. D **83** (2011) 074009 [arXiv:1010.1291 [hep-ph]]; F. Campanario, C. Englert, S. Kallweit, M. Spannowsky and D. Zeppenfeld, JHEP **1007** (2010) 076 [arXiv:1006.0390 [hep-ph]]; F. Campanario, C. Englert and M. Spannowsky, Phys. Rev. D **82** (2010) 054015 [arXiv:1006.3090 [hep-ph]]; V. Del Duca, W. Kilgore, C. Oleari, C. Schmidt and D. Zeppenfeld, Phys. Rev. Lett. **87** (2001) 122001 [hep-ph/0105129]; V. Del Duca, W. Kilgore, C. Oleari, C. Schmidt and D. Zeppenfeld, Nucl. Phys. B **616** (2001) 367 [hep-ph/0108030]; V. Del Duca, G. Klamke, D. Zeppenfeld, M. L. Mangano, M. Moretti, F. Piccinini, R. Pittau and A. D. Polosa, JHEP **0610** (2006) 016 [hep-ph/0608158]; G. Klamke and D. Zeppenfeld, JHEP **0704** (2007) 052 [hep-ph/0703202]; F. Campanario, M. Kubocz and D. Zeppenfeld, Phys. Rev. D **84** (2011) 095025 [arXiv:1011.3819 [hep-ph]]; K. Arnold, M. Bahr, G. Bozzi, F. Campanario, C. Englert, T. Figy, N. Greiner and C. Hackstein *et al.*, Comput. Phys. Commun. **180** (2009) 1661 [arXiv:0811.4559 [hep-ph]]; K. Arnold, J. Bellm, G. Bozzi, M. Brieg, F. Campanario, C. Englert, B. Feigl and J. Frank *et al.*, arXiv:1107.4038 [hep-ph].

[19] V. Hankele and D. Zeppenfeld, Phys. Lett. B **661** (2008) 103 [arXiv:0712.3544 [hep-ph]].

[20] B. Jager, C. Oleari and D. Zeppenfeld, JHEP **0607** (2006) 015 [hep-ph/0603177]; B. Jager, C. Oleari and D. Zeppenfeld, Phys. Rev. D **73** (2006) 113006 [hep-ph/0604200]; G. Bozzi, B. Jager, C. Oleari and D. Zeppenfeld, Phys. Rev. D **75** (2007) 073004 [hep-ph/0701105].

[21] F. Campanario, C. Englert, M. Rauch and D. Zeppenfeld, Phys. Lett. B **704** (2011) 515 [arXiv:1106.4009 [hep-ph]]; F. Campanario, JHEP **1110** (2011) 070 [arXiv:1105.0920 [hep-ph]].

[22] P. Nason, JHEP **0411** (2004) 040 [hep-ph/0409146]; S. Frixione, P. Nason and C. Oleari, JHEP **0711** (2007) 070 [arXiv:0709.2092 [hep-ph]]; S. Alioli, P. Nason, C. Oleari and E. Re, JHEP **1006** (2010) 043 [arXiv:1002.2581 [hep-ph]].

[23] S. Alioli, P. Nason, C. Oleari and E. Re, JHEP **0807** (2008) 060 [arXiv:0805.4802 [hep-ph]]; S. Alioli, P. Nason, C. Oleari and E. Re, JHEP **1101** (2011) 095 [arXiv:1009.5594 [hep-ph]]; S. Alioli, P. Nason, C. Oleari and E. Re, JHEP **0909** (2009) 111 [Erratum-ibid. **1002** (2010) 011] [arXiv:0907.4076 [hep-ph]]; E. Re, Eur. Phys. J. C **71** (2011) 1547 [arXiv:1009.2450 [hep-ph]]; S. Alioli, P. Nason, C. Oleari and E. Re, JHEP **0904** (2009) 002 [arXiv:0812.0578 [hep-ph]]; P. Nason and C. Oleari, JHEP **1002** (2010) 037 [arXiv:0911.5299 [hep-ph]]; S. Alioli, K. Hamilton, P. Nason, C. Oleari and E. Re, JHEP **1104** (2011) 081 [arXiv:1012.3380 [hep-ph]]; S. Frixione, P. Nason and G. Ridolfi, JHEP **0709** (2007) 126 [arXiv:0707.3088 [hep-ph]]; T. Melia, P. Nason, R. Rontsch and G. Zanderighi, Eur. Phys. J. C **71** (2011) 1670 [arXiv:1102.4846 [hep-ph]]; T. Melia, P. Nason, R. Rontsch and G. Zanderighi, JHEP **1111** (2011) 078 [arXiv:1107.5051 [hep-ph]]; C. Oleari and L. Reina, JHEP **1108** (2011) 061 [Erratum-ibid. **1111** (2011) 040] [arXiv:1105.4488 [hep-ph]]; E. Bagnaschi, G. Degrassi, P. Slavich and A. Vicini, arXiv:1111.2854 [hep-ph]; C. Bernaciak and D. Wackeroth, arXiv:1201.4804 [hep-ph]; L. Barze', G. Montagna, P. Nason, O. Nicrosini and F. Piccinini, arXiv:1202.0465 [hep-ph].

[24] B. Jager and G. Zanderighi, JHEP **1111** (2011) 055 [arXiv:1108.0864 [hep-ph]].

[25] Z. Bern, L. J. Dixon, D. C. Dunbar and D. A. Kosower, Nucl. Phys. B **425** (1994) 217 [hep-ph/9403226]; Z. Bern, L. J. Dixon, D. C. Dunbar and D. A. Kosower, Nucl. Phys. B **435** (1995) 59 [hep-ph/9409265]; Z. Bern, L. J. Dixon and D. A. Kosower, Nucl. Phys. B **513** (1998) 3 [arXiv:hep-ph/9708239]; R. Britto, F. Cachazo and B. Feng, Nucl. Phys. B **725** (2005) 275 [arXiv:hep-th/0412103]; G. Ossola, C. G. Papadopoulos and R. Pittau, Nucl. Phys. B **763** (2007) 147 [arXiv:hep-ph/0609007]; R. K. Ellis, W. T. Giele and Z. Kunszt, JHEP **0803** (2008) 003 [arXiv:0708.2398 [hep-ph]]; W. T. Giele, Z. Kunszt and K. Melnikov, JHEP **0804** (2008) 049 [arXiv:0801.2237 [hep-ph]]; R. K. Ellis, W. T. Giele, Z. Kunszt and K. Melnikov, Nucl. Phys. B **822** (2009) 270 [arXiv:0806.3467 [hep-ph]].

[26] C. F. Berger, Z. Bern, L. J. Dixon, F. Febres Cordero, D. Forde, H. Ita, D. A. Kosower and D. Maitre, Phys. Rev. D **78** (2008) 036003 [arXiv:0803.4180 [hep-ph]].

[27] G. Ossola, C. G. Papadopoulos and R. Pittau, JHEP **0803** (2008) 042 [arXiv:0711.3596 [hep-ph]].

[28] W. T. Giele and G. Zanderighi, JHEP **0806** (2008) 038 [arXiv:0805.2152 [hep-ph]]; R. K. Ellis, W. T. Giele, Z. Kunszt, K. Melnikov and G. Zanderighi, JHEP **0901** (2009) 012 [arXiv:0810.2762 [hep-ph]].

[29] P. Mastrolia, G. Ossola, T. Reiter and F. Tramontano, JHEP **1008** (2010) 080 [arXiv:1006.0710 [hep-ph]].

[30] A. van Hameren, JHEP **0907** (2009) 088 [arXiv:0905.1005 [hep-ph]]; S. Becker, C. Reuschle and S. Weinzierl, JHEP **1012** (2010) 013 [arXiv:1010.4187 [hep-ph]]; F. Cascioli, P. Maierhofer and S. Pozzorini, arXiv:1111.5206 [hep-ph].

[31] R. K. Ellis, Z. Kunszt, K. Melnikov and G. Zanderighi, arXiv:1105.4319 [hep-ph].

[32] S. Catani and M. H. Seymour, Nucl. Phys. B **485** (1997) 291 [Erratum-ibid. B **510** (1998) 503] [hep-ph/9605323]; S. Catani, S. Dittmaier, M. H. Seymour and Z. Trocsanyi, Nucl. Phys. B **627** (2002) 189 [hep-ph/0201036].

[33] S. Frixione, Z. Kunszt and A. Signer, Nucl. Phys. B **467** (1996) 399 [hep-ph/9512328]; S. Frixione, Nucl. Phys. B **507** (1997) 295 [hep-ph/9706545].

[34] D. A. Kosower, Phys. Rev. D **57** (1998) 5410 [hep-ph/9710213]; A. Gehrmann-De Ridder, T. Gehrmann and E. W. N. Glover, JHEP **0509** (2005) 056 [hep-ph/0505111]; A. Daleo, T. Gehrmann and D. Maitre, JHEP **0704** (2007) 016 [hep-ph/0612257].

[35] C. H. Chung, M. Kramer and T. Robens, JHEP **1106** (2011) 144 [arXiv:1012.4948 [hep-ph]].

[36] T. Gleisberg and F. Krauss, Eur. Phys. J. C **53** (2008) 501 [arXiv:0709.2881 [hep-ph]].

[37] R. Frederix, T. Gehrmann and N. Greiner, JHEP **0809** (2008) 122 [arXiv:0808.2128 [hep-ph]]; R. Frederix, T. Gehrmann and N. Greiner, JHEP **1006** (2010) 086 [arXiv:1004.2905 [hep-ph]].

[38] M. Czakon, C. G. Papadopoulos and M. Worek, JHEP **0908** (2009) 085 [arXiv:0905.0883 [hep-ph]].

[39] R. Frederix, S. Frixione, F. Maltoni and T. Stelzer, JHEP **0910** (2009) 003 [arXiv:0908.4272 [hep-ph]].

[40] M. H. Seymour and C. Tevlin, arXiv:0803.2231 [hep-ph].

[41] K. Hasegawa, S. Moch and P. Uwer, Comput. Phys. Commun. **181** (2010) 1802 [arXiv:0911.4371 [hep-ph]].

[42] V. Hirschi, R. Frederix, S. Frixione, M. V. Garzelli, F. Maltoni and R. Pittau, JHEP **1105** (2011) 044 [arXiv:1103.0621 [hep-ph]]; R. Frederix, S. Frixione, V. Hirschi, F. Maltoni, R. Pittau and P. Torrielli, Phys. Lett. B **701** (2011) 427 [arXiv:1104.5613 [hep-ph]]; R. Frederix, S. Frixione, V. Hirschi, F. Maltoni, R. Pittau and P. Torrielli, JHEP **1109** (2011) 061 [arXiv:1106.6019 [hep-ph]]; R. Frederix, S. Frixione, V. Hirschi, F. Maltoni, R. Pittau and P. Torrielli, arXiv:1110.4738 [hep-ph]; R. Frederix, S. Frixione, V. Hirschi,

F. Maltoni, R. Pittau and P. Torrielli, JHEP **1202** (2012) 048 [arXiv:1110.5502 [hep-ph]]; J. Alwall, M. Herquet, F. Maltoni, O. Mattelaer and T. Stelzer, JHEP **1106** (2011) 128 [arXiv:1106.0522 [hep-ph]].

[43] T. Gleisberg, S. Hoeche, F. Krauss, M. Schonherr, S. Schumann, F. Siegert and J. Winter, JHEP **0902** (2009) 007 [arXiv:0811.4622 [hep-ph]].

[44] A. van Hameren, C. G. Papadopoulos and R. Pittau, JHEP **0909** (2009) 106 [arXiv:0903.4665 [hep-ph]]; G. Bevilacqua, M. Czakon, M. V. Garzelli, A. van Hameren, A. Kardos, C. G. Papadopoulos, R. Pittau and M. Worek, arXiv:1110.1499 [hep-ph]; A. Cafarella, C. G. Papadopoulos and M. Worek, Comput. Phys. Commun. **180** (2009) 1941 [arXiv:0710.2427 [hep-ph]].

[45] G. Cullen, N. Greiner, G. Heinrich, G. Luisoni, P. Mastrolia, G. Ossola, T. Reiter and F. Tramontano, arXiv:1111.2034 [hep-ph].

[46] T. Hahn, Comput. Phys. Commun. **140** (2001) 418 [hep-ph/0012260].

[47] T. Binoth, D. Goncalves Netto, D. Lopez-Val, K. Mawatari, T. Plehn and I. Wigmore, Phys. Rev. D **84** (2011) 075005 [arXiv:1108.1250 [hep-ph]].

[48] C. Buttar, S. Dittmaier, V. Drollinger, S. Frixione, A. Nikitenko, S. Willenbrock, S. Abdullin and E. Accomando *et al.*, hep-ph/0604120.

[49] Z. Bern *et al.* [NLO Multileg Working Group Collaboration], arXiv:0803.0494 [hep-ph].

[50] J. R. Andersen *et al.* [SM and NLO Multileg Working Group Collaboration], arXiv:1003.1241 [hep-ph].

[51] S. Dittmaier, S. Kallweit and P. Uwer, Phys. Rev. Lett. **100** (2008) 062003 [arXiv:0710.1577 [hep-ph]].

[52] S. Dittmaier, S. Kallweit and P. Uwer, Nucl. Phys. B **826** (2010) 18 [arXiv:0908.4124 [hep-ph]].

[53] J. M. Campbell, R. K. Ellis and G. Zanderighi, JHEP **0712** (2007) 056 [arXiv:0710.1832 [hep-ph]].

[54] T. Binoth, T. Gleisberg, S. Karg, N. Kauer and G. Sanguinetti, Phys. Lett. B **683** (2010) 154 [arXiv:0911.3181 [hep-ph]].

[55] M. Ciccolini, A. Denner and S. Dittmaier, Phys. Rev. Lett. **99** (2007) 161803 [arXiv:0707.0381 [hep-ph]].

[56] M. Ciccolini, A. Denner and S. Dittmaier, Phys. Rev. D **77** (2008) 013002 [arXiv:0710.4749 [hep-ph]].

[57] A. Lazopoulos, K. Melnikov and F. Petriello, Phys. Rev. D **76** (2007) 014001 [arXiv:hep-ph/0703273].

[58] T. Binoth, G. Ossola, C. G. Papadopoulos and R. Pittau, JHEP **0806** (2008) 082 [arXiv:0804.0350 [hep-ph]].

[59] A. Bredenstein, A. Denner, S. Dittmaier and S. Pozzorini, Phys. Rev. Lett. **103** (2009) 012002 [arXiv:0905.0110 [hep-ph]].

[60] A. Bredenstein, A. Denner, S. Dittmaier and S. Pozzorini, JHEP **1003** (2010) 021 [arXiv:1001.4006 [hep-ph]].

[61] G. Bevilacqua, M. Czakon, C. G. Papadopoulos, R. Pittau and M. Worek, JHEP **0909** (2009) 109 [arXiv:0907.4723 [hep-ph]].

[62] C. F. Berger, Z. Bern, L. J. Dixon, F. Febres Cordero, D. Forde, T. Gleisberg, H. Ita and D. A. Kosower *et al.*, Phys. Rev. D **80** (2009) 074036 [arXiv:0907.1984 [hep-ph]].

[63] R. K. Ellis, K. Melnikov and G. Zanderighi, JHEP **0904** (2009) 077 [arXiv:0901.4101 [hep-ph]].

[64] G. Bevilacqua, M. Czakon, C. G. Papadopoulos and M. Worek, Phys. Rev. Lett. **104** (2010) 162002 [arXiv:1002.4009 [hep-ph]].

[65] T. Binoth *et al.*, PoS **RADCOR2009** (2010) 026 [arXiv:1001.4905 [hep-ph]].

[66] C. F. Berger, Z. Bern, L. J. Dixon, F. Febres Cordero, D. Forde, T. Gleisberg, H. Ita and D. A. Kosower *et al.*, Phys. Rev. Lett. **102** (2009) 222001 [arXiv:0902.2760 [hep-ph]].

[67] R. K. Ellis, K. Melnikov and G. Zanderighi, Phys. Rev. D **80** (2009) 094002 [arXiv:0906.1445 [hep-ph]].

[68] C. F. Berger, Z. Bern, L. J. Dixon, F. Febres Cordero, D. Forde, T. Gleisberg, H. Ita and D. A. Kosower *et al.*, Phys. Rev. D **82** (2010) 074002 [arXiv:1004.1659 [hep-ph]].

[69] A. Bredenstein, A. Denner, S. Dittmaier and S. Pozzorini, JHEP **0808** (2008) 108 [arXiv:0807.1248 [hep-ph]].

[70] G. Bevilacqua, M. Czakon, C. G. Papadopoulos and M. Worek, Phys. Rev. D **84** (2011) 114017 [arXiv:1108.2851 [hep-ph]].

[71] T. Binoth, N. Greiner, A. Guffanti, J. Reuter, J. P. Guillet and T. Reiter, Phys. Lett. B **685** (2010) 293 [arXiv:0910.4379 [hep-ph]]; N. Greiner, A. Guffanti, T. Reiter and J. Reuter, Phys. Rev. Lett. **107** (2011) 102002 [arXiv:1105.3624 [hep-ph]].

[72] A. Denner, S. Dittmaier, S. Kallweit and S. Pozzorini, Phys. Rev. Lett. **106** (2011) 052001 [arXiv:1012.3975 [hep-ph]].

[73] T. Melia, K. Melnikov, R. Rontsch and G. Zanderighi, JHEP **1012** (2010) 053 [arXiv:1007.5313 [hep-ph]].

[74] T. Melia, K. Melnikov, R. Rontsch and G. Zanderighi, Phys. Rev. D **83** (2011) 114043 [arXiv:1104.2327 [hep-ph]].

[75] Z. Bern, G. Diana, L. J. Dixon, F. Febres Cordero, S. Hoeche, D. A. Kosower, H. Ita and D. Maitre *et al.*, arXiv:1112.3940 [hep-ph].

[76] G. Bevilacqua, M. Czakon, A. van Hameren, C. G. Papadopoulos and M. Worek, JHEP **1102** (2011) 083 [arXiv:1012.4230 [hep-ph]].

[77] V. S. Fadin, V. A. Khoze and A. D. Martin, Phys. Rev. D **49** (1994) 2247.

[78] R. Frederix, S. Frixione, K. Melnikov and G. Zanderighi, JHEP **1011** (2010) 050 [arXiv:1008.5313 [hep-ph]].

[79] C. F. Berger, Z. Bern, L. J. Dixon, F. Febres Cordero, D. Forde, T. Gleisberg, H. Ita and D. A. Kosower *et al.*, Phys. Rev. Lett. **106** (2011) 092001 [arXiv:1009.2338 [hep-ph]].

[80] H. Ita, Z. Bern, L. J. Dixon, F. F. Cordero, D. A. Kosower and D. Maitre, arXiv:1108.2229 [hep-ph].

[81] S. Becker, D. Goetz, C. Reuschle, C. Schwan and S. Weinzierl, Phys. Rev. Lett. **108** (2012) 032005 [arXiv:1111.1733 [hep-ph]].

[82] H. Ita and K. Ozeren, arXiv:1111.4193 [hep-ph].

8.4 J-C. Winter, S. Höche, H. Hoeth, et al. - Systematic improvement of QCD parton showers

Systematic improvement of QCD parton showers

Jan Winter [1]
PH-TH Department, CERN, CH-1211 Geneva 23, Switzerland
jwinter@cern.ch

Stefan Höche
Theory Department, SLAC National Accelerator Laboratory, Menlo Park, CA 94025, USA
shoeche@slac.stanford.edu

Hendrik Hoeth, Frank Krauss, Marek Schönherr and Korinna Zapp
IPPP, Durham University, Durham DH1 3LE, UK
hendrik.hoeth@durham.ac.uk, frank.krauss@durham.ac.uk, marek.schoenherr@durham.ac.uk, k.c.zapp@durham.ac.uk

Steffen Schumann
II. Physikalisches Institut, Universität Göttingen, D-37077 Göttingen, Germany
steffen.schumann@phys.uni-goettingen.de

Frank Siegert
Physikalisches Institut, Albert-Ludwigs-Universität Freiburg, D-79104 Freiburg, Germany
frank.siegert@cern.ch

Abstract In this contribution we will give a brief overview of the progress that has been achieved in the field of combining matrix elements and parton showers. We exemplify this by focusing on the case of electron–positron collisions and by reporting on recent developments as accomplished within the SHERPA event generation framework.

1 Monte Carlo event generation at a glance

Event generators are widely used to model the multi-hadron final states of high-energy particle collisions. For a very comprehensive review, we refer the interested reader to Ref. [1]. The underlying principle for organizing the computer simulation of events is factorization, i.e. to factorize the evolution of each event into several phases ordered according to their energy domains. We broadly distinguish two major phases governed by two different physics regimes: we can apply short-distance/perturbative methods to describe the physics at the harder energy scales while for the description of soft effects, we have to rely on phenomenological models

[1] Speaker

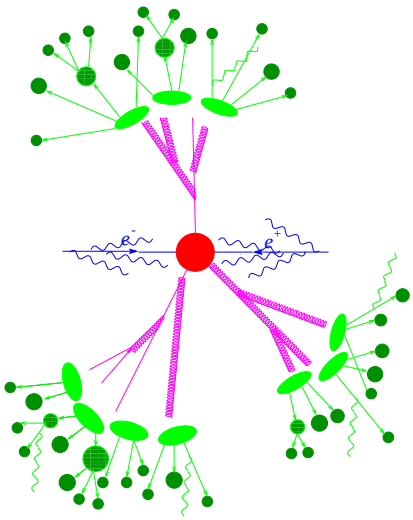

Figure 1: The various phases of Monte Carlo event generation, illustrated for lepton–lepton collisions. The outer, circular part visualizes the event evolution driven by non-perturbative dynamics (depicted by the green blobs) while the inner part shows the phases related to short-distance phenomena (depicted by the red and blue objects).

encoding our observations regarding the confinement of the collision products, a mechanism for which a rigorous understanding has not been developed yet. The separation is mainly driven by the nature of QCD where the strong coupling becomes small at large scales, such that the theory becomes asymptotically free and can be formulated in terms of partons. Contrary at scales of $\mathcal{O}(1)$ GeV, the coupling strength has increased substantially and non-perturbative dynamics dictates the evolution of the events. An extremely important property of QCD is the formation of jets, which manifest themselves as sprays of particles leaving localized energy deposits in the detectors. Correspondingly, the phases of the event generation can also be described in terms of jet production and (intra-jet) evolution, cf. e.g. Ref. [2].

Fig. 1 gives the details by showing not only the main but all phases, which we consider in Monte Carlo event generation. The phases where physics can be mastered with perturbative methods are visualized in the inner part of the figure. In blue we show the effects of initial-state radiation off the incoming leptons, which commonly are encoded in an inclusive manner by electron structure functions. The red objects visualize the hard interaction (shown by the big red blob in the middle representing the process $e^-e^+ \to q\bar{q}g$) producing energetic parton jets that give rise to subsequent QCD bremsstrahlung (shown by the branching pattern in magenta). The physics of the hard process is best described by relying on exact matrix-element expressions – with the current frontier given by n-leg tree-level ($n \sim 10$) and QCD virtual ($n \sim 5$) amplitudes – whereas all bremsstrahlung effects are described by parton showering based on matrix-element approximations that are correct in the singular phase-space regions of QCD. The phases of non-perturbative dynamics are represented by the green-coloured blobs in

the outer sphere of the figure. They depict the transition of the coloured partons into primary, unstable hadrons and their subsequent decays into stable, detectable hadrons, which can be described by phase-space or effective models. The parton–hadron conversion is "parametrized" by hadronization models, such as the renowned models of Lund string fragmentation [3] or cluster hadronization [4].

A full-fledged Monte Carlo event generator incorporates physics implementations according to all phases of event evolution, from the evaluation of scattering matrix elements to the description of hadron decays. The Monte Carlo approach is inherent to all phases: cross sections are physical objects and, hence, a probabilistic picture can be identified for each phase. We can draw events from the resulting probability densities by generating random numbers. PYTHIA [5], HERWIG [6, 7] and SHERPA [8, 9] are examples for (well) established event generators in the LHC era. Common to them is the generation of hadron-level predictions, which can be compared directly to experimental data, once the data are corrected for detector effects.

2 Parton shower basics and modern formalisms

The final states of the hard interactions often produce partons that are still sufficiently energetic to induce further radiation, because there is enough time for them to interact perturbatively before hadronization sets in. Owing to the singularity structure intrinsic to QCD, these emissions preferably populate the collinear and soft regions of phase space, and very conveniently it is in these limits that QCD amplitudes factorize. This can be taken further, i.e. be promoted to a factorization at the cross-section level:

$$d\sigma_{n+1} \;=\; d\sigma_n \;\frac{\alpha_s(t)}{2\pi}\;\frac{dt}{t}\;dz\;P_{a\to bc}(z)\;. \tag{1}$$

Here α_s, $t \equiv p_a^2$ and z respectively denote the strong coupling constant, the propagator and the momentum-fraction variable used in the splitting process. The function $P_{a\to bc}(z)$ characterizes the parton splitting $a \to bc$ (e.g. $q \to qg$) in detail, encoding the functional dependence on z, and possibly the splitting angle. For example, if one considers the leading collinear region, i.e. small-angle radiation off outgoing partons, the Altarelli–Parisi (or DGLAP) splitting functions are obtained; a nice introduction to the subject can be found in [10]. Eq. (1) expresses more than factorization of the multi-parton cross section, it ultimately forms the basis for a recursive definition of multiple emissions ordered in t. As a result collinear/soft partons can be added in an iterative procedure, and we arrive at an emission pattern as shown in Fig. 1 where the initially energetic $q\bar{q}g$ partonic ensemble has evolved down to a scale (magnitude of the ordering variable t) of the order of $t^{1/2} \sim 1$ GeV. This (i) regulates the (collinear) divergences and (ii) sets a scale conveniently close to the onset of hadronization. Emissions below this cut-off are said to be unresolvable. The iterative scheme ensures that all kinematically enhanced contributions are taken into account, which from a more formal point of view means that the leading logarithmic (LL) terms are summed up to all orders. The enhancements are manifest in the intra-jet evolution and in the rapid particle multiplicity growth, both of which being well described by the parton shower approximation.

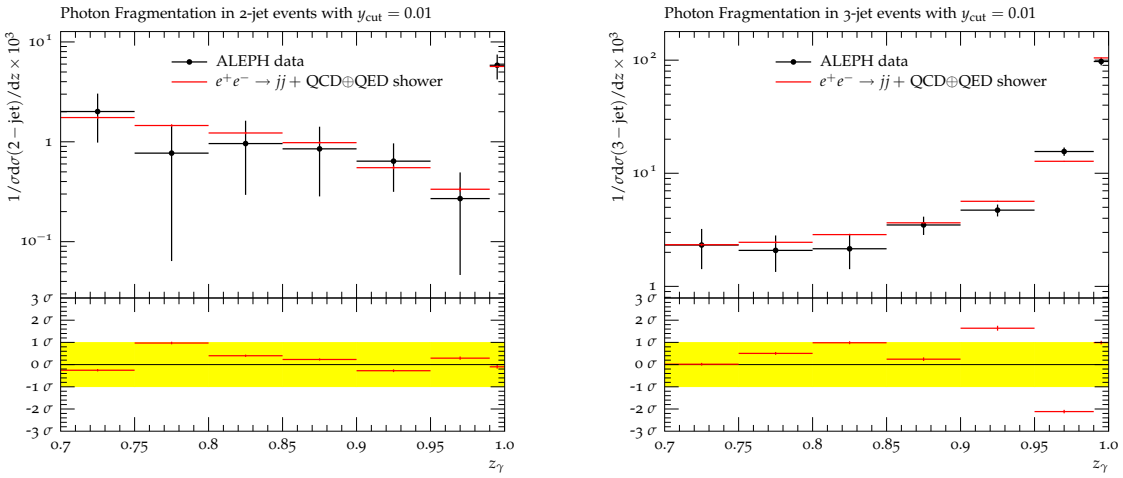

Figure 2: The z_γ distribution as measured by ALEPH in hadronic Z^0 decays at LEP1 [37] and predicted by SHERPA's QCD+QED CSSHOWER evolution added to $e^-e^+ \to q\bar{q}$ hard scatterings.

Over the last decade the activities in the field of parton shower modelling have been seen to be intensified for several reasons; there was a push for designing new Monte Carlo programs for the LHC era resulting in a careful revision of existing programs.[2] There was also a strong demand to adjust parton showers to work well with input from (multi-leg and loop) higher-order matrix elements, and furthermore to interconnect them with models for multiple parton interactions and the underlying event. These efforts led to a number of refinements in shower algorithms and, moreover, the construction of new parton showers [14, 15, 16, 17, 18, 19, 20, 21, 22, 23, 24, 25, 26, 27, 28, 29]. We want to illustrate this very briefly by presenting two selected results obtained from dipole-like shower schemes developed within the SHERPA collaboration.

2.1 Example – SHERPA's CSSHOWER

The CSSHOWER was derived from the dipole subtraction formalism used in next-to-leading order (NLO) calculations where CS stands for the names of the pioneers of this formalism, Catani and Seymour. To construct the shower algorithm, in particular its corresponding splitting functions, one exploits the dipole factorization of the real-emission matrix elements; the various CS dipole functions are translated into shower kernels by working in 4 dimensions, the large N_C limit, and averaging over spins. This was originally described in [16] and worked out in detail, as well as implemented, in Refs. [20, 21]; furthermore, dipole showers were verified to reproduce the DGLAP equation [30, 31, 32]. The CSSHOWER entails nice properties such as its Lorentz-invariant formulation, on-shell splitting kinematics with rather local recoil compensation by spectator partons, exact/complete phase-space mapping of emissions and an inherent inclusion of soft colour coherence. Nevertheless, for the production of vector bosons in hadronic collisions, one (rather minor) shortcoming of the initially proposed NLO-like recoil strategy particularly

[2] The next-generation programs PYTHIA8 [11] and HERWIG++ [12, 13] emerged from this initiative.

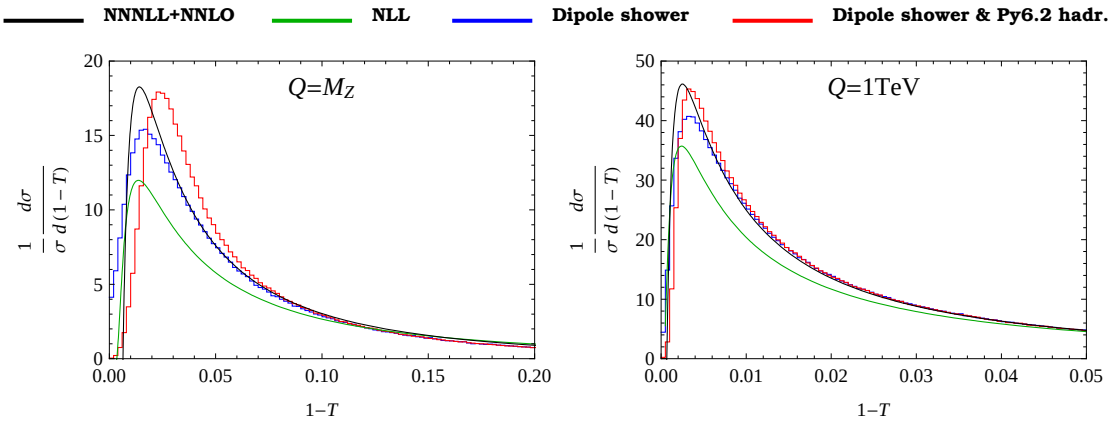

Figure 3: The all-particle one-minus-thrust event shapes in electron–positron annihilation at LEP1 and TeV energies. The comparison is between analytical results at N^{3}LL+NNLO and NLL accuracy (black and green curves), and numerical results obtained from SHERPA's colour dipole model neglecting/including hadronization corrections (blue/red histograms).

was discussed in the literature [33]. Unlike in b-space exponentiation this recoil scheme does not generate the vector boson p_T spectra continuously through each emission, but finally resolutions were put forward as in [34, 35, 36].

The CSSHOWER allows for the straightforward inclusion of QED effects; technically there is almost no difference between a $q \to q\gamma$ and $q \to qg$ splitting apart from the spectator concept (all oppositely charged particles in QED versus the colour-linked parton in large N_C QCD). The respective emission probabilities factorize trivially allowing a democratic treatment of photon and QCD parton radiation. This has been discussed in [35]. As an example we show in Fig. 2 results of a crucial benchmark for the combined QCD+QED CSSHOWER model, which is to reproduce the scale-dependent photon fragmentation function $D_\gamma(z_\gamma, y_{\rm cut})$ as measured by the ALEPH collaboration in hadronic Z^0 decays at LEP1 [37]. The events are classified by n-jet topologies and resolution measures $y_{\rm cut}$, and are required to have at least one reconstructed jet containing a photon with energy fraction $z_\gamma > 0.7$ and $E_\gamma > 5$ GeV. We observe a very nice agreement between simulation and data.

2.2 Example – SHERPA's dipole shower

While the CSSHOWER, incorporating $1 \to 2$ splittings, is said to be dipole-like owing to the spectator involvement in constructing the splitting kinematics, the currently unreleased shower model presented in [22] is based on exploiting the QCD property of antenna factorization in soft gluon emissions. This enables a complete $2 \to 3$ treatment of the splitting process employing $2 \to 3$ splitting functions and $2 \to 3$ kinematics. The original idea goes back to the pioneering work of Gustafson [38, 39] resulting in the release of the successful ARIADNE program [40].

Although, as described in Ref. [22], the goal of unifying initial- and final-state radiation into

a single perturbative framework was greatly achieved, here we only want to recall a nice result obtained during verification of the (ARIADNE-like) final-state showering of SHERPA's colour dipole model. In Fig. 3 we display various predictions for the all-particle $1 - T$ distribution in e^+e^- annihilation, where T denotes the event-shape variable thrust. By comparing directly to theoretical results from analytic resummations at next-to-LL (NLL) level and beyond, we obtain a stringent and unambiguous test of the resummation as encoded in the dipole shower without the need for hadronization corrections.[3] The pure shower results turn out to be significantly different from the NLL predictions (green curves), they actually are closer to the N^{3}LL resummed results [41], which were calculated using soft-collinear effective theory and matched to NNLO predictions [42, 43]. This is a rather remarkable result for the dipole shower.

3 Higher precision for parton shower predictions

Traditionally it was PSs (parton showers) that were used to describe any additional jet activity, including the production of further hard jets. The shower "seeds" are given by QCD LO processes for a fixed final-state multiplicity. For these reasons, parton shower algorithms are said to describe multi-jet production at the LO+LL level. But there are a number of limitations to this description. Shower algorithms only represent the semi-classical picture of the entire branching process: quantum interferences and multi-parton correlations are hardly taken into account, and the whole evolution is only formulated in the limit of a large number of colours, N_C. The application of the shower approximations outside the singular regions of QCD leads to uncontrolled behaviour and highly inaccurate predictions for rather energetic and/or large-angle radiation; shower uncertainties can therefore get large, and in general they are not easy to assess, which has the potential danger of partly compensating for missing perturbative effects via the tuning of non-perturbative parameters.

It was clear, to systematically correct for these deficiencies, the shower generators had to be improved by using more precise MEs (matrix elements). Motivated by the ground-breaking advances in efficiently calculating multi-leg MEs at tree and, more recently, even loop level, the theoretical effort in enhancing the accuracy of PSs has resulted in two new developments with significant impact on doing collider phenomenology (cf. e.g. [44]): tree-level matrix elements merged with parton showers (ME+PS), and NLO calculations interfaced (or matched) with parton showers (NLO+PS). The former primarily originated from the Catani–Krauss–Kuhn–Webber (CKKW) paper [45], with the innovative idea to correct the first few hardest shower emissions by using exact tree-level matrix-element expressions. A vast body of literature has appeared subsequently, advocating several variants, implementations and refinements to the original method (see Refs. [46, 47, 1, 48] for a review). Well-known variants include CKKW [45, 49, 50], Lönnblad-CKKW [51, 52], Mangano's MLM method [53, 54] and the versions of matrix-element and truncated-shower merging (ME&TS) [55, 56], all producing so-called *improved* LO+LL descriptions of multi-jet observables.

[3] Hadronization corrections are on the order of $1/Q$ (see Fig. 3), broaden all jets and shift the results towards smaller T as seen by comparing the red and blue histograms.

The NLO+PS development was initiated by the MC@NLO papers [57, 58] and followed later by the POWHEG proposal [59, 60]. Both approaches aim at improving the event generation of a basic process in such a way that NLO accuracy is reached for inclusive observables, while maintaining the LL accuracy of the shower approach. Essentially, this is achieved by raising the order of precision of the underlying core process. In the context of multi-jet production, we then arrive at a description accurate at NLO+LL level (see Ref. [61, 48] for a very recent review). In both cases, ME+PS and NLO+PS, we have to solve two major problems simply because MEs and PSs can describe the same final state: the emission phase space has to be covered in a way that double counting of contributions is removed and dead regions are avoided at the same time.

The theoretical effort behind these two developments has led to enormous progress in the last decade regarding the systematic embedding of higher-order QCD corrections in multi-purpose Monte Carlo event generators. PYTHIA, HERWIG and SHERPA provide solutions (partly relying on interfaces to specialized tools) and implementations to make these developments available in experimental analyses and collider studies. Using the new tools, we have found better agreement to a broad range of QCD jet data taken at lepton and hadron colliders. We have gained better control over the systematic uncertainties of the generator predictions, and generally have been able to reduce these uncertainties. In the remainder of this contribution, we will quickly summarize the status of the ME+PS and NLO+PS techniques in SHERPA.

3.1 ME&TS in SHERPA

The ME&TS implementation in SHERPA is state-of-the-art. Predictions are obtained from merging tree-level matrix elements for X plus $0, \ldots, n$-parton final states with the CSSHOWER, while preserving the LL accuracy to which soft and collinear multiple emissions are described by the CSSHOWER. The new ME&TS merging scheme was introduced in Ref. [55] and optimized as documented in Refs. [35, 36] to improve over the original SHERPA implementation based on the CKKW approach [45, 49, 62, 63]. ME&TS guarantees great compatibility between the (Q) scales used to resolve the matrix-element final states and those (t) scales ordering and driving the parton showering. In particular, truncated showering has been enabled to insert important soft emissions between resolved parton jet seeds. These shower emissions themselves do not give rise to jets but are necessary to retain the accuracy of the shower evolution, for example restore soft colour coherence. The very basic steps of the ME&TS algorithm are:

Separate phase space into a "hard" ME ($Q > Q_{\text{cut}}$) and "soft" PS ($Q < Q_{\text{cut}}$) domain according to a suitably chosen infrared-safe jet criterion. This factorizes the shower kernels similarly and regularizes the matrix elements. Via "inverted" showering one then finds the likely PS histories for the generated n-parton MEs. Based on the selected history one further evolves (using the t scales) the ME final state beyond n partons unless one encounters a shower emission above Q_{cut} resulting in the rejection of the event. This way one replaces the shower kernels in the ME domain by exact ME expressions for the hardest n jets, and ensures that rejected events are to be described by $(n+1)$-parton MEs.

We exemplify the performance of SHERPA's ME&TS merging by showing differential jet rates

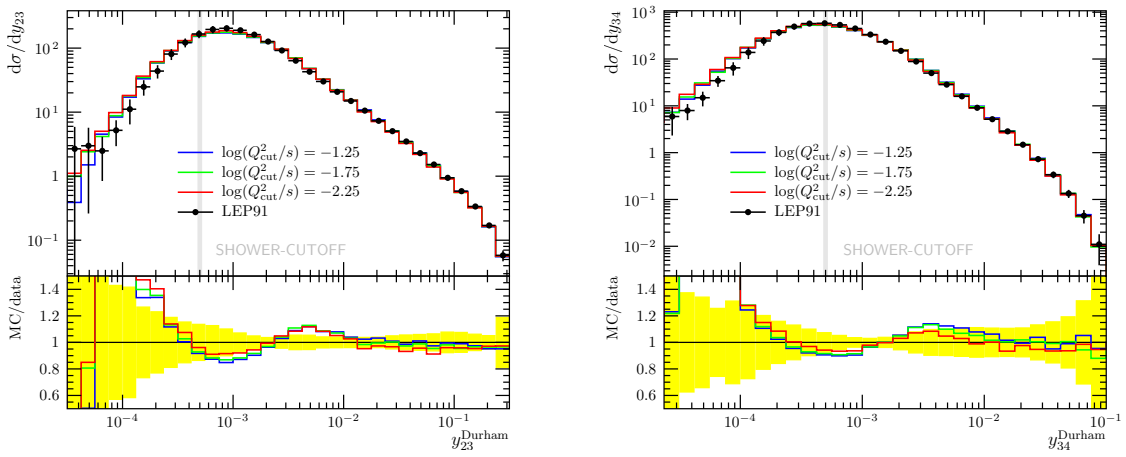

Figure 4: Differential Durham jet rates obtained from a SHERPA ME&TS sample where up to 6 jets are described by MEs. Results are shown for 3 different choices of the merging-cut parameter and compared to LEP1 data [64].

for e^+e^- annihilation into hadrons. The ME&TS sample was generated by including matrix elements with up to four extra partons (u, d, s, c, b quarks and gluons). The $y_{n\,n+1}$ distributions show at which rate, according to the Durham k_T algorithm, $n+1$ jets are clustered into n jets as a function of (the resolution parameter) $y_{n\,n+1} \approx Q^2_{n\,n+1}/s$. The observable is very sensitive to the jet emission pattern, therefore, lends itself eminently to assess the $Q_{\rm cut} = \sqrt{s\,y_{\rm cut}}$ parameter dependence of the ME&TS merging. Fig. 4 shows predictions for various $Q_{\rm cut}$, found to be in good agreement with data from LEP1 ($\sqrt{s} = 91.25$ GeV) [64]. Owing to the ME inclusion the high scales are well described, while it is very reassuring to see that the good shower behaviour is maintained at medium scales. The low scales below the (marked) shower cut-off are affected by hadronization effects and related parameter tuning (not optimized here). We therefore conclude that the merging systematics is well below the 10% level, which is a remarkable improvement over earlier merging variants.

3.2 POWHEG and MENLOPS in SHERPA

The first results of a NLO+PS effort in SHERPA were published in Ref. [65]. The implementation has been based on the POWHEG formalism, which can be understood as an advancement of earlier methods developed to correct the leading shower emission by the corresponding real-emission ME [66, 67]. This was done by invoking the Sudakov veto algorithm with an additional weight to be respected, schematically written as $w(\Phi_R) = R(\Phi_R)/R^{(\rm PS)}(\Phi_R)$ where Φ_R denotes the full real-emission phase space and R ($R^{(\rm PS)}$) stands for the real-emission ME (shower) expression. The POWHEG method reweights similarly, but at the same time accounts for a local K-factor implemented through a NLO event weight $\bar{B} = B + V + I + \int d\Phi_{R|B}(R - S)$ where $\Phi_{R|B}$ is the one-particle emission phase space. This way one generates not only observable shapes showing the Sudakov suppression and ME improvement at low and high scales, respectively, but also

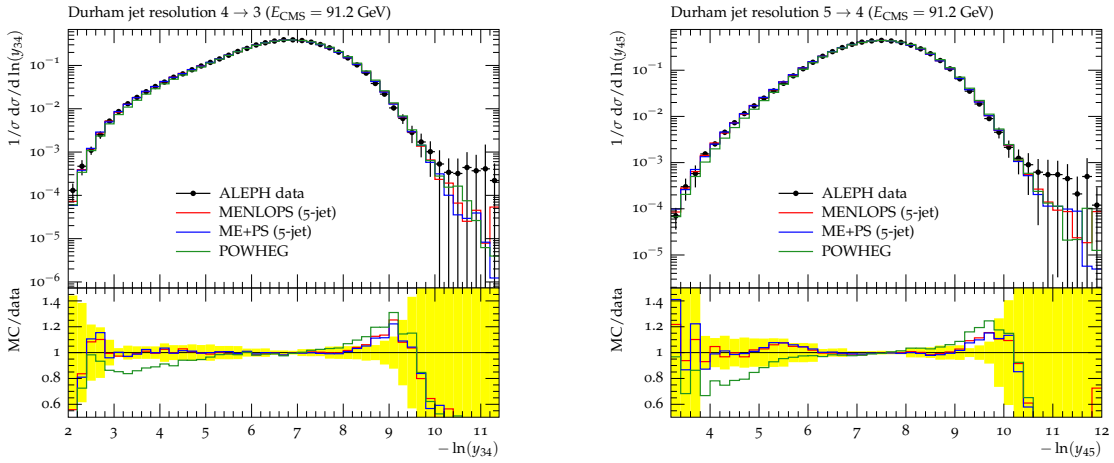

Figure 5: Differential Durham jet rates as predicted by SHERPA using three different matching schemes, POWHEG, ME&TS (up to 5 jets) and MENLOPS (up to 5 jets). The predictions are compared with LEP1 data measured by ALEPH in $e^+e^- \to$ hadrons [77].

NLO accuracy for the event sample, hence featuring a reduced scale dependence. The matching is smooth in a sense that no phase-space cut is needed as in (conventional) ME+PS methods.

SHERPA possesses almost all ingredients that make a POWHEG automation possible: automated tree-level ME generators provide the Born (B) and real-emission (R) terms [68, 69], the integrated and explicit subtraction terms (I and S) are given by the automated implementation of the CS dipole subtraction formalism [70] and the virtual contributions (V) are obtained via interfacing to one-loop ME libraries as facilitated e.g. by BLACKHAT [71], GOSAM [72] or MCFM [73] using the Binoth Les Houches Accord [74]. Last but not least the CSSHOWER is well suited for combination with the ME computations; its $R^{(\mathrm{PS})}(\Phi_R)$ often closely approximate the $R(\Phi_R)$ resulting in a very reasonable distribution of the $w(\Phi_R)$ weights.

With the ME+PS facilities in SHERPA at hand, it suggests itself to aim at fusing the POWHEG and ME+PS approaches. This effort goes under the name MENLOPS, and its key idea is to slice the POWHEG phase space in ME+PS style into two domains, the NLO core process domain and the multi-jet domain. MENLOPS has been developed very recently by two groups as documented in Ref. [75] and Ref. [76]. The method exhibits what is cutting edge in combining higher-order calculations with PSs. To understand the slicing into domains, we schematically write down the expression for an observable $\langle O \rangle$ in the MENLOPS scheme:

$$\begin{aligned}\langle O \rangle \;=\; \int d\Phi_B\, \bar{B}(\Phi_B) \Bigg[& \underbrace{\Delta^{(\mathrm{ME})}(t_0,\mu^2)\, O(\Phi_B)}_{\text{unresolved}} + \sum_{ij,k} \frac{1}{16\pi^2} \int_{t_0}^{\mu^2} dt \int_{z_-}^{z_+} dz \int_0^{2\pi} \frac{d\phi}{2\pi}\, \frac{R_{ij,k}(\Phi_R)}{B(\Phi_B)}\, O(\Phi_R) \\ \times \;& \Big(\underbrace{\Delta^{(\mathrm{ME})}(t,\mu^2)\, \Theta(Q_{\mathrm{cut}} - Q_{ij,k})}_{\text{resolved, PS domain}} + \underbrace{\Delta^{(\mathrm{PS})}(t,\mu^2)\, \Theta(Q_{ij,k} - Q_{\mathrm{cut}})}_{\text{resolved, ME domain}} \Big) \Bigg] \end{aligned} \tag{2}$$

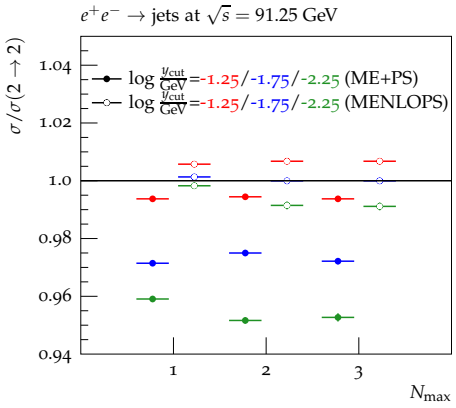

Figure 6: Parameter dependence of the total inclusive cross section as predicted by ME&TS and MENLOPS in SHERPA for $e^+e^- \to$ jets at LEP1. The cross sections are shown as a function of N_{max} for 3 different values of the merging cut. Note that the ME&TS and MENLOPS results are normalized to the LO and NLO cross sections, respectively. N_{max} denotes up to which multiplicity $(n+2)$-parton MEs are taken into account.

where Φ_B, μ^2 and t_0 denote the Born phase space, factorization/high scale and infrared cut-off, respectively. The one-particle emission phase space $\Phi_{R|B}$ is written explicitly, the sum is over the relevant CS dipoles, and the POWHEG and CSSHOWER Sudakov form factors (no-branching probabilities), $\Delta^{(\text{ME})}$ and $\Delta^{(\text{PS})}$, differ from each other by using the R/B and CSSHOWER kernels, respectively. The domains can be read off Eq. (2) pretty conveniently. The PS (or POWHEG) domain is restricted to no resolved and soft emissions ($Q < Q_{\text{cut}}$) preserving the NLO accuracy for inclusive observables. The hard (higher-order) emissions ($Q > Q_{\text{cut}}$) are described by the ME (or ME+PS) domain guaranteeing the LO+LL accuracy of each resolved jet emission. Note that before fusing the contributions, the ME+PS part has to be multiplied by the K-factor $\bar{B}(\Phi_B)/B(\Phi_B)$, as shown in Eq. (2). In SHERPA this K-factor is applied locally, i.e. on an event-by-event basis.

MENLOPS hence inherits the good features of NLO+PS and ME+PS, which we demonstrate in Figs. 5 and 6.[4] The differential jet rates for $e^+e^- \to$ hadrons in Fig. 5 prove that the shapes of MENLOPS and ME&TS essentially are identical, and in very good agreement with the data [77] over the entire perturbative regime (which is to the left in these plots). In contrast the POWHEG predictions fall short in describing the region of hard multiple jets. We display in Fig. 6 the parameter dependence of the MENLOPS and ME&TS total inclusive cross sections to show that NLO accuracy for the core process leads to a NLO-like correction and stabilization of the MENLOPS cross sections. In the POWHEG case ($Q_{\text{cut}} \to \infty$) we were to find that the term in the square bracket of Eq. (2) would integrate to one, much like as in the pure parton shower case. The phase-space slicing in ME+PS and in MENLOPS necessarily generates a mismatch in the non-logarithmic structure as given by the bracket term resulting in deviations from the

[4]The NLO predictions shown in these plots were obtained by using virtual MEs provided by BLACKHAT [71].

LO (ME+PS) and NLO (MEnloPS) cross sections.[5] As shown in Fig. 6, the parameter dependence of the MEnloPS cross section is smaller maintaining the NLO accuracy almost completely. This is where MEnloPS improves over ME+PS.

4 Conclusions and outlook

Parton showers have been continuously improved and modernized over the last years. The demand for improvement has come from measurements reaching (for) higher precision at current hadron and future linear colliders. The feasibility to aim at improvement came with the fantastic advances in efficiently computing multi-leg tree-level and one-loop amplitudes, including their integration over phase space. Two directions have been established for systematically enhancing the capabilities of parton showers:

1. Parton showers are improved by merging them with real-emission matrix elements for hard radiation (ME+PS). This is the new standard in the LHC era. Alpgen [78], MadGraph/Event [79, 80] and Sherpa are widely used. The new ME+PS scheme in Sherpa, ME&TS (available since versions 1.2), greatly helped reduce the systematic uncertainties of older Sherpa predictions. When compared to data, ME+PS predictions describe plenty of the measured shapes enabling the application of global K-factors that can be determined by higher-order calculations of the total inclusive cross section or the measurements themselves.

2. Parton showers are improved by matching them with NLO calculations (NLO+PS). Powheg [81, 82, 83] and MC@nlo [84, 85, 86] have a number of processes available.[6] For the latter, aMC@nlo [93, 94], the new, automated MC@nlo framework developed by Frixione et al. in principle allows for tackling arbitrary processes provided the necessary amount of computer resources is available. Sherpa's NLO+PS effort has been re-directed towards a MC@nlo-like strategy for many reasons; after gaining experience using a Powheg-like method [65, 76], it became clear that among other things a MC@nlo-like technique allows for much better control of the exponentiated terms, cf. [95, 96].

Both directions are very active fields of research, and MEnloPS actually emerged as a first successful attempt in fusing NLO calculations with tree-level higher-order matrix elements. While MC@nlo and Powheg give shower predictions of improved accuracy in the basic process, MEnloPS and ME+PS give improved multi-jet predictions. MEnloPS capabilities are enhanced over ME+PS regarding stability and accuracy of the total inclusive cross section.

The frontier has been pushed as documented by many recent publications [97, 98, 99, 100, 101, 102, 103, 96, 104]; for example, NLO+PS techniques were applied to calculate $W + 2$ and $W + 3$ jets. The former result was computed by aMC@nlo [103], while the latter result is a

[5] The "unitarity violations" indicate the potential size of beyond NLO corrections; note that the pure Powheg phase-space slicing effect is shown for $N_{\max} = 1$.

[6] Similar/Alternative approaches have been presented by other groups, e.g. [87, 19, 88, 89, 25, 90, 91, 92].

documentation of the remarkable capabilities of the MC@NLO implementation that has become available in SHERPA lately [96], provided efficient "one-loop engines" like BLACKHAT are interfaced as done in this $W + 3$-jet SHERPA computation.

The above examples clearly demonstrate that NLO+PS for multi-jet final states is no magic anymore, it is doable owing to the advances in NLO calculations in the multi-jet realm. This actually brings ME+PS@NLO within reach. First proposals have already appeared in the literature [105]. The naive combination in form of NLO Exclusive Sums discussed for $W + 0, \ldots, 4$ jets in [48] has been shown to work surprisingly well. To go towards ME+PS@NLO, it will be necessary to replace each naive Exclusive-Sums jet veto at the respective NLO accuracy by a jet veto at least accurate at $\mathcal{O}(\alpha_s^{m+1})$ where m is the highest LO jet multiplicity (i.e. $m = 4$ in the above example).

No matter which of these methods is finally used for phenomenological studies, in all cases it is absolutely crucial to be able to provide reliable estimates of the theoretical uncertainties of the calculations. Comparisons between N(N)LO, NLO+PS, ME+PS, MENLOPS are mandatory to broaden our understanding regarding these issues [48].

Acknowledgments

JW thanks the organizers for having created an excellent workshop experience. SH's work is supported by the US Department of Energy under contract DE-AC02-76SF00515, and in part by the US National Science Foundation, Grant NSF-PHY-0705682, (The LHC Theory Initiative). MS's work is supported by the Research Executive Agency (REA) of the European Union under the Grant Agreement number PITN-GA-2010-264564 (LHCPhenoNet). FS's is supported by the German Research Foundation (DFG) via Grant DI 784/2-1.

References

[1] A. Buckley, J. Butterworth, S. Gieseke, D. Grellscheid, S. Höche, H. Hoeth, F. Krauss and L. Lönnblad *et al.*, *Phys. Rept.* **504** (2011) 145 [arXiv:1101.2599 [hep-ph]].

[2] J. Winter, "QCD jet evolution at high and low scales", PhD thesis (2008).

[3] B. Andersson, G. Gustafson, G. Ingelman and T. Sjöstrand, *Phys. Rept.* **97** (1983) 31.

[4] B. R. Webber, *Nucl. Phys. B* **238** (1984) 492.

[5] T. Sjöstrand, S. Mrenna and P. Z. Skands, *JHEP* **0605** (2006) 026 [hep-ph/0603175].

[6] G. Corcella, I. G. Knowles, G. Marchesini, S. Moretti, K. Odagiri, P. Richardson, M. H. Seymour and B. R. Webber, *JHEP* **0101** (2001) 010 [hep-ph/0011363].

[7] G. Corcella, I. G. Knowles, G. Marchesini, S. Moretti, K. Odagiri, P. Richardson, M. H. Seymour and B. R. Webber, hep-ph/0210213.

[8] T. Gleisberg, S. Höche, F. Krauss, A. Schälicke, S. Schumann and J. Winter, *JHEP* **0402** (2004) 056 [hep-ph/0311263].

[9] T. Gleisberg, S. Höche, F. Krauss, M. Schönherr, S. Schumann, F. Siegert and J. Winter, *JHEP* **0902** (2009) 007 [arXiv:0811.4622 [hep-ph]].

[10] R. K. Ellis, W. J. Stirling and B. R. Webber, *Camb. Monogr. Part. Phys. Nucl. Phys. Cosmol.* **8** (1996) 1.

[11] T. Sjöstrand, S. Mrenna and P. Z. Skands, *Comput. Phys. Commun.* **178** (2008) 852 [arXiv:0710.3820 [hep-ph]].

[12] M. Bähr, S. Gieseke, M. A. Gigg, D. Grellscheid, K. Hamilton, O. Latunde-Dada, S. Plätzer and P. Richardson *et al.*, *Eur. Phys. J. C* **58** (2008) 639 [arXiv:0803.0883 [hep-ph]].

[13] S. Gieseke, D. Grellscheid, K. Hamilton, A. Papaefstathiou, S. Plätzer, P. Richardson, C. A. Röhr and P. Ruzicka *et al.*, arXiv:1102.1672 [hep-ph].

[14] S. Gieseke, P. Stephens and B. R. Webber, *JHEP* **0312** (2003) 045 [hep-ph/0310083].

[15] T. Sjöstrand and P. Z. Skands, *Eur. Phys. J. C* **39** (2005) 129 [hep-ph/0408302].

[16] Z. Nagy and D. E. Soper, *JHEP* **0510** (2005) 024 [hep-ph/0503053] and hep-ph/0601021.

[17] C. W. Bauer and F. J. Tackmann, *Phys. Rev. D* **76** (2007) 114017 [arXiv:0705.1719 [hep-ph]].

[18] Z. Nagy and D. E. Soper, *JHEP* **0709** (2007) 114 [arXiv:0706.0017 [hep-ph]].

[19] W. T. Giele, D. A. Kosower and P. Z. Skands, *Phys. Rev. D* **78** (2008) 014026 [arXiv:0707.3652 [hep-ph]].

[20] M. Dinsdale, M. Ternick and S. Weinzierl, *Phys. Rev. D* **76** (2007) 094003 [arXiv:0709.1026 [hep-ph]].

[21] S. Schumann and F. Krauss, *JHEP* **0803** (2008) 038 [arXiv:0709.1027 [hep-ph]].

[22] J. Winter and F. Krauss, *JHEP* **0807** (2008) 040 [arXiv:0712.3913 [hep-ph]].

[23] C. W. Bauer, F. J. Tackmann and J. Thaler, *JHEP* **0812** (2008) 010 [arXiv:0801.4026 [hep-ph]] and *JHEP* **0812** (2008) 011 [arXiv:0801.4028 [hep-ph]].

[24] R. Corke and T. Sjöstrand, *Eur. Phys. J. C* **69** (2010) 1 [arXiv:1003.2384 [hep-ph]].

[25] W. T. Giele, D. A. Kosower and P. Z. Skands, *Phys. Rev. D* **84** (2011) 054003 [arXiv:1102.2126 [hep-ph]].

[26] A. Gehrmann-De Ridder, M. Ritzmann and P. Z. Skands, *Phys. Rev. D* **85** (2012) 014013 [arXiv:1108.6172 [hep-ph]].

[27] W. Kilian, J. Reuter, S. Schmidt and D. Wiesler, *JHEP* **1204** (2012) 013 [arXiv:1112.1039 [hep-ph]].

[28] S. Plätzer and M. Sjödahl, arXiv:1201.0260 [hep-ph].

[29] Z. Nagy and D. E. Soper, arXiv:1202.4496 [hep-ph].

[30] Y. L. Dokshitzer and G. Marchesini, *JHEP* **0903** (2009) 117 [arXiv:0809.1749 [hep-ph]].

[31] Z. Nagy and D. E. Soper, *JHEP* **0905** (2009) 088 [arXiv:0901.3587 [hep-ph]].

[32] P. Z. Skands and S. Weinzierl, *Phys. Rev. D* **79** (2009) 074021 [arXiv:0903.2150 [hep-ph]].

[33] Z. Nagy and D. E. Soper, *JHEP* **1003** (2010) 097 [arXiv:0912.4534 [hep-ph]].

[34] S. Plätzer and S. Gieseke, *JHEP* **1101** (2011) 024 [arXiv:0909.5593 [hep-ph]].

[35] S. Höche, S. Schumann and F. Siegert, *Phys. Rev. D* **81** (2010) 034026 [arXiv:0912.3501 [hep-ph]].

[36] T. Carli, T. Gehrmann and S. Höche, *Eur. Phys. J. C* **67** (2010) 73 [arXiv:0912.3715 [hep-ph]].

[37] D. Buskulic *et al.* [ALEPH Collaboration], *Z. Phys. C* **69** (1996) 365.

[38] G. Gustafson, *Phys. Lett. B* **175** (1986) 453.

[39] G. Gustafson and U. Pettersson, *Nucl. Phys. B* **306** (1988) 746.

[40] L. Lönnblad, *Comput. Phys. Commun.* **71** (1992) 15.

[41] T. Becher and M. D. Schwartz, *JHEP* **0807** (2008) 034 [arXiv:0803.0342 [hep-ph]].

[42] A. Gehrmann-De Ridder, T. Gehrmann, E. W. N. Glover and G. Heinrich, *Phys. Rev. Lett.* **99** (2007) 132002 [arXiv:0707.1285 [hep-ph]].

[43] A. Gehrmann-De Ridder, T. Gehrmann, E. W. N. Glover and G. Heinrich, *JHEP* **0712** (2007) 094 [arXiv:0711.4711 [hep-ph]].

[44] J. D. Lykken, A. Martin and J. Winter, arXiv:1111.2881 [hep-ph].

[45] S. Catani, F. Krauss, R. Kuhn and B. R. Webber, *JHEP* **0111** (2001) 063 [hep-ph/0109231].

[46] J. Alwall, S. Höche, F. Krauss, N. Lavesson, L. Lönnblad, F. Maltoni, M. L. Mangano and M. Moretti *et al.*, *Eur. Phys. J. C* **53** (2008) 473 [arXiv:0706.2569 [hep-ph]].

[47] N. Lavesson and L. Lönnblad, *JHEP* **0804** (2008) 085 [arXiv:0712.2966 [hep-ph]].

[48] J. A. Maestre, S. Alioli, J. R. Andersen, R. D. Ball, A. Buckley, M. Cacciari, F. Campanario and N. Chanon *et al.*, arXiv:1203.6803 [hep-ph].

[49] F. Krauss, *JHEP* **0208** (2002) 015 [hep-ph/0205283].

[50] S. Mrenna and P. Richardson, *JHEP* **0405** (2004) 040 [hep-ph/0312274].

[51] L. Lönnblad, *JHEP* **0205** (2002) 046 [hep-ph/0112284].

[52] L. Lönnblad and S. Prestel, *JHEP* **1203** (2012) 019 [arXiv:1109.4829 [hep-ph]].

[53] M. L. Mangano, M. Moretti and R. Pittau, *Nucl. Phys. B* **632** (2002) 343 [hep-ph/0108069].

[54] M. L. Mangano, M. Moretti, F. Piccinini and M. Treccani, *JHEP* **0701** (2007) 013 [hep-ph/0611129].

[55] S. Höche, F. Krauss, S. Schumann and F. Siegert, *JHEP* **0905** (2009) 053 [arXiv:0903.1219 [hep-ph]].

[56] K. Hamilton, P. Richardson and J. Tully, *JHEP* **0911** (2009) 038 [arXiv:0905.3072 [hep-ph]].

[57] S. Frixione and B. R. Webber, *JHEP* **0206** (2002) 029 [hep-ph/0204244].

[58] S. Frixione, P. Nason and B. R. Webber, *JHEP* **0308** (2003) 007 [hep-ph/0305252].

[59] P. Nason, *JHEP* **0411** (2004) 040 [hep-ph/0409146].

[60] S. Frixione, P. Nason and C. Oleari, *JHEP* **0711** (2007) 070 [arXiv:0709.2092 [hep-ph]].

[61] P. Nason and B. R. Webber, arXiv:1202.1251 [hep-ph].

[62] F. Krauss, A. Schälicke, S. Schumann and G. Soff, *Phys. Rev. D* **70** (2004) 114009 [hep-ph/0409106] and *Phys. Rev. D* **72** (2005) 054017 [hep-ph/0503280].

[63] T. Gleisberg, F. Krauss, A. Schälicke, S. Schumann and J. Winter, *Phys. Rev. D* **72** (2005) 034028 [hep-ph/0504032].

[64] P. Pfeifenschneider *et al.* [JADE and OPAL Collaborations], *Eur. Phys. J. C* **17** (2000) 19 [hep-ex/0001055].

[65] S. Höche, F. Krauss, M. Schönherr and F. Siegert, *JHEP* **1104** (2011) 024 [arXiv:1008.5399 [hep-ph]].

[66] M. H. Seymour, *Nucl. Phys. B* **436** (1995) 443 [hep-ph/9410244].

[67] G. Miu and T. Sjöstrand, *Phys. Lett. B* **449** (1999) 313 [hep-ph/9812455].

[68] F. Krauss, R. Kuhn and G. Soff, *JHEP* **0202** (2002) 044 [hep-ph/0109036].

[69] T. Gleisberg and S. Höche, *JHEP* **0812** (2008) 039 [arXiv:0808.3674 [hep-ph]].

[70] T. Gleisberg and F. Krauss, *Eur. Phys. J. C* **53** (2008) 501 [arXiv:0709.2881 [hep-ph]].

[71] C. F. Berger, Z. Bern, L. J. Dixon, F. Febres Cordero, D. Forde, H. Ita, D. A. Kosower and D. Maitre, *Phys. Rev. D* **78** (2008) 036003 [arXiv:0803.4180 [hep-ph]].

[72] G. Cullen, N. Greiner, G. Heinrich, G. Luisoni, P. Mastrolia, G. Ossola, T. Reiter and F. Tramontano, arXiv:1111.2034 [hep-ph].

[73] J. M. Campbell, R. K. Ellis and C. Williams, *JHEP* **1107** (2011) 018 [arXiv:1105.0020 [hep-ph]].

[74] T. Binoth, F. Boudjema, G. Dissertori, A. Lazopoulos, A. Denner, S. Dittmaier, R. Frederix and N. Greiner *et al.*, *Comput. Phys. Commun.* **181** (2010) 1612 [arXiv:1001.1307 [hep-ph]].

[75] K. Hamilton and P. Nason, *JHEP* **1006** (2010) 039 [arXiv:1004.1764 [hep-ph]].

[76] S. Höche, F. Krauss, M. Schönherr and F. Siegert, *JHEP* **1108** (2011) 123 [arXiv:1009.1127 [hep-ph]].

[77] A. Heister *et al.* [ALEPH Collaboration], *Eur. Phys. J. C* **35** (2004) 457.

[78] M. L. Mangano, M. Moretti, F. Piccinini, R. Pittau and A. D. Polosa, *JHEP* **0307** (2003) 001 [hep-ph/0206293].

[79] J. Alwall, P. Demin, S. de Visscher, R. Frederix, M. Herquet, F. Maltoni, T. Plehn and D. L. Rainwater *et al.*, *JHEP* **0709** (2007) 028 [arXiv:0706.2334 [hep-ph]].

[80] J. Alwall, M. Herquet, F. Maltoni, O. Mattelaer and T. Stelzer, *JHEP* **1106** (2011) 128 [arXiv:1106.0522 [hep-ph]].

[81] S. Alioli, P. Nason, C. Oleari and E. Re, *JHEP* **1006** (2010) 043 [arXiv:1002.2581 [hep-ph]].

[82] S. Alioli, K. Hamilton and E. Re, *JHEP* **1109** (2011) 104 [arXiv:1108.0909 [hep-ph]].

[83] L. Barze, G. Montagna, P. Nason, O. Nicrosini and F. Piccinini, arXiv:1202.0465 [hep-ph].

[84] P. Torrielli and S. Frixione, *JHEP* **1004** (2010) 110 [arXiv:1002.4293 [hep-ph]].

[85] S. Frixione, F. Stoeckli, P. Torrielli and B. R. Webber, *JHEP* **1101** (2011) 053 [arXiv:1010.0568 [hep-ph]].

[86] S. Frixione, F. Stoeckli, P. Torrielli, B. R. Webber and C. D. White, arXiv:1010.0819 [hep-ph].

[87] O. Latunde-Dada, S. Gieseke and B. R. Webber, *JHEP* **0702** (2007) 051 [hep-ph/0612281].

[88] K. Hamilton, P. Richardson and J. Tully, *JHEP* **0810** (2008) 015 [arXiv:0806.0290 [hep-ph]] and *JHEP* **0904** (2009) 116 [arXiv:0903.4345 [hep-ph]].

[89] A. Kardos, C. Papadopoulos and Z. Trocsanyi, *Phys. Lett. B* **705** (2011) 76 [arXiv:1101.2672 [hep-ph]].

[90] S. Plätzer and S. Gieseke, arXiv:1109.6256 [hep-ph].

[91] S. Alioli, S.-O. Moch and P. Uwer, *JHEP* **1201** (2012) 137 [arXiv:1110.5251 [hep-ph]].

[92] M. Skrzypek, S. Jadach, A. Kusina, W. Placzek, M. Slawinska and O. Gituliar, *Acta Phys. Polon. B* **42** (2011) 2433 [arXiv:1111.5368 [hep-ph]].

[93] V. Hirschi, R. Frederix, S. Frixione, M. V. Garzelli, F. Maltoni and R. Pittau, *JHEP* **1105** (2011) 044 [arXiv:1103.0621 [hep-ph]].

[94] R. Frederix, S. Frixione, V. Hirschi, F. Maltoni, R. Pittau and P. Torrielli, *Phys. Lett. B* **701** (2011) 427 [arXiv:1104.5613 [hep-ph]].

[95] S. Höche, F. Krauss, M. Schönherr and F. Siegert, arXiv:1111.1220 [hep-ph].

[96] S. Höche, F. Krauss, M. Schönherr and F. Siegert, arXiv:1201.5882 [hep-ph].

[97] S. Alioli, K. Hamilton, P. Nason, C. Oleari and E. Re, *JHEP* **1104** (2011) 081 [arXiv:1012.3380 [hep-ph]].

[98] T. Melia, P. Nason, R. Rontsch and G. Zanderighi, *Eur. Phys. J. C* **71** (2011) 1670 [arXiv:1102.4846 [hep-ph]].

[99] C. Oleari and L. Reina, *JHEP* **1108** (2011) 061 [Erratum-ibid. **1111** (2011) 040] [arXiv:1105.4488 [hep-ph]].

[100] L. D'Errico and P. Richardson, *JHEP* **1202** (2012) 130 [arXiv:1106.3939 [hep-ph]].

[101] R. Frederix, S. Frixione, V. Hirschi, F. Maltoni, R. Pittau and P. Torrielli, *JHEP* **1109** (2011) 061 [arXiv:1106.6019 [hep-ph]].

[102] M. V. Garzelli, A. Kardos, C. G. Papadopoulos and Z. Trocsanyi, *Europhys. Lett.* **96** (2011) 11001 [arXiv:1108.0387 [hep-ph]].

[103] R. Frederix, S. Frixione, V. Hirschi, F. Maltoni, R. Pittau and P. Torrielli, *JHEP* **1202** (2012) 048 [arXiv:1110.5502 [hep-ph]].

[104] J. M. Campbell, R. K. Ellis, R. Frederix, P. Nason, C. Oleari and C. Williams, arXiv:1202.5475 [hep-ph].

[105] N. Lavesson and L. Lönnblad, *JHEP* **0812** (2008) 070 [arXiv:0811.2912 [hep-ph]].

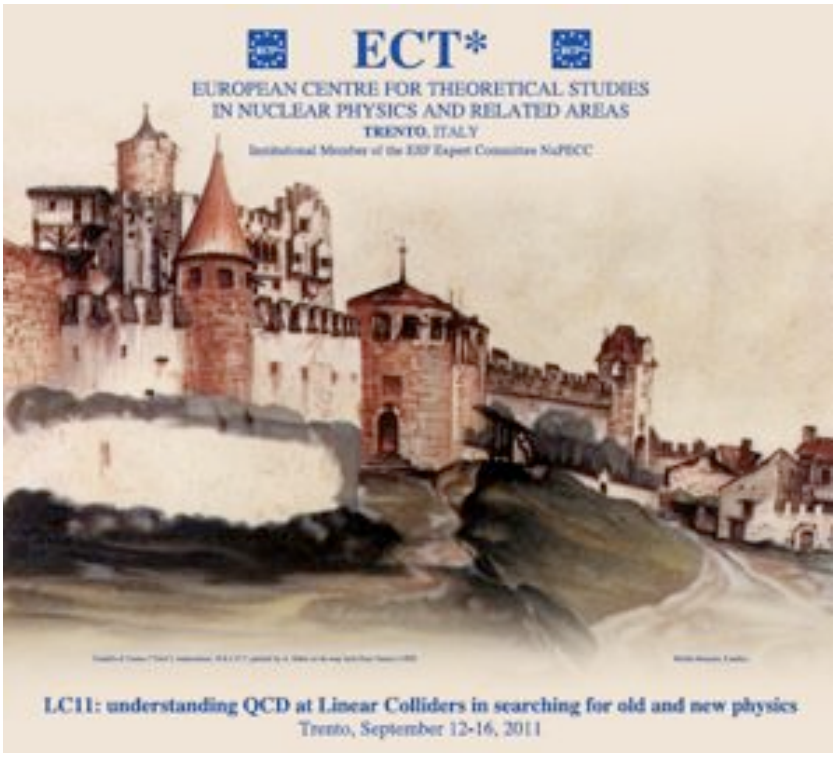

Castello di Trento painted by A. Dürer on his way back from Venice (1495).

8.5 P.F. Monni, T. Gehrmann and G. Luisoni - Thrust-distribution resummation in e^+e^- collisions

Thrust distribution resummation in e^+e^- collisions

Pier Francesco Monni [1] *and Thomas Gehrmann*
Institut für Theoretische Physik, Universität Zürich, Winterthurerstrasse 190, CH-8057 Zürich, Switzerland
E-mail: pfmonni@physik.uzh.ch, thomas.gehrmann@uzh.ch

Gionata Luisoni
Institute for Particle Physics Phenomenology, University of Durham, Science Laboratories, South Rd, Durham DH1 3LE, UK
E-mail: gionata.luisoni@durham.ac.uk

Abstract In this talk we report on the recent progresses on IR logarithms resummation for the Thrust distribution in e^+e^- collisions. Using renormalisation group (RG) evolution in Laplace space, the resummation of logarithmically enhanced corrections is performed to next-to-next-to-leading logarithmic (NNLL) accuracy. To combine the resummed expressions with the fixed-order results, we derive the $\log(R)$-matching and R-matching of the NNLL approximation to the fixed-order NNLO distribution.

1 Introduction

Event-shapes are observables which measure the geometrical properties of energy-momentum flow in a hadronic final state. They have been precisely measured over a broad range in energies at electron-positron colliders. The event-shape distributions allow for a detailed probe of the dynamics of QCD and especially for a precise determination of the strong coupling constant α_s. Owing to their infrared and collinear safety, they can be computed systematically in perturbation theory. The fixed-order description, based on a power series expansion of the distribution in the strong coupling constant, is reliable over most of the kinematical range of the event-shape. In the dijet limit, which is attained for the thrust variable [1] as $T \to 1$, the convergence of the fixed-order expansion is spoilt by large logarithmic terms $\log(1-T)$ at each order in the strong coupling constant, thus it necessitates a resummed description. During LEP times, precision studies of a standard set of six event-shapes were based on the combination of fixed-order NLO calculations [2–9] with NLL resummation [10–12]. To avoid the double counting of terms, both expansions need to be matched to each other according to matching procedures such as the R and $\log(R)$ schemes [13]. In the recent past, substantial progress

[1] Speaker

was made both on the fixed-order and the resummed description of event-shapes. Following the development of new methods for calculations of QCD jet observables at NNLO [14], the NNLO corrections to $e^+e^- \to 3$ jets and related event-shape observables were computed [15–20]. More recently, in the context of Soft-Collinear-Effective-Theory, the N^{2}LL resummation for thrust [23, 24] and the heavy jet mass [25] has been performed and applied for a precise determination of α_s, and the framework for the resummation of the jet broadening distributions has been outlined [26,27]. In these calculations, the $\mathcal{O}(\alpha_s^2)$ soft corrections were determined only up to a constant term by exploiting the renormalisation group invariance of the cross section. Such term is also needed to unambiguously match the resummed distribution to the NNLO result in the R scheme. In this talk we report on the direct computation of these corrections and we provide a new resummed formula. Finally we match the latter to the existing NNLO prediction comparing two different matching schemes.

2 Fixed-order and resummed distributions

The differential thrust distribution in perturbation theory is numerically known at NNLO [16, 19]. At a centre-of-mass energy Q and for a renormalisation scale μ it reads

$$\begin{aligned}\frac{1}{\sigma}\frac{\mathrm{d}\sigma}{\mathrm{d}\tau}(\tau,Q) = \bar{\alpha}_s(\mu)\frac{\mathrm{d}A}{\mathrm{d}\tau}(\tau) + \bar{\alpha}_s^2(\mu)\frac{\mathrm{d}B}{\mathrm{d}\tau}(\tau,x_\mu) \\ + \bar{\alpha}_s^3(\mu)\frac{\mathrm{d}C}{\mathrm{d}\tau}(\tau,x_\mu) + \mathcal{O}(\bar{\alpha}_s^4)\,,\end{aligned} \tag{1}$$

where we defined

$$\bar{\alpha}_s = \frac{\alpha_s}{2\pi}\,, \qquad x_\mu = \frac{\mu}{Q}\,, \tag{2}$$

and where σ is the total perturbative hadronic cross-section for $e^+e^- \to$ hadrons. The explicit dependence on the renormalisation scale is given by

$$\frac{\mathrm{d}B}{\mathrm{d}\tau}(\tau,x_\mu) = \frac{\mathrm{d}B}{\mathrm{d}\tau}(\tau) + 2\beta_0\,\log(x_\mu^2)\frac{\mathrm{d}A}{\mathrm{d}\tau}(\tau), \tag{3}$$

$$\begin{aligned}\frac{\mathrm{d}C}{\mathrm{d}\tau}(\tau,x_\mu) = \frac{\mathrm{d}C}{\mathrm{d}\tau}(\tau) + 2\,\log(x_\mu^2)\big(2\beta_0\frac{\mathrm{d}B}{\mathrm{d}\tau}(\tau) \\ + 2\beta_1\frac{\mathrm{d}A}{\mathrm{d}\tau}(\tau)\big) + \big(2\beta_0\,\log(x_\mu^2)\big)^2\,\frac{\mathrm{d}A}{\mathrm{d}\tau}(\tau).\end{aligned} \tag{4}$$

The QCD β-function is defined by the renormalisation group equation for the QCD coupling constant

$$\frac{d\alpha_s(\mu)}{d\log\mu^2} = -\alpha_s(\mu)\left(\frac{\alpha_s(\mu)}{\pi}\beta_0 + \frac{\alpha_s^2(\mu)}{\pi^2}\beta_1 + \dots\right). \tag{5}$$

The normalised thrust cross-section is then defined as

$$R_T(\tau) \equiv \frac{1}{\sigma}\int_0^1 \frac{d\sigma\,(\tau', Q)}{d\tau'}\Theta(\tau - \tau')d\tau', \tag{6}$$

where σ is the total cross section for $e^+e^- \to$ hadrons. In the two-jet region the fixed-order thrust distribution is enhanced by large infrared logarithms which spoil the convergence of the perturbative series. The convergence can be restored by resumming the logarithms to all orders in the coupling constant. The matched cross section can in general be written as

$$R_T(\tau) = C(\alpha_s)\Sigma(\tau, \alpha_s) + D(\tau, \alpha_s), \tag{7}$$

where

$$C(\alpha_s) = 1 + \sum_{k=1}^{\infty} C_k \bar{\alpha}_s^k, \tag{8}$$

$$\begin{aligned}\log\Sigma(\tau, \alpha_s) &= \sum_{n=1}^{\infty}\sum_{m=1}^{n+1} G_{nm}\bar{\alpha_s}^n L^m \\ &= Lg_1(\alpha_s L) + g_2(\alpha_s L) + \frac{\alpha_s}{\pi}\beta_0 g_3(\alpha_s L) + \dots\end{aligned} \tag{9}$$

where $L \equiv \log(1/\tau)$. The function g_1 encodes all the leading logarithms, the function g_2 resums all next-to-leading logarithms and so on. The constant terms C_i are required to achieve a full $\mathrm{N}^{1+i}\mathrm{LL}$ accuracy. $D(\tau, \alpha_s)$ is a remainder function that vanishes order-by-order in perturbation theory in the dijet limit $\tau \to 0$.

In view of matching the NNLL resummed distribution to the NNLO fixed order prediction using the R-matching scheme, we need to include the logarithmically subleading terms C_2, C_3 and G_{31} in the expansions (8),(9).

The resummation of the thrust distribution beyond NLL was first achieved in [23] using an effective-theory approach and revisited in [28], where the full analytic expressions for the $\mathcal{O}(\bar{\alpha}_s^2)$ constant term C_2 and the coefficient G_{31} were also obtained. The $\mathcal{O}(\bar{\alpha}_s^3)$ constant term C_3 is currently unknown, and a numerical estimate is given in [28] together with the full analytic expressions of the functions $g_i(\alpha_s L)$.

2.1 Factorisation and Resummation

Factorisation properties of event-shapes have been widely studied in the literature [33–35]. Referring to Fig. 1 we recast the cross section (6) as

$$R_T(\tau) = H\left(\frac{Q}{\mu},\alpha_s(\mu)\right)\int dk^2 d\bar{k}^2 \mathcal{J}\left(\frac{k}{\mu},\alpha_s(\mu)\right)\bar{\mathcal{J}}\left(\frac{\bar{k}}{\mu},\alpha_s(\mu)\right) \times \int dw \mathcal{S}\left(\frac{w}{\mu},\alpha_s(\mu)\right)\Theta(Q^2\tau-\bar{k}^2-k^2-wQ)+\mathcal{O}(\tau), \quad (10)$$

where we neglected terms of order $\mathcal{O}(\tau)$ which are absorbed in the remainder function $D(\tau,\alpha_s)$. We use the integral representation of the Θ-function

$$\Theta(Q^2\tau-\bar{k}^2-k^2-wQ) = \frac{1}{2\pi i}\int_C \frac{d\nu}{\nu}\,\mathrm{e}^{\nu\tau Q^2}\mathrm{e}^{-\nu k^2}\mathrm{e}^{-\nu\bar{k}^2}\mathrm{e}^{-\nu wQ}, \quad (11)$$

and the Laplace transform to recast Eq. (10) as

$$R_T(\tau) = H\left(\frac{Q}{\mu},\alpha_s(\mu)\right)\frac{1}{2\pi i}\int_C \frac{dN}{N}\,\mathrm{e}^{\tau N}\tilde{J}^2\left(\sqrt{\frac{N_0}{N}}\frac{Q}{\mu},\alpha_s(\mu)\right)\tilde{S}\left(\frac{N_0}{N}\frac{Q}{\mu},\alpha_s(\mu)\right) \quad (12)$$

where we set $N=\nu Q^2$ and $N_0 = e^{-\gamma_E}$. The soft subprocess $\tilde{S}\left(N_0/NQ/\mu,\alpha_s(\mu)\right)$ describes the

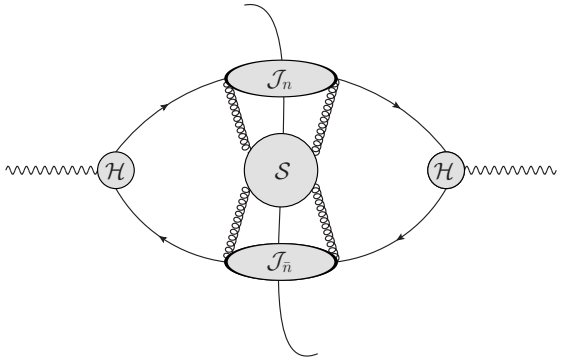

Figure 1: Leading regions in dijet factorisation.

interaction between the two jets of hard collinear particles through soft gluon exchange. It can be therefore defined in a gauge invariant way as a correlator of Wilson lines

$$\tilde{S}\left(\frac{N_0}{N}\frac{Q}{\mu},\alpha_s(\mu)\right) = \frac{Q}{N_c}\int d\tau_s \mathrm{e}^{-\tau_s N}\sum_{k_{eik}}\langle 0|W^\dagger_{\bar{n}}(0)W^\dagger_n(0)|k_{eik}\rangle\mathcal{J}_{cut}(\tau_s Q)\langle k_{eik}|W_n(0)W_{\bar{n}}(0)|0\rangle, \quad (13)$$

where we defined $\tau_s = w/Q$. W_n and $W_{\bar{n}}$ are Wilson lines

$$W_n(y) = \mathbf{P}\text{exp}\left(ig\int_0^\infty ds\, n\cdot A(ns+y)\right), \tag{14}$$

describing the eikonal interaction of soft gluons with the fast moving quarks along the light-like directions n^μ and $\bar{n}^\mu$ respectively. $A(ns+y)$ in eq. (14) denotes the gluon field in QCD. The sum runs over the final states $|k_{eik}\rangle$ involving k soft particles whose phase space is constrained according to the thrust trigger function $\mathcal{J}_{cut}(\tau Q^2)$. Both soft and soft-collinear contributions are encoded into the soft subprocess. The two-loop expression was computed analytically in [28] by performing direct phase-space cuts. The results are in agreement with those presented in [31, 32]. The collinear subprocess $\mathcal{J}$ ($\bar{\mathcal{J}}$) describes the decay of the jet-initiating hard quark (antiquark) into a jet of collinear particles moving along the n^μ ($\bar{n}^\mu$) direction. It is therefore an inclusive quantity which can be found in many other relevant QCD processes such as deep inelastic scattering and heavy quarks decay [21, 29, 36]. The short-distance hard function $H\left(Q/\mu, \alpha_s(\mu)\right) = |\mathcal{H}\left(Q/\mu, \alpha_s(\mu)\right)|^2$ takes into account the hard virtual corrections to the quark-antiquark production subprocess. It is free of large logarithms and it can be generally defined such that Eq. (10) reproduces the fixed-order cross section up to power suppressed terms.
Using the Renormalisation Group evolution of the soft and collinear subprocesses [28, 29, 36], we can recast eq. (12) as

$$\begin{aligned} R_T(\tau) =& H\left(\frac{Q}{\mu}, \alpha_s(\mu)\right)\frac{1}{2\pi i}\int_C \frac{dN}{N}\,\mathrm{e}^{\tau N}\tilde{J}^2\left(1, \alpha_s(\sqrt{\frac{N_0}{N}}Q)\right)\tilde{S}\left(1, \alpha_s(\frac{N_0 Q}{N})\right)\times \\ & \exp\Bigg\{-2\int_{\frac{N_0}{N}}^1 \frac{du}{u}\left[\int_{u^2Q^2}^{uQ^2}\frac{dk^2}{k^2}\mathcal{A}(\alpha_s(k^2)) + \mathcal{B}(\alpha_s(uQ^2))\right]\Bigg\}, \end{aligned} \tag{15}$$

where the two coefficients $\mathcal{A}(\alpha_s)$ and $\mathcal{B}(\alpha_s)$ can be computed in perturbation theory. The coefficient $\mathcal{A}(\alpha_s)$ reads

$$\mathcal{A}(\alpha_s) = \Gamma_{\text{cusp}}(\alpha_s) - \beta(\alpha_s)\frac{\partial\Gamma_{\text{soft}}(\alpha_s)}{\partial\alpha_s}, \tag{16}$$

where $\Gamma_{\text{cusp}}(\alpha_s)$ and $\Gamma_{\text{soft}}(\alpha_s)$ are the cusp and the soft anomalous dimensions respectively. The former, together with the coefficient $\mathcal{B}(\alpha_s)$ can be extracted from the asymptotic limit of the $P_{qq}(\alpha_s, z)$ splitting function [30, 37] as $z \to 1$

$$P_{qq}(\alpha_s, z) \to 2\frac{\Gamma_{\text{cusp}}(\alpha_s)}{(1-z)_+} + 2\mathcal{B}(\alpha_s)\delta(1-z) + ... \tag{17}$$

The integration countour in eq. (15) runs parallel to the imaginary axis on the right of all singularities of the integrand. From eq. (15) we see that the u-integral in the exponent is regularised by the lower bound $\frac{N_0}{N}$. Such a bound acts as an infrared regulator which prevents the strong coupling constant from being evaluated at non-perturbative scales ($\leq \Lambda_{QCD}$). Then, the contour in eq. (15) should be set away from all the singularities (in particular from the Landau pole). Nevertheless, for resummation purposes we can set the contour on the left of the Landau singularity since it would contribute with a non-logarithmic effect suppressed with some negative power of the center-of-mass energy scale. The inversion of the Laplace transform can be performed analytically by using the residue theorem as shown in [10, 28] and results in

$$R_T(\tau) = \left(1 + \sum_{k=1}^{\infty} C_k \left(\frac{\alpha_s}{2\pi}\right)^k\right) \exp\left[\log\frac{1}{\tau} g_1(\lambda) + g_2(\lambda) + \frac{\alpha_s}{\pi}\beta_0 g_3(\lambda) + \left(\frac{\alpha_s}{2\pi}\right)^3 G_{31} \log\frac{1}{\tau}\right], \quad (18)$$

where

$$\begin{aligned} g_1(\lambda) =&\ f_1(\lambda), \\ g_2(\lambda) =&\ f_2(\lambda) - \log\Gamma(1 - f_1(\lambda) - \lambda f_1'(\lambda)), \\ g_3(\lambda) =&\ f_3(\lambda) + \left(f_1' + \frac{1}{2}\lambda f_1''(\lambda)\right)\left(\psi^{(0)}(1-\gamma(\lambda))^2 - \psi^{(1)}(1-\gamma(\lambda))\right) + f_2'(\lambda)\psi^{(0)}(1-\gamma(\lambda)) \\ &+ C_F/\beta_0\left(\gamma_E\left(3/2 - \gamma_E\right) - \pi^2/6\right). \end{aligned} \quad (19)$$

The functions $f_i(\lambda)$ as well as the constants C_1, C_2 and G_{31} are defined in [28], while the C_3 constant term is still analytically unknown. We fit the latter numerically using the fixed order Monte Carlo parton-level generator `EERAD3`. The fit is performed by subtracting the $\mathcal{O}(\alpha_s^3)$ logarithmic structure from the fixed-order result and taking (numerically) the asymptotic limit $\tau \to 0$.

`EERAD3` is run with a technical cutoff $y_0 = 10^{-5}$ which affects the thrust distribution below $\tau_0 \sim \sqrt{y_0}$. This forbids us from probing the far infrared region and we perform the fit for values of τ larger than τ_0. Numerical fixed order results are obtained with 6×10^7 points for the leading colour contribution and 10^7 points for the subleading colour structures. Because of the presence of large fluctuations in the Monte Carlo results, each color contribution is fitted separately over an interval where the distribution is stable and the different results are combined to find the numerical value of C_3. As an alternative approach we first sum up all the color contributions and then fit C_3. We consider the difference between the two approaches as a systematic error and as final result we obtain

$$C_3 = -1050 \pm 180(\text{stat.}) \pm 500(\text{syst.}). \quad (20)$$

Considering that there is no statistical correlation between different bin errors, as a different possible estimate of the systematic uncertainty due to the sizeable fluctuation, we varied the fit range observing that it does not alter the result in any significant way outside the quoted systematic error margins. In Fig. 2 we vary the value of C_3 within its error band and we study its impact on the distribution. We observe that the numerical impact of C_3 on the distributions is less than 1.5‰ and it is therefore completely negligible compared the other theoretical uncertainties such that the large relative error range is tolerable for all practical purposes.

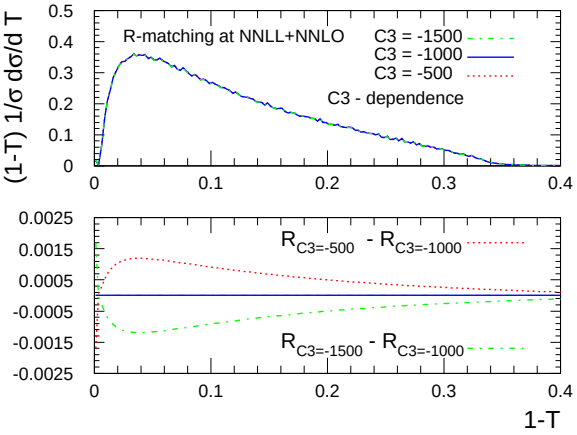

Figure 2: Impact of C_3 variation

2.2 Matching to fixed-order and numerical results

In this section we match the obtained resummed distribution (18) to the NNLO fixed order prediction. The matching formalism must avoid double counting and allow to access theoretical uncertainties. We compare the R-matching and $\log(R)$-matching schemes described in [13].

In Fig. 3 we compare the differential cross section of the new matched NNLL+NNLO results with the old NLL+NNLO derived in [41]. The correction due to the resummation is sizable, leading to a 8% increase of the distribution around the peak region. The effect of the additional resummed subleading logarithms becomes progressively less important towards the multijet region, where the increase is nevertheless of about 5%. It is interesting to note that the matching of NNLO with NNLL resummation shifts the pure NNLO result also in the multijet region (Fig. 4). This was not the case for NLL+NNLO, for which the impact of resummation in the region of large τ was negligible. This is another sign of the importance of the NNLL contribution.

The renormalisation scale dependence, which was observed to increase from pure NNLO to NLL+NNLO [41, 44] because of a mismatch in the cancellation of renormalisation scale logarithms, is obtained by varying $0.5 < x_\mu < 2$. It decreases at NNLL+NNLO by 20% in the peak region compared to NLL+NNLO. The magnitude of the scale uncertainty varies between 4% in the 3-jet region and 5% around the peak. In Fig. 5 we compare the R-matching and the $\log(R)$-matching scheme predictions at NNLL+NNLO. The difference between the two matching prescriptions is tiny and lies well below the scale uncertainty. This implies a very good stability of the theoretical predictions under variation of the matching scheme.

One further source of arbitrariness is the choice of the logarithms to be resummed. In fact, it is not clear whether powers of $\alpha_s \log(1/\tau)$ or powers of *e.g.* $\alpha_s \log(2/\tau)$ have to be resummed. The origin of this arbitrariness has to do with how much of the non-logarithmic part of the fixed-order prediction is exponentiated together with the logarithms. We can express this arbitrariness by introducing a new parameter x_L, which rescales the logarithms as [13]: $L \to \hat{L} = \log(1/(x_L \tau))$.

We can estimate the related uncertainty by varying the parameter x_L. In Ref. [13] several prescriptions are given on how to set the correct variation range for x_L for different observables. For the sake of simplicity and since we are not performing a fit of the strong coupling constant, we choose to vary x_L within the canonical interval $0.5 < x_L < 2$, similarly to what is chosen to quantify the renormalisation scale uncertainty. This choice is also close to the nominal range of variation proposed in [13]. The impact of this variation is shown in Fig. 6. The

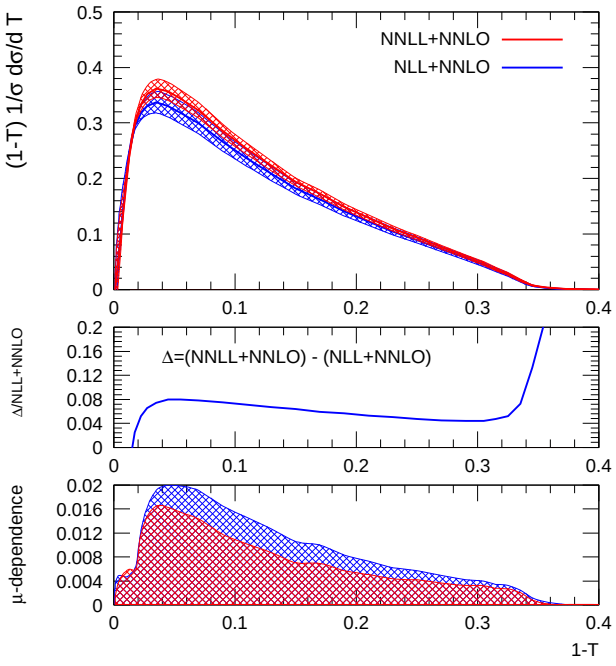

Figure 3: Comparison of the Thrust distributions with NNLL+NNLO and NLL+NNLO accuracy. The plot on the top shows the two distributions, with the uncertainty band due to scale dependence. The curve in the middle shows the difference between NNLL+NNLO and NLL+NNLO normalised to the NLL+NNLO curve. The impact of the resummation at NNLL is an increase in the distribution of order 5-8%. The lowest plot shows the absolute scale dependence of the two curves.

left plots show a comparison of the x_L-dependence between NLL+NNLO and NNLL+NNLO

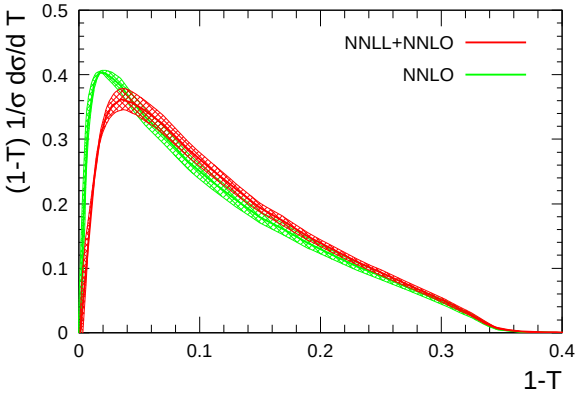

Figure 4: Comparison of the Thrust distribution at NNLO with the matched NNLL+NNLO predictions. The contribution of NNLL resummation is sizable over the full thrust range.

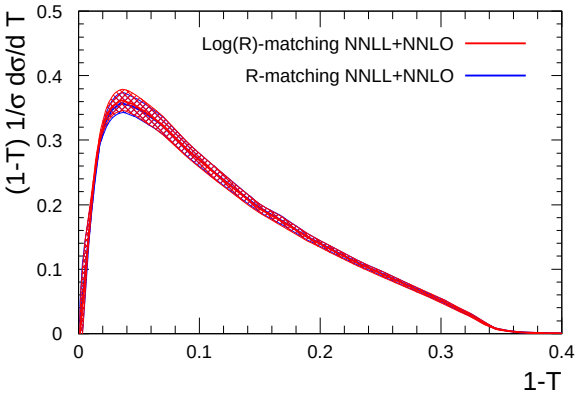

Figure 5: Comparison of the results obtained with the R-matching scheme and the $\log(R)$-matching scheme . The width of the curve shows the uncertainty related to the scale variation.

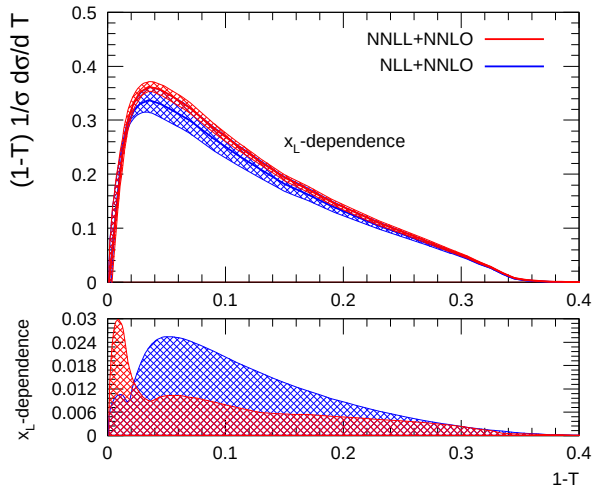

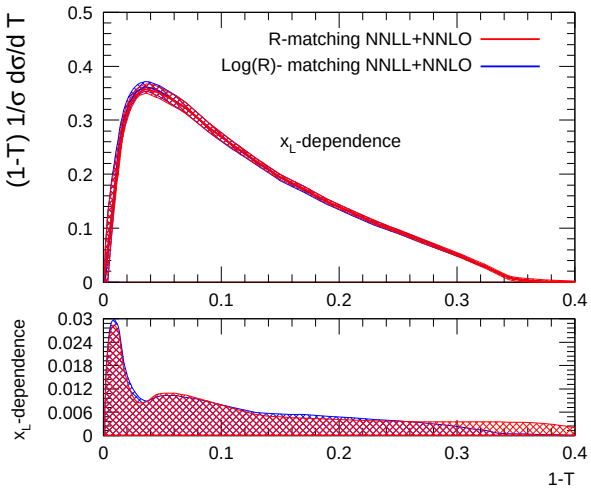

Figure 6: Dependence on the resummed logarithms, determined by varying the parameter x_L. The left plot shows the change in the x_L dependence between NLL+NNLO and NNLL+NNLO. The upper plot shows the distributions with the corresponding uncertainty band, in the lower plot we compare only the uncertainties. In the right plot the x_L dependence using the two different matching schemes is shown.

predictions. The lower plot allows to quantify the reduction of the uncertainty due to a variation x_L. Apart from the far infrared region, it is observed to decrease by 50% in the peak region. The scale-dependence reduction is smaller towards the multijet region, where the contribution of the logarithmic part becomes less important. The resummation uncertainty at NNLL+NNLO varies between 2% and 3%. In the right plot the same comparison is made at NNLL+NNLO using the R-matching and $\log(R)$-matching schemes. We observe a similar x_L-dependence in both schemes.

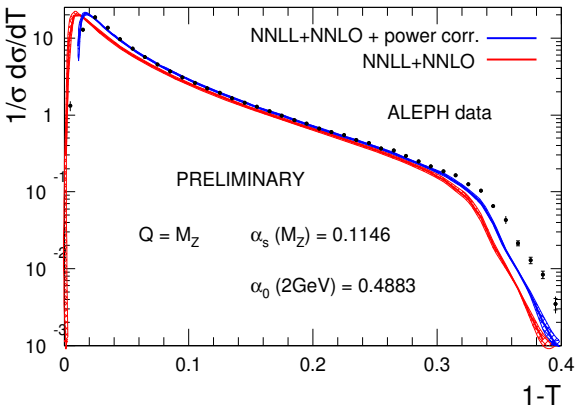

Figure 7: Theoretical prediction with (blue) and without (red) power corrections compared to ALEPH data. The non-perturbative parameter α_0 as well as the strong coupling constant α_s are fitted to experimental data.

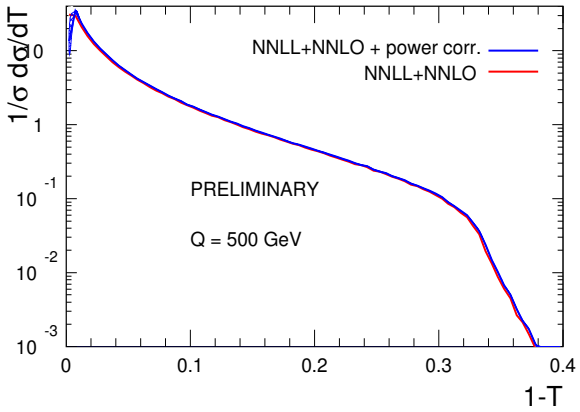

Figure 8: Comparison of the perturbative (red) and power-corrected (blue) distributions at a center of mass energy of 500 GeV. The plot shows how much hadronisation corrections get suppressed at typical future linear collider energies.

3 Outlook

The recent results on event-shape resummation improve the description of existing experimental data. In view of future work at high energy linear colliders and precise determinations of the strong coupling constant, N^{2}LL predictions for the remaining Event-Shape observables are necessary. Moreover, an additional source of uncertainty is due to power-behaving hadronisation corrections which get large in the dijet region. Currently there is no deep theoretical understanding of such corrections which constitute an important source of theoretical error. In the past, these were often computed using leading-logarithmic parton shower Monte Carlo programs, which turned out to be clearly insufficient [44] in view of the precision now attained by the perturbative description. Systematic approaches to hadronization within the

dispersive model [40, 47] or by using the shape function formalism [24, 46] are offering a more reliable description. Such corrections are quite sizeable at LEP energies (Fig. 7) while they are highly suppressed at future linear colliders energies (Fig. 8). In Fig. 7 we show what the power-corrected distribution looks like when compared to the pure perturbative answer. Non-perturbative corrections are computed with a dispersive model [47] and both the mean effective coupling α_0 and the strong coupling α_s are obtained by performing a simultaneous fit using ALEPH data at $Q = 91.2$ GeV. Such a fit is purely qualitative since the correlation matrix is degenerate when only one data set is used. To perform a meaningful fit, experimental data over a broader range of energies have to be included. We will address this issue in a future publication.

4 Acknowledgments

This research is supported in part by the Swiss National Science Foundation (SNF) under contract 200020-138206, by the UK STFC, by the European Commission through the "LHCPhenoNet" Initial Training Network PITN-GA-2010-264564 and by the National Science Foundation under grant NSF PHY05-51164.

References

[1] S. Brandt, C. Peyrou, R. Sosnowski and A. Wroblewski, Phys. Lett. **12** (1964) 57;
E. Farhi, Phys. Rev. Lett. **39** (1977) 1587.

[2] R. K. Ellis, D. A. Ross and A. E. Terrano, Nucl. Phys. B **178** (1981) 421.

[3] R. K. Ellis, D. A. Ross and A. E. Terrano, Phys. Rev. Lett. **45** (1980) 1226.

[4] Z. Kunszt, Phys. Lett. B **99** (1981) 429.

[5] J. A. M. Vermaseren, K. J. F. Gaemers and S. J. Oldham, Nucl. Phys. B **187** (1981) 301.

[6] K. Fabricius, I. Schmitt, G. Kramer and G. Schierholz, Z. Phys. C **11** (1981) 315.

[7] Z. Kunszt and P. Nason, *QCD at LEP*, CERN Yellow Report 89-08 (1989), p.373.

[8] W. T. Giele and E. W. N. Glover, Phys. Rev. D **46** (1992) 1980.

[9] S. Catani, M. H. Seymour, Phys. Lett. **B378** (1996) 287. [hep-ph/9602277];

[10] S. Catani, L. Trentadue, G. Turnock, B. R. Webber, Nucl. Phys. **B407** (1993) 3.

[11] Y.L. Dokshitzer, A. Lucenti, G. Marchesini and G.P. Salam, JHEP **9801** (1998) 011 [hep-ph/9801324].

[12] A. Banfi, G.P. Salam and G. Zanderighi, JHEP **0201** (2002) 018 [hep-ph/0112156].

[13] R. W. L. Jones, M. Ford, G. P. Salam, H. Stenzel, D. Wicke, JHEP **0312** (2003) 007. [hep-ph/0312016].

[14] A. Gehrmann-De Ridder, T. Gehrmann and E. W. N. Glover, JHEP **0509** (2005) 056 [hep-ph/0505111].

[15] A. Gehrmann-De Ridder, T. Gehrmann, E. W. N. Glover, G. Heinrich, JHEP **0711** (2007) 058 [arXiv:0710.0346].

[16] A. Gehrmann-De Ridder, T. Gehrmann, E. W. N. Glover, G. Heinrich, JHEP **0712** (2007) 094 [arXiv:0711.4711].

[17] A. Gehrmann-De Ridder, T. Gehrmann, E. W. N. Glover, G. Heinrich, Phys. Rev. Lett. **99** (2007) 132002 [arXiv:0707.1285].

[18] S. Weinzierl, JHEP **0907** (2009) 009 [arXiv:0904.1145].

[19] S. Weinzierl, JHEP **0906** (2009) 041 [arXiv:0904.1077].

[20] S. Weinzierl, Eur. Phys. J. C **71** (2011) 1565 [arXiv:1011.6247].

[21] G. F. Sterman, Nucl. Phys. B **281** (1987) 310.

[22] D. de Florian and M. Grazzini, Nucl. Phys. B **704** (2005) 387 [hep-ph/0407241].

[23] T. Becher, M.D. Schwartz, JHEP **0807** (2008) 034 [arXiv:0803.0342].

[24] R. Abbate, M. Fickinger, A. H. Hoang, V. Mateu, I. W. Stewart, Phys. Rev. **D83** (2011) 074021.

[25] Y.T. Chien, M.D. Schwartz, JHEP **1008** (2010) 058 [arXiv:1005.1644].

[26] J. -y. Chiu, A. Jain, D. Neill, I. Z. Rothstein, [arXiv:1104.0881].

[27] T. Becher, G. Bell and M. Neubert, Phys. Lett. B **704** (2011) 276 [arXiv:1104.4108 [hep-ph]].

[28] P. F. Monni, T. Gehrmann and G. Luisoni, JHEP **1108** (2011) 010 [arXiv:1105.4560 [hep-ph]].

[29] T. Becher and M. Neubert, Phys. Lett. B **637** (2006) 251 [hep-ph/0603140].

[30] T. Becher, M. Neubert and B. D. Pecjak, JHEP **0701** (2007) 076 [hep-ph/0607228].

[31] R. Kelley, M. D. Schwartz, R. M. Schabinger and H. X. Zhu, Phys. Rev. D **84** (2011) 045022.

[32] A. Hornig, C. Lee, I. W. Stewart, J. R. Walsh and S. Zuberi, JHEP **1108** (2011) 054.

[33] J.C Collins, D.E. Soper, G. Sterman, in *Perturbative Quantum Chromodynamics*, ed. A.H. Mueller (World Scientific Singapore, 1989).

[34] C. F. Berger, T. Kucs, G. F. Sterman, Phys. Rev. **D68** (2003) 014012. [hep-ph/0303051]; Int. J. Mod. Phys. **A18** (2003) 4159. [hep-ph/0212343].

[35] S. Fleming, A. H. Hoang, S. Mantry and I. W. Stewart, Phys. Rev. D **77** (2008) 074010.

[36] G. P. Korchemsky and G. F. Sterman, Phys. Lett. B **340** (1994) 96 [hep-ph/9407344].

[37] G. P. Korchemsky, Mod. Phys. Lett. A **4** (1989) 1257.

[38] G. Dissertori, A. Gehrmann-De Ridder, T. Gehrmann, E. W. N. Glover, G. Heinrich, H. Stenzel, JHEP **0802** (2008) 040. [arXiv:0712.0327].

[39] G. Dissertori, *et al.*, Phys. Rev. Lett. **104** (2010) 072002 [arXiv:0910.4283].

[40] T. Gehrmann, M. Jaquier and G. Luisoni, Eur. Phys. J. C **67** (2010) 57 [arXiv:0911.2422].

[41] T. Gehrmann, G. Luisoni, H. Stenzel, Phys. Lett. **B664** (2008) 265 [arXiv:0803.0695].

[42] R. A. Davison and B. R. Webber, Eur. Phys. J. C **59** (2009) 13 [arXiv:0809.3326].

[43] S. Bethke, S. Kluth, C. Pahl and J. Schieck [JADE Collaboration], Eur. Phys. J. C **64** (2009) 351.

[44] G. Dissertori, A. Gehrmann-De Ridder, T. Gehrmann, E. W. N. Glover, G. Heinrich, G. Luisoni, H. Stenzel, JHEP **0908** (2009) 036. [arXiv:0906.3436].

[45] G. Abbiendi *et al.* [OPAL Collaboration], Eur. Phys. J. C **71** (2011) 1733 [arXiv:1101.1470 [hep-ex]].

[46] G. P. Korchemsky and G. F. Sterman, Nucl. Phys. B **555** (1999) 335 [hep-ph/9902341].

[47] Y. L. Dokshitzer, G. Marchesini and B. R. Webber, Nucl. Phys. B **469** (1996) 93 [hep-ph/9512336].

8.6 F. Becattini - The statistical hadronisation model

The statistical hadronization model in e^+e^- collisions

F. Becattini
Dipartimento di Fisica e Astronomia, Universitá di Firenze, Italy
becattini@fi.infn.it

Abstract In this contribution I will summarize the main achievements of the statistical hadronization model in e^+e^-collisions.

1 Introduction

The idea of applying statistical concepts to the problem of multi-particle production in high energy collisions dates back to a work of Fermi [1] in 1950, who assumed that particles originated from an excited region evenly occupying all available phase space states. This was one of Fermi's favorite ideas and soon led to an intense effort in trying to work out the predictions of inclusive particle rates calculating, analytically and numerically, the involved multidimensional phase-space integrals. When it became clear that the (quasi) isotropic particle emission in the center-of-mass frame predicted by Fermi's model was ruled out by the data, an amendment was put forward by Hagedorn [2] in the '60s, who postulated the existence of two hadron emitting sources flying apart longitudinally in the center-of-mass frame of a pp collision. Thereby, one could explain the striking difference between spectra in transverse and longitudinal momentum. Hagedorn was also able to explain the almost universal slope of p_T spectra in his renowned statistical bootstrap model, assuming that resonances are made of hadrons and resonances in turn.

After QCD turned up, many phenomenological models of strong interactions were no longer pursued and the statistical model was no exception. The resurgence of interest in these ideas came about when it was argued that a completely equilibrated hadron gas would be a clear signature of the formation of a transient Quark-Gluon Plasma (QGP) in heavy ion collisions at high energy. While it has been indeed confirmed that an (almost) fully equilibrated hadron gas has been produced in those collisions, the interest in this model was also revived by the unexpected observation that it is able to accurately reproduce particle multiplicities in elementary collisions [3]. Naively, one did not expect a statistical approach to work in an environment where the number of particles is $\mathcal{O}(10)$ because it was a belief of many that a hadronic thermalization process would take a long time if driven by hadronic collisions. Apparently this is not the case and one of the burning questions, which is still waiting a generally accepted answer, is why a supposedly non-thermal system exhibits a striking thermal behavior.

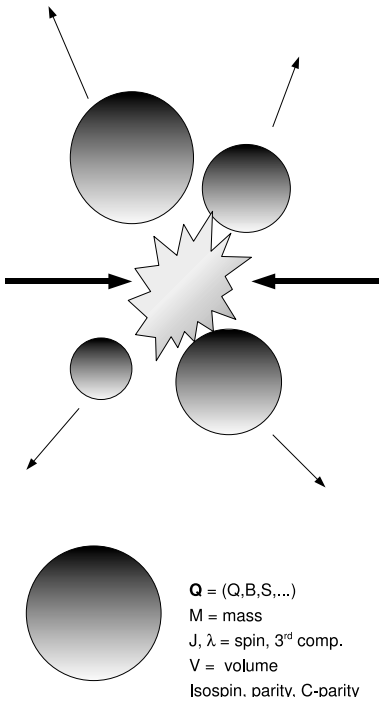

Figure 1: High energy collisions are assumed to give rise to multiple clusters at the hadronization stage [top]. Each cluster [bottom] is a colorless extended massive object endowed with abelian charges (electric, strange, baryonic etc.), intrinsic angular momentum and other quantum numbers such as parity, C-parity and isospin.

2 The model

The Statistical Hadronization Model (SHM) must be considered as an effective model describing the process of hadron formation in high energy collisions at energy (or distance) scales where perturbative QCD is no longer applicable. A high energy collision is thought of as a complex dynamical process, governed by QCD, which eventually gives rise to the formation of extended massive colorless objects defined as *clusters* or *fireballs* (see Fig. 1). While the multiplicity, masses, momenta and charges of these objects are determined by this complex dynamical process, the SHM postulates that hadrons are formed from the decay of each cluster in a purely statistical fashion, that is:

> *Every multihadronic state localized within the cluster and compatible with conservation laws is equally likely.*

This is the *urprinzip* of the SHM. The assumption of the eventual formation of massive colorless clusters is common for many hadronization models (e.g. the cluster model implemented in the Monte-Carlo code HERWIG [4]) based on the property of color preconfinement exhibited by perturbative QCD. The distinctive feature of the SHM is that clusters have a finite spacial size. This aspect of clusters as a relativistic massive extended objects coincides with that of a bag in the MIT bag model [5]. Indeed, the SHM can be considered as an effective model to calculate bag decays.

The requirement of finite spacial extension is crucial. If the SHM is to be an effective representation of the QCD-driven dynamical hadronization process, this characteristic must be ultimately related to the QCD fundamental scale $\Lambda_{\rm QCD}$. As we will see, the universal soft scale shows up in the approximately constant energy density at hadronization; in other words, the volume of clusters is in a constant ratio with their mass when hadronization takes place. It is also worth stressing here that there is clear, independent evidence of the finite size of hadronic sources in high energy collisions. Quantum interference effects in the production of identical particles, the so-called Bose-Einstein correlations or Hanbury Brown-Twiss second-order interference, is by now a firmly established phenomenon. This effect would simply be impossible without a finite volume.

3 Results in high energy collisions

Each individual cluster produced in a high energy collision (shown in Fig. 1), should be hadronized so as to fulfill conservation laws for each cluster. In a statistical mechanical language, this implies that averages are to be calculated within the microcanonical ensemble. However, this is very difficult, and if one is interested in more inclusive quantities involving all clusters, simplifying assumptions can be introduced (see ref. [3]).

In the multi-cluster averaging process, it can be shown that suitable assumptions reduce the calculation of inclusive multiplicities of particle species to those produced by one global cluster having as volume the sum of volumes of single clusters. This global cluster generally turns out to be large enough in mass and volume so that the canonical ensemble becomes a good approximation of the more fundamental microcanonical ensemble; in other words, a temperature can be introduced which replaces the *a priori* more fundamental description in terms of energy density. This "global" temperature closely mirrors the value of energy density at which clusters hadronize.

In this approach, the primary multiplicity of each hadron species j is given by [6]:

$$\langle n_j \rangle^{\rm primary} = \frac{VT(2S_j+1)}{2\pi^2} \sum_{n=1}^{\infty} \gamma_S^{N_s n} (\mp 1)^{n+1} \, \frac{m_j^2}{n} \, {\rm K}_2\left(\frac{n m_j}{T}\right) \, \frac{Z(\mathbf{Q} - n\mathbf{q}_j)}{Z(\mathbf{Q})} \qquad (1)$$

where V is the (mean) volume and T the temperature of the equivalent global cluster. Here

$Z(\mathbf{Q})$ is the canonical partition function depending on the initial abelian charges $\mathbf{Q} = (Q, N, S, C, B)$, i.e., electric charge, baryon number, strangeness, charm and beauty, respectively; m_j and S_j are the mass and the spin of the hadron j, $\mathbf{q}_j = (Q_j, N_j, S_j, C_j, B_j)$ its corresponding charges; the upper sign applies to bosons and the lower sign to fermions. The parameter γ_S in (1) is an extra phenomenological factor implementing an *ad hoc* suppression of hadrons with N_s strange valence quarks with respect to the equilibrium value. This parameter is outside a pure thermodynamical framework and it is needed to reproduce the data, as we will see.

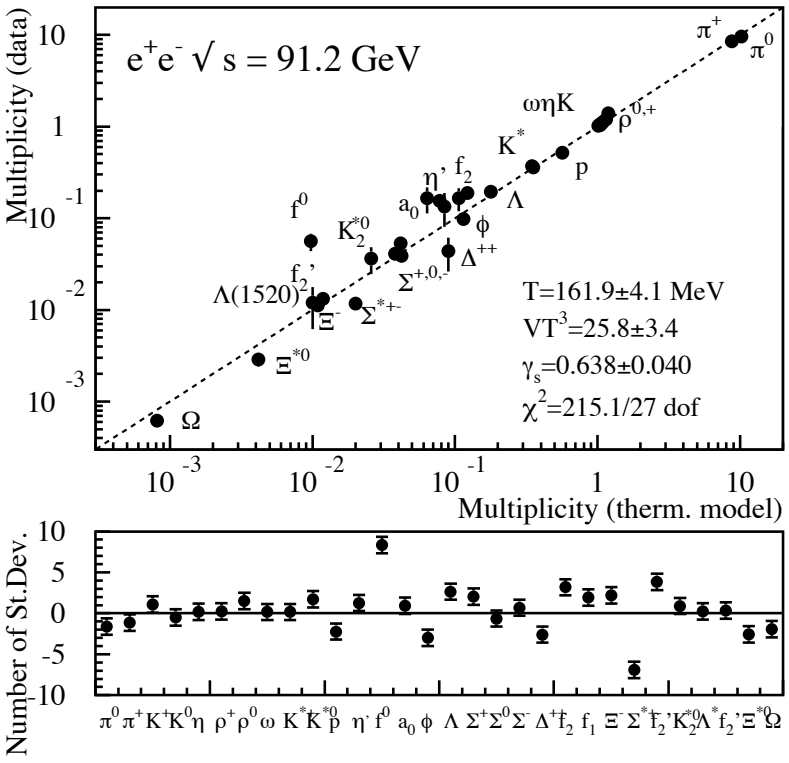

Figure 2: Upper panel: measured vs theoretical multiplicities of light-flavoured hadrons in e^+e^-collisions at $\sqrt{s} = 91.25$ GeV. Lower panel: fit residuals (from ref. [7]).

The light-flavoured multiplicities in e^+e^-show a very good agreement with the predictions of the model, as it shown in Fig. 2: the temperature value is about 160 MeV and the strangeness undersaturation parameter $\gamma_S \sim 0.7$. Similar good agreements are found for many kinds of

$\sqrt{s}$ (GeV)	ρ (GeV/fm^3)	γ_S	χ^2/dof
2.1	0.24 ± 0.17	0.66 ± 0.22	93.4/16
2.2	0.36 ± 0.20	0.86 ± 0.22	82.6/14
2.4	0.44 ± 0.30	0.78 ± 0.36	55.4/17
2.6	0.56 ± 0.36	0.62 ± 0.47	44.9/12

Table 1: Summary of the fit results to multi-hadronic exclusive channels at different centre-of-mass energies. Also shown the correlation coefficient of ρ and γ_S (from ref. [8]).

high energy elementary collisions over a large energy range [3]. Also, an excellent agreement between measured and predicted relative abundances of heavy flavoured hadronic species in e^+e^-collisions by using the model parameters fitted to light-flavoured multiplicities [3, 7].

4 Exclusive channels in e^+e^-collisions at low energy

We have recently performed a stringent test of the statistical model by comparing its predictions with the production rates of exclusive channels in e^+e^-collisions at low energy [8]. To carry out the calculation, we have taken advantage of the formalism developed in two previous papers [9, 10] where the microcanonical partition function of an ideal multi-species relativistic gas was calculated enforcing the conservation of the maximal set of observables pertaining to space-time symmetries (energy-momentum, spin, helicity, parity).

At low energy, where exclusive rates measurements are available, the formation of a single cluster at rest in the centre-of-mass frame of an e^+e^-collision is assumed. Its mass therefore coincides with $\sqrt{s}$ and the other quantum numbers are those of the initial state. Particularly, in e^+e^-collision, the hadron production is dominated by the diagram with an intermediate virtual photon, so that the hadronizing cluster is assigned with a spin, parity and C-parity $J^{PC} = 1^{--}$.

Finally, for the geometry of the cluster, we have assumed a spherical shape and a volume given by:

$$V = \frac{M}{\rho} = \frac{\sqrt{s}}{\rho} \tag{2}$$

where M is the mass and ρ the energy density; this is taken to be a free parameter to be determined by comparing the model with the data.

For our data points, we have examined the energy interval from 2 to 3 GeV, in order to avoid resonance region and not to overcome charm production threshold. Much data in this energy interval has been lately provided by the BABAR experiment which has measured the cross-sections of several multi-hadronic channels in e^+e^-collisions at several centre-of-mass energies with the method of initial state radiation. We have chosen four energy points, that is $\sqrt{s} = 2.1$,

2.2, 2.4 and 2.6 GeV and added to the available BABAR measurements older measurements performed by experiments at e^+e^-colliders run at the same centre-of-mass energies and collected in a nice review paper [11].

The fit results are summarized in table 4; the detailed comparison between data and model predictions can be found in ref. [8] Although the fit quality is not perfect in terms of statistical test, one can fairly conclude that the statistical hadronization model is able to satisfactorilty reproduce most exclusive multi-hadronic channels measured in e^+e^-collisions at low energy. Especially at 2.4 GeV, all measured channel rates lie within 2.5 standard deviations from the model values, which is quite remarkable taking into account the obvious fact that exclusive channels are a very stringent test for any model, certainly much more than inclusive multiplicities, and that the fits were done with only 4 free parameters.

Overall, the most interesting outcome of the analysis are the values of the fitted energy density ρ and strangeness suppression parameter γ_S, shown in table,4, around 0.5 GeV/fm^3 and 0.7 respectively. These values are essentially the same obtained with the analysis of inclusive hadronic multiplicities at high energy [3].

5 Conclusions

The main message I want to convey in this talk is that the statistical hadronization model is a very good hadronization model for e^+e^-collisions, capable of reproducing at a very good level of accuracy many hadronization-related observables with a minimal number of free parameters. Its modelling of hadronization process is not based on ad hoc concepts but it uses the concept of statistical equilibrium, posing intriguing questions on its origins in the non-linear regime in strong interactions (see discussion in ref. [3]). This model can be implemented in Monte-Carlo codes to replace traditional string-model based hadronization. This is an ongoing project [12], that we aim at accomplishing before the advent of the high energy e^+e^-linear collider.

Acknowledgments

I would like to thank the organizers, and especially Lia Pancheri, for their excellent work and their kind hospitality.

References

[1] E. Fermi, Prog. Th. Phys. **5** 570 (1950).

[2] R. Hagedorn, Nuovo Cim. Suppl. **3** 147 (1965).

[3] F. Becattini, *Introduction to the statistical hadronization model*, arXiv:0901.3643; F. Becattini, R. Fries in *Relativistic heavy ion physics*, Landolt-Börnstein 1-23 (2010), arXiv:0907.1031, and references therein.

[4] G. Corcella et al, J. High En. Phys., 0101:010 (2001) and references therein.

[5] A. Chodos et al, Phys. Rev. D **9** 3471.

[6] F. Becattini and G. Passaleva, Eur. Phys. J. C **23** 551 (2002).

[7] F. Becattini, P. Castorina, J. Manninen and H. Satz, Eur. Phys. J. C **56** 493 (2008).

[8] L. Ferroni and F. Becattini, Eur. Phys. J. C **71** (2011) 1824.

[9] F. Becattini and L. Ferroni, Eur. Phys. J. C **51** (2007) 899.

[10] F. Becattini and L. Ferroni, Eur. Phys. J. C **52** (2007) 597.

[11] M. R. Whalley, J. Phys. G **29** (2003) A1.

[12] C. Bignamini, F. Becattini and F. Piccinini, *A Monte-Carlo generator for statistical hadronization in high energy e+e- collisions*, arXiv:1204.2300.

8.7 F. Bigazzi and A.L. Cotrone - String theory meets QCD

String Theory meets QCD

Francesco Bigazzi [1]
Universitá di Firenze and INFN Sezione di Pisa, Italy
bigazzi@fi.infn.it

Aldo L. Cotrone
Universitá di Torino and INFN Sezione di Torino, Italy
cotrone@to.infn.it

Abstract The holographic correspondence, developed within string theory, provides a novel set of tools to address non-perturbative problems in quantum field theory. We provide a short, basic review on some informations which can be inferred, by means of this approach, on equilibrium as well dynamical properties of toy models of the strongly coupled QCD quark-gluon plasma produced in heavy ion collisions at RHIC and LHC.

1 Introduction

One of the most relevant challenges for theoretical particle physics is to provide non-perturbative tools to deduce the low energy properties of QCD. This is certainly relevant if one wants to compare QCD predictions with experimental data. Standard powerful techniques, like Lattice QCD or effective models are not always enough for this aim. The former, a first-principle approach to quantum chromodynamics, is still not optimized to address real-time problems (e.g. hydrodynamic behavior, response to perturbations, jet quenching) or to study finite baryon density regimes. The latter are not always satisfying in that they provide, for example, model-dependent predictions on many relevant features of the QCD phase diagram.

The holographic approach is emerging as a novel complementary method to address non-perturbative problems in quantum field theories in and out equilibrium. It is based on a proposed boundary-to-bulk correspondence between ordinary quantum field theories and theories of gravity (strings) in at least one higher dimension. Hints for such a correspondence came from many different directions, from QCD phenomenology (Veneziano amplitude and Regge trajectories) to black hole thermodynamics and the holographic principle, from 't Hooft's large N limit to D-brane physics and open-closed string duality. See [1] for a review.

The first explicit realization of the correspondence [2, 3, 4] involves a conformal field theory (CFT) in 4 space-time dimensions, with gauge group SU(N), 4 adjoint Weyl fermions and 6

[1] Speaker

adjoint real scalars - the $\mathcal{N} = 4$ supersymmetric Yang-Mills (SYM)- and a theory of closed strings on a 10d background given by the direct product of a non-compact Anti-de Sitter (AdS) space-time in 5 dimensions and a compact 5-sphere. This AdS/CFT connection has then been extended to other classes of models with less or no supersymmetry and with no conformal invariance (see e.g. [5] for reviews).

The most remarkable feature of the correspondence is that it works as a duality: certain regimes where a quantum field theory is strongly interacting, are mapped into the low-energy limit of a weakly interacting string model, which amounts to be a classical theory of gravity. For the explicit example given above, this is realized when the number of colors and the 't Hooft coupling of the CFT are taken to be very large: $N \gg 1$, $\lambda \equiv g^2_{YM} N \gg 1$. In these limits, therefore, holography allows to solve extremely difficult quantum problems just mapping them into classical gravity ones.

The holographic map between string and quantum field theories provides theoretically falsifiable predictions and it is supported by an enormous amount of validity checks. Moreover it is well suited to study equilibrium (e.g. vacuum structure, mass spectra and phase diagrams) as well as non-equilibrium problems (hydrodynamic behavior, response to quantum quenches, thermalization, interaction with dynamical probes) both at zero and at finite temperature and densities. It is thus an amazing achievement for theoretical physics.

Despite the fact that the applicability of the holographic approach to phenomenologically relevant theories like QCD is still technically limited to toy models, it is providing novel perspectives on various classes of phenomena for which a standard description in terms of weakly coupled quasi-particles is missing. In this short contribution, we will pick a notable example within such a class: the strongly coupled [6] quark-gluon plasma (QGP) phase of QCD emerging in high energetic heavy ion collisions such as those studied in current experiments at RHIC and LHC. This phase occurs at temperatures above the confinement-deconfinement crossover at $T_c \sim 170 MeV$.

There are solid lattice indications that the QGP is nearly conformal in the temperature window relevant for the present experiments $1.5T_c \leq T \leq 4T_c$. Our first crude approximation for the QCD plasma in that window will thus consist in modeling it by a strongly coupled 4d CFT (like the above mentioned SYM) with a holographic dual description. In the finite temperature case, the latter turns out to be a gravity model on a 5d AdS black hole background. We will see how this toy model works quite well, at least for what concerns some real-time properties of the QCD plasma, like its hydrodynamical transport coefficients. For a recent complete review on holographic methods for the QGP see [7].

2 Basic Holography and Thermal AdS/CFT

As we have pointed out, the master AdS/CFT example of [2, 3, 4] involves a 10d background with a compact part given by a five-sphere. Let us reduce the gravity model over this compact space and work from now on with a theory defined on the remaining five non-compact directions.

The holographic correspondence maps ingredients in a quantum field theory into dual ones in the gravity model. As a first relevant input, the renormalization group scale is dual to a radial extra dimension r in the gravity background. Other relevant entries of the holographic dictionary are as follows.

Field theory vacua correspond to gravity background solutions. In particular, deconfined phases at finite temperature (and charge density) correspond to (charged) black hole solutions. For an uncharged finite temperature 4d CFT in thermodynamic equilibrium, the dual gravity description [8] is provided by an AdS_5 black hole, whose metric (in Minkowski signature) can be written as

$$ds_5^2 = \frac{r^2}{L^2}\left[-b(r)dt^2 + dx_i dx_i\right] + \frac{L^2}{b(r)r^2}dr^2\,, \tag{1}$$

where $b(r) = 1-(r_h/r)^4$, L is the AdS radius and $i = 1,2,3$ label the space directions. Here r_h is the radial position of the event horizon. It defines the black hole temperature, which is in turn holographically mapped into the temperature of the CFT, by

$$T = \frac{r_h}{\pi L^2}\,. \tag{2}$$

When $r_h = 0$ one recovers the AdS_5 metric (with natural "boundary" at $r \to \infty$), dual to the CFT at zero temperature.

Holography maps the (uncharged) QFT partition function $Z_{QFT} = Tr(e^{-H/T}) = e^{-F/T}$ (where F is the free energy) into some string partition function Z_s. The latter, in the classical gravity regime where the corresponding QFT is strongly coupled, is actually replaced by its saddle point value $Z_s \sim e^{-S_g(on-shell)}$. For a CFT, S_g is the Euclidean 5d gravity action with negative cosmological constant

$$S_g = -\frac{1}{16\pi G_5}\int dt_E\, d^3x\, dr\sqrt{-g}\left[\mathcal{R} - \frac{12}{L^2}\right] + S_{GH}\,, \tag{3}$$

where S_{GH} is the Gibbons-Hawking boundary term which we leave implicit. In the above expression the Euclidean time coordinate t_E has to be compactified on a circle of length $1/T$. Moreover this action has to be evaluated on-shell, i.e. on the AdS black hole solution (1) with Euclidean signature ($t_E = it$). The result is divergent for two reasons: i) the infinite volume V_3 of the 3 non-compact space directions; ii) the divergence coming from the radial integration.

The first infinite term can be avoided by just working with volume densities; the other one can be systematically removed, either by subtracting to the action some other "reference" one (e.g. the action for the $T = 0$ case) or, equivalently, by adding suitable covariant "counterterms" following the so-called "holographic renormalization" prescription [9]. The final result, which we denote by $S_g^{ren}(on - shell)$, is finite (modulo V_3) and provides, through the map with the field theory partition function, a precise expression for the free energy density of the CFT

$$\mathcal{F} \equiv \frac{F}{V_3} = \frac{TS_g^{ren}(on - shell)}{V_3} = -\frac{1}{16\pi G_5}\frac{r_h^4}{L^5}\,. \tag{4}$$

This can be expressed in terms of field theory quantities using (2) as well as a model-dependent relation involving the AdS radius L and G_5. For the $SU(N)$ $\mathcal{N} = 4$ CFT this relation reads

$$\frac{L^3}{4G_5} = \frac{N^2}{2\pi}\,, \tag{5}$$

which clearly shows how the classical gravity regime $L \gg l_{Planck} \sim G_5^{1/3}$ is realized in the large N limit. Using the relations above we find

$$\mathcal{F} = -\frac{\pi^2}{8}N^2T^4\,. \tag{6}$$

From this expression we can deduce the whole thermodynamics of the $\mathcal{N} = 4$ SYM in the planar ($N \to \infty$) strong 't Hooft coupling regime ($\lambda \to \infty$). In particular, the entropy density

$$s \equiv \frac{S}{V_3} = -\frac{\partial \mathcal{F}}{\partial T} = \frac{\pi^2}{2}N^2T^3\,, \tag{7}$$

as well as the pressure $p = -\mathcal{F}$ and the energy density $\epsilon = \mathcal{F} + Ts$ easily follow. It turns out that $\epsilon = 3p$, consistently with the fact that the trace of the stress-energy tensor for a CFT at equilibrium is zero. Moreover, the expression in (7) is perfectly consistent with the Bekenstein-Hawking formula $S = A_h/4G_5$ for the entropy of the 5d black hole (where A_h is the horizon area, given in the present case by $A_h = (r_h/L)^3V_3$).

What is relevant in these expressions is that they are finite. Their scaling with powers of N and T would have been expected on general grounds: $N^2 \gg 1$ accounts for the number of adjoint degrees of freedom of the deconfined $SU(N)$ plasma; T is the only dimensionful scale for the CFT and the dependence of the thermodynamical quantities on the latter is dictated by dimensional analysis. What really matters are the finite overall numerical coefficients which are what holography predicts in the non-perturbative $\lambda \gg 1$ regime. Comparing the above quantities with those at zero coupling, we can also realize that the CFT thermodynamics is not so sensitive to the coupling regime. For example it turns out that $\epsilon/\epsilon_0 = 3/4$, where ϵ_0 is the

energy density of the free SYM theory (at $\lambda = 0$). Remarkably, a similar ratio is found (from Lattice QCD) for the energy density of the QGP w.r.t. that of a free gas of quarks and gluons.

Gauge invariant single trace operators $\mathcal{O}$ are mapped into gravity fields Φ. The basic formula, which allows to compute (e.g. the Euclidean) correlation functions in a quantum field theory from gravity data is [3, 4]

$$Z_{QFT}[\Phi_0(x)] \equiv \langle e^{-\int \Phi_0(x)\mathcal{O}(x)} \rangle_{QFT} = Z_s[\Phi_0(x)] \sim e^{-S_g(\Phi_0(x))}\,, \tag{8}$$

where $\Phi_0(x) \equiv \lim_{r\to\infty} r^\alpha \Phi(x,r)$ is the boundary value of the 5d gravity field Φ dual to the operator $\mathcal{O}$. For a CFT, α is precisely given in terms of the conformal dimension of $\mathcal{O}$. The Euclidean gravity action $S_g(\Phi_0)$, describing the fluctuating mode Φ over the (say, AdS black hole) background, has to be evaluated on-shell on the solution for Φ satisfying the above boundary condition as well as an appropriate one in the interior. The left hand side of the formula above is the generating functional of the (Euclidean) correlation functions of the operator $\mathcal{O}$ in the QFT. This formula thus allows to compute correlation functions at strong coupling just by solving classical equations of motion. It can be extended to real-time Minkowski correlators as well.

The map between operators and fields is also dictated by the symmetries and the requirement of Lorentz invariance on the boundary. Thus, for example, a scalar operator like TrF^2 is mapped into a massless scalar field ϕ (for a 4d CFT, there is a general holographic relation between the scalar mass in AdS_5 and the conformal dimension of the dual operator: $\Delta(\Delta - 4) = m^2 L^2$). Moreover a conserved current J_μ is mapped into a gauge field A_μ in 5d. Furthermore, the stress energy tensor $T_{\mu\nu}$ is mapped into the metric field $g_{\mu\nu}$.

3 Hydrodynamics from AdS/CFT

At long distances and times compared to some microscopical scale (like e.g. the mean free path), the fluctuations around local thermal equilibrium are described by hydrodynamics. For a (zero density) CFT at finite temperature the only relevant energy scale is provided by T, and thus the hydrodynamic approximation applies when frequencies and momenta of a perturbation are such that $\omega, |\vec{k}| \ll T$.

Due to the presence of dissipative terms, hydrodynamics is not expressed starting from an action principle. Instead it is written in terms of conservation laws for the stress energy tensor (and of currents when they are present). The latter is in turn expressed, by means of constitutive equations, in a derivative expansion in the fluid velocity and temperature. Up to first order, the expansion of the energy-momentum tensor for a relativistic uncharged fluid reads

$$T^{\mu\nu} = \varepsilon u^\mu u^\nu + p\Delta^{\mu\nu} - \eta\sigma^{\mu\nu} - \Delta^{\mu\nu}\zeta(\nabla\cdot u)\,, \tag{9}$$

where ε is the energy density, u^μ the velocity field (normalized as $u^2 = -1$), $p(\varepsilon)$ the pressure, $\Delta^{\mu\nu} = h^{\mu\nu} + u^\mu u^\nu$ with $h^{\mu\nu}$ the 4-dimensional metric. We refer to [10] for the precise definition of the first-order-in derivative expression for $\sigma^{\mu\nu}$, which is not necessary here.

The shear viscosity η is the only non trivial coefficient for a conformal fluid. Tracelessness in fact implies that the bulk viscosity ζ is zero. This is not precisely what happens for the quark-gluon plasma, especially near T_c: however ζ_{QCD} is reasonably small for larger temperatures, so that the toy-CFT model we are considering here does not come totally unjustified.

For a general strongly coupled theory, the theoretical determination of the transport coefficients is a daunting task. In the case at hand, on the contrary, they can be extracted with a reasonable amount of work from gravity. The shear viscosity, for example, can be derived in quantum field theory using linear response, via the Kubo formula

$$\eta = \lim_{\omega\to 0} \frac{1}{2\omega} \int dt\ d\vec{x}\ e^{i\omega t}\ \langle [T_{xy}(t,\vec{x}), T_{xy}(0,\vec{0})] \rangle\ . \tag{10}$$

The above stress-tensor correlator (evaluated at thermal equilibrium) can be computed from the basic holographic formula (8) focusing on the on-shell gravity action for the g_{xy} component of the metric. This gives the value of the shear viscosity over entropy density [11]

$$\frac{\eta}{s} = \frac{1}{4\pi}\ . \tag{11}$$

This result for $\mathcal{N} = 4$ SYM in the planar limit is surprisingly compatible with the experimental data at RHIC and LHC, even though experimental errors remain large. Other methods of obtaining this quantity, such as perturbative QCD or lattice, give higher values, hardly compatible with experiments.

4 Concluding remarks

The holographic approach has been employed to explore many other relevant properties of strongly coupled plasmas like second order hydrodynamic transport coefficients and jet quenching, see [7] for a review. Moreover, the original toy-model considered here, has been extended so to account for some missing crucial features of the real-world QGP, like the presence of dynamical matter fields transforming in the fundamental representation of the gauge group (the quarks), the finite baryon density or, more generally, the breaking of conformal invariance. Some of the authors' contributions in that field can be found in [12, 13, 14].

Acknowledgments

The research of A. L. C. and F. B. is supported by the European Community Seventh Framework Programme FP7/2007-2013, under grant agreements n. 253534 and 253937.

We would like to thank the Italian students, parents, teachers and scientists for their activity in support of public education and research.

References

[1] O. Aharony, S. S. Gubser, J. M. Maldacena, H. Ooguri and Y. Oz, Phys. Rept. **323**, 183 (2000).

[2] J. M. Maldacena, Adv. Theor. Math. Phys. **2**, 231 (1998) [Int. J. Theor. Phys. **38**, 1113 (1999)].

[3] S. S. Gubser, I. R. Klebanov and A. M. Polyakov, Phys. Lett. B**428**, 105 (1998).

[4] E. Witten, Adv. Theor. Math. Phys. **2**, 253 (1998).

[5] O. Aharony, "The non-AdS/non-CFT correspondence, or three different paths to QCD," arXiv:hep-th/0212193. M. Bertolini, Int. J. Mod. Phys. A **18**, 5647 (2003). F. Bigazzi, A. L. Cotrone, M. Petrini and A. Zaffaroni, Riv. Nuovo Cim. **25N12**, 1 (2002).

[6] E. V. Shuryak, Nucl. Phys. A **750**, 64 (2005).

[7] J. Casalderrey-Solana, H. Liu, D. Mateos, K. Rajagopal and U. A. Wiedemann, "Gauge/String Duality, Hot QCD and Heavy Ion Collisions", arXiv:1101.0618 [hep-th].

[8] E. Witten, Adv. Theor. Math. Phys. **2**, 505 (1998).

[9] K. Skenderis, Class. Quant. Grav. **19**, 5849 (2002).

[10] L.D. Landau and E. M. Lifshitz, "Fluid Mechanics", Pergamon Press 1987.

[11] G. Policastro, D. T. Son and A. O. Starinets, Phys. Rev. Lett.**87**, 081601 (2001).

[12] F. Bigazzi, A. L. Cotrone, J. Mas, A. Paredes, A. V. Ramallo and J. Tarrio, JHEP **0911**, 117 (2009).

[13] F. Bigazzi, A. L. Cotrone, J. Mas, D. Mayerson and J. Tarrio, JHEP **1104**, 060 (2011).

[14] F. Bigazzi, A. L. Cotrone and J. Tarrio, JHEP **1002**, 083 (2010). F. Bigazzi and A. L. Cotrone, JHEP **1008**, 128 (2010).

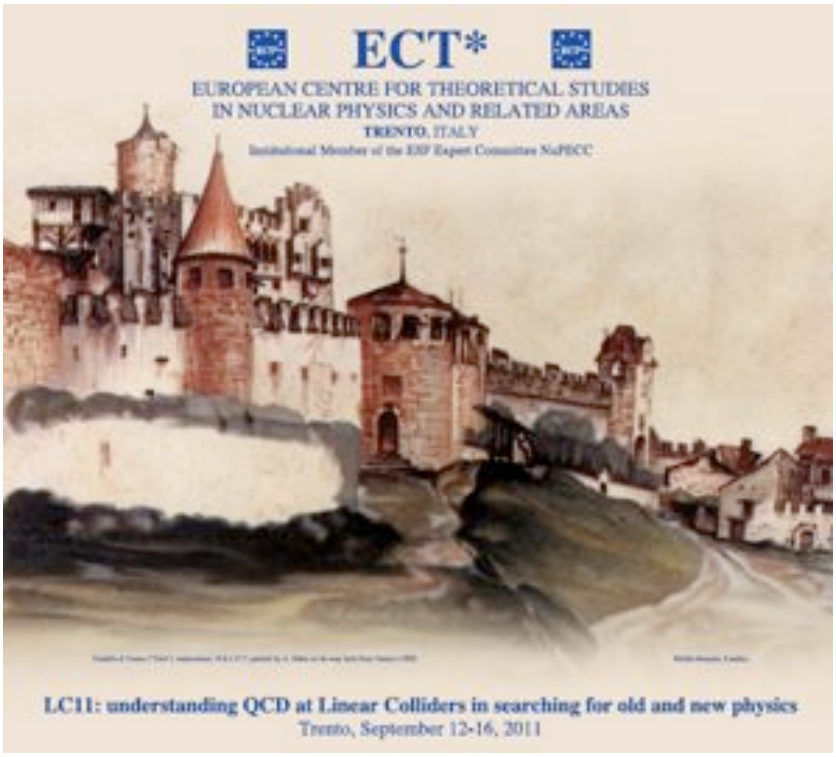

Castello di Trento painted by A. Dürer on his way back from Venice (1495).

Chapter 9

Programme

Programme

Monday 12 September
Future LC projects and theoretical appraisal

14:15 A. Masiero (University and INFN, Padova, Italy): Update on today's theoretical landscape
15.00 F. Richard (LAL, Orsay, France): Update on ILC
16.15 R. Corsini (CERN, Geneva, Switzerland): Update on CLIC
17.00 M. Ross (FNAL, Batavia, USA): Machine options for an ILC at 1 TeV
17:45 E. Eichten (FNAL, Batavia, USA): Physics prospects at a muon collider

Tuesday 13 September
Dark Matter searches

9:30 M. Cirelli (SPhT, Saclay and CERN, Geneva, Switzerland): Tools for Dark Matter indirect detection

Precision measurements at e^+e^- colliders and elsewhere

10.00 M. Spira (PSI, Villingen, Switzerland): Precision Higgs physics at the LHC and future LCs
10.30 F. Jegerlehner (Humboldt University, Berlin, Germany): Implications of low and high energy measurements on SUSY models 11:00 Coffee break

11.30 D. Nomura (Tohoku University, Japan): Muon g-2 re-evaluated using new precise data
12.00 G. Venanzoni (INFN, Frascati, Italy): Latest on g-2 from experiment Medium energy projects in future e+e- physics
12.30 M. Ciuchini (University and INFN, Roma III, Italy): SuperB

DIS and photon-photon physics

14:30 N. Armesto (Santiago de Compostela University, Spain): QCD at an electron-hadron collider at CERN: the LHeC project
15:00 A. Finch (Lancaster University, UK): Two photon physics at CLEO and LEP and a LC
15.30 G. Pancheri (INFN, Frascati, Italy): LC hadronic total cross-sections and forward physics at LHC: what to learn for LC 16:00 Coffee break
16:30 F. Kapusta (LPNHE, Paris, France): Color factors and color basis in two fermion pair production in photon-photon, photon-gluon and gluon-gluon collisions
17:00 W. da Silva (LPNHE, Paris, France): Two fermion pair production in photon-photon, photon-gluon and gluon-gluon collisions
17:30 D. Lopez-Val (University of Heidelberg, Germany): Single Higgs-boson production at a photon-photon collider: 2HDM versus MSSM 18:00 End of the session

Wednesday 14 September

QCD from partons to hadrons

9.30 N. Kauer (NExT, Royal Holloway University of London, UK): NLO automated tools for QCD and Beyond
10.00 J-C. Winter (CERN, Geneva, Switzerland): Systematic improvement of QCD parton showers
10.30 P.F. Monni (University of Zurich, Switzerland): Thrust-distribution resummation in e+e- collisions
11.30 F. Becattini (University and INFN, Firenze, Italy): The statistical hadronisation model
12.00 A.D. Martin (IPPP, Durham University, UK): Soft QCD production processes
12.30 R. di Sipio (University and INFN, Bologna, Italy): Top quarks in ATLAS and CMS

Thursday 15 September

The structure of QCD from the multi-TeV to the GeV scale

9:30 G. Bellettini (University and INFN, Pisa, Italy): QCD highlights from CDF (and D0)
10.00 N. Marinelli (University of Notre Dame, USA): QCD at LHC
10:30 I. Scimemi (University of Madrid, Spain): Latest development in SCET

Physics beyond the Standard Model

11.30 S. Bianco (INFN, Frascati, Italy): Searches for SUSY and BSM at the LHC
12.00 M. Kraemer (RWTH, Aachen, Germany): What if the LHC does not find supersymmetry in the sqrt(s)=7 TeV run?
12:30 R. Ferrari (University and INFN, Milano, Italy): Of Higgs, unitarity and other questions

Photon-photon Physics, Higgs and Top physics

14:30 R.M. Godbole (CTS/IISC, Bangalore, India): Photon-photon hadronic backgrounds at LC
15:00 S. Rosati (University and INFN, Roma, Italy): Higgs searches in ATLAS and CMS
15.30 G. Gutierrez (FNAL, Batavia, USA): Recent results on top quark physics at the Tevatron
16:30 R. Frederix (Zurich University, Switzerland): Selected topics on top quark physics at linear colliders
17:00 M. Muhlleitner (ITP, Karlsruhe, Germany): SM and BSM Higgs physics
17:30 F. Coradeschi (University and INFN, Firenze, Italy): Composite Higgs Model Phenomenology in top and bottom channels at CLIC Flavour Physics at LHC
18.00 S. Barsuk (LAL, Orsay, France): Heavy flavour and QCD results from LHCb

Friday 16 September
QCD from partons to hadrons

9:30 A.D. Martin (IPPP, Durham University, UK): Parton distributions of the proton
10:00 L. Cunqueiro Mendez (INFN, Frascati, Italy): Jet reconstruction in PbPb with ALICE Physics beyond the Standard Model
10.30 A. Crivellin (ITP, University of Bern, Switzerland): Flavour violation in the MSSM and implications for top and squark searches at colliders
11:30 F. Bigazzi (INFN, Pisa, Italy): String theory meets QCD, AdS/QCD, holography and all that The future of QCD in e+e- physics
12:00 A. Banfi (ETH, Zurich, Switzerland): QCD at work, from lepton to hadron colliders and back
12.30 S. Kluth (MPI, Munich, Germany): Experimental tests of QCD from GeV to TeV scale

Chapter 10

List of participants

Armesto Nestor - University of Santiago de Compostela, Spain
Banfi Andrea - ETH, Zurich, Switzerland
Barsuk Sergey - LAL, Orsay, France
Becattini Francesco - University and INFN, Firenze, Italy
Bellettini Giorgio - University and INFN, Pisa, Italy
Bianco Stefano - INFN, Frascati, Italy
Bigazzi Francesco - INFN, Pisa, Italy
Borzumati Francesca - Tohoku University, Japan
Cirelli Marco - SPhT, Saclay and CERN, Geneva, Switzerland
Ciuchini Marco - University and INFN, Roma III, Italy
Comelli Denis - INFN Ferrara, Italy
Coradeschi Francesco -University and INFN, Firenze, Italy
Corcella Gennaro - INFN Frascati, Italy
Corsini Roberto - CERN, Geneva, Switzerland
Crivellin Andreas - ITP, University of Bern, Switzerland
Cunqueiro Mendez Letitia - INFN, Frascati, Italy
Da Silva Wilfrid - LPNHE, Paris, France
Aldo De Andrea - Univ. Lyon, France
Di Sipio Riccardo -University and INFN, Bologna, Italy
Eichten Estia - FNAL, Batavia, USA
Ferrari Ruggero - University and INFN, Milano, Italy
Finch Alex - Lancaster University, UK
Frederix Rikkert - Zurich University, Switzerland
Godbole Rohini M. - CTS/IISC, Bangalore, India
Gutierrez Gaston - FNAL, Batavia, US
Illaryonov Alexei - U. Trento, Italy

Jegerlehner Fred - Humboldt University, Berlin, Germany
Kapusta Frederic - LPNHE, Paris, France
Kauer Nicolas - NExT, Royal Holloway University of London, UK
Kluth Stefan -MPI, Munich, Germany
Kraemer Michael - RWTH, Aachen, Germany
Lopez-Val David -University of Heidelberg, Germany
Marinelli Nancy - University of Notre Dame, USA
Martin Alan D. - IPPP, Durham University, UK
Masiero Antonio - University and INFN, Padova, Italy
Monni Pier Francesco - University of Zurich, Switzerland
Moretti Stefano - Southampton University , UK
Muhlleitner Margarete - ITP, Karlsruhe, Germany
Nomura Daisuke - Tohoku University, Japan
Pancheri Giulia - INFN Frascati, Italy
Panella Orlando - INFN Perugia, Italy
Richard Francois - LAL, Orsay, France
Rosati Stefano- University and INFN, Roma, Italy
Ross Marc - FNAL, Batavia, USA
Scimemi Ignatio - University of Madrid, Spain
Spira Michael - PSI, Villingen, Switzerland
Venanzoni Graziano - INFN, Frascati, Italy
Winter J-C. - CERN, Geneva, Switzerland